Exploration of new 17O-labeling strategies for carboxylic acids using mechanochemistry and application to high resolution NMR analyses

Jessica Spackova

THÈSE POUR OBTENIR LE GRADE DE DOCTEUR DE L'UNIVERSITÉ DE MONTPELLIER

En chimie organique, minérale, industrielle

École doctorale Sciences chimiques BALARD

Unité de recherche UMR5253

Exploration de nouvelles voies d'enrichissement d'acides carboxyliques en oxygène-17 grâce à la mécanochimie et application à des études RMN haute résolution

Présentée par Jessica ŠPAČKOVÁ

Le 9 décembre 2021

Sous la direction de Dr. Danielle LAURENCIN et Dr. Thomas-Xavier MÉTRO

Devant le jury composé de

Prof. Melinda DUER, University of Cambridge	Rapporteuse
Dr. Krunoslav UŽAREVIĆ, Ruđer Bošković Institute	Rapporteur
Dr. Myrtil KAHN, Laboratoire de Chimie de Coordination	Présidente
Dr. Céline CRAUSTE, Institut des Biomolécules Max Mousseron	Examinatrice
Dr. David TOUBOUL, Institut de Chimie des Substances Naturelles	Examinateur
Dr. Pau BERNADO, Centre de Biochimie Structurale	Examinateur
Dr. Danielle LAURENCIN, Institut Charles Gerhardt Montpellier	Directrice de thèse
Dr. Thomas-Xavier MÉTRO, Institut des Biomolécules Max Mousseron	Co-directeur de thèse

UNIVERSITÉ DE MONTPELLIER

RÉSUMÉ EN FRANÇAIS

L'oxygène est un élément omniprésent dans notre environnement, qui se trouve dans un grand nombre de composés organiques, inorganiques et hybrides. Il a trois isotopes stables: l'oxygène-16 (99.76 % d'abondance naturelle), l'oxygène-17 (0.04 %) et l'oxygène-18 (0.20 %). Les techniques analytiques qui reposent sur la signature d'isotopes stables dans des composés comprenant de l'oxygène peuvent fournir des informations intéressantes concernant leur structure et/ou leur réactivité. Malheureusement, l'abondance naturelle des isotopes ^{17}O et ^{18}O est très faible, et l'enrichissement en $^{17}O/^{18}O$ des composés peut être nécessaire pour pouvoir utiliser ces techniques.

Dans cette thèse, des voies d'enrichissement d'acides carboxyliques ont été développées, basées majoritairement sur la mécanochimie, et en utilisant de l'eau enrichie en $^{17}O/^{18}O$. Toutes les réactions mécanochimiques ont été réalisées à température et la pression ambiantes, et ont fourni des produits enrichis en $^{17}O/^{18}O$ rapidement, facilement et d'une manière peu coûteuse. Particulièrement, des acides gras ont été enrichis par deux protocoles mécanochimiques différentes: *i)* un protocole fondé sur l'activation de la fonction acide carboxylique à l'aide de CDI (1,1-carbonyldiimidazole) suivi d'une hydrolyse et *ii)* un protocole basé sur une saponification. Des acides aminés ont également été enrichis par la saponification mécanochimique, et ces protocoles ont été comparés à ceux par échange d'oxygènes en catalyse acide. Tous les produits enrichis ont été isolés purs avec des rendements corrects à élevés, et des taux d'enrichissement élevés. Ils ont été caractérisés par DRX, IR, MS et RMN multinucléaire, y compris par RMN solide ^{17}O.

Afin d'illustrer l'intérêt de ces nouvelles approches, l'acide oléique enrichi en ^{17}O a été utilisé pour la préparation de matériaux: de l'oléate de zinc et des nanoparticules d'oxyde de zinc fonctionnalisées par de l'acide oléique. La structure et la réactivé de ces composés sous irradiation UV ont été étudiées par RMN solide ^{17}O. Pour ce qui concerne les acides aminés enrichis en $^{17}O/^{18}O$, ils ont été protégés par le groupe Fmoc et utilisés dans la synthèse des peptides RGD et GRGDS enrichis en $^{17}O/^{18}O$, qui ont été charactérisés, entre autres, par RMN solide ^{17}O.

Mots clés: oxygène-17, oxygène-18, enrichissement isotopique, mécanochimie, acides gras, acides aminés, peptides, nanoparticules, RMN, MS

ABSTRACT IN ENGLISH

Oxygen is a ubiquitous element present in many inorganic, organic and hybrid compounds. It has three naturally stable isotopes: ^{16}O (99.76 % natural abundance), ^{17}O (0.04 %) and ^{18}O (0.20 %). Using analytical techniques that rely on the minor oxygen isotopes can bring additional information regarding the structure and reactivity of oxygen-containing compounds. Unfortunately, due to the very low natural abundance of $^{17}O/^{18}O$, such analyses often require to work with compounds enriched $^{17}O/^{18}O$.

In this thesis, new labeling schemes for $^{17}O/^{18}O$-enrichment of carboxylic acids based on mechanochemistry were developed using enriched water as a source of $^{17}O/^{18}O$-isotopes. All mechanochemical reactions were performed at room temperature and atmospheric pressure providing $^{17}O/^{18}O$-labeled products rapidly, in a user-friendly way and a cost-efficient manner. In particular, two different mechanochemical protocols were developed for $^{17}O/^{18}O$-labeling of fatty acids: a CDI-activation/hydrolysis approach and a saponification approach. For the labeling of amino acids, the mechanochemical saponification was applied and the results were compared to the acid-catalysed oxygen exchange approach. All the enriched products were isolated pure in moderate to high yields, and characterized by various analyses, including ^{17}O solid-state NMR spectroscopy.

In addition, ^{17}O-enriched oleic acid was used for the synthesis of two materials systems: zinc oleate and oleic acid-grafted ZnO nanoparticles. Oxygen-17 solid-state NMR was then used to explore their structure and to describe their reactivity under UV light irradiation. In parallel, the $^{17}O/^{18}O$-enriched amino acids were Fmoc-protected and used for the synthesis of the $^{17}O/^{18}O$-labeled peptides RGD and GRGDS, which were also characterized by solid-state ^{17}O NMR.

Key words: oxygen-17, oxygen-18, isotope enrichment, mechanochemistry, fatty acids, amino acids, peptides, nanoparticles, NMR, MS

ACKNOWLEDGEMENT

First of all, I would like to express my gratitude to my supervisors, Danielle Laurencin and Thomas-Xavier Métro, for giving me the opportunity to work on this project, to embrace so many different techniques and to further develop and shape my skills. I very much appreciate their constant support, optimism and catchy enthusiasm for high quality science.

The work presented on the following pages would not be possible without the assistance of colleagues from local analytical platforms, who were always available for a discussion and happy to help me solve all the puzzles I have encountered during the past few years. Specifically, I would like to thank Guillaume Cazals for the many, many MS analyses and Aurélien Lebrun for the solution NMR analyses. I would also like to thank Philippe Gaveau for his assistance with the solid-state NMR analyses, Saad Sene for the TEM analyses (and all the plastic pipet tips) and Dominique Granier for the flexible XRD time booking.

I would also like to thank Pascal Verdié and Manon Maurel from the SynBio3 platform for welcoming me in the group and providing me with their expertise in the solid-phase peptide synthesis.

I would also like to acknowledge our external collaborators: Dr. Ivan Hung, Dr. Zhehong Gan, Dr. Dinu Iuga and Dr. Julien Trébosc from the high-field NMR facilities for the high-resolution NMR analyses, Dr. Marie Hubert-Roux and Dr. Isabelle Schmitz-Afonso for the ultra-high resolution MS analyses and Prof. Christel Gervais for the *ab-initio* NMR calculations.

I am likewise grateful to the jury members Prof. Melinda Duer, Dr. Krunoslav Užarević, Dr. Myrtil Kahn, Dr. Céline Crauste, Dr. David Touboul and Dr. Pau Bernado for accepting to participate in my defence and for their valuable feedback.

I would like to thank all my colleagues from the Misotop lab, former and present, for their help with this project and for their kindness and friendship. I would especially like to thank Ieva for keeping my sugar level high with her delicious pastry, the boys from the Red Hot Milling Powders, Séb and César, for their extraordinary singing skills making me smile every time I hear them and Dorothée for her kind assistance with the difficulties the life abroad can bring.

Lastly, I would like to express my gratitude to my family who continuously supports me in my choices and especially to my partner Simon who agreed to move with me to France in the first place and who accompanied me on our many adventures.

LIST OF ABBREVIATIONS

***AA*:** Amino Acids

ATR-IR: Attenuated Total Reflectance Infrared spectroscopy

BET: Brunauer–Emmett–Teller analysis

CP: Cross Polarisation

CDI : 1,1'-carbonyldiimidazole

DCM: dichloromethane

DIEA: *N,N*-diisopropylethylamine

DFT: Density Functional Theory

DMF: *N,N*-dimethylformamide

DMSO: dimethylsulfoxide

EDX: Energy Dispersive X-Ray analysis

EL: Enrichment Level

EY: Enrichment Yield

ESI: ElectroSpray Ionisation

FA: Fatty Acids

FT-ICR: Fourier Transform Ion Cyclotron Resonance

HATU: Hexafluorophosphate Azabenzotriazole Tetramethyl Uronium

HFIP: Hexafluoroisopropyl alcohol

HPLC: High Performance Liquid Chromatography

HRMS: High Resolution Mass Spectrometry

LAG: Liquid Assisted Grinding

LCMS: Liquid Chromatography Mass Spectrometry

MAS: Magic Angle Spinning

MQMAS: Multiple Quantum Magic Angle Spinning

NMR: Nuclear Magnetic Resonance

NPs: Nanoparticles

PUFA: PolyUnsaturated Fatty Acids

SPPS: Solid Phase Peptide Synthesis

TEM: Transmission Electron Microscopy

TFA: trifluoroacetic acid

TGA: ThermoGravimetric Analysis

TIS: triisopropylsilane

VBM: Vibratory Ball Milling

XRD: X-ray Diffraction Analysis

ABBRÉVIATIONS FRANÇAISES

ATG: Analyse Thermogravimétrique

DRX: Diffraction aux Rayons X

***MET*:** Microscopie Électronique en Transmission

RMN: Résonance Magnétique Nucléaire

TABLE OF CONTENTS

RESUME EN FRANÇAIS

GENERAL INTRODUCTION

Oxygen is in mass the third most abundant element in the universe after hydrogen and helium, and the most abundant element in the earth's crust.[1] It was discovered independently by two scientists, Scheele in 1771 and Priestley in 1774, both producing a colourless gas by thermal decomposition of mercuric oxide. Priestley was first to publish his discovery, however, he never recognized the implications of his work, and used his observations to argue for the phlogiston theory instead (superseded theory describing chemical processes now known as "oxidation"). The first person who truly understood the potential of oxygen was Antoine Lavoisier, who provided oxygen with its name based on Greek roots "oxys" and "-genes", meaning "acid-forming", since he believed that it is an essential component of all acids. In a collaboration with his wife, Marie-Anne Paulze Lavoisier, he also proposed the role of oxygen in oxidizing metals and respiration processes, proving that oxygen was a chemical element, which finally discredited the phlogiston theory.

Oxygen is a highly reactive non-metallic atom that forms bonds with nearly all other elements. Due to its widespread abundance and its chemical properties, oxygen participates in a broad range of processes that build or protect our planet (*e.g.* as part of silicate materials present in the Earth's crust, or through the allotrope ozone, respectively). It is also one of the most abundant elements found in living organisms, comprising for two thirds of a mass of human body.[2] It is present in functional groups of many organic compounds, including essential molecules such as DNA, proteins, carbohydrates and lipids, but it also constitutes other structural elements such as bones and teeth, and it was therefore subjected to numerous studies.

Oxygen has three naturally occurring stable isotopes: the most abundant oxygen-16, and the minority isotopes oxygen-17 and oxygen-18 (see Table 1.1).

Table 1.1: Stable isotopes of oxygen, their natural abundance and cost of $^{17}O/^{18}O$-labeled water.

Isotope	Atomic mass[3]	Natural abundance[3]	Nuclear spin (I)	Cost of 1 mL of H_2O*
Oxygen-16	15.9949	99.757 %	0	-
Oxygen-17	16.9991	0.038 %	5/2	1800 - 2900€ (90% of ^{17}O)
Oxygen-18	17.9992	0.205 %	0	60 - 150 € (97 - 99% of ^{18}O)

Their discovery from atmospheric oxygen absorption bands in the late 1920s[4-6] triggered rapid development in many analytical techniques, especially in mass spectrometry (MS, using ^{18}O

isotope)[7] and in nuclear magnetic resonance (NMR, using ^{17}O isotope).[8] However, due to the very low natural abundance of $^{17}O/^{18}O$ isotopes, the $^{17}O/^{18}O$-enrichment of studied samples is required for a number of applications. Given the cost of $^{17}O/^{18}O$-labeled reagents (*e.g.* labeled water in Table 1.1), such treatments can turn out to be very costly, especially for ^{17}O NMR spectroscopy.

^{17}O NMR spectroscopy is an analytical technique particularly interesting for studying oxygen-containing compounds, due to the very high sensitivity of the ^{17}O NMR signal to the local environment of oxygen, and it has a great potential to bring new information regarding both structure and reactivity of studied systems.[9] However, NMR is not a sensitive technique and the only NMR active isotope, oxygen-17 (nuclear spin I = 5/2), has very low natural abundance (~ 0.04 %). Combined with its low receptivity (^{17}O is 10^{-5} less receptive compared to ^{1}H), it most-often imposes to work with ^{17}O-enriched samples. Among the few commercially available ^{17}O-enriched precursors, ^{17}O-enriched water is the most practical source of oxygen isotopes, but it is also very expensive (see Table 1.1). In addition, at the start of this work, most ^{17}O-enrichment protocols available in the literature were either very costly, due to the large excess of labeled water involved, and/or experimentally constraining, thereby preventing the development and use of this technique by a broad research community.[10] Therefore, the main objective of this thesis was to provide new, user-friendly and cost-efficient labeling schemes for $^{17}O/^{18}O$-enrichment of organic molecules, using an original synthetic approach initially proposed in Montpellier in 2017 based on mechanochemistry.[11]

The layout of this manuscript is as follows: in the *Chapter 1*, at first a literature overview of synthetic approaches available in the literature for the $^{17}O/^{18}O$-enrichment of carboxylic acid functions (which are widely present in biomolecules), will be presented. Then, generalities on mechanochemistry and how it had been employed in $^{17}O/^{18}O$-labeling schemes will be explained, followed by an overview of the analytical techniques which can be used to analyse $^{17}O/^{18}O$-enriched compounds, specifically NMR, IR and MS analyses. In the following *Chapters 2 and 3*, the specific $^{17}O/^{18}O$-enrichment protocols developed for labeling fatty acids and the application of ^{17}O-labeled oleic acid in the advanced structural characterization of materials using ^{17}O NMR spectroscopy will be described, respectively. In *Chapters 4 and 5*, the enrichment protocols for labeling amino acids and the synthesis of labeled peptides will be presented, respectively. All experimental procedures including analyses of prepared labeled compounds can be found in the attached *Annexes II-V*, related to the corresponding Chapters 2-5.

CHAPTER 1

LITERATURE OVERVIEW

INTRODUCTION

Oxygen is a ubiquitous element involved in all aspects of our daily life. It can be found in many organic as well as inorganic compounds, where it is involved in different types of bonding environments (*e.g.* forming covalent, ionic, coordination, hydrogen, and, to a lesser extent, even halogen bonds). Within the frame of this work, the emphasis will be laid solely on the oxygen-containing *organic* compounds.

Oxygen has three naturally abundant stable isotopes: the most abundant isotope ^{16}O (99.76 %), and the minority isotopes ^{17}O (0.04 %) and ^{18}O (0.20 %) (Table 1.1). In general, a heavy isotope within a molecule structure forms slightly stronger covalent bonds, which can be related to their physicochemical properties. For example, depending on the oxygen isotope content in water molecules, the water boiling point or vapour pressure are slightly affected (with $H_2{}^{16}O$ being slightly preferred to evaporate and $H_2{}^{18}O$ being slightly preferred to condensate), which leads to natural isotope fractionation during the water cycle.[12-13] The small variations in natural distribution of $^{16}O/^{18}O$ isotope ratios over the world are studied and quantified by high-resolution mass spectrometry (MS) in the fields like paleoclimatology (to determine the temperature evolution on Earth over multimillion-year timescales),[14] or in forensic science (*e.g.* to control the quality and/or geographical origin of food).[15]

For other advanced analytical techniques used to study molecules and materials, and which rely on the signature of stable isotopes, the natural abundance of oxygen isotopes is not sufficient, and the use of $^{17}O/^{18}O$-enriched species is required. For example, the ^{18}O-enriched compounds are used in MS as standards for quantitation of biologically relevant species, including peptides and proteins,[16-19] or to decipher reaction mechanisms.[20-21] On the other hand, ^{17}O is the only isotope of oxygen with a non-zero nuclear spin (I = 5/2), and is therefore the only isotope observable by nuclear magnetic resonance (NMR) spectroscopy. Due to the very high sensitivity of the ^{17}O NMR signal to the local environment of oxygen atom, and the ability of NMR spectroscopy to provide an atomic-level insight, ^{17}O NMR spectroscopy is seen as an excellent probe for investigating the structure and reactivity of complex biomolecules and materials.[22-23] However, ^{17}O is one of the more difficult nuclei for NMR spectroscopy, due to its quadrupolar nature, low-resonance frequency and mainly very low natural abundance, which all together results in low sensitivity and potentially complicated spectra.[9] It is therefore necessary to work with ^{17}O-enriched samples in order to obtain a relevant information within a reasonable amount of time.

In this chapter, an overview of the protocols currently available in the literature for $^{17}O/^{18}O$-labeling of organic compounds will first be presented, focusing on molecules with carboxylic functions. Then, general information about synthetic approaches involving mechanochemistry will be presented, including $^{17}O/^{18}O$ labeling schemes which had been developed in our laboratory, prior to the beginning of this thesis. Finally, general aspects of the analytical techniques used to characterize the enriched molecules in this work, specifically ^{17}O solid-state NMR spectroscopy, IR spectroscopy and mass spectrometry, will be briefly described.

1.1 OXYGEN LABELING OF CARBOXYLIC ACIDS

In organic compounds, oxygen is one of the most abundant elements (together with H, C and N), and constitutes many functional groups, such as hydroxyl groups (OH) in alcohols and phenols, carbonyl functions (C=O) in ketones and aldehydes, or carboxylic groups (COOH) in carboxylic acids. These oxygen-containing groups very often play key roles in terms of structure and/or reactivity of biomolecules. Indeed, oxygen has a major role in the secondary, tertiary or quaternary structure of proteins, which are stabilized by hydrogen bonds, but it is also involved in a formation of coordination bonds to metal ions, *e.g.* involvement of carboxylic functions in peptides in coordination to metal ions (such as Ca^{2+}) in the process of bio-mineralization.

Within the frame of the thesis, only the $^{17}O/^{18}O$-enrichment of oxygen atoms in carboxylic functional groups will be described. Carboxylic acid functions are found in a broad variety of biologically important families of compounds, *e.g.* fatty acids or amino acids, but also other small molecules widely employed in material science, *e.g.* organic ligands forming metal-organic frameworks (MOFs) or ligands present at the surface of nanoparticles. The carboxylic acids were selected as our primary target in this study due to the variety of their applications across many research fields, thus making them interesting subjects for labeling.

This overview is not intended to represent an exhaustive list of all enrichment protocols ever performed for enriching carboxylic acids in $^{17}O/^{18}O$, since some of them are *a priori* only applicable to certain molecules, and were used only in a very specific studies.[24-27] In addition, a review summarizing the protocols for $^{17}O/^{18}O$-enrichment of organic molecules, including a chapter on carboxylic acids, was written by Theodorou *et al.* in 2014.[10] Therefore, the aim is to summarize globally the most frequently used labeling schemes which are typically applied for $^{17}O/^{18}O$-enrichment of a wide diversity of molecules containing carboxylic acid functions, or

the procedures with a potential to be applied to a wide array of substrates, highlighting some examples related to the fatty acids and amino acids, two specific groups of organic compounds developed in details later in this work (in Chapters 2 and 4).

Among the commercially available $^{17}O/^{18}O$-enriched reagents, $^{17}O/^{18}O$-enriched water is most often used for the labeling of carboxylic functional groups.[10] It is here important to bear in mind that the ^{17}O-enriched water is much more expensive compared to the one enriched in ^{18}O (*i.e.* 1800 - 2900 € for 1 mL of 90% ^{17}O water and 60 - 150 € for 1 mL of 97 - 99 % ^{18}O water). This means, that although in theory the protocols developed for one isotope could be easily performed with the other, given the considerably higher price of ^{17}O-enriched water, not every ^{18}O-enrichment protocol can be directly applied on ^{17}O-labeling, due to the large amounts of water frequently employed in ^{18}O-enrichment protocols, which would make the ^{17}O-labeling unaffordable.

In general, the $^{17}O/^{18}O$-labeling protocols for carboxylic acids can be divided in two groups: *i)* enrichment protocols based on thermodynamic equilibrium between the substrate and enriched water, and *ii)* enrichment protocols using irreversible reactions between an activated carboxylic function and enriched water.[10] Both of these approaches will be described in more details in the following subsections. Within the whole manuscript, labeled oxygen atoms will be marked with a star (O*), and a colour code will be used as follows: red colour (for oxygen labeling in general and for ^{18}O-enrichment) and green colour (for ^{17}O-enrichment only).

1.1.1 Thermodynamic equilibrium - Acid-catalysed oxygen exchange

The protocols based on thermodynamic equilibria are very frequently used for the enrichment of carboxylic acid-containing molecules. In these procedures, a carboxylic acid function is labeled in the presence of an excess of enriched water *via* a series of oxygen exchange reactions between the non-labeled substrate and labeled water, leading eventually to an equal isotope composition in all exchangeable oxygen positions achieved *via* isotope scrambling (random mixing of the 3 oxygen isotopes between specific positions). Step by step, the substrate molecules are getting more enriched at the expense of labeled water, whose oxygen-isotope composition is in the contrary getting diluted by the non-labeled oxygen atoms coming from the substrate (see exchange reaction in Scheme 1.1). When the equilibrium is reached, each oxygen in the system (*i.e.* in the carboxylic function as well as in the water) has the same average enrichment level in ^{16}O, ^{17}O and ^{18}O.

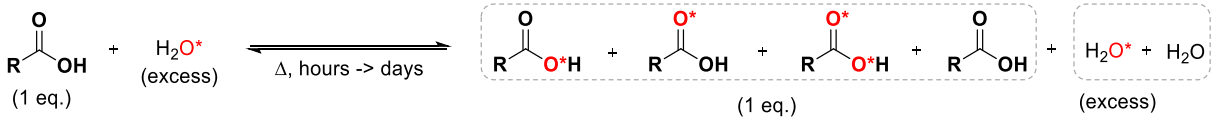

Scheme 1.1: Scheme of oxygen isotopes scrambling between non-labeled carboxylic acid substrate and enriched water. In the final sample, globally, each oxygen atom has the same probability of being enriched in ^{17}O and in ^{18}O (the average enrichment level depending on the initial composition and excess of labeled water used).

As apparent from the Scheme 1.1, during the oxygen exchange process, one or both oxygen atoms within the same carboxylic group are eventually exchanged. In the case when only one enriched oxygen is present in the molecule, the label is equally distributed between the carbonyl (C=O*) and the hydroxy (-O*H) functions. In addition, non-labeled substrate molecules are also present in the final sample, as products of back-exchange of labeled oxygen from the carboxylic group with non-labeled water molecules. Indeed, when the equilibrium is reached, the final sample contains all the possibilities (non-labeled, mono-labeled, doubly-labeled species), and their relative contribution follows a binomial statistical distribution (more details will be provided in Annexe I).

The oxygen exchange protocol can potentially provide molecules with high enrichment levels, depending on the initial composition and the excess of enriched water used. However, its widespread application is hindered by several important drawbacks:

i) Large excesses of enriched water are frequently employed (generally ~ 20 - 50 eq. per carboxylic acid), which can be explained by the aim to reach high enrichment levels (see Figure 1.1).[28-30] However, the amount of labeled water is not systematically optimized, and its overuse has implied in some cases to put additional efforts in the recovery of the labeled water (by vacuum distillation into a liquid nitrogen cooled trap) in order for the procedure to be cost-efficient (especially for ^{17}O-labeling).[28-29, 31-33] Unfortunately, this excess of enriched water is not always recovered.[34-37]

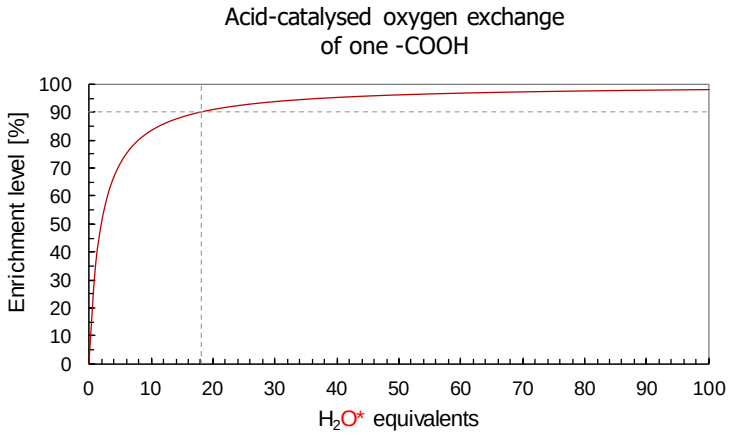

Figure 1.1: Graphical representation of theoretical maximal average enrichment level (EL) reachable per carboxylic oxygen of a mono-carboxylic acid depending on the number of enriched H_2O* equivalents used for oxygen exchange (EL = (n/(2+n))*100, where n = number of equivalents of enriched H_2O*, and supposing substrate is composed of 100 % of ^{16}O isotopes and water 100 of % ^{18}O isotopes). The grey dashed lines point out to the number of H_2O* equivalents (18 eq., 100% ^{18}O enriched) theoretically necessary to obtain 90% average enrichment level for each carboxylic oxygen.

ii) The reactions based on thermodynamic equilibria require very long time for oxygen atoms to exchange quantitatively (days up to weeks).[38-39] To accelerate the isotopic exchange process and reach the thermodynamic equilibrium more quickly (hours up to days), an acid catalysis under elevated temperatures (~ 50 - 100 °C) is applied, typically using HCl gas or an aqueous HCl (Scheme 1.2).[28, 30] However, additional constraints are related to the use of acid catalysis. To be more specific, the HCl gas is a corrosive and toxic reagent, which requires increased safety measures (hence is not user-friendly). On the other hand, the aqueous HCl is easier to work with, but its addition to the reaction mixture dilutes the label in water, and decreases the overall labeling efficiency. In addition, for many molecules, harsh heat-treatments are inconceivable as they can induce unwanted side-reactions or trigger their degradation.

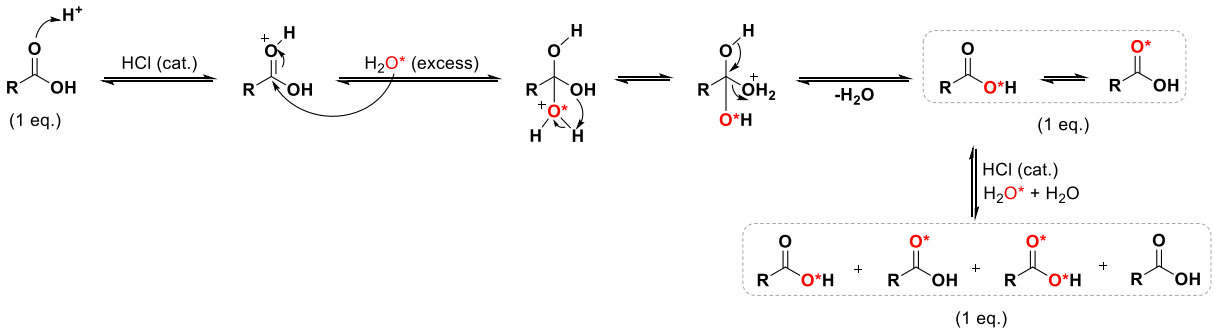

Scheme 1.2: Scheme of acid-catalysed oxygen exchange of a carboxylic acid. When the equilibrium is reached, the final sample contains non-labeled, mono-labeled and doubly-labeled products, and each oxygen atom in carboxylic function has the same average enrichment level (absolute value depends on the excess of enriched water used and its isotope composition).

iii) In some cases, the water-solubility of targeted molecule is too low, which prevents fast and efficient oxygen exchange. Therefore, an additional organic solvent (*e.g.* dioxane) is used to help solubilize the substrate, and thus to facilitate and accelerate the exchange reaction.[28-29, 31] However, this organic solvent has to be pre-dried to avoid introducing non-labeled water molecules in the reaction mixture, and the reactions are performed under inert atmosphere to prevent label dilution with the non-labeled water vapour in air.[29, 40]

In the literature, there are several examples of applications of exchange reactions for the ^{17}O or ^{18}O enrichment of two important families of molecules with COOH functions discussed in this thesis, namely fatty acids and amino acids.[10, 28, 31-33, 35-36, 41-42] To provide a few examples, L-serine was ^{17}O-enriched by acid-catalysed exchanged in ^{17}O-labeled water (90% ^{17}O-content, 23 eq. excess).[40] A concentrated HCl solution was used here for the catalysis, and the reaction medium was heated in a sealed vial under inert atmosphere at 55 °C during 8 days. Under these conditions, L-serine was ^{17}O-labeled solely at the carboxylic function with the enrichment level determined by MS as 80%, however, the isolated yield was not provided.[40] In another work, Fmoc-protected amino acids with aliphatic side-chains were labeled in ^{18}O using acidified $H_2{}^{18}O$/dioxane (2/3, V/V) mixture (~ 90% of ^{18}O content, > 100 eq. excess of H_2O^*, 0.1 M HCl).[29] The reaction mixture was heated under inert atmosphere at 100 °C for 3 - 30 hours (depending on the substrate). When the reaction was repeated twice, the ^{18}O-enrichment level of Fmoc-protected amino acids was 95 - 96 % and the isolated yield was 80 - 90 %.[29] In both examples, the excess of enriched water was recovered by distillation and reused.

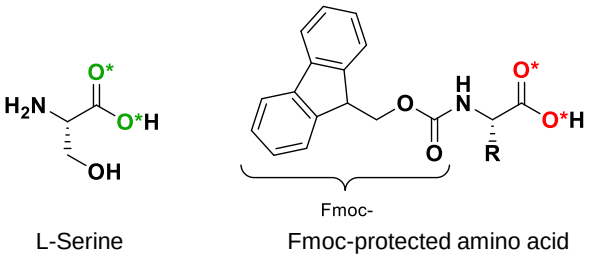

Figure 1.2: Examples of molecules enriched by oxygen exchange enrichment protocols described above, *i.e.* L-serine enriched in ^{17}O and a Fmoc-protected amino acid enriched in ^{18}O (R = aliphatic side-chain).

Overall, the acid-catalysed oxygen exchange reactions can be applied to relatively broad variety of substrates, and they can lead to highly enriched molecules. However, the large excesses of labeled water employed, the use of hazardous HCl (often as a gas),[28, 31-33, 35, 43] and the necessity of long reactions time at elevated temperatures hamper their widespread use.

1.1.2 Irreversible reactions - Hydrolysis

The second group of protocols commonly used for enrichment of carboxylic acids is based on an irreversible hydrolysis reaction between an activated carboxylic acid derivative (*e.g.* esters or acid halides) and a labeled water, using in some cases acidic or basic reaction conditions (Scheme 1.3).[44-47] In general, these hydrolytic reactions require only small amounts of labeled water (used in stoichiometric proportions or in a small excess), and are therefore cheaper in terms of the cost of labeled water employed compared to the oxygen exchange protocols (especially for ^{17}O-labeling). However, during this reaction, only one labeled oxygen atom is introduced per molecule of carboxylic acid.

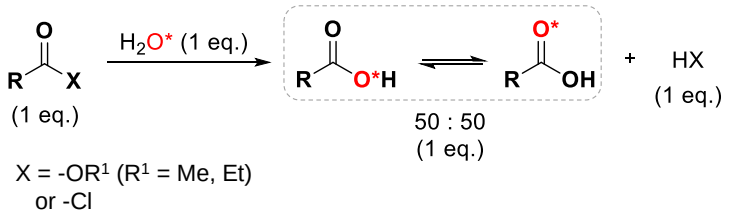

Scheme 1.3: Scheme of oxygen enrichment *via* irreversible reaction between a reactive carboxylic acid derivative (ester, acid halide) and labeled water. Due to the equilibrium in carboxylic group, both oxygen atoms (*i.e.* C=O* and C-O*H) are equally enriched.

As mentioned above, the use of esters or acid halides as activated precursors only allows to introduce one labeled oxygen per carboxylic function, which decreases the maximal potential overall enrichment level of the molecule compared to the oxygen exchange protocols. Yet, since these hydrolytic reactions proceed quantitatively even under mild conditions,[44-47] the average ^{17}O-enrichment level per carboxylic oxygen can easily reach up to 45 % (using 90% ^{17} -enriched water), which is a value sufficient for conducting ^{17}O NMR analyses.

For other applications, which require enrichment levels higher than 45 %, other reaction schemes based on irreversible reactions were proposed, yet, with additional drawbacks. One possibility is to reactivate the isolated hydrolysed labeled product, and then repeat the hydrolysis step.[44] Performing six repetitions of the activation/hydrolysis cycle can lead up to 98% labeling efficiency, which results in 98% enrichment level per carboxylic oxygen when using 100% ^{18}O-enriched water (see Figure 1.3). The reactivation can be also performed *in-situ*, which allows to avoid isolation of mono-labeled intermediate.[48] On the other hand, the repetition of the reaction steps again requires to work with excess of labeled water and it also prolongs the reaction times (see details in examples below).

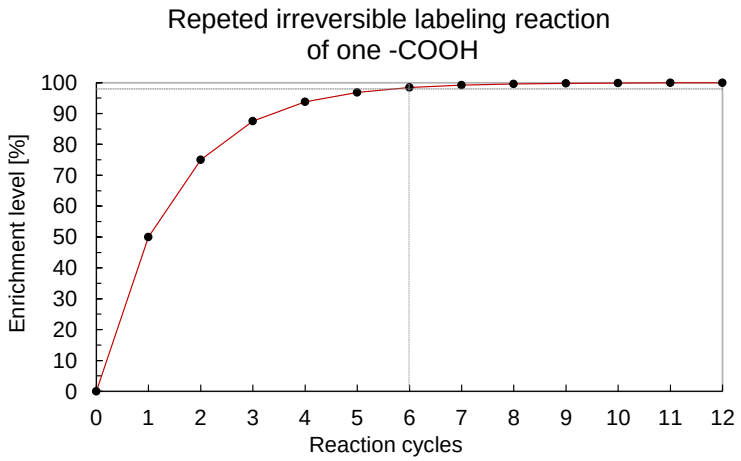

Figure 1.3: Graphical representation of theoretical maximal average enrichment level reachable per carboxylic oxygen of a mono-carboxylic acid depending on the number of reaction cycles (activation/hydrolysis), supposing substrate is composed of 100% ^{16}O isotopes and water 100% of ^{18}O isotopes (EL = $(1-(1/2)^n)*100$, where n = number of reaction cycles). One equivalent of water is consumed per reaction cycle, *i.e.* number of reaction cycles is equal to number of water equivalents theoretically necessary. Grey dashed lines point to the number of reaction cycles necessary to achieve 98% labeling efficiency.

An efficient labeling scheme based on hydrolysis under mild conditions was developed by Yamada *et al.*, where pentafluorophenyl esters of Fmoc-protected amino acids were hydrolysed in labeled water (4 eq.) at room temperature and nearly neutral pH.[44] The hydrolysis was performed under inert atmosphere and took several days. The final products were purified by column chromatography and isolated in ~ 70% yield. When the labeled product was re-activated (*i.e.* to form again pentafluorophenyl ester) and the hydrolysis was repeated, the final enrichment level reported was ~ 80 % (when using 85% ^{17}O-enriched water), suggesting that several repetitions of the activation/hydrolysis steps were performed.

In a distinct approach first proposed by Seyfried *et al.*,[48] the carboxylic acid function was activated by the 1-ethyl-3-(3-dimethylaminopropyl) carbodiimide hydrochloride (EDC) producing reactive *O*-acylisourea intermediate, which was afterwards hydrolysed by labeled water (Scheme 1.4a). The activating agent EDC as well as the labeled water were used in excess, which allowed to perform the subsequent reactivation/hydrolysis cycles (turnovers) *in-situ* without the isolation of the labeled intermediate. In every subsequent turnover, half of the mono-labeled acid reacts with the labeled water producing doubly-labeled product, and the other half stays mono-labeled producing ^{18}O-labeled urea side-product instead (Scheme 1.4b). Letting the carboxylic acid to undergo enough reaction cycles results in the isolation of final products with enrichment level close to the one of the labeled water used. This labeling scheme was originally developed for ^{18}O-enrichment of protected amino acids,[48] but due to its high labeling efficiency it was adapted by other researches, including for the ^{17}O-labeling.[49-51]

Specifically, using this approach, protected amino acids were $^{17}O/^{18}O$-enriched *via* kinetically enhanced multiple-turnover reaction sequence in the presence of large excesses of a carbodiimide (in total 30 eq.), used for activation, and labeled water (~ 20 - 50 eq.), used for hydrolysis (Scheme 1.4). The carbodiimide was added gradually to the reaction mixture (3x 10 eq.) to push the conversion forward, while the water was only introduced once at the beginning, and the reaction mixture was stirred for ~ 24 - 96 h at room temperature under inert atmosphere and mildly acidic conditions. In doing so, the $^{17}O/^{18}O$-labeled products were isolated in high yields (88 - 95 %),[48] and high enrichment levels (*e.g.* 92 - 95 % using 95% ^{18}O-enriched water, and 35 - 40 % using 40% ^{17}O-enriched water).[48-51]

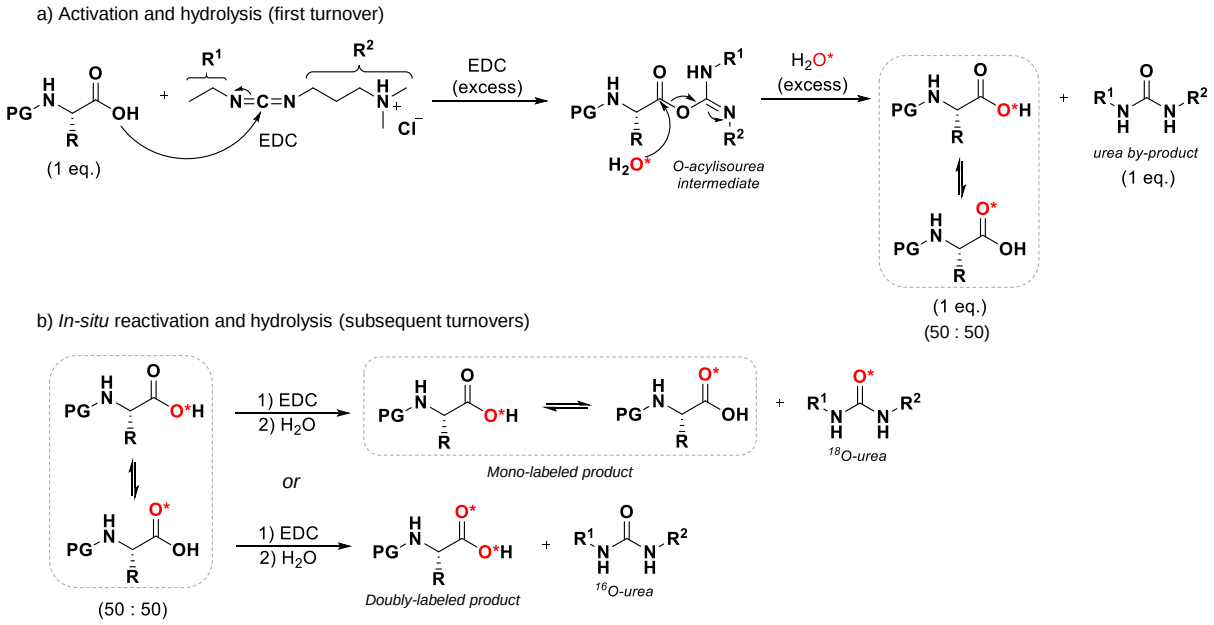

Scheme 1.4: Non-equilibrium, kinetically enhanced multiple-turnover $^{17}O/^{18}O$-labeling scheme of protected amino acids. a) The first activation and hydrolysis cycle, b) *In-situ* reactivation and subsequent hydrolysis. EDC = 3-(3-dimethylaminopropyl) carbodiimide hydrochloride, PG = protective group, R = amino acid side-chain.

Another way of enriching both carboxylic oxygens, is to hydrolyse a nitrile derivative of the targeted carboxylic acid. However, this procedure often requires to work with hazardous HCl gas at elevated temperatures, as illustrated in examples below. In addition, not all nitrile derivatives are commercially available, and their preparation often involves additional work with highly reactive and dangerous reagents (*e.g.* potassium cyanides and alkyl iodides).[21, 52]

To provide an example of the nitrile hydrolysis protocol for the labelling of fatty acids, octanoic acid was ^{18}O-enriched *via* hydrolysis of octanenitrile in acidified labeled water (7 eq.)/dioxane (1/7, V/V, 4M HCl) mixture. The medium was stirred in a sealed container under inert atmosphere for 4 h, while heated at 100 °C. The labeled product was isolated after

column chromatography in 61% yield with 87% enrichment level (using 97% ^{18}O-enriched water).[20] In this case, the starting nitrile derivative was commercially available. In another work, hexanoic acid was ^{18}O-enriched *via* hydrolysis of hexanenitrile in the presence of labeled water (2.6 eq.), *tert*-butoxide (1 eq.) and *tert*-butanol (1 eq.).[21] The mixture was stirred under inert atmosphere for 2 h while heating at reflux. The final product was isolated in 45% yield with 60% enrichment level (using 98% ^{18}O-enriched water). Here, the hexanenitrile was synthesised before the hydrolysis step, starting from 1-iodopentane and potassium cyanide. However, these reaction conditions might not be applicable to unsaturated fatty acids.

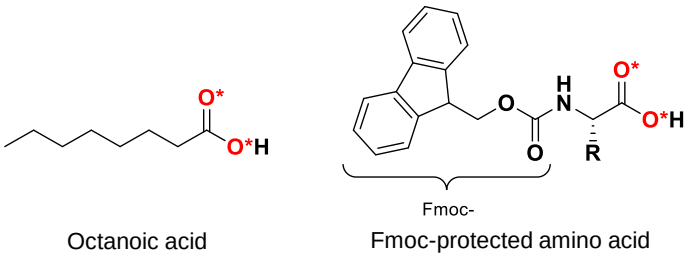

Figure 1.4: Examples of molecules enriched by irreversible reactions described above, *i.e.* octanoic acid and a Fmoc-protected amino acid, both enriched in ^{18}O (R = aliphatic side-chain).

Overall, the reaction schemes based on irreversible reactions represent an attractive cost-efficient approach for the labeling of carboxylic-acid systems for which the ^{17}O-enrichment level around 40 - 45 % is sufficient, as they can be performed under mild conditions using small amounts of water. However, in order to reach higher enrichment levels (above 80 %), working under elevated temperature with hazardous reagents, or longer reaction times and higher consumption of ^{17}O/^{18}O-labeled water will be required.

The overall summary of advantages and disadvantages of enrichment protocols described above follows. The self-evident advantage of presented protocols is the high enrichment level (> 80 % per carboxylic oxygen), which can be achieved using either oxygen exchange scheme, or by repeating irreversible reactions. However, it is redeemed by high consumption of labeled water (~ 20 - 50 eq.) long reaction times (hours - days) under inert atmosphere and elevated temperature (~ 50 - 100 °C), and last but not least, by the work with hazardous reagents (such as HCl gas).

In addition, despite the variety of procedures already available for ^{17}O/^{18}O-enrichment of carboxylic acids, only a limited number of protocols actually contains all the important experimental details, as was shown on the chosen examples above. Indeed, a majority of labeling procedures proposed in the literature are lacking some of the important synthetic information, such as the amount, enrichment level and/or the number of equivalents of labeled

water used,[24, 33, 53-54] work-up procedures employed,[42, 53, 55] and/or the isolated yield of labeled product.[28, 33, 35-36, 42-43, 45, 49, 51, 53, 56] Also the enrichment level of the final molecules is not determined regularly.[24, 28, 33, 36, 57] Some of these missing points could be justified by the intended application of the labeled compounds. For example, the final product isolation may not be required for the ^{18}O-enriched species used as MS standards, and the absolute enrichment level of ^{17}O-labeled samples used in ^{17}O NMR studies is not crucial for many researches as long as the ^{17}O signal comes out relatively quickly and provides the desired information. However, all the missing information then impedes the application of these protocols by other researchers, since all these details are necessary for a procedure to be adapted by a broad research community.

The lack of experimental details coupled with the drawbacks of the well-described protocols (*i.e.* large excess of water required, work with hazardous compounds, long reaction times and elevated temperatures), create a room for further improvement. As a response to the need for alternative labeling routes, which could be performed under mild conditions, in fast, safe and cost-efficient manner, and could be applied on a broad range of substrates, a new ^{17}O/^{18}O-enrichment methodology based on mechanochemistry was developed in our laboratory. A general introduction to mechanochemistry as well as its employment in ^{17}O/^{18}O-labeling procedures will be presented in the following section.

1.2 MECHANOCHEMISTRY

1.2.1 Generalities on mechanochemistry

Mechanochemistry is a rapidly developing field of chemistry offering *alternative* synthetic routes to the conventional solution-based syntheses.[58-61] By definition, mechanochemical reaction is a reaction induced by direct and indirect absorption of mechanical energy.[62-63] Although known for centuries, the first systematic studies were performed only at the end of 19th century, and in the next years the mechanochemistry was mostly used for the preparation of inorganic materials, such as alloys or metal oxides.[64] It is only a few decades since mechanochemistry is applied also to the syntheses of an increasing variety of organic and organometallic compounds, including coordination compounds or self-assembled supramolecular structures.[65-67] This increasing attention to mechanochemistry is partly driven by the demand for more ecological, atom- and cost-efficient chemical processes. In addition, in some cases mechanochemistry enables to produce compounds inaccessible *via* traditional solution-based techniques.[68-70] The most typical feature of mechanochemistry is that the reactions under mechanochemical conditions proceed without the need for a *bulk solvent* (solvent used for reaction*)*, which has many important impacts, for example:

- Generation of solvent waste of a given process can be significantly reduced.[58, 71]
- Working with insoluble reagents is enabled under mechanochemical conditions.[72-75]
- Reaction proceeds in highly concentrated systems, which generally results in faster conversions compared to the reactions performed in solution.[58, 76-78]
- Reaction mechanisms can be modified, resulting in increased selectivity of some processes, or in formation of products inaccessible *via* a solvent-based approach.[58, 72, 75]
- Control of reactants stoichiometry is easier compared to the solution-based processes (*e.g.* in the formation of coordination compounds or co-crystals).[79-80]

As mentioned above, a mechanochemical reaction is a reaction induced by absorption of mechanical energy. This mechanical energy can be imposed to the system by two main types of mechanical action: impact and friction, which are imposed alone or in combination on the reacting particles, causing different modes of mechanical stress (Figure 1.5).[81] For solid reagents, this results in particle size reduction and generation of fresh active surfaces for the particles to react.[62] In some cases, a partial melting of one or several reagents was observed (specifically for organic reactions where reagents with low melting points are often engaged).[62, 82-83]

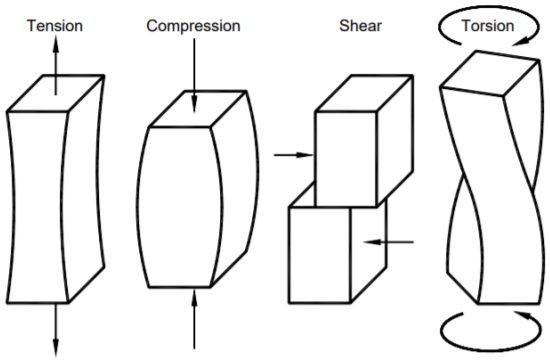

Figure 1.5: Different types of mechanical stress imposed on the solid particles during mechanochemistry.[84]

Probably the most widespread mechanochemical process is grinding solid compounds using a mortar and a pestle (Figure 1.6). However, the outcome of such process is strongly operator dependent, as each individual may apply different kinds of force in different ways, providing the system with different levels of energy, which, in addition, can vary in time.[85] This manual approach is also not convenient for compounds sensitive to the exposure to atmosphere, such as moisture sensitive substrates, which could react with the humidity in the air,[86] thereby reducing the efficiency of the reaction or inducing the formation of side-products. In order to provide more controllable and reproducible environment, the mechanochemical reactions are nowadays preferentially performed in automatized electronic devices (Figure 1.6). The most widespread equipment used in view of performing synthetic chemistry are ball-mills (Figure 1.6 and Figure 1.7a).

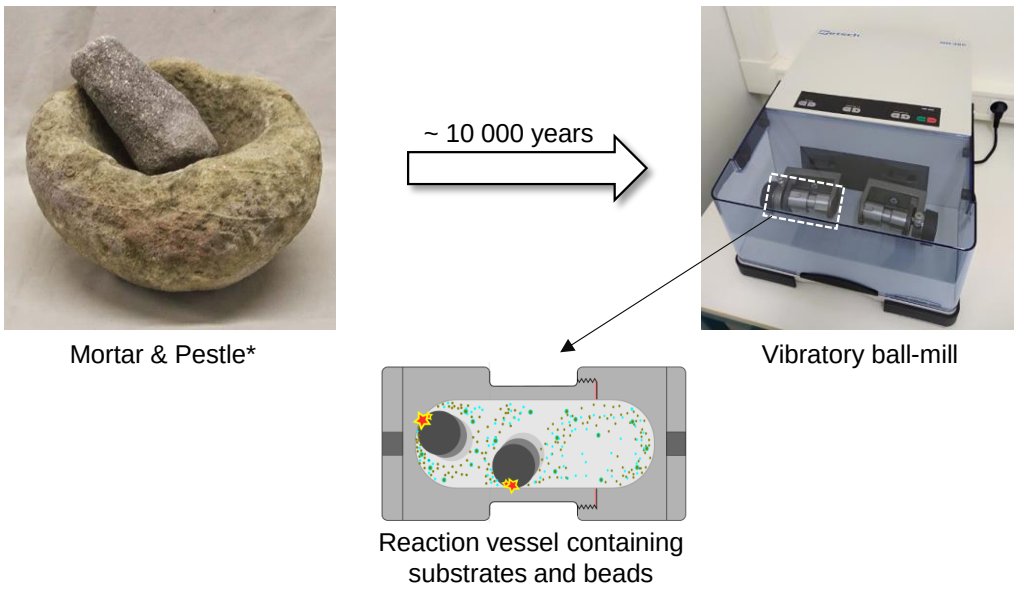

Figure 1.6: Evolution of mechanochemistry apparatus from a mortar and a pestle to automatized ball-mill devices. *Photo taken from ref.[87]

Using automatized ball-mills, the reactions are carried out in closed reaction vessels (also named jars or reactors) containing beads and reagents. When placed in a ball-mill machine, the vessels are shaken, which induces a movement of the beads inside of a vessel and they fulfil the same role as the pestle in the mortar, but in reproducible and long-term efficient manner.

To perform chemical reactions, two main types of ball-mills are used: vibratory and planetary ball-mills (Figure 1.7a), and they mainly differ in the type of movements of the vessel inside the ball mill and the scale at which the reactions can be performed.[61] In vibratory ball-mills, the jars are rapidly oscillating from side to side (horizontally or vertically), and are suitable for lab-scale syntheses, providing products on milligram up to gram scale. On the other hand, in planetary mills, the jars generally spin counter-directionally to the spinning disk that they are mounted on, causing the beads to roll over the reagents. The central spinning disk is sometimes called the "sun wheel", and the jars orbit around their central spinning axis, hence the name planetary (see Figure 1.7a). The planetary mills are often employed for scaled-up reactions producing compounds on milligram up to the multigram scale.[88-89] In both cases, the composition of mechanical forces (impact or friction) applied on the reagents can vary depending on the reaction parameters used (developed later in this subsection).[90]

Both vibratory and planetary ball-mills can be equipped with jars of different volumes, which are made of various materials, *e.g.* stainless steel, polytetrafluoroethylene (PTFE, Teflon), transparent material polymethylmethacrylate (PMMA), tungsten carbide, agate, sintered aluminium oxide, silicon nitride, zirconia and more (Figure 1.7b). The beads are also available in different materials, and in different diameters (Figure 1.7b). Mechanochemical reactions can be also applied to reaction mixtures under continuous flow by using extruders, which are especially useful in terms of industrial scale-up. However, the latter were not applied in this thesis, and are therefore not discussed in this section.

Figure 1.7: a) Commercial ball-mill machines used during this thesis, with the red arrows symbolizing the induced movement, and the product brand names indicated below the instruments, *i.e.* MM400 (horizontal shaking), P23 (vertical shaking), P7 (planetary movement). b) Examples of mechanochemical equipment available at the laboratory during the course of this thesis: reaction vessels (jars) and milling beads of different size, and made of different materials.

As mentioned above, automatization of mechanochemical processes has enabled reproducible performance under a more controlled environment. Similarly to the classical solution chemistry, the mechanochemical reaction proceeds when a sufficient amount of energy is provided (*i.e.* energy input), and when the reagents are in close contact (*i.e.* efficient mixing). Regarding the first aspect, the energy input can be easily modified by changing the milling time, the milling frequency, or the nature of the material composing the jar and beads.[91-93] Specifically, more energetic milling conditions can be achieved by increasing the milling frequency, and/or working with a jar and beads made of stainless steel (hard, dense material, density ~ 7.5 g/mL). On the other hand, a softer mechanochemical conditions can be provided by reducing the milling frequency, and/or by employing jars made of softer materials, such as Teflon (density ~ 2.3 g/mL), and beads of smaller diameter or those made of a less dense

material. However, more energetic milling does not always lead to shorter times and higher yields, as it is strongly reaction-dependent.[91, 94]

Regarding the second key aspect of a successful reaction (the mass transfer), mechanochemistry in general enables a highly efficient mixing of solid reagents, but also solid-liquid or liquid-liquid mixtures. Yet, in some cases, inhomogeneous mixtures are obtained, and reaction conditions need to be optimized. There exists many possibilities, how to enhance the mixing efficiency in mechanochemical reactions. For example, a reduction of the amount of reagents (filling factor) or an increase of the number of beads employed while reducing their size, can be considered.[89, 92-94] In some cases of reaction mixtures containing one or more liquid components (starting material, intermediate or product), the reaction mixture can become sticky, or have pasty or rubber-like aspects, which prevents efficient mass and energy transfer.[78, 94] Indeed, it was observed, that a different texture of reaction mixtures can lead to different kinetics.[95] To counter this issue, an inert solid milling agent (auxiliary), such as silica, alumina or inorganic salts can be applied as milling auxiliaries or adsorbents.[78, 94-96]

On the other hand, adding a small amount of liquid can also have a beneficial impact on the course of certain mechanochemical reactions improving the mixing efficiency.[59, 77, 79, 97-99] This technique is now commonly addressed as "Liquid Assisted Grinding" (LAG), and is characterized by a parameter η, which is defined as a ratio of volume of liquid added (in µL) to the total mass of solid reagents (in mg).[97] Generally speaking, it has been observed that LAG can have beneficial effects when η ranges between 0 and 1 (Figure 1.8). In this LAG range, it has been observed in certain cases that reactivity appears independent from the solubility of the reagents, and that the added liquid mainly serves as a lubricant facilitating the particles diffusion, whereas for the reactions occurring in a « slurry » or in a homogenous solution (corresponding to η >> 1), the low solubility does hinder reactivity.[97] Moreover, in some cases, the added liquid can influence the reaction outcome, for example by inducing the formation of a different phase or a polymorph.[100-102]

Figure 1.8: Scale of the parameter η (µL/mg) describing mechanochemical processes with liquid additive to solid reagents, LAG = liquid assisted grinding.

Despite the significant progress in the field of mechanochemistry in terms of instrumentation and synthetic applications, some aspects in mechanochemical processes still remain challenging, compared to the solution-based chemistry, in particular: a possibility to control easily the temperature evolution in the reaction vessel and a possibility of a real-time follow-up of the conversion of reactions without interrupting the milling process. However, both of these points are currently of high interest of several research groups.[103-105]

Regarding the temperature evolution in the jar, it was observed that temperature can play a critical role in mechanochemical transformations.[106-108] During the milling process, a frictional heat is generated due to the multiple collisions between the beads, reagents and the walls of the jar, and its extent depends on many parameters, such as a duration of the experiment, material of the jar and beads, or the physical aspect of the reaction mixture.[109-110] The evolution of temperature during the reaction can be monitored by measuring the external temperature of the jar using IR camera.[108, 110] While endothermic reactions could benefit from this additional source of energy, an excessive temperature increase could also result in the loss of selectivity, formation of by-products, or even decomposition of temperature sensitive compounds. In order to prevent excessive temperature build-up, reactions can be performed in a cryo-mill, *i.e.* ball-mill operating under liquid nitrogen temperatures (-196 °C).[111-112] However, more work needs to be done to provide methods for easy and precise temperature control in a wide temperature range.[61]

Regarding the real time monitoring of the conversion of mechanochemical reactions, such option is not yet generally available on commercial equipment, and to establish the duration of the majority of reactions requires to perform ex-situ measurements. Indeed, mechanochemical reactions occur commonly in a “black-box” and the standard procedure for conversion evaluation requires to stop the milling process, open the jar, and finally analyse the medium. The use of solid-state analytical techniques is recommended to follow organic reactions, in order to avoid unwanted evolution of the reaction medium, when analysed in a solution state. However, extensive efforts have been made to develop and implement platforms to conduct *in-situ* measurements, using X-ray powder diffraction (coupled to synchrotron-based radiation sources), or more laboratory-friendly Raman spectroscopy monitoring. [103-105, 108, 113-114] The use of *in-situ* monitoring enables to measure reaction kinetics, to study the effect of temperature or to observe and characterize reaction intermediates, providing insights into the mechanism of the mechanochemical processes.[68, 76]

Mechanochemistry has proven to be a beneficial synthetic alternative to classical solution-based reactions in a vast array of either chemical reaction types (*e.g.* catalysis, oxidation, reduction and nucleophilic addition) or molecule types (*e.g.* coordination complexes, lipids, nucleotides, peptides and heterocycles).[60, 65, 67] Mechanochemistry has also been applied to the synthesis of isotopically enriched compounds, which is discussed in the following subsection.

1.2.2 Isotope labeling using mechanochemistry

One of the first applications of mechanochemistry for isotope labeling was performed by Bowmaker in 2010.[115] In this work, an N-H bond in 1-methylimidazole-2-thione was deuterated mechanochemically when grinded with D_2O in a mortar and a pestle.

In a more recent work, mechanochemistry was used for deuteration of the carboxylic function in benzoic acid (Scheme 1.5).[116] Almost full deuteration was achieved by repeated milling of benzoic acid in the presence of D_2O (3x 2 eq.), and the conversion towards thermodynamic equilibrium was followed by tandem *in-situ* monitoring (coupled powder XRD and Raman spectroscopy). By employing this mechanochemical approach, the solvent consumption was reduced at least 60-times, compared to a conventional deuteration in solution.[116] In addition, deuteration of benzoic acid by ball-milling was also performed by other groups for the purpose of NMR studies.[117]

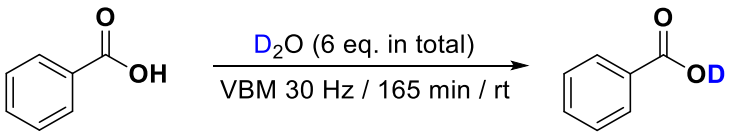

Scheme 1.5: Reaction scheme of benzoic acid deuteration using mechanochemistry, VBM = vibratory ball-milling.[116]

In 2017, a new method for ^{17}O-labeling was proposed by our laboratory, applying for the first time mechanochemistry to the ^{17}O-enrichment of inorganic as well as organic compounds, in view of NMR analyses.[11] Water enriched in ^{17}O was used here as a source of ^{17}O isotope, and it played the role of being both a liquid assistant (LAG technique described in previous section) and a ^{17}O-labeled reagent at the same time.

Regarding the inorganic products, several metal hydroxides (*e.g.* calcium, magnesium and aluminium hydroxides) were ^{17}O-enriched simply by milling the non-labeled commercial hydroxides in the presence of ^{17}O-enriched water (< 2 eq., 41% ^{17}O-content), during 30 min at 25 Hz (Scheme 1.6). The labeled metal hydroxides were then converted to metal oxides by

heat-treatment under argon atmosphere, and characterized by XRD and ^{17}O solid-state NMR spectroscopy. The final labeled metal oxides were obtained in high yields (> 85 %). The enrichment level of CaO phase was determined by ^{17}O solid-state NMR measurements to be ~ 5 %, when compared to the non-labeled equivalent. Following this initial work, further developments of the ^{17}O-labeling of various oxides using mechanochemistry have been reported.[118-120]

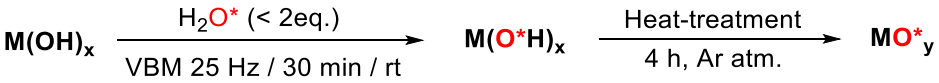

Scheme 1.6: Initial strategy for the ^{17}O-enrichment of metal hydroxides using mechanochemistry, and their subsequent conversion to ^{17}O-labeled metal oxides, VBM = vibratory ball-milling.[11]

In terms of the ^{17}O-labeling of organic compounds, in the initial publication,[11] several carboxylic acids were ^{17}O-enriched using mechanochemistry, including terephthalic and trimesic acids, two ligands widely employed in the field of metal-organic frameworks (MOFs), a protected amino acid Boc-phenylalanine (Boc- being *tert*-butyloxycarbonyl protection group), and ibuprofen. For their ^{17}O-enrichment, two-steps reaction scheme based on mechanochemical activation of the carboxylic function followed by its subsequent hydrolysis using labeled water was applied (Scheme 1.7). In the case of ibuprofen,[11] the carboxylic function was activated with 1,1-carbonyldiimidazole (CDI, 1.0 eq.), providing reactive acyl-imidazol within 10 min of milling at 25 Hz. Subsequently, the active intermediate was hydrolysed in the presence of ^{17}O-labeled water (1.5 eq., 41% ^{17}O-content) during 5 min of milling at 25 Hz. The pure ^{17}O-labeled ibuprofen was recovered after the work-up in high yield (75 %). The average enrichment level per carboxylic oxygen was determined by mass spectrometry to be ~ 8 %.

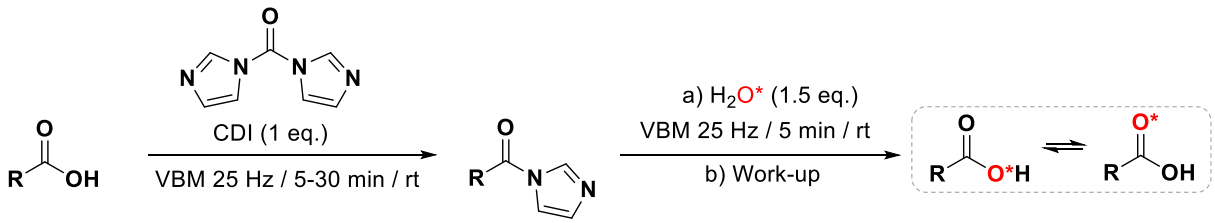

Scheme 1.7: Initial strategy for the ^{17}O-enrichment of carboxylic acids using mechanochemistry,[11] VBM = vibratory ball-milling. In the enriched product, the label is equally distributed between both oxygens (*i.e.* C=O* and C-O*H), as confirmed by ^{17}O solid-state NMR.

Employing mechanochemistry for ^{17}O-labeling enabled to prepare ^{17}O-enriched species in short time (less than 2 hours), in a cost-efficient and user-friendly manner, reaching enrichment levels sufficient to record ^{17}O solid-state NMR spectra in just a few hours. Overall,

these results represented a significant progress among the so far available ^{17}O-labeling strategies. Since then, the enrichment conditions used in this first study were further optimized by our group (including a study I participated in involving terephthalic acid enrichment, published in 2021),[121] which led to higher enrichment levels. In addition, new developments and applications of the ^{17}O/^{18}O-enrichment strategies on the carboxylic groups of other families of molecules were achieved within this thesis and are described in the following Chapters 2-5.

1.3 ANALYSES OF ^{17}O/^{18}O-OXYGEN LABELED ORGANIC MOLECULES

1.3.1 ^{17}O solid-state NMR spectroscopy

Nuclear magnetic resonance (NMR) spectroscopy is a powerful and versatile analytical technique frequently used to obtain information regarding the local environment of studied nucleus, and hence to inform on the chemical bonding, and the structure and dynamics in molecular or materials systems on atomic level. For example, NMR can be used to study complex biomolecules (such as lipid bilayers or proteins),[122-123] inorganic materials (such as borophosphate glasses or some electrodes for lithium batteries),[124-125] as well as hybrid systems (such as metal organic frameworks (MOFs) or calcium-phosphate-based biomaterials).[126]

Only those nuclei, which have a non-zero nuclear spin (I) interact with the external magnetic fields: B_0 (Zeeman interaction) and B_1 (RF excitation field), and are therefore observable by NMR.[127] The Zeeman interaction causes the separation of spin systems into different energy levels. For spin I = ½ nuclei, the RF field is subsequently applied to excite the spin population from the lower to the higher energy level, and during their relaxation (returning to equilibrium state), the decay of an NMR signal is recorded.[127]

The majority of NMR studies of bio-organic compounds focus on the nuclei with a nuclear spin I = ½, such as ^{1}H, ^{13}C and ^{15}N (see Table 1.2 for more details). However, similar studies of oxygen environments remain scarce, despite the fact that oxygen-containing functional groups often play key roles in maintaining both structures and functions of organic (macro)molecules, and that exploring their local environment could provide complementary information about the structure and reactivity of the systems.

Table 1.2: NMR active nuclei present in biomolecules with their spins, natural abundance, Larmor frequency (at 14.1 T), receptivity with respect to ^{1}H, and typical chemical shift range for organic molecules.

Nucleus	Nuclear spin (I)	Natural abundance[3]	Larmor frequency[a]	Receptivity[b]	Chemical shift range[c]
^{1}H	1/2	99.989 %	600 MHz	1.0	~ 12 ppm
^{13}C	1/2	1.078 %	151 MHz	1.7×10^{-4}	~ 200 ppm
^{14}N	1	99.636 %	43 MHz	1.0×10^{-3}	~ 500 ppm
^{15}N	1/2	0.365 %	61 MHz	3.8×10^{-6}	~ 500 ppm
^{17}O	5/2	0.038 %	81 MHz	1.1×10^{-5}	~ 1000 ppm

[a] Larmor frequency of nuclei at B_0 = 14.1 T, [b] Receptivity of nuclei with respect to ^{1}H,[128] [c] Range of ppm values typical for organic compounds.[51, 129]

The only stable isotope of oxygen which is active in NMR is oxygen-17, which has a nuclear spin of I = 5/2 and a natural abundance of 0.04 %. Despite the high interest in studying oxygen, few ^{17}O NMR studies are available compared to the other nuclei present in biomolecules, due to its inherently low sensitivity. This low sensitivity is related predominantly to the very low natural abundance of oxygen-17 (which requires to work with ^{17}O-enriched samples in the majority of applications), and, to a lesser extent, to its relatively low Larmor frequency. Altogether, oxygen has very low receptivity compared to the other nuclei present in biomolecules (see Table 1.2).[9]

Another important and potentially constraining aspect for NMR analyses comes from the quadrupolar nature of oxygen (having a nuclear spin I > 1/2). Indeed, a quadrupolar nucleus like ^{17}O will experience a nuclear quadrupole interaction between the quadrupole moment of the nucleus and the electric field gradient (EFG) around it. The quadrupolar interaction is often much larger than the other nuclear spin interactions encountered (*i.e.* magnetic shielding, dipolar interactions, and J-coupling) (Table 1.3). As a result, the quadrupolar interaction can give rise to broad NMR signals, thereby affecting the spectral resolution.[130] The NMR parameters related to the quadrupolar interaction are the quadrupole coupling constant (C_Q) and the asymmetry parameter (η_Q), and they can be extracted from the experimental NMR spectra. The quadrupole coupling constant C_Q is related to the magnitude of the quadrupolar interaction, and the asymmetry parameter η_Q is reflected in the shape of a resonance, and varies between 0 and 1 (see later in Figure 1.12b). Together with the isotropic chemical shift δ_{iso}, which is related to the magnetic shielding caused by neighbouring nuclei, the quadrupole parameters contain information about the electronic environment of the nucleus, its symmetry or distortions.

Table 1.3: Internal nuclear spin interactions observed in NMR spectroscopy.

Type of interaction	Origin	Information provided	Order of magnitude
Magnetic shielding	neighbouring atoms effecting electronic environment of a nucleus	δ_{iso}, chemical bonding, coordination number, coordination symmetry	~ 10s of kHz
Dipolar interaction	direct dipolar interaction (through space)	internuclear distance	~ kHz
Quadrupolar interaction	interaction of quadrupole moment with EFG	C_Q, η_Q symmetry of electron distribution, coordination	~ 1 - 10 MHz
J-coupling	indirect spin-spin interaction (through bonds)	bond connectivity	~ Hz

Despite the experimental constraints, the research studies reported so far demonstrate that ^{17}O NMR spectroscopy is an excellent tool to probe the structure and dynamics of organic compounds.[131-132] Oxygen-17 is a nucleus that is very sensitive to subtle changes in its local environment or bonding modes, with a chemical shift range exceeding 1400 ppm (see Figure 1.9), which provides sufficient resolution of common organic functional groups like carbonyls (270 to 350 ppm, C=**O**), carboxylic acids (with a particular range between 160 to 260 ppm for the hydroxyl CO-**O**H) or alcohols (50 to 110 ppm, -**O**H).[51] In addition, ^{17}O exhibits a vast range of variation of quadrupolar parameters, *e.g.* for organic compounds C_Q is typically ~ 5 - 12 MHz (see Figure 1.10).

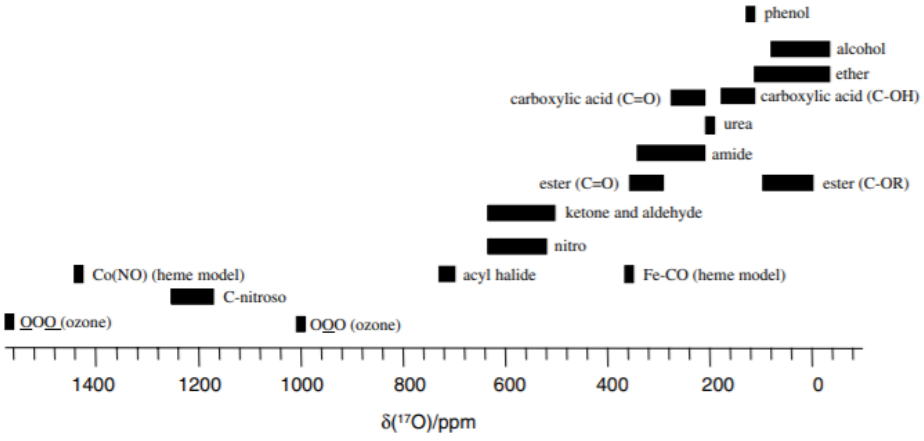

Figure 1.9: Typical ^{17}O chemical shifts measured from liquid water ($\delta = 0$ ppm) for organic compounds. Adapted from ref.[132]

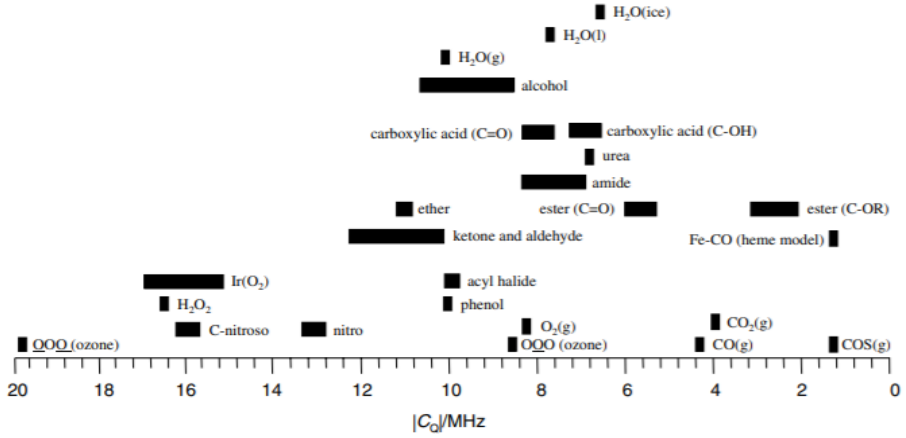

Figure 1.10: Typical ^{17}O nuclear quadrupole coupling constants found for organic molecules. Adapted from ref.[132]

The nuclear spin interactions mentioned above are anisotropic, which means that they are dependent on the relative orientation of the molecules or crystallites with respect to the external magnetic field B_0. In the solid-state NMR, the solid crystallites of the sample are present in many different orientations with respect to B_0, and the recorded spectra contain both the isotropic and anisotropic components of all interactions present (Figure 1.11a). This causes that a given spin population resonates in solid-state NMR spectra generally over a broader range of frequencies (see Figure 1.11b, blue spectrum). In contrast, in the solution NMR, rapid tumbling of molecules averages out all possible orientations. Thus, only the isotropic component of each interaction remains, and consequently each spin resonates in a narrow band of frequency, resulting in a rather narrow peak in the NMR spectrum (see Figure 1.11b, black spectrum).

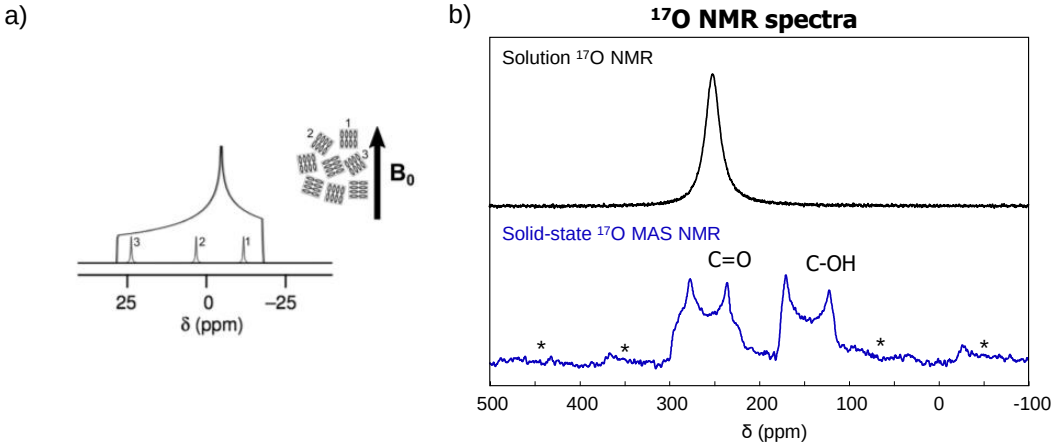

Figure 1.11: a) Hypothetical 1D spectrum of a powder sample composed of resonance frequencies of individual crystallites (adapted from ref),[133] b) Comparison of experimental ^{17}O NMR spectra of ^{17}O-labeled oleic acid recorded in solution (black line) or in solid-state (blue line, MAS = magic angle spinning). In the solid state, two oxygen resonances were resolved (*i.e.* C=O and C-OH). "*" symbols correspond to spinning sidebands.

A number of ^{17}O solution NMR spectroscopy studies of organic biomolecules, such as amino acids or monosaccharides, have been reported in the literature.[36, 134-135] However, they have been rather limited to small organic molecules.[136] For large molecules of biological interest, molecular tumbling motion in solution is usually slow, which combined with the quadrupolar interaction results in short relaxation times, causing severe line broadening of the NMR signals, and finally a loss of resolution.[132] Only recently, the implementation of a new methodology based on ^{17}O quadrupole-central-transition (QCT) enabled to obtain high-resolution ^{17}O solution NMR spectra of larger biomolecules (*e.g.* yeast ubiquitin or tryptophan synthase proteins).[30, 40, 137]

Solid-state ^{17}O NMR analyses have been for a long time preferred alternative for studying large biomolecules, since they are not limited by the molecular weight of the studied system.[131-132, 136] Despite the fact that the quadrupolar interaction causes NMR resonances from a powdered sample to spread out over a large frequency range (Figure 1.11 and Figure 1.12), the relaxation times are longer, and the resolution in solid-state NMR spectra of quadrupolar nuclei can be higher compared to the solution NMR.

To increase the resolution in ^{17}O solid-state NMR spectra, magical angle spinning (MAS), which, simply speaking, tends to emulate the molecular tumbling in solution, is typically applied. In MAS, a solid sample is packed into a rotor, which is then spun at tens of kHz around its axis, which is inclined by the magic angle 54.74 ° with respect to B_0 (Figure 1.12a). However, the quadrupolar interaction is not completely averaged out under MAS. Although ~ 3 - 4 times narrower signals are obtained (see Figure 1.12b), they are still burdened by the second order quadrupolar broadening, with distinct NMR lineshapes. On the other hand, this means that the quadrupolar parameters (C_Q and η_Q) can still be extracted by fitting the experimental spectra, providing information on the local environment of the nucleus.

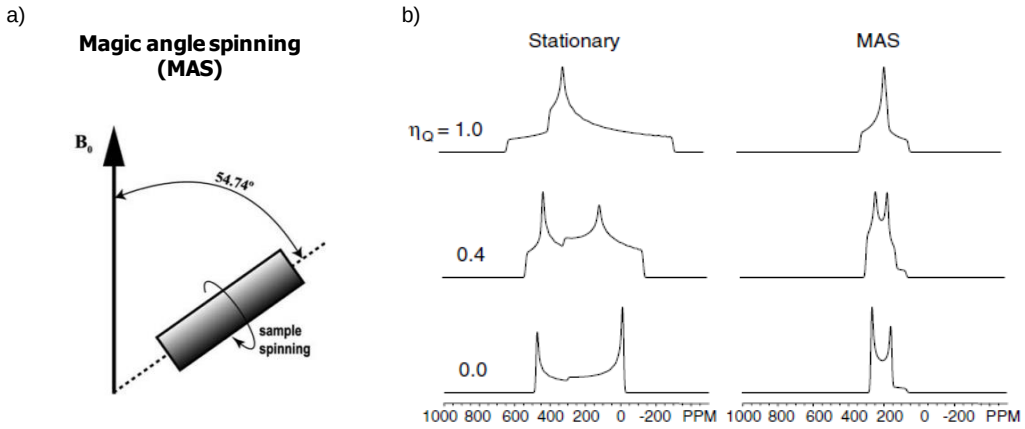

Figure 1.12: a) Schematic representation of the MAS technique. The spinning axis of the sample is at an angle of 54.74° (magic angle) with respect to the static magnetic field B_0 (figure adapted from ref),[138] b) Simulated ^{17}O stationary and MAS NMR spectra. Parameters used in the simulations are: B_0 = 11.75 T, C_Q = 8.5 MHz (figure adapted from ref).[132]

As previously mentioned, the quadrupolar interactions are not completely removed under MAS, and the 1D spectra of quadrupolar nuclei can be often composed of broad overlapping peaks. Additional increase in resolution is necessary to resolve and assign all overlapping sites in the analysed sample, and to extract the NMR parameters. This can be done, for example, by performing multiple field analyses (Figure 1.13a). Indeed, because the second-order quadrupolar broadening is inversely proportional to the applied magnetic field, it is particularly advantageous to perform solid-state NMR experiments of quadrupolar nuclei at higher magnetic fields ($B_0 \geq 20$ T), which tremendously increases both sensitivity and resolution (see Figure 1.13a).

Higher resolution can also be achieved by performing a two-dimensional multiple-quantum magic-angle spinning (MQMAS) experiment.[139] MQMAS is a sequence which removes completely the anisotropic components of the quadrupolar interactions, and therefore the lineshapes that appear broadened and overlapping in 1D MAS spectra, can be resolved in the indirect dimension in this 2D experiment (Figure 1.13b). Moreover, the resolved signals can be individually studied and fitted to extract the relevant NMR parameters.

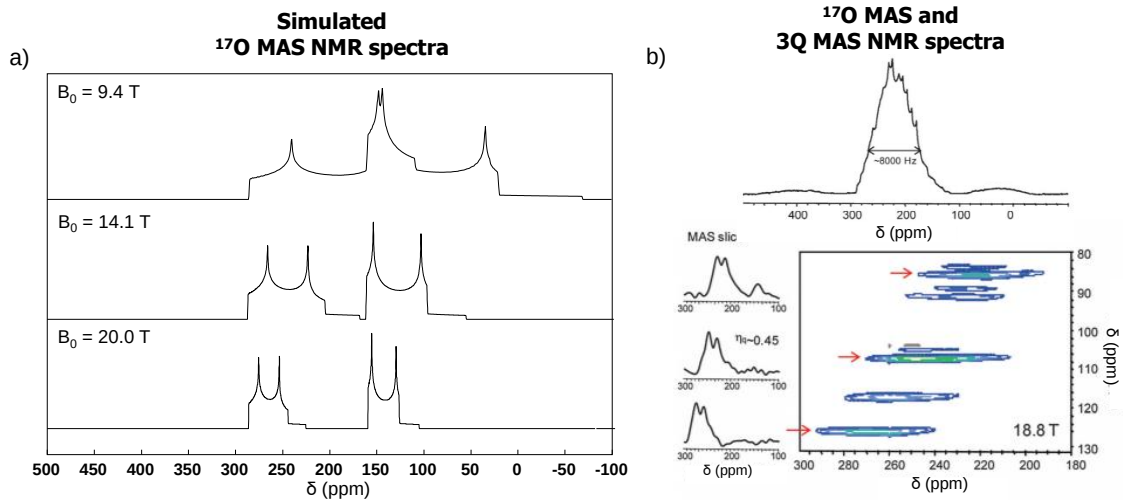

Figure 1.13: a) Simulation of ^{17}O MAS NMR spectra of oleic acid at multiple fields (9.4, 14.1 and 20.0 T), parameters used for simulation can be found in Table 2.5 in the next Chapter 2, in section 2.3.4, b) 1D ^{17}O MAS NMR spectrum of monosodium L-glutamate recorded at 14.1 T (top) and the 2D 3Q MAS NMR spectrum of the same compound recorded at 18.8 T (adapted from ref).[140]

To be able to increase the sensitivity of ^{17}O NMR and to achieve high resolution are aspects particularly important for studying organic and biological molecules, for which many different oxygen-containing functional groups may be present, but also because the weight percentage of enriched ^{17}O nuclei can be exceedingly low (*e.g.* in proteins labeled in ^{17}O only in a specific amino acid).[30, 141] Many other techniques for increasing the sensitivity and/or resolution of quadrupolar nuclei can be found in the literature, such as DFS (Double Frequency Sweep),[142] DOR (Double Orientation Rotation)[143] or DNP (Dynamic Nuclear Polarization),[144-145] just to name a few.

1.3.2 IR spectroscopy

Infrared (IR) spectroscopy is an analytical technique, which can be used to identify specific functional groups within a studied compound/material, or to explore its structure and dynamics. In IR spectroscopy, broadly speaking, an electromagnetic radiation in the range between 14000 - 10 cm^{-1} can be applied. However, the mid-infrared range (4000 - 400 cm^{-1}) is used the most frequently. After irradiation, a molecule absorbs energy associated with different frequencies that are characteristic of its structure, and the IR spectrum then represents a summary of all vibration bands of a given molecule, which can be assigned to vibration modes involving specific bonds and/or functional groups. However, for a vibration mode to be observable by IR, it has to exhibit a change in a dipole moment during vibration. With respect to the directions of a vibrational movements, one typically distinguishes between stretching vibrations (ν, changes in bond lengths) and bending vibrations (changes in angles). The bending

vibrations can be further divided in scissoring (δ), rocking (ρ), twisting (τ) and wagging (ω) modes (Figure 1.14).[127]

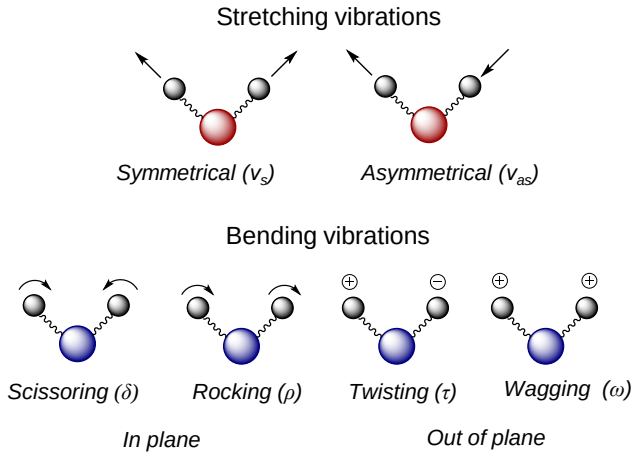

Figure 1.14: Common vibration modes observed in IR spectroscopy.

IR spectroscopy is frequently used to study the structure of biologically active compounds, such as proteins or peptides. However, the resolution of IR spectrum is low and with more bonded atoms and more functional groups present in large biomolecules, it becomes more complicated to interpret, and results in many overlapping vibration bands. In order to resolve the overlapping bands, isotope labeling is often employed. [31, 43, 146-147] In principle, when a specific atom is replaced by its isotope of larger mass, the bonded atoms vibrate at lower frequency, which results in a red-shift (towards smaller wavenumbers) of the vibration band related to the isotopically modified bond (see Figure 1.15).

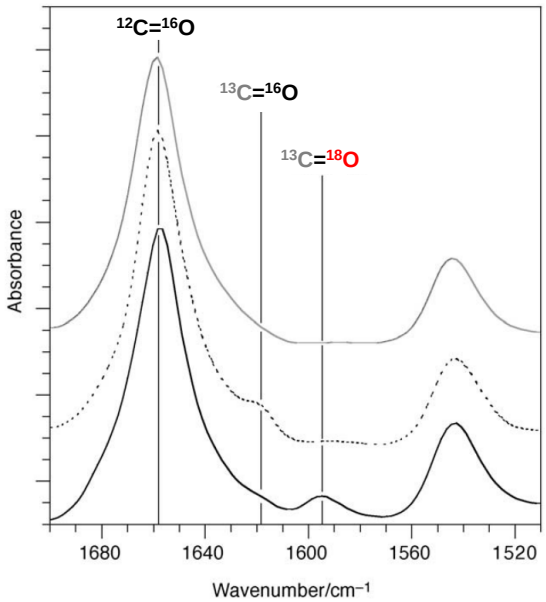

Figure 1.15: Zoomed IR spectra of a protein (Influenza A M2) adapted from reference.[146] The spectra shown here are of samples with no label (grey line), a single $^{13}C=^{16}O$ label (dashed line) or a double $^{13}C=^{18}O$ label (black line). The location of the non-labeled and labeled peaks are shown.

Such isotope effects have been frequently used in biological studies of peptides and proteins, where individual bonds could be spectroscopically resolved, such as the backbone carbonyl groups that create the so-called amide I vibrational band.[148] In this context, $^{13}C{=}^{18}O$ labels have been shown to provide site-specific secondary structure and orientational information in proteins without size-limitation, due to an increase in resolution.[31, 146, 148] Indeed, when only $^{13}C{=}O$ label is used, the amide I vibration band shifts by ~ 40 cm^{-1}, which is sufficient for deconvolution and fitting of the spectra of small peptides. However, this shift is not large enough for bigger structures, where the spectral resolution is hampered by a more intense resonance arising from natural abundance of ^{13}C isotope (1.1 %), whose contribution becomes significant for large protein molecules containing a lot of carbon atoms. On the other hand, the $^{13}C{=}^{18}O$ label induces a shift of ~ 65 cm^{-1}, which further increases the resolution and results in baseline separation of the studied vibration bands (see example in Figure 1.15).

Except for the standard FTIR (Fourier transform IR) studies,[31, 43, 146] the $^{13}C{=}^{18}O$ labeled has been used also in advanced two-dimensional IR analyses.[148] 2D IR spectra provide 2D lineshapes that give information on the environment of the label, and cross peaks that report on the secondary structure, and are also used to follow rapid structural changes and proteins dynamics.[149-150] Yet, this technique was not used in the frame of this work, and will thus not be further discussed here.

1.3.3 Mass spectrometry

Within the frame of this subsection, the emphasis will be laid on the use/application of mass spectrometry to study small organic (bio)molecules, as it was used during this thesis.

Mass spectrometry (MS) is an analytical technique which can be used to identify the amount and/or nature of chemical substances present in a sample. It has become an essential technique in many research fields, such as proteomics, metabolomics, or in pharmaceutical industry, due to its high sensitivity, potentially high resolution, broad molecular coverage, and ability to provide structural information.[16, 151-152]

In MS, only ions can be analysed (both positively or negatively charged), since neutral molecules are not affected by the electric and/or magnetic field applied by mass analyser during the analysis. This means, that in order to be measurable, the neutral molecules in the sample have to be first ionized, before being transferred in a gas-phase to a mass analyser, which separates the ions based on their respective m/z ratio, and to finally be detected, providing the MS spectrum as a function of relative abundance (intensity) of mass-to-charge ratios (m/z) of the generated ions (see Figure 1.16). From the MS spectra, the mass of a molecular ion and/or

molecular fragments are used to determine, for example, the elemental composition or isotopic signature of a compound.[153]

Figure 1.16: Simplified description of mass spectrometry analysis.

The information contained in an MS spectrum depends, among others, on the type of ionization technique used and on the resolution of the instrument. Specifically, mainly molecular ions can be expected when a soft ionization mode, such as electrospray ionization (ESI) is used, while an extensive fragmentation of a molecule is observed using a hard ionization technique, such as electron ionization (EI), or chemical ionization (CI). To be able to determine the elemental or even isotopic composition of a molecule, it is essential to use an analyser which can provide high mass accuracy (a difference between m/z measured and the one theoretically expected), and high resolution (the minimal m/z difference between two ions, which results in two separate peaks, $R = m/\Delta m$).

To be more specific, a resolution (R) required to resolve a monoisotopic molecular ion (composed only of the most abundant isotopes of each element, see Table 1.4) of stearic acid (SA, $C_{18}H_{35}O_2^-$, 283.26 g/mol) from an ion of the same molecule containing one isotope ^{13}C is R > 800, and it can be easily provided by commonly used analysers, such as quadrupole or time-of-flight (TOF). However, in order to resolve molecular ions with smaller mass difference, such as isotopic fine structures (molecular ions varying in other isotopes than only ^{13}C),[154] much higher resolution is required. To give a specific example, a resolution R > 300 000 is needed to resolve SA molecular ions containing either two ^{13}C isotopes or one ^{18}O isotope, and R > 1 000 000 is necessary to resolve SA molecular ions containing one ^{13}C or one ^{17}O isotope. The two mass analysers, which can provide such high resolution and which are frequently used in biological studies to determine the isotope composition, are referred to as orbitrap and Ion Cyclotron Resonance (ICR).[153]

Table 1.4: List of common elements contained in organic molecules and their stable isotopes, including their isotopic mass and natural abundance.[3]

Stable isotopes	Atomic mass [u]	Natural abundance [%]
^{1}H	1.007825	99.99
^{2}H	2.014102	0.01
^{12}C	12.000000	98.93
^{13}C	13.003355	1.07
^{14}N	14.003074	99.64
^{15}N	15.000109	0.36
^{16}O	15.994915	99.76
^{17}O	16.999132	0.04
^{18}O	17.999161	0.20

To provide a specific example, in Figure 1.17a, the high-resolution MS pattern (HRMS) recorded on a commercially available stearic acid sample (SA, analysed in negative mode under the form of the stearate ion, $C_{18}H_{35}O_2^-$) is displayed. In this case, the highest peak corresponds to the monoisotopic mass of stearate ion, and is composed of the most abundant isotopes of all elements contained in the SA structure, *i.e.* its isotope composition is: $^{12}C_{18}\ ^{1}H_{35}\ ^{16}O_2^-$. The following peaks detected with sufficient sensitivity, corresponding here only to the *p+1* and *p+2* masses, then reflect different isotope compositions of the same molecule (Table 1.4). In this case, they are mainly related to the presence of one or two naturally abundant ^{13}C isotopes in the molecule (natural abundance of ^{13}C is 1.1 %), with a very small contribution of naturally abundant ^{18}O isotope (0.2 %) in the peak *p+2*. Specifically, the isotope composition of *p+1* is mainly: $^{12}C_{17}\ ^{13}C\ ^{1}H_{35}\ ^{16}O_2^-$, and the isotope composition of *p+2* includes mainly: $^{12}C_{16}\ ^{13}C_2\ ^{1}H_{35}\ ^{16}O_2^-$ and $^{12}C_{18}\ ^{1}H_{35}\ ^{16}O\ ^{18}O^-$. The contribution of molecular ions composed of the other stable isotopes, such as ^{2}H and ^{17}O, is negligible due to their very low natural abundance (< 0.05 %, see Table 1.4). It is worth noting that the probability of detecting molecular ions containing ^{13}C isotopes increases with increasing number of carbon atoms in the structure, resulting in an increase in the relative intensity of *p+1*, *p+2* peaks on the mass spectrum, with respect to the monoisotopic peak. This is illustrated in the Figure 1.17, comparing the MS spectra of stearic acid (C_{18}) and valeric acid (C_5), both recorded in natural abundance.

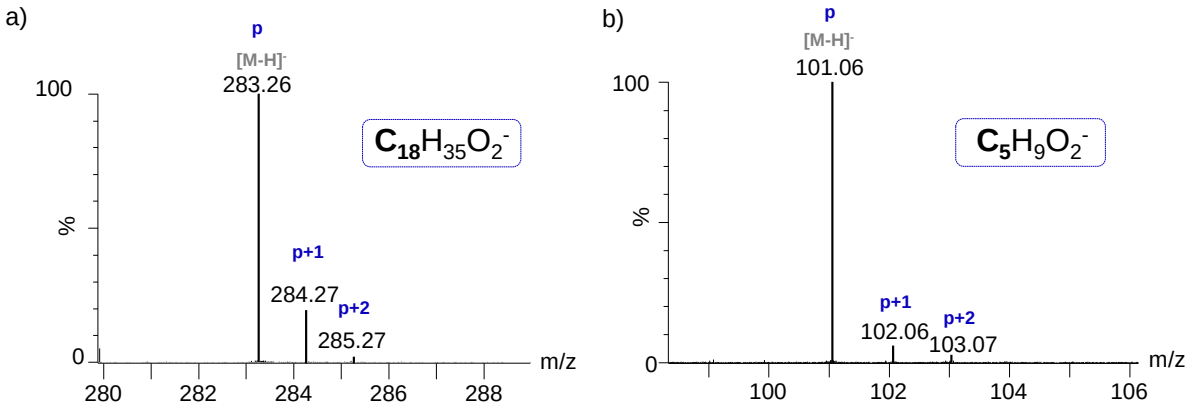

Figure 1.17: HRMS (ESI^-) patterns of a) stearate ($C_{18}H_{35}O_2^-$) and b) aspartate ($C_4H_6O_4^-$) ions in natural abundance, zoomed regions, recorded on a Waters Synapt G2-S spectrometer (negative mode, TOF analyser, R = 40 000).

In the case of $^{17}O/^{18}O$-enriched species, such as those which will be described in this thesis, the interpretation of the MS patterns (recorded using the same conditions as those shown in Figure 1.17), now requires taking into account molecular ions enriched in $^{17}O/^{18}O$ at m/z corresponding to peaks *p+1*, *p+2*, p+3, etc., as far as they are detected with sufficient intensity. This is illustrated in the Figure 1.18, where the MS pattern of ^{17}O-labeled stearic acid is compared to the one of non-labeled commercial SA (natural abundance). In the MS pattern of the ^{17}O-labeled compound, the monoisotopic peak has the same mass as in the non-labeled molecule, however, its relative intensity significantly decreased. Now, the highest peak is shifted by one m/z unit (*p+1*), and is mainly composed of stearate ions containing one ^{17}O isotope (*i.e.* $^{12}C_{18}\,^{1}H_{35}\,^{16}O\,^{17}O^-$), and anions containing one ^{13}C isotope (*i.e.* $^{12}C_{17}\,^{13}C\,^{1}H_{35}\,^{16}O_2^-$).

With further increasing m/z, the isotope composition determination becomes more and more complex, due to the increasing number of species to consider. For example, the *p+2* peak then corresponds to SA anions comprising mainly the following isotope compositions: 1x ^{17}O + 1x ^{13}C isotope (*i.e.* $^{12}C_{17}\,^{13}C\,^{1}H_{35}\,^{16}O^{17}O^-$), 1x ^{18}O isotope (*i.e.* $^{12}C_{18}\,^{1}H_{35}\,^{16}O\,^{18}O^-$), 2x ^{13}C isotopes (*i.e.* $^{12}C_{16}\,^{13}C_2\,^{1}H_{35}\,^{16}O_2^-$) and 2x ^{17}O isotopes (*i.e.* $^{12}C_{18}\,^{1}H_{35}\,^{17}O_2^-$). Analogously, different isotope contributions can be assigned to the *p+3* peak, and some of the possibilities are shown in the table below the spectrum. The contribution of ^{2}H isotopes was not considered here, due to their very low natural abundance (0.01 %), and thus a negligible contribution.

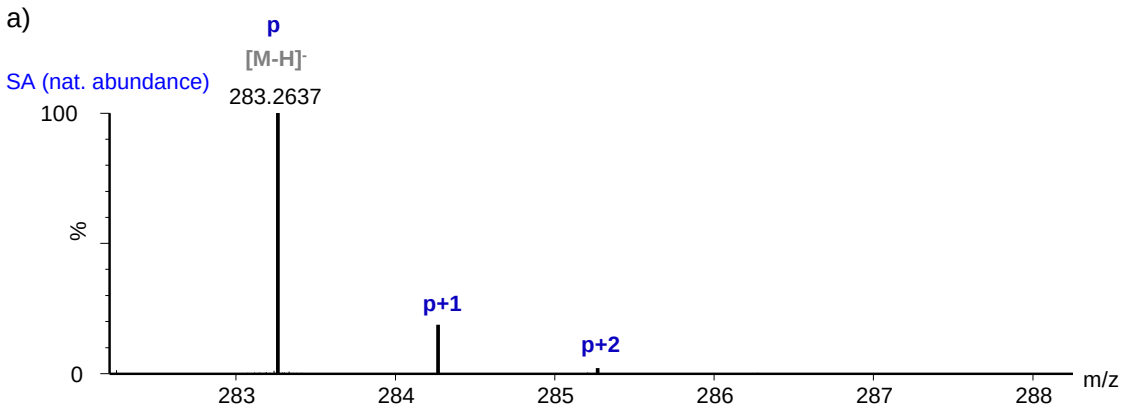

p	p+1	p+2	p+3
$^{12}C_{18}\,^{1}H_{35}\,^{16}O_2^-$	$^{12}C_{17}\,^{13}C\,^{1}H_{35}\,^{16}O_2^-$	$^{12}C_{16}\,^{13}C_2\,^{1}H_{35}\,^{16}O_2^-$	$^{12}C_{17}\,^{13}C\,^{1}H_{35}\,^{16}O\,^{18}O^-$
		$^{12}C_{18}\,^{1}H_{35}\,^{16}O\,^{18}O^-$	$^{12}C_{15}\,^{13}C_3\,^{1}H_{35}\,^{16}O_2^-$

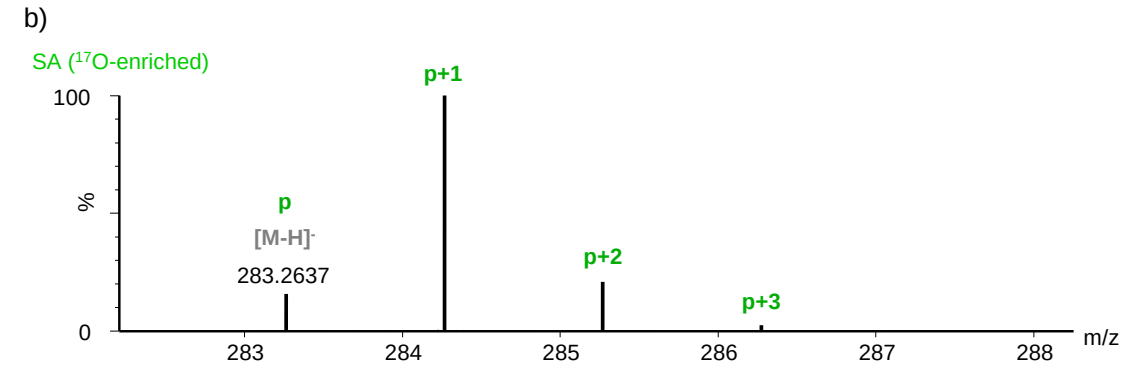

p	p+1	p+2	p+3
$^{12}C_{18}\,^{1}H_{35}\,^{16}O_2^-$	$^{12}C_{18}\,^{1}H_{35}\,^{16}O\,^{17}O^-$	$^{12}C_{18}\,^{1}H_{35}\,^{16}O\,^{18}O^-$	$^{12}C_{17}\,^{13}C\,^{1}H_{35}\,^{16}O\,^{18}O^-$
	$^{12}C_{17}\,^{13}C\,^{1}H_{35}\,^{16}O_2^-$	$^{12}C_{17}\,^{13}C\,^{1}H_{35}\,^{16}O\,^{17}O^-$	$^{12}C_{16}\,^{13}C_2\,^{1}H_{35}\,^{16}O\,^{17}O^-$
		$^{12}C_{16}\,^{13}C_2\,^{1}H_{35}\,^{16}O_2^-$	$^{12}C_{18}\,^{1}H_{35}\,^{17}O\,^{18}O^-$
		$^{12}C_{18}\,^{1}H_{35}\,^{17}O_2^-$	$^{12}C_{17}\,^{13}C\,^{1}H_{35}\,^{17}O_2^-$

Figure 1.18: HRMS (ESI^-) spectra of stearic acid (SA), zoomed regions, a) non-labeled commercial, b) ^{17}O-enriched, recorded on a Waters Synapt G2-S spectrometer (negative mode, TOF analyser, R = 40 000). Some of the possible ions contributions to the resolved peaks are in the tables below each spectrum.

As already mentioned above, using commonly available mass spectrometers (*e.g.* with time-of-flight (TOF) analyser), the resolution is not high enough to resolve the isotopic fine structures comprised within the individual m/z peaks. However, such resolution can be achieved by using other mass analysers, including Fourier Transform Ion Cyclotron Resonance mass spectrometer (FT-ICR), which can reveal the elemental composition of compounds by exquisite mass accuracy and mass resolution (R > 500 000), thus, by capturing isotopic fine structures.[151,

[154-156] Such instruments are not widely available in research laboratories, yet enable very high resolution analyses. As an example, in Figure 1.19, the MS spectrum of ^{17}O-enriched lauric acid ($C_{14}H_{24}O_2$) using an FT-ICR instrument is shown. The isotopic fine structures are resolved and assigned in the zoomed regions of peaks *p+1*, *p+2* and *p+3* displayed below.

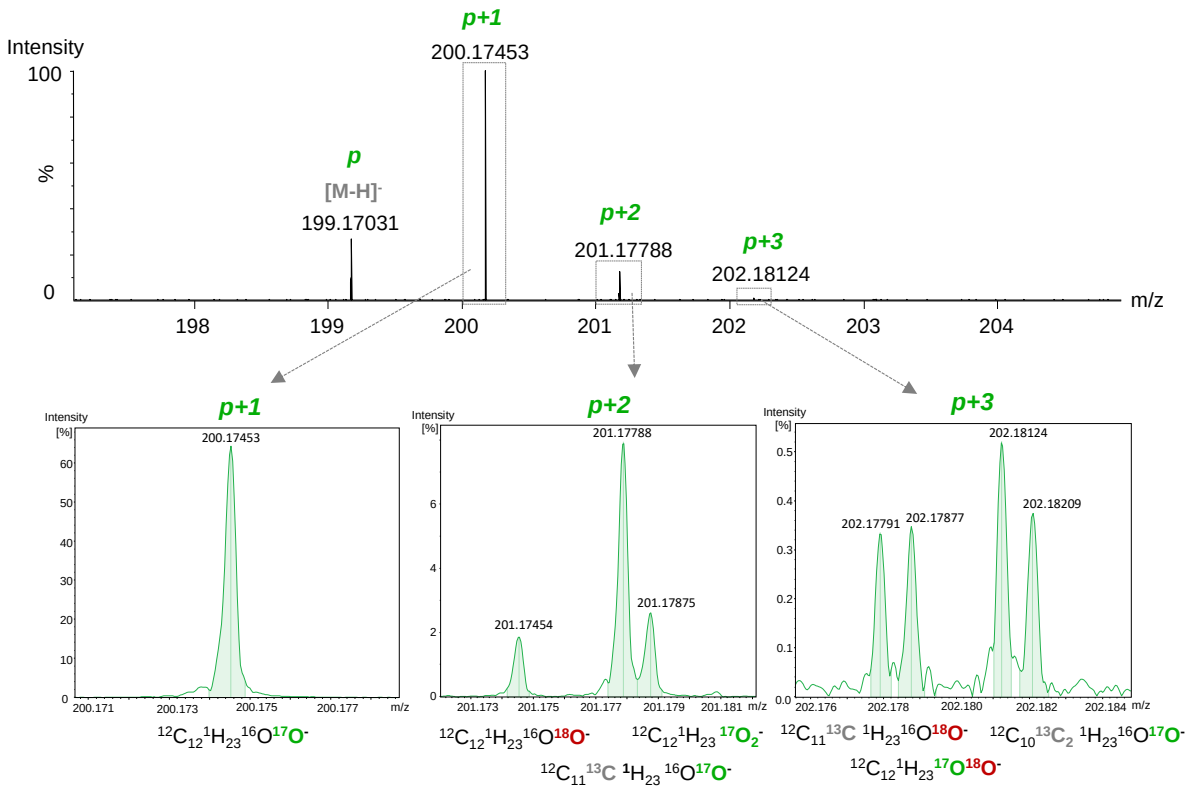

Figure 1.19: HRMS (ESI^-) spectrum of ^{17}O-enriched lauric acid recorded in negative mode using a Fourier Transform Ion Cyclotron Resonance (FT-ICR) mass spectrometer (R = 500 000 at m/z 277). The analysis was performed in COBRA laboratory in Rouen (France).[157] The resolved individual peaks of isotopic fine structures are displayed in the zoomed regions.

Within this thesis, the $^{17}O/^{18}O$-labeled products were routinely analysed using a Waters Synapt G2-S spectrometer, which is a part of IBMM analytical platform accessible to chemistry laboratories locally. The samples were analysed using electrospray ionization (ESI, in negative or positive mode), and the time-of-flight analyser (TOF, R = 40 000). This mass spectrometer provided resolution sufficient to estimate the enrichment level of $^{17}O/^{18}O$-labeled compounds and the enrichment yield of proposed labeling schemes. The methodology for calculating the enrichment level/yield is described in Annexe I. Complementary FT-ICR analyses were also performed on selected fatty acids in the COBRA laboratory in Rouen,[157] as a part of a measurement session I participated in during my thesis, in collaboration with Dr. Marie Hubert-Roux and Dr. Isabelle Schmitz-Afonso. Some of the FT-ICR MS results will be discussed in Chapter 2.3.1.

1.4 OBJECTIVES OF THE THESIS

The main objective of this thesis was to develop new labeling procedures using mechanochemistry, for enriching in $^{17}O/^{18}O$ key families of (bio)molecules containing carboxylic acid functions: fatty acids (Chapter 2) and amino acids (Chapter 4). It was envisaged for these protocols to be cost-efficient, consuming minimal amounts of labeled water, and to produce pure products in high yields with high enrichment levels. Because it was observed that many $^{17}O/^{18}O$ labeling procedures of carboxylic-acid molecules in the literature were very often poorly described (when not absent), the goal was to develop protocols that would be reproducible and accompanied with detailed experimental descriptions and thorough analyses (Annexes II and IV). This would enable the scientific community to build over these reliable protocols, and to initiate and catalyse a faster development of the analyses allowed by the ^{17}O or ^{18}O isotopic labeling, such as ^{17}O NMR.

Another key objective of this thesis was to illustrate the interest of these newly developed procedures for the synthesis of complex ^{17}O-containing compounds, and their analysis by high-resolution ^{17}O NMR spectroscopy, in view of answering key scientific questions regarding their structure or reactivity. In Chapter 3, this is illustrated through the study of ^{17}O-enriched zinc oleate coordination polymer and zinc oxide nanoparticles grafted with ^{17}O-labeled oleic acid, and in Chapter 5 through the synthesis of $^{17}O/^{18}O$-labeled peptides RGD and GRGDS.

REFERENCES

1. Yaroshevsky, A. A., Abundances of chemical elements in the Earth's crust. *Geochem. Int.* **2006,** *44* (1), 48-55.
2. Wang, Z. M.; Pierson, R. N., Jr; Heymsfield, S. B., The five-level model: a new approach to organizing body-composition research. *Am. J. Clin. Nutr.* **1992,** *56* (1), 19-28.
3. Haynes, W. M., *Handbook of Chemistry and Physics*. 92nd ed.; 2011-2012.
4. Giauque, W. F.; Johnston, H. L., An Isotope of Oxygen, Mass 18. *Nature* **1929,** *123* (3096), 318-318.
5. Giauque, W. F.; Johnston, H. L., An isotope of oxygen, mass 17, in the earth's atmosphere. *J. Am. Chem. Soc.* **1929,** *51* (12), 3528-3534.
6. Giauque, W. F.; Johnston, H. L., An isotope of oxygen, mass 18. Interpretation of the atmospheric absorption bands. *J. Am. Chem. Soc.* **1929,** *51* (5), 1436-1441.
7. McKinney, C. R.; McCrea, J. M.; Epstein, S.; Allen, H. A.; Urey, H. C., Improvements in Mass Spectrometers for the Measurement of Small Differences in Isotope Abundance Ratios. *Rev. Sci. Instrum.* **1950,** *21* (8), 724-730.
8. Alder, F.; Yu, F. C., On the Spin and Magnetic Moment of 17O. *Phys. Rev.* **1951,** *81* (6), 1067-1068.
9. Gerothanassis, I., Oxygen-17 NMR spectroscopy: Basic principles and applications (Part I). *Prog. Nucl. Magn. Reson. Spectrosc.* **2010,** *56*, 95-197.
10. Theodorou, V.; Skobridis, K.; Alivertis, D.; Gerothanassis, I. P., Synthetic methodologies in organic chemistry involving incorporation of [17O] and [18O] isotopes. *J. Labelled Comp. Radiopharm.* **2014,** *57* (8), 481-508.
11. Métro, T. X.; Gervais, C.; Martinez, A.; Bonhomme, C.; Laurencin, D., Unleashing the potential of 17O NMR spectroscopy using mechanochemistry. *Angew. Chem., Int. Ed.* **2017,** *56* (24), 6803-6807.
12. Aggarwal, P. K.; Dillon, M. A.; Tanweer, A., Isotope fractionation at the soil-atmosphere interface and the 18O budget of atmospheric oxygen. *Geophys. Res. Lett.* **2004,** *31* (14).
13. Barbour, M. M., Stable oxygen isotope composition of plant tissue: a review. *Funct. Plant Biol.* **2007,** *34* (2), 83-94.
14. Pearson, P. N., Oxygen isotopes in foraminifera: Overview and historical review. *The Paleontological Society Papers* **2012,** *18*, 1-38.
15. Benson, S.; Lennard, C.; Maynard, P.; Roux, C., Forensic applications of isotope ratio mass spectrometry—A review. *Forensic Sci. Int.* **2006,** *157* (1), 1-22.
16. Stewart, I. I.; Thomson, T.; Figeys, D., 18O Labeling: a tool for proteomics. *Rapid Comm. Mass Spectrom.* **2001,** *15* (24), 2456-2465.
17. Kozmin, Y. P.; Manoilov, A.; Serebryakova, M.; Mirgorodskaya, O., A direct introduction of 18 O isotopes into peptides and proteins for quantitative mass spectroscopy analysis. *Russ. J. Bioorg. Chem.* **2011,** *37* (6), 719-731.
18. Bergmann, D.; Hübner, F.; Humpf, H.-U., Stable Isotope Dilution Analysis of Small Molecules with Carboxylic Acid Functions Using 18O Labeling for HPLC-ESI-MS/MS: Analysis of Fumonisin B1. *J. Agr. Food Chem.* **2013,** *61* (33), 7904-7908.
19. Pickett, W. C.; Murphy, R. C., Enzymatic preparation of carboxyl oxygen-18 labeled prostaglandin F2α and utility for quantitative mass spectrometry. *Anal. Biochem.* **1981,** *111* (1), 115-121.
20. Izgu, E. C.; Björkbom, A.; Kamat, N. P.; Lelyveld, V. S.; Zhang, W.; Jia, T. Z.; Szostak, J. W., N-Carboxyanhydride-Mediated Fatty Acylation of Amino Acids and Peptides for Functionalization of Protocell Membranes. *J. Am. Chem. Soc.* **2016,** *138* (51), 16669-16676.
21. Brobst, S. W.; Townsend, C. A., The potential role of fatty acid initiation in the biosynthesis of the fungal aromatic polyketide aflatoxin B1. *Can. J. Chem.* **1994,** *72* (1), 200-207.
22. Lemaître, V.; Smith, M. E.; Watts, A., A review of oxygen-17 solid-state NMR of organic materials—towards biological applications. *Solid State Nucl. Magn. Reson.* **2004,** *26* (3), 215-235.
23. Wu, G., Solid-State 17O NMR studies of organic and biological molecules: Recent advances and future directions. *Solid State Nucl. Magn. Reson.* **2016,** *73*, 1-14.
24. de Gracia Retamosa, M.; Ruiz-Olalla, A.; Bello, T.; de Cózar, A.; Cossío, F. P., A Three-Component Enantioselective Cyclization Reaction Catalyzed by an Unnatural Amino Acid Derivative. *Angew. Chem., Int. Ed.* **2018,** *57* (3), 668-672.
25. Marcé, P.; Lynch, J.; Blacker, A. J.; Williams, J. M. J., Conversion of nitroalkanes into carboxylic acids via iodide catalysis in water. *Chem. Commun.* **2016,** *52* (5), 1013-1016.
26. Westcott, J. Y.; Clay, K. L.; Murphy, R. C., Preparation of oxygen-18-labeled lipoxygenase metabolites of arachidonic acid. *Biomed. Mass Spectrom.* **1985,** *12* (12), 714-718.
27. Jiang, X.; Zhai, Y.; Chen, J.; Han, Y.; Yang, Z.; Ma, S., Iron-Catalyzed Aerobic Oxidation of Aldehydes: Single Component Catalyst and Mechanistic Studies. *Chin. J. Chem.* **2018,** *36* (1), 15-19.

28. Pike, K. J.; Lemaitre, V.; Kukol, A.; Anupõld, T.; Samoson, A.; Howes, A. P.; Watts, A.; Smith, M. E.; Dupree, R., Solid-State 17O NMR of Amino Acids. *J. Phys. Chem. B* **2004,** *108* (26), 9256-9263.
29. Marecek, J.; Song, B.; Brewer, S.; Belyea, J.; Dyer, R. B.; Raleigh, D. P., A Simple and Economical Method for the Production of 13C,18O-Labeled Fmoc-Amino Acids with High Levels of Enrichment: Applications to Isotope-Edited IR Studies of Proteins. *Org. Lett.* **2007,** *9* (24), 4935-4937.
30. Lin, B.; Hung, I.; Gan, Z.; Chien, P.-H.; Spencer, H. L.; Smith, S. P.; Wu, G., 17O NMR studies of yeast ubiquitin in aqueous solution and in the solid state. *Chem. Bio. Chem.* **2021,** *22* (5), 826.
31. Torres, J.; Kukol, A.; Goodman, J. M.; Arkin, I. T., Site-specific examination of secondary structure and orientation determination in membrane proteins: The peptidic 13C=18O group as a novel infrared probe. *Biopolymers* **2001,** *59* (6), 396-401.
32. Steinschneider, A.; Burgar, M. I.; Buku, A.; Fiat, D., Labeling of mamino acids and peptides with isotopic oxygen as followed by 17O-NMR. *Int. J. Pept. Protein Res.* **1981,** *18* (3), 324-333.
33. Wong, A.; Hung, I.; Howes, A. P.; Anupõld, T.; Past, J.; Samoson, A.; Brown, S. P.; Smith, M. E.; Dupree, R., The determination of 17O NMR parameters of hydroxyl oxygen: A combined deuteration and DOR approach. *Mag. Reson. Chem.* **2007,** *45* (S1), S68-S72.
34. Xia, H.; Zhang, Y.; Attygalle, A. B., Experimental and Theoretical Studies on Gas-Phase Fragmentation Reactions of Protonated Methyl Benzoate: Concomitant Neutral Eliminations of Benzene, Carbon Dioxide, and Methanol. *J. Am. Soc. Mass Spectrom.* **2018,** *29* (8), 1601-1610.
35. Murphy, R. C.; Clay, K. L., Synthesis and back exchange of 18O labeled amino acids for use as internal standards with mass spectrometry. *Biomed. Mass Spectrom.* **1979,** *6* (7), 309-314.
36. Gerothanassis, I. P.; Hunston, R. N.; Lauterwein, J., 17O NMR chemical shifts of the twenty protein amino acids in aqueous solution. *Magn. Res. Chem.* **1985,** *23* (8), 659-665.
37. Yano, Y.; Kondo, K.; Watanabe, Y.; Zhang, T. O.; Ho, J.-J.; Oishi, S.; Fujii, N.; Zanni, M. T.; Matsuzaki, K., GXXXG-Mediated Parallel and Antiparallel Dimerization of Transmembrane Helices and Its Inhibition by Cholesterol: Single-Pair FRET and 2D IR Studies. *Angew. Chem. Int. Edit.* **2017,** *56* (7), 1756-1759.
38. Kong, X.; Terskikh, V. V.; Khade, R. L.; Yang, L.; Rorick, A.; Zhang, Y.; He, P.; Huang, Y.; Wu, G., Solid-State 17O NMR Spectroscopy of Paramagnetic Coordination Compounds. *Angew. Chem., Int. Ed.* **2015,** *54* (16), 4753-4757.
39. Zhu, J.; Ye, E.; Terskikh, V.; Wu, G., Solid-State 17O NMR Spectroscopy of Large Protein–Ligand Complexes. *Angew. Chem. Int. Ed. Engl.* **2010,** *49* (45), 8399-8402.
40. Young, R. P.; Caulkins, B. G.; Borchardt, D.; Bulloch, D. N.; Larive, C. K.; Dunn, M. F.; Mueller, L. J., Solution-State 17O Quadrupole Central-Transition NMR Spectroscopy in the Active Site of Tryptophan Synthase. *Angew. Chem. Int. Ed. Engl.* **2016,** *55* (4), 1350-1354.
41. Hill, E.; Murphy, R. C., Quantitation of 20-hydroxy-5,8,11,14-eicosatetraenoic acid (20-HETE) produced by human polymorphonuclear leukocytes using electron capture ionization gas chromatography/mass spectrometry. *Biol. Mass Spectrom.* **1992,** *21* (5), 249-253.
42. Mears, W. H., The Oxygen Exchange Reaction of Glycine Hydrochloride and Water. *J. Chem. Phys.* **1938,** *6* (5), 295-295.
43. Laulicht, I.; Pinchas, S.; Samuel, D.; Wasserman, I., The Infrared Absorption Spectrum of Oxygen-18-Labeled Glycine. *J. Phys. Chem.* **1966,** *70* (9), 2719-2725.
44. Kazuhiko, Y.; Toshio, Y.; Miwako, A.; Hiroshi, H.; Naoki, Y.; Yasuhiro, K., Solid-state 17O NMR in Biological Solids: Efficient 17O Labeling of Amino Acids and Peptides. *Chem. Lett.* **2007,** *36* (1), 192-193.
45. Valentine, B.; Amour, T. S.; Walter, R.; Fiat, D., pH dependence of oxygen-17 chemical shifts and linewidths of l-alanine and glycine. *J. Magn. Reson.* **1980,** *38* (3), 413-418.
46. Kovacs, J.; Kisfaludy, L.; Ceprini, M. Q.; Johnson, R. H., Investigations on the stereospecificity of peptide active phenyl ester formation and coupling. *Tetrahedron* **1969,** *25* (12), 2555-2573.
47. Huang, B.; Zeng, L.; Shen, Y.; Cui, S., One-Pot Multicomponent Synthesis of β-Amino Amides. *Angew. Chem. Int. Ed.* **2017,** *56* (16), 4565-4568.
48. Seyfried, M. S.; Lauber, B. S.; Luedtke, N. W., Multiple-Turnover Isotopic Labeling of Fmoc- and Boc-Protected Amino Acids with Oxygen Isotopes. *Org. Lett.* **2010,** *12* (1), 104-106.
49. Keeler, E. G.; Michaelis, V. K.; Colvin, M. T.; Hung, I.; Gor'kov, P. L.; Cross, T. A.; Gan, Z.; Griffin, R. G., 17O MAS NMR Correlation Spectroscopy at High Magnetic Fields. *J. Am. Chem. Soc.* **2017,** *139* (49), 17953-17963.
50. Carnahan, S. L.; Lampkin, B. J.; Naik, P.; Hanrahan, M. P.; Slowing, I. I.; VanVeller, B.; Wu, G.; Rossini, A. J., Probing O–H Bonding through Proton Detected 1H–17O Double Resonance Solid-State NMR Spectroscopy. *J. Am. Chem. Soc.* **2019,** *141* (1), 441-450.
51. Klein, B. A.; Tkachuk, D. G.; Terskikh, V. V.; Michaelis, V. K., Expanding the NMR toolkit for biological solids: oxygen-17 enriched Fmoc-amino acids. *New J. Chem.* **2021,** *45* (28), 12384-12398.
52. Cane, D. E.; Hasler, H.; Liang, T.-C., Macrolide biosynthesis. Origin of the oxygen atoms in the erythromycins. *J. Am. Chem. Soc.* **1981,** *103* (19), 5960-5962.

53. Ponnusamy, E.; Eckert, H.; Fiat, D., Synthesis of 17O isotope labeled Leu-enkephalin and 17O n.m.r.*. *Int. J. Pept. Protein Res.* **1988,** *32* (1), 21-27.
54. Ponnusamy, E.; Jones, C. C.; Fiat, D., Synthesis of oxygen-18 isotope labeled amino acids and dipeptides and its effects on carbon-13 NMR. *J. Labelled Compd. Rad.* **1987,** *24* (7), 773-778.
55. Tsikas, D.; Fauler, J.; Frölich, J., *Chemical synthesis of dioxygen-18 labelled ω-/β-oxidized cysteinyl leukotrienes: analysis by gas chromatography-mass spectrometry and gas chromatography-tandem mass spectrometry*. 1995; Vol. 667, p 209-21.
56. Waddell, K. W.; Chekmenev, E. Y.; Wittebort, R. J., Peptide 17O Chemical Shielding and Electric Field Gradient Tensors. *J. Phys. Chem. B* **2006,** *110* (45), 22935-22941.
57. Yamada, K.; Dong, S.; Wu, G., Solid-State 17O NMR Investigation of the Carbonyl Oxygen Electric-Field-Gradient Tensor and Chemical Shielding Tensor in Amides. *J. Am. Chem. Soc.* **2000,** *122* (47), 11602-11609.
58. Howard, Joseph L.; Cao, Q.; Browne, D. L., Mechanochemistry as an emerging tool for molecular synthesis: what can it offer? *Chem. Sci.* **2018,** *9* (12), 3080-3094.
59. Friščić, T.; Mottillo, C.; Titi, H. M., Mechanochemistry for synthesis. *Angew. Chem.* **2020,** *132* (3), 1030-1041.
60. Tan, D.; García, F., Main group mechanochemistry: from curiosity to established protocols. *Chem. Soc. Rev.* **2019,** *48* (8), 2274-2292.
61. Andersen, J.; Mack, J., Mechanochemistry and organic synthesis: from mystical to practical. *Green Chem.* **2018,** *20* (7), 1435-1443.
62. Boldyreva, E., Mechanochemistry of inorganic and organic systems: what is similar, what is different? *Chem. Soc. Rev.* **2013,** *42* (18), 7719-7738.
63. Michalchuk, A. A. L.; Boldyreva, E. V.; Belenguer, A. M.; Emmerling, F.; Boldyrev, V. V., Tribochemistry, Mechanical Alloying, Mechanochemistry: What is in a Name? *Front. Chem.* **2021,** *9* (359).
64. Takacs, L., The historical development of mechanochemistry. *Chem. Soc. Rev.* **2013,** *42* (18), 7649-7659.
65. James, S. L.; Adams, C. J.; Bolm, C.; Braga, D.; Collier, P.; Friščić, T.; Grepioni, F.; Harris, K. D.; Hyett, G.; Jones, W., Mechanochemistry: opportunities for new and cleaner synthesis. *Chem. Soc. Rev.* **2012,** *41* (1), 413-447.
66. Friščić, T., Supramolecular concepts and new techniques in mechanochemistry: cocrystals, cages, rotaxanes, open metal–organic frameworks. *Chem. Soc. Rev.* **2012,** *41* (9), 3493-3510.
67. Leonardi, M.; Villacampa, M.; Menéndez, J. C., Multicomponent mechanochemical synthesis. *Chem. Sci.* **2018,** *9* (8), 2042-2064.
68. Štrukil, V.; Gracin, D.; Magdysyuk, O. V.; Dinnebier, R. E.; Friščić, T., Trapping Reactive Intermediates by Mechanochemistry: Elusive Aryl N-Thiocarbamoylbenzotriazoles as Bench-Stable Reagents. *Angew. Chem. Int. Edit.* **2015,** *54* (29), 8440-8443.
69. Tan, D.; Mottillo, C.; Katsenis, A. D.; Štrukil, V.; Friščić, T., Development of C□N Coupling Using Mechanochemistry: Catalytic Coupling of Arylsulfonamides and Carbodiimides. *Angew. Chem. Int. Edit.* **2014,** *53* (35), 9321-9324.
70. Shi, Y. X.; Xu, K.; Clegg, J. K.; Ganguly, R.; Hirao, H.; Friščić, T.; García, F., The First Synthesis of the Sterically Encumbered Adamantoid Phosphazane P4(NtBu)6: Enabled by Mechanochemistry. *Angew. Chem. Int. Edit.* **2016,** *55* (41), 12736-12740.
71. Yeboue, Y.; Jean, M.; Subra, G.; Martinez, J.; Lamaty, F.; Métro, T.-X., Epimerization-Free C-Term Activation of Peptide Fragments by Ball Milling. *Org. Lett.* **2021,** *23* (3), 631-635.
72. Karki, S.; Fábián, L.; Friščić, T.; Jones, W., Powder X-ray Diffraction as an Emerging Method to Structurally Characterize Organic Solids. *Org. Lett.* **2007,** *9* (16), 3133-3136.
73. Beillard, A.; Métro, T.-X.; Bantreil, X.; Martinez, J.; Lamaty, F., Cu(0), O2 and mechanical forces: a saving combination for efficient production of Cu–NHC complexes. *Chem. Sci.* **2017,** *8* (2), 1086-1089.
74. Zhu, S.-E.; Li, F.; Wang, G.-W., Mechanochemistry of fullerenes and related materials. *Chem. Soc. Rev.* **2013,** *42* (18), 7535-7570.
75. Hernández, J. G.; Bolm, C., Altering Product Selectivity by Mechanochemistry. *J. Org. Chem.* **2017,** *82* (8), 4007-4019.
76. Juribašić, M.; Užarević, K.; Gracin, D.; Ćurić, M., Mechanochemical C–H bond activation: rapid and regioselective double cyclopalladation monitored by in situ Raman spectroscopy. *Chem. Comm.* **2014,** *50* (71), 10287-10290.
77. Howard, J. L.; Sagatov, Y.; Repusseau, L.; Schotten, C.; Browne, D. L., Controlling reactivity through liquid assisted grinding: the curious case of mechanochemical fluorination. *Green Chem.* **2017,** *19* (12), 2798-2802.
78. Howard, J. L.; Sagatov, Y.; Browne, D. L., Mechanochemical electrophilic fluorination of liquid beta-ketoesters. *Tetrahedron* **2018,** *74* (25), 3118-3123.
79. Karki, S.; Friščić, T.; Jones, W., Control and interconversion of cocrystal stoichiometry in grinding: stepwise mechanism for the formation of a hydrogen-bonded cocrystal. *Cryst. Eng. Comm* **2009,** *11* (3), 470-481.

80. Trask, A. V.; van de Streek, J.; Motherwell, W. D. S.; Jones, W., Achieving Polymorphic and Stoichiometric Diversity in Cocrystal Formation: Importance of Solid-State Grinding, Powder X-ray Structure Determination, and Seeding. *Cryst. Growth. Des.* **2005,** *5* (6), 2233-2241.
81. Michalchuk, A. A. L.; Tumanov, I. A.; Drebushchak, V. A.; Boldyreva, E. V., Advances in elucidating mechanochemical complexities via implementation of a simple organic system. *Faraday Discuss.* **2014,** *170* (0), 311-335.
82. Yamashita, H.; Hirakura, Y.; Yuda, M.; Teramura, T.; Terada, K., Detection of Cocrystal Formation Based on Binary Phase Diagrams Using Thermal Analysis. *Pharm. Res.* **2013,** *30* (1), 70-80.
83. Rothenberg, G.; Downie, A. P.; Raston, C. L.; Scott, J. L., Understanding Solid/Solid Organic Reactions. *J. Am. Chem. Soc.* **2001,** *123* (36), 8701-8708.
84. Frank M. Marlow, P. E., *Welding Fabbrication and Repair: Questions and Answers*. Industrial Press Inc.: 2002.
85. Schneider, F.; Szuppa, T.; Stolle, A.; Ondruschka, B.; Hopf, H., Energetic assessment of the Suzuki–Miyaura reaction: a curtate life cycle assessment as an easily understandable and applicable tool for reaction optimization. *Green Chem.* **2009,** *11* (11), 1894-1899.
86. Tumanov, I. A.; Michalchuk, A.; Politov, A.; Boldyreva, E.; Boldyrev, V. V., Inadvertent liquid assisted grinding: a key to "dry" organic mechano-co-crystallisation? *Cryst. Eng. Comm.* **2017,** *19* (21), 2830-2835.
87. http://oldeuropeanculture.blogspot.com.
88. Singh, V. K.; Chamberlain-Clay, A.; Ong, H. C.; León, F.; Hum, G.; Par, M. Y.; Daley-Dee, P.; García, F., Multigram Mechanochemical synthesis of a Salophen Complex: A Comparative Analysis. *ACS Sustain. Chem. Eng.* **2021,** *9* (3), 1152-1160.
89. Stolle, A.; Schmidt, R.; Jacob, K., Scale-up of organic reactions in ball mills: process intensification with regard to energy efficiency and economy of scale. *Faraday Discuss.* **2014,** *170*, 267-286.
90. Burmeister, C. F.; Kwade, A., Process engineering with planetary ball mills. *Chem. Soc. Rev.* **2013,** *42* (18), 7660-7667.
91. Stolle, A.; Szuppa, T.; Leonhardt, S. E. S.; Ondruschka, B., Ball milling in organic synthesis: solutions and challenges. *Chem. Soc. Rev.* **2011,** *40* (5), 2317-2329.
92. Thorwirth, R.; Bernhardt, F.; Stolle, A.; Ondruschka, B.; Asghari, J., Switchable Selectivity during Oxidation of Anilines in a Ball Mill. *Chem. Eur. J.* **2010,** *16* (44), 13236-13242.
93. Michalchuk, A. A. L.; Tumanov, I. A.; Boldyreva, E. V., Ball size or ball mass – what matters in organic mechanochemical synthesis? *Cryst. Eng. Comm.* **2019,** *21* (13), 2174-2179.
94. Szuppa, T.; Stolle, A.; Ondruschka, B.; Hopfe, W., An Alternative Solvent-Free Synthesis of Nopinone under Ball-Milling Conditions: Investigation of Reaction Parameters. *Chem. Sus. Chem.* **2010,** *3* (10), 1181-1191.
95. Hutchings, B. P.; Crawford, D. E.; Gao, L.; Hu, P.; James, S. L., Feedback kinetics in mechanochemistry: the importance of cohesive states. *Angew. Chem., Int. Ed.* **2017,** *56* (48), 15252-15256.
96. Do, J.-L.; Mottillo, C.; Tan, D.; Štrukil, V.; Friščić, T., Mechanochemical Ruthenium-Catalyzed Olefin Metathesis. *J. Am. Chem. Soc.* **2015,** *137* (7), 2476-2479.
97. Friščić, T.; Childs, S. L.; Rizvi, S. A. A.; Jones, W., The role of solvent in mechanochemical and sonochemical cocrystal formation: a solubility-based approach for predicting cocrystallisation outcome. *Cryst. Eng. Comm* **2009,** *11* (3), 418-426.
98. Friščić, T.; Fabian, L.; Burley, J. C.; Reid, D. G.; Duer, M. J.; Jones, W., Exploring the relationship between cocrystal stability and symmetry: is Wallach's rule applicable to multi-component solids? *Chem. Comm.* **2008,** (14), 1644-1646.
99. Bowmaker, G. A.; Skelton, B. W.; White, A. H., Structural and Infrared Spectroscopic Studies of Some Novel Mechanochemically Accessed Adducts of Silver(I) Oxoanion Salts with Thiourea. *Inorg. Chem.* **2009,** *48* (7), 3185-3197.
100. Weyna, D. R.; Shattock, T.; Vishweshwar, P.; Zaworotko, M. J., Synthesis and Structural Characterization of Cocrystals and Pharmaceutical Cocrystals: Mechanochemistry vs Slow Evaporation from Solution. *Cryst. Growth Des.* **2009,** *9* (2), 1106-1123.
101. Trask, A. V.; Shan, N.; Motherwell, W. D. S.; Jones, W.; Feng, S.; Tan, R. B. H.; Carpenter, K. J., Selective polymorph transformation via solvent-drop grinding. *Chem. Commun.* **2005,** (7), 880-882.
102. Hasa, D.; Miniussi, E.; Jones, W., Mechanochemical Synthesis of Multicomponent Crystals: One Liquid for One Polymorph? A Myth to Dispel. *Cryst. Growth. Des.* **2016,** *16* (8), 4582-4588.
103. Batzdorf, L.; Fischer, F.; Wilke, M.; Wenzel, K. J.; Emmerling, F., Direct In Situ Investigation of Milling Reactions Using Combined X-ray Diffraction and Raman Spectroscopy. *Angew. Chem.* **2015,** *127* (6), 1819-1822.
104. Friščić, T.; Halasz, I.; Beldon, P. J.; Belenguer, A. M.; Adams, F.; Kimber, S. A. J.; Honkimäki, V.; Dinnebier, R. E., Real-time and in situ monitoring of mechanochemical milling reactions. *Nat. Chem.* **2013,** *5* (1), 66-73.
105. Užarević, K.; Halasz, I.; Friščić, T., Real-Time and In Situ Monitoring of Mechanochemical Reactions: A New Playground for All Chemists. *J. Phys. Chem. Lett.* **2015,** *6* (20), 4129-4140.

106. Takacs, L.; McHenry, J. S., Temperature of the milling balls in shaker and planetary mills. *J. Mater. Sci.* **2006,** *41* (16), 5246-5249.
107. Schmidt, R.; Burmeister, C. F.; Baláž, M.; Kwade, A.; Stolle, A., Effect of Reaction Parameters on the Synthesis of 5-Arylidene Barbituric Acid Derivatives in Ball Mills. *Org. Process Res. Dev.* **2015,** *19* (3), 427-436.
108. Uzarevic, K.; Štrukil, V.; Mottillo, C.; Julien, P. A.; Puškarić, A.; Friščić, T.; Halasz, I., Exploring the effect of temperature on a mechanochemical reaction by in situ synchrotron powder X-ray diffraction. *Cryst. Growth Des.* **2016,** *16* (4), 2342-2347.
109. Užarević, K.; Ferdelji, N.; Mrla, T.; Julien, P. A.; Halasz, B.; Friščić, T.; Halasz, I., Enthalpy vs. friction: heat flow modelling of unexpected temperature profiles in mechanochemistry of metal–organic frameworks. *Chem. Sci.* **2018,** *9* (9), 2525-2532.
110. Kulla, H.; Wilke, M.; Fischer, F.; Röllig, M.; Maierhofer, C.; Emmerling, F., Warming up for mechanosynthesis–temperature development in ball mills during synthesis. *Chem. Commun.* **2017,** *53* (10), 1664-1667.
111. Kumar, N.; Biswas, K., Fabrication of novel cryomill for synthesis of high purity metallic nanoparticles. *Rev. Sci. Instrum.* **2015,** *86* (8), 083903.
112. Huot, J.; Cuevas, F.; Deledda, S.; Edalati, K.; Filinchuk, Y.; Grosdidier, T.; Hauback, B. C.; Heere, M.; Jensen, T. R.; Latroche, M.; Sartori, S., Mechanochemistry of Metal Hydrides: Recent Advances. *Materials* **2019,** *12* (17), 2778.
113. Kulla, H.; Haferkamp, S.; Akhmetova, I.; Röllig, M.; Maierhofer, C.; Rademann, K.; Emmerling, F., In Situ Investigations of Mechanochemical One-Pot Syntheses. *Angew. Chem., Int. Ed.* **2018,** *57* (20), 5930-5933.
114. Gracin, D.; Štrukil, V.; Friščić, T.; Halasz, I.; Užarević, K., Laboratory Real-Time and In Situ Monitoring of Mechanochemical Milling Reactions by Raman Spectroscopy. *Angew. Chem. Int. Ed.* **2014,** *53* (24), 6193-6197.
115. Bowmaker, G. A.; Pakawatchai, C.; Saithong, S.; Skelton, B. W.; White, A. H., Novel complexes of silver (i) sulfate with 1-methylimidazole-2-thione: structures and vibrational spectroscopy. *Dalton Trans.* **2010,** *39* (28), 6542-6550.
116. Lukin, S.; Tireli, M.; Stolar, T.; Barišić, D.; Blanco, M. V.; di Michiel, M.; Užarević, K.; Halasz, I., Isotope Labeling Reveals Fast Atomic and Molecular Exchange in Mechanochemical Milling Reactions. *J. Am. Chem. Soc.* **2019,** *141* (3), 1212-1216.
117. Altenhof, A. R.; Wi, S.; Schurko, R. W., Broadband adiabatic inversion cross-polarization to integer-spin nuclei with application to deuterium NMR. *Magn. Reson. Chem.* **2021,** *59* (9-10), 1009-1023.
118. Chen, C.-H.; Gaillard, E.; Mentink-Vigier, F.; Chen, K.; Gan, Z.; Gaveau, P.; Rebière, B.; Berthelot, R.; Florian, P.; Bonhomme, C.; Smith, M. E.; Métro, T.-X.; Alonso, B.; Laurencin, D., Direct 17O Isotopic Labeling of Oxides Using Mechanochemistry. *Inorg. Chem.* **2020,** *59* (18), 13050-13066.
119. Chen, C.-H.; Mentink-Vigier, F.; Trébosc, J.; Goldberga, I.; Gaveau, P.; Thomassot, E.; Iuga, D.; Smith, M. E.; Chen, K.; Gan, Z., Labeling and probing the silica surface using mechanochemistry and 17O NMR spectroscopy. **2021**.
120. Rainer, D. N.; Rice, C. M.; Warrender, S. J.; Ashbrook, S. E.; Morris, R. E., Mechanochemically assisted hydrolysis in the ADOR process. *Chem. Sci.* **2020,** *11* (27), 7060-7069.
121. Chen, C.-H.; Goldberga, I.; Gaveau, P.; Mittelette, S.; Špačková, J.; Mullen, C.; Petit, I.; Métro, T.-X.; Alonso, B.; Gervais, C.; Laurencin, D., Looking into the dynamics of molecular crystals of ibuprofen and terephthalic acid using 17O and 2H nuclear magnetic resonance analyses. *Magn. Reson. Chem.* **2021,** *59* (9-10), 975-990.
122. Yu, X.; Chu, S.; Hagerman, A. E.; Lorigan, G. A., Probing the Interaction of Polyphenols with Lipid Bilayers by Solid-State NMR Spectroscopy. *J. Agr. Food Chem.* **2011,** *59* (12), 6783-6789.
123. Ladizhansky, V., Applications of solid-state NMR to membrane proteins. *Biochim. Biophys. Acta Proteins Proteom.* **2017,** *1865* (11, Part B), 1577-1586.
124. Tricot, G.; Alpysbay, L.; Doumert, B., Solid State NMR: A Powerful Tool for the Characterization of Borophosphate Glasses. *Molecules* **2020,** *25* (2), 428.
125. Kitada, K.; Pecher, O.; Magusin, P. C. M. M.; Groh, M. F.; Weatherup, R. S.; Grey, C. P., Unraveling the Reaction Mechanisms of SiO Anodes for Li-Ion Batteries by Combining in Situ 7Li and ex Situ 7Li/29Si Solid-State NMR Spectroscopy. *J. Am. Chem. Soc.* **2019,** *141* (17), 7014-7027.
126. Bonhomme, C.; Gervais, C.; Laurencin, D., Recent NMR developments applied to organic–inorganic materials. *Prog. Nucl. Magn. Reson. Spectrosc.* **2014,** *77*, 1-48.
127. Gauglitz, G.; Moore, D. S., *Handbook of spectroscopy*. Wiley-Vch Weinheim: 2014; Vol. 1.
128. Harris, R. K.; Becker, E. D.; Menezes, S. M. C. d.; Goodfellow, R.; Granger, P., NMR nomenclature. Nuclear spin properties and conventions for chemical shifts(IUPAC Recommendations 2001). *Pure Appl. Chem.* **2001,** *73* (11), 1795-1818.
129. Thorn, K. A., 13C and 15N NMR identification of product compound classes from aqueous and solid phase photodegradation of 2,4,6-trinitrotoluene. *PLOS ONE* **2019,** *14* (10), e0224112.

130. Wasylishen, R. E.; Ashbrook, S. E.; Wimperis, S., *NMR of quadrupolar nuclei in solid materials*. John Wiley & Sons: 2012.
131. Lemaître, V.; de Planque, M. R. R.; Howes, A. P.; Smith, M. E.; Dupree, R.; Watts, A., Solid-State 17O NMR as a Probe for Structural Studies of Proteins in Biomembranes. *J. Am. Chem. Soc.* **2004,** *126* (47), 15320-15321.
132. Wu, G., Solid-state 17O NMR studies of organic and biological molecules. *Prog. Nucl. Magn. Reson. Spectrosc.* **2008,** *52* (2), 118-169.
133. Nardelli, F.; Borsacchi, S.; Calucci, L.; Carignani, E.; Martini, F.; Geppi, M., Anisotropy and NMR spectroscopy. *Rend. Lincei Sci. Fis. Nat.* **2020,** *31* (4), 999-1010.
134. D'Souz, F. W.; Lowary, T. L., A New Route to Carbohydrates Enriched with Oxygen Isotopes. *J. Org. Chem.* **1998,** *63* (10), 3166-3167.
135. Shen, J. Solid-state 17O NMR studies of glucose and development of 17O NMR as a new probe of glucose metabolism in HeLa cancer cells. Queen's University, Kingston, Ontario, Canada, 2020.
136. Wu, G., 17O NMR studies of organic and biological molecules in aqueous solution and in the solid state. *Prog. Nucl. Magn. Reson. Spectrosc.* **2019,** *114-115*, 135-191.
137. Zhu, J.; Wu, G., Quadrupole Central Transition 17O NMR Spectroscopy of Biological Macromolecules in Aqueous Solution. *J. Am. Chem. Soc.* **2011,** *133* (4), 920-932.
138. Alia, A.; Ganapathy, S.; de Groot, H. J. M., Magic angle spinning (MAS) NMR: a new tool to study the spatial and electronic structure of photosynthetic complexes. *Photosynth. Res.* **2009,** *102* (2), 415.
139. Medek, A.; Harwood, J. S.; Frydman, L., Multiple-quantum magic-angle spinning NMR: A new method for the study of quadrupolar nuclei in solids. *J. Am. Chem. Soc.* **1995,** *117* (51), 12779-12787.
140. Wong, A.; Howes, A. P.; Yates, J. R.; Watts, A.; Anupõld, T.; Past, J.; Samoson, A.; Dupree, R.; Smith, M. E., Ultra-high resolution 17O solid-state NMR spectroscopy of biomolecules: A comprehensive spectral analysis of monosodium L-glutamate·monohydrate. *Phys. Chem. Chem. Phys.* **2011,** *13* (26), 12213-12224.
141. Wong, A.; Beevers, A. J.; Kukol, A.; Dupree, R.; Smith, M. E., Solid-state 17O NMR spectroscopy of a phospholemman transmembrane domain protein: Implications for the limits of detecting dilute 17O sites in biomaterials. *Solid State Nucl. Magn. Reson.* **2008,** *33* (4), 72-75.
142. Perras, F. A.; Viger-Gravel, J.; Burgess, K. M.; Bryce, D. L., Signal enhancement in solid-state NMR of quadrupolar nuclei. *Solid State Nucl. Magn. Reson.* **2013,** *51*, 1-15.
143. Samoson, A.; Lippmaa, E., Synchronized double-rotation NMR spectroscopy. *J. Mag. Reson.* **1989,** *84* (2), 410-416.
144. Carver, T. R.; Slichter, C. P., Polarization of nuclear spins in metals. *Phys. Rev.* **1953,** *92* (1), 212.
145. Rossini, A. J.; Zagdoun, A.; Lelli, M.; Lesage, A.; Copéret, C.; Emsley, L., Dynamic Nuclear Polarization Surface Enhanced NMR Spectroscopy. *Accounts. Chem. Res.* **2013,** *46* (9), 1942-1951.
146. Arkin, I. T., Isotope-edited IR spectroscopy for the study of membrane proteins. *Curr. Opin. Chem. Biol.* **2006,** *10* (5), 394-401.
147. Haris, P. I.; Robillard, G. T.; Van Dijk, A. A.; Chapman, D., Potential of carbon-13 and nitrogen-15 labeling for studying protein-protein interactions using Fourier-transform infrared spectroscopy. *Biochemistry* **1992,** *31* (27), 6279-6284.
148. Ghosh, A.; Ostrander, J. S.; Zanni, M. T., Watching Proteins Wiggle: Mapping Structures with Two-Dimensional Infrared Spectroscopy. *Chem. Rev.* **2017,** *117* (16), 10726-10759.
149. Middleton, C.; Woys, A.; Mukherjee, S.; Zanni, M., Residue-Specific Structural Kinetics of Proteins through the Union of Isotope Labeling, Mid-IR Pulse Shaping, and Coherent 2D IR Spectroscopy. *Methods* **2010,** *52*, 12-22.
150. Marek, P.; Woys, A. M.; Sutton, K.; Zanni, M. T.; Raleigh, D. P., Efficient Microwave-Assisted Synthesis of Human Islet Amyloid Polypeptide Designed to Facilitate the Specific Incorporation of Labeled Amino Acids. *Org. Lett.* **2010,** *12* (21), 4848-4851.
151. Samarah, L. Z.; Khattar, R.; Tran, T. H.; Stopka, S. A.; Brantner, C. A.; Parlanti, P.; Veličković, D.; Shaw, J. B.; Agtuca, B. J.; Stacey, G.; Paša-Tolić, L.; Tolić, N.; Anderton, C. R.; Vertes, A., Single-Cell Metabolic Profiling: Metabolite Formulas from Isotopic Fine Structures in Heterogeneous Plant Cell Populations. *Anal. Chem.* **2020,** *92* (10), 7289-7298.
152. Geoghegan, K. F.; Kelly, M. A., Biochemical applications of mass spectrometry in pharmaceutical drug discovery. *Mass Spectrom. Rev.* **2005,** *24* (3), 347-366.
153. E. Hoffmann, V. S., *Mass Spectrometry Principles and Applications*. Wiley: 2007.
154. Miladinović, S. M.; Kozhinov, A. N.; Gorshkov, M. V.; Tsybin, Y. O., On the Utility of Isotopic Fine Structure Mass Spectrometry in Protein Identification. *Anal. Chem.* **2012,** *84* (9), 4042-4051.
155. Bogdanov, B.; Smith, R. D., Proteomics by FTICR mass spectrometry: Top down and bottom up. *Mass Spectrom. Rev.* **2005,** *24* (2), 168-200.
156. Leavell, M. D.; Leary, J. A., Fatty Acid Analysis Tool (FAAT): An FT-ICR MS Lipid Analysis Algorithm. *Anal. Chem.* **2006,** *78* (15), 5497-5503.

157. Drebushchak, V. A.; Boldyreva, E. V.; Drebushchak, T. N.; Shutova, E. S., Synthesis and calorimetric investigation of unstable β-glycine. *J. Cryst. Growth* **2002,** *241* (1), 266-268.

ANNEXE I

ENRICHMENT CALCULATIONS

INTRODUCTION

When performing $^{17}O/^{18}O$-enrichment experiments, the proportion of ^{17}O or ^{18}O isotopes in the final isolated molecule is a critical parameter enabling to evaluate the efficiency of a labeling scheme. In the following paragraphs, the methods used to determine $^{17}O/^{18}O$-enrichment of carboxylic acids will be explained in relation to the labeling schemes proposed in this thesis. However, the general concept can be adapted to *carboxylic acids* obtained by other enrichment schemes, and also to other oxygen-containing molecules.

I-A) TERMINOLOGY AND GENERAL CONCEPT

In general, the isotopic composition of oxygen atoms in the final products can be discussed in terms of enrichment *level* and enrichment *yield*.

- The enrichment *level* (EL) is a characteristic of the isolated product, and it stands for the average absolute value of the ^{17}O (or ^{18}O) isotope contribution per oxygen atom present in the structure of the enriched molecule. For example, if the ^{17}O-enrichment level of carboxylic acid function is equal to 40 %, this means that on average in the sample 40 % of all oxygen atoms are in fact the isotope ^{17}O. The absolute value of EL is related to the type of labeling scheme, and to the isotope composition of the water used for labeling.
- The enrichment *yield* (EY), on the other hand, is a characterization of the enrichment process, describing how efficient was the labeling reaction. It corresponds to the amount of ^{17}O or ^{18}O isotope successfully incorporated in the structure of the final product, with respect to the maximal amount possible (depending on the type of the reaction, and/or the initial isotope content of the enriched water). For example, if the ^{17}O-enrichment yield of a reaction is 90%, it means that 90 % of the oxygen atoms introduced to the molecule originated from the labeled water, while the remaining 10 % correspond to oxygen atoms of natural abundance (*i.e.* predominantly ^{16}O isotope), which may come, for example, from the air humidity. The absolute value of EY is independent from the water isotope composition, supposing no isotope effects during the labeling.

In this thesis, the $^{17}O/^{18}O$-enrichment *yields* and *level*s of the isolated products were determined from HRMS analyses, performed locally at the University of Montpellier (at IBMM analytical platform) using a Waters Synapt G2-S spectrometer, with electrospray ionization source (ESI) and time-of-flight analyser (TOF, R = 40 000). Each analysis provided an MS spectrum with m/z peaks of individual molecular ions and their relative intensities (see Figure I-1). The errors in EY and EL, related to MS measurements themselves, and to variations between synthetic batches, will be discussed later in the text.

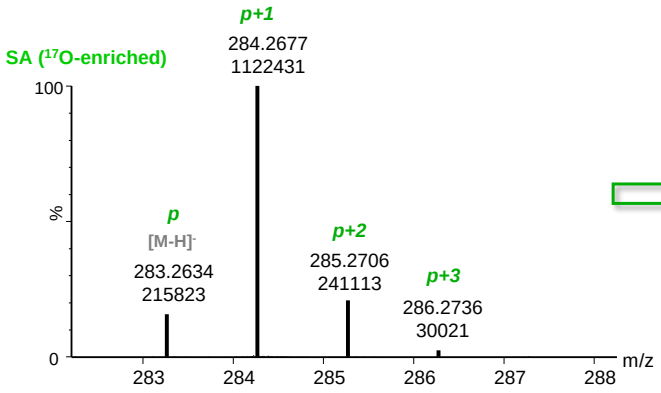

HRMS analysis

m/z	Intensity (I) (a.u.)	Relative I [%]
283.2634	215823	13
284.2677	1122431	70
285.2706	241113	15
286.2736	30021	2

Figure I-1: HRMS (ESI$^-$) spectrum of ^{17}O-enriched stearic acid (SA), zoomed region, recorded on a Waters Synapt G2-S spectrometer (negative mode, TOF analyser, R = 40 000) and table summarizing the values of m/z and intensity extracted from the MS spectrum.

Having the processed MS data, at first an "average molar mass" of the labeled product is calculated from the measured masses of the relevant molecular ions (*p*, *p+1*, *p+2*, *p+3*, etc.) and their relative contributions. In the next step, the theoretical average molar mass of the all the elements in labeled product *except oxygen atoms* is substracted (this value being calculated from all stable isotopes of the elements and their natural abundances – aside oxygen), providing the apparent molar mass of oxygen atoms (with variable contribution of ^{16}O, ^{17}O and ^{18}O isotopes). In the subsequent calculations of the enrichment level/yield, the molar mass of oxygen isotopes and the isotopic composition of water used for the labeling are involved, and an assumption is made, that no isotope effects take place during the labeling. This calculation method is graphically represented in the Figure I-2.

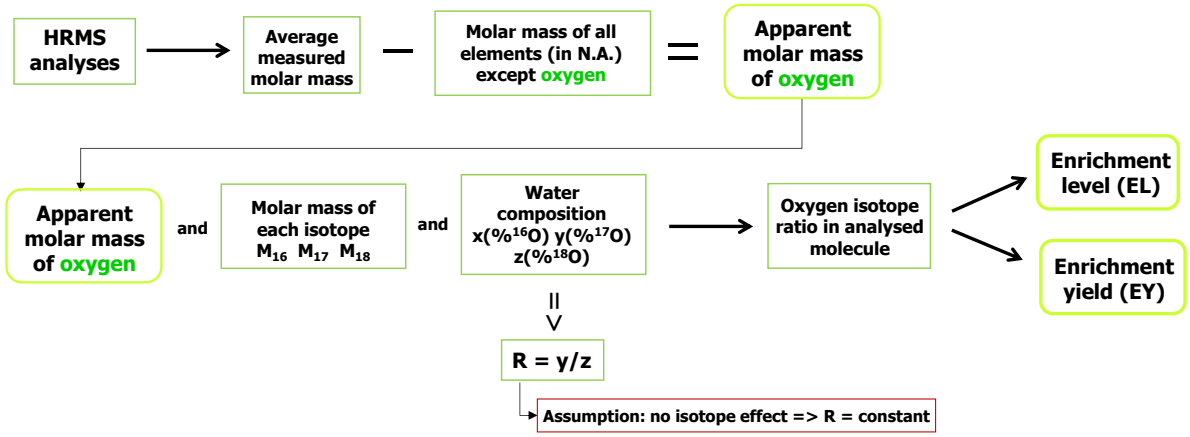

Figure I-2: Schematic description of enrichment calculation process, starting with recorded MS data and providing the enrichment level or yield, N.A. = natural abundance.

I-B) ENRICHMENT LEVEL CALCULATION

The enrichment *level* (EL) of labeled molecule is calculated from a system of three equations with three unknowns *x*, *y*, *z*, as shown below. The first equation (1) describes the oxygen mass equation in the labeled product, the second equation (2) describes that the sum of relative proportions of each oxygen isotope is equal to 1, and the third equation (3) represents the isotope composition of enriched water used for the labeling (as declared in the certificate of its analysis provided by a supplier), and it is used here with the assumption that the relative

ratio of ^{17}O / ^{18}O isotopes remains constant during the labeling process (*i.e.* the potential presence of isotope effects during the labeling reaction are neglected).

$$n \cdot x \cdot M_{16} + n \cdot y \cdot M_{17} + n \cdot z \cdot M_{18} = M_{(ox.app)} \quad (1)$$

$$x + y + z = 1 \quad (2)$$

$$R = \frac{y}{z} \quad (3)$$

Where the variables and parameters are as follows:

- *n* corresponds to the number of oxygen atoms in the structure susceptible to enrichment
- M_{16}, M_{17}, M_{18} stands for the isotopic mass of ^{16}O, ^{17}O and ^{18}O isotopes
- *x*, *y*, *z* represent the relative proportions (fractional abundances) of each oxygen isotope (*x* for ^{16}O, *y* for ^{17}O, *z* for ^{18}O)
- $M_{(ox.app)}$ corresponds to the apparent oxygen mass derived from the MS data
- *R* is a constant, expressing the $^{17}O/^{18}O$ isotope ratio (given by the water isotope composition given by the provider, and the one expected in the labeled product).

By solving the system of three equations, the relative proportions of ^{16}O, ^{17}O and ^{18}O isotopes, expressed as *x*, *y*, *z* can be determined as shown below (equations 4, 5, 6). The enrichment levels are finally obtained by multiplying the *x*, *y*, *z* values by 100, providing EL in percentage.

$$z = \frac{M_{(ox.app)} - n \cdot M_{16}}{n \cdot M_{18} + n \cdot R \cdot M_{17} - n \cdot R \cdot M_{16} - n \cdot M_{16}} \quad (4)$$

$$y = z \cdot R \quad (5)$$

$$x = 1 - y - z \quad (6)$$

I-C) ENRICHMENT YIELD CALCULATION

Regarding the enrichment *yield* (EY), the calculation method depends on the type of reaction used for labeling, *i.e.* irreversible reaction, supposing only one oxygen is introduced per molecule (*e.g.* saponification, CDI-activation/hydrolysis), or reaction based on thermodynamic equilibrium, supposing equilibrium enrichment state of all oxygen atoms (*e.g.* oxygen exchange), as further developed in this section.

a) Irreversible reaction (CDI-activation/hydrolysis, saponification)

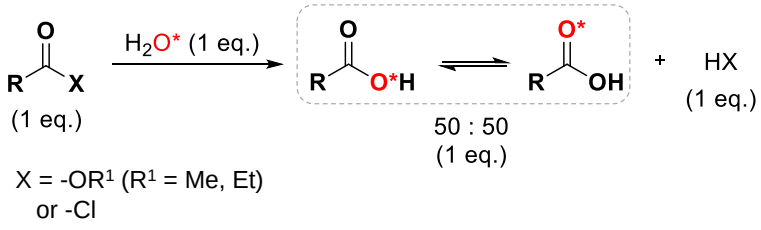

Scheme I-1: Scheme of oxygen enrichment *via* irreversible reaction between a reactive carboxylic acid derivative (ester, acid halide) and labeled water. Due to the equilibrium in carboxylic group, both oxygen atoms (*i.e.* C=O* and C-O*H) are equally enriched.

In the case of the irreversible labeling schemes (Scheme I-1), such as those applied for enrichment in this thesis (*i.e.* CDI-activation/hydrolysis and saponification), the assumption

was made that only one labeled oxygen can be introduced in the molecule, and the possibility of obtaining doubly oxygen labeled products was not considered for its very small probability. The validity of this assumption is illustrated in the Figure I-3, where the MS pattern of L-lysine ^{18}O-labeled *via* saponification (using 99% ^{18}O-enriched water), is displayed. This MS spectrum demonstrates that the analysed sample is composed predominantly of molecules containing one ^{18}O isotope with the major peak being the *p+2*, which corresponds to the ^{18}O-mono-labeled lysine. The remaining small peaks can be attributed to the monoisotopic mass of lysine (peak *p*), and the rest mainly to presence of one ^{13}C (natural abundance) within the ^{18}O-labeled lysine structure.

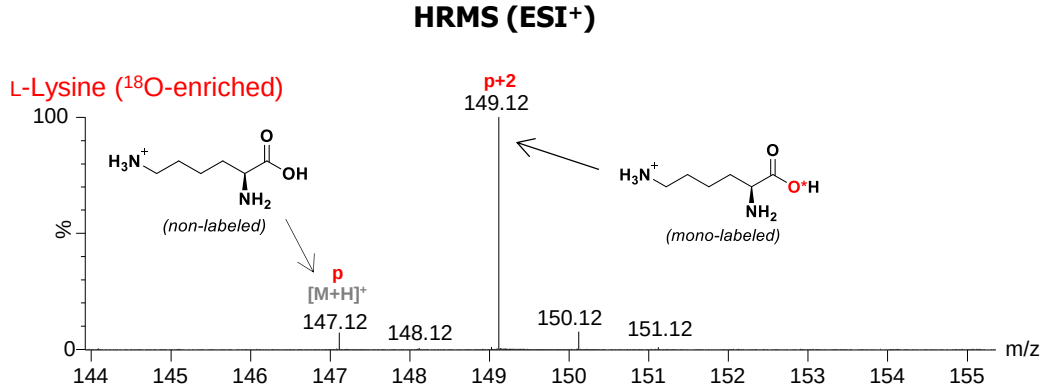

Figure I-3: HRMS (ESI$^+$) patterns of L-lysine enriched in ^{18}O *via* saponification, recorded on a Waters Synapt G2-S spectrometer (positive mode, TOF analyser, R = 40 000). The peak *p* corresponds to the monoisotopic mass of lysine, and the peak *p+2* mainly belongs to the lysine molecules containing 1x^{18}O isotope.

The assumption of only one labeled oxygen being introduced in the carboxylic function described above is also applied in the enrichment *yield* calculations, neglecting the very low contribution of doubly-labeled molecules in the overall enrichment yield. After obtaining the apparent molar mass of oxygens from the MS data, as described previously, the molar mass of the non-labeled oxygen (natural abundance) is substracted from the apparent mass of all oxygens in the sample, providing the apparent molar mass of the labeled oxygen only (with a variable contribution of ^{16}O, ^{17}O and ^{18}O isotopes). Then, using the equations (4), (5), (6) shown above (with *n* being here equal to 1), the isotope composition of the one labeled oxygen is provided. To provide the enrichment *yield*, this value is finally divided by the corresponding isotope content in the enriched water and multiplied by 100 to be expressed in percentage. This calculation concept is graphically represented in the Figure I-4.

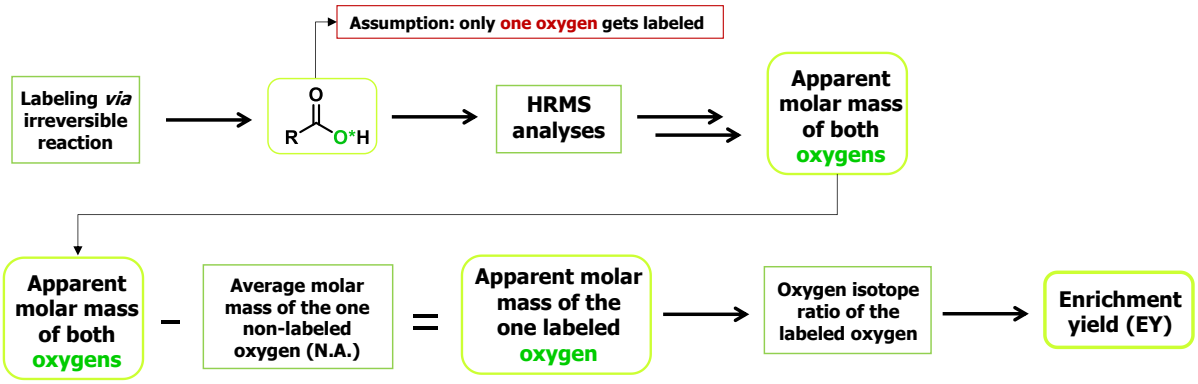

Figure I-4: Schematic description of enrichment yield calculation process when using irreversible reaction schemes for the enrichment (for the labeling protocols developed in this thesis). N.A. = natural abundance.

b) Thermodynamic equilibrium (oxygen exchange)

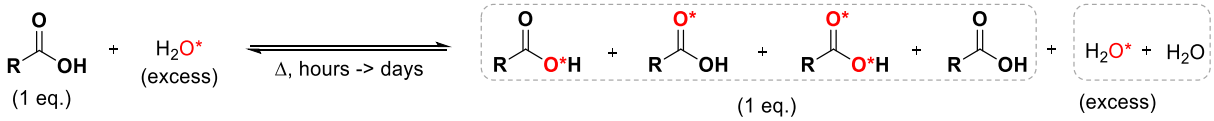

Scheme I-2: Scheme of oxygen isotopes scrambling between non-labeled carboxylic acid substrate and enriched water. In the final sample, globally, each oxygen atom has the same probability of being enriched in ^{17}O and in ^{18}O (the average enrichment level depending on the initial composition and excess of labeled water used).

An alternative approach for labeling was used in a small number of cases in this thesis, which is based on successive oxygen isotopic exchanges with enriched water, reaching a thermodynamic equilibrium (Scheme I-2). As already mentioned in the Chapter 1.1.1, when the equilibrium is reached, assuming there are no significant isotope effects, the final product contains all the possibilities (*i.e.* non-labeled, mono-labeled, doubly-labeled species), and their relative contribution follows a binomial statistical distribution X ~ *Bin*(n,p), where *n* is the number of oxygen atoms susceptible to be enriched and *p* is the probability of enrichment of an arbitrary oxygen (*i.e.* enrichment level). This is illustrated in the Figure I-5, where the MS pattern of L-lysine ^{18}O-labeled *via* oxygen exchange (using 99% ^{18}O-enriched water), is displayed. In this MS spectrum, the major peaks *p*, *p+2* and *p+4* correspond to the non-labeled (monoisotopic mass), ^{18}O-mono-labeled and $^{18}O_2$-doubly-labeled lysine molecules, respectively). The remaining small peaks can be attributed mainly to presence of ^{13}C (natural abundance) within the ^{18}O-labeled lysine, and to much lesser extent to ^{17}O coming from the ^{18}O-enriched water.

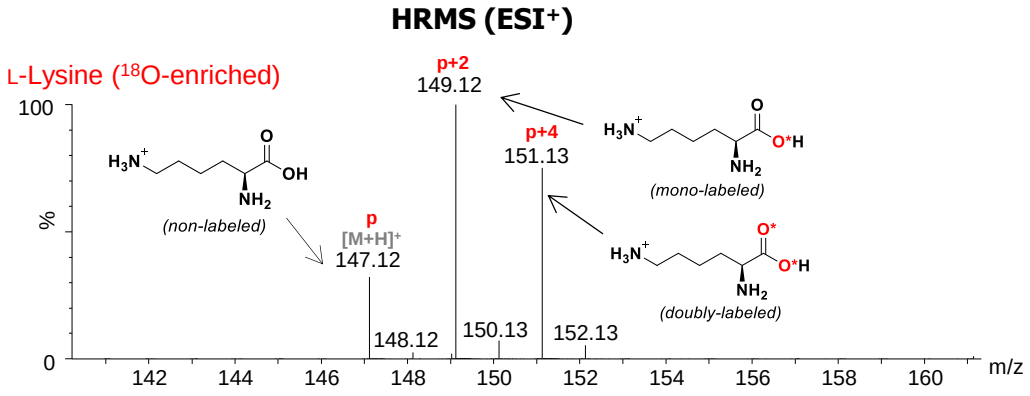

Figure I-5: HRMS (ESI⁺) patterns of L-lysine enriched in ^{18}O *via* oxygen exchange, recorded on a Waters Synapt G2-S spectrometer (positive mode, TOF analyser, R = 40 000). The peak *p* corresponds to the monoisotopic mass of lysine, while peaks *p+2* and *p+4* mainly belong to the molecules containing $1x^{18}O$ and $2x^{18}O$, respectively.

Regarding the enrichment *yield* calculation, here the calculated EY reflects whether the thermodynamic equilibrium was reached or not. It is determined as enrichment level per oxygen calculated from the MS data (as described previously) with respect to the maximal theoretical enrichment level possible. The maximal theoretical enrichment level is related to a system in the state of equilibrium, and is calculated from the oxygen isotope composition in the reagents (*i.e.* carboxylic acid and water, see Figure I-6). When multiplied by 100, the EY is provided in percentage, and it can be described as quantitative, when the equilibrium was reached (*i.e.* EY = 100 %). This calculation concept is graphically represented in the Figure I-6.

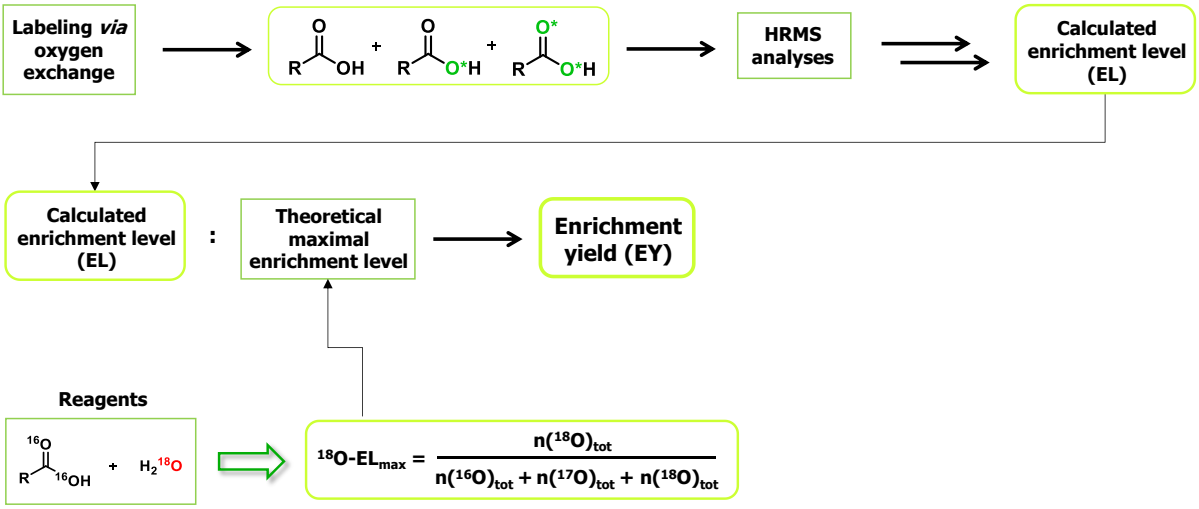

Figure I-6: Schematic description of enrichment yield calculation process when using oxygen exchange labeling scheme for the enrichment, including the theoretical maximal enrichment level equation.

I-D) ERROR BARS CALCULATION

The mass accuracy of the MS instrument used regularly for the analysis of labeled products (*i.e.* Waters Synapt G2-S spectrometer, with electrospray ionization source (ESI) and time-of-flight analyser (TOF, R = 40 000)), is 0.001 Da (based on instrument specification).

The statistical error of the MS measurement itself was calculated from repeated measurements of non-labeled palmitic acid (PA, natural abundance, n = 6 x 10 measurements)

and ^{18}O-enriched PA sample (n = 6 x 10 measurements). The standard deviation of the measured average mass for the non-labeled PA was determined as 255.392 ± 0.002 g/mol, and for the ^{18}O-labeled PA as 257.311 ± 0.013 g/mol. For the ^{18}O-enriched PA, the related standard error of the calculated enrichment yield/level then corresponded to EY = 97.00 ± 0.04 %, and EL = 46.50 ± 0.04 %.

However, more significant difference in enrichment yield/level comes from the different synthetic batches. Therefore, in this manuscript, the error bars of calculated ^{17}O/^{18}O-enrichment yields/levels correspond to standard deviations of the average enrichment yields/levels from repeated synthesis (typical number of repetitions n = 2 - 4). In general, for ^{17}O/^{18}O-labeled fatty acids, the calculated EY variation was ± 1 - 3 %, the EL variation was ± 1 - 2 %, and for ^{17}O/^{18}O-labeled amino acids, the calculated EY variation was ± 1 - 2 %, the EL variation was ± 1 %. More details can be found in Annexe II, section II-D, Table II-4 (for fatty acids), and in Chapter 4, section 4.2.5, Table 4.8 (for amino acids).

REFERENCES

1. Samarah, L. Z.; Khattar, R.; Tran, T. H.; Stopka, S. A.; Brantner, C. A.; Parlanti, P.; Veličković, D.; Shaw, J. B.; Agtuca, B. J.; Stacey, G.; Paša-Tolić, L.; Tolić, N.; Anderton, C. R.; Vertes, A., Single-Cell Metabolic Profiling: Metabolite Formulas from Isotopic Fine Structures in Heterogeneous Plant Cell Populations. *Anal. Chem.* **2020,** *92* (10), 7289-7298.
2. Stewart, I. I.; Thomson, T.; Figeys, D., 18O Labeling: a tool for proteomics. *Rapid Comm. Mass Spectrom.* **2001,** *15* (24), 2456-2465.
3. Geoghegan, K. F.; Kelly, M. A., Biochemical applications of mass spectrometry in pharmaceutical drug discovery. *Mass Spectrom. Rev.* **2005,** *24* (3), 347-366.
4. E. Hoffmann, V. S., *Mass Spectrometry Principles and Applications*. Wiley: 2007.
5. Miladinović, S. M.; Kozhinov, A. N.; Gorshkov, M. V.; Tsybin, Y. O., On the Utility of Isotopic Fine Structure Mass Spectrometry in Protein Identification. *Anal. Chem.* **2012,** *84* (9), 4042-4051.
6. Haynes, W. M., *Handbook of Chemistry and Physics*. 92nd ed.; 2011-2012.
7. Bogdanov, B.; Smith, R. D., Proteomics by FTICR mass spectrometry: Top down and bottom up. *Mass Spectrom. Rev.* **2005,** *24* (2), 168-200.
8. Leavell, M. D.; Leary, J. A., Fatty Acid Analysis Tool (FAAT): An FT-ICR MS Lipid Analysis Algorithm. *Anal. Chem.* **2006,** *78* (15), 5497-5503.
9. https://www.insa-rouen.fr/en/recherche/laboratoires/cobra.

CHAPTER 2

$^{17}O/^{18}O$-ENRICHMENT OF FATTY ACIDS

INTRODUCTION

The content of this Chapter 2 is based on part of the work published in:

- Špačková, J.; Fabra, C.; Cazals, G.; Hubert-Roux, M.; Schmitz-Afonso, I.; Goldberga, I.; Berthomieu, D.; Lebrun, A.; Métro, T.-X.; Laurencin, D., Cost-efficient and user-friendly $^{17}O/^{18}O$ labeling procedures of fatty acids using mechanochemistry. *Chem. Commun.* **2021**, *57*, 6812-6815
- Špačková, J.; Fabra, C.; Mittelette, S.; Gaillard, E.; Chen, C.-H.; Cazals, G.; Lebrun, A.; Sene, S.; Berthomieu, D.; Chen, K.; Gan, Z.; Gervais, C.; Métro, T.-X.; Laurencin, D., Unveiling the Structure and Reactivity of Fatty-Acid Based (Nano)materials Thanks to Efficient and Scalable ^{17}O and ^{18}O-Isotopic Labeling Schemes. *J. Am. Chem. Soc.* **2020**, *142* (50), 21068-21081.

Fatty acids (FAs) represent a substantial class of biomolecules with multiple applications. Because of their biological importance, they are widely studied in the fields of lipidomics and metabolomics, as well as in human nutrition research, especially the essential ω-3 and ω-6 polyunsaturated fatty acids (PUFAs)[1] like α-linolenic acid (ALA) or linoleic acid (LA) (Figure 2.1).[2] Furthermore, because of their amphiphilic character they are also used in materials science, for example as surfactants in nanoparticles synthesis, where they can direct the final shape and properties of nanoparticles.[3-4]

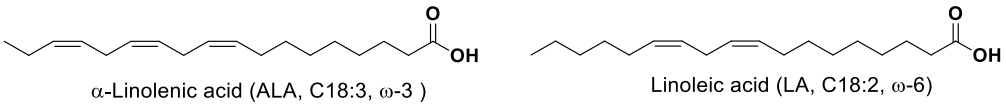

Figure 2.1: Examples of ω-3 and ω-6 polyunsatured fatty acids (PUFAs).

The labeling of free FAs and their ester derivatives in stable isotopes (^{2}H, ^{13}C and $^{17}O/^{18}O$) is of high interest as it allows to better understand the structure and reactivity of the complex (bio)molecules and materials systems. For example, by deuteration, the influence of the chain length of free FAs on the phase behaviour of stratum corneum membranes could be explored by ^{2}H NMR.[5] Using ^{13}C labeling, in-vivo ^{13}C NMR spectroscopy could be used to study the metabolism of polyunsaturated fatty acid methyl esters in the neonatal rat brains.[6] When labeled in ^{18}O, FA derivatives could be used as internal standards in mass spectrometry (MS) for metabolites quantitation or to elucidate reaction mechanisms.[7-9] Lastly, regarding the application of labeled FAs in material science, ^{13}C isotopic labeling was found to be valuable for studying by ^{13}C solid state NMR the mode of binding of the carboxylic group of stearic acid at the surface of zirconia as a function of temperature,[10] or the partitioning of myristate and

hexanoate ligands at the surface of CdSe nanocrystals.[11] The application of ^{17}O-labeled oleic acid in the structural study of zinc-oleate soap, and the study of surface reactivity under UV light irradiation of oleic acid functionalized zinc oxide nanoparticles will be described in the next Chapter 3.

Despite the great potential that $^{17}O/^{18}O$-labeled FAs could offer to the research community, their use remains scarce compared to ^{2}H and ^{13}C labeled species. One of the reasons to this comes from the limited access to $^{17}O/^{18}O$-labeled FAs, which are not commercially available and require to be synthesized. The very few oxygen enrichment protocols found in the literature almost exclusively focus on the ^{18}O-labeling of specific FA derivatives used as standards in GC-MS analyses. In these protocols, the carboxylic oxygen atoms are labeled *via* hydrolysis of the corresponding esters (under basic or enzymatically catalysed conditions), or by acid catalysed oxygen exchange in labeled water.[7-8, 12] These syntheses engage large excesses (> 500 eq.) of H_2O^* (^{18}O-enriched) in order to produce only μg quantities of labeled products. Although such low amounts of product are adequate for applications in GC-MS analyses, they are absolutely insufficient for the synthesis of (nano)materials, and a simple scale-up of the protocols would be very costly considering the price of enriched water (1800 - 2900 € for 1 mL of 90% ^{17}O-H_2O^*, and 60 - 150 € for 1 mL of 97 - 99% ^{18}O-H_2O^*). To the best of our knowledge, the only "high-scale" ^{18}O-enrichment protocol published previously for free FA was the labeling of octanoic acid, which was obtained *via* hydrolysis of octanenitrile using small excess of $H_2{}^{18}O$ (8 eq.).[9] In this procedure, ~ 300 mg of labeled acid (61% yield) with high enrichment level (87 %) were isolated. The drawbacks of this method lied however in the necessity to use nitrile derivatives of FA, which are not widely available, and to apply high temperature (110 °C) for the reaction, which is not suitable for sensitive substrates, such as PUFAs (as already discussed in the Chapter 1.1).

In order to address the need for efficient and scalable $^{17}O/^{18}O$ labeling protocols which would be generally applicable to a broad range of FA substrates, we have developed alternative synthetic approaches using mechanochemistry (see Chapter 1, section 1.2.2),[13] where the $^{17}O/^{18}O$ enrichment is performed at ambient temperature and pressure using low amounts of H_2O^* (typically a few μL per synthesis).[14]

In the first part of this chapter, $^{17}O/^{18}O$-enrichment protocols for labeling of saturated FAs and also unsaturated FAs containing up to four double bonds, will be discussed (Figure 2.2a). For their labeling, the CDI-activation/hydrolysis protocol using mechanochemistry (vibratory ball-milling, VBM) developed in our group had to be adapted and optimized.[14] In the second part, a new enrichment protocol based on saponification of the

fatty acid ester derivatives will be described and applied on the $^{17}O/^{18}O$-labeling of the longest and highly sensitive PUFAs with five and six double bonds (eicosapentaenoic acid (EPA) and DHA, respectively) (Figure 2.2b). In the final part of this chapter, analyses of $^{17}O/^{18}O$-enriched products will be also discussed.

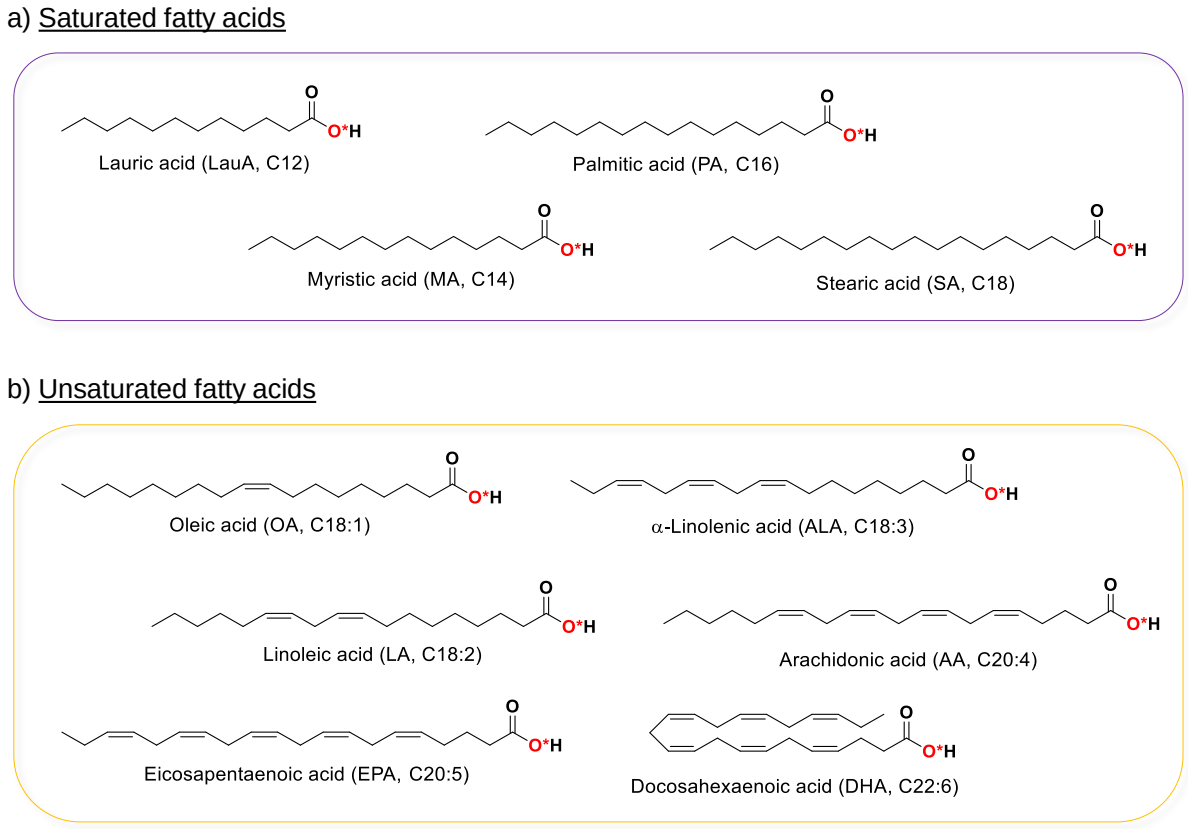

Figure 2.2: The scope of saturated and unsaturated fatty acids enriched in $^{17}O/^{18}O$ in this work. Both carboxylic oxygens (*i.e.* C=O* and C-O*H) are equally enriched (50 :50).

2.1 FATTY ACIDS ENRICHED *VIA* CDI-ACTIVATION/HYDROLYSIS

2.1.1 $^{17}O/^{18}O$-Enrichment of saturated fatty acids

At first, the enrichment protocols for saturated FAs with the chain-length varying between C12 to C18 were developed. Experiments were initially tested on small quantities of material, with less than 100 mg of fatty acid introduced in the stainless-steel 10 mL jar containing two stainless-steel beads (using a mixer mill, Retsch MM 400) and the reaction conditions were first optimized using $H_2{}^{18}O$, due to the lower purchasing price of ^{18}O-enriched water, before producing ^{17}O-labeled equivalents. Here, the enrichment consisted of two mechanochemical steps: activation with small excess of 1,1'-carbonyldiimidazole (CDI, 1.1 eq.), followed by hydrolysis of the activated acyl-imidazole intermediate using labeled

water (2 - 3 eq.) (Scheme 2.1). The course of the reaction was monitored by Attenuated total reflectance infrared spectroscopy (ATR-IR) looking at the shift of carbonyl stretching vibration band. The homogeneity of the reaction mixture was controlled by analysing samples from different parts of the reaction vessel at each synthetic step. After complete hydrolysis, products were recovered from the jar using non-labeled water, the medium was acidified with aqueous HCl (6M) and the labeled FAs were finally recovered by extraction with ethyl acetate (see Annexe II for detailed protocols).

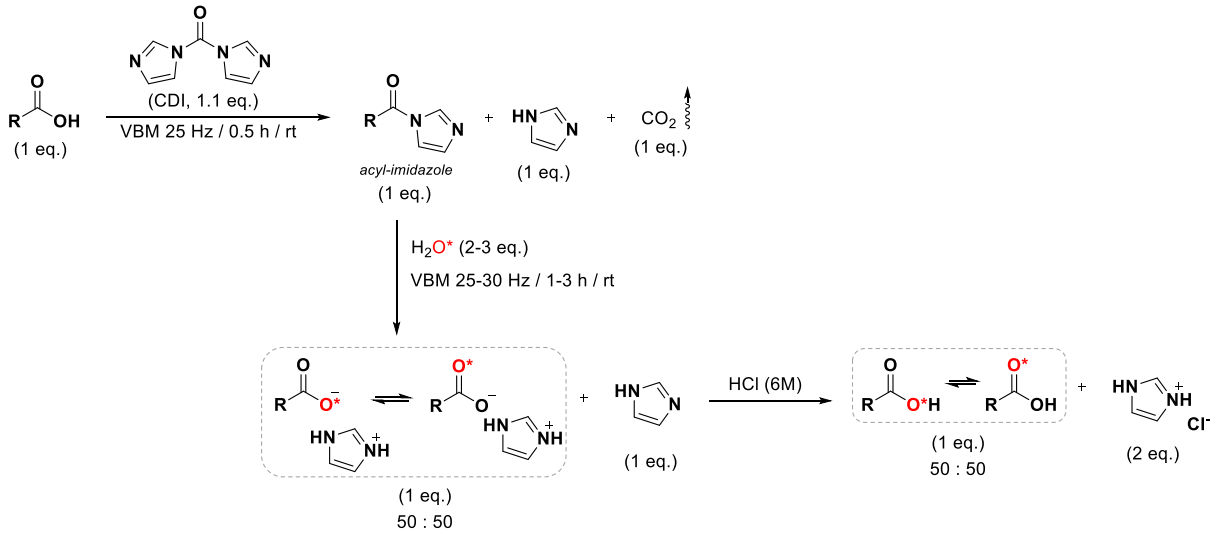

Scheme 2.1: Enrichment protocol for FAs using CDI-activation/hydrolysis approach. R = aliphatic chain specific of each fatty acid. Work-up process is not detailed in the scheme and can be found in the Annexe II.

Enriched products were isolated in good synthetic yields (80 - 91 %), with high enrichment yields (91 - 97 %), and high enrichment levels (average per carboxylic oxygen, 44 - 47 % and 42 - 44 %, for the ^{18}O-labeled products using 97% ^{18}O-enriched water, and for the ^{17}O-labeled products using 90% ^{17}O-enriched water, respectively) (Table 2.1). The purity of isolated phases was confirmed by solution ^{1}H and ^{13}C NMR spectroscopy and LCMS analyses.[15-16] The ^{17}O-labeled saturated FAs were also analysed by ^{17}O solid-state NMR, showing that on average, the ^{17}O-label is distributed equally among the two oxygen sites (*i.e.* "C=O" and "C-OH") in the isolated product (see subsection 2.3.4).

Table 2.1: Summary of saturated fatty acids $^{17}O/^{18}O$-enriched *via* CDI-activation-hydrolysis.

Enriched product	Isolated yield [%]	EY[a] [%]	^{18}O-EL[b] [%]	^{17}O-EL[c] [%]
Lauric acid (LauA, C12)	82	97	47	44
Myristic acid (MA, C14)	80	96	46	44
Palmitic acid (PA, C16)	88	96	47	43
Stearic acid (SA, C18)	84	91	44	42
^{13}C-Stearic acid (^{13}C-SA, C18)	91	94	44	43

[a] Average $^{17}O/^{18}O$-enrichment yield, [b] Enrichment level using 97% ^{18}O-enriched water, [c] Enrichment level using 90% ^{17}O-enriched water. All values represent average of multiple experiments (see Annexe II for details).

For the labeling of saturated FAs, concerning the activation step, full conversion was achieved for all molecules within 30 min of milling at 25 Hz. The hydrolysis step, in contrast, was found to be strongly substrate dependent, and needed to be optimized for each acid separately. Indeed, it was observed that the milling time required to achieve complete hydrolysis highly correlates with the increasing chain-length of activated acids. Specifically, milling for 1 h at 30 Hz was sufficient to fully hydrolyse lauroyl-imidazole (LauA, C12), whereas the complete hydrolysis of palmitoyl-imidazole (PA, C16) was achieved only after 3 h at 30 Hz. In the case of activated stearic acid (SA, C18), full conversion was not observed even after 6 h of milling at 30 Hz. Here, it was necessary to add a base (K_2CO_3, 1 eq.) to the reaction mixture after activation, to accelerate the hydrolysis of the stearyl-imidazole intermediate, reaching full conversion in 3 h of milling at 30 Hz (Table 2.2). The addition of this base favoured the formation of labeled hydroxide ions (H^*O^-) in the reaction medium, which was more reactive toward the acyl-imidazole.

Table 2.2: Melting points of non-labeled saturated FAs and their activated intermediates mixtures, and reaction conditions used for activation and hydrolysis steps.

Substrate	Chemical formula	M.p. [°C]	CDI-activation		M.p. (activ. interm.) [°C]	Hydrolysis		
			Time [min]	Freq. [Hz]		H_2O eq.	Time [min]	Freq. [Hz]
Saturated fatty acids		*(n = 2)*			*(n = 3)*			
LauA	$C_{12}H_{24}O_2$	43.4-46.3	30	25	58.4-62.3	3	60	30
MA	$C_{14}H_{28}O_2$	54.2-56.0	30	25	66.3-70.9	3	150	30
PA	$C_{16}H_{32}O_2$	62.4-64.4	30	25	73.5-78.1	3	180	30
SA	$C_{18}H_{36}O_2$	67.3-71.0	30	25	77.0-82.0	3	180*	30

*hydrolysis complete only when using K_2CO_3 (1 eq.); n = 2 and 3 corresponds to the number of repetitions of the analysis.

To further explain such differences, the melting points of the media isolated after activation were measured. These were found to follow the same trend as for the starting acids, with the melting points increasing with the length of the organic chain (Table 2.2). Additionally, it was found that the higher these melting points, the longer the time needed for hydrolysis. The evolution of the physical aspect of the reaction mixture is also worth mentioning: only when the reaction mixture had an oily aspect after hydrolysis was the hydrolysis found to be complete (Figure 2.3). It can be hypothesized that the long milling times at 30 Hz (required for the full conversion of the longer chain fatty acyl-imidazoles) enabled to reach a temperature high enough to change the physical state of the reaction mixture, resulting in higher mobility of the molecules, which could accelerate the hydrolysis. These observations may be related to the progressive temperature increase during the ball-milling which has been described previously.[17-19]

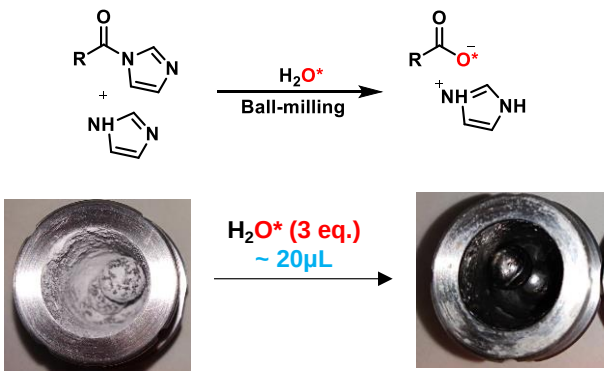

Figure 2.3: Photos of reactors showing the typical evolution of the physical state of the reaction mixtures before and after hydrolysis, when starting from solid FAs (LauA, MA, PA).

2.1.2 $^{17}O/^{18}O$-Enrichment of unsaturated fatty acids

For the labeling of unsaturated FAs containing up to four double bonds, the same two-steps protocol was applied (see Scheme 2.1 above). Compared to saturated FAs, no difference in reactivity related to the chain length was observed during hydrolysis, and overall reaction times were reduced. In particular, oleic acid was activated in 30 min of milling at 25 Hz and fully hydrolysed in 60 min of milling at 25 Hz in a stainless-steel jar using ball-mill MM400. For the remaining polyunsaturated fatty acids (PUFAs), in order to avoid potential side-reaction on the double bonds, the molecules were enriched using a different ball-mill (Fritsch, Pulverisette 23) with a jar made of polytetrafluoroethylene (PTFE) and a PTFE-coated bead (see Annexe II, for more details). Here, the PUFAs were completely activated in 20 min of ball-milling at 25 Hz, and fully hydrolysed in 90 min of milling at 25 Hz. The reduction of reaction

times is most probably caused by the different physical state of non-labeled unsaturated FAs reactants that are viscous oils at ambient temperature.

No impurities were detected in the enriched products, which were isolated in good yields (88 - 90 %) (see Table 2.3).[15-16] However, the enrichment yield achieved for the labeled PUFAs was slightly lower (81 - 87 %) compared to the one of oleic acid and other saturated FAs (90 - 97 %), which resulted in slightly lower enrichment levels determined (39 - 44 % compared to 44 - 47%, for ^{18}O-labeled products). This can be explained by the choice of the milling equipment used for the labeling of PUFAs, where part of the reaction mixture remains unreacted due to a non-optimal design of the milling jar (see Annexe II, section D, for details). Nevertheless, overall, it was shown here that the CDI-activation procedure can be easily optimized and generally applied to a variety of saturated and unsaturated FAs, allowing pure ^{17}O/^{18}O-enriched compounds to be produced in high yields.

Table 2.3: Summary of unsaturated fatty acids ^{17}O/^{18}O-enriched using CDI-activation/hydrolysis.

Enriched product	**Isolated yield [%]**	**EY[a] [%]**	**^{18}O-EL[b] [%]**	**^{17}O-EL[c] [%]**
Oleic acid (OA, C18:1)	90	90	44	42
Linoleic acid (LA, C18:2)	90	87	41	40
α-Linolenic acid (ALA, C18:3)	88	87	43	40
Arachidonic acid (AA, C20:4)	89	81	39	37

[a] Average ^{17}O/^{18}O-enrichment yield, [b] Enrichment level using 97% ^{18}O-enriched water, [c] Enrichment level using 90% ^{17}O-enriched water. All values represent an average of multiple experiments (see Annexe II for details).

2.1.3 Scale-up protocols

In order to be able to use the ^{17}O/^{18}O-enriched fatty acids in "routine" molecular and materials science applications, it was necessary to be able to produce up to gram quantities of enriched compounds. Scale-up procedures were therefore developed for saturated stearic acid (SA, C18) and unsaturated oleic acid (OA, C18:1), both molecules being of major interest in biology and (nano)materials science,[20-25] notably for the synthesis of functional nanoparticles. In both cases, given that the activation step leads to the release of CO_2, larger volume milling jars were used, to avoid any excessive build-up of internal pressure inside the reactors.

Scale-up experiments were first tested in a ball-mill MM400 using 50 mL milling jars. The oleic acid was activated with CDI within 15 min of milling at 25 Hz, and the acyl-imidazole intermediate was then fully hydrolysed using 2 equivalents of H_2O* within 30 min of milling at 25 Hz. This allowed the production of ~ 1 g of ^{17}O-enriched oleic acid with very good

synthetic yield (~ 92%) and enrichment level (average ^{17}O-enrichment per carboxylic oxygen ~ 43%) in just 2 hours of experimental time (work-up included), and required only ~ 150 µL of H_2*O (which corresponds to a cost of less than 300 € if 90% ^{17}O-enriched $H_2{}^{17}O$ is used). In the case of stearic acid, scale-up experiments were also attempted in the mixer-mill MM400 under similar conditions, but the hydrolysis step was again problematic, despite the presence of additional K_2CO_3. Even by decreasing the amount of sample to ~ 500 mg, or by modifying the number of beads used during the milling, the hydrolysis remained incomplete after 6 h of milling at 30 Hz (using 3 eq. H_2O*), according to ATR-IR and mass spectrometry analyses (~ 80% conversion). In order to change the type of mixing of the reaction medium during the hydrolysis, the enrichment of stearic acid was then studied on a planetary mill, using 20 mL jars.

Here, the stearic acid was activated within 2x 10 minutes cycle (500 rpm, 30 min break), and after careful optimization of the milling parameters (see Annexe II for details), it was possible to reduce the hydrolysis time to just 1 h (700 rpm, no break) in the presence of K_2CO_3 (1 eq.) using 3 equivalents of H_2O*. This allowed to produce ~ 500 mg of ^{18}O-enriched stearic acid with very good synthetic yield (~ 95%) and enrichment level (average ^{18}O-enrichment per carboxylic oxygen ~ 46%). To the best of our knowledge, it is the first time that the enrichment of oleic and stearic acids in ^{17}O or ^{18}O is reported on such a large scale and with such a high efficiency, both in terms of time and cost.

2.2 FATTY ACIDS ENRICHED *VIA* SAPONIFICATION

In order to reach other important PUFAs, such as eicosapentaenoic acid (EPA) and docosahexaenoic acid (DHA), and to further extend the substrate scope, a new enrichment procedure was developed: a one-pot mechanochemical saponification (Scheme 2.2).[26-27] This appeared as a potentially attractive strategy considering that many fatty acids are commercially available in the form of esters. In this enrichment protocol, ethyl ester derivatives of fatty acids were introduced into the reaction jar together with labeled water (3 eq.) and sodium ethoxide (1.5 eq.). After only 30 min of milling at 25 Hz, full conversion was observed by ATR-IR (see Annexe II). In this one-pot synthesis, labeled hydroxide anions were most probably first formed *in-situ via* acid-base reaction between labeled water and sodium ethoxide, and subsequently reacted with the ester function in the substrate, producing the labeled molecule (as carboxylate) and ethanol side-product. The same work-up as for the CDI-activation/hydrolysis, described above, was used here (*i.e.* acidification with HCl (6M) and extraction with ethyl acetate).

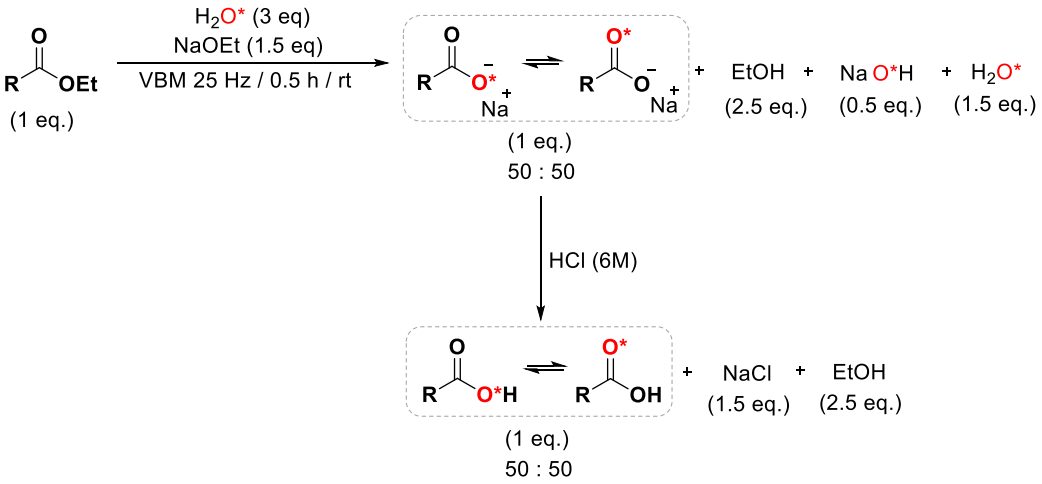

Scheme 2.2: Enrichment protocol for PUFAs using mechanochemical saponification approach. R = aliphatic chain specific for each acid. The dilution of labeled water after acidification with aqueous HCl is not shown in the scheme. Work-up process is not detailed in the scheme and can be found in the Annexe II.

Using saponification, all PUFAs were obtained in high synthetic yield (93 - 96 %) with high enrichment yields (91 - 93 %) and high enrichment levels (average per carboxylic oxygen: 45 % and 41 - 42 %, for the ^{18}O-labeled products using 97% ^{18}O-enriched water, and for the ^{17}O-labeled products using 90% ^{17}O-enriched water, respectively) (see Table 2.4). The purity of PUFAs prepared *via* saponification was confirmed by ^{1}H and ^{13}C solution NMR and by LCMS analyses, and no degradation was observed (see Supporting Information in the published work).[15-16] Hence, this work demonstrates for the first time that saponification reactions are highly attractive enrichment protocols for oxygen labeling of carboxylic functions of FAs, starting from the ester derivatives.

Table 2.4: Summary of unsaturated fatty acids ^{17}O/^{18}O-enriched using saponification.

Enriched product	Isolated yield [%]	EY[a] [%]	^{18}O-EL[b] [%]	^{17}O-EL[c] [%]
α-Linolenic acid (ALA, C18:3)	96	93	45	42
Eicosapentaenoic acid (EPA, C20:5)	96	92	45	42
Docosahexaenoic acid (DHA, C22:6)	93	91	45	41

[a] Average ^{17}O/^{18}O-enrichment yield, [b] Enrichment level using 97% ^{18}O-enriched water, [c] Enrichment level using 90% ^{17}O-enriched water. All values represent average of multiple experiments (see Annexe II for details).

2.3 ANALYSES OF ISOTOPICALLY LABELED PRODUCTS

2.3.1 Ultra-high resolution FT-ICR mass spectrometry

In comparison to previously published ^{18}O-enrichment protocols in which both oxygen atoms in carboxylic function are labeled (enrichment > 80% per carboxylic oxygen), the reaction mechanisms of both our mechanochemical enrichment protocols allows only one oxygen isotope per carboxylic function to be introduced. This is apparent from the MS spectra of ^{18}O-labeled products (see Annexe II), where the main molecular peak is shifted by two *m/z* units (*p+2*), and from ^{13}C solution NMR analyses, where the main resonance of carboxylic function appears shielded by ~ 0.025 ppm in comparison with the non-labeled molecule due to the ^{18}O isotope effect (see subsection 2.3.2). However, when looking at the whole MS pattern of unsaturated FA enriched *via* CDI-activation/hydrolysis procedure, we noticed that a molecular peak shifted by four *m/z* units (*p+4)* exhibits higher intensity than expected from simulations (Figure 2.4), suggesting a non-negligible presence of doubly labeled molecules.

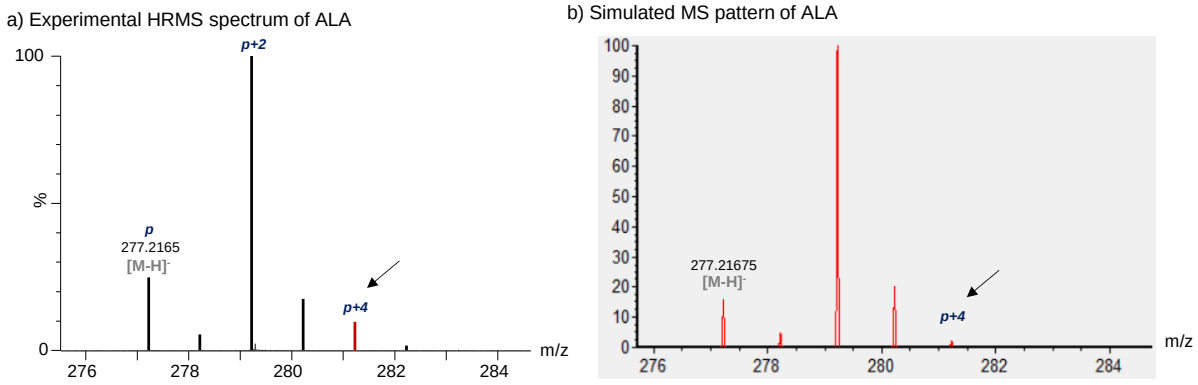

Figure 2.4: Experimentally measured HRMS (ESI$^-$, negative mode) spectrum of α-linolenic acid (ALA) prepared by CDI-activation/hydrolysis procedure is compared to a simulated MS pattern (simulated with IsoPro 3.1 using oxygen isotope content calculated from the measured spectrum, and considering that only 1 oxygen gets enriched).

The presence of doubly labeled product became even more obvious when MS spectra of ^{18}O-labeled α-linolenic acid (ALA) prepared by the two mechanochemical protocols were compared. Indeed, as shown in Figure 2.5, the ultra-high resolution FT-ICR (Fourier-Transform Ion Cyclotron Resonance) mass spectra enabled us to resolve the "*p+4*" peak (isotopic fine structures)[28] and to differentiate the relative contribution of doubly-labeled molecules in each method. More specifically, it was observed that in the case of saponification, the "*p+4*" peak mainly consists of molecules containing two ^{13}C and one ^{18}O isotope as expected, with only very little amount of doubly ^{18}O-labeled product, whereas in the case of CDI-activation/hydrolysis, ~ 10 times more of doubly ^{18}O-labeled molecules was formed

compared to saponification, representing the dominant contribution. It can be hypothesized that doubly labeled products result predominantly from a CDI-reactivation of already enriched acid molecules due to the presence of remaining unreacted CDI reagent in the reaction mixture.

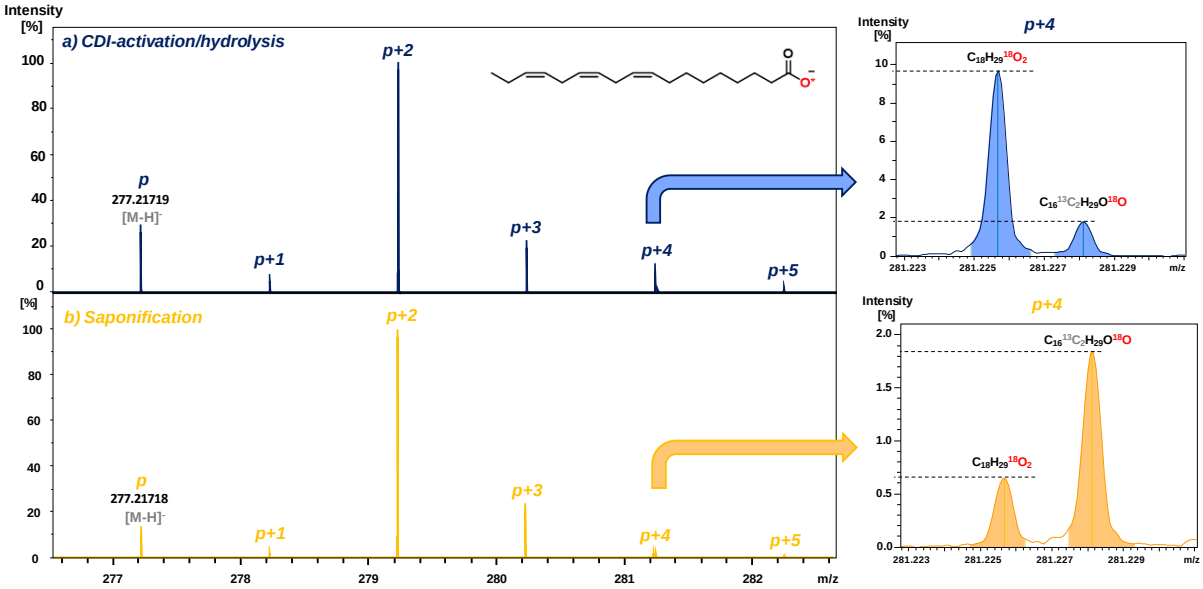

Figure 2.5: Ultra-high resolution mass spectra in ESI$^-$ (negative mode) of α-linolenic acid (ALA) enriched in ^{18}O a) *via* CDI-activation or b) saponification procedure recorded in COBRA laboratory in Rouen (France).[29] Relative content of doubly-labeled product is compared in *p+4* zoom on the right side; p = monoisotopic mass of ALA.

2.3.2 Oxygen-18 isotope effect on ^{13}C solution NMR

As already mentioned above, the presence of predominantly one enriched oxygen per molecule caused that the main resonance of carboxylic carbon appeared shielded in ^{13}C solution NMR (by ~ 0.025 ppm), compared to the non-labeled precursor, and represents a –C^{18}O^{16}OH head-group (Figure 2.6). This value is within a range of shifts previously reported in the literature for ^{18}O-enriched carboxylic acids.[30-31] Moreover, a third very small peak shielded in comparison to the non-labeled precursor (by ~ 0.05 ppm), was also resolved for some of the ^{18}O-labeled compounds. This peak was assigned to the doubly labeled carboxylic group -C^{18}O^{18}OH. Although this peak was not resolved in all ^{18}O-labeled molecules, at least a lower-frequency shoulder was always apparent for unsaturated fatty acids labeled *via* CDI-activation/hydrolysis procedure (see Annexe II).[15-16]

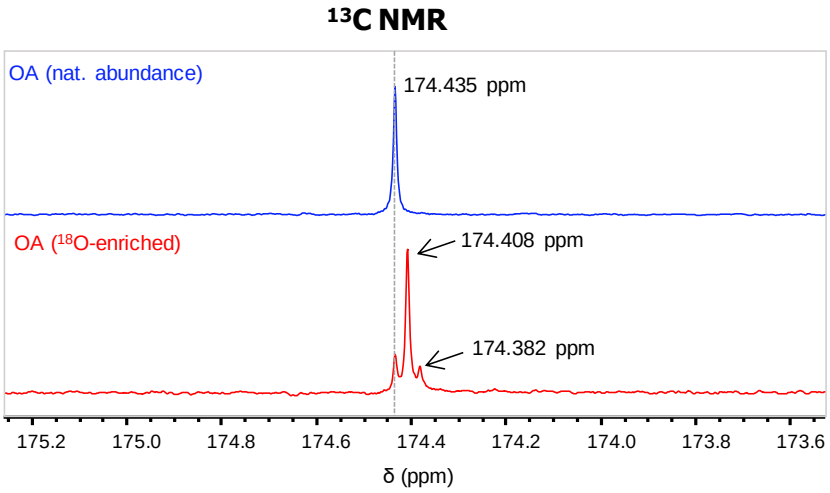

Figure 2.6: Oxygen-18 isotope effect on the carboxylic carbon resonance in ^{13}C solution NMR of ^{18}O-labeled oleic acid (OA) enriched *via* CDI-activation/hydrolysis procedure using 97% ^{18}O-enriched water for hydrolysis.

2.3.3 IR assignment of vibration bands

The labeling of the carboxylic functions in ^{17}O or ^{18}O is particularly advantageous for the direct assignment of several IR vibrations associated to the carboxylic group. This is illustrated by the ATR-IR spectrum in Figure 2.7 in the case of stearic acid (top 3 spectra). For this molecule, the most significant shifts after isotopic labeling concern the vibration bands at ~ 1699, 689 and 549 cm^{-1}, which decrease by ~ 6, ~ 5 and ~ 2 cm^{-1}, respectively, after replacement of one of the two carboxylic ^{16}O atoms by a ^{17}O. These shifts were even more pronounced in the case of ^{18}O-labeled product. These vibrations correspond to C=O stretching (at 1699 cm^{-1}), CO_2 bending/deformation (at 689 cm^{-1}), and CO_2 wagging modes (at 549 cm^{-1}), respectively.[32-35]

Such straightforward identification of carboxylic vibration frequencies following isotopic substitutions on the oxygen sites is complementary to experimental analyses on molecules enriched in ^{13}C. Indeed, the extent of isotopic shifts varies depending on which carboxylic atom(s) has been enriched (C or O), as illustrated in Figure 2.7 (bottom spectra) for a commercial stearic acid molecule labeled in ^{13}C on the carboxylic group. For example, the main C=O stretching band is now centred at 1655 cm^{-1}, and is further shifted by 6 cm^{-1} after ^{17}O labeling. Overall, this means that the oxygen labeling of fatty acids offers new possibilities to confirm IR spectral assignments, and/or help resolve vibration bands which may overlap.

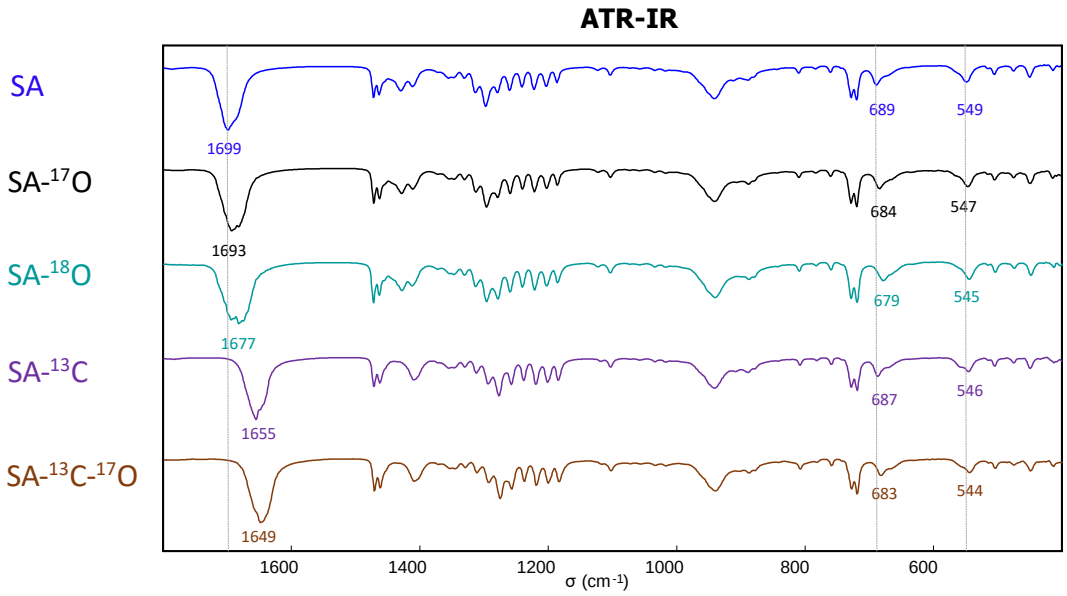

Figure 2.7: IR spectra of stearic acid (SA), at natural abundance (dark blue spectrum), enriched in ^{17}O (average ^{17}O-labeling ~ 42%; black spectrum), enriched in ^{18}O (average ^{18}O-labeling ~ 44%; light blue spectrum), enriched in ^{13}C on the carboxylic group (^{13}C labeling ~ 99 %; purple spectrum), and enriched in ^{13}C and ^{17}O on the carboxylic group (^{13}C labeling ~ 99 % and average ^{17}O-labeling ~ 42%; brown spectrum). Different synthetic batches of each ^{17}O or ^{18}O enriched molecule were analysed by ATR-IR and revealed similar wavenumbers, indicating that the trends reported here are robust.

2.3.4 ^{17}O MAS NMR of fatty acids

The saturated fatty acids and unsaturated oleic acid (OA) enriched in ^{17}O were analysed by ^{17}O magic-angle spinning (MAS) solid-state NMR spectroscopy.[15-16] In the case of oleic acid, the enriched sample was frozen and the measurement was performed at low temperature (- 40 °C). Since the increase of temperature inside of a rotor during spinning at 16 kHz is about 20 °C (estimated from the dependence of ^{207}Pb shift in the lead nitrate on the temperature),[36] and the melting point of the oleic acid is ~ 13 °C, performing the analyses at -40 °C ensured that oleic acid remained in the frozen solid form. However, this analysis was not performed for the polyunsaturated fatty acids due to their very low melting points (-5 to -55 °C), which would require even lower temperature for the analyses.

The ^{17}O MAS NMR spectra of stearic acid (SA) and oleic acid (OA) recorded at 14.1 T are compared in Figure 2.8. Although predominant contributions from "C=O*" and "C-O*H" like environments can be clearly distinguished on the MAS NMR spectra of both molecules,[37-38] a more significant overlap of these resonances is observed in the case of stearic acid. Given that fatty acids have been shown to crystallize with the polar head-chains forming H-bonded dimers,[39-43] such differences are likely to arise from discrepancies in the average localization of the OH hydrogen atoms,[42] and hence in relative energy of the two interconverting tautomeric

forms, as this can significantly impact ^{17}O MAS NMR spectra.[44-46] From a more practical point of view, both of these ^{17}O NMR spectra could be recorded with very good signal-to-noise ratio in short time (less than 4 hours on a 14.1 T NMR instrument), making these enriched molecules highly promising precursors for helping elucidate the structure of more complex molecular and materials systems. Quadrupolar parameters were extracted from the ^{17}O MAS NMR spectra of the studied ^{17}O-labeled FAs, and are summarized below in Table 2.5.

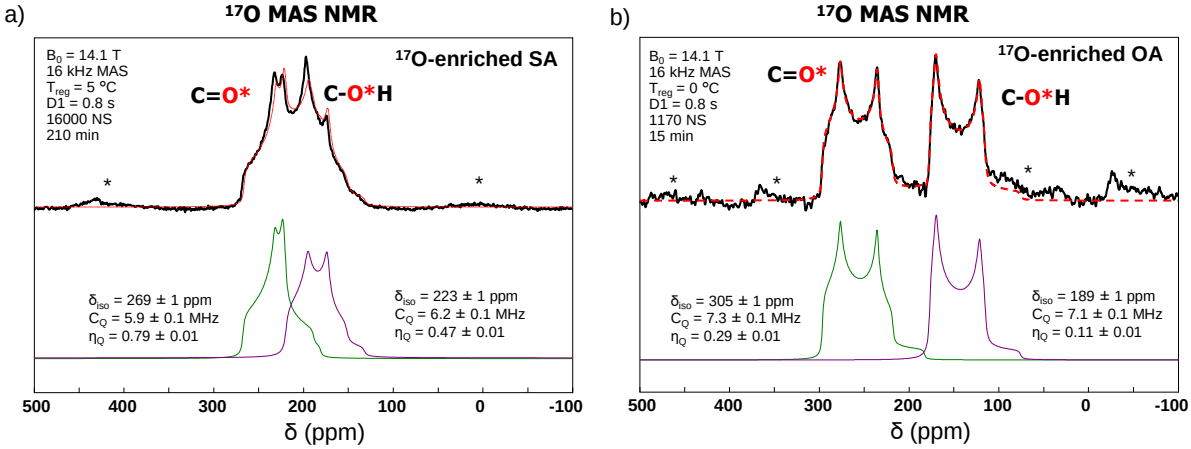

Figure 2.8: ^{17}O MAS NMR spectra of a) ^{17}O-labeled stearic acid and b) oleic acid (right), together with the fit (dashed red line), showing the contributions from the "C=O*" and "C-O*H" -like environments (50 :50, green and purple spectra). The average ^{17}O-enrichment of the carboxylic groups in the molecules studied here by NMR was ~ 42 % for stearic acid and ~ 19 % for oleic acid. "*" symbols correspond to spinning sidebands.

Table 2.5: Summary table of the extracted quadrupolar parameters (δ_{iso}, C_Q and η_Q) from the ^{17}O MAS NMR spectra of ^{17}O-labeled FAs (Site A = C=O* like, Site B = C-O*H like).

^{17}O-labeled FA	**Oxygen sites**	**δ_{iso} (ppm)**	**C_Q (MHz)**	**η_Q**
Lauric acid (LauA, C12)	Site A	278 ± 1	6.3 ± 0.1	0.68 ± 0.01
	Site B	217 ± 1	6.4 ± 0.1	0.38 ± 0.01
Myristic acid (MA, C14)	Site A	274 ± 1	6.1 ± 0.1	0.75 ± 0.01
	Site B	219 ± 2	6.1 ± 0.2	0.43 ± 0.02
Palmitic acid (PA, C16)	Site A	270 ± 1	5.9 ± 0.1	0.77 ± 0.02
	Site B	223 ± 3	6.3 ± 0.3	0.47 ± 0.01
Stearic acid (SA, C18)	Site A	269 ± 1	5.9 ± 0.1	0.79 ± 0.01
	Site B	223 ± 1	6.2 ± 0.1	0.47 ± 0.01
^{13}C-Stearic acid (^{13}C-SA, C18)	Site A	267 ± 1	5.7 ± 0.1	0.82 ± 0.01
	Site B	225 ± 1	6.2 ± 0.1	0.50 ± 0.01
Oleic acid (OA, C18:1)	Site A	305 ± 1	7.3 ± 0.1	0.29 ± 0.01
	Site B	189 ± 1	7.1 ± 0.1	0.11 ± 0.01

CONCLUSION

Overall, it was shown here that mechanochemistry is a versatile approach that stands out from currently available oxygen enrichment protocols for carboxylic acids, thanks to the simplicity, rapidity and cost-efficiency of proposed procedures. It was demonstrated that the reaction conditions can be easily optimized to extend the scope of $^{17}O/^{18}O$-labeled fatty acids using CDI-activation/hydrolysis. A variety of saturated as well as unsaturated free FAs was for the first time enriched in $^{17}O/^{18}O$ and isolated pure in high yields (80 - 91 %), with no need for column chromatography, in less than a half-day. Moreover, the newly developed mechanochemical saponification enabled to reach other important and highly sensitive PUFAs, including EPA and DHA. Using simple work-up, $^{17}O/^{18}O$-enriched PUFAs were isolated pure, in high yields (93 - 96 %) and with high enrichment levels (45% and 41 - 42% average per carboxylic oxygen, for ^{18}O-labeling and ^{17}O-labeling, respectively). Moreover, enrichment was found to be stable over a 1-year storage period (see Annexe II, section II-D).

The greater availability of the ^{17}O or ^{18}O enriched fatty acids is expected to also favour the development and use of other structural characterization techniques which are sensitive to the stable isotopes of oxygen, such as vibrational spectroscopies (IR and Raman), mass spectrometry (including high-resolution FT-ICR - Fourier Transform Ion Cyclotron Resonance),[47] as well as ^{17}O QCT (quadrupole central transition) and ^{17}O DNP-enhanced NMR spectroscopies.[48] Although, in average, only one oxygen per carboxylic function is labeled, the enrichment levels provided by this methodology are perfectly suitable for (nano)materials science applications[49-51] for gaining deeper insight into the structure and reactivity of different systems *via* IR (using ^{18}O-labeled species) or high-resolution ^{17}O NMR analyses. This will be illustrated in the following Chapter 3. More generally, saponification under ball-milling represents a new, simple, fast and cost-efficient $^{17}O/^{18}O$ labeling strategy, which has great potential to be applied for oxygen enrichment of other organic molecules containing carboxylic functions, and this will be illustrated in the Chapter 4.

REFERENCES

1. Saini, R. K.; Keum, Y.-S., Omega-3 and omega-6 polyunsaturated fatty acids: Dietary sources, metabolism, and significance — A review. *Life Sci* **2018,** *203*, 255-267.
2. De Carvalho, C. C.; Caramujo, M. J., The various roles of fatty acids. *Molecules* **2018,** *23* (10), 2583.
3. Yang, Y.; Qin, H.; Jiang, M.; Lin, L.; Fu, T.; Dai, X.; Zhang, Z.; Niu, Y.; Cao, H.; Jin, Y.; Zhao, F.; Peng, X., Entropic Ligands for Nanocrystals: From Unexpected Solution Properties to Outstanding Processability. *Nano Lett.* **2016,** *16* (4), 2133-2138.
4. Wang, H.; Lian, Y., A mechanistic study of oleic acid-mediated solvothermal shape controllable preparation of zinc oxide nanostructures. *J. Alloys Compd.* **2014,** *594*, 141-147.
5. Chen, X.; Kwak, S.; Lafleur, M.; Bloom, M.; Kitson, N.; Thewalt, J., Fatty Acids Influence "Solid" Phase Formation in Models of Stratum Corneum Intercellular Membranes. *Langmuir* **2007,** *23* (10), 5548-5556.
6. Cun-nane, S. C.; Williams, S. C. R.; Bell, J. D.; Brookes, S.; Craig, K.; Iles, R. A.; Crawford, M. A., Utilization of Uniformly Labeled 13C-Polyunsaturated Fatty Acids in the Synthesis of Long-Chain Fatty Acids and Cholesterol Accumulating in the Neonatal Rat Brain. *J. Neurochem.* **1994,** *62* (6), 2429-2436.
7. Pickett, W. C.; Murphy, R. C., Enzymatic preparation of carboxyl oxygen-18 labeled prostaglandin F2α and utility for quantitative mass spectrometry. *Anal. Biochem.* **1981,** *111* (1), 115-121.
8. Hill, E.; Murphy, R. C., Quantitation of 20-hydroxy-5,8,11,14-eicosatetraenoic acid (20-HETE) produced by human polymorphonuclear leukocytes using electron capture ionization gas chromatography/mass spectrometry. *Biol. Mass Spectrom.* **1992,** *21* (5), 249-253.
9. Izgu, E. C.; Björkbom, A.; Kamat, N. P.; Lelyveld, V. S.; Zhang, W.; Jia, T. Z.; Szostak, J. W., N-Carboxyanhydride-Mediated Fatty Acylation of Amino Acids and Peptides for Functionalization of Protocell Membranes. *J. Am. Chem. Soc.* **2016,** *138* (51), 16669-16676.
10. Pawsey, S.; Yach, K.; Halla, J.; Reven, L., Self-Assembled Monolayers of Alkanoic Acids: A Solid-State NMR Study. *Langmuir* **2000,** *16* (7), 3294-3303.
11. Pang, Z.; Zhang, J.; Cao, W.; Kong, X.; Peng, X., Partitioning surface ligands on nanocrystals for maximal solubility. *Nat. Commun.* **2019,** *10* (1), 2454.
12. Westcott, J. Y.; Clay, K. L.; Murphy, R. C., Preparation of oxygen-18-labeled lipoxygenase metabolites of arachidonic acid. *Biomed. Mass Spectrom.* **1985,** *12* (12), 714-718.
13. James, S. L.; Adams, C. J.; Bolm, C.; Braga, D.; Collier, P.; Friščić, T.; Grepioni, F.; Harris, K. D.; Hyett, G.; Jones, W., Mechanochemistry: opportunities for new and cleaner synthesis. *Chem. Soc. Rev.* **2012,** *41* (1), 413-447.
14. Métro, T. X.; Gervais, C.; Martinez, A.; Bonhomme, C.; Laurencin, D., Unleashing the potential of 17O NMR spectroscopy using mechanochemistry. *Angew. Chem., Int. Ed.* **2017,** *56* (24), 6803-6807.
15. Špačková, J.; Fabra, C.; Mittelette, S.; Gaillard, E.; Chen, C.-H.; Cazals, G.; Lebrun, A.; Sene, S.; Berthomieu, D.; Chen, K.; Gan, Z.; Gervais, C.; Métro, T.-X.; Laurencin, D., Unveiling the Structure and Reactivity of Fatty-Acid Based (Nano)materials Thanks to Efficient and Scalable 17O and 18O-Isotopic Labeling Schemes. *J. Am. Chem. Soc.* **2020,** *142* (50), 21068-21081.
16. Špačková, J.; Fabra, C.; Cazals, G.; Hubert-Roux, M.; Schmitz-Afonso, I.; Goldberga, I.; Berthomieu, D.; Lebrun, A.; Métro, T.-X.; Laurencin, D., Cost-efficient and user-friendly 17O/18O labeling procedures of fatty acids using mechanochemistry. *Chem. Comm.* **2021,** *57* (55), 6812-6815.
17. Kulla, H.; Haferkamp, S.; Akhmetova, I.; Röllig, M.; Maierhofer, C.; Rademann, K.; Emmerling, F., In Situ Investigations of Mechanochemical One-Pot Syntheses. *Angew. Chem., Int. Ed.* **2018,** *57* (20), 5930-5933.
18. Užarević, K.; Ferdelji, N.; Mrla, T.; Julien, P. A.; Halasz, B.; Friščić, T.; Halasz, I., Enthalpy vs. friction: heat flow modelling of unexpected temperature profiles in mechanochemistry of metal–organic frameworks. *Chem. Sci.* **2018,** *9* (9), 2525-2532.
19. Hutchings, B. P.; Crawford, D. E.; Gao, L.; Hu, P.; James, S. L., Feedback kinetics in mechanochemistry: the importance of cohesive states. *Angew. Chem., Int. Ed.* **2017,** *56* (48), 15252-15256.
20. Hermans, J. J.; Baij, L.; Koenis, M.; Keune, K.; Iedema, P. D.; Woutersen, S., 2D-IR spectroscopy for oil paint conservation: Elucidating the water-sensitive structure of zinc carboxylate clusters in ionomers. *Science Advances* **2019,** *5* (6), eaaw3592.
21. Zherebetskyy, D.; Scheele, M.; Zhang, Y.; Bronstein, N.; Thompson, C.; Britt, D.; Salmeron, M.; Alivisatos, P.; Wang, L.-W., Hydroxylation of the surface of PbS nanocrystals passivated with oleic acid. *Science* **2014,** *344* (6190), 1380-1384.
22. Yin, H.; Casey, P. S.; McCall, M. J.; Fenech, M., Effects of Surface Chemistry on Cytotoxicity, Genotoxicity, and the Generation of Reactive Oxygen Species Induced by ZnO Nanoparticles. *Langmuir* **2010,** *26* (19), 15399-15408.
23. Ha, S.-T.; Su, R.; Xing, J.; Zhang, Q.; Xiong, Q., Metal halide perovskite nanomaterials: synthesis and applications. *Chem. Sci.* **2017,** *8* (4), 2522-2536.

24. Cai, J.; Miao, Y. Q.; Yu, B. Z.; Ma, P.; Li, L.; Fan, H. M., Large-Scale, Facile Transfer of Oleic Acid-Stabilized Iron Oxide Nanoparticles to the Aqueous Phase for Biological Applications. *Langmuir* **2017,** *33* (7), 1662-1669.
25. Shah, R. M.; Rajasekaran, D.; Ludford-Menting, M.; Eldridge, D. S.; Palombo, E. A.; Harding, I. H., Transport of stearic acid-based solid lipid nanoparticles (SLNs) into human epithelial cells. *Colloids Surf. B* **2016,** *140*, 204-212.
26. Štrukil, V., Highly Efficient Solid-State Hydrolysis of Waste Polyethylene Terephthalate by Mechanochemical Milling and Vapor-Assisted Aging. *Chem. Sus. Chem.* **2021,** *14* (1), 330-338.
27. Yeboue, Y.; Jean, M.; Subra, G.; Martinez, J.; Lamaty, F.; Métro, T.-X., Epimerization-Free C-Term Activation of Peptide Fragments by Ball Milling. *Org. Lett.* **2021,** *23* (3), 631-635.
28. Samarah, L. Z.; Khattar, R.; Tran, T. H.; Stopka, S. A.; Brantner, C. A.; Parlanti, P.; Veličković, D.; Shaw, J. B.; Agtuca, B. J.; Stacey, G.; Paša-Tolić, L.; Tolić, N.; Anderton, C. R.; Vertes, A., Single-Cell Metabolic Profiling: Metabolite Formulas from Isotopic Fine Structures in Heterogeneous Plant Cell Populations. *Anal. Chem.* **2020,** *92* (10), 7289-7298.
29. https://www.insa-rouen.fr/en/recherche/laboratoires/cobra.
30. Risley, J. M.; Van Etten, R. L., Oxygen-18 isotope effect in carbon-13 nuclear magnetic resonance spectroscopy. 2. The effect of structure. *J. Am. Chem. Soc.* **1980,** *102* (14), 4609-4614.
31. Risley, J. M.; Van Etten, R. L., Oxygen-18-isotope effect in carbon-13 nuclear magnetic resonance spectroscopy. 3. Additivity effects and steric effects. *J. Am. Chem. Soc.* **1980,** *102* (22), 6699-6702.
32. Kaneko, F.; Simofuku, T.; Miyamoto, H.; Kobayashi, M.; Suzuki, M., Vibrational spectroscopic study on the occurrence of stearic acid B and E forms: heterogeneous nucleation of the B form on the surface of E crystals and the topotactic phase transition from E to B. *J. Phys. Chem.* **1992,** *96* (25), 10554-10559.
33. Pudney, P. D. A.; Mutch, K. J.; Zhu, S., Characterising the phase behaviour of stearic acid and its triethanolamine soap and acid–soap by infrared spectroscopy. *Phys. Chem. Chem. Phys.* **2009,** *11* (25), 5010-5018.
34. Zerbi, G.; Conti, G.; Minoni, G.; Pison, S.; Bigotto, A., Premelting phenomena in fatty acids: an infrared and Raman study. *J. Phys. Chem.* **1987,** *91* (9), 2386-2393.
35. Robinet, L.; Corbeil, M.-C., The Characterization of Metal Soaps. *Stud. Conserv.* **2003,** *48* (1), 23-40.
36. Bielecki, A.; Burum, D. P., Temperature Dependence of207Pb MAS Spectra of Solid Lead Nitrate. An Accurate, Sensitive Thermometer for Variable-Temperature MAS. *J. Magn. Reson. A* **1995,** *116* (2), 215-220.
37. Wong, A.; Poli, F., Chapter Three - Solid-State ^{17}O NMR Studies of Biomolecules. In *Annu. Rep. NMR Spectrosc.* Webb, G. A., Ed. Academic Press: 2014; Vol. 83, pp 145-220.
38. Wu, G., Solid-State 17O NMR studies of organic and biological molecules: Recent advances and future directions. *Solid State Nucl. Magn. Reson.* **2016,** *73*, 1-14.
39. Moreno-Calvo, E.; Gbabode, G.; Cordobilla, R.; Calvet, T.; Cuevas-Diarte, M. À.; Negrier, P.; Mondieig, D., Competing Intermolecular Interactions in the High-Temperature Solid Phases of Even Saturated Carboxylic Acids ($C_{10}H_{19}O_2H$ to $C_{20}H_{39}O_2H$). *Chem. Eur. J.* **2009,** *15* (47), 13141-13149.
40. Kaneko, F.; Yamazaki, K.; Kitagawa, K.; Kikyo, T.; Kobayashi, M.; Kitagawa, Y.; Matsuura, Y.; Sato, K.; Suzuki, M., Structure and Crystallization Behavior of the β Phase of Oleic Acid. *J. Phys. Chem. B* **1997,** *101* (10), 1803-1809.
41. Moreno, E.; Cordobilla, R.; Calvet, T.; Cuevas-Diarte, M. A.; Gbabode, G.; Negrier, P.; Mondieig, D.; Oonk, H. A. J., Polymorphism of even saturated carboxylic acids from n-decanoic to n-eicosanoic acid. *New J. Chem.* **2007,** *31* (6), 947-957.
42. Wang, L.; Uribe-Romo, F. J.; Mueller, L. J.; Harper, J. K., Predicting anisotropic thermal displacements for hydrogens from solid-state NMR: a study on hydrogen bonding in polymorphs of palmitic acid. *Phys. Chem. Chem. Phys.* **2018,** *20* (13), 8475-8487.
43. Gbabode, G.; Negrier, P.; Mondieig, D.; Moreno, E.; Calvet, T.; Cuevas-Diarte, M. À., Fatty acids polymorphism and solid-state miscibility: Pentadecanoic acid–hexadecanoic acid binary system. *J. Alloys Compd.* **2009,** *469* (1), 539-551.
44. Kong, X.; Shan, M.; Terskikh, V.; Hung, I.; Gan, Z.; Wu, G., Solid-State 17O NMR of Pharmaceutical Compounds: Salicylic Acid and Aspirin. *J. Phys. Chem. B* **2013,** *117* (33), 9643-9654.
45. Wu, G.; Hung, I.; Gan, Z.; Terskikh, V.; Kong, X., Solid-State ^{17}O NMR Study of Carboxylic Acid Dimers: Simultaneously Accessing Spectral Properties of Low- and High-Energy Tautomers. *J. Phys. Chem. A* **2019,** *123* (38), 8243-8253.
46. Chen, C.-H.; Goldberga, I.; Gaveau, P.; Mittelette, S.; Špačková, J.; Mullen, C.; Petit, I.; Métro, T.-X.; Alonso, B.; Gervais, C.; Laurencin, D., Looking into the dynamics of molecular crystals of ibuprofen and terephthalic acid using 17O and 2H nuclear magnetic resonance analyses. *Magn. Reson. Chem.* **2021,** *59* (9-10), 975-990.
47. Griffiths, W. J.; Wang, Y., Mass spectrometry: from proteomics to metabolomics and lipidomics. *Chem. Soc. Rev.* **2009,** *38* (7), 1882-1896.

48. Wu, G., 17O NMR studies of organic and biological molecules in aqueous solution and in the solid state. *Prog. Nucl. Magn. Reson. Spectrosc.* **2019,** *114-115*, 135-191.
49. Sut, T. N.; Park, S.; Yoon, B. K.; Jackman, J. A.; Cho, N.-J., Supported Lipid Bilayer Formation from Phospholipid-Fatty Acid Bicellar Mixtures. *Langmuir* **2020,** *36* (18), 5021-5029.
50. Modugno, F.; Di Gianvincenzo, F.; Degano, I.; van der Werf, I. D.; Bonaduce, I.; van den Berg, K. J., On the influence of relative humidity on the oxidation and hydrolysis of fresh and aged oil paints. *Sci. Rep.* **2019,** *9* (1), 5533.
51. Kwak, G.; Seol, M.; Tak, Y.; Yong, K., Superhydrophobic ZnO nanowire surface: chemical modification and effects of UV irradiation. *J. Phys. Chem. C* **2009,** *113* (28), 12085-12089.

ANNEXE II

FATTY ACIDS LABELING - EXPERIMENTAL PART

II-A) MATERIALS AND METHODS

II-A1) Reagents

The following reagents were used as received: stearic acid ($C_{18}H_{36}O_2$, Sigma-Aldrich, 95%, noted here SA), ^{13}C-stearic acid ($C_{17}H_{35}{}^{13}COOH$, Sigma-Aldrich, 99 atom% ^{13}C, noted here ^{13}C-SA), palmitic acid ($C_{16}H_{32}O_2$, Sigma, ≥ 99%, noted here PA), myristic acid ($C_{14}H_{28}O_2$, Sigma, ≥ 99%, noted here MA), lauric acid ($C_{12}H_{24}O_2$, Acros Organics, 99%, noted here LauA), oleic acid ($C_{17}H_{33}COOH$, Sigma-Aldrich, ≥ 99%, noted here OA), linoleic acid ($C_{18}H_{32}O_2$, Sigma, ≥ 99%, noted here LA), α-linolenic acid ($C_{18}H_{30}O_2$, Sigma, ≥ 99%, noted here ALA), arachidonic acid ($C_{20}H_{32}O_2$, Sigma, > 95%, noted here AA), ethyl-linolenate ($C_{20}H_{34}O_2$, Sigma, ≥ 98%), 1,1'-carbonyldiimidazole ($C_7H_6N_4O$, TCI, > 97%, noted here CDI), potassium carbonate anhydrous (K_2CO_3, Alfa Aesar, 99%), sodium ethanolate (C_2H_5ONa, Sigma-Aldrich, 95%). Ethyl-eicosapentaenoate ($C_{22}H_{34}O_2$) and ethyl-docosahexaenoate ($C_{24}H_{36}O_2$) were kindly offered by Dr. Céline Crauste (IBMM, Montpellier). Reagent grade solvents were used in all purification protocols.

^{17}O-labeled water with ~ 90% ^{17}O-enrichment was purchased from CortecNet. ^{18}O-labeled water was purchased from Eurisotop (its isotopic composition, as indicated in the certificate of analysis, is 97.1 % ^{18}O, 1.1 % ^{17}O, 1.8 % ^{16}O) or CortecNet (its isotopic composition, as indicated in the certificate of analysis, is 97.1 % ^{18}O, 1.4 % ^{17}O, 1.5 % ^{16}O).

II-A2) Synthetic equipment

Milling treatments were carried out in a Retsch Mixer Mill 400 apparatus, using 50 mL, 10 mL or 5 mL screw-type stainless steel grinding jars, containing 10 mm or 7 mm diameter stainless steel beads or in a Fritsch mini-mill Pulverisette 23 apparatus, using 5 mL screw-type Teflon jar containing one 10 mm diameter Teflon-coated bead. Some milling experiments for the scale-up of stearic-acid labeling were performed on a Fristch planetary mill apparatus (P7), using 20 mL inner-volume jars, containing 5 mm diameter beads. All protocols were first tested using non-labeled water and then optimized using ^{18}O-labeled water, before performing experiments with ^{17}O-labeled H_2O.

Zirconia milling jars and beads were not employed in the enrichment protocols of saturated fatty acids described below. Indeed, zirconia being a less dense material than stainless steel, longer milling times would probably be required to complete hydrolysis, during which more debris could shed off the milling equipment. This could imply a simultaneous loss of enrichment in the final material, because we have shown that zirconia particles can be labeled in ^{17}O using mechanochemistry.[1]

II-A3) Characterization protocols

Infrared (IR) spectra were recorded on a Perkin Elmer Spectrum 2 FT-IR instrument. The attenuated total reflectance (ATR) measurement mode was used (diamond crystal), and measurements were performed in the 400-4000 cm^{-1} range. All ATR-IR figures are available in the supporting information of the published work.[2-3]

Powder XRD analyses were carried out on a X'Pert MPD diffractometer using Cu $K_{\alpha 1}$ radiation (λ = 1.5406 Å) with the operation voltage and current maintained at 40 kV and 25 mA, respectively. Diffractograms were recorded between 5°and 60° in 2θ, with step size of 0.017°, and a time per step of 40 s. The XRD figures of final products are available in the supporting information of the published work.[2-3]

Melting points were measured on BÜCHI Melting Point B-540 instrument with temperature gradient 2 °C/1 min.

EDXS analyses were carried out on a Zeiss Evo HD15 scanning electron microscope equipped with an Oxford Instruments X-MaxN SDD 50 mm2 EDX detector. Powdered samples were deposited on double sided conducting carbon tape.

Mass spectrometry (MS) analyses were performed on a Waters Synapt G2-S apparatus, using electrospray ionization in negative or positive mode in a range of 50-1500 Da. Capillary and cone voltage were 2000 V and 30 V, respectively. The source temperature was 100 °C and desolvation temperature was set to 50°C. Data were processed by MassLynxV4.1 software. For each product three solutions were prepared (in acetonitrile or methanol, depending on the solubility), which were analyzed five-times by ESI-MS.

The ^{18}O-enrichement levels (EL) were estimated based on the calculation of an apparent average atomic weight for oxygen in the isolated phase, from which enrichment level per carboxylic oxygen was subsequently derived using ^{18}O enrichment and $^{18}O/^{17}O$ isotopic ratio of the labeled water. Reported error bars for ^{18}O labeling correspond to the standard deviation between different synthetic batches, each batch having been analyzed 5 times. Error bars for ^{17}O labeling were estimated to ~1 - 3%.

Enrichment yields (EY) correspond to the ratio between the average enrichment level per carboxylic oxygen determined by MS and the maximum average enrichment level per carboxylic oxygen which could have been obtained, considering the composition of enriched water used for the hydrolysis, and assuming that each carboxylic group is enriched on one of the 2 oxygen atoms (based on the hydrolysis of the acyl-imidazole intermediate, or the saponification of the ester).

LC-MS (liquid chromatography-mass spectrometry) analyses were done using an Acquity H-Class (Waters) system equipped with a Kinetex EVO C18 column (1.7 µm particle size, 50 x 2.1 mm, Phenomenex). Mobile phase A consisted of water while mobile phase B was acetonitrile, both containing 0.1% formic acid. The gradient started at 50% mobile phase B and increased to 100% mobile phase B over 5 min. After holding for 2 min the gradient returned to 50% B before re-equilibration for 3 min, to give a total run time of 10 min. The flow rate was 0.2 mL/min and the eluent was directed to the atmospheric pressure ionization source of a Synapt G2-S (Waters) operating under the conditions described above. The LCMS figures of final products are available in the supporting information of the published work.[2-3]

Ultra-high resolution mass spectrometry analyses were carried out on a FTICR instrument (SolariX XR FTMS, Bruker Daltonics) equipped with a 12 Tesla superconducting magnet and a dynamically harmonized ICR cell. The instrument is equipped with an electrospray (ESI) ionization source. Each sample was diluted in methanol, introduced in the ESI source at 200 □L/hr and analyzed in negative ion mode. Source parameters were as follows: nebulizer gas: 1 bar, dry gas 3 L/min and dry temperature 200 °C. Acquisition was realized with a 1.4 s transient length, with an accumulation time of 0.02 s and 50 scans accumulation. Resolution was 500 000 at *m/z* 277. FTICR-MS data were treated with Data Analysis 5.0 (Bruker). Molecular formulae were attributed considering $[M–H]^-$ deprotonated molecules. Isotopic fine structures were deciphered including ^{13}C and ^{18}O isotopes.

^1H and ^{13}C solution NMR spectra were recorded on an Avance III Bruker 600 MHz NMR spectrometer equipped with a TCI Prodigy cryoprobe or on an Avance III Bruker 500 MHz NMR spectrometer equipped with a BBO Helium cryoprobe, using DMSO-d_6 as a solvent. Chemical shifts were referenced to the residual solvent peaks at 2.50 ppm (^1H NMR spectra) and 39.52 ppm (^{13}C NMR spectra).

^{17}O solid state NMR experiments were performed on a VNMRS 600 MHz (14.1 T) NMR spectrometer, using a 3.2 mm probe tuned to ^{1}H (599.82 MHz) and ^{17}O (81.31 MHz). Two types of probes were used, depending on the availability of the equipment: a 3.2 mm Varian HX probe, or a 3.2 mm Varian HXY probe equipped with a 3.2 mm probe head. Spectra were recorded under MAS (Magic Angle Spinning) conditions, using a spinning frequency 16 kHz. ^{17}O NMR experiments were recorded using DFS (Double Frequency Sweep)[4] excitation scheme followed by a rotor-synchronized echo (one rotor period, 62.5 µs delay) to enhance the ^{17}O signal. The parameters were as following: DFS pulse of 500 µs, with sweep between 200 and 80 kHz, followed by a 90° "solid" pulse of 2 µs and a 180° pulse of 4 µs. ^{1}H decoupling (RF ~ 62.5 kHz) (SPINAL-64) was applied during acquisition. More details on acquisition conditions are reported in Table II-1. ^{17}O chemical shifts were referenced to D_2O at -2.7 ppm (which corresponds to tap-water at 0 ppm). All ^{17}O MAS NMR spectra were fitted and presented using DMfit software (using Q mas ½ model).[5]

Table II-1: ^{17}O solid state NMR acquisition parameters.

Sample	MAS frequency [kHz]	Temp. reg. [°C]	Recycle delay (D1) [s]	Acq. time [ms]	Number of scans (NS)	Exp. time
Lauric acid						
LauA	16	5	0.8	6	1850	~ 0h30
Myristic acid						
MA	16	5	0.8	6	6950	~ 1h30
Palmitic acid						
PA	16	5	0.8	20	6950	~ 1h30
Stearic acid						
SA	16	5	0.8	6	16000	~ 3h30
^{13}C-SA	16	5	0.8	6	10000	~ 2h15
Oleic acid						
OA	16	-40	0.8	6	1170	~ 0h15

II-B) SYNTHESES AND CHARACTERIZATIONS OF $^{17}O/^{18}O$-LABELED FA PREPARED *VIA* CDI-ACTIVATION/HYDROLYSIS PROCEDURE

II-B1) Lauric acid (LauA, $C_{12}H_{24}O_2$)

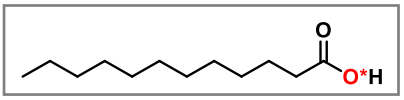

II-B1-a) Optimized labeling protocol

Lauric acid (79.4 mg, 0.40 mmol, 1.0 eq.) and CDI (70.7 mg, 0.44 mmol, 1.1 eq.) were introduced into the stainless-steel grinding jar (10 mL inner volume) containing two stainless-steel balls (10 mm diameter). The jar was closed and subjected to grinding for 30 min in the MM400 mixer mill operated at 25 Hz. ^{18}O-labeled water (97.1%, 21.5 µL, 1.2 mmol, 3.0 eq.) was then added into the jar, and the mixture was subjected to further grinding for 120 min at 25 Hz. To help recover the product, non-labeled water (1 mL) was added into the jar, and the content was subjected to grinding for 2 min at 25 Hz. Then, the medium ("milky" solution with a foam on top) was transferred to a beaker (together with sufficient amount of non-labeled water (10 mL) used here to rinse the jar). The medium was acidified to pH ~ 1 with an aqueous solution of HCl (6M, 12 drops) and extracted with ethyl acetate (1x 20 mL, 3x 10 mL). Combined organic phases were dried over Na_2SO_4 and filtered. Solvent was evaporated giving white solid, which was re-dissolved in diethyl ether and finally dried under vacuum to yield the product as white microcrystalline solid. Average yield (n = 3): 64 ± 10 mg, 80 ± 12 %, m. p. 43.7 - 45.7 °C.

For the ^{17}O-labeling, exactly the same reaction/work-up conditions as for ^{18}O-labeling were employed with 90% ^{17}O-enriched water (21.5 µL, 3.0 eq.) used at the hydrolysis step. After addition of ^{17}O-labeled water, the mixture was subjected to grinding for 150 min at 25 Hz. Yield (n = 1): 68 mg, 85 %.

Figure II-1: ATR-IR analysis of the starting material, reaction intermediates, and final products. The dashed line shows that the C=O stretching frequency of $^{18}O/^{17}O$-enriched product is shifted to lower wavenumbers in comparison with non-labeled precursor.

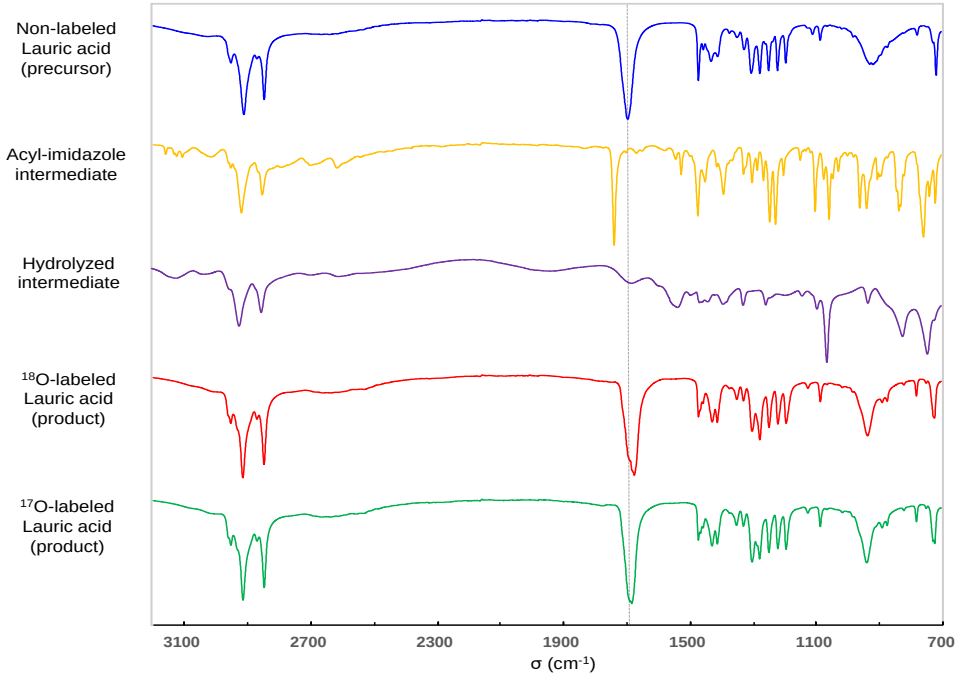

II-B1-b) Characterization of the ^{18}O-labeled LauA

Figure II-2: MS analyses of the non-labeled precursor in comparison to the ^{18}O-enriched product. Average enrichment per carboxylic oxygen determined by MS: 46.9 ± 0.5 % (n = 3), enrichment yield: ~ 96 %.

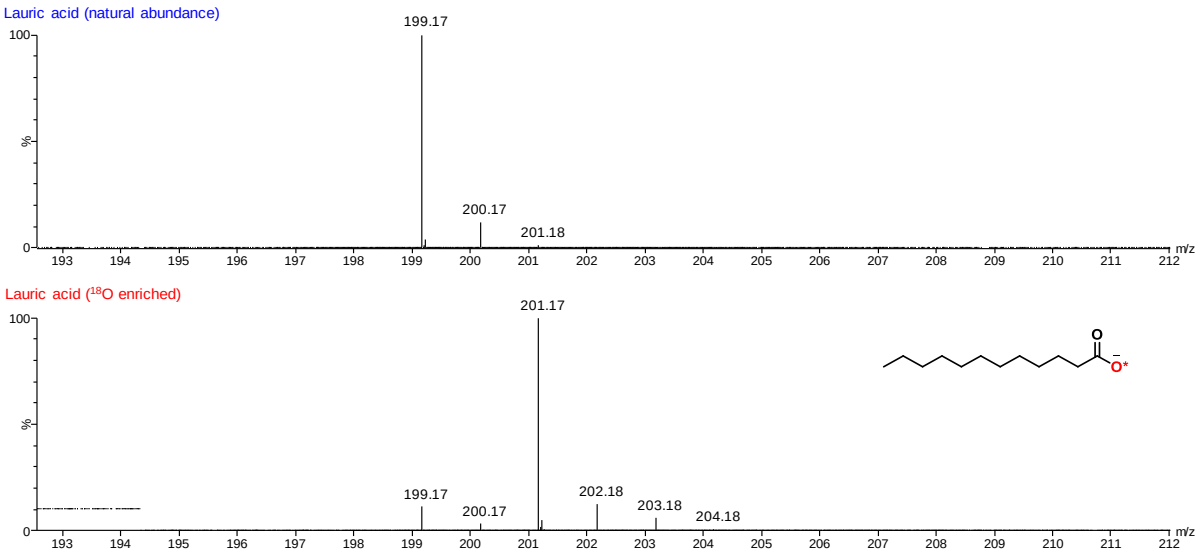

Figure II-3: ^{13}C NMR study of ^{18}O-isotope effect on the ^{13}C-carboxylic resonance in solution NMR. The non-labeled precursor is compared to the ^{18}O-enriched product, both having been mixed in different ratios, as indicated above each spectrum (DMSO-d_6, 600 MHz).

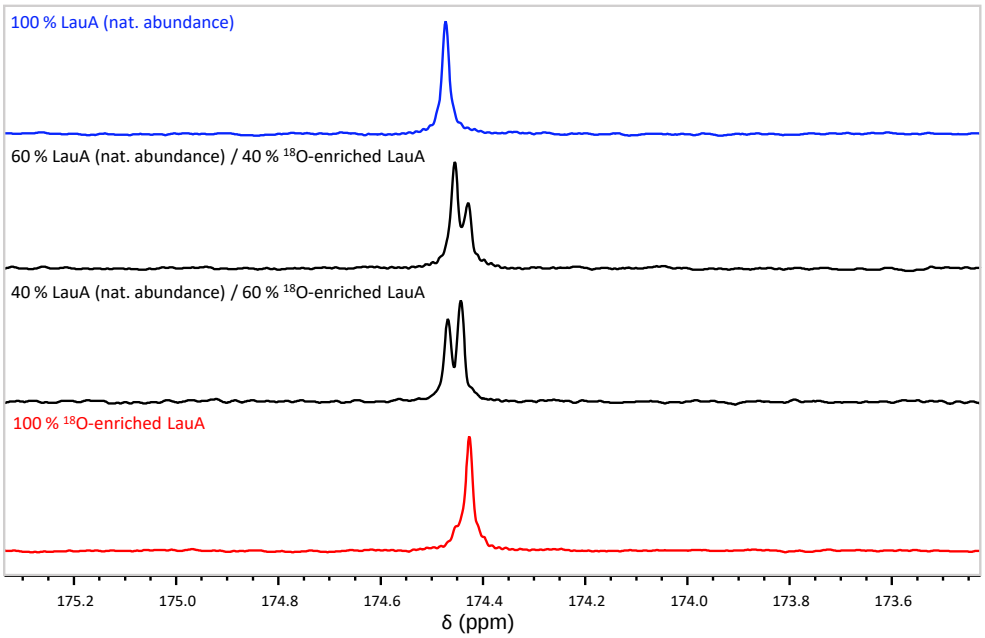

II-B1-c) Characterization of the ^{17}O-labeled LauA

Figure II-4: MS analyses of the non-labeled precursor in comparison to the ^{17}O-enriched product. Average enrichment per carboxylic oxygen determined by MS: 44 % (n = 1).

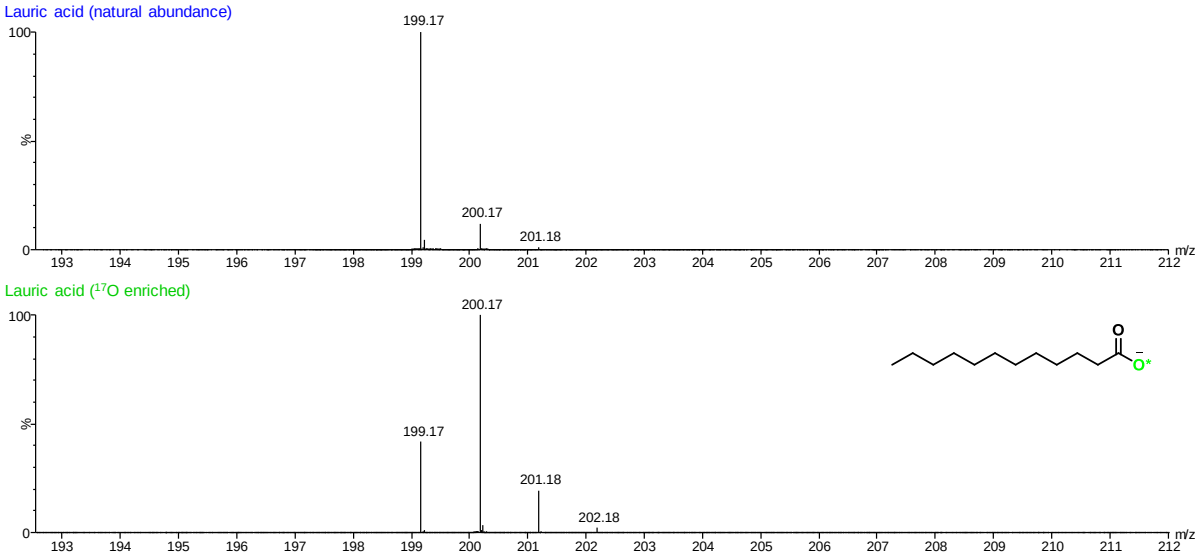

Figure II-5: ^{17}O MAS NMR spectrum of ^{17}O-labeled LauA (black) and its fit (dashed red line), considering the presence of C=O (green) and C-OH (purple) contributions.

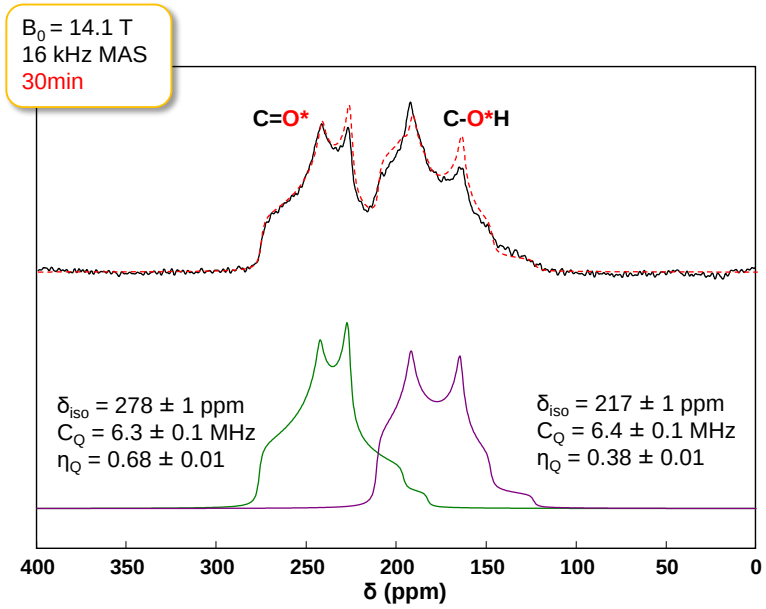

II-B2) Myristic acid (MA, $C_{14}H_{28}O_2$)

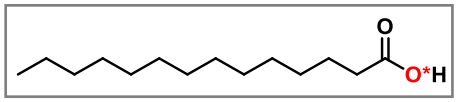

II-B2-a) Optimized labeling protocol

Myristic acid (84.2 mg, 0.37 mmol, 1.0 eq.) and CDI (65.8 mg, 0.41 mmol, 1.1 eq.) were introduced into the stainless-steel grinding jar (10 mL inner volume) containing two stainless-steel balls (10 mm diameter). The jar was closed and subjected to grinding for 30 min in the MM400 mixer mill operated at 25 Hz. ^{18}O-labeled water (97.1%, 20 µL, 1.1 mmol, 3.0 eq.) was then added into the jar, and the mixture was subjected to further grinding for 150 min at 30 Hz. To help recover the product, non-labeled water (1 mL) was added into the jar, and the content was subjected to grinding for 2 min at 25 Hz. Then, the medium ("milky" solution with a foam on top) was transferred to a beaker (together with sufficient amount of non-labeled water (10 - 12 mL) used here to rinse the jar). The medium was acidified to pH ~ 1 with an aqueous solution of HCl (6M, 10 drops) and extracted with ethyl acetate (1x 20 mL, 3x 10 mL). Combined organic phases were washed with HCl (1M, 15 mL), dried over Na_2SO_4 and filtered. Solvent was evaporated giving white solid, which was re-dissolved in diethyl ether and finally dried under vacuum to yield the product as white microcrystalline solid. Average yield (n = 3): 70 ± 4 mg, 82 ± 5 %, m. p. 53.1-55.6 °C.

For the ^{17}O-labeling, exactly the same reaction/work-up conditions as for ^{18}O-labeling were employed with 90% ^{17}O-enriched water (20 µL, 3.0 eq.) used at the hydrolysis step. Yield (n = 1): 63 mg, 75 %.

II-B2-b) Characterization of the ^{18}O-labeled MA

Figure II-6: MS analyses of the non-labeled precursor in comparison to the ^{18}O-enriched product. Average enrichment per carboxylic oxygen determined by MS: 46.4 ± 0.8 % (n = 3), enrichment yield: ~ 97 %.

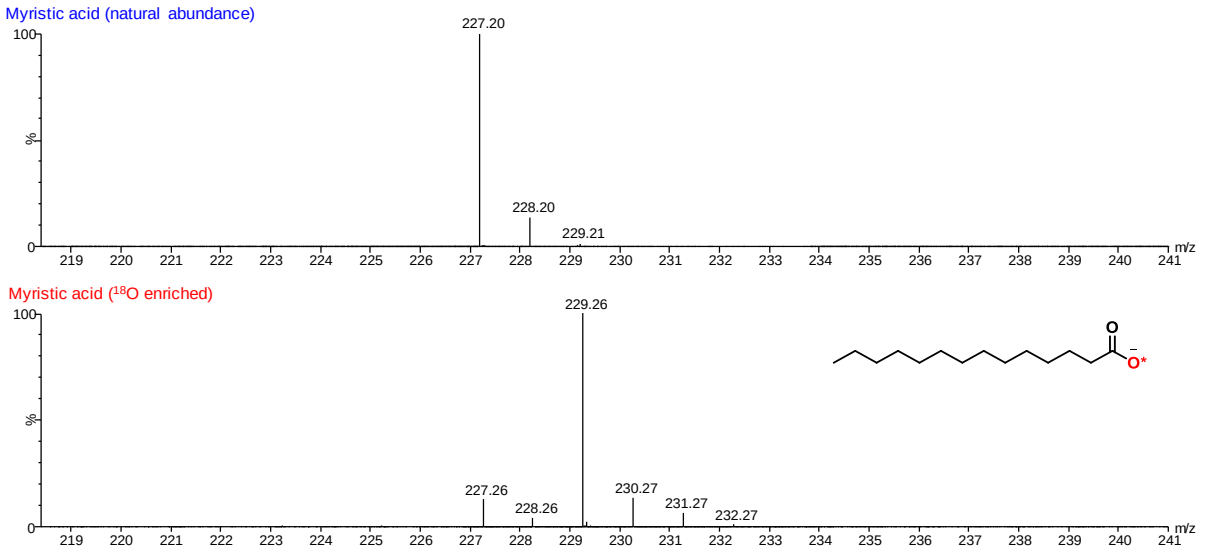

Figure II-7: ^{13}C NMR study of ^{18}O-isotope effect on the ^{13}C-carboxylic resonance in solution NMR. The non-labeled precursor is compared to the ^{18}O-enriched product, both having been mixed in different ratios, as indicated above each spectrum (DMSO-d_6, 600 MHz).

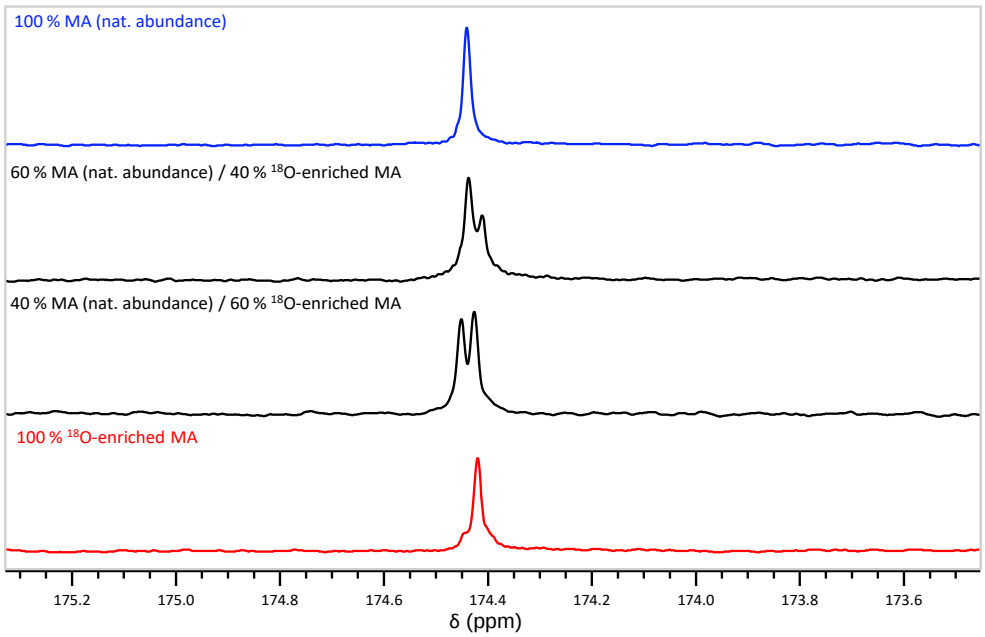

II-B2-c) Characterization of the ^{17}O-labeled MA

Figure II-8: MS analyses of the non-labeled precursor in comparison to the ^{17}O-enriched product. Average enrichment per carboxylic oxygen determined by MS: 44 % (n = 1).

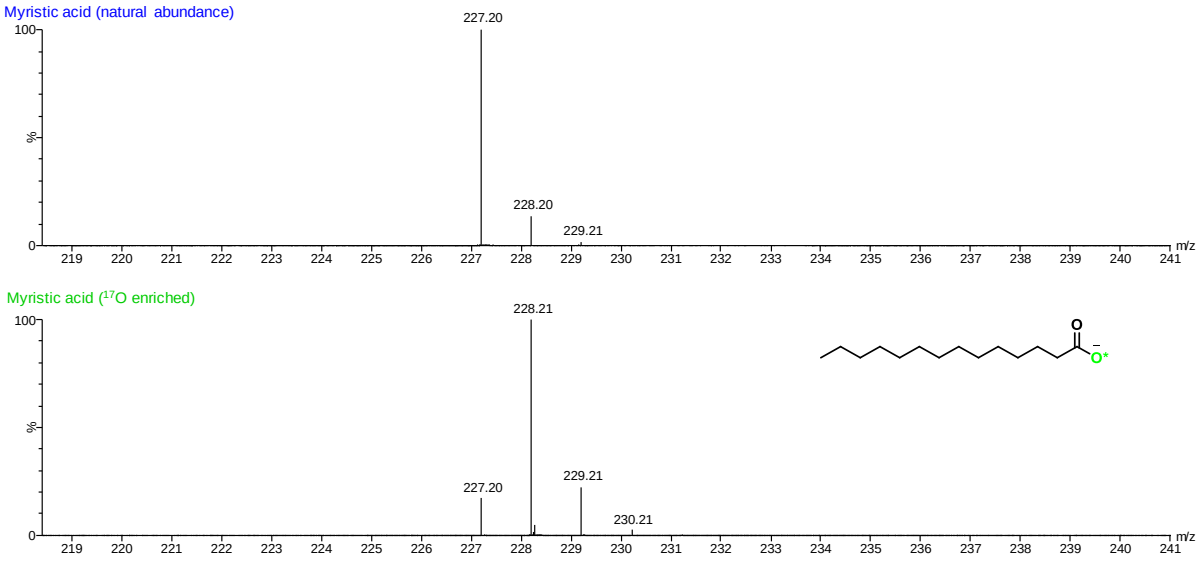

Figure II-9: ^{17}O MAS NMR spectrum of ^{17}O-labeled MA (black) and its tentative fit (dashed red line), considering the presence of C=O (green) and C-OH (purple) contributions.

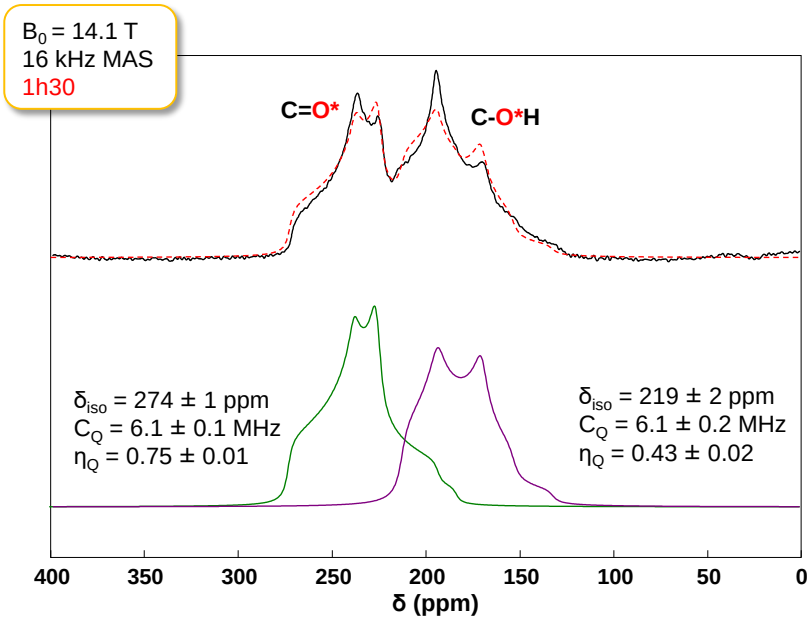

II-B3) Palmitic acid (PA, $C_{16}H_{32}O_2$)

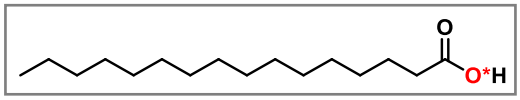

II-B3-a) Optimized labeling protocol

Palmitic acid (88.5 mg, 0.35 mmol, 1.0 eq.) and CDI (61.5 mg, 0.38 mmol, 1.1 eq.) were introduced into the stainless-steel grinding jar (10 mL inner volume) containing two stainless-steel balls (10 mm diameter). The jar was closed and subjected to grinding for 30 min in the MM400 mixer mill operated at 25 Hz. ^{18}O-labeled water (97.1%, 18.5 µL, 1.03 mmol, 3.0 eq.) was then added into the jar, and the mixture was subjected to further grinding for 180 min at 30 Hz. To help recover the product, non-labeled water (1 mL) was added into the jar, and the content was subjected to grinding for 2 min at 25 Hz. Then, the medium ("milky" solution with a foam on top) was transferred to a beaker (together with sufficient amount of non-labeled water (10-15 mL) used here to rinse the jar), poured into a separatory funnel, diluted and acidified with an aqueous solution of HCl (1M, 15 mL), and finally extracted with ethyl acetate (1x 20 mL, 2x 10 mL). Combined organic phases were dried over Na_2SO_4, filtered, and finally dried under vacuum to yield the product as white microcrystalline solid. Average yield (n = 3): 78 ± 3 mg, 88 ± 3 %, m. p. 62.0-64.5 °C.

For the ^{17}O-labeling, overall the same reaction/work-up conditions as for ^{18}O-labeling were employed with 90% ^{17}O-enriched water (18.5 µL, 3.0 eq.) used at the hydrolysis step. After addition of ^{17}O-labeled water, the mixture was subjected to grinding for 270 min at 30 Hz. Yield (n = 1): 78 mg, 87 %.

II-B3-b) Characterization of the ^{18}O-labeled PA

Figure II-10: MS analyses of the non-labeled precursor in comparison to the ^{18}O-enriched product. Average enrichment per carboxylic oxygen determined by MS: 46.9 ± 0.2 % (n = 3), enrichment yield: ~ 98 %.

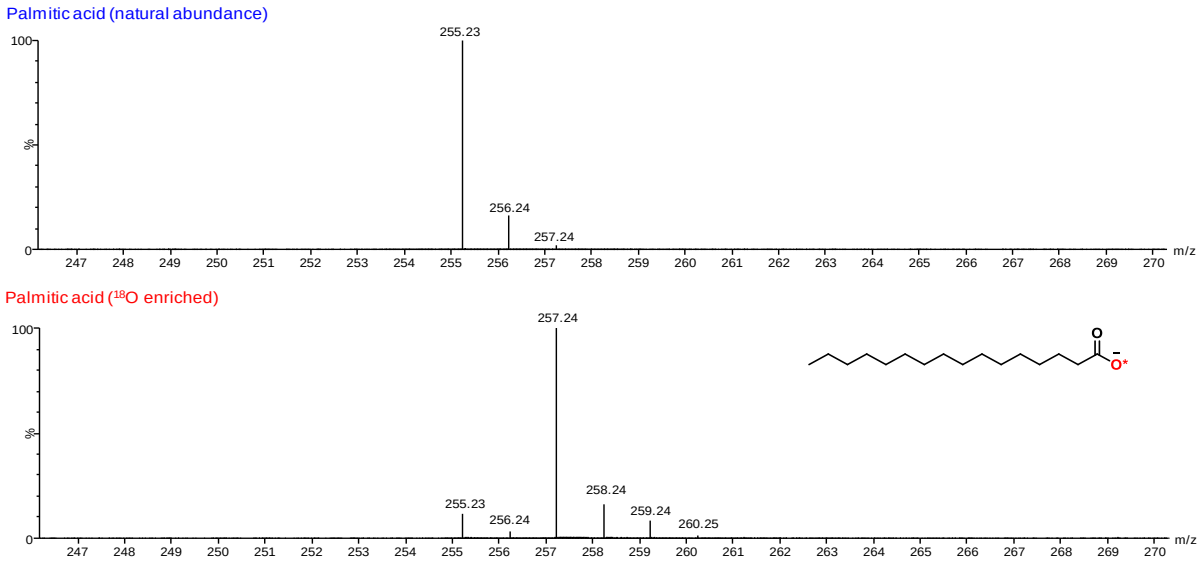

Figure II-11: ^{13}C NMR study of ^{18}O-isotope effect on the ^{13}C-carboxylic resonance in solution NMR. The non-labeled precursor is compared to the ^{18}O-enriched product, both having been mixed in different ratios, as indicated above each spectrum (DMSO-d_6, 600 MHz).

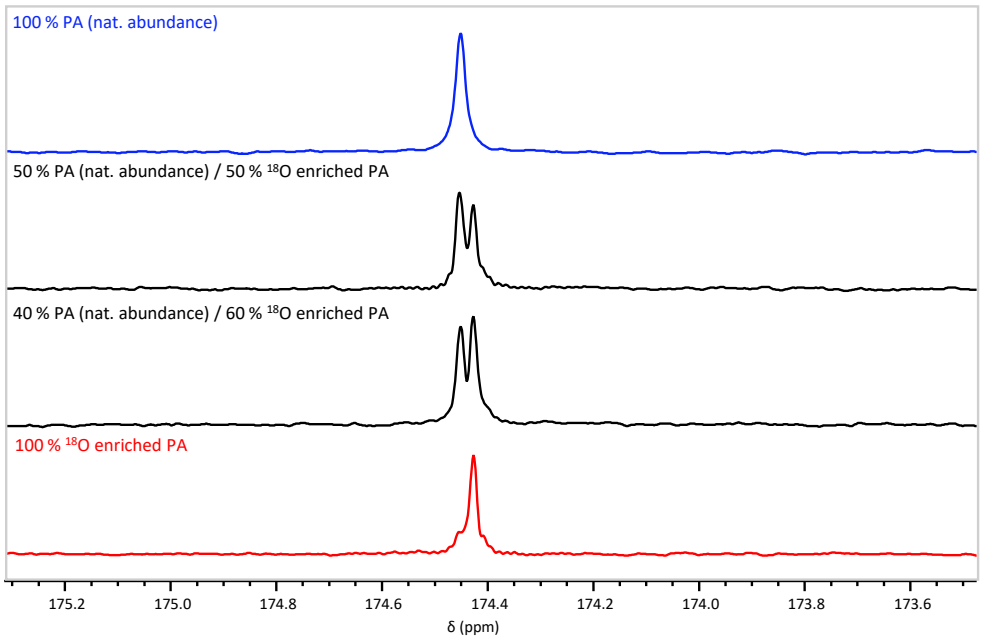

II-B3-c) Characterization of the ^{17}O-labeled PA

Figure II-12: MS analyses of the non-labeled precursor in comparison to the ^{17}O-enriched product. Average enrichment per carboxylic oxygen determined by MS: 43 % (n = 1).

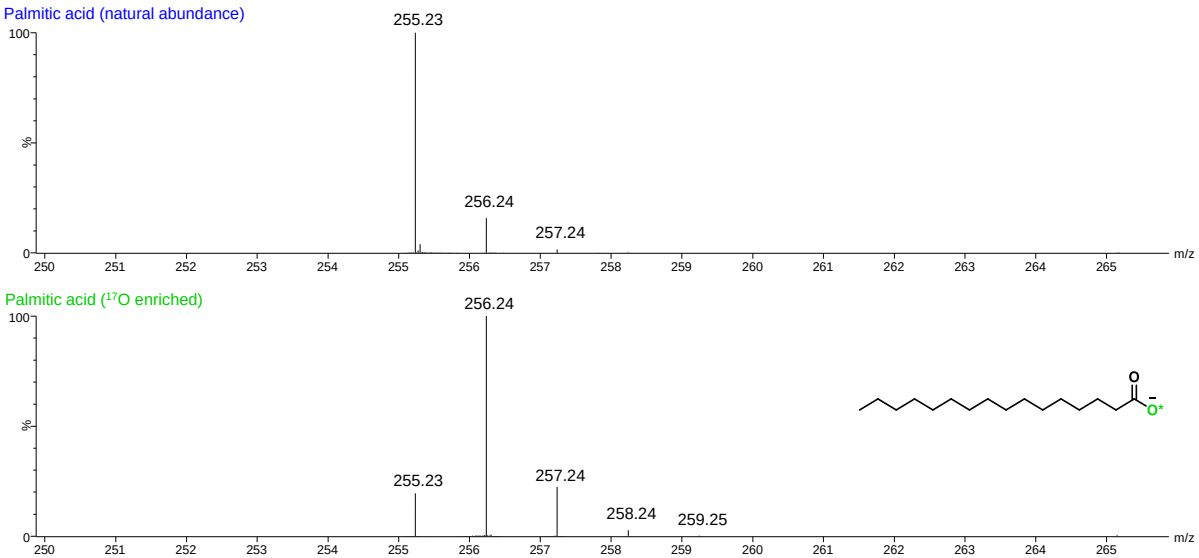

Figure II-13: ^{17}O MAS NMR spectrum of ^{17}O-labeled PA (black) and its fit (dashed red line), considering the presence of C=O (green) and C-OH (purple) contributions.

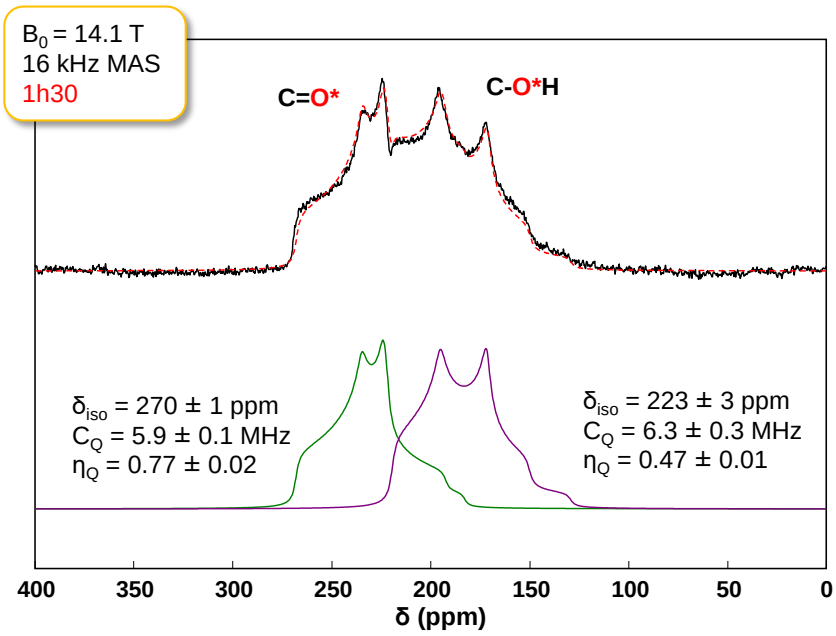

Figure II-14: SEM/EDX analyses of ^{17}O-labeled PA.

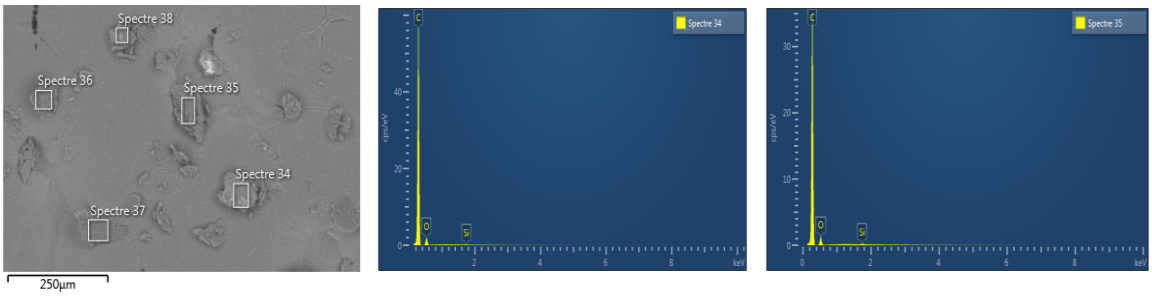

II-B4) Stearic acid (SA, $C_{18}H_{36}O_2$)

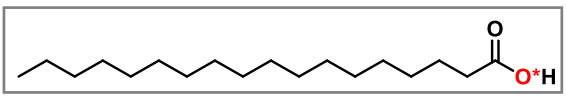

II-B4-a) Optimized labeling protocol

Stearic acid (92.2 mg, 0.32 mmol, 1.0 eq) and CDI (57.8 mg, 0.36 mmol, 1.1 eq.) were introduced into a Retsch MM400 stainless steel grinding jar (10 mL inner volume) containing two stainless steel beads (10 mm diameter). The jar was closed and subjected to grinding for 30 min in the MM400 mixer mill operated at 25 Hz. Potassium carbonate (44.8 mg, 0.32 mmol, 1.0 eq.) and ^{18}O-labeled water (97.1%, 17.5 µL, 0.97 mmol, 3.0 eq.) were then added subsequently into the jar, and the mixture was subjected to further grinding for 180 min at 30 Hz. To help recover the product, non-labeled water (1 mL) was added into the jar, and the content was subjected to grinding for 2 min at 25 Hz. Then, the suspension was transferred to a beaker (together with a sufficient amount of non-labeled water (10 mL) used here to rinse the jar). The medium was then acidified under stirring to pH ~ 1 with an aqueous solution of HCl (6M, 12 drops) and extracted with ethyl acetate (1x 20 mL, 3x 10 mL). Combined organic phases were washed with HCl (1M, 15 mL), dried over Na_2SO_4, filtered, and finally dried under vacuum. The product was collected as a white microcrystalline solid. Average yield (n = 3): 77 ± 2 mg, 83 ± 2 %.

For the ^{17}O-labeling, 90.4% ^{17}O-labeled water (17.5 µL, 3.0 eq.) was used at the hydrolysis step. Yield (n= 1): 78 mg, 85 %.

- *Scale-up procedure:*

For the scale-up, stearic acid (555 mg, 1.95 mmol, 1.0 eq.) and CDI (348,7 mg, 2.15 mmol, 1.1 eq) were introduced into a Fristch P7 stainless steel grinding jar (20 mL inner volume), and eighty stainless steel beads (5 mm diameter) were added. The jar was closed and subjected to grinding in the P7 planetary mill for two cycles of 10 min at 500 rpm, with a break of 30 min between each cycle. Anhydrous potassium carbonate (269.5 mg, 1.95 mmol, 1.0 eq.) and ^{18}O-labeled water (99.3%, 104 µL, 5.85 mmol, 3.0 eq.) were then added subsequently into the jar, and the mixture was subjected to further grinding for 60 min at 700 rpm. To help recover the product, non-labeled water (6 mL) was added into the jar, and the content was subjected to grinding for 1 min at 500 rpm. Then, the suspension was transferred to an Erlenmeyer flask, using non-labeled water and ethyl acetate to rinse the jar and lid (~ 3x 20 mL of each in total, alternating between both solvents). The medium was acidified under stirring to pH ~ 1 with an aqueous solution of HCl (6M, ~ 3.3 mL or 75 drops) and extracted with ethyl acetate (1x 40 mL, 3x 30 mL). Combined organic phases were washed with HCl (1M, 40 mL), dried over Na_2SO_4, filtered, and finally dried under vacuum to yield the product as white microcrystalline solid. Average yield (n = 3): 529 ± 7 mg, 95 ± 1 %.

Further details on the optimization of the hydrolysis step in MM400 and P7 labeling schemes are provided in section II-B4-d.

II-B4-b) Characterization of the ^{18}O-labeled SA

Figure II-15: MS analyses of the non-labeled precursor in comparison to the ^{18}O-enriched product. Average enrichment per carboxylic oxygen determined by MS: 44.1 ± 1.1 % (n = 3), enrichment yield: ~ 90 %.

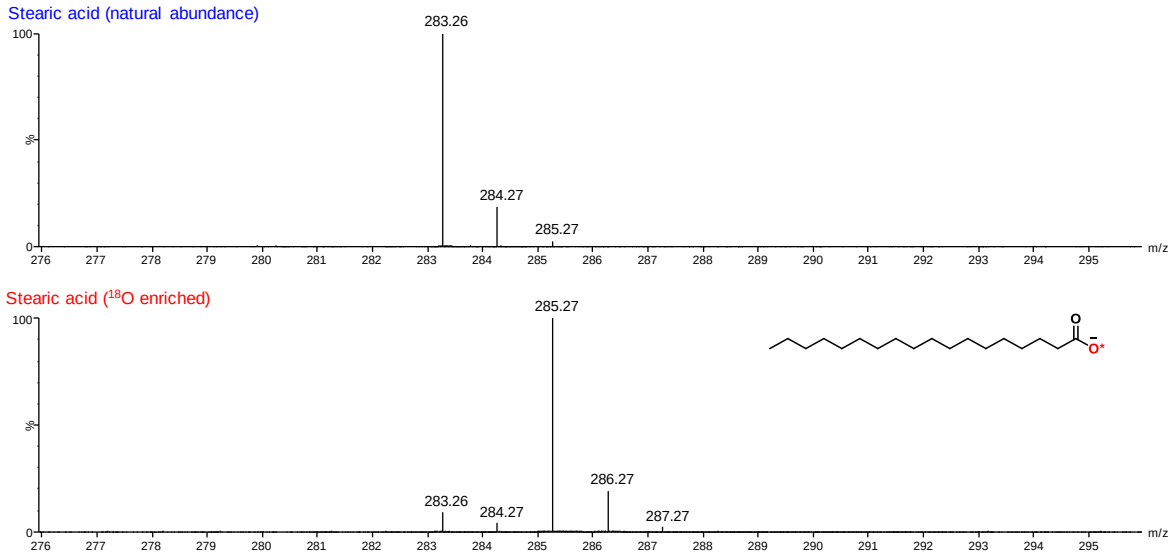

Figure II-16: ^{13}C NMR study of the ^{18}O-isotope effect on the ^{13}C-carboxylic resonance in solution NMR. The non-labeled precursor is compared to the ^{18}O-enriched product, both having been mixed in different ratios, as indicated above each spectrum (DMSO-d_6, 600 MHz).

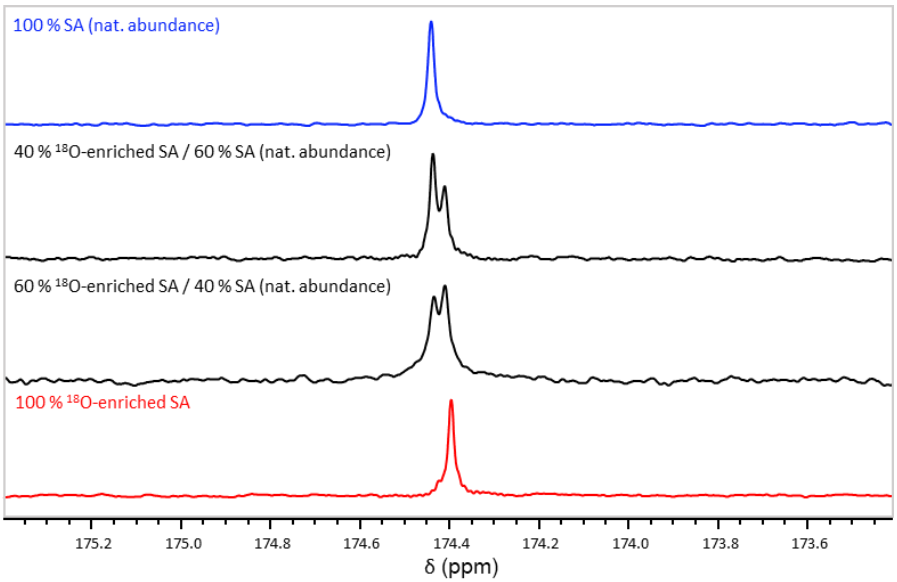

II-B4-c) Characterization of the ^{17}O-labeled SA

Figure II-17: MS analyses of the non-labeled precursor in comparison to the ^{17}O-enriched product. Average enrichment per carboxylic oxygen determined by MS: 42 % (n = 1).

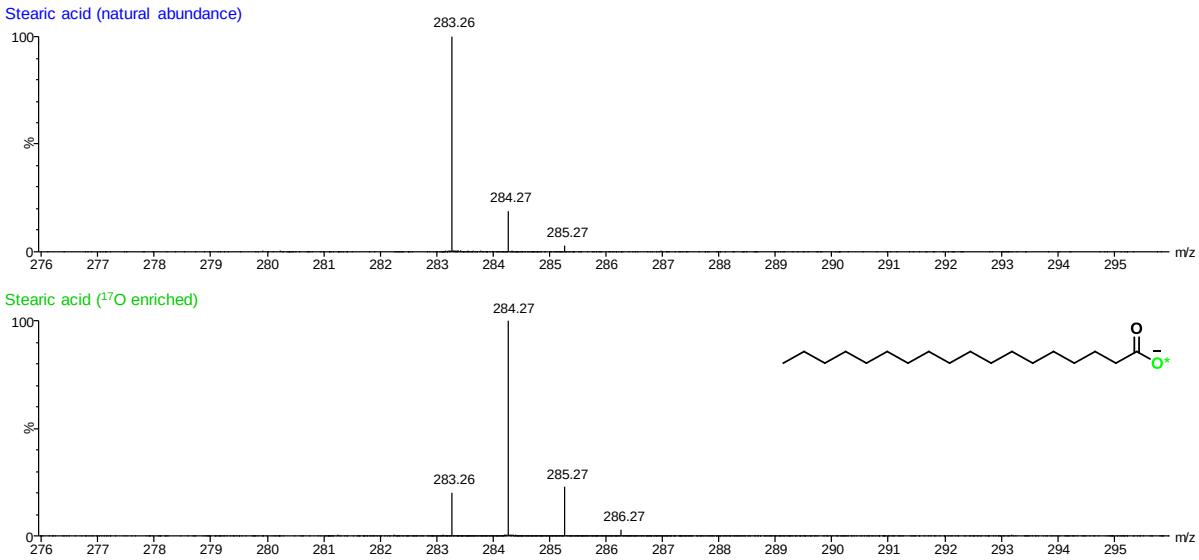

II-B4-d) Optimization of the hydrolysis conditions for the labeling of SA

The optimisation of the scale-up procedure for the labeling of SA was performed by Sébastien Mittelette.

Table II-2: Optimization of the hydrolysis step for the small-scale synthesis of enriched SA (MM400 ball-mill; 10 mL inner-volume jar containing two 10 mm diameter beads; stainless steel).

Test	$n_{(eq)}$ (H_2*O)	$n_{(eq)}$ (K_2CO_3)	Milling time (h)	Milling frequency (Hz)	Yield (%)	Enrichment yield (%)
1	3.0	0	> 5.5 h[a]	30	N.D.[b]	N.M.[c]
2	3.0	1.0	3.0 h	30	82-84	91-94
3	2.0	1.0	3.5 h	30	82	85
4	2.0	2.0	3.0 h	30	81	N.M.[c]

[a] Hydrolysis incomplete after 5.5 h
[b] N.D. = Not Determined
[c] N.M. = Not measured because non-enriched water was used in this test.

In absence of K_2CO_3 base (test #1), the hydrolysis time exceeded 5.5 h, despite the use of 3 equivalents of H_2*O in the hydrolysis step. By adding 1 equivalent of K_2CO_3 during the hydrolysis step (test #2), the milling time could be reduced to only 3 hours, and the enriched molecule was isolated with good synthetic and enrichment yields. When trying to further reduce the number of equivalents of H_2*O in presence of 1 equivalent of K_2CO_3 (test #3), the milling time had to be re-increased to 3.5 h, and the overall enrichment yield of the isolated product was lower. Addition of a second equivalent of base only slightly reduced the milling time (test #4).

Overall, the optimal milling conditions which were chosen, allowing the best enrichment and synthetic yields to be reached in minimal time, are those of test #2. These conditions were found to be reproducible.

Table II-3: Optimization of the milling conditions during the hydrolysis step in larger-scale syntheses of enriched SA (P7 planetary mill; 20 mL inner-volume jar containing 5 mm diameter beads; stainless steel). Tests #1-5 (grey lines) correspond to syntheses performed starting from ~ 310 mg of stearic acid reagent. Test #6 (blue line) corresponds to tests performed starting from ~ 555 mg of stearic acid reagent.

Test	Rotation speed (rpm)	Number of milling beads	Effective milling time (h)	Hydrolysis step (estimated by IR)	Medium homogeneity (estimated by IR)	Yield (%)	Enrichment yield (%)
1	500	80	2 h[a]	incomplete	homogeneous	96[c]	67
2	500	80	3 h[b]	incomplete	homogeneous	95[c]	84
3	800	80	1 h	incomplete	heterogeneous	N.D.[d]	N.M.[e]
4	**700**	**80**	**1 h**	**complete**	**homogeneous**	**95± 3[f]**	**88± 3[f]**
5	800	50	1 h	incomplete	heterogeneous	89	77
6	**700**	**80**	**1 h**	**complete**	**homogeneous**	**95 ± 1[f]**	**92 ± 2[f]**

[a] Four cycles of 15 min, with a 30 min break between each cycle), followed by 1 cycle of 60 min.
[b] Three cycles of 60 min, with a 30 min break between each cycle.
[c] Traces of imidazolium in the product.
[d] N.D. = Not determined.
[e] N.M. = Not measured (non-enriched water was used).
[f] Average value over 3 independent experiments (n = 3).

Larger-scale experiments were all performed using the optimal relative stoichiometries between reagents established in the MM400 (Table II-2, test #2). As reported in Table II-3, using the planetary mill, the milling conditions of the hydrolysis step also required optimization. Tests were first performed on an intermediate scale (~ 310 mg of stearic acid reagent, tests #1 to 5), before switching to larger quantities (~ 555 mg of stearic acid reagent, test #6). At 500 rpm, the hydrolysis was found to be incomplete, even after 3 hours of milling (Table II-3, tests #1 and 2). Using a higher rotation speed of 800 rpm (test #3), although a higher hydrolysis rate was globally achieved, the mixing of reagents was found to be heterogeneous, based on IR analyses. This could be explained by a "rolling effect" occurring during the milling, as can be seen in Figure II-18a. In order to counter this, two options were looked into: reducing the rotation speed (test #4) or the number of beads (test #5). The former solution was found to be the most efficient, as shown in Table II-3 (test #4) and Figure II-18b, and was used in subsequent scale-up labeling tests for stearic acid. Indeed, using the same conditions, it was possible to reproducibly perform the labeling starting from 555 mg of stearic acid, as shown in Table II-3 (test #6) and Figure II-18c.

It is worth noting that experiments were performed here using only one of the two P7 reactors. Had both reactors been used, it would have been possible to double the amount of enriched stearic acid produced (and hence obtain ~ 1 g of enriched product).

Figure II-18: Photo of the reaction mixture at the end of the hydrolysis step **a)** at 800 rpm (Table II-3, test #3, ~ 310 mg of stearic acid reagent); **b)** at 700 rpm (Table II-3, test #4, ~ 310 mg of stearic acid reagent); and **c)** at 700 rpm (Table II-3, test #6, ~ 555 mg of stearic acid reagent).

a)

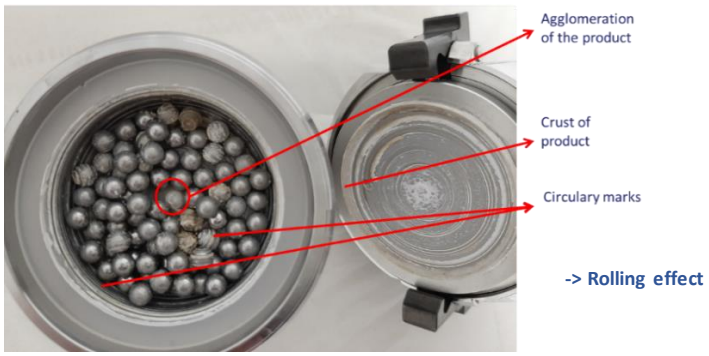

b)

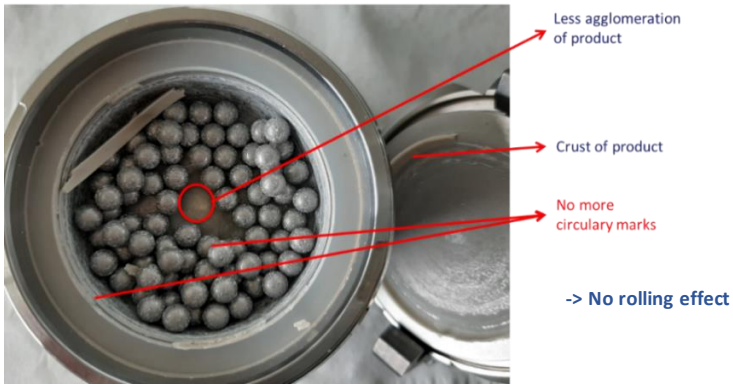

c)

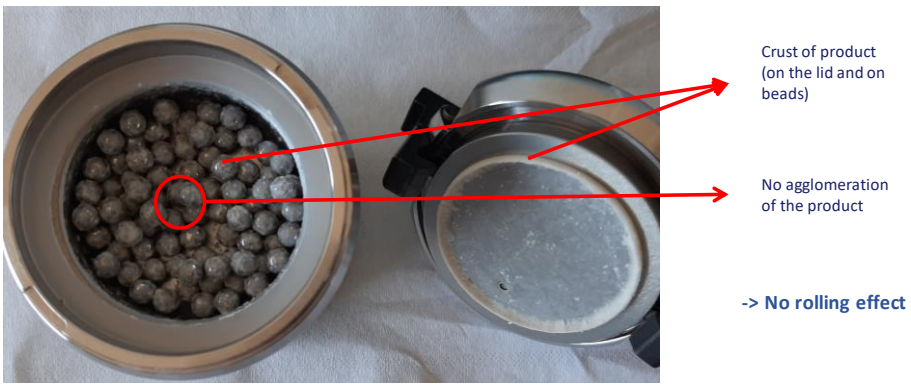

II-B5) ^{13}C-Stearic acid (^{13}C-SA, $C_{18}H_{36}O_2$)

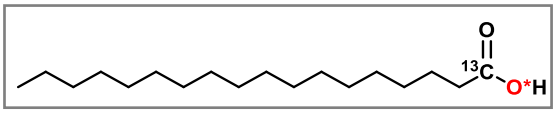

II-B5-a) Optimized labeling protocol

^{13}C-Stearic acid (92.3 mg, 0.32 mmol, 1.0 eq.) and CDI (57.7 mg, 0.36 mmol, 1.1 eq.) were introduced into a stainless-steel grinding jar (10 mL inner volume) containing two stainless steel beads (10 mm diameter). The jar was closed and subjected to grinding for 30 min in the MM400 mixer mill operated at 25 Hz. Anhydrous potassium carbonate (44.7 mg, 0.32 mmol, 1.0 eq.) and ^{18}O-labeled water (97.1%, 17.5 µL, 0.97 mmol, 3.0 eq.) were then added subsequently into the jar, and the mixture was subjected to further grinding for 180 min at 30 Hz. To help recover the product, non-labeled water (1 mL) was added into the jar, and the content was subjected to grinding for 2 min at 25 Hz. Then, the suspension was transferred to a beaker (together with a sufficient amount of non-labeled water (15 mL) used here to rinse the jar). The medium was acidified to pH ~ 1 with an aqueous solution of HCl (6M, 12 drops) and extracted with ethyl acetate (1x 20 mL, 3x 10 mL). Combined organic phases were washed with HCl (1M, 15 mL), dried over Na_2SO_4, filtered, and finally dried under vacuum to yield the product as white microcrystalline solid. Yield (n = 1): 81 mg, 89 %.

For the ^{17}O-labeling, 90.4% water (17.5 µL, 3.0 eq.) was used at the hydrolysis step. Average yield (n = 3): 86 ± 4 mg, 92 ± 2 %.

II-*B5-b) Characterization of the ^{18}O-labeled ^{13}C-SA*

Figure II-19: MS analyses of the non-labeled precursor in comparison to the ^{18}O-enriched product. Average enrichment per carboxylic oxygen determined by MS: 44.2 ± 0.3 % (n = 1), enrichment yield: ~ 91 %.

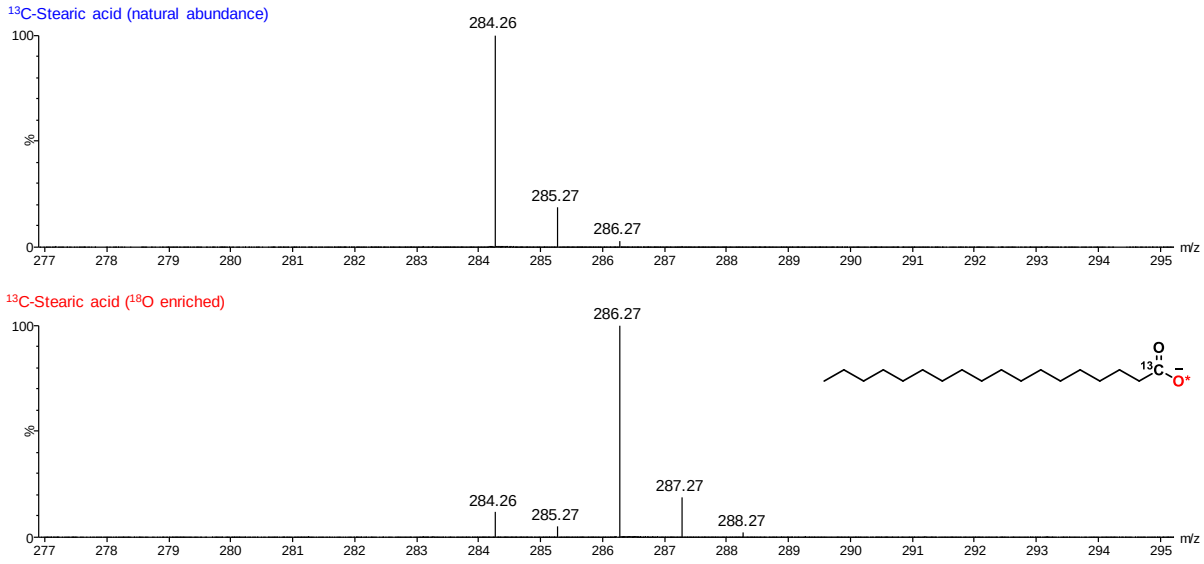

II-B5-c) Characterization of the ^{17}O-labeled ^{13}C-SA

Figure II-20: MS analyses of the non-labeled precursor in comparison to the ^{17}O-enriched product. Average enrichment per carboxylic oxygen determined by MS: 42.9 ± 1.2 % (n = 3), enrichment yield: ~ 94 %.

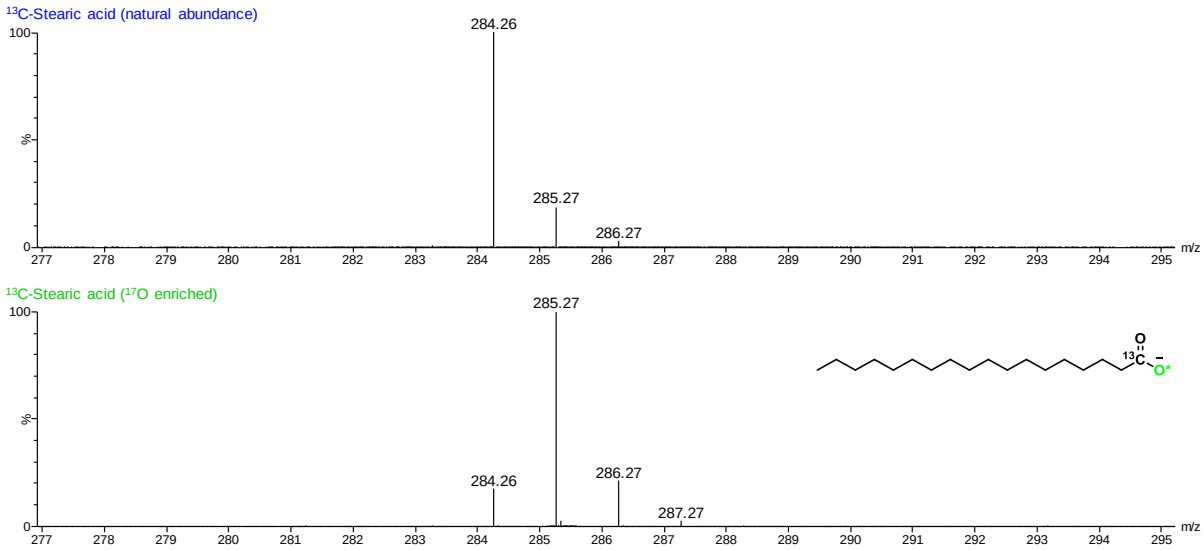

Figure II-21: ^{17}O MAS NMR spectrum of ^{17}O- and ^{13}C-labeled SA (black) and its fit (dashed red line), considering the presence of C=O (green) and C-OH (purple) contributions.

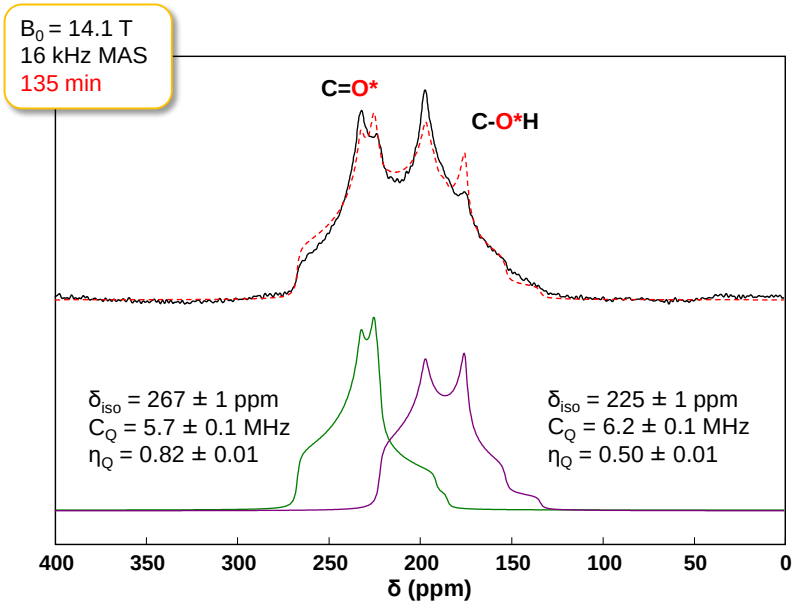

II-B6) Oleic acid (OA, $C_{18}H_{34}O_2$)

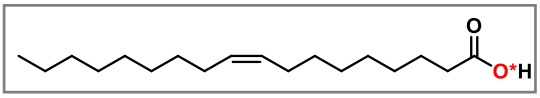

II-B6-a) Optimized labeling protocol

Oleic acid (92 mg, 0.33 mmol, 1.0 eq.) and CDI (58 mg, 0.36 mmol, 1.1 eq.) were introduced into the stainless-steel grinding jar (10 mL inner volume) containing two stainless steel beads (10 mm diameter). The jar was closed and subjected to grinding for 30 min in the MM400 mixer mill operated at 25 Hz. ^{18}O-labeled water (97.1%, 12 µL, 0.66 mmol, 2.0 eq.) was then added into the jar, and the mixture was subjected to further grinding for 60 min at 25 Hz. To help recover the product, non-labeled water (1 mL) was added into the jar, and the content was subjected to grinding for 2 minutes at 25 Hz. Then, the content was transferred to a beaker (together with a sufficient amount of non-labeled water (13 - 15 mL), used here to rinse the jar). The medium was acidified to pH ~ 1 with an aqueous solution of HCl (6M, 14 - 18 drops) and extracted with ethyl acetate (1x 20 mL, 2x 10 mL). Combined organic phases were dried over Na_2SO_4, filtered and finally dried under vacuum giving the product as a colourless oil. Average yield (n = 3): 84 ± 1 mg, 91 ± 2 %.

For the ^{17}O-labeling, 39.3% or 90.4% enriched water (12 µL, 2.0 eq.) was used at the hydrolysis step. Average yield (n = 2): 83 ± 1 mg, 90 ± 2 %.

- *Scale-up procedure:*

For the scale-up, a 50 mL stainless steel jar with eight stainless steel beads (10 mm diameter) was used. Oleic acid (1.2 g, 4.3 mmol, 1.0 eq.) and CDI (0.8 g, 4.7 mmol, 1.1 eq.) were introduced into the jar and reacted for 15 min in the MM400 mixer mill operated at 25 Hz. For hydrolysis, 90% $H_2{}^{17}O$ (154 µL, 8.5 mmol, 2 eq.) was added and reaction took place for 30 min at 25 Hz. To recover the product, 50 mL of non-labeled water and 5 mL of ethyl acetate were used to rinse the jar and transfer the content to a beaker. The medium was acidified to pH ~1 with an aqueous solution of HCl (6M, 2.5 mL) and extracted with ethyl acetate (4x 15 mL). Combined organic phases were dried over Na_2SO_4, filtered and finally dried under vacuum. The product was isolated as a colourless oil. Average yield (n = 2): 1.10 ± 0.02 g, 92 ± 2 %.

II-B6-b) Characterization of the ^{18}O-labeled OA

Figure II-22: MS analyses of the non-labeled precursor in comparison to the ^{18}O-enriched product. Average enrichment per carboxylic oxygen determined by MS: 43.8 ± 1.5 % (n = 3), enrichment yield: ~ 90 %.

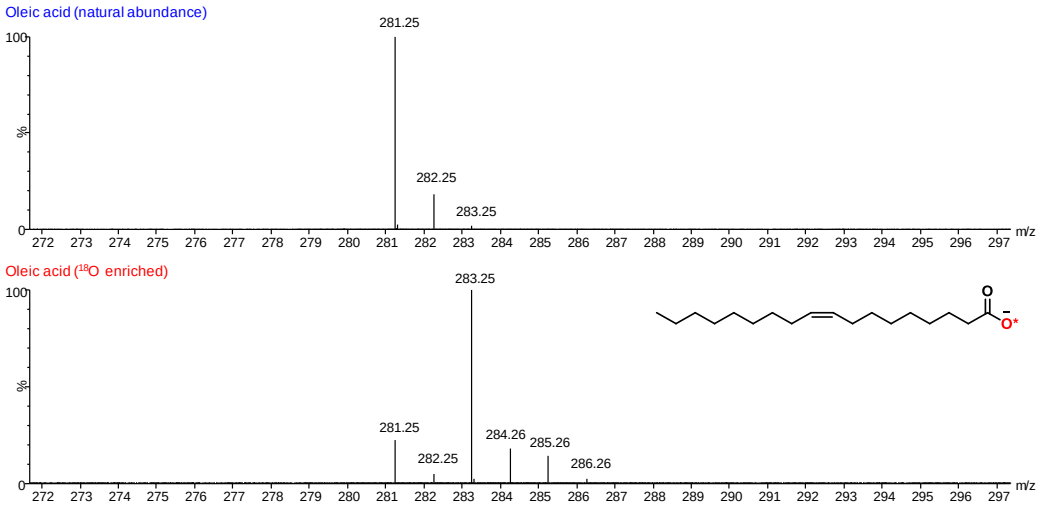

Figure II-23: ^{13}C NMR study of the ^{18}O-isotope effect on the ^{13}C-carboxylic resonance in solution NMR. The non-labeled precursor is compared to the ^{18}O-enriched product, both having been mixed in different ratios, as indicated above each spectrum (DMSO-d_6, 600 MHz).

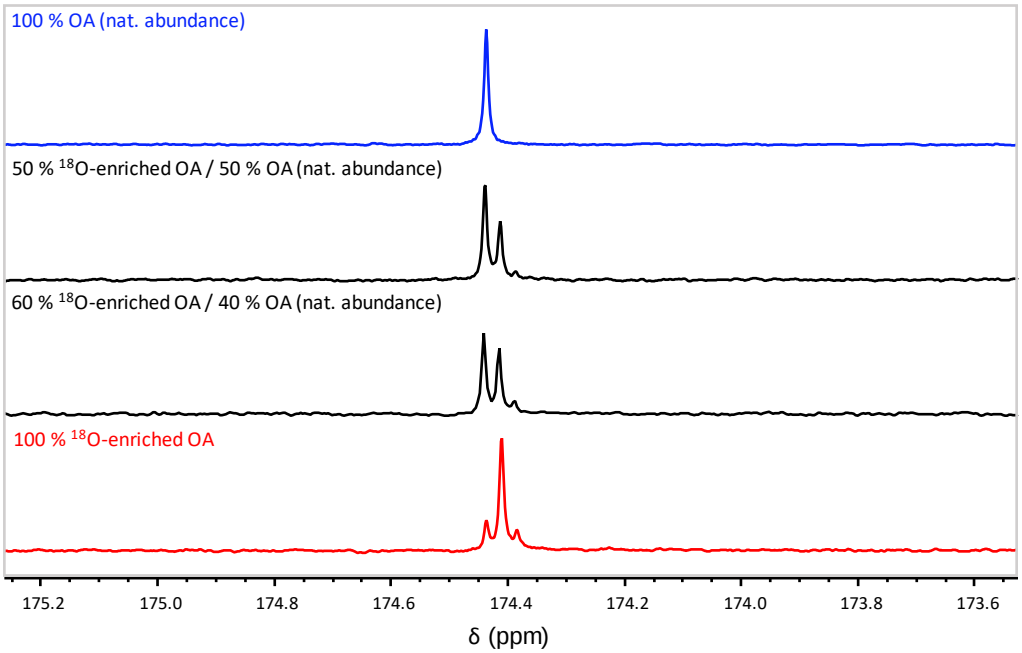

II-B6-c) Characterization of the ^{17}O-labeled OA

Figure II-24: MS analyses of the non-labeled precursor in comparison to the ^{17}O-enriched product (scale-up synthesis). Average enrichment per carboxylic oxygen determined by MS: 42 % (n = 1).

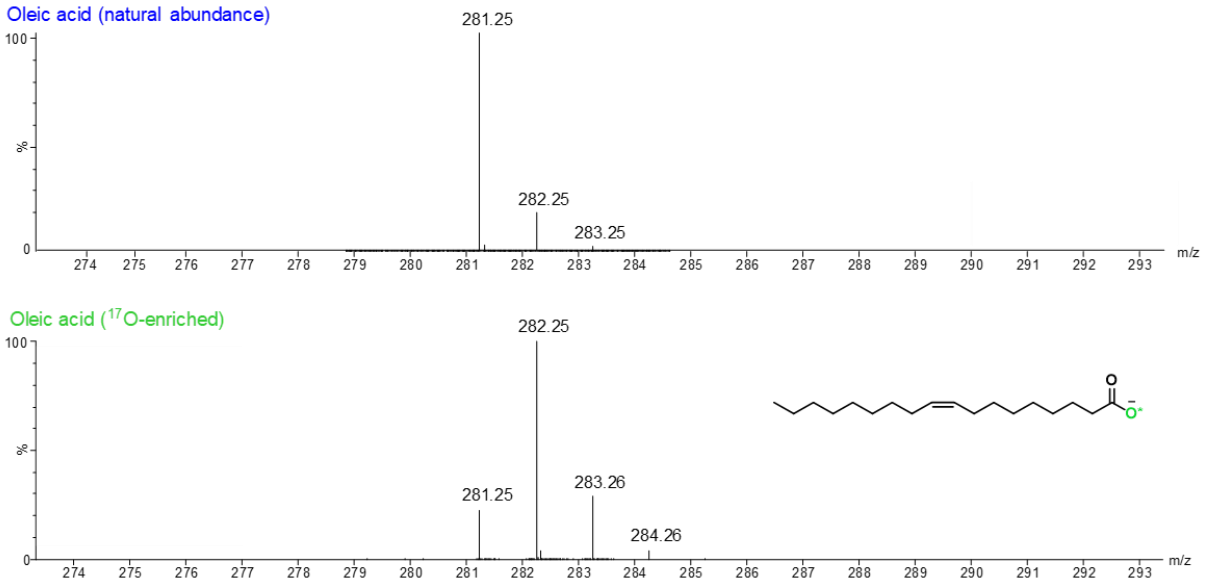

II-B7) Linoleic acid (LA, $C_{18}H_{32}O_2$)

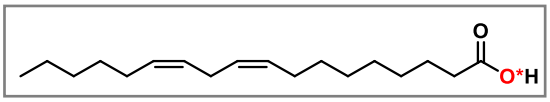

II-B7-a) Optimized labeling protocol

Linoleic acid (46 mg, 0.16 mmol, 1.0 eq.) and CDI (29 mg, 0.18 mmol, 1.1 eq.) were introduced into the PTFE grinding jar (5 mL inner volume) containing one PTFE ball (10 mm diameter). The jar was closed and subjected to grinding for 20 min in the P23 ball-mill operated at 25 Hz. ^{18}O-labeled water (97.1%, 6 µL, 0.33 mmol, 2.0 eq.) was then added into the jar, and the mixture was subjected to further grinding for 3x30 min at 25 Hz. In order to enable complete hydrolysis, the jar was opened after each 30 min of grinding and material stuck at the inner edge was scratched into the jar. To help recover the product, non-labeled water (1 mL) was added into the jar, and the content was subjected to grinding for 1 min at 25 Hz. Then, the colorless emulsion was transferred to a beaker (together with sufficient amount of non-labeled water (6 - 8 mL) used here to rinse the jar). The medium was acidified to pH ~ 1 with an aqueous solution of HCl (6M, 9 - 10 drops) and extracted with ethyl acetate (1x 10 mL, 3x 6 mL). Combined organic phases were dried over Na_2SO_4, filtered and finally dried under vacuum giving the product as a colorless oil. Average yield (n = 2): 42 ± 1 mg, 90 ± 3 %.

For the ^{17}O-labeling, exactly the same reaction/work-up conditions as for ^{18}O-labeling were employed with 90% ^{17}O-enriched water (6 µL, 2.0 eq.) used at the hydrolysis step. Yield (n = 1): 41 mg, 90 %.

II-B7-b) Characterization of the ^{18}O-labeled LA

Figure II-25: MS analyses of the non-labeled precursor in comparison to the ^{18}O-enriched product. Average enrichment per carboxylic oxygen determined by MS: 41.3 ± 0.4 % (n = 2), enrichment yield: ~ 82 %.

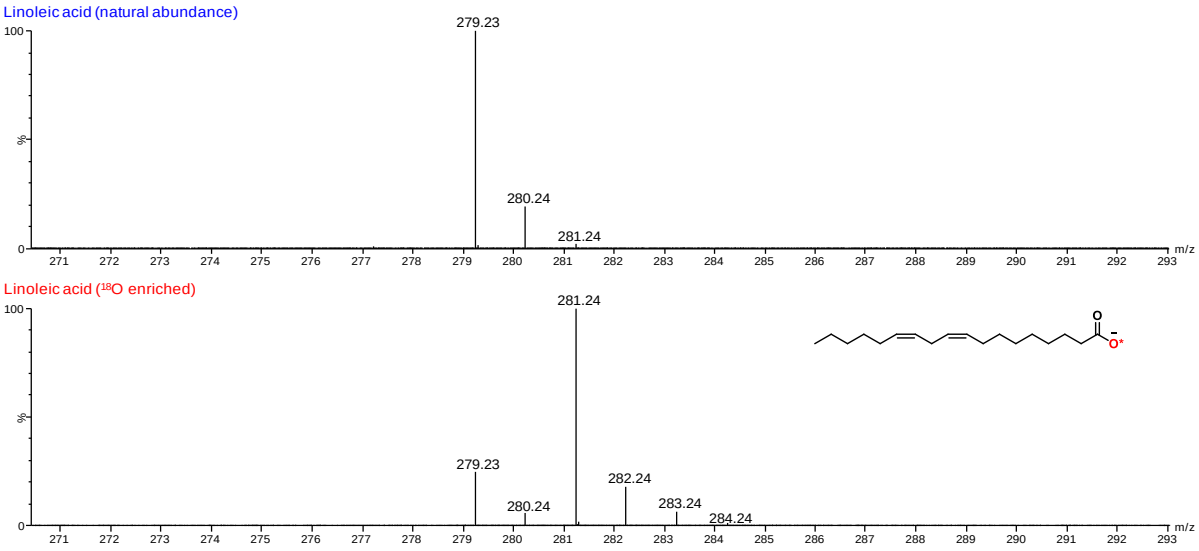

Figure II-26: ^{13}C NMR study of ^{18}O-isotope effect on the ^{13}C-carboxylic resonance in solution NMR. The non-labeled precursor is compared to the ^{18}O-enriched product, both having been mixed in different ratios, as indicated above each spectrum (DMSO-d_6, 600 MHz).

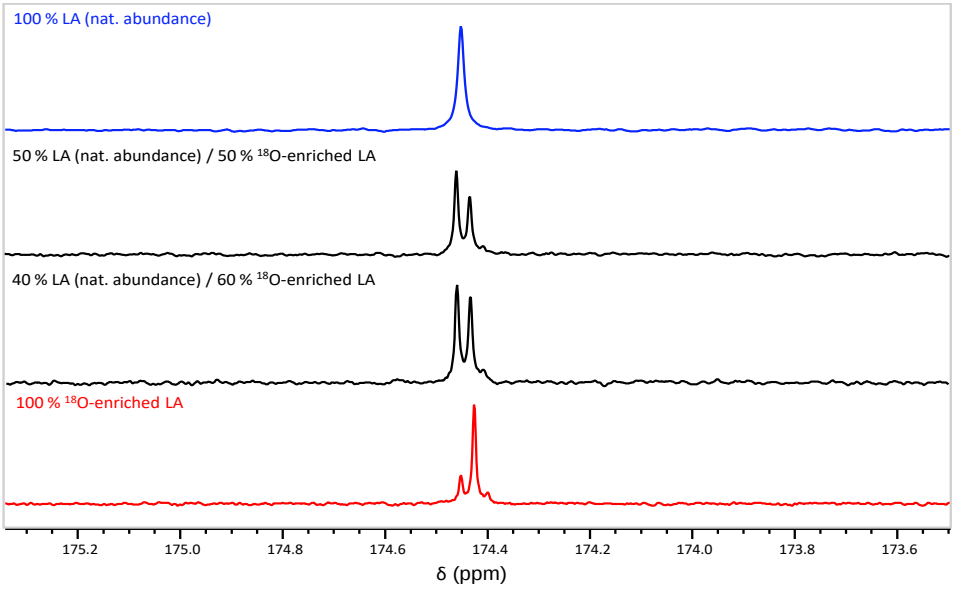

II-B7-c) Characterization of the ^{17}O-labeled LA

Figure II-27: MS analyses of the non-labeled precursor in comparison to the ^{17}O-enriched product. Average enrichment per carboxylic oxygen determined by MS: 40 % (n = 1).

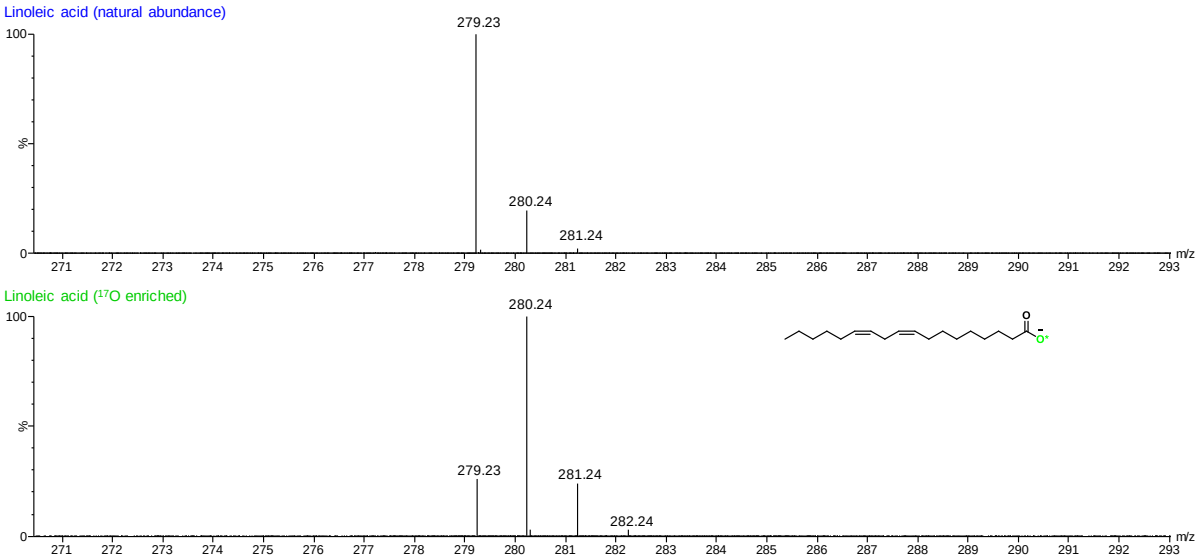

II-B8) α-Linolenic acid (ALA, $C_{18}H_{30}O_2$)

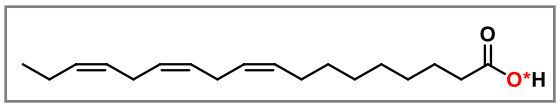

II-B8-a) Optimized labeling protocol

α-Linolenic acid (46 mg, 0.16 mmol, 1.0 eq.) and CDI (29 mg, 0.18 mmol, 1.1 eq.) were introduced into the PTFE grinding jar (5 mL inner volume) containing one PTFE ball (10 mm diameter). The jar was closed and subjected to grinding for 20 min in the P23 ball-mill operated at 25 Hz. ^{18}O-labeled water (97.1%, 6 µL, 0.33 mmol, 2.0 eq.) was then added into the jar, and the mixture was subjected to further grinding for 3x30 min at 25 Hz. In order to enable complete hydrolysis, the jar was opened after each 30 min of grinding and material stuck at the inner edge was scratched into the jar). To help recover the product, non-labeled water (1 mL) was added into the jar, and the content was subjected to grinding for 1 min at 25 Hz. Then, the yellow emulsion was transferred to a beaker (together with sufficient amount of non-labeled water (7 - 8 mL) used here to rinse the jar). The medium was acidified to pH ~ 1 with an aqueous solution of HCl (6M, 9 - 12 drops), leading to a cloudy mixture which was extracted with ethyl acetate (1x 10 mL, 2x 6 mL). Aqueous phase was diluted with brine and extracted with ethyl acetate (6 mL) one more time. Combined organic phases were dried over Na_2SO_4, filtered and finally dried under vacuum giving the product as a yellow oil. Average yield (n = 2): 40 ± 3 mg, 87 ± 7 %.

For the ^{17}O-labeling, exactly the same reaction/work-up conditions as for ^{18}O-labeling were employed with 90% ^{17}O-enriched water (6 µL, 2.0 eq.) used at the hydrolysis step. Yield (n = 1): 41 mg, 89 %.

II-B8-b) Characterization of the ^{18}O-labeled ALA

Figure II-28: MS analyses of the non-labeled precursor in comparison to the ^{18}O-enriched product. Average enrichment per carboxylic oxygen determined by MS: 42.5 ± 0.3 % (n = 2), enrichment yield: ~ 88 %.

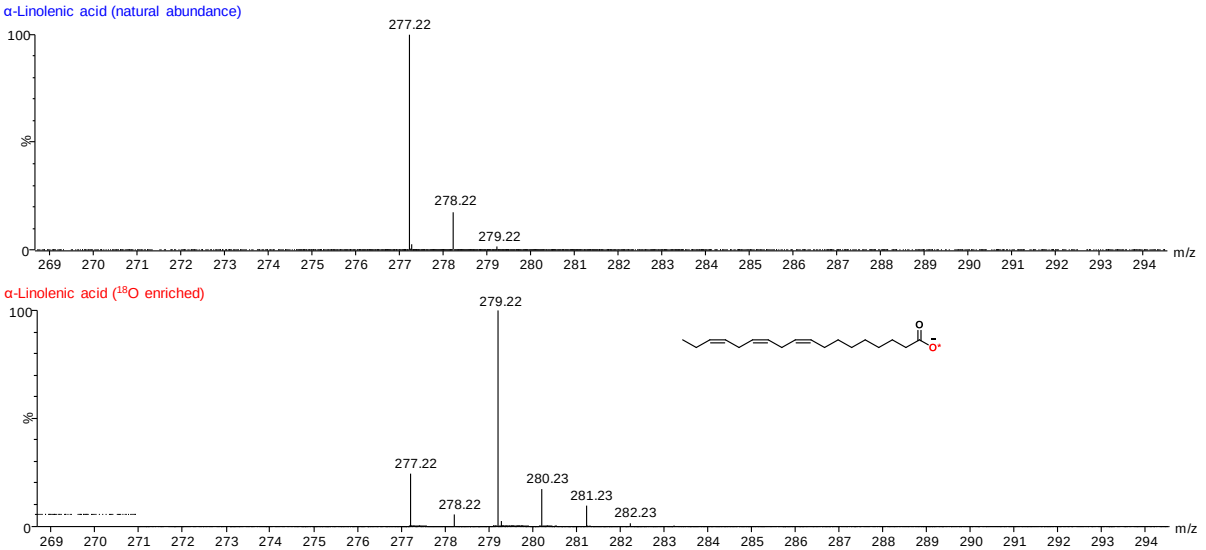

Figure II-29: ^{13}C NMR study of ^{18}O-isotope effect on the ^{13}C-carboxylic resonance in solution NMR. The non-labeled precursor is compared to the ^{18}O-enriched product, both having been mixed in different ratios, as indicated above each spectrum (DMSO-d_6, 600 MHz).

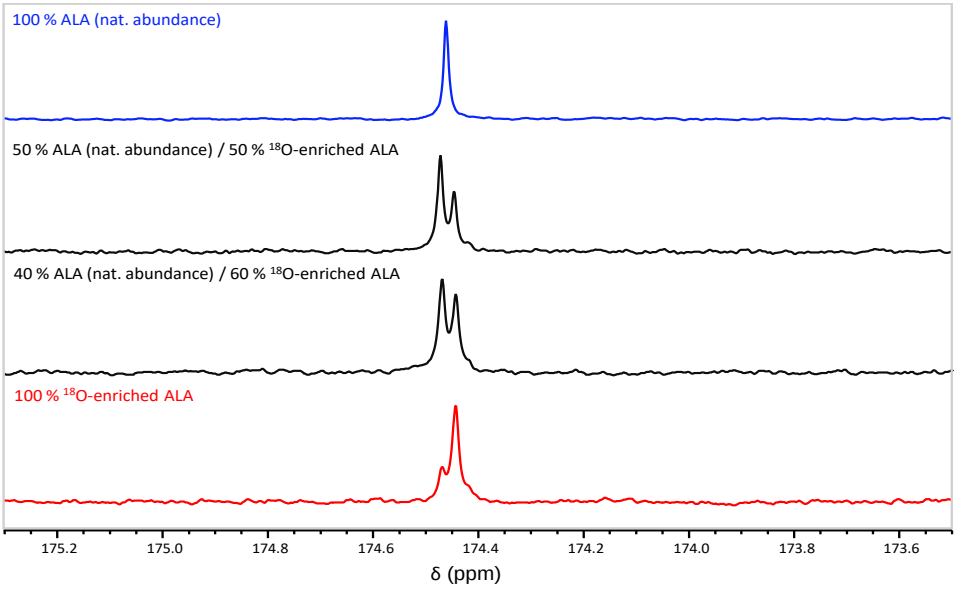

II-B8-c) Characterization of the ^{17}O-labeled ALA

Figure II-30: MS analyses of the non-labeled precursor in comparison to the ^{17}O-enriched product. Average enrichment per carboxylic oxygen determined by MS: 40 % (n = 1).

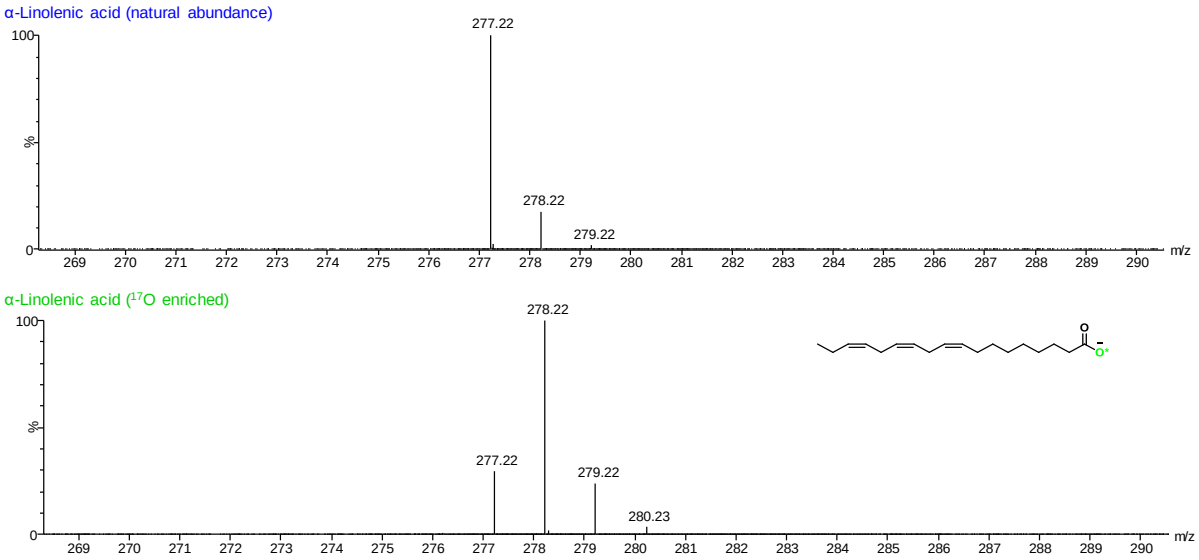

II-B9) Arachidonic acid (AA, $C_{20}H_{32}O_2$)

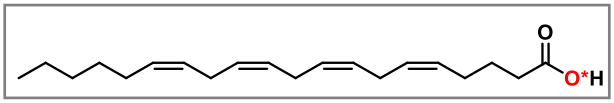

II-B9-a) Optimized labeling protocol

Arachidonic acid (47 mg, 0.15 mmol, 1.0 eq.) and CDI (28 mg, 0.17 mmol, 1.1 eq.) were introduced into the PTFE grinding jar (5 mL inner volume) containing one PTFE ball (10 mm diameter). The jar was closed and subjected to grinding for 20 min in the P23 ball-mill operated at 25 Hz. ^{18}O-labeled water (97.1%, 5.75 µL, 0.32 mmol, 2.0 eq.) was then added into the jar, and the mixture was subjected to further grinding for 3x30 min at 25 Hz. In order to enable complete hydrolysis, the jar was opened after each 30 min of grinding and material stuck at the inner edge was scratched into the reactor). To help recover the product, non-labeled water (1 mL) was added into the jar, and the content was subjected to grinding for 1 min at 25 Hz. Then, the yellow emulsion was transferred to a beaker (together with sufficient amount of non-labeled water (6 - 7 mL) used here to rinse the jar). The medium was acidified to pH ~ 1 with an aqueous solution of HCl (6M, 7 - 9 drops), leading to a cloudy mixture, which was diluted with brine (10 mL) and then extracted with ethyl acetate (1x 10 mL, 3x 6 mL). Combined organic phases were dried over Na_2SO_4, filtered and finally dried under vacuum giving the product as a yellow oil. Average yield (n = 3): 44 ± 1 mg, 90 ± 2 %.

For the ^{17}O-labeling, exactly the same reaction/work-up conditions as for ^{18}O-labeling were employed with 90% ^{17}O-enriched water (5.75 µL, 2.0 eq.) used at the hydrolysis step. Yield (n = 1): 42 mg, 88 %.

II-B9-b) Characterization of the ^{18}O-labeled AA

Figure II-31: MS analyses of the non-labeled precursor in comparison to the ^{18}O-enriched product. Average enrichment per carboxylic oxygen determined by MS: 38.8 ± 1.5 % (n = 3), enrichment yield: ~ 84 %.

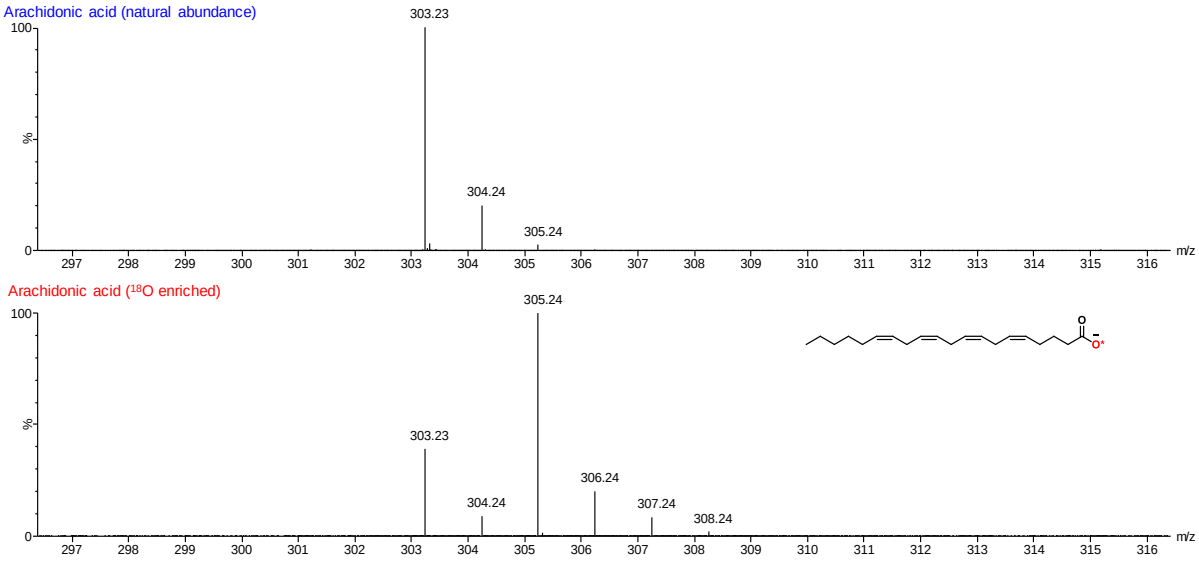

Figure II-32: ^{13}C NMR study of ^{18}O-isotope effect on the ^{13}C-carboxylic resonance in solution NMR. The non-labeled precursor is compared to the ^{18}O-enriched product, both having been mixed in different ratios, as indicated above each spectrum (DMSO-d_6, 600 MHz).

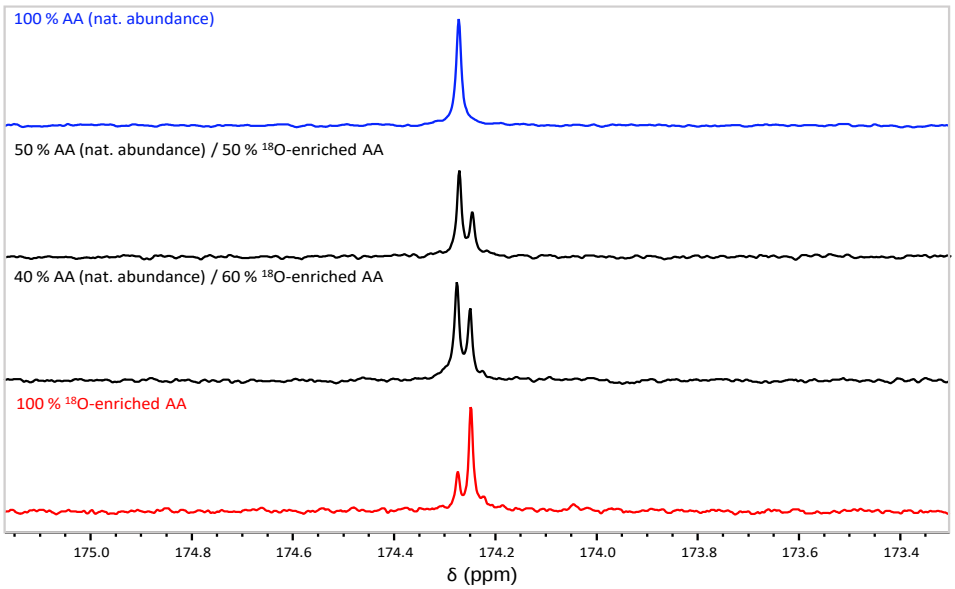

II-B9-c) Characterization of the ^{17}O-labeled AA

Figure II-33: MS analyses of the non-labeled precursor in comparison to the ^{17}O-enriched product. Average enrichment per carboxylic oxygen determined by MS: 37 % (n = 1).

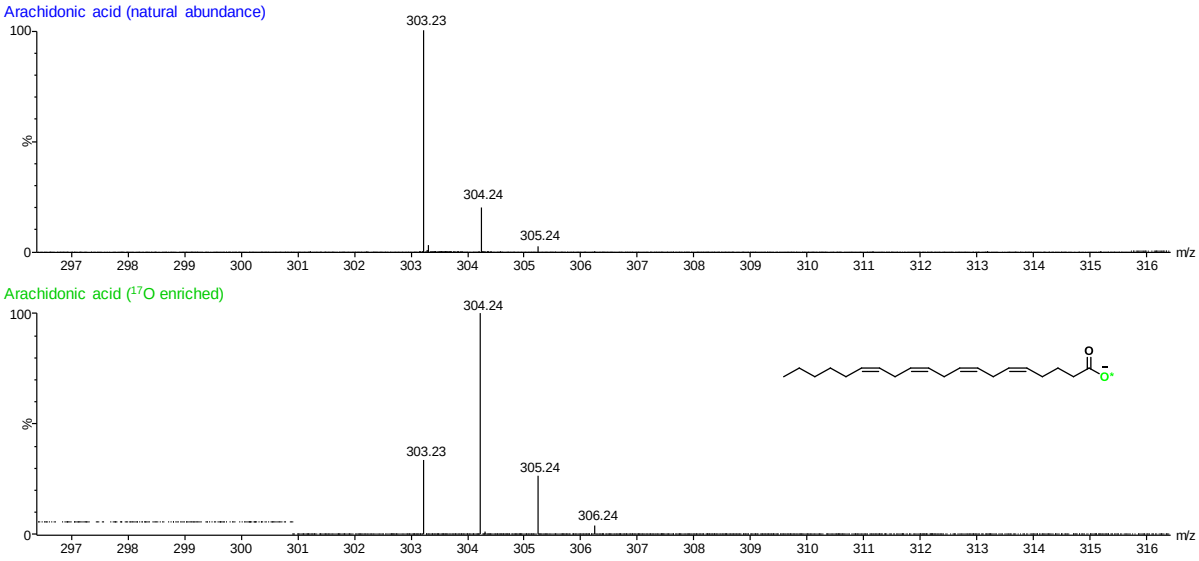

II-C) SYNTHESES AND CHARACTERIZATIONS OF $^{17}O/^{18}O$-LABELED FA PREPARED *VIA* SAPONIFICATION

II-C1) α-Linolenic acid (ALA, $C_{18}H_{30}O_2$)

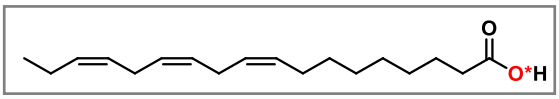

II-C1-a) Optimized labeling protocol

Ethyl linolenate (56 mg, 0.18 mmol, 1.0 eq.), ^{18}O-labeled water (97.1%, 9.5 µL, 0.52 mmol, 3.0 eq.) and sodium ethoxide (19 mg, 0.27 mmol, 1.5 eq.) were introduced successively into the stainless-steel grinding jar (5 mL inner volume) containing two stainless steel balls (7 mm diameter). The jar was closed and subjected to grinding for 30 min in the MM400 mixer mill operated at 25 Hz. To help recover the product, non-labeled water (1 mL) was added into the jar, and the content was subjected to grinding for 2 min at 25 Hz. Then, the yellow solution (with foam-like texture) was transferred to a beaker (together with sufficient amount of non-labeled water (3 - 5 mL) used here to rinse the jar). The medium was acidified to pH ~ 1 with an aqueous solution of HCl (6M, 8 - 9 drops), leading to a cloudy suspension, which was diluted with brine and extracted with ethyl acetate (1x 10 mL, 3x 6 mL). Combined organic phases were dried over Na_2SO_4, filtered and finally dried under vacuum giving the product as a yellow oil. Average yield (n = 2): 48 ± 1 mg, 96 ± 1 %.

For the ^{17}O-labeling, overall the same reaction/work-up conditions as for ^{18}O-labeling were employed with 90% ^{17}O-enriched water (9.75 µL, 3.0 eq.) used at the hydrolysis step. After addition of ^{17}O-labeled water, the mixture was subjected to grinding for 45 min at 25 Hz. Yield (n = 1): 47 mg, 95 %.

Figure II-34: ATR-IR analysis of the starting material, reaction intermediate, and final products. The dashed line shows that the C=O stretching frequency of $^{18}O/^{17}O$-enriched product is shifted to lower wavenumbers in comparison with non-labeled precursor.

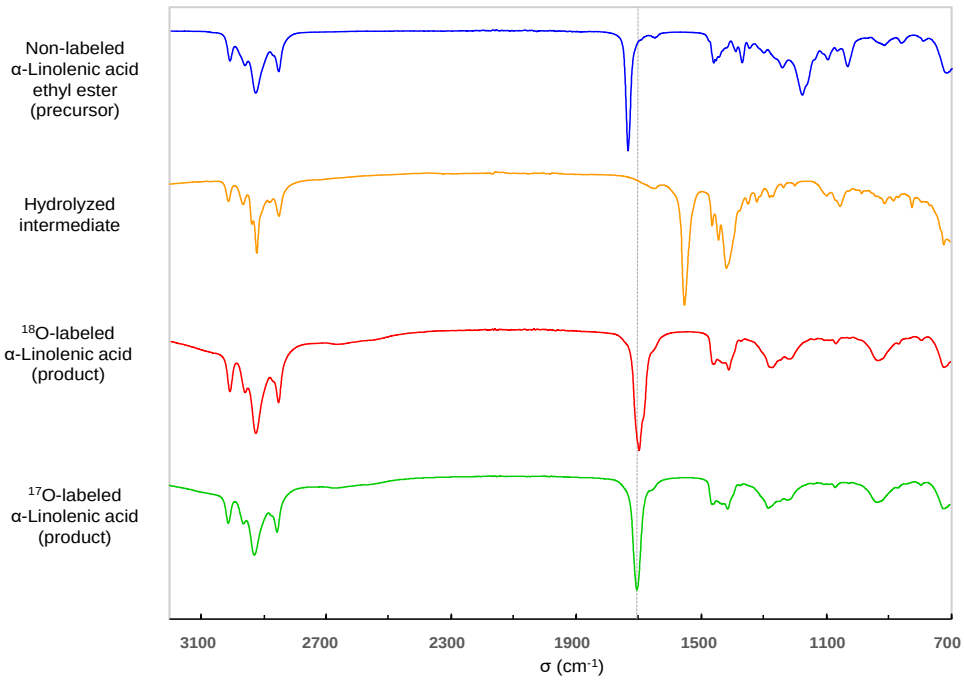

II-C1-b) Characterization of the ^{18}O-labeled ALA

Figure II-35: MS analyses of the non-labeled acid in comparison to the ^{18}O-enriched product. Average enrichment per carboxylic oxygen determined by MS: 44.5 ± 1.0 % (n = 2), enrichment yield: ~ 91 %.

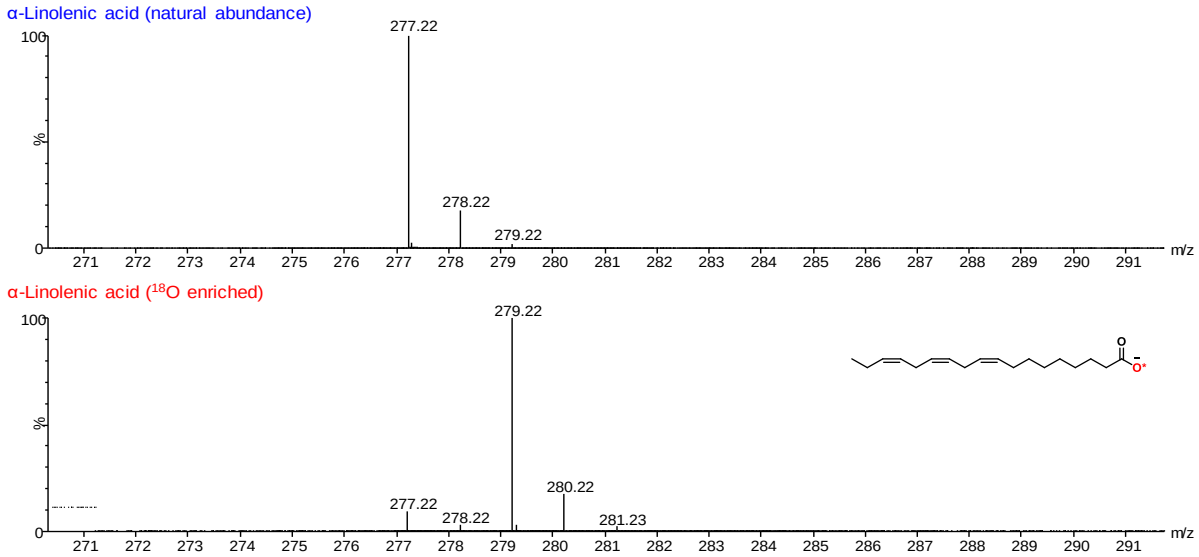

Figure II-36: ^{13}C NMR study of ^{18}O-isotope effect on the ^{13}C-carboxylic resonance in solution NMR. The non-labeled precursor is compared to the ^{18}O-enriched product, both having been mixed in different ratios, as indicated above each spectrum (DMSO-d_6, 600 MHz).

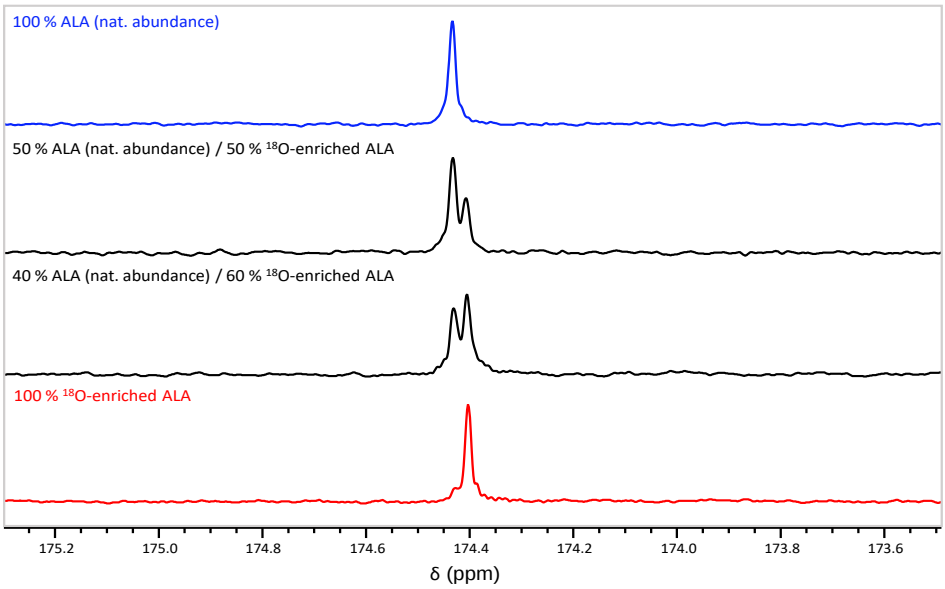

II-C1-c) Characterization of the ^{17}O-labeled ALA

Figure II-37: MS analyses of the non-labeled acid in comparison to the ^{17}O-enriched product. Average enrichment per carboxylic oxygen determined by MS: 42 % (n = 1).

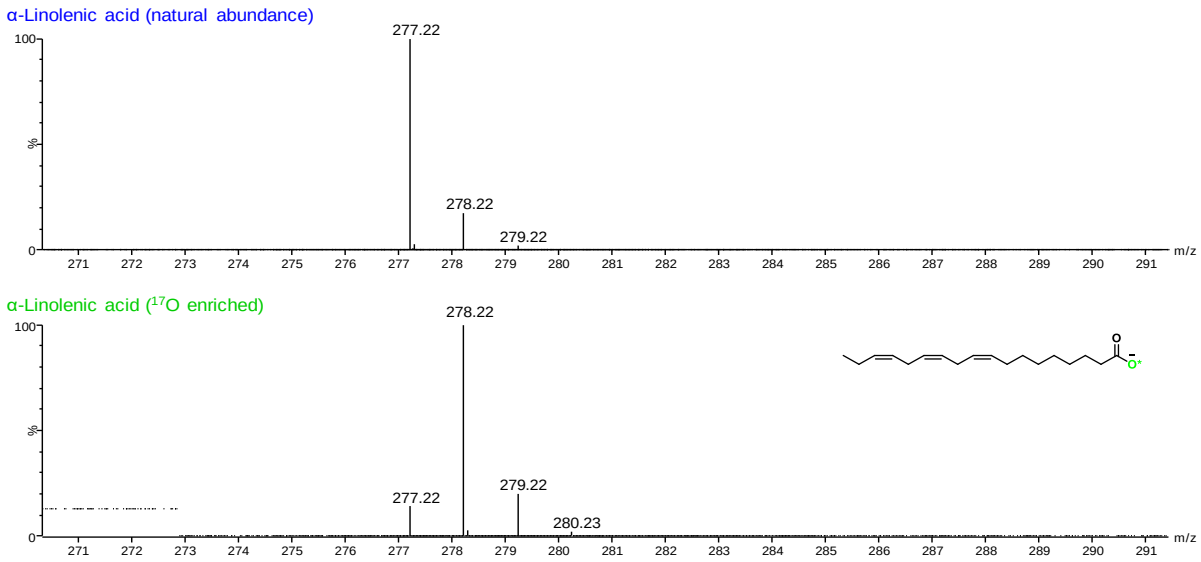

II-C2) Eicosapentaenoic acid (EPA, $C_{20}H_{30}O_2$)

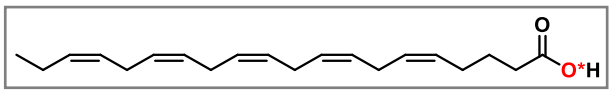

II-C2-a) Optimized labeling protocol

Ethyl eicosapentaenoate (57 mg, 0.17 mmol, 1.0 eq.), ^{18}O-labeled water (97.1%, 9 µL, 0.50 mmol, 3.0 eq.) and sodium ethoxide (18 mg, 0.26 mmol, 1.5 eq.) were introduced successively into the stainless-steel grinding jar (5 mL inner volume) containing two stainless steel balls (7 mm diameter). The jar was closed and subjected to grinding for 30 min in the MM400 mixer mill operated at 25 Hz. To help recover the product, non-labeled water (1 mL) was added into the jar, and the content was subjected to grinding for 2 min at 25 Hz. Then, the yellow solution (with a foam-like texture) was transferred to a beaker (together with sufficient amount of non-labeled water (4 mL) used here to rinse the jar). The medium was acidified to pH ~ 1 with an aqueous solution of HCl (6M, 9 drops), leading to a cloudy suspension, which was diluted with brine and extracted with ethyl acetate (1x 10 mL). Combined organic phases were dried over Na_2SO_4, filtered and finally dried under vacuum giving the product as a yellow oil. Average yield (n = 2): 48 ± 1 mg, 94 ± 1 %.

For the ^{17}O-labeling, exactly the same reaction/work-up conditions as for ^{18}O-labeling were employed with 90% ^{17}O-enriched water (9.25 µL, 3.0 eq.) used at the hydrolysis step. Yield (n = 1): 51 mg, 99 %.

II-C2-b) Characterization of the ^{18}O-labeled EPA

Figure II-38: MS analyses of the non-labeled acid in comparison to the ^{18}O-enriched product. Average enrichment per carboxylic oxygen determined by MS: 44.7 ± 1.2 % (n = 2), enrichment yield: ~ 92 %.

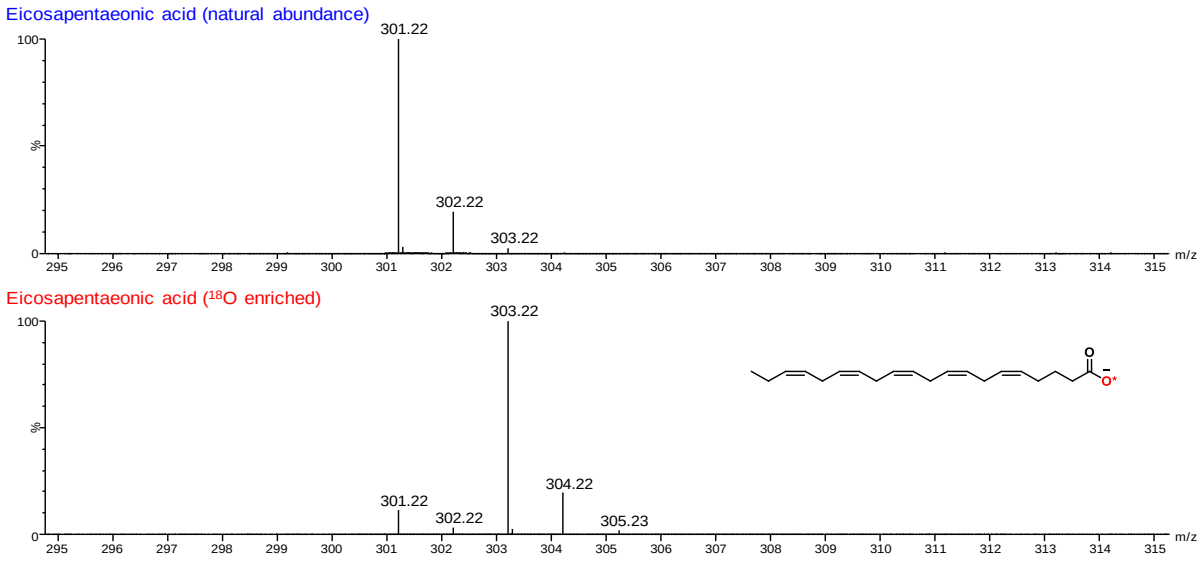

Figure II-39: ^{13}C NMR study of ^{18}O-isotope effect on the ^{13}C-carboxylic resonance in solution NMR. The non-labeled precursor is compared to the ^{18}O-enriched product, both having been mixed in different ratios, as indicated above each spectrum (DMSO-d_6, 600 MHz).

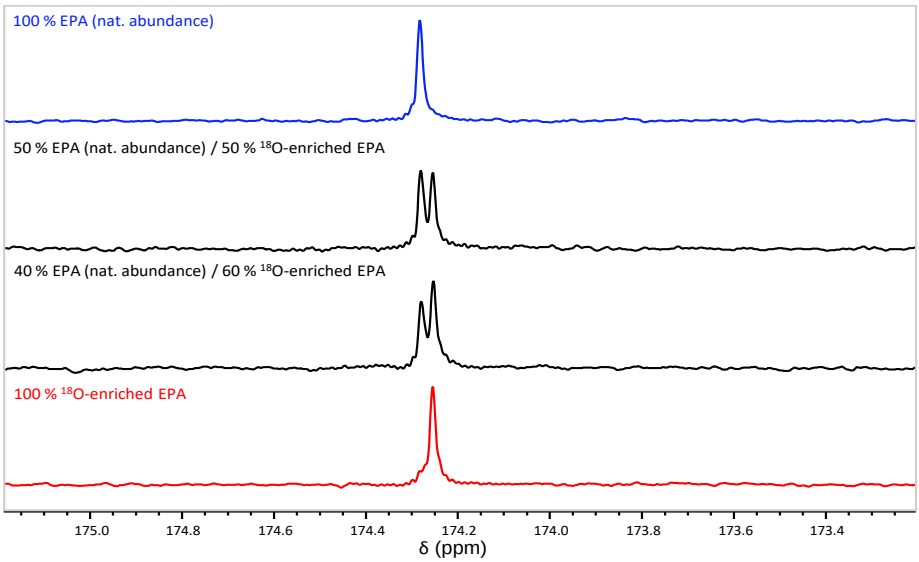

II-C2-c) Characterization of the ^{17}O-labeled EPA

Figure II-40: MS analyses of the non-labeled acid in comparison to the ^{17}O-enriched product. Average enrichment per carboxylic oxygen determined by MS: 42 % (n = 1).

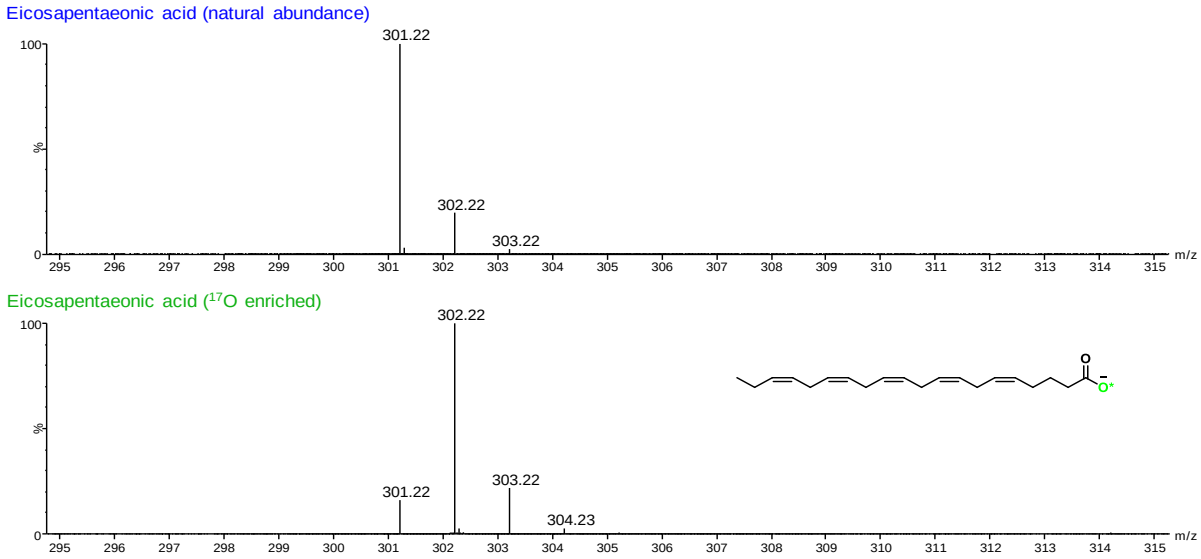

II-C3) Docosahexaenoic (DHA, $C_{22}H_{32}O_2$)

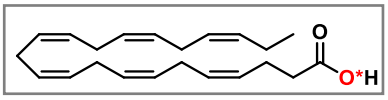

II-C3-a) Optimized labeling protocol

Ethyl docosahexaenoate (58 mg, 0.16 mmol, 1.0 eq.), ^{18}O-labeled water (97.1%, 8.75 µL, 0.49 mmol, 3.0 eq.) and sodium ethoxide (17 mg, 0.25 mmol, 1.5 eq.) were introduced successively into the stainless-steel grinding jar (5 mL inner volume) containing two stainless steel balls (7 mm diameter). The jar was closed and subjected to grinding for 30 min in the MM400 mixer mill operated at 25 Hz. To help recover the product, non-labeled water (1 mL) was added into the jar, and the content was subjected to grinding for 2 min at 25 Hz. Then, the yellow solution (with a foam-like aspect) was transferred to a beaker (together with sufficient amount of non-labeled water (4 mL) used here to rinse the jar). The medium was acidified to pH ~ 1 with an aqueous solution of HCl (6M, 9 drops), and the cloudy suspension was diluted with brine and extracted with ethyl acetate (1x 10 mL). Combined organic phases were dried over Na_2SO_4, filtered and finally dried under vacuum giving the product as a yellow oil. Average yield (n = 2): 50 ± 1 mg, 95 ± 1 %.

For the ^{17}O-labeling, exactly the same reaction/work-up conditions as for ^{18}O-labeling were employed with 90% ^{17}O-enriched water (8.75 µL, 3.0 eq.) used at the hydrolysis step. Yield (n = 1): 48 mg, 90 %.

II-C3-b) Characterization of the ^{18}O-labeled DHA

Figure II-41: MS analyses of the non-labeled acid in comparison to the ^{18}O-enriched product. Average enrichment per carboxylic oxygen determined by MS: 44.5 ± 0.9 % (n = 2), enrichment yield: ~ 91 %.

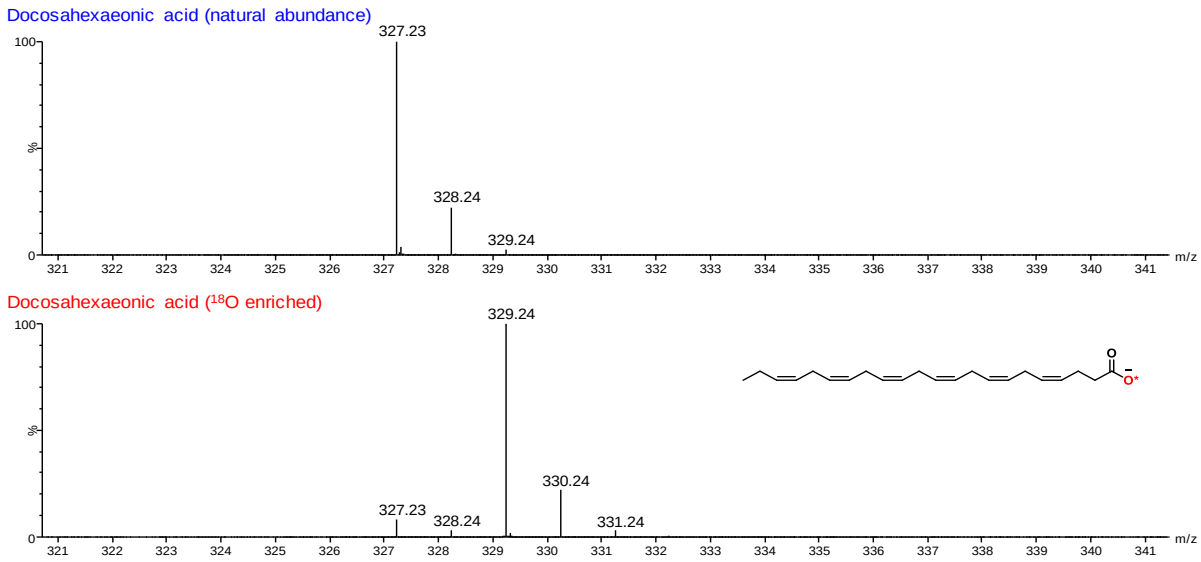

Figure II-42: ^{13}C NMR study of ^{18}O-isotope effect on the ^{13}C-carboxylic resonance in solution NMR. The non-labeled precursor is compared to the ^{18}O-enriched product, both having been mixed in different ratios, as indicated above each spectrum (DMSO-d_6, 600 MHz).

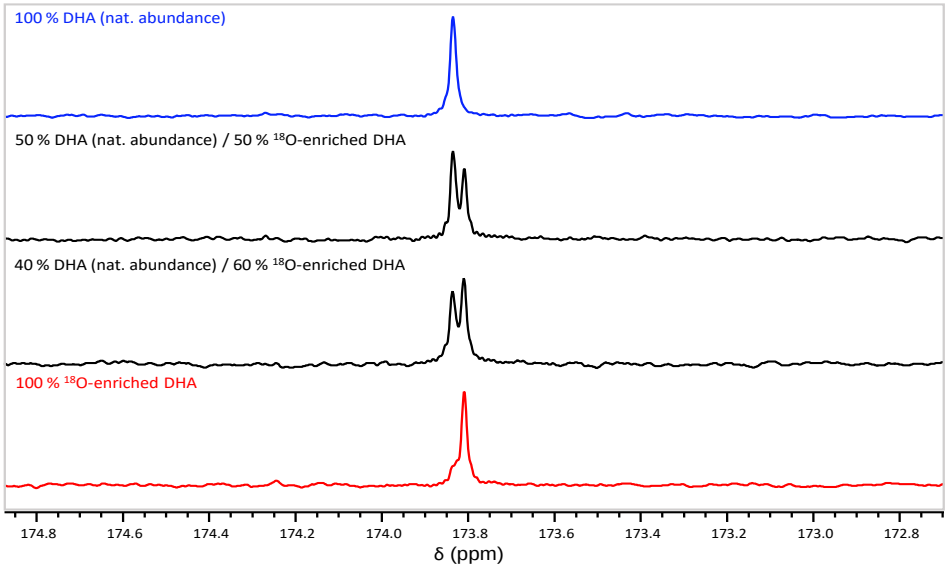

II-C3-c) Characterization of the ^{17}O-labeled DHA

Figure II-43: MS analyses of the non-labeled acid in comparison to the ^{17}O-enriched product. Average enrichment per carboxylic oxygen determined by MS: 41 % (n = 1).

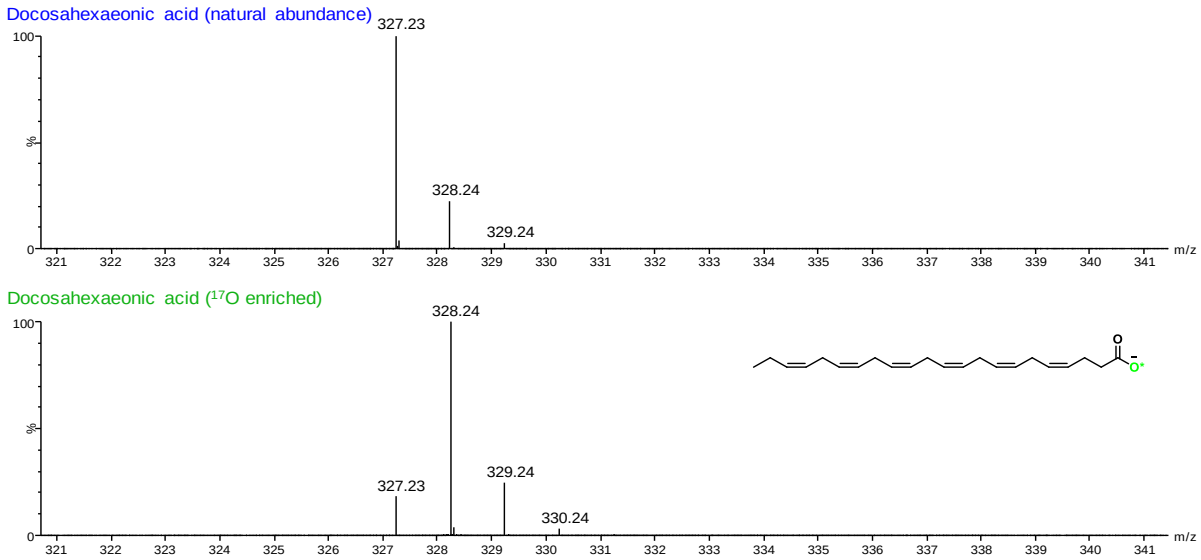

II-D) ADDITIONAL TABLES AND FIGURES

Table II-4: Summary of $^{17}O/^{18}O$-labeled fatty acids enriched using mechanochemical protocols (CDI-activation/hydrolysis or saponification). Average synthetic yields and enrichment level with including error bars were calculated from repeated experiments (where nx = average of x repetitions).

Entry	Product	Enrichment procedure	Isolated yield [%]	Enrichment yield [%]	^{18}O-Enrich. level [%]	^{17}O-Enrich. level [%]
Saturated fatty acids						
1	Lauric acid (LauA, C12)	CDI-activation	82 ± 10 (n4)	97.3 ± 2.0 (n4)	44.1 ± 1.1 (n3)	44 (n1)
2	Myristic acid (MA, C14)	CDI-activation	80 ± 6 (n4)	96.1 ± 2.0 (n4)	47.2 ± 0.2 (n3)	44 (n1)
3	Palmitic acid (PA, C16)	CDI-activation	88 ± 2 (n4)	95.6 ± 0.7 (n4)	46.4 ± 0.8 (n3)	43 (n1)
4	Stearic acid (SA, C18)	CDI-activation	84 ± 2 (n4)	90.8 ± 1.9 (n4)	46.9 ± 0.5 (n3)	42 (n1)
5	^{13}C-Stearic acid (^{13}C-SA, C18)	CDI-activation	91 ± 22 (n4)	93.7 ± 2.7 (n4)	44 (n1)	42.9 ± 1.2 (n3)
Unsaturated fatty acids						
6	Oleic acid (OA, C18:1)	CDI-activation	90 ± 2 (n4)	90.4 ± 2.7 (n4)	43.8 ± 1.5 (n3)	42 (n2)
7	Linoleic aicd (LA, C18:2)	CDI-activation	90 ± 2 (n3)	86.6 ± 0.8 (n4)	41.3 ± 0.4 (n2)	40 (n1)
8	α-Linolenic aicd (ALA, C18:3)	CDI-activation	88 ± 5 (n3)	87.4 ± 0.5 (n4)	42.5 ± 0.3 (n2)	40 (n1)
9	α-Linolenic aicd (ALA, C18:3)	Saponification	96 ± 1 (n3)	92.5 ± 2.4 (n3)	44.5 ± 1.0 (n2)	42 (n1)
10	Arachidonic acid (AA, C20:4)	CDI-activation	89 ± 2 (n4)	80.9 ± 3.4 (n3)	38.8 ± 1.5 (n2)	37 (n1)
11	Eisocapentaeonic acid (EPA, C20:5)	Saponification	96 ± 3 (n3)	91.9 ± 1.7 (n3)	44.7 ± 1.2 (n2)	42 (n1)
12	Docosahexaeonic acid (DHA, C22:6)	Saponification	93 ± 3 (n3)	91.2 ± 1.3 (n3)	44.5 ± 0.9 (n2)	41 (n1)

Table II-5: Measured enrichment levels of $^{17}O/^{18}O$-labeled FAs (n = 1) after 1 year of storage in parafilmed vials in a freezer (average enrichment per carboxylic oxygen, as determined by MS). ^{rt} Samples stored in parafilmed vials at room temperature. 40% ^{17}O-enriched water was used here for PA and OA labeling.

	Enrichment level [%]	
Fatty acid	**t_0**	**t_0 + 1 year**
Saturated fatty acids		
Lauric acid-^{18}O	47.4	47.6^{rt}
Lauric acid-^{17}O	44	45
Myristic acid-^{18}O	47.2	46.9
Myristic acid-^{17}O	44	45
Palmitic acid-^{18}O	47.2	47.3^{rt}
Palmitic acid-^{17}O	19.6	19.9^{rt}
Stearic acid-^{18}O	44.0	44.0^{rt}
Stearic acid-^{17}O	42	42
Unsaturated fatty acids		
Oleic acid-^{18}O	45.4	45.4
Oleic acid-^{17}O	18.6	18.7
Linoleic acid-^{18}O	41.6	41.4
Linoleic acid-^{17}O	40	41
α-Linolenic acid-^{18}O	42.2	42.2
α-Linolenic acid-^{17}O	40	41
Arachidonic acid-^{18}O	38.0	38.0
Arachidonic acid-^{17}O	37	39
Eicosapentaeonic acid-^{18}O	43.9	43.6
Eicosapentaeonic acid-^{17}O	42	42
Docosahexaeonic acid-^{18}O	45.1	45.1
Docosahexaeonic acid-^{17}O	41	42

Table II-6: Study of evolution of enrichment before work-up (*i.e.* right after hydrolysis by $H_2{}^{18}O$), and after work-up (*i.e.* recovery, acidification, extraction and drying steps). Average ^{18}O-enrichment levels including error bars were calculated from repeated experiments (where n=x is average of x repetitions).

Fatty acid	^{18}O-EL [%] before work-up	^{18}O-EL [%] after work-up
Palmitic acid (PA, C16)	46.5 ± 0.4 (n=3)	46.8 ± 0.5 (n=3)
α-Linolenic acid (ALA, C18:3)	42.3 ± 2.2 (n=2)	42.4 ± 0.5 (n=2)

Figure II-44: Photos of reactors showing the typical evolution of the physical state of the reaction mixtures before and after hydrolysis; a) starting from solid FAs (LauA, MA, PA, SA) - white powdery mixture is converted to colorless viscous oil only when the hydrolysis step is complete, b) starting from oily FAs (LA, ALA, AA) - white/yellowish suspension is converted to colorless oil when hydrolysis step is complete.

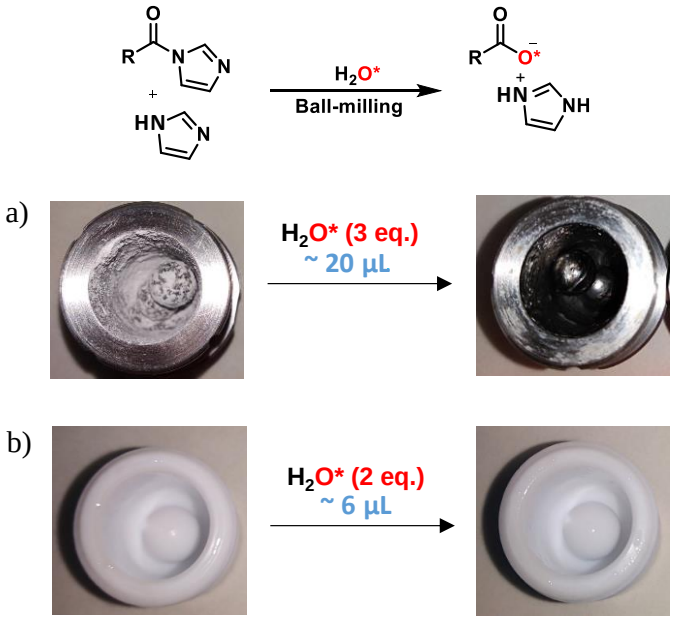

Figure II-45: Photos and a scheme of PTFE (5 mL inner volume, Fritsch) jar used for enrichment of unsaturated FAs (LA, ALA, AA). Due to the beveled edge at the contact planes of both parts of the jar, a gap is created where the two parts of the jar meet. During the milling experiments, small portion of a reaction mixture remains stuck in this gap and cannot interact with the labeled water, thus remains not labeled. During the work-up, this non-labeled portion is included into the final product and very probably causes a decrease of the overall enrichment of isolated products.

REFERENCES

1. Chen, C.-H.; Gaillard, E.; Mentink-Vigier, F.; Chen, K.; Gan, Z.; Gaveau, P.; Rebière, B.; Berthelot, R.; Florian, P.; Bonhomme, C.; Smith, M. E.; Métro, T.-X.; Alonso, B.; Laurencin, D., Direct 17O Isotopic Labeling of Oxides Using Mechanochemistry. *Inorg. Chem.* **2020,** *59* (18), 13050-13066.
2. Špačková, J.; Fabra, C.; Mittelette, S.; Gaillard, E.; Chen, C.-H.; Cazals, G.; Lebrun, A.; Sene, S.; Berthomieu, D.; Chen, K.; Gan, Z.; Gervais, C.; Métro, T.-X.; Laurencin, D., Unveiling the Structure and Reactivity of Fatty-Acid Based (Nano)materials Thanks to Efficient and Scalable 17O and 18O-Isotopic Labeling Schemes. *J.Am.Chem.Soc.* **2020,** *142* (50), 21068-21081.
3. Špačková, J.; Fabra, C.; Cazals, G.; Hubert-Roux, M.; Schmitz-Afonso, I.; Goldberga, I.; Berthomieu, D.; Lebrun, A.; Métro, T.-X.; Laurencin, D., Cost-efficient and user-friendly 17O/18O labeling procedures of fatty acids using mechanochemistry. *Chem.Comm.* **2021,** *57* (55), 6812-6815.
4. Perras, F. A.; Viger-Gravel, J.; Burgess, K. M.; Bryce, D. L., Signal enhancement in solid-state NMR of quadrupolar nuclei. *Solid State Nucl. Magn. Reson.* **2013,** *51*, 1-15.
5. Massiot, D.; Fayon, F.; Capron, M.; King, I.; Le Calvé, S.; Alonso, B.; Durand, J.-O.; Bujoli, B.; Gan, Z.; Hoatson, G., Modelling one- and two-dimensional solid-state NMR spectra. *Magn. Res. Chem.* **2002,** *40* (1), 70-76.

CHAPTER 3

APPLICATION OF ^{17}O-LABELED OLEIC ACID IN STRUCTURAL ELUCIDATION OF MATERIALS

INTRODUCTION

The content of this Chapter 3 is based on part of the work published in:

- Špačková, J.; Fabra, C.; Mittelette, S.; Gaillard, E.; Chen, C.-H.; Cazals, G.; Lebrun, A.; Sene, S.; Berthomieu, D.; Chen, K.; Gan, Z.; Gervais, C.; Métro, T.-X.; Laurencin, D., Unveiling the Structure and Reactivity of Fatty-Acid Based (Nano)materials Thanks to Efficient and Scalable ^{17}O and ^{18}O-Isotopic Labeling Schemes. *J. Am. Chem. Soc.* **2020**, *142* (50), 21068-21081.

As mentioned in Chapter 2, fatty acids are not only important in biological processes, but they are also widely applied in (nano)materials science. The amphiphilic nature of these molecules has been widely exploited for the preparation of soaps,[1] the formation of vesicles and drug-carrier systems,[2-4] and the surface-functionalization of inorganic materials and nanoparticles (NPs).[5-10]

Due to the importance of fatty acids, the synthesis of their isotopically-labeled versions has been looked into, with the aim to investigate in more detail their structure and reactivity.[11-14] In particular, ^{13}C isotopic labeling was found to be valuable for studying by ^{13}C solid-state NMR the mode of binding of the carboxylic group of stearic acid at the surface of zirconia as a function of temperature,[11] or the partitioning of myristate and hexanoate ligands at the surface of CdSe nanocrystals.[10, 15] However, although such high-sensitivity NMR analyses are of general interest for gaining insight into the nature of organic-mineral interfaces between fatty acids and inorganic phases, their use has been scarce. This can be explained by several factors, including the cost and limited availability of some of the commercial fatty acids enriched in ^{13}C, and the time and experimental constraints for performing the labeling (whether using chemical or biological synthetic routes).[16-20] In this context, being able to have access more straightforwardly to isotopically-enriched fatty acids to perform high resolution spectroscopic analyses of the local binding mode of carboxylic functions at materials interfaces appears as a major objective.

When considering the different enrichment possibilities for NMR studies of fatty acids, oxygen-17 is a highly attractive target. Indeed, high-resolution ^{17}O NMR spectroscopy is increasingly being used for structural elucidation purposes,[21-26] due to high sensitivity of oxygen-17 to its local environment expressed on a very broad range of variation of ^{17}O chemical shift (which exceeds 2000 ppm) and quadrupolar parameters (oxygen-17 has a nuclear spin of 5/2).[21-22, 27] However, the major drawback of this isotope is its very poor natural abundance (only 0.04%), meaning that the synthesis of ^{17}O-labeled species is generally necessary.

In our case, it was shown that it is possible to use mechanochemistry and ball-milling to provide ^{17}O-enriched carboxylic acids in a cost-efficient and user-friendly manner. The synthetic protocols for ^{17}O-enriched saturated and unsaturated fatty acids using ball-milling were described in the previous Chapter 2. Scaling-up these protocols producing ~ 1 g quantities of labeled species was seen as a pre-requisite for their general application in (nano)materials synthesis, and it was also discussed in the previous chapter (for details see section 2.1.3).

In this chapter, application of ^{17}O-labeled oleic acid (OA) in structural investigations using ^{17}O NMR spectroscopy will be demonstrated for two related systems shown in Figure 3.1: *i)* zinc oleate ($Zn(C_{18}H_{33}O_2)_2$, Zn-OA), a metal soap which crystallizes as a coordination polymer (but for which no crystal structure has yet been reported), despite of its interest notably in art-preservation sciences[28-30] and for the synthesis of quantum-dots,[31-32] and *ii)* zinc oxide (ZnO) nanoparticles functionalized by oleic acid, which have been studied in fields like toxicology and pharmacy (*e.g.* sunscreens),[33-35] art (*e.g.* oil paints),[36-38] as well as for the elaboration of nanocomposite materials,[39] but for which no direct experimental evidence into the binding mode of the fatty acid on the nanoparticle surface had been provided so far (see Figure 3.1). The high resolution ^{17}O solid-state NMR spectroscopy was used to study the structure and reactivity of these materials, including their evolution after UV-light irradiation, and it will be discussed in detail in the second part of this chapter.

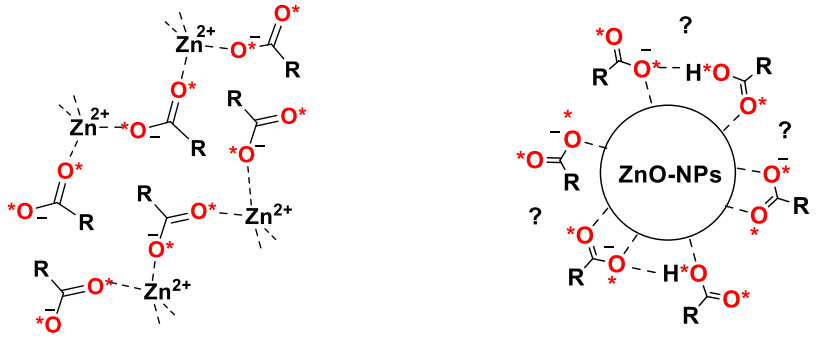

Figure 3.1: Schematic representation of ^{17}O-labeled zinc oleate ($Zn(C_{18}H_{33}O_2)_2$, Zn-OA, on the left), which crystallizes as a coordination polymer, and ZnO nanoparticles (NPs) functionalized with ^{17}O-labeled oleic acid (on the right). R = aliphatic chain of oleic acid.

3.1 ZINC OLEATE COORDINATION POLYMER

3.1.1 Synthesis of ^{17}O-labeled zinc oleate

According to the literature, zinc oleate ($Zn(C_{18}H_{33}O_2)_2$, Zn-OA) can be prepared by various routes, including *i)* by reaction of $ZnCl_2$ with sodium oleate (which can be formed

in-situ from oleic acid and NaOH) in solution,[40-46] *ii)* by reaction of oleic acid with Zn-acetate,[47] or *iii)* by reaction of $Zn(Et)_2$ and oleic acid.[31]

Here, an alternative protocol for the synthesis of Zn-OA was developed using ball-milling. At first, a sodium oleate salt was formed by reacting the oleic acid with 1 equivalent of NaOH for 10 minutes at 25 Hz in a vibratory mixer-mill (VBM) containing two beads. Zinc oleate was then obtained by adding 0.5 equivalents of $ZnCl_2$ into the jar, milling for 15 min at 25 Hz, and then drying the sample under vacuum (see Scheme 3.1). Both reaction steps could be followed by IR spectroscopy (see Annexe III). Using ^{17}O-labeled oleic acid as a precursor led to the preparation of ^{17}O-labeled Zn-OA. Due to the mild conditions used in these rapid ball-milling steps, no loss of enrichment was expected.

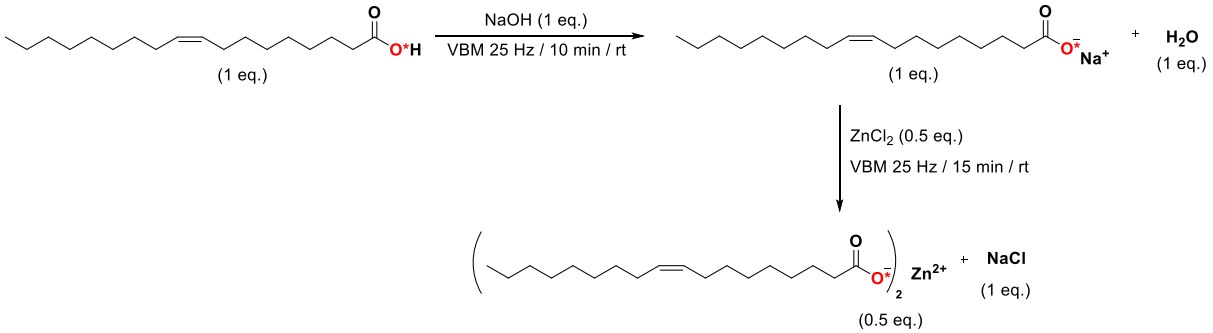

Scheme 3.1: Mechanochemical synthesis of ^{17}O-labeled Zn-OA. Both oxygens are enriched equally in the final product. The final product was isolated as a mixture with NaCl.

With this ball-milling procedure, the labeled material was recovered as a mixture of the Zn-oleate salt and NaCl, as shown by X-ray diffraction (Figure 3.2a). No attempt was made to wash off the NaCl, as its presence in the material was actually found to be advantageous for characterization purposes (especially for solid-state NMR). Indeed, it allows the sample to have a more powdery texture, making it easier to manipulate than the pasty/waxy precipitates which can be isolated for metal soap phases.[46] It is worth noting that the ^{23}Na solid-state NMR spectrum of the product recovered after ball-milling only shows the distinct sharp signature of crystalline NaCl at 7.2 ppm (see Figure 3.2b), but no other sodium environments, which proves that this phase is not a mixed Na,Zn oleate salt.

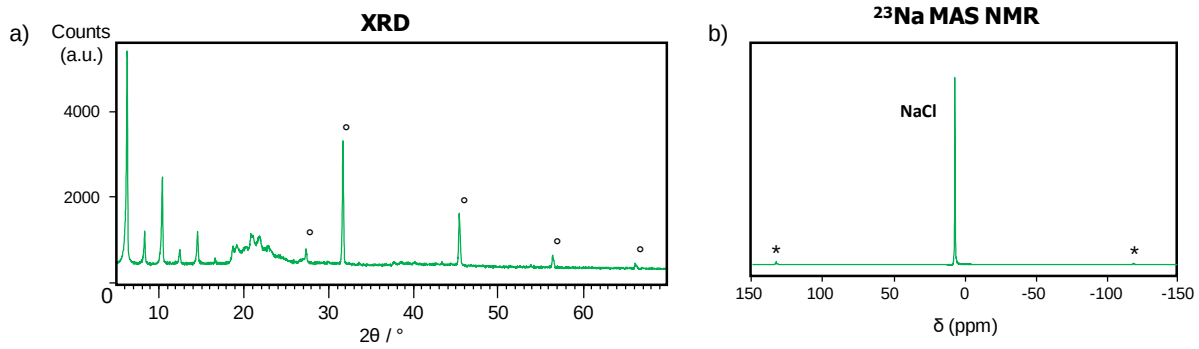

Figure 3.2: a) XRD powder pattern of Zn-OA (which matches the pattern previously reported in the literature),[41, 48] diffraction peaks marked with "°" correspond to the NaCl by-product, b) ^{23}Na solid-state NMR spectrum of Zn-OA/NaCl mixture recovered from the jar, spinning side bands are marked with "*".

In view of isolation and characterization of a phase-pure compound (without NaCl), attempts to synthesize Zn-OA by ball-milling starting from oleic acid and ZnO precursors directly were also performed. Although the formation of zinc oleate could be achieved in some cases, syntheses were more difficult to reproduce, and yields were generally lower. Moreover, the product was difficult to remove from the reactor due to its waxy texture. Hence, this second synthetic route was not pursued.

2.1.2 Advanced structural analyses of zinc oleate soap

The crystalline ^{17}O-labeled Zn-OA was studied by ATR-IR spectroscopy, as well as ^{13}C and ^{17}O solid-state NMR analyses, with the aim to describe the binding mode of oleate ligands to Zn^{2+}.

The IR spectra of this enriched phase and its non-labeled analogue were first analyzed in detail and compared (see Figure 3.3). This allowed to *i)* assign (or re-assign) the carboxylate vibration frequencies, and *ii)* demonstrate the presence of at least two oleate environments in the crystal structure, because of the observation of 2 resolved ν_{as}(COO) bands at 1546 and 1525 cm^{-1}. The difference in frequency between the ν_{as}(COO) and ν_{s}(COO) stretching modes was found to be consistent with a bidentate coordination mode of the carboxylate groups.[49] Moreover, the low-frequency band at 550 cm^{-1} (carboxylate rocking mode) was observed at a wavenumber close to the one reported for anhydrous zinc acetate and zinc stearate, in which the carboxylate group adopts a bridging bidentate coordination mode. Hence, it appears that the carboxylate functions in Zn-OA also adopts a similar binding mode, with each oxygen of a given carboxylate being bound to a different Zn^{2+} cation (see Figure 3.3).[50] This is in line with what has been observed for other Zn-soap phases for which X-ray structures are available.[51]

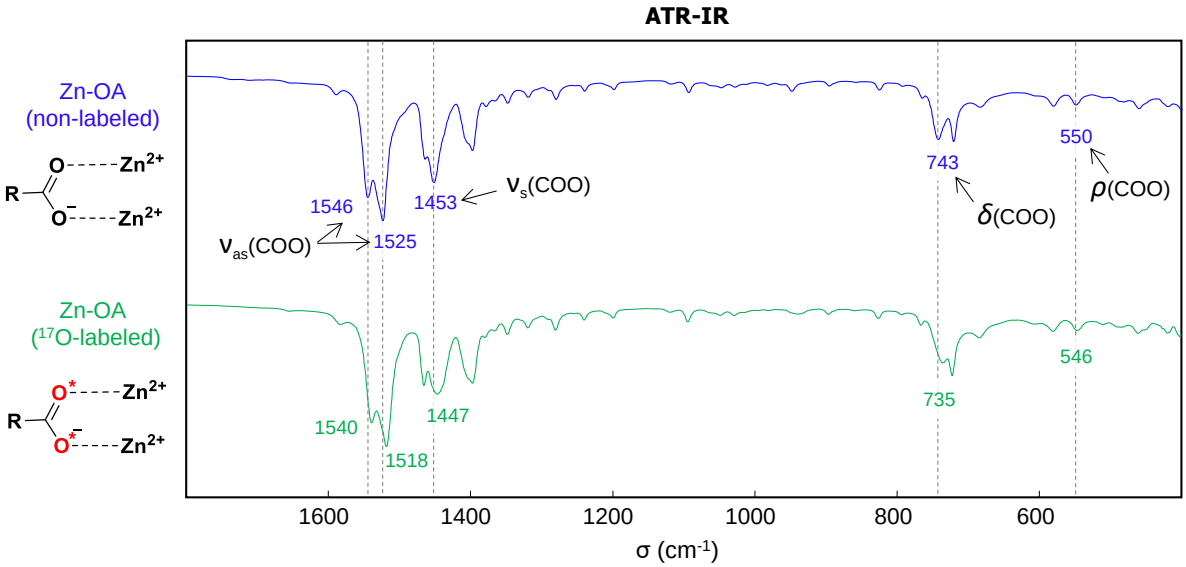

Figure 3.3: ATR-IR spectra of non-labeled and ^{17}O-labeled Zn-OA phase with carboxylate vibration bands assigned based on the isotope shifts observed (ν_{as} = asymmetric stretching, ν_s = symmetric stretching, δ = bending and ρ = rocking vibration bands).

High resolution ^{13}C and ^{17}O MAS NMR experiments were then performed, in order to gain deeper insight into the carboxylate environments of Zn-OA. First, in ^{13}C NMR, two carboxylate resonances of equal intensity were observed (separated by only ~ 0.2 ppm), as well as two α-CH_2 resonances (Figure 3.4a), which confirms that two non-equivalent carboxylate ligands are present in the crystal structure.[52] Second, in ^{17}O NMR, two different oxygen environments could be clearly resolved by performing a two-dimentional 3QMAS experiment (triple quantum magic angle spinning). These were found to be in a relative proportion of 3:1, with a difference in ^{17}O isotropic chemical shifts of ~ 6 ppm (Figure 3.4b).

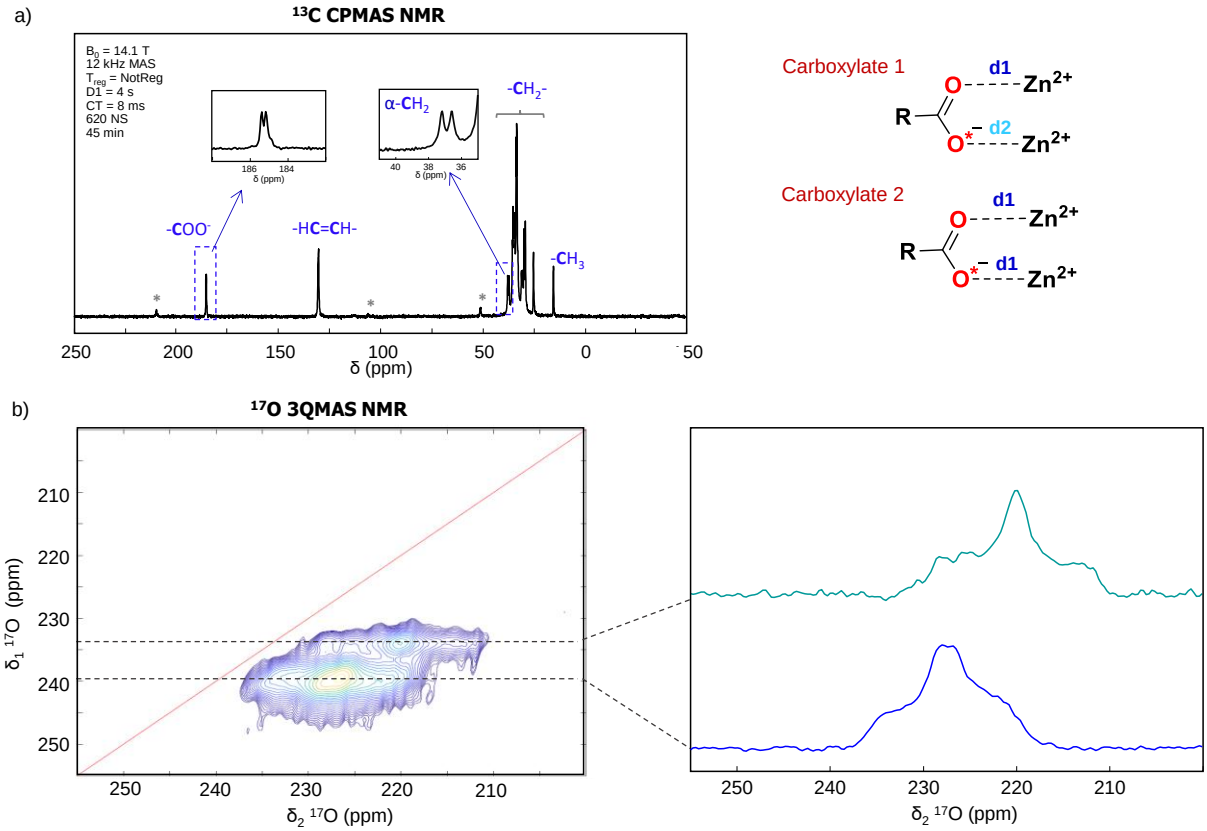

Figure 3.4: a) ^{13}C CPMAS NMR spectrum of ^{17}O-labeled Zn-OA recorded at 14.1 T, showing the presence of 2 inequivalent carboxylate and α-CH_2 environments (zoomed regions), b) Ultra-high field ^{17}O 3QMAS NMR spectrum (recorded at 35.2 T, spinning speed 18 kHz, left), and resolved sites (right). A possible fit of the resolved ^{17}O sites is proposed in Annexe III, section III-B2.

Such observations could be consistent with 3 of the oxygen atoms of the two inequivalent carboxylates having similar binding modes to Zn^{2+}, and one being slightly different, possibly because of a change in the Zn···O distance, as schematized also in Figure 3.4. In order to confirm this hypothesis, a computational study was performed on Zn-carboxylate phases for which a crystal structure had already been reported (zinc pentanoate ($Zn(C_5H_9O_2)_2$) and zinc octanoate ($Zn(C_8H_{15}O_2)_2$), and in which the Zn^{2+} also adopts a bridging bidentate coordination (*i.e.* with each carboxylate oxygen linked to one Zn^{2+} ion). For these phases, *ab initio* calculations of the ^{17}O NMR parameters were performed in collaboration with Prof. Christel Gervais (LCMCP, Paris) using the GIPAW DFT method (Gauge-Including Projector Augmented Wave – Density Functional Theory),[53-54] and calculated values were confronted to the local geometry around the oxygen (details in Annexe III, section B3). This enabled to demonstrate a strong dependence between the isotropic chemical shift of ^{17}O and the Zn···O distance. Indeed, $\delta_{iso}(^{17}O)$ values were found to span over ~ 40 ppm, with the isotropic shift increasing as the Zn···O distance increased (Figure 3.5). More specifically, based on the calculations, a change as small as 0.08 Å in this distance could lead to an increase by ~ 40 ppm

in $\delta_{iso}(^{17}O)$. No other relationship could be found between the local structure around oxygen and the calculated $\delta_{iso}(^{17}O)$ values. This implies that the ~ 6 ppm difference observed between the two sets of ^{17}O resonances in Zn-oleate must be due to a very small difference in Zn···O distances, which can be estimated to ~ 0.01 Å on the basis of the GIPAW-DFT calculations.

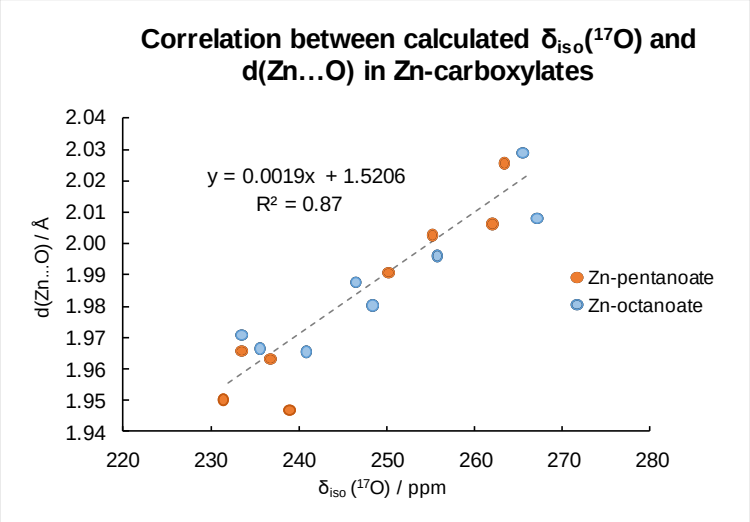

Figure 3.5: Correlation between the calculated ^{17}O isotropic chemical shifts (δ_{iso}, ppm) in Zn-pentanoate ($Zn(C_5H_9O_2)_2$) and Zn-octanoate ($Zn(C_8H_{15}O_2)_2$) using H-relaxed and fully-relaxed models, see Annexe III, section B3 for details, and the Zn…O distance (d, Å) in the corresponding models.

Such detailed level of insight had never been reached so far for Zn-oleate, and could only be achieved by looking at ^{17}O, thanks to the very high ^{17}O-isotopic labeling of oleic acid. Indeed, more conventional ^{13}C solid-state NMR analyses could not have provided such level of information, because *i)* they inform on the number of inequivalent carboxylate ligands (but not on the binding modes of the individual carboxylate oxygen atoms), and *ii)* the range of variation of ^{13}C NMR parameters in Zn-carboxylates is more limited compared to oxygen (with notably isotropic shifts of carboxylate groups spanning only over ~ 10 ppm for ^{13}C, compared to 40 ppm for ^{17}O), meaning that it is less sensitive to geometrical changes in the coordination. Hence, on a more general perspective, similar high–resolution ^{17}O NMR studies would be worth performing on other metal soaps of unknown structure.

3.2 ZnO NPs functionalized with ^{17}O-OA

Oleic acid is one of the main surfactant molecules involved in the synthesis of metal and metal oxide NPs.[55-59] Therefore, our next step was to show how using ^{17}O-enriched species can help to elucidate their mode of attachment and reactivity at the surface of NPs. Here, we focused on functionalized ZnO NPs. Indeed, previous investigations based on XRD, TEM, IR and/or

XPS (X-ray photoelectron spectroscopy) analyses had shown that oleic acid is present at the surface of ZnO nanoparticles and can influence nanoparticle sizes and shapes, but with no clear experimental insight into its exact mode of binding, nor on how it can be affected by exposure to heat or UV light.[60-63]

3.2.1 Synthesis of OA-functionalized ZnO NPs

A "post-grafting" synthetic approach was used here to prepare oleic-acid capped ZnO NPs. At first, non-functionalized ZnO nanoparticles were obtained as nanorods (NRs), by reacting Zn-acetate dihydrate (1 eq.) with KOH (2 eq.) in methanol at 60°C overnight (see detailed protocol in Annexe III).[64-65] Then, the surface of the nanoparticles was functionalized by oleic acid, using either ^{17}O-labeled oleic acid, prepared using scale-up protocol described in previous chapter (section 2.1.3), or non-labeled oleic acid, used here for the preparation of "control" samples (see detailed protocol in Annexe III). Finally, the grafted particles were washed, dried under vacuum, and characterized by XRD, TGA, TEM, ATR-IR and multinuclear solid-state NMR spectroscopies (^{1}H, ^{13}C and ^{17}O NMR).

3.2.2 Analyses of OA-functionalized ZnO NPs

The oleic acid grafted nanoparticles were at first analysed by common analytical techniques to describe their size and shape, and to estimate the grafting density (number of ligands per nm^2 of NPs surface). Then, more thorough analyses were performed with the aim to elucidate the bonding mode of carboxylate ligands on the surface of ZnO.

Based on the TEM and XRD analyses, the size and shape of the ZnO nanorods was not altered by the surface functionalization process (Figure 3.6a,b). X-ray diffraction powder patterns displayed the characteristic features expected for nanorods, with a sharper peak at 34.4° in 2θ,[64] and no new diffraction peaks at lower angles. The latter point was important to verify, as it confirmed that no "dissolution-recrystallization" process had taken place during the grafting, and hence that no zinc oleate by-product had formed (see Annexe III, Figure III-8, for direct comparison with Zn-OA). Based on TGA, the average grafting density was estimated to ~ 2 molecules per nm^2. The presence of oleic acid at the surface of the nanorods was detectable by ATR-IR spectroscopy, through the appearance of C-H stretching vibrations around 2900 cm^{-1} (Figure 3.6c). The aliphatic carbon peaks of oleic acid could also be observed in ^{13}C solid-state NMR, with the ^{13}C resonance at ~ 130 ppm corresponding to the carbons of the alkene bond, and those between 10 and 45 ppm to the carbons in CH_2 and CH_3 groups (Figure 3.6d).

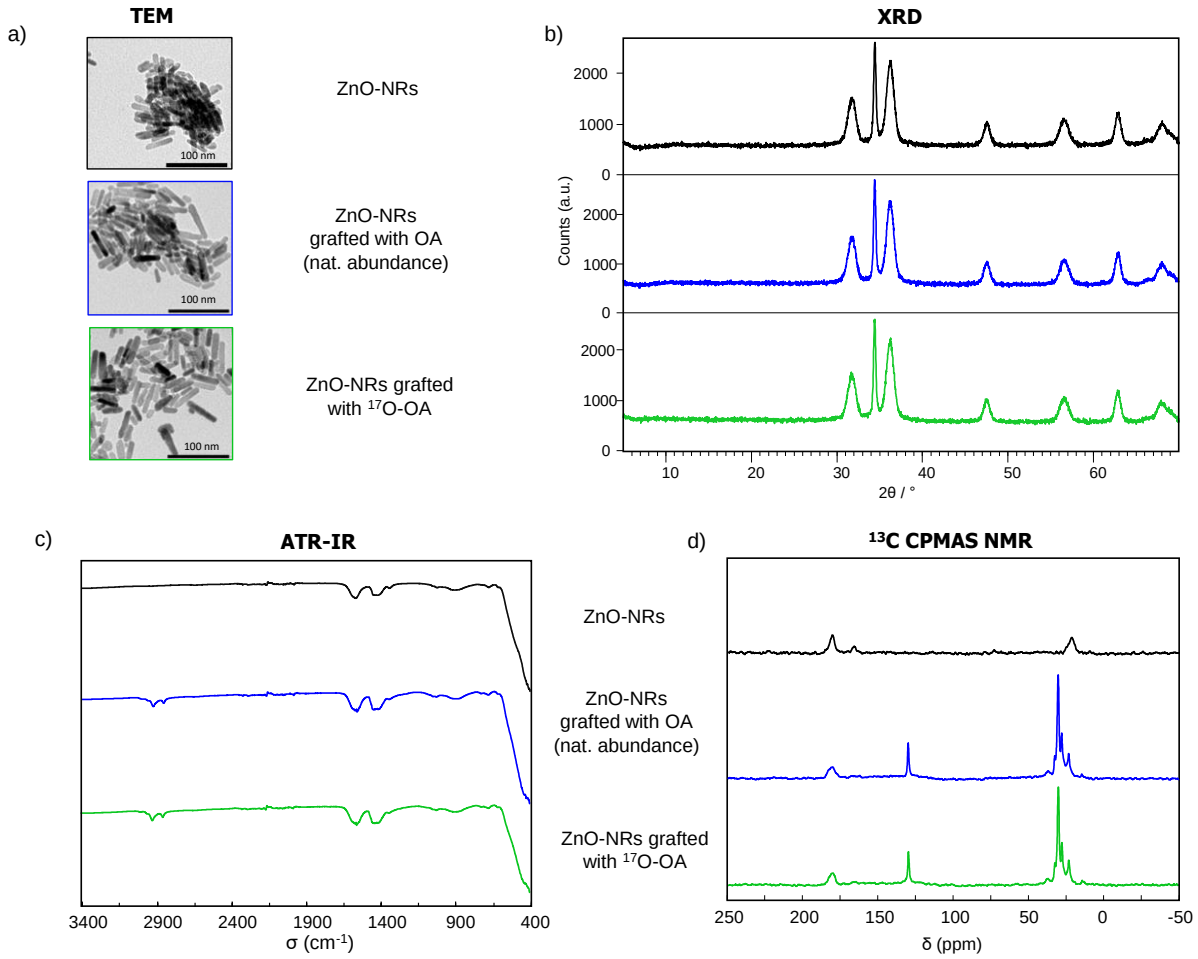

Figure 3.6: a) TEM, b) XRD, c) ATR-IR and d) ^{13}C CPMAS NMR characterization of bare ZnO nanorods (black), nanorods grafted with non-labeled OA (blue) and nanorods grafted with ^{17}O-labeled OA (green).

To understand the mode of binding of oleic acid at the ZnO surface, the spectroscopic signatures of the carboxylic group were analyzed. In IR spectroscopy, the broad vibration bands observed in the C=O stretching region were found at similar positions before and after functionalization of the nanorods, *i.e.* centered around 1430 and 1565 cm^{-1}. For the starting ZnO nanorods, the observation of these broad bands can be explained by the presence of residual acetate and carbonate ions at the surface of the particles, as confirmed by ^{13}C solid-state NMR, with the distinct ^{13}C resonances at 180.5 and 21.9 ppm (acetate) and at 166.2 ppm (carbonate) (Figure 3.6d, black spectrum). It is worth noting that previous studies on ZnO nanoparticles have reported the presence of these anions, for syntheses carried out using zinc acetate as precursor,[65-66] or following exposure of ZnO nanoparticles to CO_2 (including at atmospherically relevant pressures).[67-68] For the OA-functionalized nanorods, the lack of significant shift in the C=O stretching region and the absence of a new band around 1700 cm^{-1} (which is characteristic for the acidic form of oleic acid), suggests that it is mainly the oleate

which is present at the surface of the particles (see Annexe III, Figure III-9, for a comparison of the IR spectra of zinc oleate, oleic acid, and the functionalized nanorods).[10,11,61]

Because previous works on oleic acid-grafted ZnO nanoparticles had proposed that either protonated or deprotonated forms of oleic acid can attach to the surface of the nanoparticles,[63, 69-70] additional solid-state NMR analyses were performed. In ^{13}C solid-state NMR, only one broad resonance was observed in the high-frequency region of the functionalized nanoparticles, centred at ~ 181.1 ppm (Figure 3.6d, blue and green spectra). This ^{13}C resonance is broader than those of the rest of the organic chain, as expected for a grafting process occurring through the carboxylic moiety.[11, 71] Although its chemical shift was found to be closer to the one observed for pure oleic acid (carboxylic resonance is centred at ~ 181.4 ppm, as measured by ^{13}C CPMAS NMR while regulating temperature at -20°C),[61, 72] than for zinc oleate (carboxylate resonances centred at ~ 185.3 ppm), it is still compatible with a deprotonated function, because the ^{13}C chemical shift range of grafted carboxylates can vary depending on their binding mode and distance to the surface of nanoparticles.[11] As a matter of fact, when recording a 2D ^{1}H-^{13}C heteronuclear correlation experiment, the ^{13}C resonance at 181.1 ppm was not found to correlate with any ^{1}H resonances characteristic of acidic protons, which are generally expected above 10 ppm. Moreover, no distinct ^{1}H carboxylic resonance could be observed in ^{1}H MAS NMR, even when performing the analyses at temperatures as low as -100°C (Figure 3.7). Therefore, these complementary NMR characterizations also tend to confirm that it is mainly the oleate form which is present at the surface of the nanoparticles.

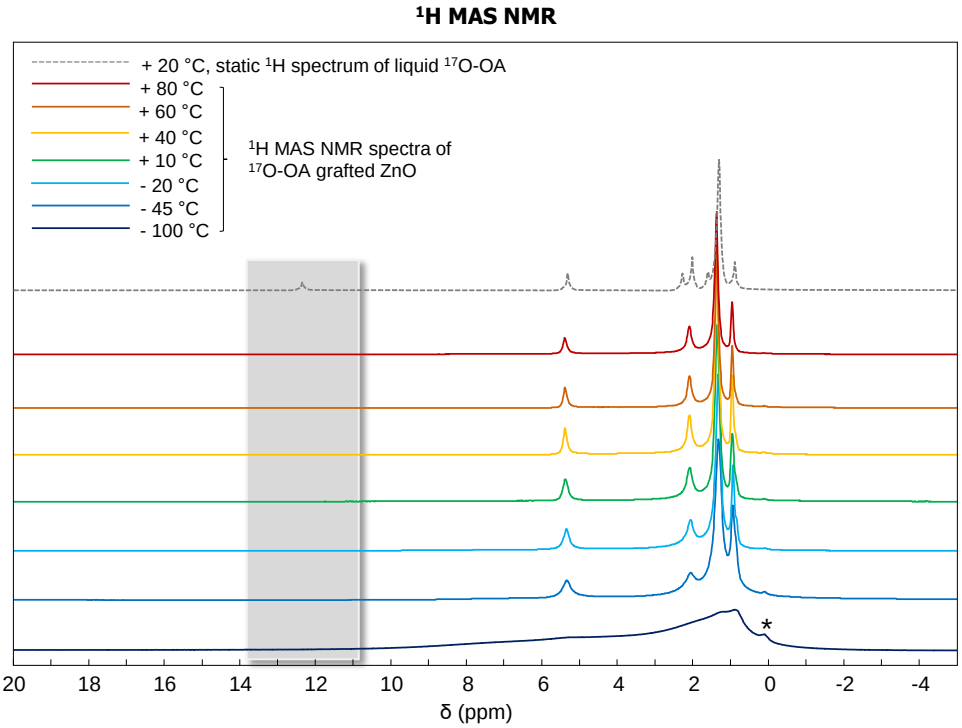

Figure 3.7: Variable-temperature ^{1}H MAS NMR spectra of the ^{17}O-OA grafted nanorods (B_0 = 14.1 T, 16 kHz spinning speed, Hahn-echo sequence with an echo delay of 4 rotor periods). The shaded grey region corresponds to the chemical shift range where COOH signals are expected, as shown by comparison to the ^{1}H NMR spectrum of pure oleic acid, recorded on the same instrument (dashed grey line). The "*" symbol indicates a background resonance.

In view of reaching deeper insight into the mode of binding of the fatty acid at the surface of ZnO, ^{17}O solid-state NMR analyses were carried out. As shown in Figure 3.8 (green spectrum), the ^{17}O NMR spectrum of the grafted nanoparticles presents one main broad signal, centred at ~ 200 ppm (at 14.1 T). This signal was not observed for the starting nanoparticles, nor for those which were reacted using non-labeled oleic acid, and can therefore be assigned to the enriched carboxylic function of oleic acid. The spectrum was obtained overnight with a good signal-to-noise ratio at 14.1 T, which is all the more noteworthy that the analysis was performed on just ~ 35 mg of sample. Indeed, this corresponds to only ~ 0.1 mg of ^{17}O from the oleic acid head-group, based on the initial enrichment of the molecule used in the grafting and on the grafting density determined from TGA analyses of the functionalized nanoparticles. Other weaker resonances were also observed on the ^{17}O NMR spectrum, at ~ -18 ppm (natural abundance signal corresponding to the core of the ZnO nanoparticles)[73-74] and at ~ 380 ppm (natural abundance signal of the zirconia rotor used for the analyses), which were also present on the spectra of the non-grafted nanoparticles and those grafted using non-labeled oleic acid (Figure 3.8, black and blue spectra).

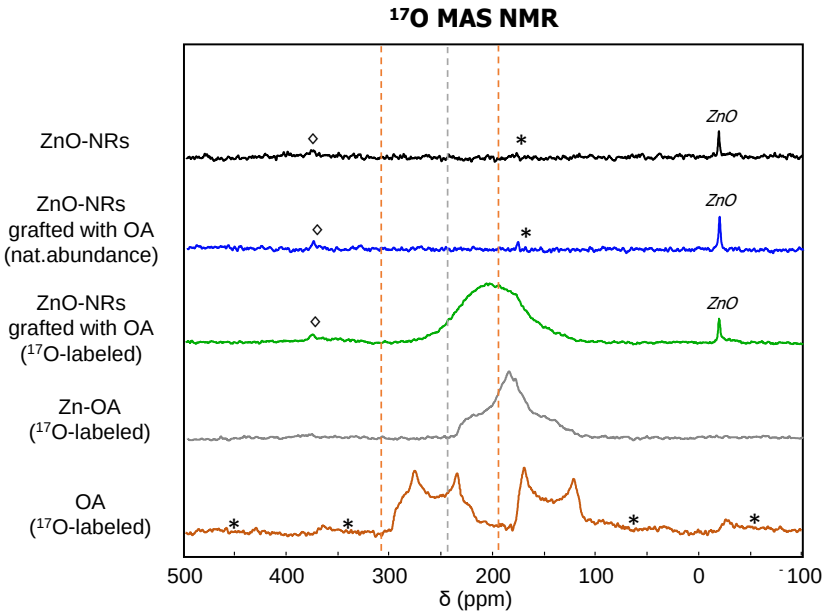

Figure 3.8: ^{17}O MAS NMR characterization of bare ZnO nanorods (black), nanorods grafted with non-labeled oleic acid (blue) and nanorods grafted with ^{17}O-labeled oleic acid (green), compared to ^{17}O-labeled zinc oleate (Zn-OA, grey) and oleic acid (OA, brown), all recorded at 14.1 T. All NMR acquisition parameters can be found in Annexe III (Table III-2). "*" symbols correspond to spinning sidebands, and "◊" symbols to the natural abundance signal of the zirconia rotor. The dashed vertical lines indicate the isotropic peak positions of the C=O and C-OH resonances of OA (brown) and the high frequency carboxylate resonance of Zn-OA (grey).

The ^{17}O NMR signal centred at ~ 200 ppm falls in the range expected for carboxylic acids and carboxylates,[21, 75] as shown in Figure 3.8 when comparing it to oleic acid and Zn-oleate (brown and grey spectra). However, when cooling the sample down to -100 °C, only a slight shift and broadening of the ^{17}O NMR signal was observed, but no splitting into distinct C=O and C-OH contributions as for oleic acid (see Figure 3.9). Moreover, when heating up to +60 °C, the signal is slightly narrower and more symmetric (as expected if the molecules become somewhat more mobile at the nanoparticle surface), but its maximum position increases by less than 15 ppm, thereby remaining very distinct to that of liquid oleic acid. This could reflect the fact that the grafted OA species remain relatively well attached to the ZnO surface even at high temperatures, through coordination bonds between Zn^{2+} and the carboxylate, and that there are only few more weakly bound species interacting through hydrogen bonding (as may have been expected upon grafting of the oleic acid form). Overall, these variable-temperature ^{17}O NMR analyses also appear to be consistent with the predominance of oleate anions at the surface of the nanoparticles.

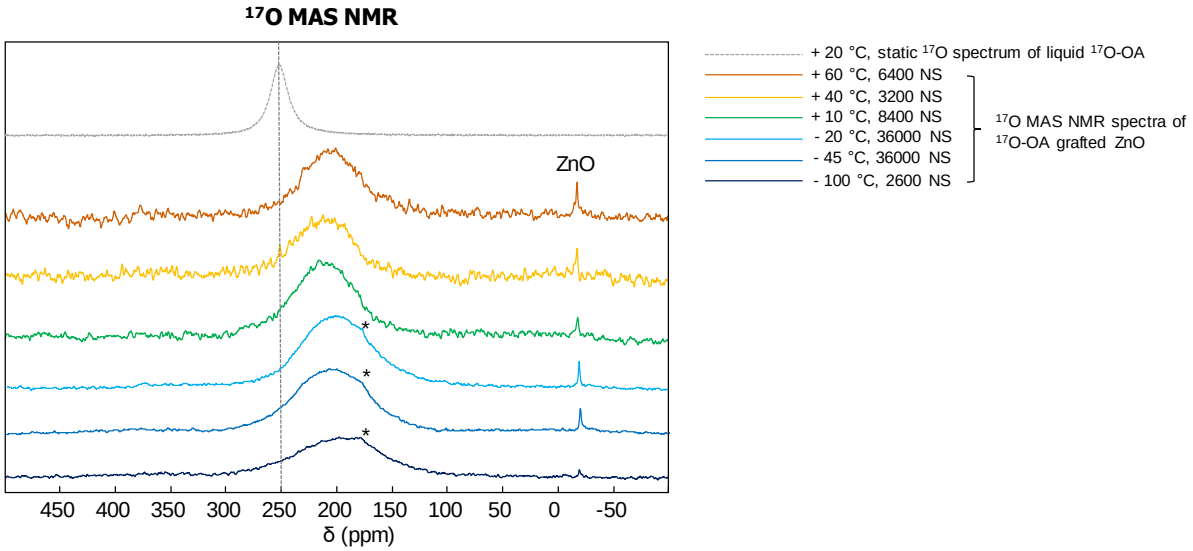

Figure 3.9: Variable-temperature ^{17}O MAS NMR spectra of the ^{17}O-OA grafted nanorods (B_0 = 14.1 T, 16 kHz spinning speed, DFS-onepulse sequence). The "*" symbol indicates a spinning sideband of ZnO.

Because of the wide range of chemical shifts covered by this ^{17}O signal, which spreads over ~ 180 ppm at 14.1 T (between ~ 110 and 290 ppm), additional characterizations were also performed at ultra-high magnetic field at the MagLab in Tallahassee (B_0 = 35.2 T), in order to try to achieve better resolution and gain further insight into the grafting mode. Indeed, ^{17}O being a quadrupolar nucleus, going to higher fields decreases significantly the broadening caused by the quadrupolar interaction, the second-order quadrupolar broadening being inversely proportional to B_0. At 35.2 T, the main resonance spreads over ~ 90 ppm only (between ~ 200 and 290 ppm), and is now shifted at higher frequency (peak maximum at ~ 250 ppm), as expected considering the field dependence of the maximum peak-position of solid-state NMR spectra of quadrupolar nuclei (Figure 3.10). Although no additional resolution could be obtained, this 1D ^{17}O MAS NMR spectrum nevertheless shows that there are several oxygen local environments at the surface of the nanoparticles, because the linewidth expected for ^{17}O resonances from "single" carboxylic or carboxylate oxygen atoms is less than 20 ppm at 35.2 T. Moreover, on the spectrum recorded at this field, the ^{17}O peak maximum position is very clearly positioned at higher frequencies compared to the Zn-oleate model compound. This demonstrates that the main mode of binding of oleate to the ZnO nanorod surface is different compared to Zn-oleate, meaning that there are very few oleate ligands coordinated through a bidentate bridging mode to the surface Zn^{2+} ions. Considering the results of the DFT calculations reported in Annexe III (section III-B3), the higher frequency of the maximum peak position in the functionalized nanorods may suggest that Zn…O distances between the oleate and the nanoparticle surface are not only more distributed but also on average slightly longer

than in crystalline zinc oleate. More specifically, an average increase in distance ~ 0.04 Å can be proposed.

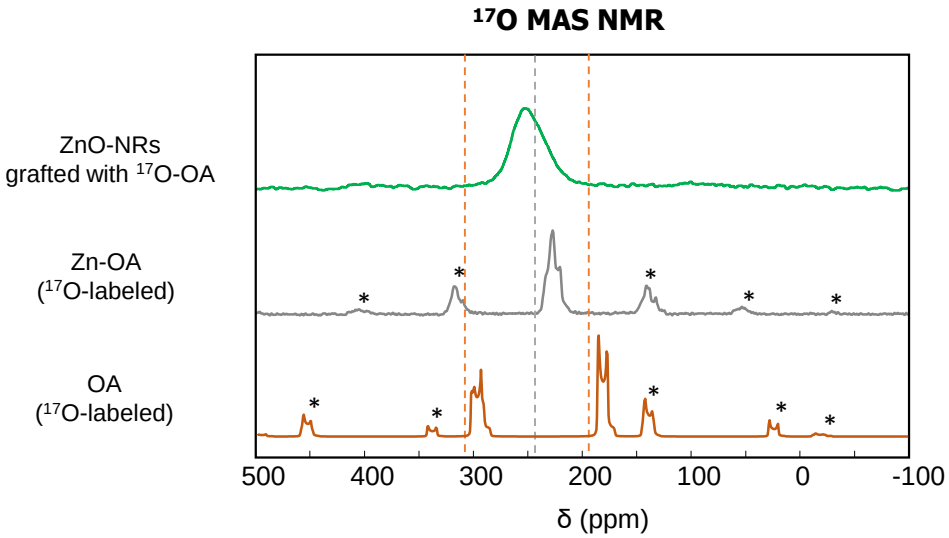

Figure 3.10: Ultra high-field ^{17}O MAS NMR characterization of nanorods grafted with ^{17}O-labeled oleic acid (green) and ^{17}O-labeled zinc oleate (Zn-OA, grey) recorded at 35.2 T, compared to the simulated spectrum oleic acid (OA, brown, simulated for 32 kHz spinning speed, as was used for the nanoparticles at this field, and estimating the CSA parameters from GIPAW-DFT calculations). For the ^{17}O-OA grafted nanorods, the lack of natural abundance ZnO signal at 35.2 T is ascribed to the difference in acquisition conditions used in comparison to the study at 14.1 T. "*" symbols correspond to spinning sidebands. The dashed vertical lines indicate the isotropic peak positions of the C=O and C-OH resonances of oleic acid (brown) and the high frequency carboxylate resonance of Zn-OA (grey).

Taken together, the observations made by IR and variable-temperature ^{1}H and ^{17}O NMR suggest the predominance of oleate species at the surface of the nanoparticles. Moreover, the ^{13}C NMR and ultra-high field ^{17}O NMR spectra point to the attachment of the oleates through the carboxylate function, with a heterogeneity of local environments at the surface of the nanorods. The aliphatic carbon atoms of the oleate chain interact much more weakly with the surface, as shown by the sharper resonances in ^{13}C NMR,[81] and by the similar chemical shifts as for liquid oleic acid (see Annexe III, Figure III-10). As a matter of fact, the mobility of the aliphatic chains only significantly decreases below -45°C, as shown above by the variable-temperature ^{1}H NMR data (Figure 3.7). Considering that it is the acidic form of oleic acid which was initially introduced in THF for the post-functionalization procedure used here, and that the lateral facets of the nanorods (which are parallel to the *c* axis) are apolar,[60, 76] a direct attachment of oleate species is unlikely. However, it can be proposed that the grafting occurs by exchange with acetate ligands initially present at the surface of the nanorods, which would be released in THF under the form of acetic acid upon coordination of the oleate, thereby ensuring the charge balancing.[82] A schematic representation of possible modes of attachment of oleates is given in Figure 3.11. While this binding mode to ZnO nanorods was proposed here, it is possible that

other synthetic strategies for the functionalization of ZnO nanoparticles may lead to different binding configurations, depending on the size and shape of the particles, and whether a direct-grafting strategy or post-grafting strategy is used.

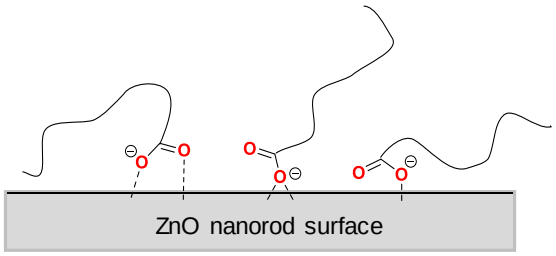

Figure 3.11: Schematic representation of possible binding modes of OA ligands to the surface of ZnO NPs.

3.3 Reactivity of OA-functionalized ZnO NPs under UV-irradiation

Because of the photocatalytic properties of ZnO, the stability of the oleate coating upon exposure to UV-vis radiation was investigated. More specifically, a batch of grafted nanorods taken in their powdered form was irradiated for 6 hours, after which X-ray diffraction, TEM, ATR-IR spectroscopy, ^{13}C NMR and ^{17}O NMR analyses were carried out. In order to distinguish the evolutions coming from heating or irradiation, a separate batch of the grafted nanorods was heated at 60 °C in a closed furnace for the same period of time as this temperature was estimated as representative of the heating occurring within the apparatus used for irradiation. Moreover, for comparison purposes, the other two sets of samples described above (*i.e.* bare nanorods and nanorods coated with non-labeled oleic acid), as well as the crystalline zinc oleate phase, were also exposed to the same treatments (irradiation and heating), and subsequently characterized by the same techniques (Figure 3.12).

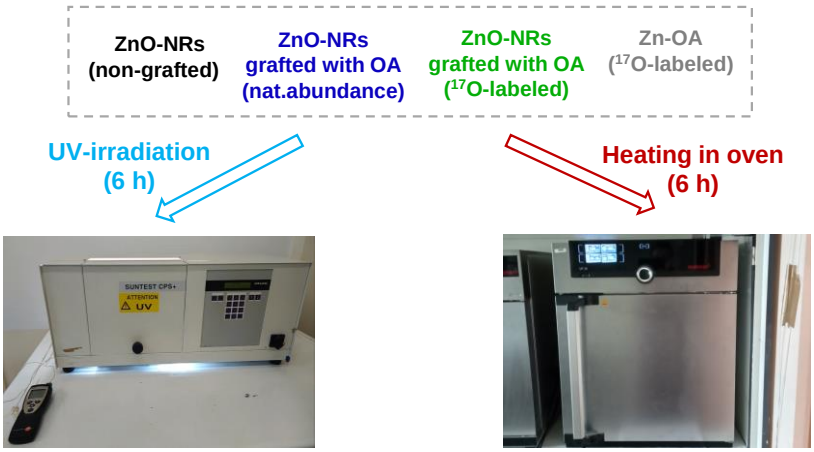

Figure 3.12: Photos of the instruments used for UV irradiation and heat treatment studies, performed on the ZnO NPs (non-grafted, grafted with OA (nat. abundance) and with ^{17}O-enriched OA), and on the ^{17}O-enriched Zn-OA phase.

While the heating of the non-grafted and grafted ZnO samples at 60 °C for 6 h did not lead to noticeable changes in TEM, XRD, IR, ^{13}C NMR or ^{17}O NMR (Figures III-12 and III-13 in Annexe III, Figure 3.13), significant differences were observed upon irradiation. First, regarding crystal morphologies, the irradiation step was found to strongly affect the *non-grafted* nanorods, as shown by TEM (more ill-defined crystal morphologies) and XRD (decrease in the relative intensity of the (002) diffraction peak at ~ 34.4° in 2θ). In contrast, no strong changes in shape and morphology of the *grafted* nanorods was observed in TEM and XRD after irradiation (Figures 3.13a and 3.13b). The OA surface coating thus appears to have had some protective effect for ZnO nanorods under the irradiation conditions used here.

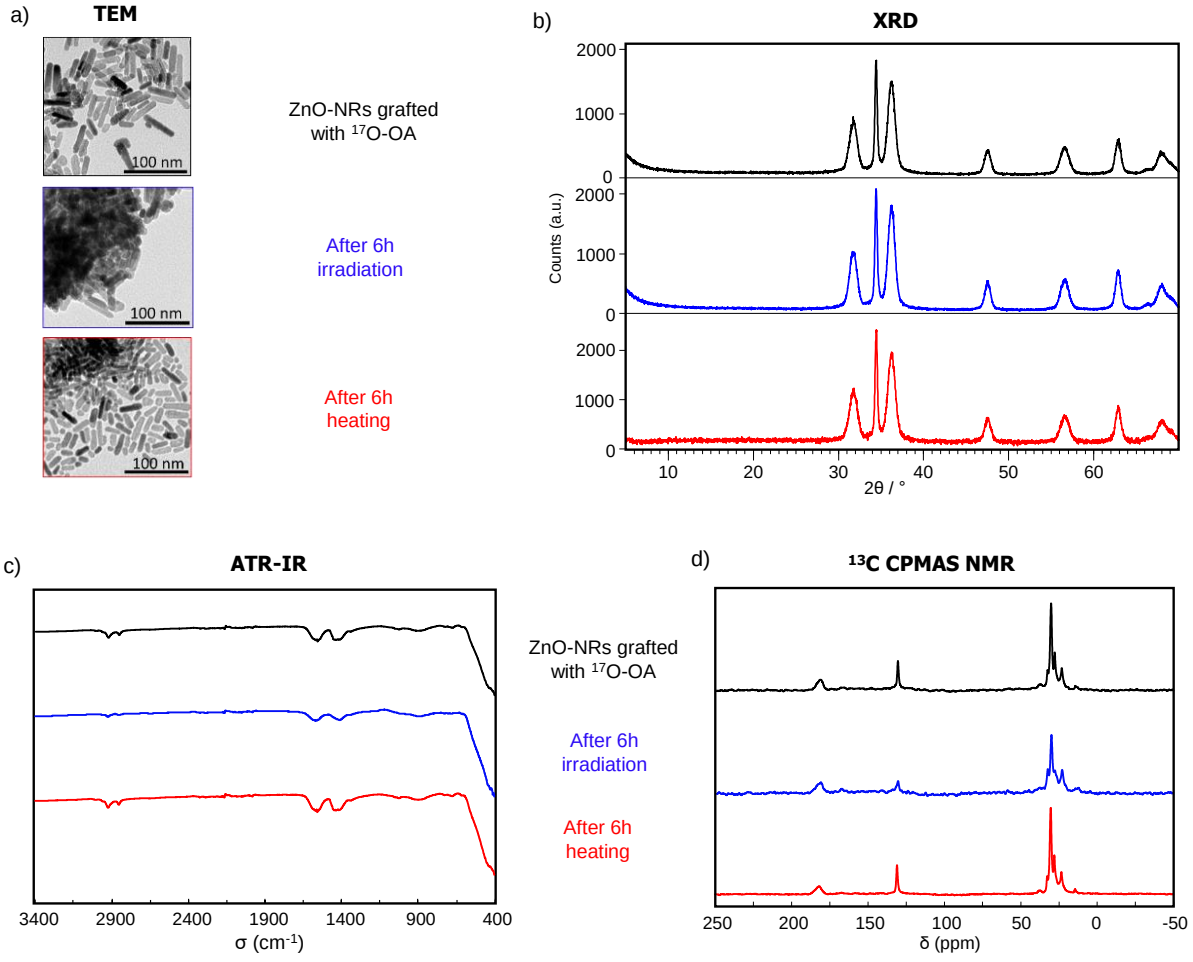

Figure 3.13: a) TEM, b) XRD,[77] c) IR, d) ^{13}C CPMAS NMR characterization of ZnO nanorods functionalized by with ^{17}O-enriched oleic acid (OA), before (black) and after 6h hours of irradiation (blue) or heat-treatment (red).

Nevertheless, the grafted molecules did not remain unaffected by the UV-vis treatment, as visible from the TEM, where more significant agglomeration of the crystallites was observed (Figure 3.13a), but also from the results of other analyses after irradiation, such as ATR-IR, solid-state NMR, and TGA. Indeed, TGA data shows that the weight loss due to the combustion

of the organic coating is less significant after irradiation (see Figure III-15 in Annexe III), in agreement with the degradation of some of the fatty acid molecules. ATR-IR spectroscopy shows a broadening of the carboxylate stretching vibrations after irradiation, as well as a decrease in relative intensity of the CH stretching vibrations (Figure 3.13c). Such a decrease in the CH bands had also been reported in previous studies of the photodegradation of fatty-acids coated at the surface of ZnO.[78] Changes in the ^{13}C CPMAS NMR spectra also point to the degradation of surface oleic acid molecules. Indeed, an overall decrease in signal-to-noise ratio in comparison to the non-irradiated grafted nanorods was observed, together with a reduction in intensity of the ^{13}C resonances of the aliphatic chain relative to the carboxylate ones, the decrease being more pronounced for the C atoms of the alkene bond (at ~ 130 ppm) than those of the CH_2 and CH_3 groups (between 5 and 45 ppm) (Figure 3.13d). It is worth noting that the changes in IR and NMR signatures of OA observed here appear to be caused by the ZnO nanorods and not the photoreactivity of OA alone, because no variations were observed by IR or ^{13}C NMR for the Zn-OA coordination polymer under similar irradiation conditions (see Annexe III, Figure III-14). Taken together, all these observations are in line with previous investigations on the photodecomposition of organic molecules at the surface of ZnO, which can lead to a shortening of the organic chain of fatty acids,[7] and eventually to the formation of CO_2 and H_2O.[79]

^{17}O MAS NMR analyses were found to provide further information on the reactions occurring at the surface of the grafted nanorods upon irradiation (Figure 3.14a). Indeed, while no strong difference was noticed after simple heating, a decrease in the relative intensity of the carboxylic resonances with respect to the signal coming from the ZnO nanoparticles core signal at ~ -18 ppm was observed after irradiation, which is consistent with the photodegradation of part of the organic molecules at the surface of ZnO. More interestingly, a new signal was observed at ~ -28 ppm, which can be assigned to oxygen surface sites, based on previous ^{17}O NMR studies of ZnO nanorods.[73-74] Considering the small number of oxygen surface sites in comparison to bulk for this size of nanorods, such surface sites are not expected to be readily detectable in absence of isotopic labeling. As a matter of fact, this new signal was found to be absent from the ^{17}O MAS NMR spectra of the bare nanorods and nanorods grafted with non-labeled OA after 6 h irradiation (see Annexe III, Figures III-12 and III-13). Overall, this shows that these surface oxygen atoms have become enriched in ^{17}O as a consequence of the irradiation of the grafted ^{17}O-labeled OA, as schematically illustrated in Figure 3.14b.

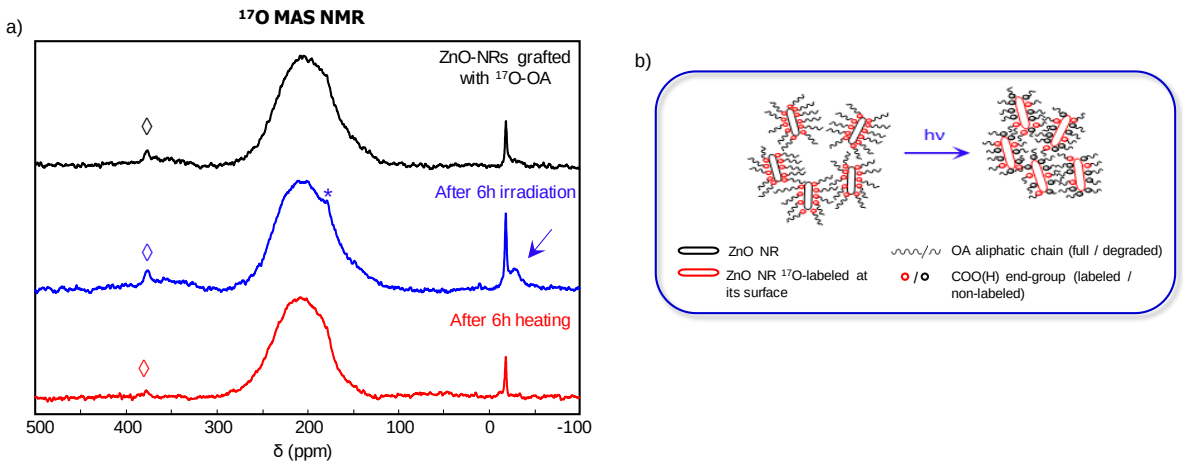

Figure 3.14: a) ^{17}O MAS NMR characterization of ZnO nanorods functionalized by with ^{17}O-enriched oleic acid (OA), before (black) and after 6 h hours of irradiation (blue) or heat-treatment (red). For the ^{17}O MAS NMR spectrum recorded after UV irradiation, the blue arrow points to the enriched surface sites. "*" symbols correspond to spinning sidebands, and "◊" symbols to the natural abundance signal of the zirconia rotor. All NMR acquisition parameters can be found in Annexe III (Tables III-2). b) Schematic illustration of the different processes occurring upon irradiation of the grafted nanorods.

To the best of our knowledge, direct experimental evidence of oxygen exchange/transfer processes occurring during the photodecomposition of organic molecules at the surface of ZnO had not been provided so far, and could not have been revealed by other characterization techniques like XPS, IR or photoluminescence spectroscopy. This clearly shows the added value of having synthesized ^{17}O-enriched molecules for reaching atomic-level insight into the different photocatalytic reactions at the surface of ZnO. More generally speaking, considering the complexity of (photo)catalytic processes, and the numerous challenges related to rationalizing and optimizing the properties of catalysts, similar strategies would be of interest for other catalytic reactions which can involve oxygen exchange/transfer steps.

CONCLUSION

In this chapter, new levels of structural insight were reached for two systems which have been studied and used in a many research fields: [31, 33, 35, 37-38, 60] crystalline Zn oleate, and OA functionalized ZnO nanoparticles. The high level of ^{17}O-labeling enabled high-resolution NMR analyses to be performed in reasonable experimental time, from which fine structural information could be obtained for the first time. In the former case, different bidentate bridging modes of oleate ligands to Zn^{2+} could be resolved, which were shown to differ in very small changes in the Zn···O distances, estimated to only ~ 0.01 Å. Such level of insight could not have been reached by more standard ^{13}C solid-state NMR analyses, which points to the added value of performing ^{17}O NMR studies for helping understanding the structure of fatty-acid phases for which no crystal structure is yet available. In the latter case, direct insight into the mode of binding and reactivity of oleic acid molecules at the surface of ZnO was reached, by looking at the carboxylic oxygen atoms. The predominance of the oleate form at the nanoparticle surface was thereby demonstrated, and structural changes occurring after irradiation were evidenced, including the ^{17}O-isotopic enrichment of the nanoparticle surface, which occurs in addition to the photodegradation processes of grafted ^{17}O-labeled oleic acid molecules. This type of information on the reactivity of organic-mineral interfaces had not been provided so far, and could only have been accessed using ^{17}O NMR. Given the number of studies aiming at understanding and optimizing photocatalytic processes taking place at the surface of ZnO nanoparticles, depending on their size and shape, being able to achieve such atomic-level insight will clearly be beneficial, by allowing to go one step further in comparison to more conventional spectroscopic analyses.[7, 78, 80]

The fine structural investigations described here were made possible by the high level of enrichment oxygen-isotope enrichment of the fatty acids, and the possibility to produce these enriched molecules on a large scale. Mechanochemistry was found to be very well suited for this purpose, allowing up to gram quantities of these labeled molecules to be obtained in high yield and at reasonable cost in just a few hours (~1/2 day of manipulation). Considering that very few protocols had been proposed so far for the oxygen-isotopic labeling of fatty acids, none of which was as efficient for ^{17}O NMR purposes, this work clearly opens new perspectives for advanced structural studies of other complex molecular and materials systems involving fatty acids, such as other metal soaps, grafted nanoparticles (including with other photocatalysts like TiO_2), or even more complex (nano)formulations, such as those developed for oil-paints, sunscreens, or nanolubricants.

REFERENCES

1. Lynch, M. L., Acid-soaps. *COCIS* **1997,** *2* (5), 495-500.
2. de Mul, M. N. G.; Davis, H. T.; Evans, D. F.; Bhave, A. V.; Wagner, J. R., Solution Phase Behavior and Solid Phase Structure of Long-Chain Sodium Soap Mixtures. *Langmuir* **2000,** *16* (22), 8276-8284.
3. Mehnert, W.; Mäder, K., Solid lipid nanoparticles: production, characterization and applications. *Adv. Drug Deliv. Rev.* **2012,** *64*, 83-101.
4. Izgu, E. C.; Björkbom, A.; Kamat, N. P.; Lelyveld, V. S.; Zhang, W.; Jia, T. Z.; Szostak, J. W., N-Carboxyanhydride-Mediated Fatty Acylation of Amino Acids and Peptides for Functionalization of Protocell Membranes. *J. Am. Chem. Soc.* **2016,** *138* (51), 16669-16676.
5. Ulman, A., Formation and Structure of Self-Assembled Monolayers. *Chem. Rev.* **1996,** *96* (4), 1533-1554.
6. Zherebetskyy, D.; Scheele, M.; Zhang, Y.; Bronstein, N.; Thompson, C.; Britt, D.; Salmeron, M.; Alivisatos, P.; Wang, L.-W., Hydroxylation of the surface of PbS nanocrystals passivated with oleic acid. *Science* **2014,** *344* (6190), 1380-1384.
7. Kwak, G.; Seol, M.; Tak, Y.; Yong, K., Superhydrophobic ZnO nanowire surface: chemical modification and effects of UV irradiation. *J. Phys. Chem. C* **2009,** *113* (28), 12085-12089.
8. Oliva-Puigdomènech, A.; De Roo, J.; Kuhs, J.; Detavernier, C.; Martins, J. C.; Hens, Z., Ligand Binding to Copper Nanocrystals: Amines and Carboxylic Acids and the Role of Surface Oxides. *Chem. Mater.* **2019,** *31* (6), 2058-2067.
9. Zhang, J.; Zhang, H.; Cao, W.; Pang, Z.; Li, J.; Shu, Y.; Zhu, C.; Kong, X.; Wang, L.; Peng, X., Identification of Facet-Dependent Coordination Structures of Carboxylate Ligands on CdSe Nanocrystals. *J. Am. Chem. Soc.* **2019,** *141* (39), 15675-15683.
10. Pang, Z.; Zhang, J.; Cao, W.; Kong, X.; Peng, X., Partitioning surface ligands on nanocrystals for maximal solubility. *Nat. Commun.* **2019,** *10* (1), 2454.
11. Pawsey, S.; Yach, K.; Halla, J.; Reven, L., Self-Assembled Monolayers of Alkanoic Acids: A Solid-State NMR Study. *Langmuir* **2000,** *16* (7), 3294-3303.
12. Rowat, A. C.; Kitson, N.; Thewalt, J. L., Interactions of oleic acid and model stratum corneum membranes as seen by 2H NMR. *Int. J. Pharm.* **2006,** *307* (2), 225-231.
13. Catalano, J.; Murphy, A.; Yao, Y.; Zumbulyadis, N.; Centeno, S. A.; Dybowski, C., Molecular dynamics of palmitic acid and lead palmitate in cross-linked linseed oil films: Implications from deuterium magnetic resonance for lead soap formation in traditional oil paintings. *Solid State Nucl. Magn. Res.* **2018,** *89*, 21-26.
14. Catalano, J.; Di Tullio, V.; Wagner, M.; Zumbulyadis, N.; Centeno, S. A.; Dybowski, C., Review of the use of NMR spectroscopy to investigate structure, reactivity, and dynamics of lead soap formation in paintings. *Magn. Res. Chem.* **2020,** *58* (9), 798-811.
15. Chen, Y.; Dorn, R. W.; Hanrahan, M. P.; Wei, L.; Blome-Fernández, R.; Medina-Gonzalez, A. M.; Adamson, M. A. S.; Flintgruber, A. H.; Vela, J.; Rossini, A. J., Revealing the Surface Structure of CdSe Nanocrystals by Dynamic Nuclear Polarization-Enhanced 77Se and 113Cd Solid-State NMR Spectroscopy. *J. Am. Chem. Soc.* **2021,** *143* (23), 8747-8760.
16. El'man, A. R.; Batov, A. E. Process for preparation of carbon-13-labeled saturated aliphatic carboxylic acids by hydrocarboxylation of α-olefins with labeled carbon monoxide and water and processes for preparing their derivatives. Patent # RU2311402C1, **2007**.
17. Le, P. M.; Fraser, C.; Gardner, G.; Liang, W.-W.; Kralovec, J. A.; Cunnane, S. C.; Windust, A. J., Biosynthetic production of universally 13C-labelled polyunsaturated fatty acids as reference materials for natural health product research. *Anal. Bioanal. Chem.* **2007,** *389* (1), 241-249.
18. Tortajada, A.; Duan, Y.; Sahoo, B.; Cong, F.; Toupalas, G.; Sallustrau, A.; Loreau, O.; Audisio, D.; Martin, R., Catalytic Decarboxylation/Carboxylation Platform for Accessing Isotopically Labeled Carboxylic Acids. *ACS Catalysis* **2019,** *9* (7), 5897-5901.
19. Vereshchagin, A. L.; Gorshkov, A. G.; Glyzina, O. Y.; Belikova, A. S.; Basharina, T. N.; Lyubochko, S. A.; Volokitina, N. A. Method for obtaining ^{13}C isotope labeled polyunsaturated fatty acids. Patent #RU2361922C1, **2009**.
20. Sparrow, J. T.; Patel, K. M.; Morrisett, J. D., Synthesis of carbon-13-labeled tetradecanoic acids. *J. Lipid Res.* **1983,** *24* (7), 938-941.
21. Wu, G., ^{17}O NMR studies of organic and biological molecules in aqueous solution and in the solid state. *Progr. Nucl. Magn. Res. Spectrosc.* **2019,** *114-115*, 135-191.
22. Wu, G., Solid-State ^{17}O NMR studies of organic and biological molecules: Recent advances and future directions. *Solid State Nucl. Magn. Res.* **2016,** *73*, 1-14.
23. Keeler, E. G.; Michaelis, V. K.; Wilson, C. B.; Hung, I.; Wang, X.; Gan, Z.; Griffin, R. G., High-Resolution ^{17}O NMR Spectroscopy of Structural Water. *J. Phys.Chem. B* **2019,** *123* (14), 3061-3067.

24. Perras, F. A.; Wang, Z.; Naik, P.; Slowing, I. I.; Pruski, M., Natural Abundance ^{17}O DNP NMR Provides Precise O−H Distances and Insights into the Brønsted Acidity of Heterogeneous Catalysts. *Angew. Chem. Int. Ed.* **2017,** *56* (31), 9165-9169.
25. Bignami, G. P. M.; Davis, Z. H.; Dawson, D. M.; Morris, S. A.; Russell, S. E.; McKay, D.; Parke, R. E.; Iuga, D.; Morris, R. E.; Ashbrook, S. E., Cost-effective ^{17}O enrichment and NMR spectroscopy of mixed-metal terephthalate metal–organic frameworks. *Chem. Sci.* **2018,** *9* (4), 850-859.
26. Martins, V.; Xu, J.; Wang, X.; Chen, K.; Hung, I.; Gan, Z.; Gervais, C.; Bonhomme, C.; Jiang, S.; Zheng, A.; Lucier, B. E. G.; Huang, Y., Higher Magnetic Fields, Finer MOF Structural Information: ^{17}O Solid-State NMR at 35.2 T. *J. Am. Chem. Soc.* **2020**.
27. Ashbrook, S. E.; Smith, M. E., Solid state ^{17}O NMR—an introduction to the background principles and applications to inorganic materials. *Chem. Soc. Rev.* **2006,** *35* (8), 718-735.
28. Otero, V.; Sanches, D.; Montagner, C.; Vilarigues, M.; Carlyle, L.; Lopes, J. A.; Melo, M. J., Characterisation of metal carboxylates by Raman and infrared spectroscopy in works of art. *J. Raman Spectrosc.* **2014,** *45* (11-12), 1197-1206.
29. Robinet, L.; Corbeil, M.-C., The Characterization of Metal Soaps. *Stud. Conserv.* **2003,** *48* (1), 23-40.
30. Maines, C. A.; Rogala, D.; Lake, S.; Mecklenburg, M., Deterioration in Abstract Expressionist Paintings: Analysis of Zinc Oxide Paint Layers in Works from the Collection of the Hirshhorn Museum and Sculpture Garden, Smithsonian Institution. *MRS Proceedings* **2011,** *1319*, mrsf10-1319-ww04-01.
31. Glassy, B. A.; Cossairt, B. M., Ternary synthesis of colloidal Zn_3P_2 quantum dots. *Chem. Commun.* **2015,** *51* (25), 5283-5286.
32. Zhang, L.; Yin, L.; Wang, C.; lun, N.; Qi, Y.; Xiang, D., Origin of Visible Photoluminescence of ZnO Quantum Dots: Defect-Dependent and Size-Dependent. *J. Phys. Chem. C* **2010,** *114* (21), 9651-9658.
33. Fang, X.; Jiang, L.; Gong, Y.; Li, J.; Liu, L.; Cao, Y., The presence of oleate stabilized ZnO nanoparticles (NPs) and reduced the toxicity of aged NPs to Caco-2 and HepG2 cells. *Chem. Biol. Interact.* **2017,** *278*, 40-47.
34. Smijs, T. G.; Pavel, S., Titanium dioxide and zinc oxide nanoparticles in sunscreens: focus on their safety and effectiveness. *Nanotechnol. Sci. Appl.* **2011,** *4*, 95-112.
35. Yin, H.; Casey, P. S.; McCall, M. J.; Fenech, M., Effects of Surface Chemistry on Cytotoxicity, Genotoxicity, and the Generation of Reactive Oxygen Species Induced by ZnO Nanoparticles. *Langmuir* **2010,** *26* (19), 15399-15408.
36. Artesani, A.; Gherardi, F.; Nevin, A.; Valentini, G.; Comelli, D., A Photoluminescence Study of the Changes Induced in the Zinc White Pigment by Formation of Zinc Complexes. *Materials* **2017,** *10* (4), 340.
37. Hermans, J. J.; Baij, L.; Koenis, M.; Keune, K.; Iedema, P. D.; Woutersen, S., 2D-IR spectroscopy for oil paint conservation: Elucidating the water-sensitive structure of zinc carboxylate clusters in ionomers. *Sci. Adv.* **2019,** *5* (6), eaaw3592.
38. Baij, L.; Hermans, J. J.; Keune, K.; Iedema, P., Time-Dependent ATR-FTIR Spectroscopic Studies on Fatty Acid Diffusion and the Formation of Metal Soaps in Oil Paint Model Systems. *Angew. Chem. Int. Ed.* **2018,** *57* (25), 7351-7354.
39. Fanelli, F.; Mastrangelo, A. M.; Fracassi, F., Aerosol-Assisted Atmospheric Cold Plasma Deposition and Characterization of Superhydrophobic Organic–Inorganic Nanocomposite Thin Films. *Langmuir* **2014,** *30* (3), 857-865.
40. Barman, S.; Vasudevan, S., Mixed Saturated−Unsaturated Alkyl-Chain Assemblies: Solid Solutions of Zinc Stearate and Zinc Oleate. *J. Phys. Chem. B* **2007,** *111* (19), 5212-5217.
41. Barman, S.; Vasudevan, S., Contrasting Melting Behavior of Zinc Stearate and Zinc Oleate. *J. Phys. Chem. B* **2006,** *110* (2), 651-654.
42. Choi, S.-H.; Kim, E.-G.; Park, J.; An, K.; Lee, N.; Kim, S. C.; Hyeon, T., Large-Scale Synthesis of Hexagonal Pyramid-Shaped ZnO Nanocrystals from Thermolysis of Zn−Oleate Complex. *J. Phys. Chem. B* **2005,** *109* (31), 14792-14794.
43. Reinoso, D. M.; Damiani, D. E.; Tonetto, G. M., Zinc carboxylic salts used as catalyst in the biodiesel synthesis by esterification and transesterification: Study of the stability in the reaction medium. *Appl. Catal. A-Gen.* **2012,** *449*, 88-95.
44. Xiangrong, K.; Jun, Z.; Xiaowei, Y.; Yanwei, Z., Ethanol-assisted synthesis of $Zn_{0.5}Fe_{2.5}O_4$ nanocrystals in thermal solvent of paraffin. *J. Alloys Compd.* **2008,** *464* (1), 418-421.
45. Sehmi, S. K.; Noimark, S.; Bear, J. C.; Peveler, W. J.; Bovis, M.; Allan, E.; MacRobert, A. J.; Parkin, I. P., Lethal photosensitisation of Staphylococcus aureus and Escherichia coli using crystal violet and zinc oxide-encapsulated polyurethane. *J. Mater. Chem. B* **2015,** *3* (31), 6490-6500.
46. Corbeil, M.-C.; Robinet, L., X-ray powder diffraction data for selected metal soaps. *Powder Diffr.* **2002,** *17* (1), 52-60.
47. Kim, T.; Jung, Y. K.; Lee, J.-K., The formation mechanism of CdSe QDs through the thermolysis of Cd(oleate)2 and TOPSe in the presence of alkylamine. *J. Mater. Chem. C* **2014,** *2* (28), 5593-5600.

48. Dong, J.; Weiss, R. A., Shape Memory Behavior of Zinc Oleate-Filled Elastomeric Ionomers. *Macromolecules* **2011,** *44* (22), 8871-8879.
49. Zeleňák, V.; Vargová, Z.; Györyová, K., Correlation of infrared spectra of zinc(II) carboxylates with their structures. *Spectrochim. Acta A Mol. Biomol. Spectrosc.* **2007,** *66* (2), 262-272.
50. Ishioka, T.; Shibata, Y.; Takahashi, M.; Kanesaka, I., Vibrational spectra and structures of zinc carboxylates II. Anhydrous zinc acetate and zinc stearate. *Spectrochim. Acta A Mol. Biomol. Spectrosc.* **1998,** *54* (12), 1811-1818.
51. Mesbah, A. I) Cristallochimie des Carboxylates Métalliques Inhibiteurs de la Corrosion de Métaux et II) Structure et Magnétisme de Dicarboxylates (téréphtalate et thiophène) de Métaux de Transition. PhD thesis, **2008**.
52. Kim, Y. S.; Hochstrasser, R. M., Applications of 2D IR Spectroscopy to Peptides, Proteins, and Hydrogen-Bond Dynamics. *J. Phys. Chem. B* **2009,** *113* (24), 8231-8251.
53. Pickard, C. J.; Mauri, F., All-electron magnetic response with pseudopotentials: NMR chemical shifts. *Phys. Rev. B* **2001,** *63* (24), 245101.
54. Charpentier, T., The PAW/GIPAW approach for computing NMR parameters: A new dimension added to NMR study of solids. *Solid State Nucl. Magn. Reson.* **2011,** *40* (1), 1-20.
55. Harris, R. A.; van der Walt, H.; Shumbula, P. M., Engineered Inorganic/Organic-Core/Shell Magnetic Fe_xO_y Nanoparticles with Oleic Acid and/or Oleylamine As Capping Agents. *Curr. Pharm. Des.* **2015,** *21* (37), 5369-5388.
56. Sun, S.; Zeng, H.; Robinson, D. B.; Raoux, S.; Rice, P. M.; Wang, S. X.; Li, G., Monodisperse MFe_2O_4 (M = Fe, Co, Mn) Nanoparticles. *J. Am. Chem. Soc.* **2004,** *126* (1), 273-279.
57. Sun, S.; Murray, C. B.; Weller, D.; Folks, L.; Moser, A., Monodisperse FePt Nanoparticles and Ferromagnetic FePt Nanocrystal Superlattices. *Science* **2000,** *287* (5460), 1989.
58. Sun, S.; Zeng, H., Size-Controlled Synthesis of Magnetite Nanoparticles. *J. Am. Chem. Soc.* **2002,** *124* (28), 8204-8205.
59. Wu, N.; Fu, L.; Su, M.; Aslam, M.; Wong, K. C.; Dravid, V. P., Interaction of Fatty Acid Monolayers with Cobalt Nanoparticles. *Nano Lett.* **2004,** *4* (2), 383-386.
60. McLaren, A.; Valdes-Solis, T.; Li, G.; Tsang, S. C., Shape and Size Effects of ZnO Nanocrystals on Photocatalytic Activity. *J. Am. Chem. Soc.* **2009,** *131* (35), 12540-12541.
61. Wang, H.; Lian, Y., A mechanistic study of oleic acid-mediated solvothermal shape controllable preparation of zinc oxide nanostructures. *J. Alloys Compd.* **2014,** *594*, 141-147.
62. Chen, L.; Holmes, J. D.; Ramírez-García, S.; Morris, M. A., Facile Synthesis of Monodisperse ZnO Nanocrystals by Direct Liquid Phase Precipitation. *J. Nanomater.* **2011,** *2011*, 853832.
63. Chen, L.; Xu, J.; Holmes, J. D.; Morris, M. A., A Facile Route to ZnO Nanoparticle Superlattices: Synthesis, Functionalization, and Self-Assembly. *J. Phys. Chem. C* **2010,** *114* (5), 2003-2011.
64. Pacholski, C.; Kornowski, A.; Weller, H., Self-Assembly of ZnO: From Nanodots to Nanorods. *Angew. Chem. Int. Ed.* **2002,** *41* (7), 1188-1191.
65. Sun, B.; Sirringhaus, H., Solution-Processed Zinc Oxide Field-Effect Transistors Based on Self-Assembly of Colloidal Nanorods. *Nano Lett.* **2005,** *5* (12), 2408-2413.
66. Lee, D.; Wolska-Pietkiewicz, M.; Badoni, S.; Grala, A.; Lewiński, J.; De Paëpe, G., Disclosing Interfaces of ZnO Nanocrystals Using Dynamic Nuclear Polarization: Sol-Gel versus Organometallic Approach. *Angew. Chem. Int. Ed.* **2019,** *58* (48), 17163-17168.
67. Noei, H.; Wöll, C.; Muhler, M.; Wang, Y., Activation of Carbon Dioxide on ZnO Nanoparticles Studied by Vibrational Spectroscopy.*J. Phys. Chem. C* **2011,** *115* (4), 908-914.
68. Gankanda, A.; Cwiertny, D. M.; Grassian, V. H., Role of Atmospheric CO_2 and H_2O Adsorption on ZnO and CuO Nanoparticle Aging: Formation of New Surface Phases and the Impact on Nanoparticle Dissolution. *J. Phys. Chem. C* **2016,** *120* (34), 19195-19203.
69. Andelman, T.; Gong, Y.; Polking, M.; Yin, M.; Kuskovsky, I.; Neumark, G.; O'Brien, S., Morphological Control and Photoluminescence of Zinc Oxide Nanocrystals. *J. Phys. Chem. B* **2005,** *109* (30), 14314-14318.
70. Hong, R.; Pan, T.; Qian, J.; Li, H., Synthesis and surface modification of ZnO nanoparticles. *Chem. Eng. J.* **2006,** *119* (2), 71-81.
71. Hsiao, C. Y. Y.; Ottaway, C. A.; Wetlaufer, D. B., Preparation of fully deuterated fatty acids by simple method. *Lipids* **1974,** *9* (11), 913-915.
72. Lebail, P.; Buleon, A.; Shiftan, D.; Marchessault, R. H., Mobility of lipid in complexes of amylose–fatty acids by deuterium and 13C solid state NMR. *Carbohydr. Polym.* **2000,** *43* (4), 317-326.
73. Champouret, Y.; Coppel, Y.; Kahn, M. L., Evidence for Core Oxygen Dynamics and Exchange in Metal Oxide Nanocrystals from In Situ 17O MAS NMR. *J. Am. Chem. Soc.* **2016,** *138* (50), 16322-16328.
74. Spataro, G.; Champouret, Y.; Florian, P.; Coppel, Y.; Kahn, M. L., Multinuclear solid-state NMR study: a powerful tool for understanding the structure of ZnO hybrid nanoparticles. *Phys. Chem. Chem. Phys.* **2018,** *20* (18), 12413-12421.

75. Gerothanassis, I. P., Oxygen-17 NMR spectroscopy: Basic principles and applications (Part I). *Progr. Nucl. Mag. Res. Spectrosc.* **2010,** *56* (2), 95-197.
76. Peng, Y.-K.; Tsang, S. C. E., Facet-dependent photocatalysis of nanosize semiconductive metal oxides and progress of their characterization. *Nano Today* **2018,** *18*, 15-34.
77. In panel b, the slight increase in intensity observed between 5° and 10° on the powder patterns on the grafted NRs (black) and after 6 h of irradiation (blue) is due to the nature of the sample holder used for these analyses.
78. Kenanakis, G.; Giannakoudakis, Z.; Vernardou, D.; Savvakis, C.; Katsarakis, N., Photocatalytic degradation of stearic acid by ZnO thin films and nanostructures deposited by different chemical routes. *Catal. Today* **2010,** *151* (1), 34-38.
79. Ong, C. B.; Ng, L. Y.; Mohammad, A. W., A review of ZnO nanoparticles as solar photocatalysts: Synthesis, mechanisms and applications. *Renew. Sust. Energ. Rev.* **2018,** *81*, 536-551.
80. Yin, M.; Gu, Y.; Kuskovsky, I. L.; Andelman, T.; Zhu, Y.; Neumark, G. F.; O'Brien, S., Zinc Oxide Quantum Rods. *J. Am. Chem. Soc.* **2004,** *126* (20), 6206-6207.
81. It is worth noting that the CH_2 resonance in alpha of the carboxylic group was also found to be broad and clearly shifted to high frequencies compared to a concentrated solution of oleic acid in DMSO-*d6* (37.5 vs 33.8 ppm), as expected upon grafting of fatty acids at the surface of oxide nanoparticles (cf. ref 11). This implies that this CH_2 moiety is not as mobile as the others.
82. Although the ^{13}C chemical shift of the grafted acetate groups is very similar to the one of oleic acid-functionalized NPs (180.5 vs 181.1 ppm), the amount of residual surface acetates after functionalization by oleic acid is small, as shown in the Annexe III (Figure III-11).

ANNEXE III

ZN-OA AND ZNO NPS - EXPERIMENTAL PART

III-A) MATERIALS AND METHODS

III-A1) Reagents

The following reagents were used as received: zinc chloride ($ZnCl_2$, Aldrich, 99.99%), and sodium hydroxide (NaOH, Acros Organics), zinc acetate dihydrate ($C_4H_{10}O_6Zn$, Sigma-Aldrich), potassium hydroxide (KOH, Sigma-Aldrich, ≥ 85%), methanol (HPLC - isocratic grade, VWR), tetrahydrofurane (THF, ≥ 99.8%, Fisher Chemical). Reagent grade solvents were used in purification protocols.

^{17}O-labeled oleic acid was prepared via mechanochemistry using CDI-activation/hydrolysis procedure. The average enrichment level per carboxylic oxygen was ~ 42 %, as determined by MS.

III-A2) Synthetic equipment

The milling treatments were carried out in a Retsch Mixer Mill 400 apparatus (MM400), using 10 mL stainless-steel grinding jars, containing 10 mm diameter beads. All protocols were first tested using non-labeled water, before performing experiments with ^{17}O-labeled water.

Accelerated ageing tests upon irradiation of ZnO nanorods and Zn-oleate were performed in an ATLAS/SUNTEST CPS+ apparatus. The spectrum of this apparatus between 300 and 800 nm mimics that of solar light, but with more powerful radiation (~ 60 mW/cm^2). Powdered samples were deposited such that they cover the inside surface of a closed quartz cuvettes, and then irradiated for 6 h. Samples were then characterized by ATR-IR, XRD, TEM and solid state NMR.

Accelerated ageing tests upon heat-treatment of ZnO nanorods and Zn-oleate were performed in an oven at 60°C, in absence of light. Powdered samples were placed in glassy vials and heated for 6h, after which they were characterized by ATR-IR, XRD, TEM and solid-state NMR.

III-A3) Characterization protocols

Infrared (IR) spectra were recorded on a Perkin Elmer Spectrum 2 FT-IR instrument. The attenuated total reflectance (ATR) measurement mode was used (diamond crystal), and measurements were performed in the 400-4000 cm^{-1} range.

Powder XRD analyses were carried out on an X'Pert MPD diffractometer using Cu $K_{\alpha 1}$ radiation (λ = 1.5406 Å) with the operation voltage and current maintained at 40 kV and 25 mA, respectively. Diffractograms were recorded between 5° and 70° in 2θ, with a step size of 0.017°, and a time per step of 20 to 40 s.

Transition electron microscopy (TEM) analyses were performed on a LaB6 JEOL 1400 Plus electron microscope operating at 100 kV. Samples for TEM were prepared by depositing a dispersed suspension of nanorods in THF onto carbon-supported copper grids, and left to dry overnight at air, prior to analyses.

Thermal gravimetric analyses (TGA) were carried out under air on a TA instrument Q500, at a heating rate of 10 °C/min up to 600 °C, with a flow rate of 60 mL/min.

The Brunauer-Emmett-Teller (BET) specific surface area of ZnO NRs was measured using a Tristar surface area and porosity analyzer. The measurement was performed by N_2 adsorption at liquid nitrogen temperature after degassing for 16 h at 80 °C.

The majority of ^{13}C solid state NMR experiments were performed on a VNMRS 300 MHz (7.05 T) NMR spectrometer, using a Varian 3.2 mm HX probe tuned to ^{1}H (299.99 MHz) and ^{13}C (75.43 MHz). Oleic acid was analyzed on a VNMRS 400 MHz (9.4 T)

NMR spectrometer, using a Varian 3.2 mm HXY probe tuned to ^{1}H (399.92 MHz) and ^{13}C (100.56 MHz), and setting the temperature unit to –20°C to freeze the sample. A high resolution ^{13}C NMR spectrum of enriched Zn-oleate was also recorded on a Varian VNMRS 600 MHz (14.1 T) NMR spectrometer, using a Varian 3.2 mm HX probe tuned to ^{1}H (599.82 MHz) and ^{13}C (150.81 MHz). All 1D ^{13}C NMR spectra were recorded under MAS (Magic Angle Spinning) conditions, with a spinning frequency 12 kHz. A $^{1}H \rightarrow ^{13}C$ CPMAS NMR sequence was used with a 4 µs ^{1}H excitation pulse, followed by a ramped CP pulse of 8 ms contact time, and applying spinal-64 ^{1}H-decoupling during acquisition (~ 63 kHz RF). This long contact time was used to suppress the background signals from the probe, caps and inserts (as verified by control experiments performed in the same conditions on the empty rotors). All acquisition parameters for 1D CPMAS experiments are summarized in Table III-1. ^{1}H and ^{13}C chemical shifts were referenced to adamantane at 1.8 ppm and 38.5 ppm (high frequency peak), respectively.

Table III-1: ^{13}C solid state NMR acquisition parameters.

Sample	Magnetic field B_0 [T]	MAS frequency [kHz]	Temp. set [°C]	Recycle delay (D1) [s]	Contact time [ms]	Acq. time [ms]	Number of scans (NS)	Exp. time
Oleic acid								
OA	9.4	12	-20	3	8	40	2000	~ 1h45
Zn-OA								
as-prepared	7.1	12	No reg.	2	8	40	4700	~ 2h45
	14.1	12	No reg.	4	8	40	620	~ 0h45
irradiated	7.1	12	No reg.	2	8	40	4700	~ 2h45
heated	7.1	12	No reg.	2	8	40	4700	~ 2h45
^{17}O-OA grafted NRs								
as-prepared	7.1	12	No reg.	2	8	40	4700	~ 2h45
irradiated	7.1	12	No reg.	2	8	40	8000	~ 4h30
heated	7.1	12	No reg.	2	8	40	6500	~ 3h45
Non-labeled OA-grafted NRs								
as-prepared	7.1	12	No reg.	2	8	40	6500	~ 3h45
irradiated	7.1	12	No reg.	2	8	40	6500	~ 3h45
heated	7.1	12	No reg.	2	8	40	6500	~ 3h45
Bare NRs								
as-prepared	7.1	12	No reg.	2	8	40	8400	~ 4h45
irradiated	7.1	12	No reg.	2	8	40	8200	~ 4h45
heated	7.1	12	No reg.	2	8	40	8400	~ 4h45

^{17}O solid state NMR experiments were performed on a VNMRS 600 MHz (14.1 T) NMR spectrometer, using a 3.2 mm probe tuned to ^{1}H (599.82 MHz) and ^{17}O (81.31 MHz). Three types of probes were used, depending on the availability of the equipment: a 3.2 mm Varian HX probe, a 3.2 mm Varian HXY probe, or a Phoenix NMR HXY probe equipped with a 3.2 mm probe head. Spectra were recorded under MAS conditions, using a spinning frequency 16 kHz. A double frequency sweep (DFS)[1] excitation scheme was used for ^{17}O-signal enhancement, followed by an excitation pulse of 1 to 2 µs (1 µs pulse for all spectra recorded on the ZnO NRs, corresponding to a $\pi/12$ excitation for $H_2O_{(l)}$). No ^{1}H-decoupling was applied during acquisition (as no significant impact of ^{1}H decoupling on the ^{17}O lineshapes was observed). More details on the acquisition conditions are reported in Table III-2. For the variable-temperature ^{17}O NMR study of the grafted ZnO-NRs (between -100°C and +60°C), similar acquisition conditions were used as for the as-prepared NRs. For the study on grafted ZnO-NRs under ageing conditions, ^{17}O MAS NMR spectra were recorded with the temperature

regulation unit set to -20°C. ^{17}O chemical shifts were referenced to D_2O at –2.7 ppm (which corresponds to tap-water at 0 ppm).

Additional ^{17}O solid state NMR experiments were performed at ultra-high magnetic field on the 1.5 GHz (35.2 T) SCH-instrument in Tallahassee.[2] For the Zn-oleate coordination polymer, a 3.2 mm single-channel MAS probe was used, which was tuned to ^{17}O (ν_0 = 203.4 MHz), and spun at 18 kHz. A Hahn-echo spectrum was acquired using 4 and 8 µs pulses, an echo delay of 1 rotor period, and a recycle delay of 0.5 s, and collecting 508 transients. A 3QMAS NMR spectrum was acquired using a shifted-echo pulse sequence with the SPAM conversion scheme.[3] The 3Q excitation and conversion pulses are 3.75 and 1.25 µs with about 100 kHz rf field, respectively, and the soft echo pulses are 4 and 8 µs. 192 scans were acquired for each of the rotor synchronized t_1 increments. For the ^{17}O-OA grafted nanorods, experiments were performed on a 2.0 mm HX MAS probe, spinning at 32 kHz (and without temperature regulation). A WURST-enhancement was used,[1] followed by a Hahn echo, which was acquired using 3 and 6 µs pulses, and an echo delay of 1 rotor period. The recycle delay was set to 0.5 s, and 10240 transients were collected. All ^{17}O chemical shifts were referenced to D_2O at -2.7 ppm.

Table III-2: ^{17}O solid state NMR acquisition parameters used at 14.1 T.

Sample	MAS frequency [kHz]	Temp. reg. [°C]	Recycle delay (D1) [s]	Acq. time [ms]	Number of scans (NS)	Exp. time
Oleic acid						
OA	16	-40	0.8	6	1170	~ 0h15
Zn-OA						
as-prepared	16	Not reg.	2	5	2400	~ 1h15
irradiated	16	-20	2	20	2800	~ 1h30
heated	16	-20	2	20	4000	~ 2h15
^{17}O-OA grafted NRs						
as-prepared	16	-20	1	20	65500	~ 18h30
irradiated	16	-20	1	20	80000	~ 22h45
heated	16	-20	1	20	36000	~ 10h15
Non-labeled OA-grafted NRs						
as-prepared	16	-20	1	20	44400	~ 12h30
irradiated	16	-20	1	20	36000	~ 10h15
heated	16	-20	1	20	36000	~ 10h15
Bare NRs						
as-prepared	16	-20	1	20	5840	~ 1h30
irradiated	16	-20	1	20	5840	~ 1h30
heated	16	-20	1	20	5840	~ 1h30

The ^{23}Na solid state NMR spectrum of Zn-oleate was recorded on a VNMRS 600 MHz (14.1 T) NMR spectrometer, using a 3.2 mm Varian HXY probe tuned to ^{23}Na (158.66 MHz) and ^{1}H (599.82 MHz), and spinning at 20 kHz. A single-pulse experiment was performed using a 0.5 µs excitation pulse (corresponding to a $\pi/12$ excitation for NaCl in solution), and spinal-64 ^{1}H decoupling during acquisition. Spectra were referenced to a 1 mol.L^{-1} solution of NaCl at 0 ppm.

Variable temperature ^{1}H MAS NMR spectra of ^{17}O-enriched OA-grafted nanorods were recorded using a Varian NMR HXY probe, and spinning at 16 kHz. A Hahn-echo spectrum was recorded using a 4 µs 90° pulse. Up to 128 transients were acquired with a recycle delay of 2 to 4 s. Spectra were referenced to adamantane at 1.8 ppm.

Solid state NMR spectra are presented (and fitted) using the DMfit software.[4]

III-A4) GIPAW-DFT calculations

The unit cell parameters were set to the single-crystal XRD parameters[5-6] and kept fixed during geometry optimizations to ensure consistency between experimental and optimized structures. Proton or all atomic positions were then optimized using the VASP (Vienna Ab-initio Simulation Package) code[7] based on the Kohn-Sham Density Functional Theory (DFT) and using a plane-wave pseudopotential approach. The NMR parameters were then calculated within Kohn-Sham DFT using the QUANTUM-ESPRESSO code.[8] The PBE generalized gradient approximation[9] was used and the valence electrons were described by norm-conserving pseudopotentials[10] in the Kleinman Bylander form.[10] The wave functions were expanded on a plane wave basis set with a kinetic energy cut-off of 80 Ry. The integral over the first Brillouin zone was performed using a Monkhorst–Pack 2 × 2 × 2 k-point grid for the charge density and chemical shift tensor calculation. The shielding tensor was computed using the Gauge-Including Projector Augmented Wave (GIPAW) approach,[11] which enables the reproduction of the results of a fully converged all-electron calculation. The isotropic chemical shift δ_{iso} is defined as $\delta_{iso} = [\sigma_{iso} - \sigma_{iso}(ref)]$, where σ_{iso} is the isotropic magnetic shielding and $\sigma_{iso}(ref)$ is the isotropic magnetic shielding of the same nucleus in a reference compound. In the present case, the fit of the linear correlation between the experimental δ_{iso} and the calculated σ_{iso} values of ^{17}O for Na_2SiO_3, α-$Na_2Si_2O_5$, α- and γ-glycine, and α-$SrSiO_3$ enabled the determination of the relation between δ_{iso} and calculated σ_{iso} for the ^{17}O nucleus, as described previously.[12] Diagonalization of the symmetric part of the calculated tensor then provides its principal components σ_{11}, σ_{22}, σ_{33} from which the chemical shift components δ_{11}, δ_{22}, δ_{33} can be calculated. δ_{11}, δ_{22} and δ_{33} are defined such as $|\delta_{33} - \delta_{iso}| \geq |\delta_{11} - \delta_{iso}| \geq |\delta_{22} - \delta_{iso}|$, and $\delta_{iso} = 1/3(\delta_{11} + \delta_{22} + \delta_{33})$. The principal components V_{xx}, V_{yy}, and V_{zz} of the electric field gradient (EFG) tensor defined as $|V_{zz}| \geq |V_{xx}| \geq |V_{yy}|$ are obtained by diagonalization of the tensor. The quadrupolar interaction can then be characterized by the quadrupolar coupling constant C_Q and the asymmetry parameter η_Q, which are defined as: $C_Q = eQV_{zz}/h$ and $\eta_Q = (V_{yy} - V_{xx})/V_{zz}$ (e is the proton charge, h Planck's constant and Q the quadrupole moment of the considered nucleus). The experimental value of the quadrupole moment of ^{17}O ($Q = -25 \times 10^{-30}$ m^2) was used to calculate C_Q.

III-B) SYNTHESIS AND CHARACTERIZATION OF ZN-OLEATE (ZN-OA)

III-B1) Optimized synthetic protocol

Oleic acid labeled in oxygen-17 (83 mg, 0.3 mmol, 2.0 eq.) and sodium hydroxide (12 mg, 0.3 mmol, 2.0 eq.) were introduced successively into a stainless steel grinding jar (10 mL inner volume) containing two stainless steel beads (10 mm diameter). The jar was closed and subjected to grinding for 10 min in the MM400 mixer mill operated at 25 Hz. Zinc chloride (20 mg, 0.15 mmol, 1.0 eq.) was then added into the jar, and the mixture was subjected to further grinding for 15 minutes at 25 Hz. The light grey powder was recovered from the jar and dried under vacuum. Average mass recovered (n = 2): 95 ± 12 mg. The sample was stored in the freezer to avoid potential structural changes, prior to any further analyses or ageing tests.

The OA precursor used here in the synthesis of Zn-oleate had an average ^{17}O-enrichment per carboxylic oxygen of ~ 19%, because it had been prepared using ~ 39.3% ^{17}O-enriched water.

Figure III-1: ATR-IR analysis of zinc oleate synthesis using mechanochemistry.

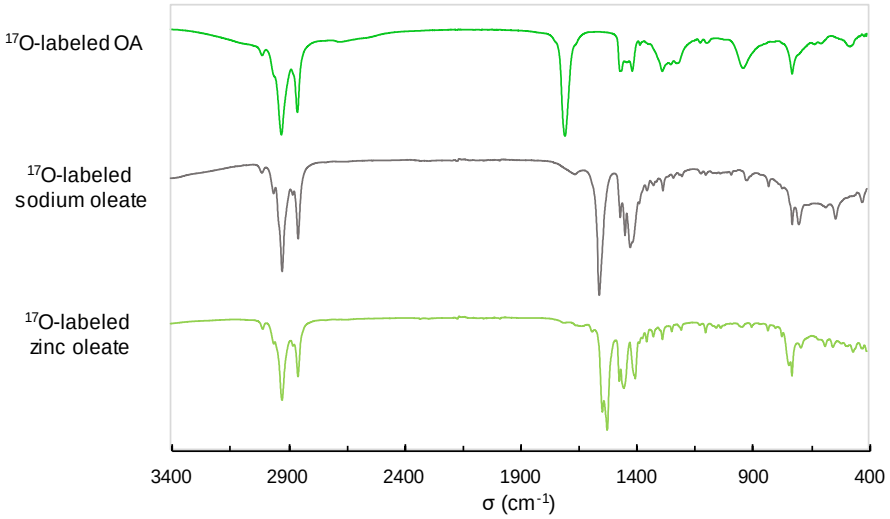

III-B2) Structural analyses

Figure III-2: Multinuclear solid state NMR study of the recovered ^{17}O-enriched Zn-oleate product at 14.1T: a) ^{13}C CPMAS NMR (*inset*: expansion of the α-CH_2 region; see main text for the expansion of the carboxylate region), b) ^{17}O MAS NMR, c) ^{23}Na MAS NMR. Acquisition conditions can be found in section A. "*" symbols correspond to spinning sidebands.

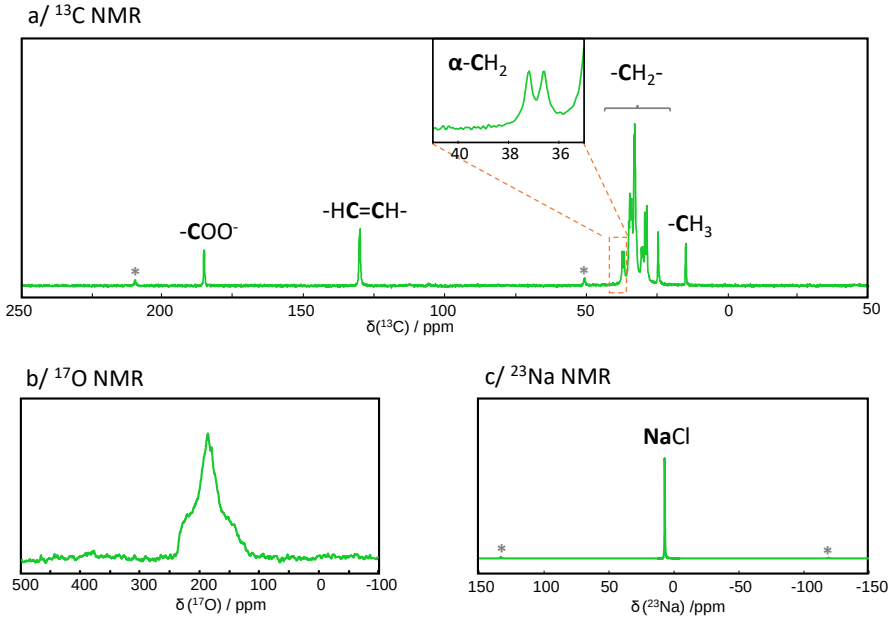

Figure III-3: ATR-IR spectra of Zn-oleate phases prepared by ball-milling, using non-labeled (top) and ^{17}O-enriched (bottom) oleic acid. The wavenumbers of the IR bands which shift upon enrichment are indicated on the spectra.

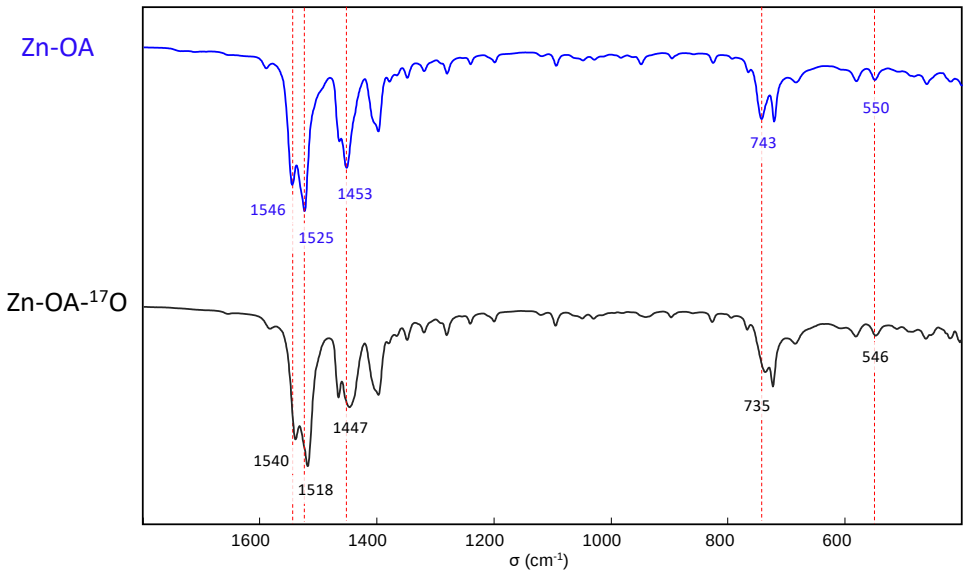

Carboxylate stretching region

In previous IR studies of Zn-oleate, the following assignments can be found:[13-14]

- 1548 and 1526 cm^{-1} : ν_a(COO) vibration modes,
- 1407 and 1398 cm^{-1} : ν_s(COO) vibration modes,
- 1467 and 1455 cm^{-1} : $\delta(CH_2)$ vibration modes.

We observed that in the C=O stretching region, the bands which shift upon ^{17}O labeling are those at 1546, 1525 and 1453 cm^{-1}. In contrast, no shift or broadening is observed in the band centered at 1466 cm^{-1}, nor in the composite band at ~ 1398 cm^{-1}. Hence, based on the IR-band shifts we observed after oxygen-isotopic labeling, we propose the following new assignments in this region:
- 1546 and 1525 cm^{-1}: ν_a(COO) vibration modes,
- ~ 1453 cm^{-1} (broad): ν_s(COO) vibration modes,
- 1466 and 1398 cm^{-1}: $\delta(CH_2)$ vibration modes.

It is worth noting that the re-assignment of the 1453 cm^{-1} band to a ν_s(COO) vibration mode is actually consistent with an IR and Raman study of Zn-acetate.[15]

Low frequency region (400-800 cm^{-1})

In the low frequency region, the bands which shift upon ^{17}O labeling are those at 743 and 550 cm^{-1}, which had not been assigned previously for Zn-oleate.[13] Here, the shifts observed after enrichment show that they both correspond to carboxylate vibration modes. By analogy to studies on Zn-acetate and Zn-stearate, they can be assigned to carboxylate bending and rocking modes, respectively.[15]

Figure III-4: Ultra-high field ^{17}O MAS NMR spectrum of ^{17}O-labeled Zn-oleate at 35.2 T: comparison of the experimental spectrum (black) and of a possible fit (red dashed line), which was performed considering the presence of 2 types of oxygen sites in a 3:1 ratio (purple and green lines). The full spectrum showing spinning sidebands is to the left, and a zoom into the central part of the spectrum to the right. Fits were performed using the int2QUAD option in the DMFit program (and hence CSA and Euler angles are defined as implemented in this program).[4]

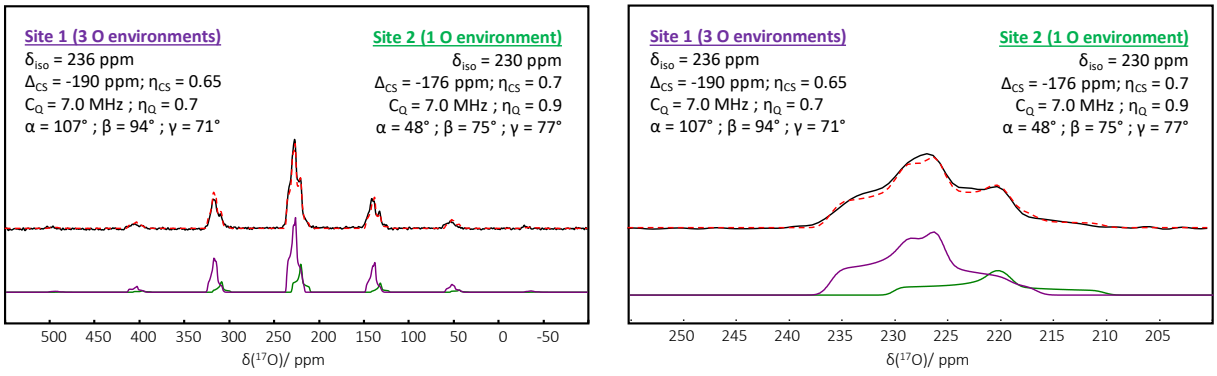

The fits shown above were carried out using δ_{iso}, Δ_{CS}, η_{CS}, C_Q and η_Q values which are globally consistent with *i)* the slices extracted from the high-resolution 3QMAS analysis, and *ii)* the GIPAW-DFT calculations performed on Zn-carboxylates adopting similar coordination modes (see section B3 below). However, further analyses under static conditions at different fields would be needed to confirm/refine the fitted parameters, especially for the high-frequency component of the spectrum, which results from the overlap of 3 different carboxylate oxygens (as described in the main text), which do not necessarily have all ^{17}O NMR parameters and Euler angles identical. This is however beyond the purpose of the current study.

III-B3) GIPAW-DFT calculations of NMR parameters in Zn-carboxylates

Investigations performed so far have shown that the ^{17}O isotropic shifts of carboxylate groups in coordination polymers and MOFs vary depending on the binding mode of the oxygen atoms (μ_1-O, μ_2-O…), the nature of the metal to which they are bound (Al^{3+}, Ga^{3+}, Sc^{3+}, Zr^{4+}, Mg^{2+}…), and the presence of additional water molecules in close proximity to the carboxylate function.[16-17] Hence, it appeared difficult to rationalize the difference in shift observed between the two ^{17}O sites of Zn-oleate by analogy to previously published studies on coordination compounds or MOFs. A computational study was thus performed to determine the sensitivity of ^{17}O NMR parameters to the local environment of oxygen in Zn-carboxylate crystalline phases in which the ligands adopt a bidentate bridging mode, with each carboxylate oxygen linked to one Zn^{2+} ion only, like for Zn-oleate.

The two structures used in the computational study were Zn-pentanoate and Zn-octanoate.[5-6] In both cases, prior to the GIPAW-DFT calculations of NMR parameters,[11] the geometry was optimized by DFT using the VASP software package,[7] keeping the cell parameters fixed, and relaxing either H-positions only, or all atomic positions. Calculated ^{17}O δ_{iso}, C_Q and η_Q values are shown in Table III-3, together with the ^{13}C chemical shifts of the carboxylate groups. The plot of $\delta_{iso}(^{17}O)$ as a function of d(Zn…O) for H-relaxed and fully relaxed models of Zn-pentanoate and Zn-octanoate is shown in Figure III-5. Moreover, the CSA parameters calculated for H-relaxed models of Zn-pentanoate and Zn-octanoate are shown in Table III-4.

Table III-3: GIPAW DFT-calculated ^{17}O NMR parameters and ^{13}C chemical shifts (for the carboxylate), for Zn-pentanoate and Zn-octanoate.

	δ_{iso}/ppm	C_Q/MHz	η_Q			δ_{iso}/ppm	C_Q/MHz	η_Q
Zn-pentanoate (H-relaxed)					**Zn-octanoate (H-relaxed)**			
O1	231.6	6.92	0.99		O11	233.6	-7.09	0.95
O2	239.1	6.98	0.90		O12	241.1	6.79	0.77
O3	233.7	-6.81	0.90		O21	246.7	6.22	0.95
O4	236.9	6.48	0.92		O22	235.8	-6.83	0.87
C1	183.5				C11	182.8		
C6	181.6				C21	184.1		
Zn-pentanoate (all relaxed)					**Zn-octanoate (all relaxed)**			
O1	250.3	-7.20	0.89		O11	248.5	-7.24	0.91
O2	262.1	6.73	0.94		O12	267.2	6.80	0.88
O3	255.3	-7.02	0.80		O21	265.6	-6.29	0.97
O4	263.4	-6.35	0.96		O22	255.8	-6.96	0.79
C1	190.7				C11	191.4		
C6	190.1				C21	190.6		

Figure III-5. Correlation between the calculated ^{17}O isotropic chemical shifts in Zn-pentanoate and Zn-octanoate (H-relaxed and fully-relaxed models), & the Zn…O distance in the corresponding models.

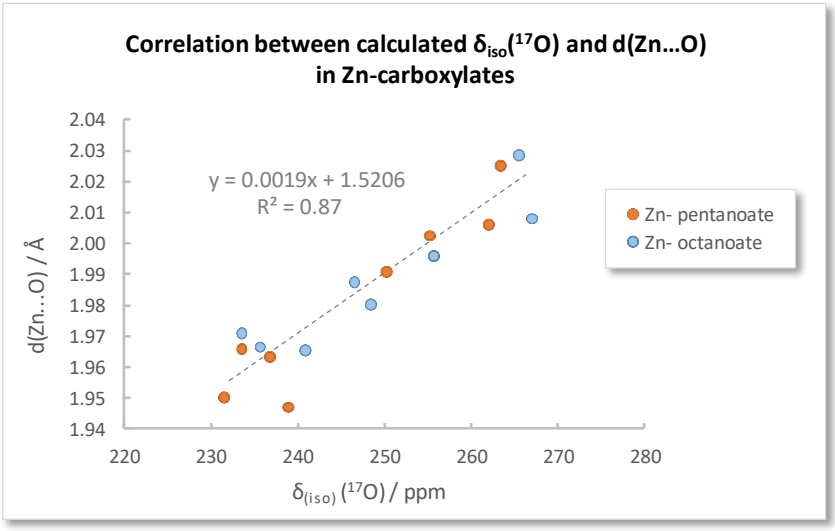

Table III-4. Complete set of GIPAW DFT-calculated ^{17}O NMR parameters for H-relaxed models of Zn-pentanoate and Zn-octanoate, including Euler angles, as defined for fitting NMR spectra with the DMFit program (int2QUAD model).[4]

	δ_{iso}/ppm	δ_{11}/ppm	δ_{22}/ppm	δ_{33}/ppm	C_Q/MHz	η_Q	α/°	β/°	γ/°
Zn-pentanoate (H-relaxed)									
O1	233.6	418.7	230.1	52.1	-7.09	0.95	95	-125	175
O2	241.1	393.6	290.7	38.9	6.79	0.77	0	80	85
O3	246.7	409.4	278.7	51.9	6.22	0.95	175	-85	95
O4	235.8	418.4	236.2	52.8	-6.83	0.87	-55	90	95
Zn-octanoate (H-relaxed)									
O11	231.6	421.6	241.5	31.6	6.92	0.99	35	-95	85
O12	239.1	399.6	278.1	39.5	6.98	0.90	180	100	85
O21	233.7	419.4	235.4	46.2	-6.81	0.90	55	90	-90
O22	236.9	396.4	275.6	38.7	6.48	0.92	175	-95	85

III-C) SYNTHESIS, CHARACTERIZATION AND REACTIVITY STUDIES OF OLEIC-ACID GRAFTED ZNO NANORODS

III-C1) Synthesis of OA-grafted ZnO nanorods (NRs)

III-C1-a) Optimized synthesis of ZnO nanorods

ZnO nanorods (NRs) were prepared by adapting a published method.[18-20] Glassware used for the synthesis was first washed with HCl (1M), and rinsed with distilled water and acetone, and then left to dry at air. Zinc acetate dihydrate (1.9 g, 8.7 mmol, 1.0 eq.) was dissolved in 84 mL of methanol, to which 180 µL of demineralized water were added. Potassium hydroxide (1.0 g, 17.8 mmol, 2.0 eq.) was separately dissolved in 46 mL of methanol, and then added dropwise (during 15 min) into the zinc acetate solution, which was heated in an oil bath at 60 °C and stirred at 750 rpm. After 5 min of addition (1/3 of KOH solution), the reaction mixture turned white. Within 5 minutes after the end of addition, the solution became transparent again. It was stirred in the oil bath for an additional ~ 2h30min (it turned white again after 1h30min). The reaction mixture was then concentrated using a rotary evaporator to ~ 20 - 25 mL volume, and the resulting cloudy solution was left to stir at 250 rpm at 60 °C overnight (~ 18 - 19 h, to be more specific). The white reaction mixture was then cooled down to room temperature and centrifuged for 15 min at 20000 rpm. The supernatant was discarded, and the white powder was washed twice using 20 mL of methanol, followed by centrifugation at 20000 rpm for 15 min, and then dried under vacuum for 2h. The as-formed nanorods (NRs) were obtained with the aspect of brittle transparent crystals, and stored in the freezer wrapped in aluminum foil. They were ground manually before the different analyses (TEM, XRD, BET, IR, solid state NMR) and the subsequent grafting procedure. Their surface area was found to be ~ 100 m^2/g (as measured by N_2 adsorption and BET analysis), and the particle size was on average ~32 ± 7 nm length and 7 ± 2 nm diameter (according to TEM). Average yield (n = 4): 614 ± 21 mg, 85 ± 3 %.

III-C1-b) Optimized ZnO-NR grafting procedure

ZnO-NRs (100 mg) were sonicated in 45 mL of THF for 30 - 60 min (temperature in the ultra-sound bath controlled to be below 30 °C). A solution of ^{17}O-oleic acid in THF (c = 0.073 M, 10.9 mg of OA, V = 524 µL) was then added to the suspension of NRs while stirring at 325 rpm. The reaction vessel was closed, parafilmed, covered with aluminum foil, and stirred at room temperature overnight (~ 17 - 18 h, to be more specific). After reaction, the white suspension was evaporated almost to dryness (leaving ~ 1 mL in the flask) using a rotary evaporator. The grafted NRs were then washed twice using 20 mL of n-hexane, followed by centrifugation at 20000 rpm for 20 min, and finally dried under vacuum for 2 h. NRs were obtained as a white soft waxy solid, and stored in the freezer wrapped in aluminum foil. Average yield (n = 4): 75 ± 4 mg.

A "control" experiment was also performed using the same protocol, but with a solution of non-labeled oleic acid in THF (c = 0.073 M, 10.9 mg of OA, V=527 µL), which was added to the suspension of NRs in view of the grafting. Average yield (n = 2): 71 ± 6 mg.

III-C2) Characterizations of OA-grafted ZnO nanorods (NRs)

Figure III-5: ATR-IR analysis of ZnO-NRs before and after the grafting procedure.

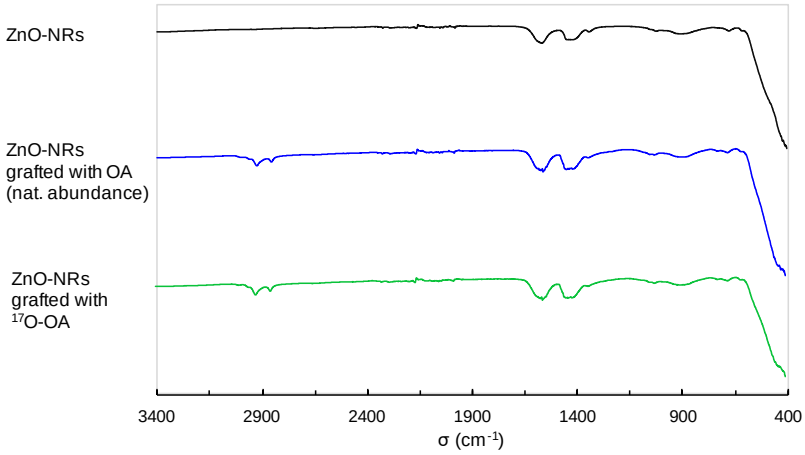

Figure III-6: XRD analysis of ZnO-NRs before and after grafting procedure.

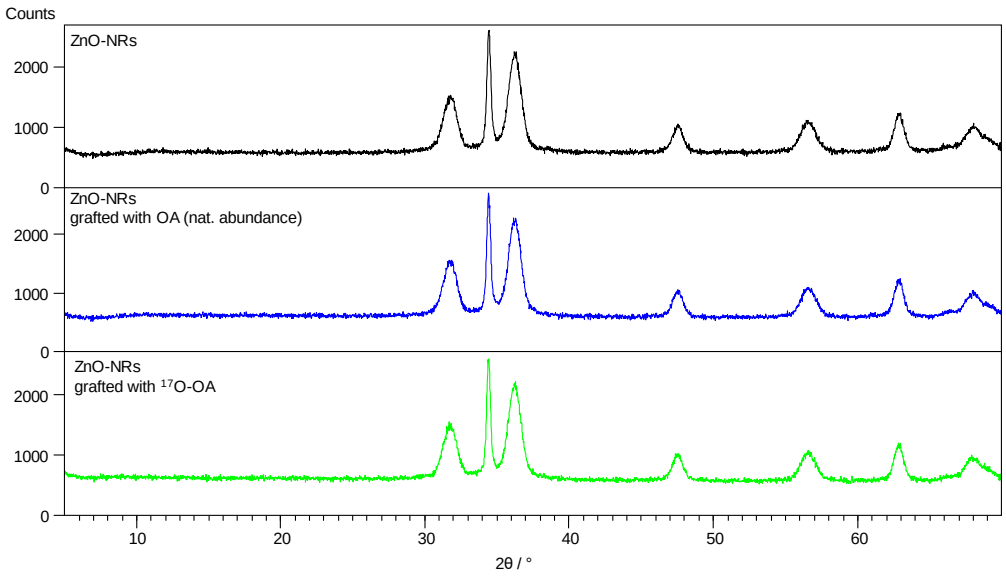

Figure III-7: TEM analysis of ZnO-NRs: a) bare NRs, b) grafted with OA (nat. abundance), c) grafted with ^{17}O-labeled OA.

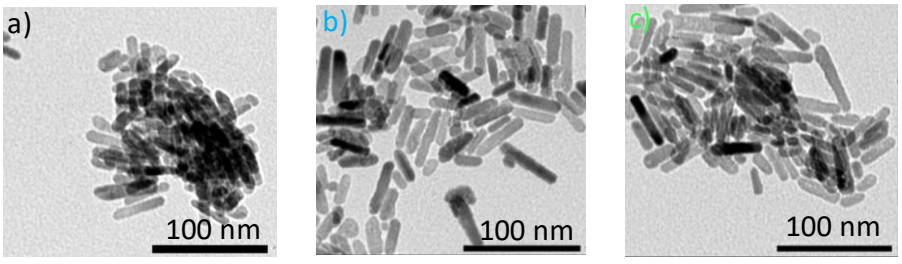

Figure III-8: XRD analysis of ^{17}O-labeled Zn-oleate and ZnO-NRs grafted with ^{17}O-labeled OA ("*" symbols correspond to NaCl.

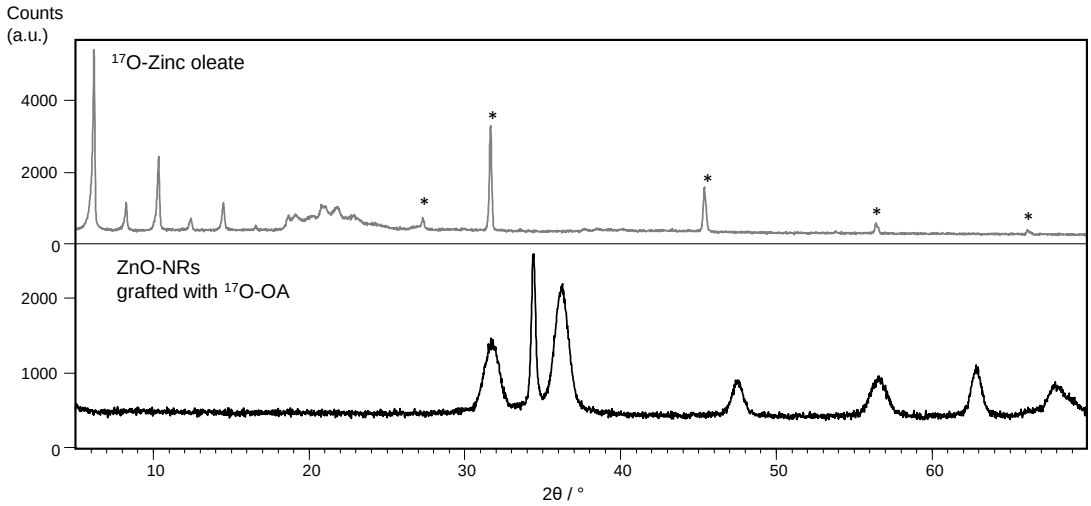

Figure III-9: Comparison of the IR spectra of ^{17}O-labeled oleic acid (green), ^{17}O-labeled zinc oleate (grey), bare ZnO NRs (black), and ZnO NRs grafted with ^{17}O-labeled OA (navy). The region shaded in orange shows where C=O stretching vibrations are expected, and the dashed red line is characteristic of an acidic COOH group.

The lack of vibration band at ~ 1700 cm^{-1} in the grafted nanorods can be seen as evidence of the predominant presence of the deprotonated oleate at the surface, in line with previous IR studies of grafted nanoparticles.[21-22]

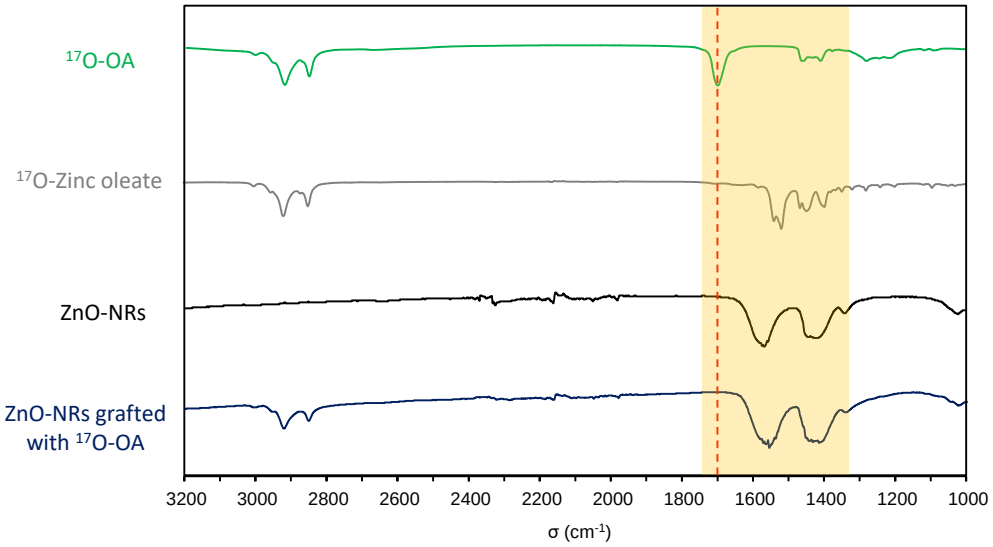

Figure III-10: ^{13}C NMR spectra of oleic acid (^{13}C solution NMR of a concentrated solution, OA/DMSO-d_6 96/4 v/v; orange), ^{17}O-labeled Zn-oleate (^{13}C solid state CPMAS NMR, grey) and grafted nanorods (^{13}C solid state CPMAS NMR, black).

The ^{13}C CPMAS NMR spectrum of grafted nanorods shows that the aliphatic chains of the oleic acid molecules are mobile, because *i)* the chemical shifts of the methylene resonances are more similar to those of liquid oleic acid than crystalline Zn-oleate, attesting of the presence of more gamma-gauche and trans-gauche conformations at the surface of the grafted nanoparticles,[23] and *ii)* the very weak signal of the methyl end-group in CPMAS.

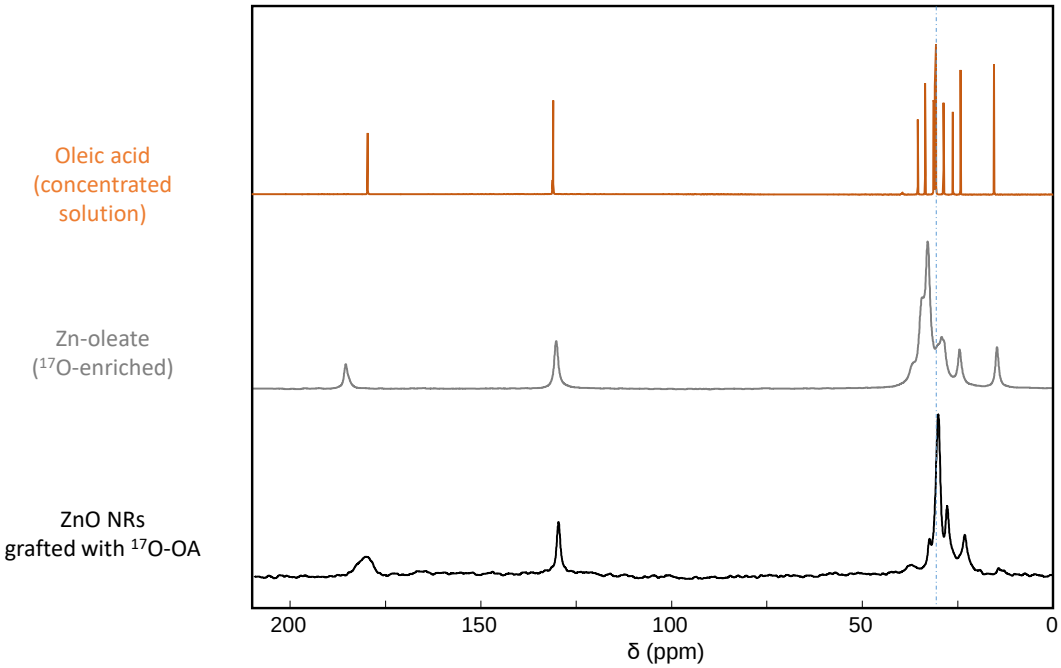

Figure III-11:. ^{13}C CPMAS NMR spectra of ZnO-NRs, before (black) after (green) grafting of ^{17}O-labeled OA. Spectra were purposely super-imposed here with a similar intensity in the carboxylic region (where the signals from grafted acetate and oleate can overlap). The comparison of these spectra shows that after OA-grafting the amount of residual acetates is small, as a much stronger intensity in the $-CH_3$ region would have been observed, if this were not the case.

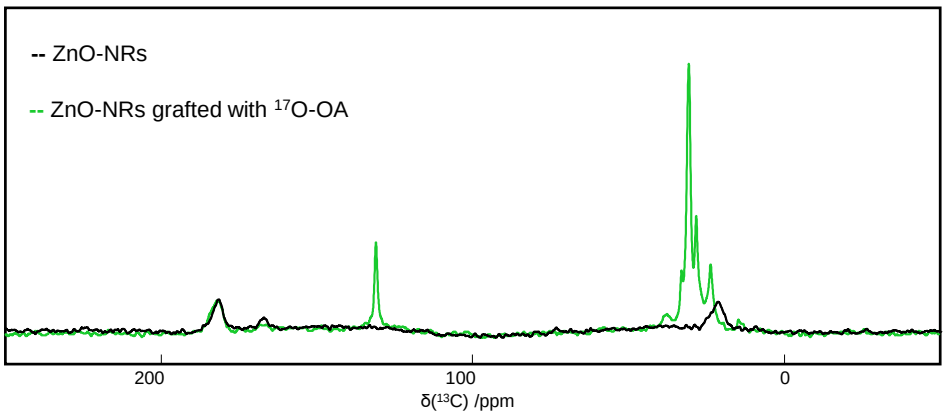

III-C3) Characterizations after accelerated ageing by irradiation or heat-treatment

Figure III-12: Analyses of non-grafted ZnO-NRs, before (black) and after irradiation (blue) and heat-treatment (red). ^{13}C and ^{17}O NMR acquisition parameters can be found in Tables II-1 and II-2 in the section. It is worth noting that for bare nanorods, the irradiation treatment induces a change in nanorod size and shape (as shown by XRD and TEM) and an increase in the relative amount of carbonates detected by ^{13}C CPMAS NMR (signal at ~ 166 ppm, blue spectrum).

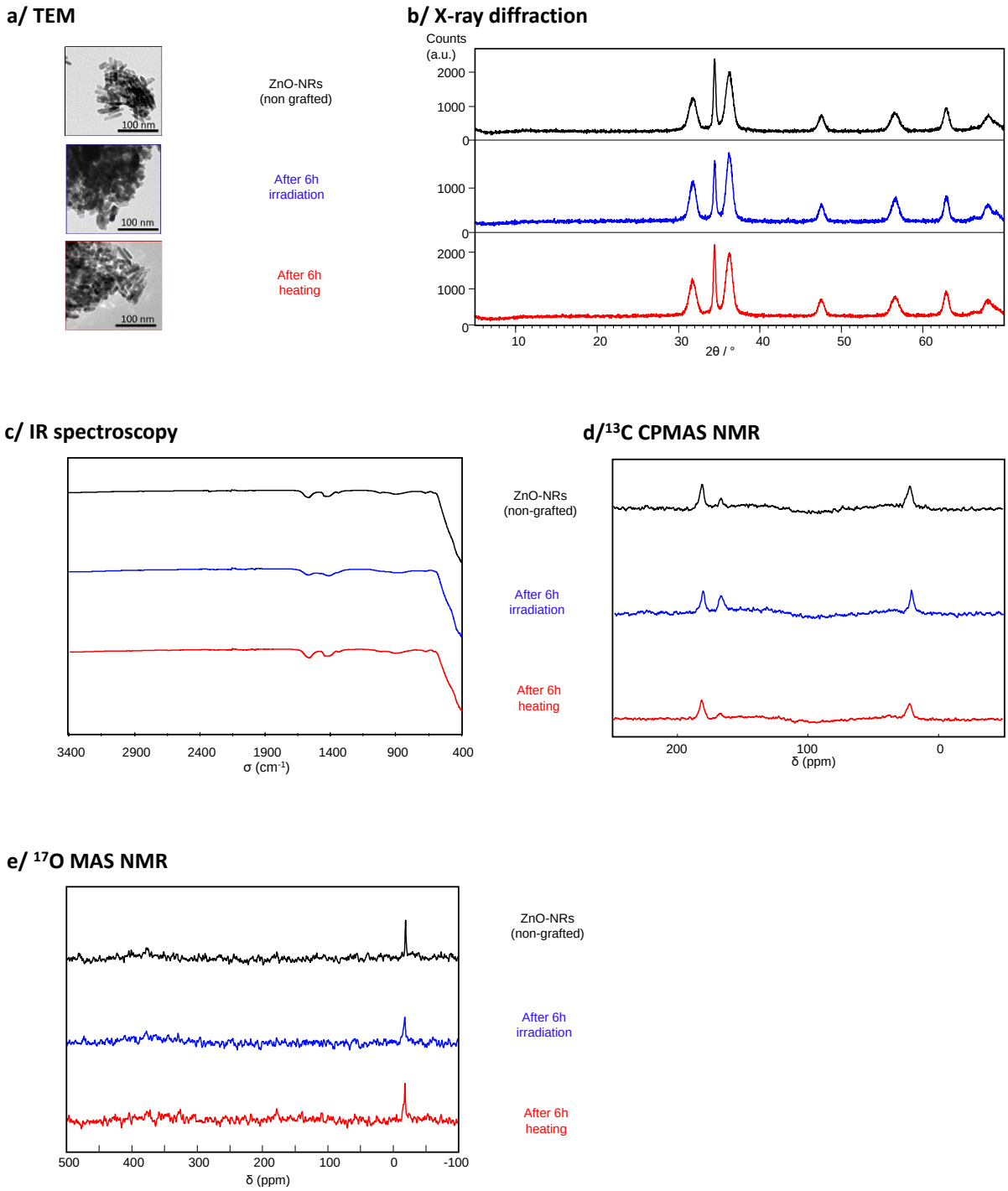

Figure III-13: Analyses of ZnO-NRs grafted with non-labeled OA, before (black) and after irradiation (blue) and heat-treatment (red). ^{13}C and ^{17}O NMR acquisition parameters can be found in Tables II-1 and II-2 in the section A. For the ^{17}O MAS NMR data, "*" symbols correspond to a ZnO spinning sideband, and "◊" symbols to the ZrO_2 rotor.

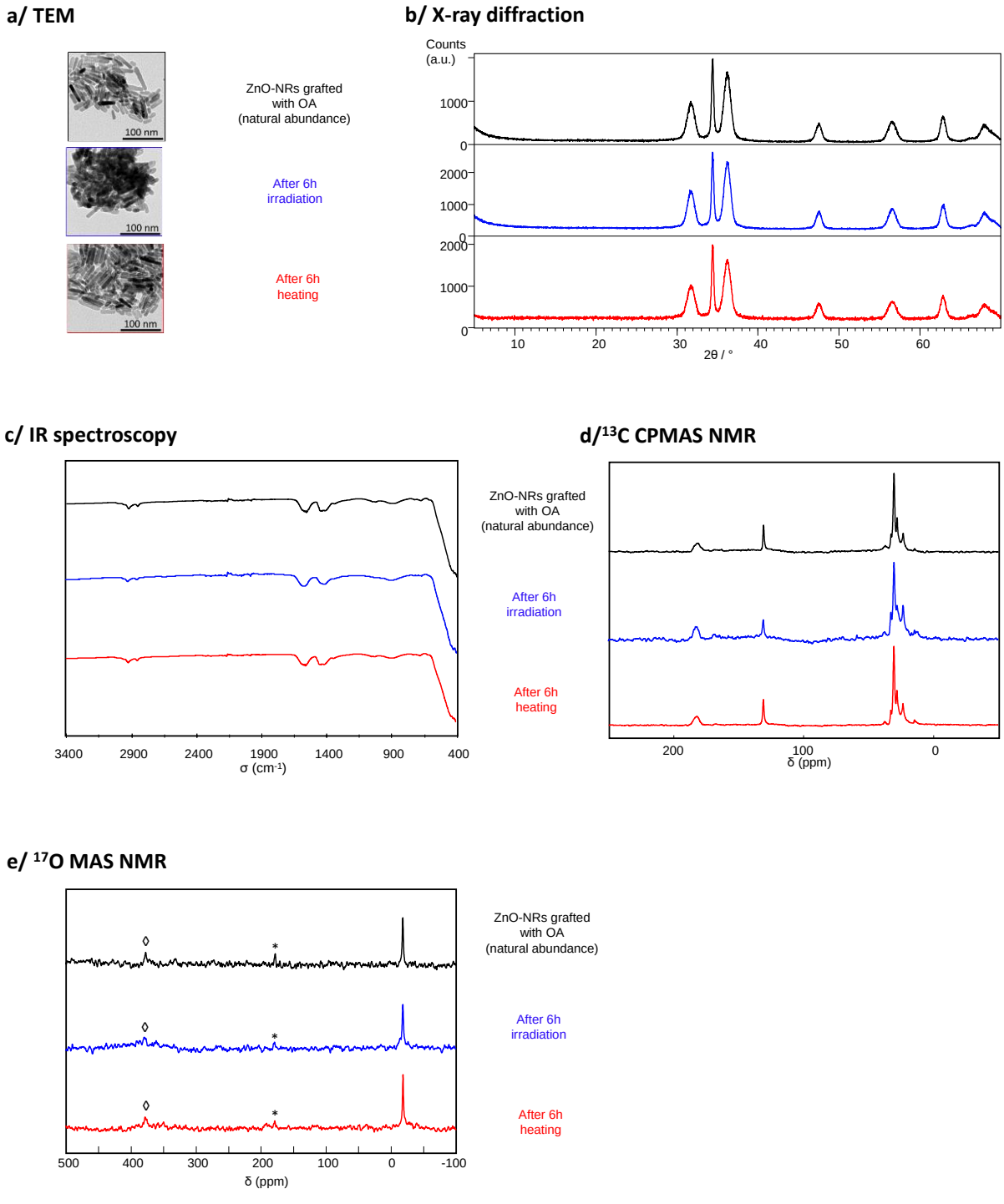

Figure III-14: Analyses of Zn-OA, before (black) and after irradiation (blue) and heat-treatment (red). ^{13}C and ^{17}O NMR acquisition parameters can be found in Tables II-1 and II-2 in the section. ("*" symbols on the X-ray diffraction powder patterns correspond to NaCl). It was found that the heating of the Zn-OA phase globally leads to a significant increase in its crystallinity, as shown by X-ray diffraction (stronger intensity of the diffraction peaks) and ^{17}O MAS NMR (more features on the NMR spectra).

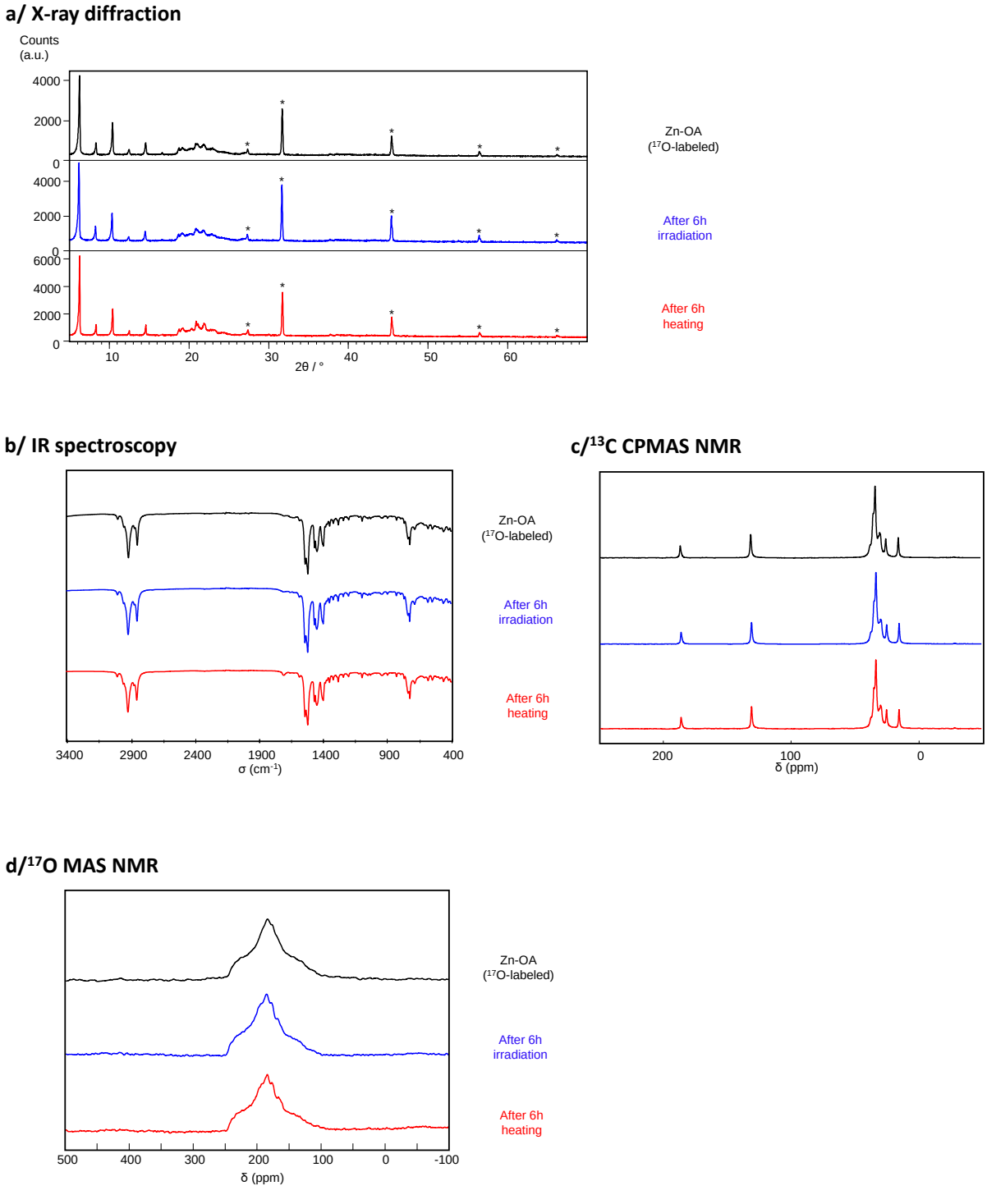

Figure III-15: TGA of OA-grafted NRs before (black) and after 6h irradiation (blue). Weight loss before irradiation is 10.1 % and corresponds to grafting density of ~ 2 molecules per nm^2. Weight loss after irradiation is 8.6 %.

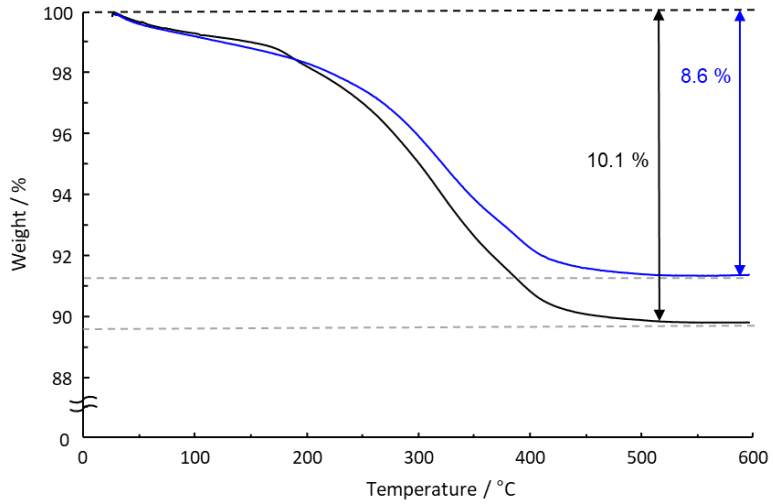

REFERENCES

1. Perras, F. A.; Viger-Gravel, J.; Burgess, K. M. N.; Bryce, D. L., Signal enhancement in solid-state NMR of quadrupolar nuclei. *Solid State Nucl. Magn. Reons.* **2013,** *51-52*, 1-15.
2. Gan, Z.; Hung, I.; Wang, X.; Paulino, J.; Wu, G.; Litvak, I. M.; Gor'kov, P. L.; Brey, W. W.; Lendi, P.; Schiano, J. L.; Bird, M. D.; Dixon, I. R.; Toth, J.; Boebinger, G. S.; Cross, T. A., NMR spectroscopy up to 35.2T using a series-connected hybrid magnet. *J. Magn. Reson.* **2017,** *284*, 125-136.
3. Gan, Z.; Gor'kov, P. L.; Brey, W. W.; Sideris, P. J.; Grey, C. P., Enhancing MQMAS of low-γ nuclei by using a high B_1 field balanced probe circuit. *J. Magn. Reson.* **2009,** *200* (1), 2-5.
4. Massiot, D.; Fayon, F.; Capron, M.; King, I.; Le Calvé, S.; Alonso, B.; Durand, J.-O.; Bujoli, B.; Gan, Z.; Hoatson, G., Modelling one- and two-dimensional solid-state NMR spectra. *Magn. Reson. Chem.* **2002,** *40* (1), 70-76.
5. Taylor, R. A.; Ellis, H. A., Anhydrous polymeric zinc(II) pentanoate. *Acta Crystallogr.E* **2008,** *64* (7), m895.
6. Lacouture, F.; Peultier, J.; Francois, M.; Steinmetz, J., Anhydrous polymeric zinc(II) octanoate. *Acta Crystallogr. C* **2000,** *56* (5), 556-557.
7. Hafner, J., Ab-initio simulations of materials using VASP: Density-functional theory and beyond. *J. Comput. Chem.* **2008,** *29* (13), 2044-2078.
8. Giannozzi, P.; Baroni, S.; Bonini, N.; Calandra, M.; Car, R.; Cavazzoni, C.; Ceresoli, D.; Chiarotti, G. L.; Cococcioni, M.; Dabo, I.; Dal Corso, A.; de Gironcoli, S.; Fabris, S.; Fratesi, G.; Gebauer, R.; Gerstmann, U.; Gougoussis, C.; Kokalj, A.; Lazzeri, M.; Martin-Samos, L.; Marzari, N.; Mauri, F.; Mazzarello, R.; Paolini, S.; Pasquarello, A.; Paulatto, L.; Sbraccia, C.; Scandolo, S.; Sclauzero, G.; Seitsonen, A. P.; Smogunov, A.; Umari, P.; Wentzcovitch, R. M., QUANTUM ESPRESSO: a modular and open-source software project for quantum simulations of materials. *J. Phys. Condens. Matter* **2009,** *21* (39), 395502.
9. Perdew, J. P.; Burke, K.; Ernzerhof, M., Generalized Gradient Approximation Made Simple. *Phys. Rev. Lett.* **1996,** *77* (18), 3865-3868.
10. Troullier, N.; Martins, J. L., Efficient pseudopotentials for plane-wave calculations. *Phys. Rev. B* **1991,** *43* (3), 1993-2006.
11. Pickard, C. J.; Mauri, F., All-electron magnetic response with pseudopotentials: NMR chemical shifts. *Phys. Rev. B* **2001,** *63* (24), 245101.
12. Métro, T.-X.; Gervais, C.; Martinez, A.; Bonhomme, C.; Laurencin, D., Unleashing the Potential of ^{17}O NMR Spectroscopy Using Mechanochemistry. *Angew. Chem.* **2017,** *129* (24), 6907-6911.
13. Robinet, L.; Corbeil, M.-C., The Characterization of Metal Soaps. *Stud. Conserv.* **2003,** *48* (1), 23-40.
14. Otero, V.; Sanches, D.; Montagner, C.; Vilarigues, M.; Carlyle, L.; Lopes, J. A.; Melo, M. J., Characterisation of metal carboxylates by Raman and infrared spectroscopy in works of art. *J. Raman Spectrosc.* **2014,** *45* (11-12), 1197-1206.
15. Ishioka, T.; Shibata, Y.; Takahashi, M.; Kanesaka, I., Vibrational spectra and structures of zinc carboxylates II. Anhydrous zinc acetate and zinc stearate. *Spectrochim. Acta A Mol. Biomol. Spectrosc.* **1998,** *54* (12), 1811-1818.
16. He, P.; Xu, J.; Terskikh, V. V.; Sutrisno, A.; Nie, H.-Y.; Huang, Y., Identification of Nonequivalent Framework Oxygen Species in Metal–Organic Frameworks by 17O Solid-State NMR. *J. Phys. Chem. C* **2013,** *117* (33), 16953-16960.
17. Bignami, G. P. M.; Davis, Z. H.; Dawson, D. M.; Morris, S. A.; Russell, S. E.; McKay, D.; Parke, R. E.; Iuga, D.; Morris, R. E.; Ashbrook, S. E., Cost-effective ^{17}O enrichment and NMR spectroscopy of mixed-metal terephthalate metal–organic frameworks. *Chem. Sci.* **2018,** *9* (4), 850-859.
18. Sun, B.; Sirringhaus, H., Solution-Processed Zinc Oxide Field-Effect Transistors Based on Self-Assembly of Colloidal Nanorods. *Nano Lett.* **2005,** *5* (12), 2408-2413.
19. Pacholski, C.; Kornowski, A.; Weller, H., Self-Assembly of ZnO: From Nanodots to Nanorods. *Angew. Chem. Int,. Ed.* **2002,** *41* (7), 1188-1191.
20. Awada, H.; Medlej, H.; Blanc, S.; Delville, M.-H.; Hiorns, R. C.; Bousquet, A.; Dagron-Lartigau, C.; Billon, L., Versatile functional poly(3-hexylthiophene) for hybrid particles synthesis by the grafting onto technique: Core@shell ZnO nanorods. *J. Polym. Sci. A* **2014,** *52* (1), 30-38.
21. Oliva-Puigdomenech, A.; De Roo, J.; Kuhs, J.; Detavernier, C.; Martins, J. C.; Hens, Z., Ligand binding to copper nanocrystals: amines and carboxylic acids and the role of surface oxides. *Chem. Mater.* **2019,** *31* (6), 2058-2067.
22. Kauffman, D. R.; Ohodnicki, P. R.; Kail, B. W.; Matranga, C., Selective electrocatalytic activity of ligand stabilized copper oxide nanoparticles. *J. Phys. Chem. Lett.* **2011,** *2* (16), 2038-2043.
23. Pawsey, S.; Yach, K.; Halla, J.; Reven, L., Self-Assembled Monolayers of Alkanoic Acids: A Solid-State NMR Study. *Langmuir* **2000,** *16* (7), 3294-3303.

CHAPTER 4

$^{17}O/^{18}O$-ENRICHMENT OF AMINO ACIDS

INTRODUCTION

Amino acids (AA) are an important class of organic molecules, which contain in their structure an amine group (-NH_2), a carboxylic group (-COOH), and a side-chain (R-) specific for each amino acid (Figure 4.1). The biologically most relevant amino acids possess an amine group at the α-position relative to the carboxylic group, commonly named α-amino acids. They include 20-proteinogenic AA, which serve as building blocks of peptides and proteins. Except for glycine, all proteinogenic amino acids are optically active, with a chiral centre located at the asymmetric α-carbon, and all proteins are primarily made up of the L-stereoisomers.[1] Due to the irreplaceable role of peptides and proteins in the living organisms, a lot of effort was invested to better understand their reactivity and to explore their structure, as a crucial prerequisite for the development of new drugs[2] or biomimetic materials.[3] Such studies have required in some cases, the preparation of species labeled in stable isotopes, such as in ^{2}H, ^{13}C, ^{15}N, and to lesser extent, oxygen-^{17}O/^{18}O,[4] which were subsequently characterized by IR,[5-6] MS[7-8] or NMR analyses.[9]

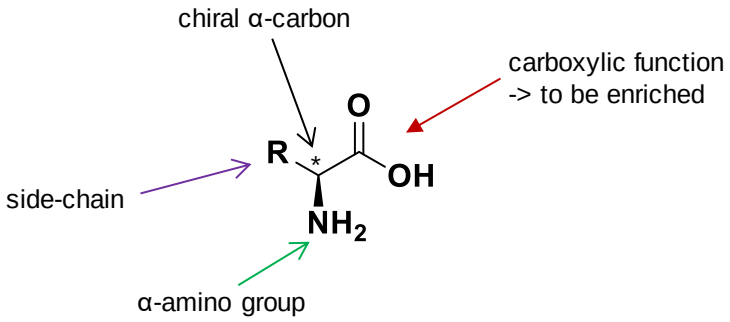

Figure 4.1: General scheme of an L-α-amino acid.

For the ^{17}O/^{18}O-labeling of carboxylic acids in general, a Brönsted-acid catalysed oxygen exchange in presence of an excess (~ 40 - 100 equivalents) of labeled water is the most common ^{17}O/^{18}O-oxygen enrichment protocol used so far in the literature (see Chapter 1.1.1).[10] It is also the strategy used the most for oxygen enrichment of free (unprotected) amino acids.[11-15] It typically involves working at elevated temperatures, during long equilibration times (few hours up to several days), and requires the use of a strong acid for catalysis (*e.g.* concentrated aqueous HCl, which unfortunately dilutes the label in the water, or toxic and corrosive HCl gas, which is streamed through the reaction medium). Most of the time, the amino acids are isolated under their hydrochloride salt form, and require additional anion exchange procedure to provide the "pure" zwitterionic form of the amino acid. Alternatively, the protocols for amino acids enrichment *via* hydrolysis of their ester derivatives under basic or acidic conditions were

described, using smaller excess of labeled water (~ 5 equivalents) and they typically led to lower enrichment levels, as only one oxygen in carboxylic function is labeled.[12, 16-17] Also, when non-labeled NaOH was used to create basic environment in labeled water, the oxygen isotopes were diluted and overall enrichment efficiency of labeling scheme was further reduced. In a view of developing more user-friendly and cost-efficient labeling schemes, we have decided to turn our attention to mechanochemistry.

In this chapter, at first, the protocols used for $^{17}O/^{18}O$-enrichment of amino acids via mechanochemistry using vibratory ball-mill (VBM) are described, and compared to acid-catalysed exchange procedures. The amino acids were selected for this study based on their different physicochemical properties and reactivity, related to their side-chains. The amino acids which were looked into in particular are the following: Glycine (Gly, G), as the simples and the most studied amino acid, L-Aspartic acid (Asp, D) and L-Glutamic acid (Glu, E), as examples of amino acids with acidic side-chain, L-Lysine (Lys, K), that contain a basic side-chain, and finally L-Leucine (Leu, L) and L-Phenylalanine (Phe, F) as representatives of amino acids with non-polar side-chains (Figure 4.2).

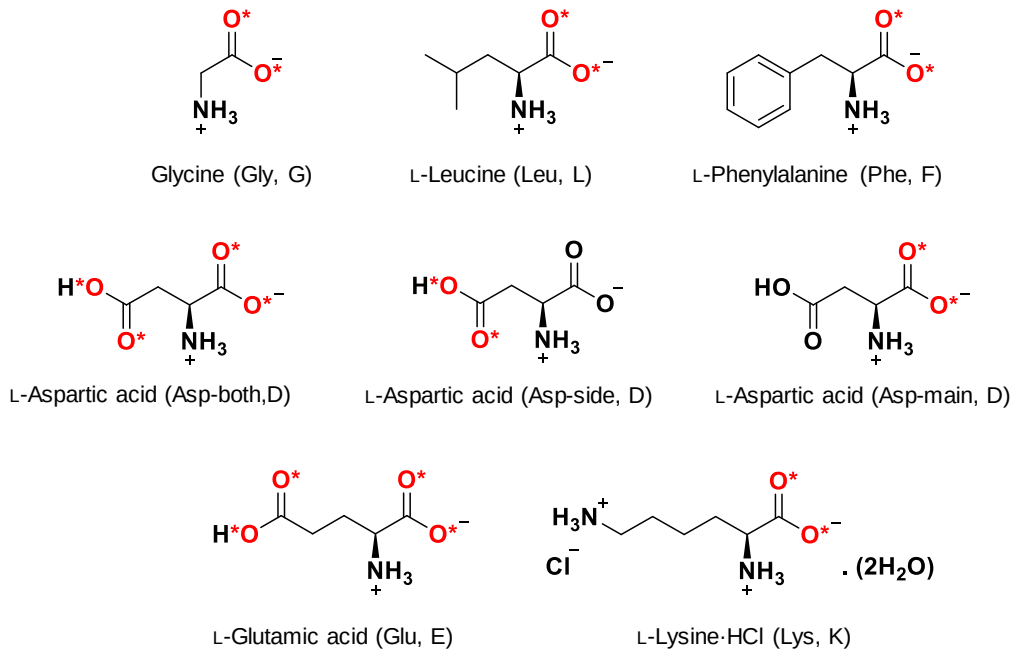

Figure 4.2: Amino acids enriched in $^{17}O/^{18}O$ in this work. Depending on the labeling strategy used, one or both oxygens per carboxylic function were enriched.

The physicochemical properties as well as the specific aspects for the synthesis and the work-up of each group of amino acids are highlighted, in relation with the need to isolate each of these phases in high yields, high enrichment levels and high enantiomeric excesses (when

relevant). Scale-up procedures are also discussed. Comparisons with other $^{17}O/^{18}O$ enrichment protocols, when available, are also proposed, and the ^{17}O solid state NMR spectra are presented and discussed.

In the second part, the protection of labeled amino acids at their amine group(s) by fluorenylmethyloxycarbonyl (Fmoc) group using common solution-based protocols is described (Figure 4.3). This protection was necessary not only for the purpose of further application of labeled amino acids in solid-phase peptide synthesis (SPPS) (described in Chapter 5), but also to check the potential evolution of enantiomeric excess of the optically active compounds upon mechanochemical or acid-catalysed syntheses. All optimized protocols with full characterizations of final products are included in the Annexe IV.

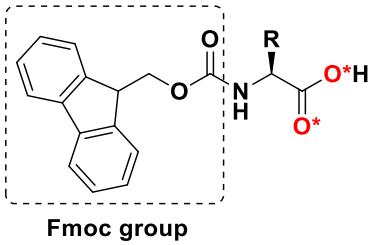

Figure 4.3: $^{17}O/^{18}O$-Enriched Fmoc-protected amino acid, R = side-chain. Depending on the labeling strategy, one or both oxygens per carboxylic function can be enriched.

4.1 $^{17}O/^{18}O$-LABELING STRATEGIES

Two different $^{17}O/^{18}O$-labeling strategies were applied in the frame of this work for enrichment of amino acids. The first method employed was a mechanochemical strategy developed for the enrichment of fatty acids based on the saponification of methyl ester derivatives (see Chapter 2.2).[18] The second strategy was inspired by the published enrichment protocol for glycine based on acid-catalysed exchange of its hydrochloride salt (Gly·HCl) in labeled water, by involving either a Brönsted or a Lewis acid.[19] In both cases, the work-up conditions were optimized at first using non-labeled water for these syntheses. Regarding the saponification, reaction conditions were optimized using $H_2{}^{18}O$ water (99 % of ^{18}O content), due to its lower purchasing price, and only then, fully optimized protocols were applied for the preparation of ^{17}O-labeled amino acids (using 70% or 90% ^{17}O-enriched H_2O*).

4.1.1 Enrichment *via* VBM saponification

The method we selected for the oxygen labeling of amino acids was the mechanochemical saponification developed as an alternative to CDI activation/hydrolysis

procedure for the enrichment of fatty acids (for details see Chapter 2.2). Indeed, the CDI-activation/hydrolysis scheme could not have been applied directly on free amino acids (with the aim to provide directly their labeled equivalents) due to the presence of unprotected amino group, which could react as a competitive nucleophile in the CDI-activation/hydrolysis scheme.[20] Using the CDI-activation/hydrolysis approach would have required having a protective group on the alpha-nitrogen atom, such as a *tert*-butyloxycarbonyl group (Boc), as was demonstrated by our group earlier on the ^{17}O-enrichment of Boc-Phenylalanine.[21] An additional deprotection step would then had to be performed in order to isolate free amino acid.

For the mechanochemical procedures developed here, a vibratory ball-mill MM400 equipped with a stainless-steel jar (10 mL inner volume) containing two stainless-steel beads (1 cm diameter) was used. The saponification experiments took 30 min of milling at 25 Hz. As a starting point, the initial mass of amino acid methyl (or ethyl) ester reagents was set to 150 mg, and the synthesis on this scale will be referred to as "low-scale synthesis" within this chapter. In contrast to the esters of fatty acids, the amino acids ester derivatives are typically commercially available in a form of hydrochloride salts (AA-OR·HCl, R = Me, Et). This results in an increase of number of equivalents of sodium ethoxide (NaOEt, > 2 eq.) base necessary, out of which one equivalent is consumed simply by reacting with the hydrochloride salt (Scheme 4.1).

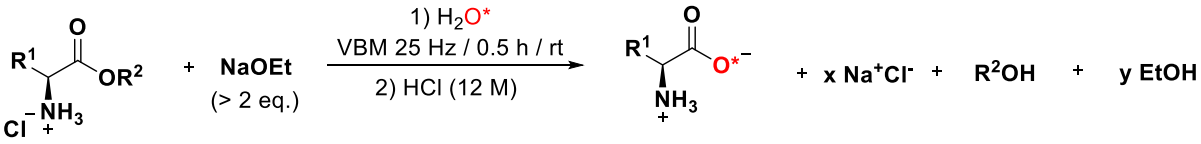

R_1 = AA specific side-chain
R_2 = Me (or Et)

Scheme 4.1: General scheme of $^{17}O/^{18}O$-enrichment protocol for labeling amino acids using VBM saponification; x, y = stoichiometry coefficients. The work-up conditions for final pure AA isolation are not shown in this schematic. More detailed schemes (including stoichiometries of reagents) are presented in each amino acid subsection.

It is important to state here, that an impact of the quality of the NaOEt precursor used for the saponification on the enrichment level of targeted molecules was observed. Sodium ethoxide is a hygroscopic compound, which reacts with the humidity from the air resulting in formation of sodium hydroxide. The hydroxide anions coming from this reaction are not labeled and therefore dilute the labeled hydroxide anions formed i*n-situ* by reaction with $^{17}O/^{18}O$ labeled water during saponification. In order to slow down this decay, a small container of NaOEt (5 g) was repeatedly ordered, and after every use, the NaOEt was straight away

covered with argon atmosphere (in the product bottle) and the container was stored in a desiccator (repetitively degassed and filled with argon). When a decrease of enrichment yield higher than 5 % was observed for several consecutive reactions, a new bottle of NaOEt was re-ordered. Indication of a beginning of degradation of the NaOEt precursor (resulting in decreases in labeling efficiency) was its colour change. Indeed, the newly opened sodium ethoxide had typically only a slightly yellowish colour, and it was found to turn more and more orange over the time, probably due to the presence of yet unidentified impurities coming from the degradation of the NaOEt. Fortunately, the presence of these yellow contaminants had no effect on the purity of the isolated amino acids.

Last but not least, another significant difference with the procedures developed for fatty acids lies in the work-up step, which turned to be a critical point in terms of isolating the enriched products pure and in high yields in a reproducible manner. Unlike for the fatty acids, which were acidified and extracted with an organic solvent after acidification of the reaction medium, leaving the sodium chloride (NaCl) in the aqueous phase, the amino acids remain fairly water-soluble over the whole pH range and their separation from Na^+ and Cl^- ions is therefore more challenging. For each amino acid, work-up conditions were optimized specifically to ensure the highest yield possible (Table 4.9 in summary section 4.2.5).

4.1.2 Enrichment *via* acid-catalysed exchange

In order to compare our mechanochemical approach with more classical protocols used for amino acids labeling, we have decided to adapt a published protocol for enrichment of amino acids by acid catalysed oxygen exchange, which should be relatively efficient and could be easily performed in our laboratory. The aim was to compare the results in terms of yield and purity of the isolated compounds, but also in terms of labeling efficiency (in time and cost).

As mentioned previously, the $^{17}O/^{18}O$ enrichment of amino acids has been frequently performed by Brönsted-acid catalysed exchange in excess of labeled water, using HCl gas at elevated temperatures.[22-23] The starting procedure we selected was the one performed by Maers,[19] in which the source of HCl comes with the amino acid itself, when it is used as hydrochloride salt (AA·HCl). This allowed to avoid having to produce HCl gas (which is experimentally constraining) or having to add aqueous HCl (which would reduce the labeling efficiency) (Scheme 4.2).

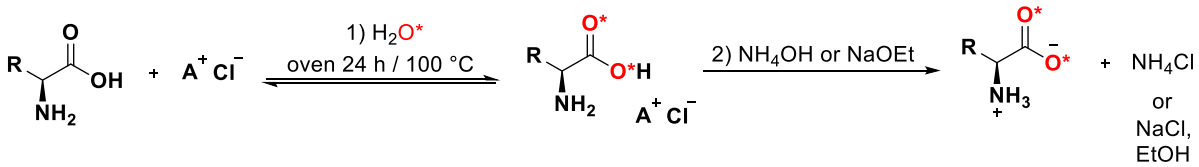

R = AA specific side-chain
$A^+ = H^+$ (Brönsted acid)
or Li^+ (Lewis acid)

Scheme 4.2: General scheme of $^{17}O/^{18}O$-enrichment protocol for labeling amino acids using acid catalysed oxygen exchange. The work-up conditions for final pure AA isolation are not shown in this schematic. More detailed scheme is presented in each amino acid subsection.

In this work, this protocol was first tested on glycine, and later adapted and applied to the other studied amino acids. As further developed below, one of the important adaptations concerned the use of a Lewis acid, LiCl, in cases where the amino acid was not commercially available as HCl salt, thereby offering a potentially attractive labeling alternative. To favour full comparison of both synthetic strategies (VBM and acid-catalysis), particular care was made to isolate the amino acids under the same form. Hence, some of the aspects of the work-up procedures optimized for the saponification were taken into consideration when isolating labeled molecules after acid catalysis.

4.2 SPECIFIC $^{17}O/^{18}O$-LABELING PROTOCOLS FOR AMINO ACIDS

4.2.1 Physicochemical properties of selected amino acids

The physicochemical properties of amino acids, specifically their pKa values and solubility in water and alcohols, turned out to be crucial for the isolation of the labeled compounds in their desired form and had strong impact on the final yield. These properties are therefore summarized and discussed here prior to the specific enrichment protocols (Table 4.1).

Table 4.1: The pKa and pI (isoelectric point) values of the targeted amino acids and their solubilities in water, methanol and ethanol (25 °C).

	pKa_1 (COOH)[24]	**pKa_2 (NH_2)[24]**	**pKa_3 (side-chain)[24]**	**pI[24]**	**Solubility in H_2O [mg/mL]**	**Solubility in MeOH [mg/mL]**	**Solubility in EtOH [mg/mL]**
Gly	2.34	9.58	-	5.97	256[25]	0.3[26]	0.1[26]
Leu	2.36	9.60	-	5.98	22[25]	-	0.21[27]
Phe	1.83	9.13	-	5.48	28[25]	2.9[28]	0.3[27]
Asp	1.95	9.66	3.77	2.77	5[25]	-	0.00006[27]
Glu	2.19	9.67	4.25	3.22	9[29]	0.06[29]	0.05[29]
Lys	2.15	9.16	10.67	9.74	246[25]	-	0.17[27]
Lys·HCl	-	-	-	-	670[30]	0.01[30]	0.0002[30]
NaCl	-	-	-	-	361[31]	14[32]	0.4[33]

The first key property is the pKa value of different functional groups of amino acids (COOH, NH_2 and the functional group in the side-chain). Targeting specific pH can affect the final isolated yield (as further described below), and can also allow to isolate amino acids in the form desired. In this work, it was mainly the neutral zwitterionic form, except for L-lysine isolated as HCl salt (Figure 4.4).

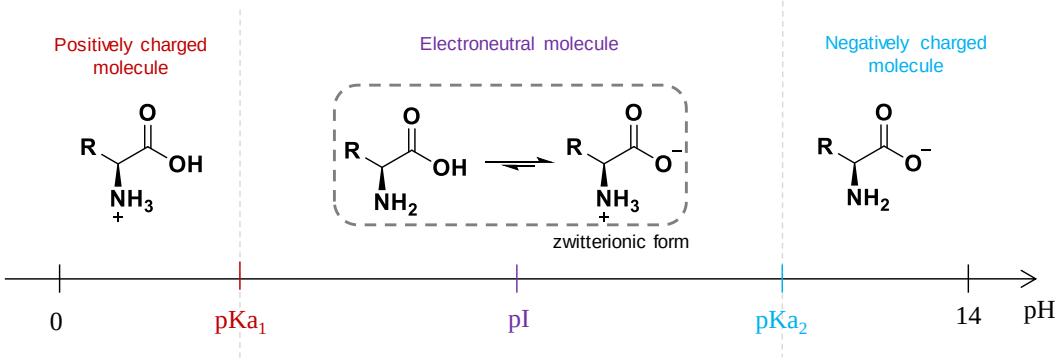

Figure 4.4: The chemical formulas of predominant amino acid form in pure water depending on the pH.

The second key property is the solubility of the amino acids. In Table 4.1, the solubility of neutral amino acids in water and alcohols (methanol/ethanol, used as anti-solvents during the work-up) is provided. It is known that the water solubility of amino acids varies depending not only on pH, but also on the temperature, and the presence of other species in the solution (cosolutes). For example, based on the literature, the solubility of amino acids generally increases with increasing temperature.[25]

The lowest solubility is expected at around pH = pI, where the amino acids occur in neutral zwitterionic form. Specifically, for the neutral side-chain amino acids (Gly, Leu, Phe) the solubility remains constant around neutral pH = 4 - 9, and increases under strongly acidic or basic conditions.[34-35] For the amino acids with acidic side-chains (Asp, Glu), the solubility in water remains constant up to pH < 3 and then increases substantially with pH > 4, as the side-chain gets deprotonated.[25] The opposite effect can be observed for the amino acids with basic side-chains (Lys), with the lowest solubility at pH > 10, increasing dramatically with pH < 9 as the side-chain gets protonated.[25]

In Table 4.1, the solubility of NaCl is also included, as the elimination of NaCl from the isolated $^{17}O/^{18}O$-labeled product turned out to be challenging in some cases. Moreover, because of the presence of other cosolutes (*e.g.* salts), phenomena of salting-in or salting-out of the amino acids can occur, and this is strongly system dependent (Figure 4.5). For example, based on the literature, the increasing NaCl concentration had no effect on glycine solubility, whereas the solubility of L-leucine was decreased (salting-out)[34] and the solubility of L-aspartic acid was

increased (salting-in)[36] (see Figure 4.5). It is important to note, that the values reported in Table 4.1 correspond to those of pure saturated amino acids solutions, measured at 25 °C, and could thus only be used as guidelines in the developed protocols.

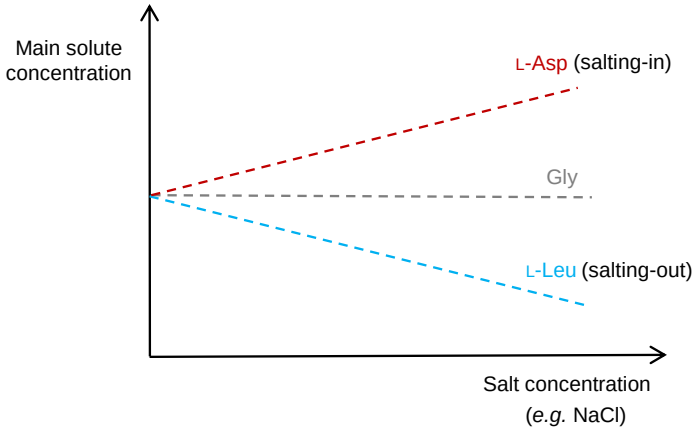

Figure 4.5: Schematic representation of the effect of a salt concentration on the solubility of a main solute (illustrated on examples of Gly, L-Leu and L-Asp in aqueous solution of NaCl).[34, 36]

4.2.2 Neutral side-chain amino acids

4.2.2.1 Glycine (Gly, G)

Glycine is the simplest amino acid with no side-chain, and thus, no stereogenic centre. So far, three polymorphs were described in the literature for anhydrous glycine: α, β and γ, all of which are highly soluble in water.[37-38]

The α-form is the kinetically favoured polymorph of glycine, which crystallizes easily from neutral aqueous glycine solutions, and then transforms gradually to the thermodynamically most stable γ-polymorph.[39] For a direct crystallization of γ-glycine from neutral solutions, additives, such as racemic methionine[40] or sodium chloride,[41] are typically required. The γ-glycine polymorph can be as well directly prepared by slow cooling of glycine solutions made acidic with acetic acid, or basic with ammonium hydroxide.[42-43] The preferential growth of the γ-polymorph was also observed from heavy water solutions.[43] The unstable β-polymorph is typically prepared from a saturated solution of glycine with the addition of ethanol as anti-solvent and transforms readily to the α-form when exposed to air/humidity.[44] This transformation can be prevented if β-glycine is stored under dry conditions. It was also shown that β-glycine forms preferentially and remains stable in nanoconfined environments.[45]

Overall, based on the literature, it can be concluded that selective synthesis of only one glycine polymorph is not that simple and typically mixtures with lower or higher content of other polymorphs are obtained.[37] Because polymorphism is an important topic of research in

the general field of amino acids,[42, 46-47] and this can affect the nature of the solid-state NMR spectra recorded, attention was made to the nature of the glycine polymorph isolated after isotopic labeling, as further detailed below.

a) $^{17}O/^{18}O$-Labeled glycine enriched by mechanochemical saponification

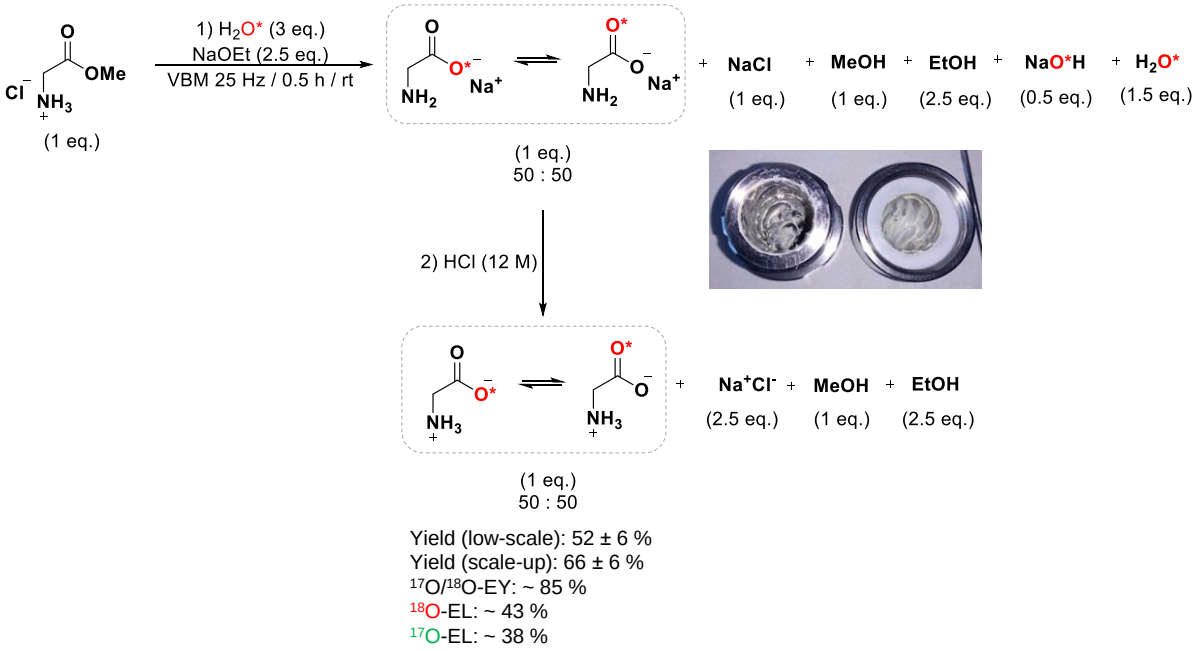

Scheme 4.3: Reaction scheme of glycine labeled using mechanochemistry. The dilution of labeled water after acidification with aqueous HCl is not shown in the scheme. The yields provided here are those of the isolated pure compounds (see Annexe IV for work-up and purification conditions). The enrichment yield (EY) and levels (EL) were measured for Fmoc-protected glycine (synthesis described later in section 4.3) and are estimated to be the same for unprotected glycine molecules. For the $^{17}O/^{18}O$-enrichment, 90% ^{17}O and 99% ^{18}O-enriched water was used, respectively.

The $^{17}O/^{18}O$-labeled glycine was prepared by mechanochemical saponification starting at low-scale from 150 mg of Gly-OMe·HCl (Scheme 4.3). The methyl ester was hydrolysed in the presence of 2.5 equivalents of NaOEt base and 3 equivalents of labeled water (65 µL, 99 % of ^{18}O content for ^{18}O-enriched H_2O* and 70% or 90% of ^{17}O content for ^{17}O-enriched H_2O*). After 30 min of milling at 25 Hz, the reaction mixture in the jar was in a form of yellowish paste, homogeneously distributed over the inner surface of the jar and on the balls. To confirm the homogeneity and full conversion of the reaction, small amounts of reaction mixture were taken from different parts of the jar and analysed by ATR-IR spectroscopy, focusing on the shifts of C=O stretching vibration bands moving from 1742 to 1609 cm^{-1}, due to the presence of heavier ^{18}O-isotope in the carboxyl group (see Annexe IV).

To recover the product from the jar, a minimum amount of non-labeled water was used to dissolve the paste, and the resulting basic solution (pH = 13.5) containing labeled glycine,

Na^+ and Cl^- ions, and potentially residual MeOH and EtOH (some of which probably already evaporated) was transferred to a round-bottom flask and acidified. For the subsequent crystallization step to be efficient, the aqueous glycine solution should be as concentrated as possible. Therefore, only 400 µL of water was introduced into the jar to dissolve the paste (the medium being homogenized using ball-milling for 2 min at 25 Hz), and another 400 µL was then used to wash the jar. Moreover, a concentrated HCl solution (12M) was used for the acidification in order to introduce the smallest amount of extra water possible. Here, the solution was acidified to pH ~ 3 - 4, transforming glycine to its zwitterionic form (Figure 4.6). When the acidification was followed more precisely with a pH probe, the pH decreased gradually as expected with no abnormalities. The acidified solution was finally sonicated for 5 min to ensure complete dissolution of the reaction mixture.

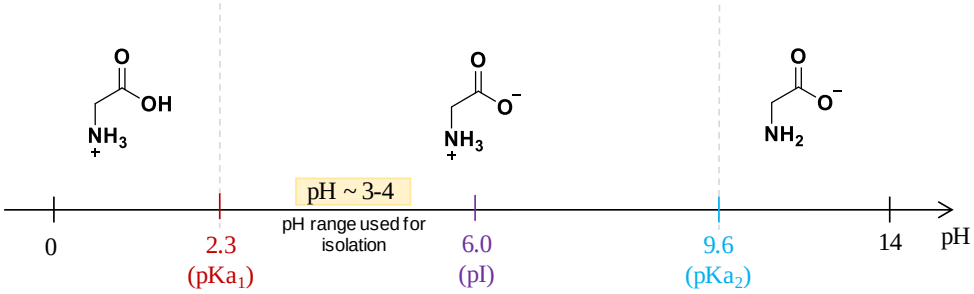

Figure 4.6: pH scale with pKa values of glycine and the chemical formulas of the predominant form of glycine in pure water depending on the pH. In the orange rectangle, the pH range at which glycine was isolated here is highlighted.

As mentioned earlier in this chapter, it was not possible to simply acidify and extract amino acids into an organic solvent. Glycine is a small polar molecule, highly soluble in water and no organic solvents could be used to extract the zwitterionic form of glycine from the aqueous phase. Therefore, another approach had to be applied. One of the possible ways of isolating glycine (and other amino acids) is to induce the precipitation from its aqueous solution using "anti-solvents", such as methanol, ethanol or isopropylalcohol (*i*-PrOH).[19, 48-49] The role of the anti-solvent lies in lowering the solubility of glycine and thus promoting its precipitation (Figure 4.7).

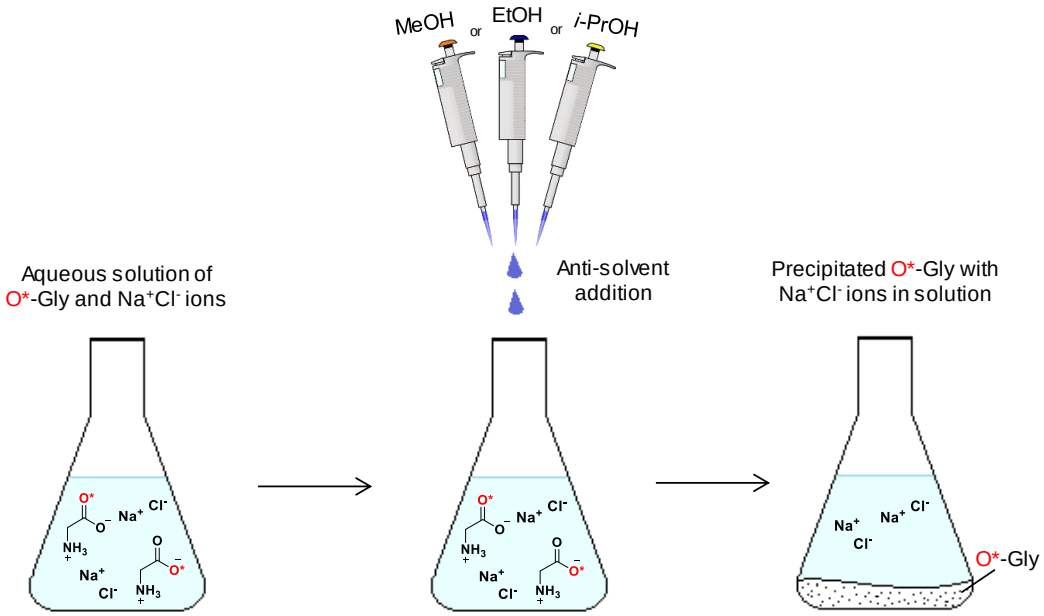

Figure 4.7: A schematic representation of anti-solvent induced precipitation of $^{17}O/^{18}O$-labeled glycine.

Looking at the relative solubilities of glycine and sodium chloride in water and alcohols (Table 4.1), the idea was to precipitate the glycine while avoiding the simultaneous precipitation of NaCl. Several different anti-solvents used in the literature were tested for glycine isolation and the results are summarized in the Table 4.2. In each case, the anti-solvent was added dropwise to the stirred solution of glycine inducing its precipitation. The suspension was then stirred in an ice-bath with the aim to increase the amount of glycine precipitated. Finally, the product was collected by filtration and dried under vacuum (for details see experimental section in Annexe IV).

The most effective in terms of inducing the precipitation was EtOH, anti-solvent typically used for amino acids isolation, where the precipitate appeared almost instantly. Unfortunately, using EtOH both glycine and NaCl precipitated and subsequent recrystallization was required in order to obtain pure glycine. Similar results were observed using *i*-PrOH, anti-solvent employed for glycine isolation after enrichment *via* acid catalysed exchange.[50] The best results in terms of both yield and purity were obtained when using MeOH. For efficient crystallization, at least six times the volume of water + aqueous HCl had to be added, and the precipitate formed only when more than half of the MeOH volume was introduced into the mixture.

Table 4.2: Different anti-solvents used and their effect on the yield and purity of the isolated compound

Anti-solvent	Volume [µL]	Calculated yield[a]	XRD purity	RC necessary	Final yield
MeOH	7880	55 mg / 58 %	pure β-Gly	-	55 mg / 58 %
EtOH	6820	195 mg / 207 %	Gly + NaCl	yes	45 mg / 48 %
i-PrOH	5880	142 mg / 121 %	Gly + NaCl	yes	not processed

[a] Yield for an individual synthesis initially calculated before recrystallization assuming no NaCl contamination (which explains why values > 100 % are reported), RC = recrystallization.

By using MeOH as an anti-solvent, labeled glycine was isolated reproducibly as pure β-polymorph with rather lower yield (52 ± 6 %) but with no NaCl contamination and therefore with no need for additional recrystallization. The ^{17}O-labeled glycine was then studied by solid-state NMR spectroscopy.

Unfortunately, it was not possible to determine the enrichment of free unprotected glycine by standard HRMS analysis. The small glycine molecule (M = 76 g/mol) was difficult to ionize and the low-intensity signals obtained were not reliable enough to calculate the enrichment. The glycine enrichment was estimated subsequently from the measurements of labeled Fmoc-Glycine molecules (synthesis discussed below in section 4.3) as no loss of enrichment was expected during Fmoc protection (as was confirmed for the other amino acids in this work, see details in section 4.3 or Annexe IV). The estimated enrichment yield of the saponification procedure was ~ 85%. The estimated enrichment level of glycine was ~ 43 % for ^{18}O-labeled products and ~ 38% for ^{17}O-labeled products.

Scale-up procedure:

For the future application of labeled amino acids in the peptide synthesis, it was necessary to scale-up the enrichment protocol in view of producing bigger amounts of labeled compounds. Keeping the same jar-size (10 mL inner volume) and the same number and size of balls (2x, 1 cm diameter), the amount of reagents in the jar was at first doubled and finally tripled (starting from 450 mg of Gly-OMe·HCl and using 195 µL of enriched water). The 30 min of milling at 25 Hz was found to be sufficient to provide full conversion, and the same enrichment level was achieved (~ 43 % for ^{18}O-labeled products). The amount of non-labeled water and MeOH used for the work-up was re-optimized leading to the NaCl free, pure β-glycine isolated with overall higher yields compared to the low-scale synthesis (66 ± 6 %, compared to 52 ± 6 % for the low-scale synthesis).

Scaling-up the procedure and doing two reactions at the same time (*i.e.* using both jars of the MM400 ball-mill), allowed to prepare around 400 mg of ^{17}O (or ^{18}O) labeled glycine in only half of a day, with the yield and the enrichment level mentioned above.

b) ^{18}O-Labeled glycine enriched via acid catalysed exchange

As part of this study, a previously published enrichment procedure based on Brönsted-acid catalyses was also reproduced,[50] with the aim to compare the results with the newly developed labeling scheme based on mechanochemical saponification. The original ratio of reagents used in the paper (Gly·HCl : H_2O^* = 2 : 3) was modified for the protocol to be directly comparable with the saponification (Gly-OMe·HCl : H_2O^* = 1 : 3), in terms of cost and final enrichment (with respect to the amount of enriched water engaged). Also, the amount of starting Gly·HCl was adjusted to provide the same theoretical mass of labeled glycine (Scheme 4.4).

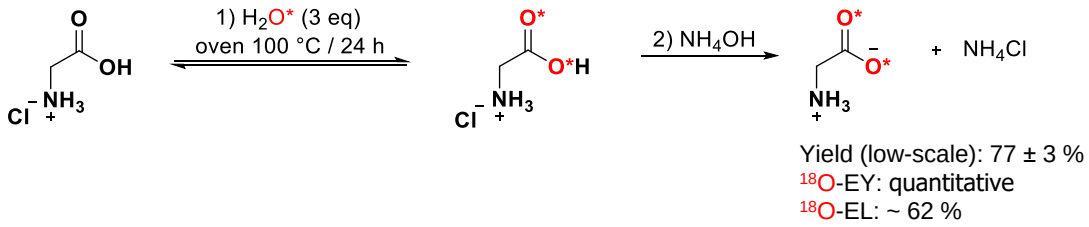

Scheme 4.4: Reaction scheme for labeling glycine using acid catalysed exchange. The yields provided here are those of the isolated pure compounds (see Annexe IV for work-up and purification conditions). The enrichment yield (EY) and level (EL) was measured for Fmoc-protected glycine and is estimated to be the same for unprotected glycine molecules. For the ^{18}O-enrichment, 99% ^{18}O-enriched water was used.

In this protocol, Gly·HCl was placed in a small HPLC vial and 3 equivalents of labeled H_2O^* were added. The vial was closed and placed in an oven heated at 100 °C for 24 h. The water introduced was not sufficient to dissolve the Gly·HCl substrate at room temperature, but with increasing temperature all Gly·HCl eventually dissolved.

For the work-up, the same amount of non-labeled water as for the saponification (800 µL) was used. The pH was set to 3 - 4 using an aqueous solution of NH_4OH, and glycine was precipitated here using *i*-PrOH as anti-solvent. The enrichment level (estimated from the results of Fmoc-Gly-O*H) was ~ 62 %, which is a value slightly higher than the theoretical enrichment level expected in the reaction conditions used (~ 60 %) and corresponds to the quantitative exchange of oxygens. The small difference is probably caused by small inaccuracies in the experimental conditions (in the exact mass of Gly·HCl and exact volume of H_2O^* used). The labeled glycine was obtained pure as mixture of polymorphs in overall higher

yield (77 ± 3 %, compared to ~ 55 % obtained using mechanochemical saponification), and with no traces of NH_4Cl by-product.

The two enrichment protocols for glycine are compared in Table 4.3. In contrast to the mechanism of enrichment *via* saponification, where only one oxygen per carboxylic molecule is labeled, using the H^+ catalytic exchange protocol glycine can be enriched on both oxygens in one carboxylic function simultaneously, resulting in the increase of overall enrichment level (considering the number of equivalents of enriched water per glycine used here). On the other hand, the mechanochemical saponification takes only 30 min of reaction time and about 45 min for the work-up (compared to more than 24 h for H^+ catalytic exchange), and provides the labeled glycine purely as β-polymorph. Based on the intended application and material/instrumentation/time availabilities, both protocols can be seen as complementary.

Table 4.3: Comparison of the two labeling schemes proposed here for glycine enrichment (low-scale conditions).

Enrichment method	Reagents	Reaction conditions	Overall time[a]	Yield	EL[b] [%]	XRD purity
Saponification (VBM)	Gly-OMe·HCl /NaOEt/H_2O*	VBM (25 Hz / 0.5 h / rt)	< 1.5 h	52 mg 55%	43	pure β-form
H^+ catalysed exchange	Gly·HCl /H_2O*	furnace (24 h / 100 °C)	> 24 h	72 mg 77%	62	mixture of polymorphs

[a] Overall time = reaction time + time spent on the work-up, [b] EL = ^{18}O-enrichment level using 99% ^{18}O-enriched water.

c) Solid-state NMR analyses

Glycine belongs to the amino acids frequently studied by solid-state NMR spectroscopy, where it also serves as a reference or a set-up sample for different NMR experiments. The studies available in the literature focus mainly on the analyses of ^{1}H, ^{13}C and ^{15}N nuclei. The commercially available ^{13}C or ^{15}N enriched compounds have been used for example to study glycine polymorphism,[51-53] or to investigate its coordination to the inorganic surfaces.[54] On the other hand, ^{17}O solid-state NMR studies of glycine are much less common.[55-56] This is mainly caused due to the general commercial unavailability of ^{17}O-labeled glycine, and the necessity of pre-labeling the sample before conducting ^{17}O NMR study.

The ^{17}O solid-state NMR spectra reported in the literature are mainly those of the ^{17}O-labeled Gly·HCl form,[11, 57-58] resulting from the typical way of glycine enrichment *via* HCl catalysed exchange. Only one previous study of β-glycine was performed by Yamada *et al.* in 2008, in which 1D ^{17}O MAS NMR spectra of β-glycine at 11.7 and 16.4 T were reported.[56]

In the Figure 4.8e, the ^{17}O MAS NMR spectrum of ^{17}O-labeled β-glycine synthesized by mechanochemical saponification and recorded at 14.1 T is compared to the spectrum simulated from the previously published data.[56] Based on the crystal structure of β-glycine and the work by Yamada, two distinct ^{17}O NMR signals were expected with very similar NMR parameters. However, they could not be resolved in our case at 14.1 T. Moreover, on our spectrum, it looks like the signal consists of two or more components, one of which is the expected β-glycine, and the other is a higher frequency shoulder (marked with a "?" symbol in Figure 4.8). This was a surprising result, since based on the XRD analysis only the β-form of glycine should be present. Also, in the ^{13}C CPMAS NMR spectrum, the β-glycine form was clearly the predominant component (Figure 4.8c). When looking closely at the main carboxylic peak in ^{13}C NMR, a small shoulder of another yet unidentified compound can be noticed at higher frequency (Figure 4.8c). However, the amount of this component does not appear sufficient to explain the high-frequency contribution observed in the ^{17}O NMR spectrum.

In order to try to understand the origin of this unexpected ^{17}O resonance, a series of experiments varying the relaxation time (D1) from 0.5 to 32 s was performed, but no difference in relaxation of the respective signal contributions was observed. Additional experiments were then performed at higher field (20.0 T) analysing the same sample. The 1D ^{17}O MAS spectrum (recorded in just 34 min) is shown in Figure 4.8f. Although in this spectrum the additional high-frequency contribution is also visible, its intensity with respect to the β-Gly signal seems to be lower compared to the spectrum recorded previously at 14.1 T. A 2D MQMAS experiment was attempted, but unfortunately, due to a lack of experimental time, it did not lead to completion. Another possibility could be effects related to the preferential orientation of the crystallites in the rotor.

Although further analyses would be needed to fully interpret the solid-state NMR data, it can be concluded that the results presented here demonstrate that the ^{17}O-enrichment level of β-glycine prepared by mechanochemical saponification is high enough to record 1D ^{17}O MAS NMR spectra in short time with very good signal-to-noise ratio. This is actually an important parameter required for the preparation and study of more complex structures, such as peptides.

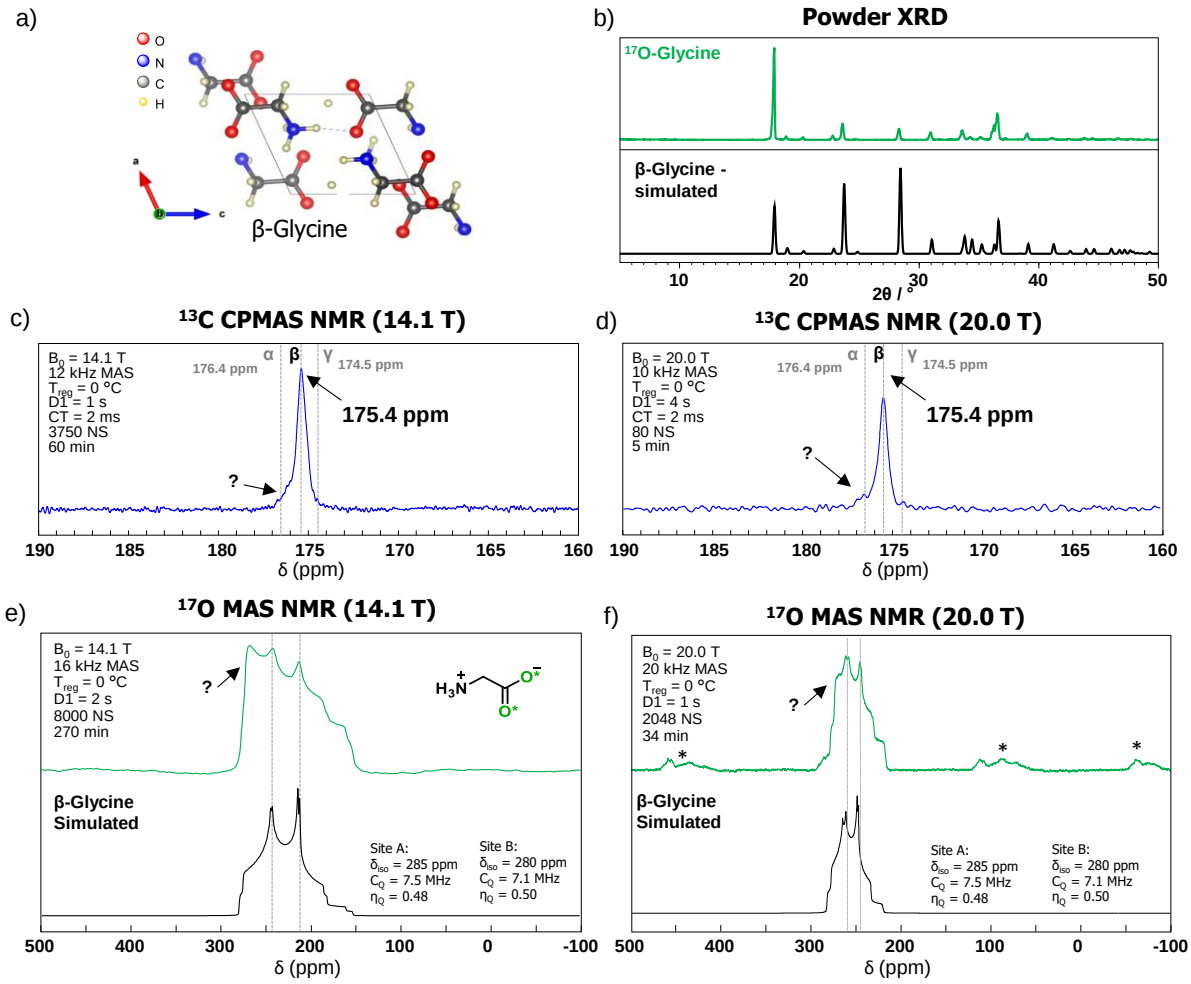

Figure 4.8: a) Crystal structure of β-glycine, b) XRD powder pattern of ^{17}O-labeled Gly compared to simulated powder pattern of β-glycine (COD-5000008), c) and d) ^{13}C CPMAS NMR spectrum of ^{17}O-labeled Gly recorded at 14.1 T and 20.0 T, respectively, e) and f) ^{17}O MAS NMR spectrum of ^{17}O-labeled Gly recorded at 14.1 T and 20.0 T, respectively, compared to the one simulated using previously reported NMR parameters for β -glycine.[56] Analyses at 20.0 T were performed by Dr. Dinu Iuga. Symbol "*" stands for spinning side bands. Only one carboxylic oxygen was labeled per molecule using mechanochemistry, but globally both C=O and C-OH sites are labeled (50 : 50).

4.2.2.2 L-Leucine (Leu, L) and L-Phenylalanine (Phe, F)

L-Leucine and L-Phenylalanine belong to the group of amino acids with neutral hydrophobic side-chains: an isobutyl chain (for Leu) and a benzylic group (for Phe). Unlike for glycine, due to the presence of the specific side-chains, all the other amino acids contain a stereogenic centre at the α-carbon position, making the molecules optically active. For each enantiomer of amino acids (D- or L-), different reactivity can be observed when placed in a chiral environment, such as when in interaction with other chiral molecules. It was therefore important to examine enantiomeric purity of ^{17}O/^{18}O-labeled amino acids after enrichment procedures.

Contrary to glycine, only one polymorph of L-Leu is stable at room temperature and atmospheric pressure. It can be obtained either by crystallization from a mildly acidic aqueous solution of leucine, or by precipitation using an anti-solvent.[59-60] However, a number of structural phase transitions as a function of temperature between ~ -123 and ~ 97 °C was observed.[61] On the other hand, the polymorphism of L-Phe at ambient conditions is still under investigation, and up to four different forms were crystallographically refined so far, all of which were likewise typically obtained by crystallization from acidic or neutral L-Phe solutions.[62-64]

In this chapter, only the $^{17}O/^{18}O$-enrichment of L-Leu and L-Phe using VBM saponification at low-scale will be discussed. The scale-up procedures and acid-catalysed exchange were not performed yet on these two molecules, as the priority was set on some of the other amino acids described in this chapter.

a) $^{17}O/^{18}O$-Labeled L-Leu and L-Phe enriched by VBM saponification

Due to the very similar physicochemical properties of L-leucine and L-phenylalanine, the reaction and work-up conditions were optimized for the two molecules simultaneously. Both amino acids were enriched in $^{17}O/^{18}O$ *via* VBM saponification of their respective methyl ester derivatives (Schemes 4.5 and 4.6). Full hydrolysis was achieved within 30 min of milling at 25 Hz in the presence of NaOEt (2.5 eq.) and labeled H_2O^* (2 - 3 eq.), as demonstrated by the shift of the C=O stretching vibration bands (from 1738 to 1556 cm^{-1} for L-Leu and from 1744 to 1552 cm^{-1} for L-Phe) by IR spectroscopy (see Annexe IV).

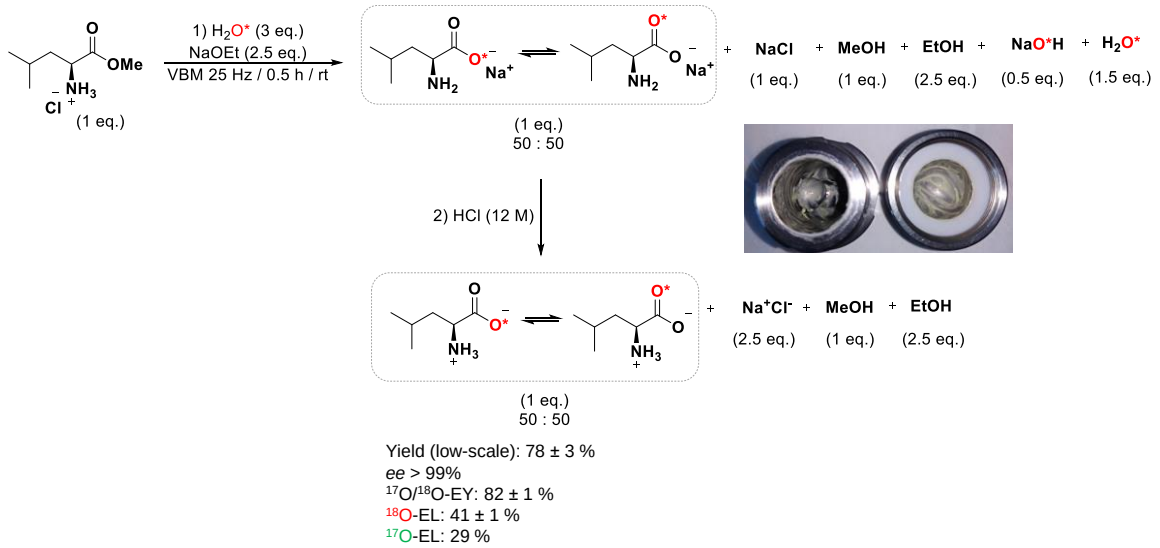

Scheme 4.5: Reaction scheme for enrichment of L-leucine using mechanochemistry. The dilution of labeled water after acidification with aqueous HCl is not shown in the scheme. The yields provided here are those of the isolated pure compounds (see Annexe IV for work-up and purification conditions). For the $^{17}O/^{18}O$-enrichment, 70% ^{17}O and 99% ^{18}O-enriched water was used, respectively.

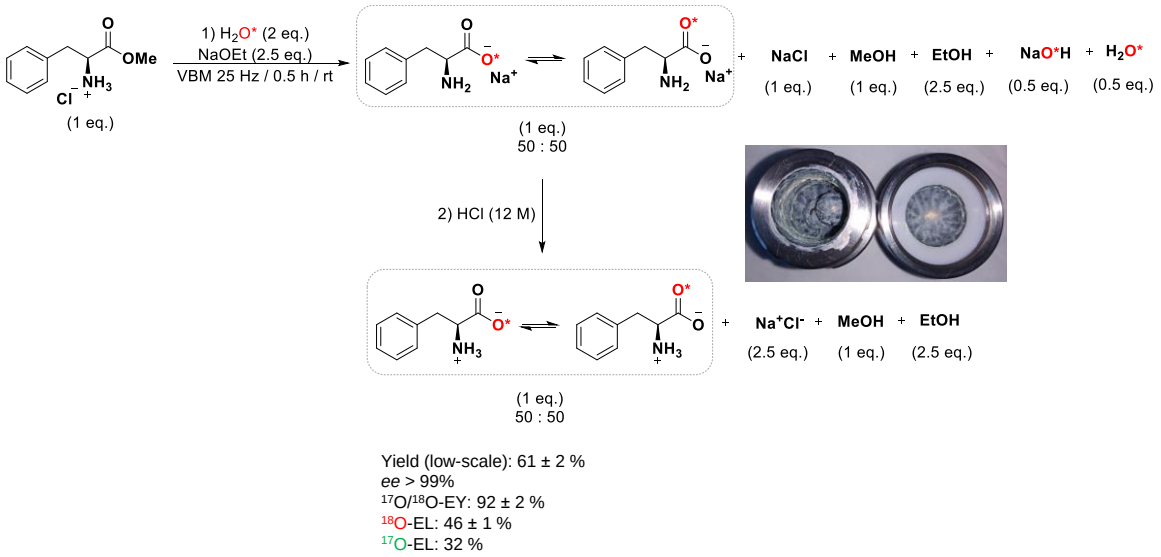

Scheme 4.6: Reaction scheme for enrichment of L-phenylalanine using mechanochemistry. The dilution of labeled water after acidification with aqueous HCl is not shown in the scheme. The yields provided here are those of the isolated pure compounds (see Annexe IV for work-up and purification conditions). For the $^{17}O/^{18}O$-enrichment, 70% ^{17}O and 99% ^{18}O-enriched water was used, respectively.

Unexpectedly, a lower enrichment yield (~ 83 %) was obtained for L-Leu, leading to only 41 % average enrichment level of the carboxylic oxygens, even when using 3 equivalents of ^{18}O-labeled H_2O^* (44.5 µL). Under these operating conditions, based on our other results, a value closer to 46 % would have been expected. This decrease is probably caused by the presence of non-labeled water or non-labeled L-Leu·HCl in the commercial L-Leu-OMe·HCl phase, as the lower enrichment could not be compensated by further increasing the amount of labeled water used. Noteworthy, in the case of L-Phe, only two equivalents of labeled H_2O^* (25 µL) were sufficient to reach full conversion with high enrichment yield (~ 93 %) and with the corresponding enrichment level (~ 46 % for ^{18}O-labeled L-Phe).

Due to the relatively low water solubility of Leu and Phe in a wide range of pH ($4 < pH < 9$), especially in comparison to NaCl, the straightforward work-up strategy was to dissolve the reaction mixtures in a minimal amount of water (as for the glycine), and then to set the pH to pI ~ 5 - 6 in order to induce the precipitation of the amino acid (Figure 4.9). As expected, the low water solubility of neutral molecules caused rapid precipitation when pH decreased below ~ 10. Unfortunately, the sponge-like precipitate absorbed all the water making it impossible to set the pH correctly. Moreover, the voluminous precipitates were found to be contaminated by NaCl in the end.

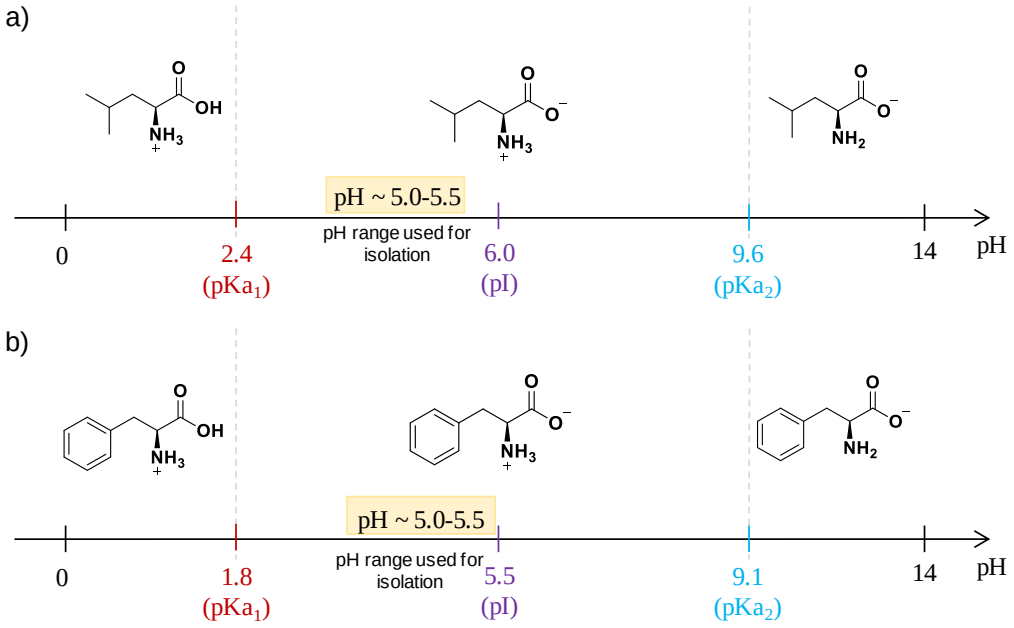

Figure 4.9: pH scale with pKa values and the chemical formulas of the predominant forms of a) L-leucine, b) L-phenylalanine in pure water depending on the pH zone. In the orange rectangle, the pH range at which L-Leu and L-Phe were isolated is highlighted.

To solve this problem, reaction mixtures were dissolved in a larger volume of non-labeled water and properly acidified to the pH ~ 5.0 - 5.5. When the acidification was followed more precisely with a pH probe, the pH decreased gradually as expected with no abnormalities. In order to avoid NaCl contaminations in the voluminous precipitates of Leu and Phe, the aqueous solutions were lyophilized and then re-dispersed in a mixture of MeOH/water and sonicated. After sonication, the suspensions were allowed to cool down to room temperature, and were placed in the fridge for another hour to enhance the precipitation of amino acids.

Using these optimized protocols, pure $^{17}O/^{18}O$-labeled L-Leu and L-Phe were isolated reproducibly in medium to high yields (~ 60 - 80 %), and with high enrichment levels (> 40 %) (see Schemes 4.5, 4.6). The optical purity of ^{18}O-labeled amino acids was first analysed by polarimetry, suggesting no racemization had occurred. The enantiomeric excess was then determined more precisely by chiral HPLC using Fmoc-protected ^{18}O-labeled compounds (their syntheses will be discussed later in Chapter 4.3). No loss of enantiomeric excess was observed (*ee* > 99%, see Annexe IV).

As mentioned above, in this work, $^{17}O/^{18}O$-labeled L-Leu and L-Phe were isolated as pure free amino acids, which contrasts to some of the previous enrichment studies, in which they had been obtained in the forms of HCl salts (typical products of HCl catalysed exchange procedures),[11, 65] or as amino acids already protected by Fmoc or Boc protection groups.[21, 23] To the best of our knowledge, only in two previous works, ^{17}O-labeled L-Leu[66] and L-Phe[17]

were isolated as free neutral amino acids (as in our case), but due to the lack of experimental details in the two publications, these studies could not be used for comparison of the labeling strategies.

Regarding the enrichment, in most of the protocols available so far, L-Leu and L-Phe had been typically enriched by Brönsted-acid catalysed exchange in the presence of an excess of labeled water acidified with HCl gas,[11, 65] which led to the labeling of both oxygens and thus higher enrichment levels (~ 60 - 80%). Here, the use of mechanochemical saponification, where only one oxygen per carboxylic function was labeled, resulted in lower average enrichment levels (~ 40 - 46%). However, these lower enrichment levels achieved were compensated by the lower amount of labeled water consumed, where only 2 - 3 equivalents of H_2O* were used in saponification compared to more than 40 - 100 equivalents excess of H_2O* necessary for efficient acid catalysed exchange.[14]

In the future, it is planned to perform a more direct comparison of VBM saponification and acid-catalysed exchange procedures for the L-Leu and L-Phe, by adapting the acid-catalysed protocol used for glycine enrichment (see Chapters 4.1.2 and 4.2.2.1-section b). The HCl salt of L-Phe would serve as starting materials in this procedure. However, in the case of L-Leu, due to the commercial unavailability of L-Leu·HCl, the acid catalysed exchange of L-Leu would require to employ an external acid (such as HCl gas, aqueous HCl or a Lewis acid catalyst, as developed further below) for the catalysis.

b) Solid-state NMR analyses

Both L-Leu and L-Phe had been previously studied by solid-state NMR spectroscopy. For example, when incorporated in a peptide, the dynamics and orientation of leucine side-chains in collagen-fibrils,[67] or the interactions of the phenylalanine ring with the hydroxyapatite surface[68-69] were studied by ^{2}H, ^{13}C and ^{15}N solid-state NMR spectroscopy. Moreover, the ring dynamics of L-Phe samples crystallized from different solvents were as well explored by ^{2}H and ^{13}C NMR.[70-71]

Regarding the available ^{17}O NMR data of free L-Leu and L-Phe in their neutral forms, one example of 1D ^{17}O MAS NMR spectrum was previously published for each of the two amino acids.[66, 72] Although based on the crystal structures, four different oxygen sites were expected for both molecules, only two sites were actually assigned on the ^{17}O NMR spectrum of L-Leu recorded at 9.4 T in the work of Prasad *et al.*,[66] and also on the ^{17}O NMR spectrum of L-Phe recorded at 14.1 T and 16.4 T in the work published by Yamada *et al*.[72]

In the Figures 4.10 and 4.12, the crystal structures, the ^{13}C CPMAS NMR spectra recorded at 14.1 T and the ^{17}O MAS NMR spectra recorded at multiple fields (9.4, 14.1 and 18.8 T) of L-Leu and L-Phe labeled in ^{17}O *via* VBM saponification are presented.

The ^{13}C CPMAS NMR spectrum of the ^{17}O-labeled L-Leu clearly shows two sets of signals resolved for all the carbons except for the methyl groups (Figure 4.10b). The ^{17}O MAS NMR spectra recorded at three different fields (9.4, 14.1 and 18.8 T) show multiple overlapping signals (Figure 4.10c).

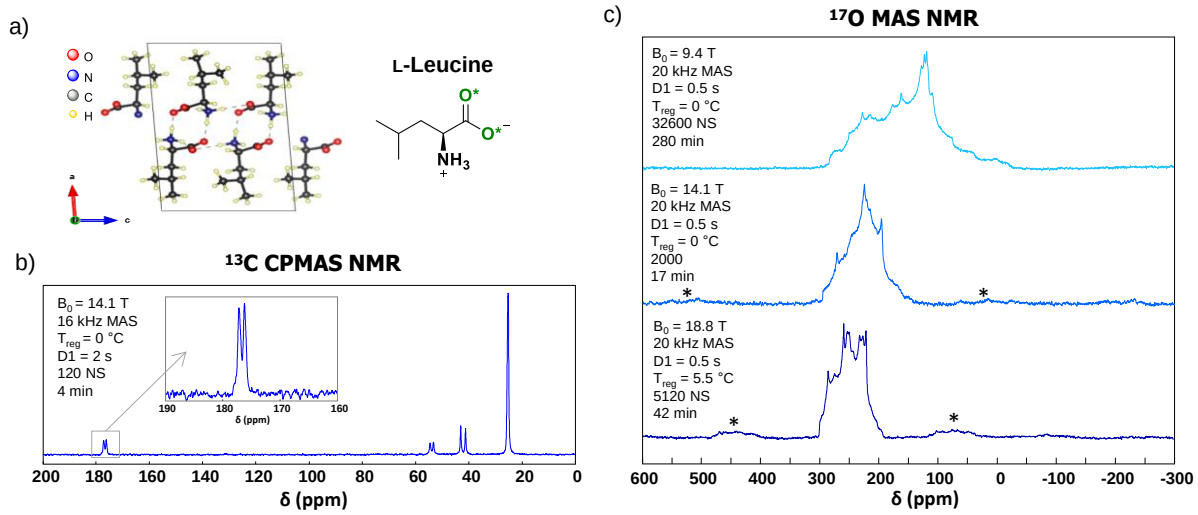

Figure 4.10: a) Crystal structure of L-Leu (CCDC number: 1206031), b) ^{13}C CPMAS NMR spectrum of L-Leu recorded at 14.1 T, and c) ^{17}O MAS NMR spectra of L-Leu recorded at 9.4, 14.1 and 18.8 T. Analyses at 9.4 and 14.1 T were performed by Dr. Ieva Goldberga, analysis at 18.8 T was performed by Dr. Julien Trébosc. Symbol "*" stands for spinning side-bands. Only one carboxylic oxygen was labeled per molecule using mechanochemistry, but globally both C=O and C-OH sites are labeled (50 : 50).

With the aim to distinguish the overlapping sites, a series of ^{17}O Hahn-echo experiments was first performed at 14.1 T (data not shown), from which ^{17}O NMR parameters of only one oxygen site could be tentatively extracted. A 2D MQMAS experiment was also recorded at 14.1 T, in which the contribution of four different sites could be suspected in the indirect dimension (data not shown). Yet, none of the sites could be resolved with sufficient sensitivity, under the acquisition conditions used. When a 2D MQMAS experiment was performed at 18.8 T without a temperature regulation (Figure 4.11a), two oxygen sites were successfully resolved, and parameters were tentatively extracted (see Figure 4.11). Yet, this 2D MQMAS spectrum showed a "smearing" of the signals between the two resolved sites. The observed "smearing" could result from dynamics occurring at the oxygen sites. This would be consistent with the fact that the 1D ^{17}O lineshape actually changes depending on the acquisition temperature (Figure 4.11b).

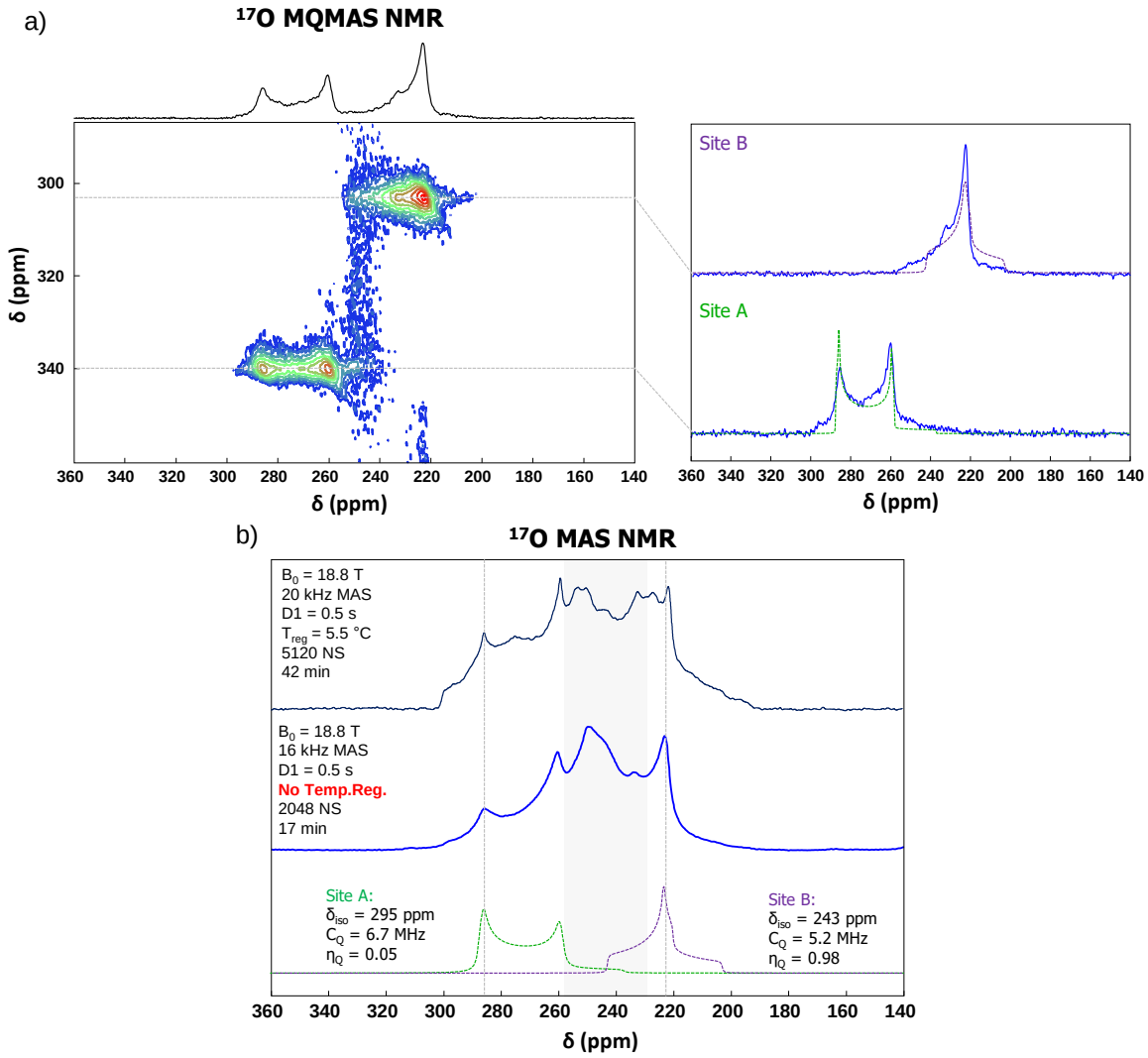

Figure 4.11: a) ^{17}O MQMAS NMR spectrum of L-Leu recorded at 18.8 T by Dr. Ivan Hung, with no temperature regulation, and with two extracted oxygen sites (shown on the right, with a tentative fit below). b) Comparison of 1D ^{17}O MAS NMR spectra of L-Leu, both recorded at 18.8 T, with and without temperature regulation (top and middle spectrum, respectively).

As already mentioned above for L-Leu, phase transitions have been described to take place between -123 and 97 °C.[61] For most of the ^{17}O and ^{13}C NMR analyses of ^{17}O-enriched L-Leu described above, except for some of the ones performed at 18.8 T (Figure 4.11a and 4.11b-middle), the temperature had been regulated during the measurements between 0 and 5 °C (temperature of regulation), ensuring that a single phase is present. In contrast, the changes in ^{17}O lineshapes observed in absence of the temperature regulation appear to be caused by the sample heating, which may enable the "activation" of different movements around the oxygen atoms within the crystal structure, which may eventually lead to the phase transitions. Thus, in order to better understand the phase transitions occurring in leucine, and help further resolve the different oxygen sites (when possible), additional ^{17}O NMR experiments, including at variable temperature and using MQMAS, are planned at high field.

Overall, the high ^{17}O-enrichment level of L-Leu prepared by mechanochemistry enabled to record a 1D ^{17}O MAS NMR spectrum with a good signal-to-noise ratio in only 17 min at 14.1 T. Compared to the literature,[66] the spectra recorded here (including the one at 9.4 T) are clearly composed of more than two overlapping oxygen sites, out of which two resonances could be resolved and the related quadrupolar parameters were extracted. This discrepancy with previously reported data could be explained by a different temperature used for the ^{17}O NMR experiments. Yet, this point could not be verified due to the absence of temperature specification in the published work.

In the case of ^{17}O-labeled L-Phe, in the ^{13}C CPMAS NMR spectrum (Figure 4.12b), two sets of signals are observed in the aromatic and aliphatic regions. These two sets of signals correspond to the two types of molecules present in the ^{17}O-labeled L-Phe: where one type is undergoing rapid ring flips, while the other type has more constrained rings.[70-71] In addition, a broad asymmetric carboxylic peak was observed suggesting two unresolved components. This is in agreement with the ^{13}C NMR data published previously for a L-Phe sample crystallized from water.[70] Using the^{17}O MAS NMR spectra recorded at multiple magnetic fields (9.4, 14.1 and 18.8 T), the parameters for three oxygen sites were tentatively extracted, and the fits with corresponding values are presented in Figure 4.12c,d. However, the remaining fourth site was not resolved, although its contribution is reflected in the ratio of the fitted sites (1:1:2). Due to a very long relaxation time (D1 > 4 s), and lack of sufficient instrument time, no MQMAS experiments were performed at this stage.

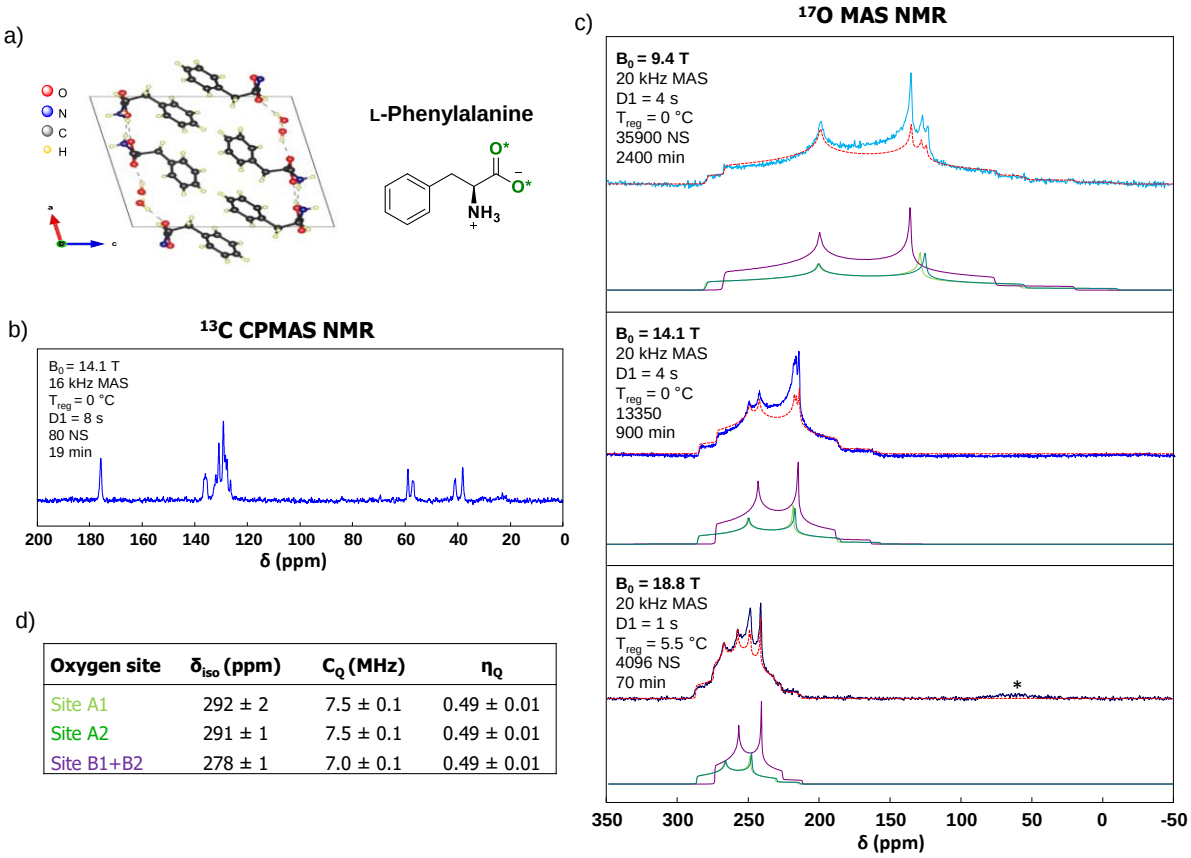

d)

Oxygen site	δ_{iso} (ppm)	C_Q (MHz)	η_Q
Site A1	292 ± 2	7.5 ± 0.1	0.49 ± 0.01
Site A2	291 ± 1	7.5 ± 0.1	0.49 ± 0.01
Site B1+B2	278 ± 1	7.0 ± 0.1	0.49 ± 0.01

Figure 4.12: a) Crystal structure of L-Phe (CCDC number: 1012154), b) ^{13}C CPMAS NMR spectrum of L-Phe recorded at 14.1 T and c) ^{17}O MAS NMR spectra of L-Phe recorded at 9.4, 14.1 and 18.8 T. Analyses at 9.4 and 14.1 T were performed by Dr. Ieva Goldberga, analysis at 20.0 T was performed by Dr. Julien Trébosc. Symbol "*" stands for spinning side bands. Only one carboxylic oxygen was labeled per molecule using mechanochemistry, but globally both C=O and C-OH sites are labeled (50 : 50).

Overall, thanks to the high enrichment level of ^{17}O-labeled L-Phe, the 1D spectra were recorded with a good signal-to-noise ratio in a very short time (70 min at 18.8 T), despite the rather longer relaxation time (D1) (compared to other amino acids in this study). The tentatively extracted parameters for three oxygen sites are close to the values reported by Yamada,[72] although in the previously published work, only two sites had been resolved. The presence of a remaining unresolved oxygen site is apparent from our spectra, and recording a 1D ^{17}O spectrum at an even higher field (like 35.2 T) or performing a 2D NMR experiment should help with its final deconvolution.

4.2.3 Acidic side-chain amino acids

L-Asp and L-Glu both contain a second carboxylic function in their side-chains and therefore belong to the group of acidic amino acids. Both of these molecules are also optically active, due to the presence of a chiral centre at the α-carbon position. Only one crystalline form of L-aspartic acid was reported so far, and was crystallized from its aqueous solution.[73] On the

other hand, two polymorphs are known to form from aqueous L-glutamic acid solutions, a metastable α-form which transforms gradually to the stable β-form. The rate of this transformation depends on various conditions: it can be promoted with increasing temperature or inhibited with additives (*e.g.* trimesic acid).[74]

When present in peptide/protein chains, the carboxylic group in the side-chain is in general not involved in the backbone peptide bond formation, instead it remains free and often plays an essential role interacting with the binding site of substrates.[75-76] Proteins with unusually acidic segments have been found in almost all mineralized tissues.[77] For example, depending on the concentration, aspartic acid rich proteins were found to inhibit or accelerate growth of calcium oxalate phases and to alter the crystallization pathway of calcium carbonate leading to different polymorphs.[78-79] Therefore, it would be very interesting to study by ^{17}O NMR the mode of binding of these proteins at the surface of different mineral phases.

4.2.3.1 L-Aspartic acid (Asp, D)

Two different enrichment protocols were applied for the enrichment of aspartic acid: saponification under mechanochemical conditions and Lewis acid catalysed oxygen exchange. Moreover, selective labeling schemes targeting only one of the two carboxylic functions present in the structure of aspartic acid were also developed (Figure 4.13).

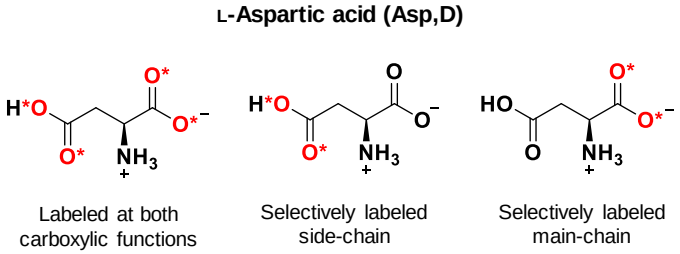

Figure 4.13: L-Aspartic acid enriched in $^{17}O/^{18}O$ at both carboxylic functions or selectively either at the side-chain or the main-chain carboxylic function. Depending on the labeling strategy used, one or both oxygens per carboxylic function were enriched.

a) $^{17}O/^{18}O$-Labeled L-Aspartic acid enriched by mechanochemical saponification

At first, a protocol for the labeling of both carboxylic functions was developed and optimized before being adapted for selective labeling. In this case, the L-aspartic acid dimethyl ester derivative was hydrolysed under basic conditions using 4 equivalents of labeled H_2O^*. As evident from the photo in the Scheme 4.7, the reaction mixture was not distributed homogeneously after saponification, but instead a sticky rubber-like paste was located at one spot in the top part of the jar and in the middle of the bottom part of the jar. Moreover, a liquid phase was also observed at the bottom of the jar. Despite this inhomogeneous aspect of the

reaction medium, full conversion was observed by ATR-IR analyses of samples taken from different parts of the jar after 30 min of milling at 25 Hz, and this observation was later confirmed by high enrichment level measured by HRMS (44 % for ^{18}O-enriched products).

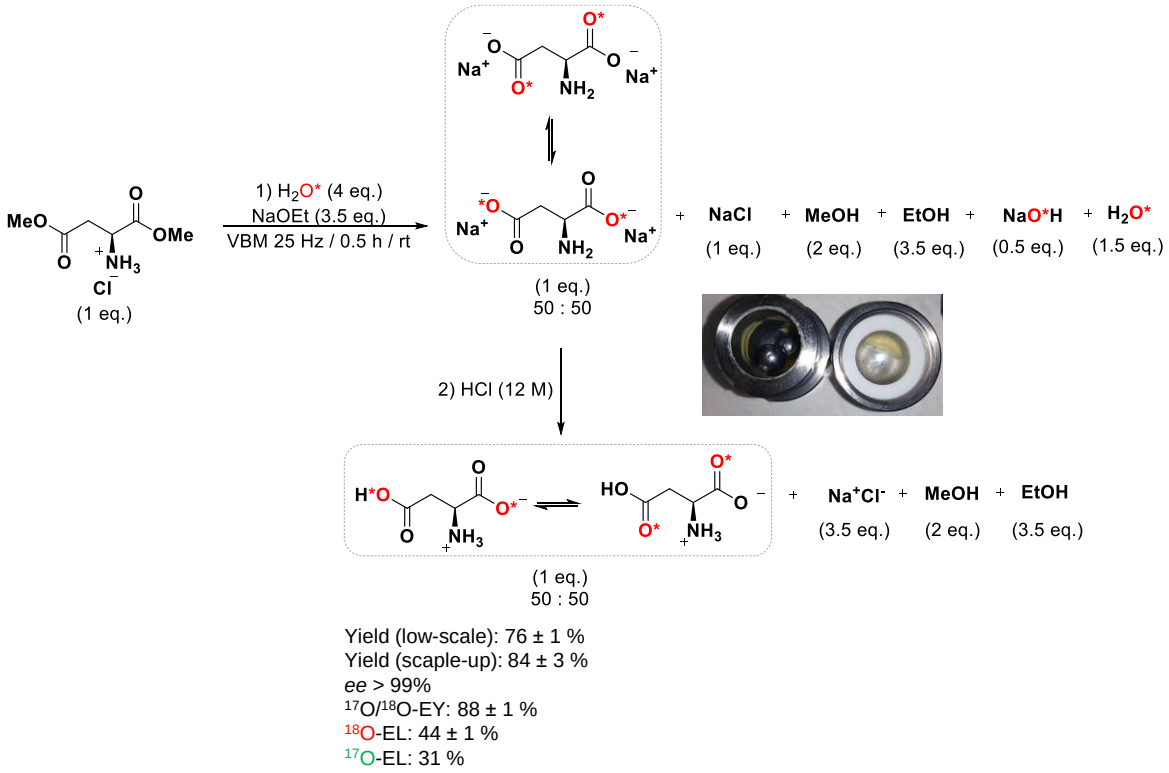

Scheme 4.7: Reaction scheme for the enrichment of L-aspartic acid at both carboxylic functions using mechanochemistry. The dilution of labeled water after acidification with aqueous HCl is not shown in the scheme. The yields provided here are those of the isolated pure compounds (see Annexe IV for work-up and purification conditions). For the ^{17}O/^{18}O-enrichment, 70% ^{17}O and 99% ^{18}O-enriched water was used, respectively.

In its zwitterionic form, L-aspartic acid has the lowest solubility in water of all amino acids in this study (Table 4.1). Therefore, it should be simple to precipitate labeled L-Asp while avoiding the simultaneous precipitation of NaCl. Similarly to glycine, a minimal amount of water was used to dissolve the reaction mixture in the jar, and the solution was acidified using concentrated HCl solution (12M). The acidification was followed by ordinary pH paper and when reaching pH ~ 3 - 4, a voluminous precipitate formed. The suspension was stirred at room temperature for 30 min and then filtered. When washing the solid on the frit with MeOH and Et_2O, a significant amount of precipitate formed in the filtrate suggesting that substantial part of the aspartic acid had not precipitated initially, but had stayed dissolved in the aqueous solution, and was only being precipitated by the anti-solvents now. It is worth noting that the initial product isolated was not contaminated by NaCl, but the yield was not reproducible and reached only around 50 %.

To understand better this behavior, acidification was followed continuously with a pH probe. After the addition of 120 µL of HCl (12M), the pH dropped from 13.5 to ~ 3.9 and a precipitate started to form. This precipitation induced an increase of pH, up to a value of ~ 4.7. Under these conditions, the carboxylic group on the side-chain probably remained partially in the form of sodium salt and together with aspartic acid, already protonated on the side chain, the suspension behaved as a "buffer". Subsequent addition of more HCl (12M) in several steps (total volume of ~ 60 - 120 µL added) was necessary to fully protonate the side-chain carboxylic function, resulting in the pH = 1.25 - 1.52. Although this pH range is well below the pKa_1 of L-aspartic acid (see Figure 4.14), the L-Asp isolated was always in its zwitterionic form, as confirmed by multiple analyses: no additional Cl^- ions were detected by EDX, no additional diffraction peaks were observed in XRD and no shift of ^1H and ^{13}C signals was observed in solution NMR, when compared to the commercial compound. Using this acidification protocol, the average yield increased to 76 ± 1 % for a low-scale synthesis with no NaCl contamination, and the procedure was reproducible.

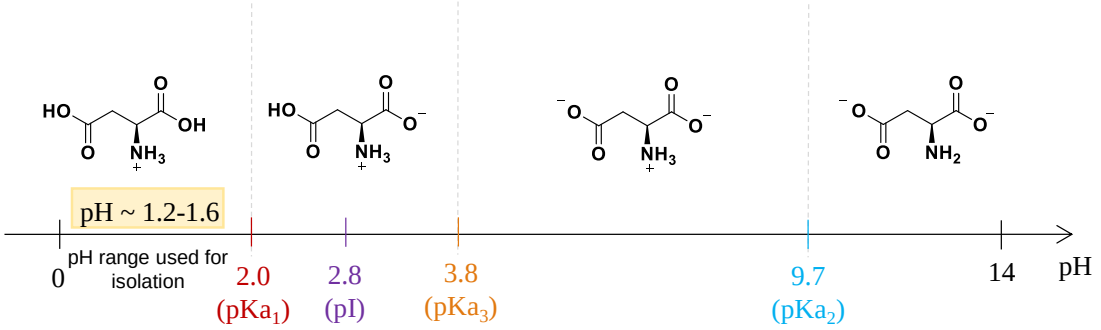

Figure 4.14: pH scale with the pKa values of L-Asp and its predominant chemical formulas in pure water depending on the pH zone. In the orange rectangle, the pH range at which L-Asp was isolated is highlighted.

To evaluate the optical purity of prepared products, ^{18}O-labeled L-aspartic acid was analysed by polarimetry, showing no racemization. The enantiomeric excess was then precisely determined by chiral HPLC using Fmoc-protected ^{18}O-labeled product (synthesis discussed later in this chapter in section 4.3). No loss of enantiomeric excess was observed (*ee* > 99%).

Scale-up procedure:

For the future application of labeled amino acids, it was necessary to scale-up the enrichment protocol producing larger amounts of labeled compounds. Keeping the same jar-size (10 mL inner volume) and the same number and size of balls (2x, 1 cm diameter), the amount of reagents was doubled (*i.e.* starting from 300 mg of L-Asp(OMe)-OMe·HCl and using 110 µL of enriched water). Milling at 25 Hz for 30 min was found sufficient to provide full

conversion, and a slightly higher enrichment level could be achieved (~ 47 % for ^{18}O-labeled products). By doubling also the amount of non-labeled water used for the work-up, and by following the acidification *in-situ*, pure labeled L-Asp could be isolated with overall higher yields compared to the low-scale synthesis (84 ± 3 %, compared to 76 ± 1 % at low scale).

Scaling-up the procedure and doing two reactions at the same time (*i.e.* using both jars of MM400 mixer-mill), allowed around 350 mg of labeled L-Asp to be prepared in only half of a day.

Site-selective ^{17}O/^{18}O-enrichment of L-Asp:

The optimized protocol for L-Asp enrichment described above was then adapted with success for the selective ^{17}O/^{18}O-labeling of the side-chain or main-chain carboxylic groups starting from L-aspartic acid derivatives with only one carboxylic function protected with a methyl ester group (Schemes 4.8 and 4.9).

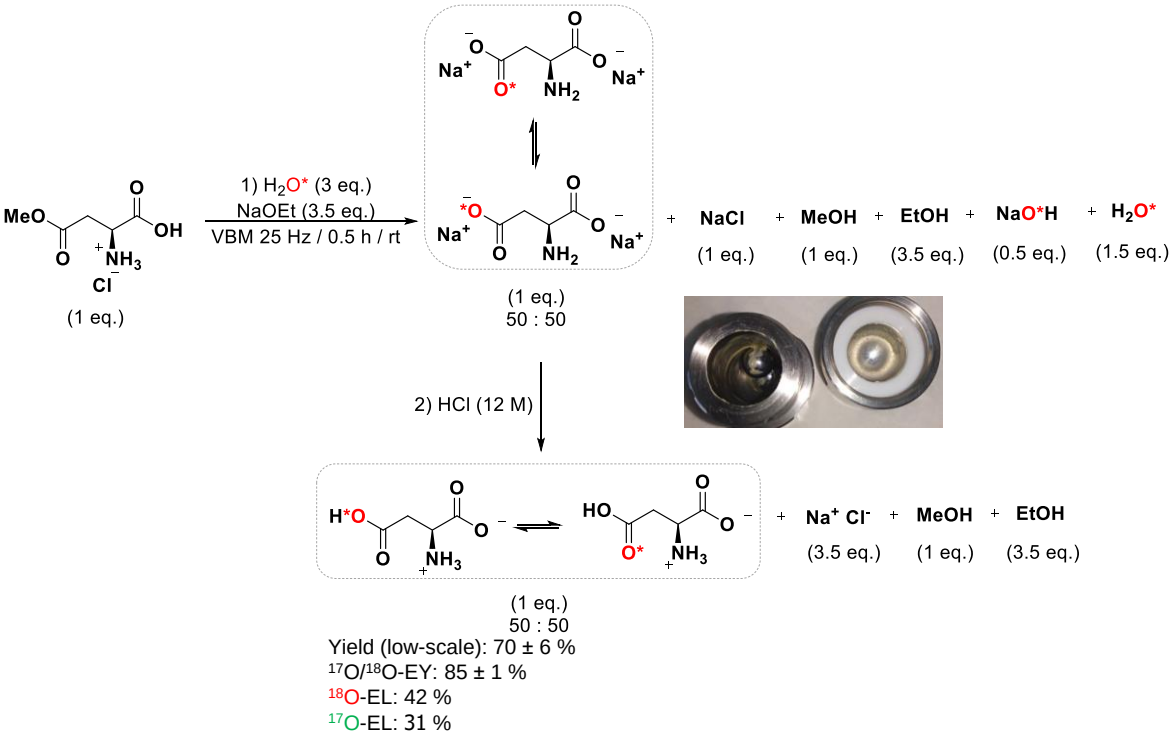

Scheme 4.8: Reaction scheme for the enrichment of L-Aspartic acid selectively at the side-chain carboxylic function using mechanochemistry. The dilution of labeled water after acidification with aqueous HCl is not shown in the scheme. The yields provided here are those of the isolated pure compounds (see Annexe IV for work-up and purification conditions). For the ^{17}O/^{18}O-enrichment, 70% ^{17}O and 99% ^{18}O-enriched water was used, respectively.

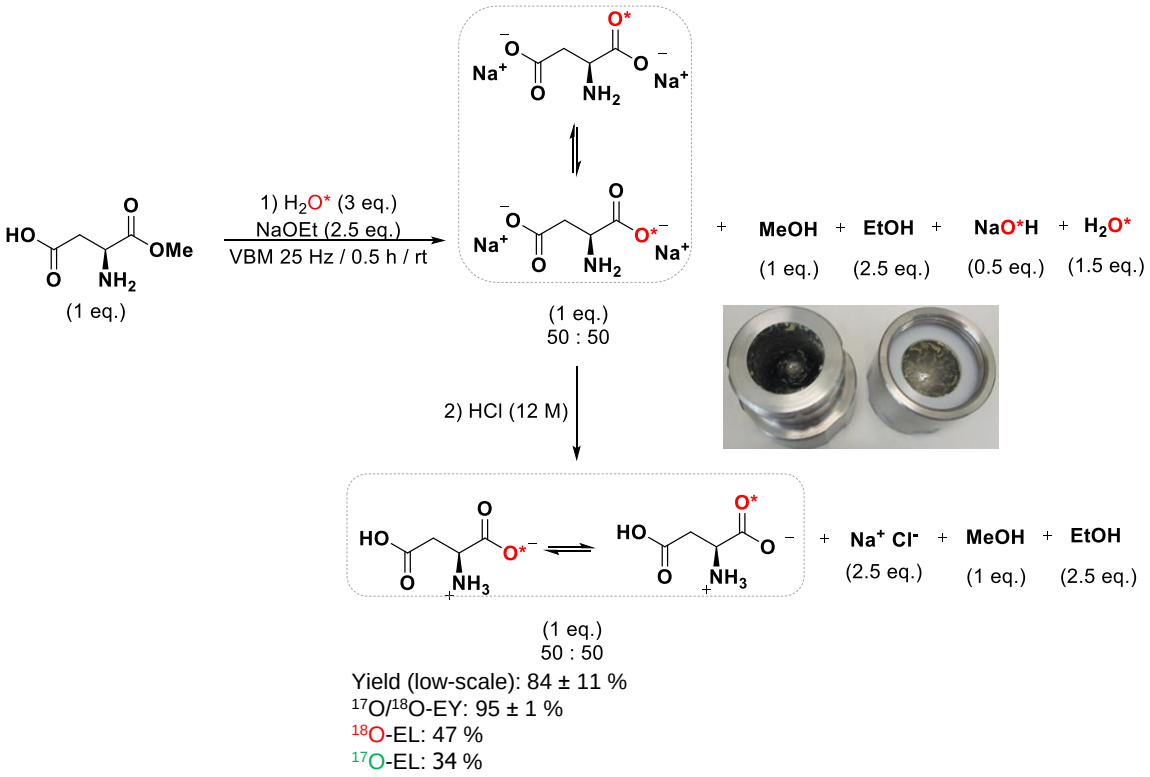

Scheme 4.9: Reaction scheme for the enrichment of L-Aspartic acid selectively at the main-chain carboxylic function using mechanochemistry. The dilution of labeled water after acidification with aqueous HCl is not shown in the scheme. The yields provided here are those of the isolated pure compounds (see Annexe IV for work-up and purification conditions). For the $^{17}O/^{18}O$-enrichment, 70% ^{17}O and 99% ^{18}O-enriched water was used, respectively.

The selectively enriched products were as well isolated pure, with similar or even higher yields and enrichment levels compared to L-Asp enriched at both sides (see Table 4.4). A possible explanation for the overall better results of L-Asp selectively labeled at the main-chain might be in the substrate used here for the enrichment. Indeed, for the main-chain labeling, the L-Asp-OMe used was not in a form of hydrochloride salt (compared to the other two L-Asp substrates). This means that less NaOEt equivalents was required for the reaction and therefore less Na^+Cl^- was subsequently produced in the work-up. As mentioned above in section 4.1.2, the solubility of L-Asp increases with increasing concentration of Na^+Cl^- ions (salting-in), which can explain the higher isolated yield. Regarding the higher enrichment, this can also be caused by the substrate, since the hydrochloride salts might be more hygroscopic, reducing the efficiency of labeling process. All the ^{17}O-labeled products were analysed by ^{17}O solid-state NMR spectroscopy, as further detailed below.

Table 4.4: Summary of results for L-Asp enriched in $^{17}O/^{18}O$ on both carboxylic functions and selectively enriched only at the main/side-chain

Enriched product	Isolated yield	$^{17}O/^{18}O$-EY	^{18}O-EL[a]	^{17}O-EL[b]
Asp-both[c]	80 mg 76 %	88 %	44 %	31 %
Asp-side	77 mg 70 %	85 %	42 %	31 %
Asp-main	113 mg 84 %	95 %	47 %	34 %

Asp-both, Asp-side and Asp-main correspond to L-Asp labeled either on both carboxylic functions, on the side-chain only or main-chain only, [a] Enrichment level using 99% ^{18}O-enriched water, [b] Enrichment level using 70% ^{17}O-enriched water, [c] results for low-scale synthesis.

b) ^{18}O-Labeled L-Aspartic acid enriched via acid catalysed exchange

After having synthesized the L-Asp by mechanochemical saponification, it was envisaged to compare the results with the classical acid-catalysed enrichment protocol. Yet, the only procedure found for the labeling of aspartic acid *via* acid-catalysed exchange in ^{18}O labeled water was not selected for the comparison, as in this work only 1 - 4 mg of amino acids was dissolved in enormous excesses of labeled water (> 740 eq.), which had been acidified with dry HCl gas.[13] Moreover, labeled amino acids were not isolated.[13] This implies that in order to have the same theoretical yield of labeled compound as in our saponification tests, 10 mL of ^{18}O labeled water would have been necessary, which is prohibitively expensive. Therefore, an alternative enrichment procedure adapted from the protocol described above for glycine enrichment was applied here for the labeling of L-aspartic acid (Scheme 4.10).

Due to the commercial unavailability of L-Asp as a hydrochloride salt, the advantage of having the most acidic form of the molecule directly available as a substrate could not be used. In order to avoid using concentrated HCl solution, which would dilute the oxygen-label, the possibility of using a Lewis acid (Li^+) instead to catalyse the isotopic exchange was thus tested. The Li^+ cation is a "hard" Lewis acid with small ionic size witch should interact readily with a carboxylic oxygen ("hard" base), and was therefore chosen here for the activation of carboxylic group.

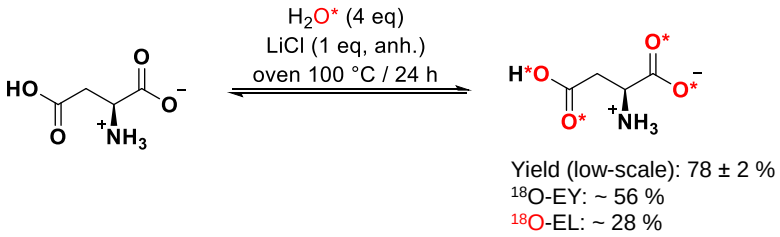

Scheme 4.10: Reaction scheme for enrichment of L-aspartic acid using LiCl catalysed exchange. The yields provided here are those of the isolated pure compounds (see Annexe IV for work-up and purification conditions). For the ^{18}O-enrichment, 99% ^{18}O-enriched water was used.

Here, L-Asp was mixed with anhydrous LiCl (1 eq.) in a vial, and 4 equivalents of ^{18}O-labeled water were added. The vial was closed and placed in an oven heated at 100 °C for 24 h. The pure L-Asp was isolated by filtration, with a yield of 78 ± 2 %, comparable to the yield of saponification (76 ± 1 %) (see Table 4.5). The MS analysis of the recovered product showed an average ^{18}O-enrichment level equal to 28 % (compared to 47 % reached by ball-milling), which corresponds to an enrichment yield of ~ 56 % (table 4.5). The enrichment level could be possibly increased up to 50 % (using the same amount of labeled water) by prolonging the reaction time.

Table 4.5: Comparison of the two labeling schemes proposed here for L-Asp enrichment of both main-chain and side-chain (low-scale conditions).

Enrichment method	Reagents	Reaction conditions	Overall time[a]	Yield	EY[b] [%]	EL[c] [%]
Saponification (VBM)	L-Asp(OMe)-OMe·HCl/ NaOEt/H_2O*	VBM (25 Hz / 0.5 h / rt)	< 1.5 h	80 mg 77%	88	47
Li^+ catalysed exchange	L-Asp/LiCl/H_2O*	furnace (24 h / 100 °C)	> 24 h	81 mg 78%	56	28

[a] Overall time = reaction time + time spent on the work-up, [b] EY = enrichment yield, [c] EL = ^{18}O-enrichment level using 99% ^{18}O-enriched water.

Looking at the MS pattern of L-Asp ^{18}O-labeled *via* acid catalysed exchange (Figure 4.15, bottom), we can clearly see that part of the aspartic molecules contains carboxylic functions labeled at both oxygens (peak "p+6" and "p+8"). Compared to the product labeled *via* saponification (Figure 4.15, top), where the most abundant peak "p+4" represents 2x^{18}O per molecule of L-Asp, but only one in each carboxylic function. Although the enrichment level is not as high as for the saponification, this reaction still offers a very attractive approach. Indeed, for the first time, Lewis catalysis was used here for the enrichment of amino acids, opening new possibilities for the ^{17}O/^{18}O-enrichment of carboxylic acids avoiding the use of corrosive acids such as HCl (aqueous or as a gas) and potentially applicable to amino acids for which hydrochloride salts are not available.

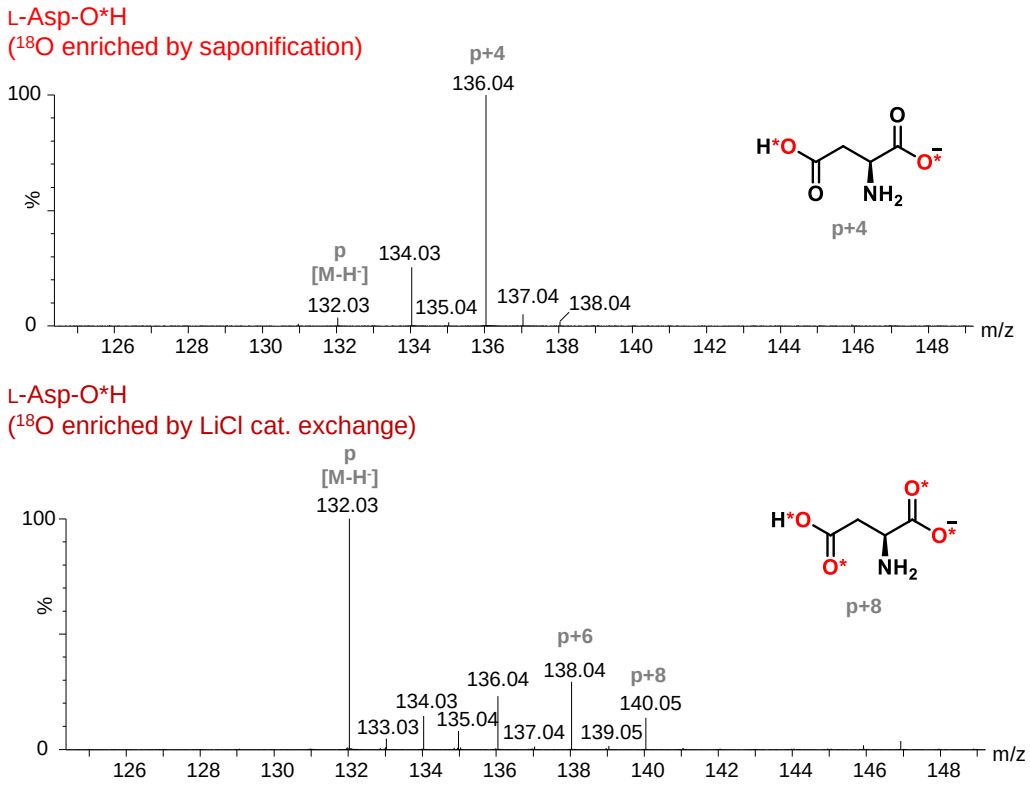

Figure 4.15: Comparison of HRMS (ESI$^-$) patterns of L-Asp-O*H enriched in ^{18}O *via* saponification (top) or Lewis acid-catalysed exchange (bottom). The "p [M-H$^-$]" stands for monoisotopic mass, "p+4" (top) marks the most abundant peak belonging to 2x^{18}O introduced in the molecule (1x^{18}O per carboxylic function), "p+6" and "p+8" (bottom) stands for 3x^{18}O and 4x^{18}O in a molecule, where one COOH has 2x^{18}O and both COOH have 2x^{18}O, respectively.

c) Solid-state NMR analyses

Aspartic acid was previously subjected to solid-state NMR studies to explore its crystallization pathways[80] or its role in bio-mineralization processes.[81] The only ^{17}O NMR data published so far were reported by Yamada *et al.* in 2007 for L-Aspartic acid labeled *solely* at the main-chain and measured at 16.4 T.[82] Based on the L-Asp crystal structure, four oxygen sites in total are expected: two for the main-chain and two for the side-chain carboxylic function. In the previously published work, the two sites corresponding to the main-chain carboxylic group were resolved performing MQMAS experiment.[82] The spectrum simulated from these published parameters is shown in Figure 4.16b, where it is compared to the experimental spectrum we measured at 14.1 T in this study for the same molecule (enriched at main-chain only, by VBM saponification). Here, the recorded spectrum does not match completely with the published data. The different lineshapes may result from a different form of L-Asp studied or a difference in the temperature used for the analyses. Unfortunately, neither the information regarding temperature used for NMR experiments, nor the XRD pattern of the

analysed labeled L-Asp, was provided in the previously published work.[82] Performing 1D ^{17}O MAS NMR experiments at multiple fields (14.1 and 20.0 T) enabled to fit the main-chain signal, and the tentatively extracted parameters are compared to the ones published previously[82] in Figure 4.16b,c. In addition, ^{13}C MAS NMR spectrum of L-Asp labeled at the main-chain was also recorded and is shown in the Figure 4.16a.

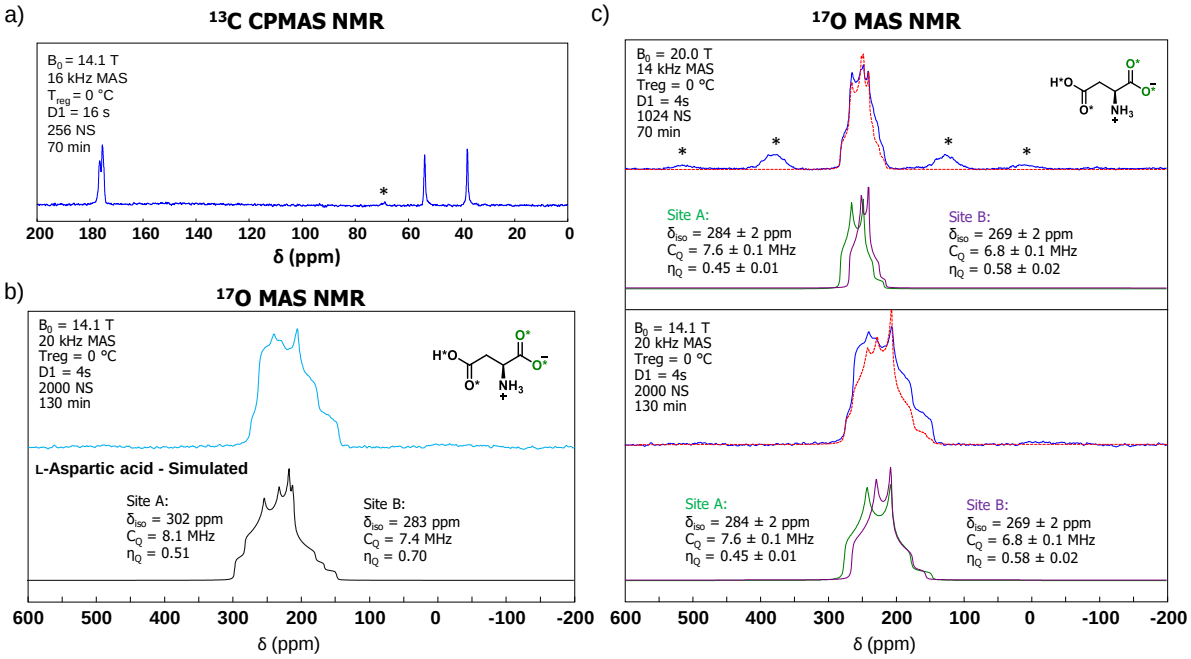

Figure 4.16: a) ^{13}C CP MAS NMR of L-Asp labeled only on the main-chain (recorded at 14.1 T by Dr. Ieva Goldberga), b) ^{17}O MAS NMR spectrum of L-Asp labeled only on the main-chain (recorded at 14.1 T) compared to a spectrum simulated from published data,[82] c) ^{17}O MAS NMR spectra of L-Asp labeled on the main-chain recorded at 14.1 and 20.0 T with extracted parameters. Analysis at 20.0 T was performed by Dr. Ieva Goldberga and Dr. César Leroy. Symbol "*" above the blue curve stands for spinning side-bands. Only one carboxylic oxygen was labeled per molecule using mechanochemistry, but globally both C=O and C-OH sites are labeled (50 : 50).

In addition to the main-chain enriched L-Asp, the ^{17}O MAS NMR spectra of fully-enriched L-Asp and the side-chain enriched L-Asp enriched by VBM saponification were also reported here for the first time (Figure 4.17). Being able to selectively label only one of the two carboxylic functions turned out to be particularly useful to help resolve the four overlapping oxygen sites of L-Asp, when labeled at both carboxylic groups. For the side-chain carboxylic group, the two resonances for C-O*H and C=O* can be clearly distinguished and their ^{17}O parameters were also extracted. It is the first time that a complete analysis of neutral L-Asp is reported.

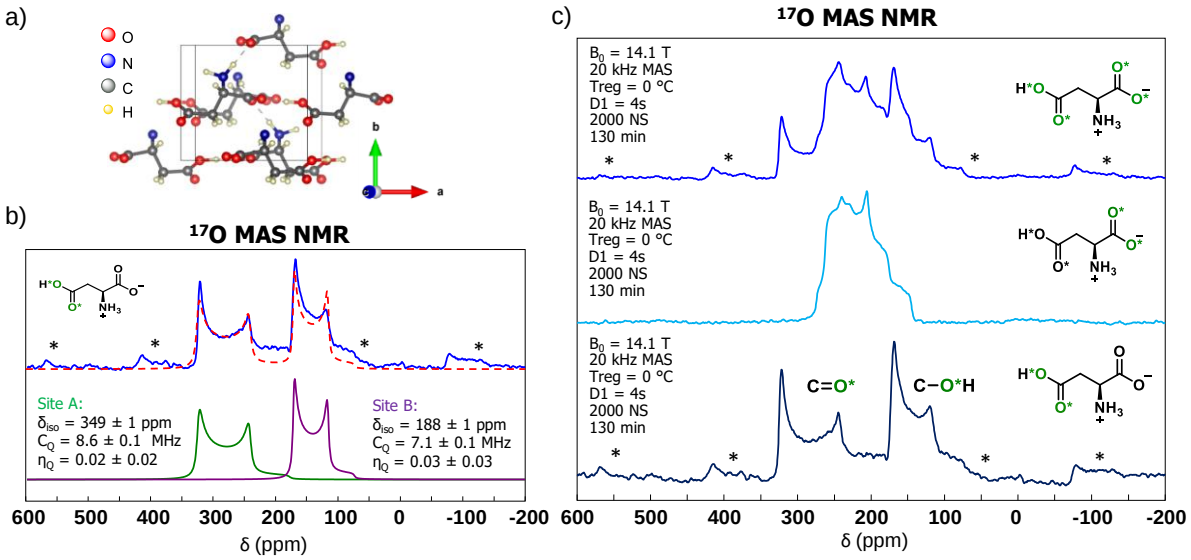

Figure 4.17: a) Crystal structure of L-Asp (CCDC number: 1203754), b) ^{17}O MAS NMR spectrum of L-Asp labeled on the side-chain (recorded at 14.1 T), together with fitted parameters, b) ^{17}O MAS NMR spectra of L-Asp labeled on both carboxylic functions, in comparison with the phases labeled selectively on the main or side-chain carboxylic function. Symbol "*"stands for spinning side-bands. Only one carboxylic oxygen was labeled per molecule using mechanochemistry, but globally both C=O and C-OH sites are labeled (50 : 50) as apparent from the ^{17}O NMR spectrum in b).

4.2.3.2 L-Glutamic acid (Glu, E)

a) ^{17}O/^{18}O-Labeled L-Glutamic acid enriched by mechanochemical saponification

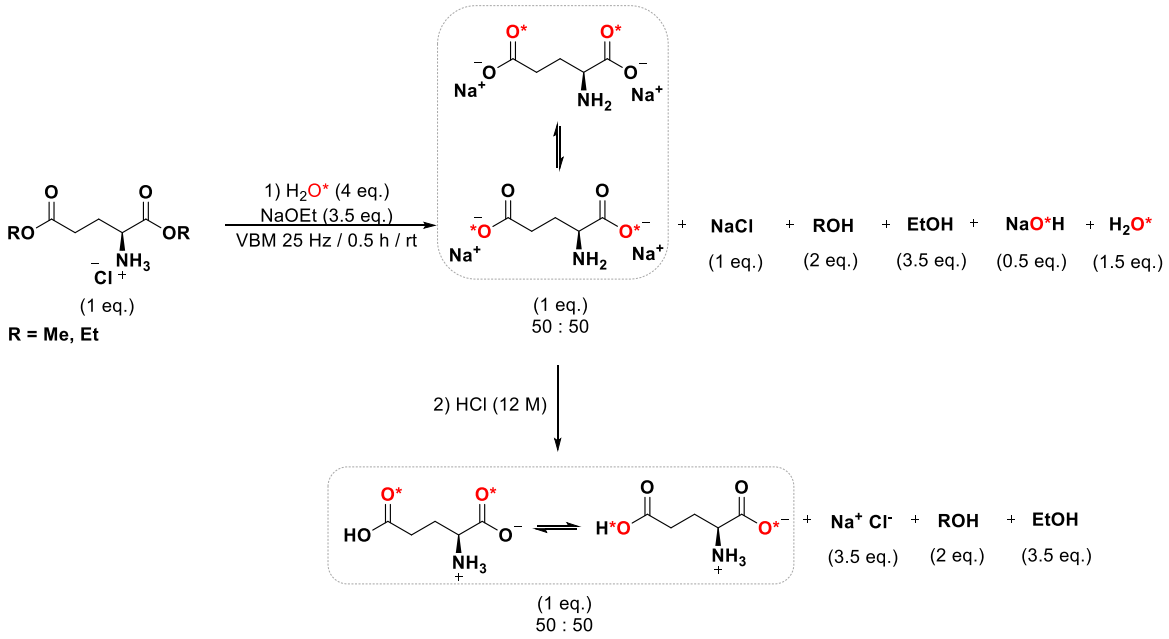

Scheme 4.11: Reaction scheme for the enrichment of L-glutamic acid *via* saponification. 99% ^{18}O-enriched water was used. The dilution of labeled water after acidification with aqueous HCl is not shown in the scheme.

Compared to the L-Asp, the L-glutamic acid has only one more carbon in its side chain and its physicochemical properties are very similar to those of L-Asp. The same reaction

conditions optimized for L-Asp ^{18}O-labeling were therefore applied for L-Glu enrichment. L-Glu(OMe)-OMe·HCl was saponified with ^{18}O-labeled water under basic conditions (4 eq. H_2O*, 3.5 eq. of NaOEt, Scheme 4.11). After 30 min of milling at 25 Hz, the full conversion was observed by ATR-IR. After recovery of the reaction mixture from the jar, the acidification step was closely monitored with a pH probe. The pH was easily set with HCl solution (12M) to a value close to pI = 3.2 (see Figure 4.18), and, unlike for aspartic acid, no "buffering effect" was observed. However, the precipitation of L-Glu was not spontaneous and had to be induced by addition of an anti-solvent (MeOH and/or EtOH). The precipitated solid was collected by filtration and dried under vacuum.

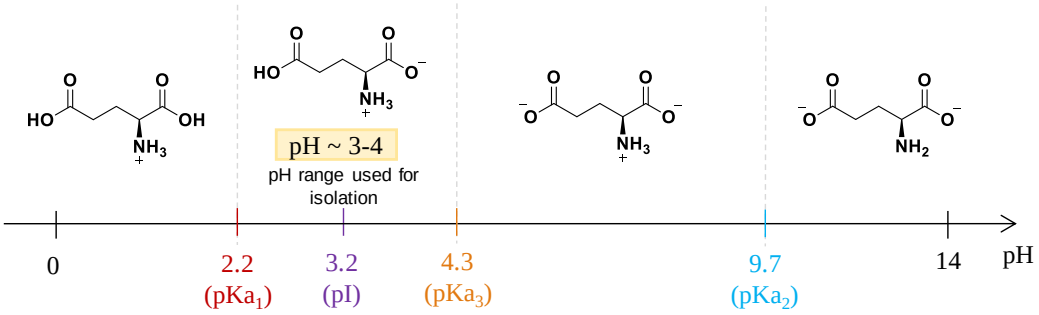

Figure 4.18: pH scale with the pKa values of L-Glu and its predominant chemical formulas in pure water depending on the pH zone. In the orange rectangle, the pH range at which L-Glu was isolated is highlighted.

Despite the use of an anti-solvent, L-Glu was obtained in very small yield (~ 28 %). The enrichment level measured was also atypically low, around 22 % (for the ^{18}O-enriched product), and was not improved when more labeled water was used for the synthesis. This very low enrichment was assigned to the high hygroscopicity of the starting methyl ester. To achieve better enrichment, a less hygroscopic reagent L-Glu(OEt)-OEt·HCl, was used. This time, ^{18}O-enrichment level increased to ~ 34 %, but it was still low compared to the other amino acids. Moreover, starting from the diethyl ester, the isolation of final molecules was even more difficult resulting in only ~ 7 % synthetic yield (Table 4.6).

Table 4.6: Summary of current results for L-Glu enrichment via saponification using different substrates

Substrate	Reaction conditions	Crude mixture[a] pyroGlu : L-Glu (eq.)	L-Glu Yield	L-Glu EL[b]	L-pyroGlu EL[c]
L-Glu(OMe)-OMe·HCl	VBM 25 Hz / 0.5 h / rt	2 : 1	31 mg 29 %	22%	39 %
L-Glu(OEt)-OEt·HCl	VBM 25 Hz / 0.5 h / rt	6.7 : 1	6 mg 7 %	34%	N.D.

[a] Reaction mixture analysed by solution ^1H NMR directly from the jar, [b] EL = enrichment level of isolated L-Glu, [c] EL = enrichment level of L-pyroGlu in reaction mixture, N.D. = not determined.

In order to understand the origin of the low isolated yields, the filtrates were lyophilised and analysed by solution ^{1}H NMR spectroscopy. It was found, that while the solid isolated by filtration represents pure glutamic acid, the solid resulting from lyophilisation of the filtrate mainly consists of pyroglutamic acid (pyroGlu), a five-membered cyclic derivative of glutamic acid (Figure 4.19).

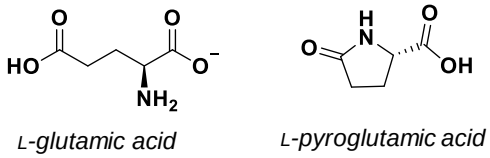

Figure 4.19: Semi-developed chemical structure of L-Glu and L-pyroGlu acid.

This cyclic by-product was also detected by ^{1}H NMR, when analysing the crude mixture present in the jar directly after saponification. It can be therefore assumed, that this side-product was formed during the saponification step and not during the work-up. In addition, based on the HRMS analyses, the pyroglutamic acid was also enriched in ^{18}O, with average enrichment level per carboxylic oxygen around 39 % (mechanism discussed later, Scheme 4.12). Due to the high water solubility of L-pyroglutamic acid (865 mg/mL compared to 9 mg/mL for L-Glu), it stayed dissolved in the solution during the work-up, and only remaining L-Glu was isolated. It was also observed, that the ratio of pyroGlu : Glu after saponification was higher when the diethyl ester was used as a substrate, which correlates with the lower yield isolated (Table 4.6).

In the Scheme 4.12, a mechanism of pyroGlu formation under the basic conditions of saponification is proposed. Due to an acid-base reaction between the HCl salt and either NaOEt, or OH^{-} anions, which is supposed to be faster than the saponification, the amino group is deprotonated and reacts intramolecularly with the ester of the side-chain, which results in the intramolecular formation of the five-membered ring. Afterwards, the main-chain ester is saponified with the ^{18}O-labeled hydroxide anions. This is in agreement with the MS pattern of the labeled L-pyroGlu phase, showing one labeled oxygen was introduced per molecule.

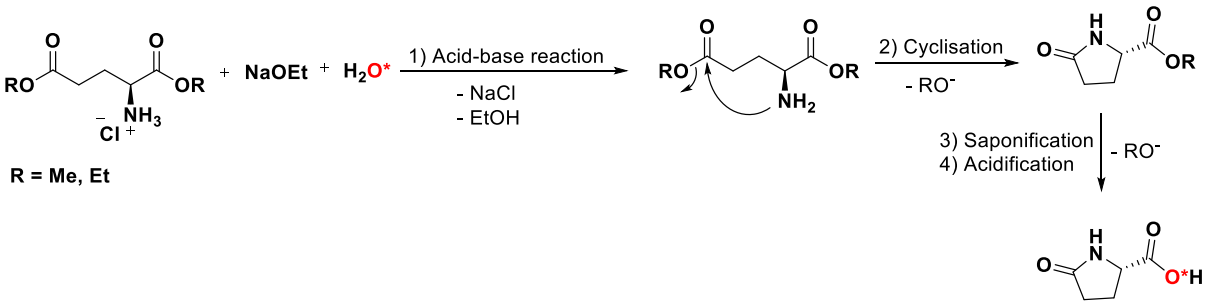

Scheme 4.12: Reaction scheme of a probable mechanism of L-pyroGlu formation during saponification step.

The formation of L-pyroglutamic acid was an unexpected phenomenon, and it was favoured here due to an intramolecular reaction resulting in 5-membered ring, compared to the L-Asp, for which such a reaction would impose a formation of 4-membered ring, which is more constrained and therefore less favoured. However, this side-reaction could be prevented, for example by using L-Glu substrate with the amine function protected with a Boc- protective group. Yet, no additional studies were performed at this stage.

4.2.4 Basic side-chain amino acid

4.2.4.1 L-Lysine hydrochloride (Lys, K)

L-Lysine represents an example of a basic amino acid containing a nitrogen atom in its side-chain. Due to the presence of a chiral centre at the α-carbon position, lysine is also an optically active amino acid. $^{17}O/^{18}O$-labeled L-Lysine prepared in this work was isolated as a monohydrochloride salt. L-Lys·HCl crystallises readily from its saturated aqueous solutions as a dihydrate.[83] Except for this hydrated form, two anhydrous crystalline phases were as well described: an α-form, derived from the L-Lys·HCl·$2H_2O$ by dehydration at higher temperatures (> 115 °C), and a β-form, formed at lower temperatures under reduced pressure.[84]

As mentioned above for L-Asp, the reactivity of the function held by the side-chain of L-Lys (here a primary amine group) can play a role in various transformations. For instance, this amino group is involved in bio-mineralization processes effecting the shape of growing calcium carbonate crystals.[85] In another study, the side-chain amine group of lysine immobilized on solid support served as a catalyst for Knoevenagel synthesis.[86]

a) $^{17}O/^{18}O$-Labeled L-Lysine hydrochloride enriched by mechanochemical saponification

A standard saponification procedure was used for the $^{17}O/^{18}O$-enrichment of L-Lys. Due to the presence of a second amine group in the molecule, the starting lysine methyl ester was in a form of a dihydrochloride. Because of this, the number of NaOEt equivalents was increased to 3.5 equivalents, out of which 2 equivalents were consumed simply to react with the hydrochlorides. Based on the ATR-IR analyses, the saponification reaction was complete after 30 min of milling at 25 Hz using 3 equivalents of $^{17}O/^{18}O$-labeled water (35 μL) (Scheme 4.13).

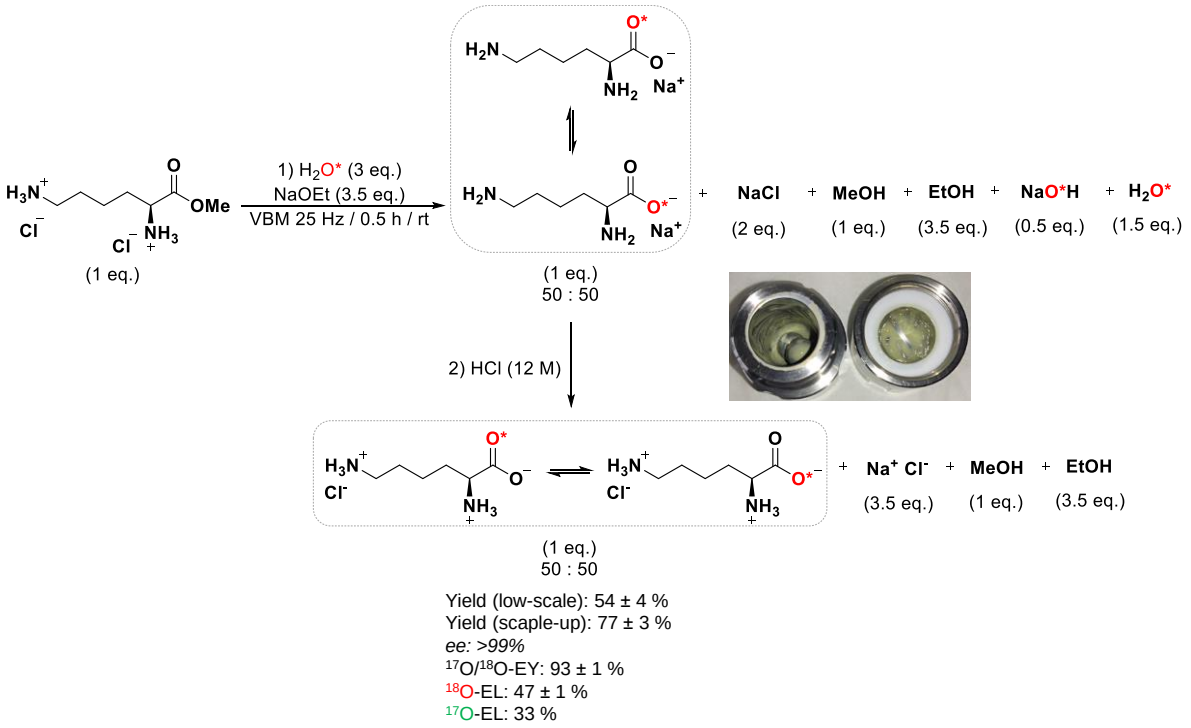

Scheme 4.13: Reaction scheme for enrichment of L-Lys·HCl using mechanochemistry. The dilution of labeled water after acidification with aqueous HCl is not shown in the scheme. The yields provided here are those of the isolated pure compounds (see Annexe IV for work-up and purification conditions). For the $^{17}O/^{18}O$-enrichment, 70% ^{17}O and 99% ^{18}O-enriched water was used, respectively.

Due to the high water solubility of L-Lys·HCl (670 mg/mL), the yellowish paste was recovered from the jar using the minimal amount of water possible, and the solution was acidified with concentrated HCl solution (12M) to pH ~ 3 - 4. Since the pKa of the amine group in the side-chain is higher than the one of the α-NH_2 group (pKa_3 = 10.67, pKa_1 = 9.16), the side-chain was protonated before reaching the pI, and the final L-lysine was isolated in the form of hydrochloride salt (Figure 4.20). No attempt was made her to isolate the molecule under its neutral form. Similarly to glycine isolation, the final product was precipitated by addition of MeOH, used here as an anti-solvent.

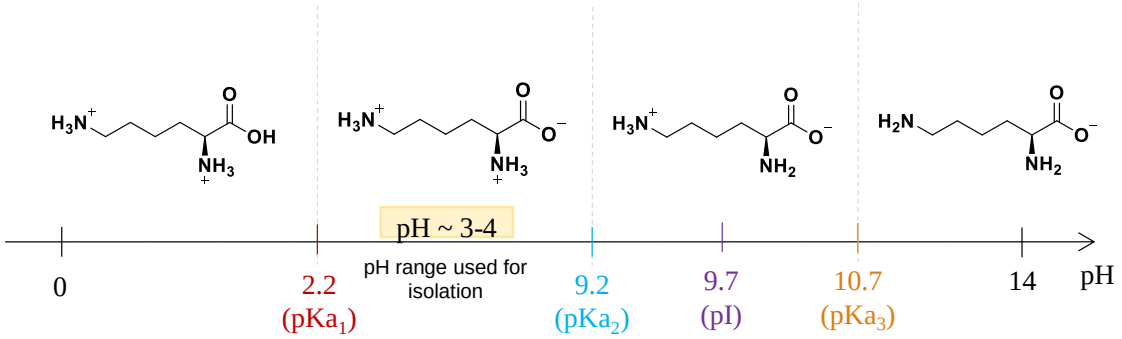

Figure 4.20: pH scale with the pKa values of L-Lys and its predominant chemical formulas depending on the pH zone. In the orange rectangle, the pH range at which L-Lys was isolated is highlighted.

Using an optimized ratio of water and MeOH, the product was isolated with no NaCl contamination (according to XRD analysis). However, 0.8 equivalents of MeOH per L-Lys·HCl molecule was always detected by solution ^{1}H NMR. It was not possible to evaporate the residual methanol under vacuum, even when increasing the temperature (up to 80 °C). The MeOH was eventually eliminated by re-dissolving the sample in water and performing lyophilisation. The product isolated upon lyophilisation was an anhydrous form of L-Lys·HCl as observed by ATR-IR and TGA analyses (Figure 4.21). The anhydrous product was converted to its dihydrate form by placing the sample into a desiccator with a controlled relative humidity of ~ 85 % for 24 h. The formation of dihydrate was observed by ATR-IR spectroscopy, where OH stretching vibration bands from H_2O molecules appeared at 3497, 3472 and 3558 cm^{-1}. This was confirmed by TGA analysis, where a loss of mass equal to the expected 16 weight % was measured at ~ 100 °C.[84]

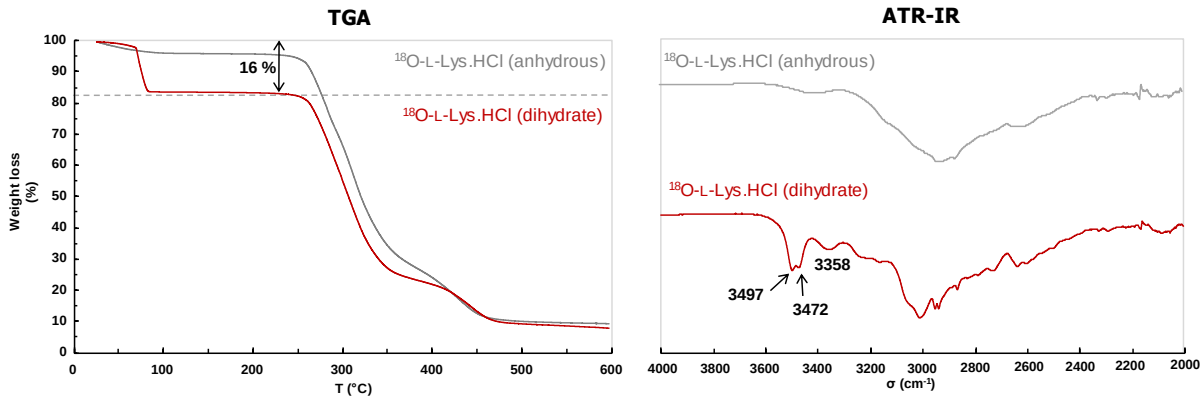

Figure 4.21: The TGA (left) and ATR-IR (right) analyses of ^{18}O-labeled L-lysine·HCl in its anhydrous and dihydrate forms.

For the low-scale procedure, anhydrous L-lysine monohydrochloride anhydrous was reproducibly isolated with a moderate yield of 54 ± 4 %, but in high enrichment yields (93 ± 1 %) and levels (47 ± 1 % and 33 %, for ^{18}O- and ^{17}O-enriched products, respectively). The optical purity of ^{18}O-labeled L-Lys·HCl was first measured by polarimetry, showing no racemization. The enantiomeric excess was then precisely determined by chiral HPLC after protection of the amines by Fmoc groups (synthesis discussed further below in Chapter 4.3). No loss of enantiomeric excess was observed (*ee* > 99%).

Scale-up procedure:

For future applications of ^{17}O/^{18}O-labeled L-lysine, it was necessary to scale-up and optimize the enrichment protocol. Keeping the same jar-size (10 mL inner volume) and the same number and size of balls (2x, 1 cm diameter), the amount of reagents was doubled keeping

the same stoichiometric ratios (starting from 300 mg of Lys-OMe·2HCl and using 70 µL of enriched water). Milling at 25 Hz for 30 min was found sufficient to provide full conversion with the same enrichment yield (~ 93 %). By optimizing the amount of non-labeled water and MeOH used for the work-up, pure labeled anhydrous L-Lys·HCl was obtained in a higher overall yield (77 ± 3 %, comparted to the 54 ± 4 % for the low-scale synthesis).

Scaling-up the procedure and doing two reactions at the same time (*i.e.* using both jars of the MM400 mixer-mill), allowed ~ 400 mg of labeled L-Lys·HCl·2H_2O to be prepared at once.

b) ^{18}O-Labeled L-Lysine hydrochloride enriched via acid-catalysed exchange

Acid-catalysed exchange was also tested for the enrichment of L-lysine as an alternative approach to the mechanochemical saponification. The anhydrous L-Lys is commercially available in a form of mono- or di-hydrochloride, and both substrates were tested. The amount of lysine hydrochloride salt was adjusted to give theoretically the same amount of labeled compound, so that direct comparison with the saponification protocol could be made. Also the amount of ^{18}O-labeled water (35 µL, 3 eq.) was set to be the same. Here, L-Lysine mono- or di-hydrochloride were introduced in a vial and $H_2{}^{18}O$ was added. The vial was closed and placed in an oven heated to 100 °C for 24 h (Scheme 4.14). The work-up conditions in terms of solvents used were identical to the conditions applied after saponification.

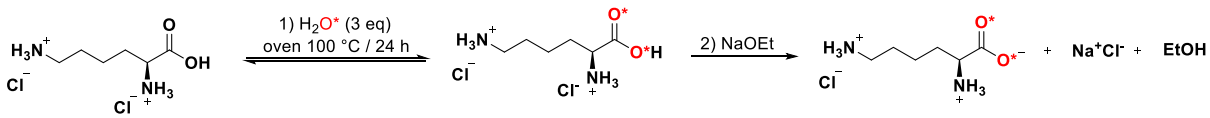

Yield (low-scale): 62 ± 5 %
ee > 99%
^{18}O-EY: quantitative
^{18}O-EL: 60 ± 1 %

Scheme 4.14: Reaction scheme for enrichment of L-Lys starting from L-Lys·2HCl using H^+ catalysed exchange. The yields provided here are those of the isolated pure compounds (see Annexe IV for work-up and purification conditions). For the ^{18}O-enrichment, 99% ^{18}O-enriched water was used.

When starting from L-Lys·HCl, the reaction mixture remained in a solid form after 24 h of heating. The solid was dissolved in a minimal amount of non-labeled water, and transferred to a flask. No pH modification was necessary as the pH value (pH ~ 6) was already in the zone of the desired form of lysine. The product precipitated upon addition of MeOH, and was isolated by filtration. However, no enrichment was detected by HRMS analyses.

On the other hand, when starting from L-Lys·2HCl, the reaction mixture transformed to a viscous liquid after 24 h of heating. It was diluted in a minimal amount of non-labeled

water, and the pH of the acidic solution was increased using NaOEt up to pH ~ 3 - 4. The product then precipitated upon addition of MeOH (anti-solvent), and was collected by filtration. Also here, the labeled L-Lys·HCl product was re-dissolved in water and then lyophilised to eliminate the residual MeOH. The optical purity of thus enriched lysine was evaluated by chiral HPLC analysis of its Fmoc-derivative (synthesis described later in Chapter 4.3), showing no loss of enantiomeric excess (*ee* > 99%).

Using L-Lys·2HCl as a substrate for acid-catalysed exchange in labeled water turned out to be a highly efficient labeling strategy. The anhydrous form of L-Lys·HCl was isolated in higher yield ~ 62 % (compared to saponification yield ~ 54 %), together with a higher enrichment level equal to 60 ± 1 % (compared to 47 ± 1 % by saponification), and this level corresponds to the quantitative oxygen exchange (Table 4.7).

Table 4.7: Comparison of the two labeling schemes proposed here for L-Lys enrichment (low-scale conditions).

Enrichment method	Reagents	Reaction conditions	Overall time[a]	Yield	EL [%]
Saponification (VBM)	L-Lys-OMe·2HCl/ NaOEt/H_2O*	VBM (25 Hz / 0.5 h / rt)	~ 15 h	64 mg 54%	47
H^+ catalysed exchange	L-Lys·2HCl/H_2O*	furnace (24 h / 100 °C)	~ 36 h	73 mg 62%	60

[a] Overall time = reaction time + time spent on the work-up producing anhydrous form of L-Lys·HCl, EL = enrichment level using 99% ^{18}O-enriched water.

From the HRMS spectra of ^{18}O-labeled L-Lys enriched by two different protocols (Figure 4.22), we can clearly see that only one ^{18}O is introduced per molecule of lysine doing saponification (the major peak being "p+2"), whereas both oxygens in one carboxylic function can be labeled via acid-catalysed exchange (peak "p+4"), which leads to the overall higher enrichment level.

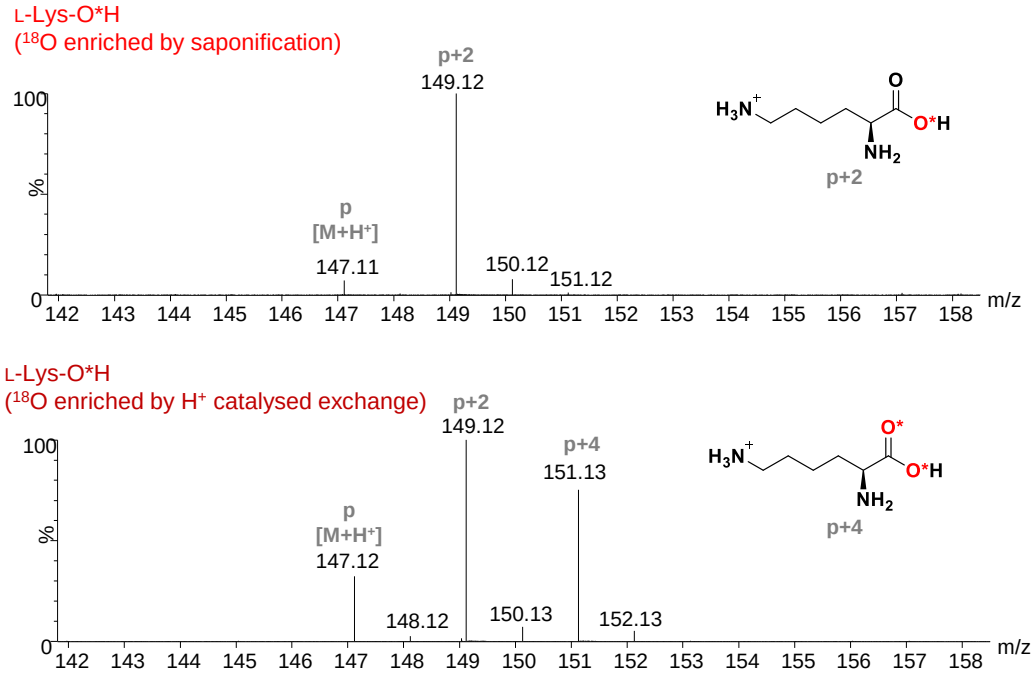

Figure 4.22: Comparison of HRMS (ESI^+) patterns of L-Lys enriched in ^{18}O *via* saponification (top) or acid-catalysed exchange (bottom). The "p $[M+H^+]$" stands for the monoisotopic mass, "p+2" (top) marks the most abundant peak belonging to 1x^{18}O introduced in the molecule (1x ^{18}O per carboxylic function), "p+4" (bottom) stands for 2x^{18}O in a molecule (2x ^{18}O per carboxylic function).

In terms of enrichment yield, the acid-catalysed exchange procedure described above is comparable with the classical oxygen exchange protocols reported in the literature (often reaching quantitative oxygen exchange).[13] However, the protocol used here is more user friendly, as it does not require to generate and use HCl gas, and it is also more cost-efficient, since the enriched water consumption is significantly lower, using only 3 equivalents of H_2O^* for the quantitative exchange, compared to the water excess (> 40 equivalents) traditionally employed.[14] The only downside of this approach is the rather long reaction time (more than 24 h). However, it is important to mention, that the reaction time for quantitative exchange was not optimized, thus it could possibly be reduced.

It is also worth mentioning that to the best of our knowledge, and based on our analysis of the available literature, the $^{17}O/^{18}O$-labeled L-Lysine was most probably isolated as pure monohydrochloride salt for the first time. Indeed, it seems, that in the previously reported protocols using H^+ catalysed oxygen exchange, L-Lys was prepared as dihydrochloride salt, since no additional information about adjusting the pH accordingly prior to the final product isolation was mentioned in these works.[11, 13] The only pH adjustment is mentioned in the procedure of Gerothanassis *et al.*,[87] where the final solution was brought to pH ~ 6 (pH corresponding to the L-Lys monohydrochloride), but the product was finally not isolated from the reaction mixture.

c) Solid-state NMR analyses

L-Lysine was previously studied by solid-state NMR spectroscopy, focusing mainly at ^{13}C and ^{15}N nuclei.[88-90] The only ^{17}O solid-state NMR study of a phase referred to as lysine hydrochloride published so far was performed by Pike *et al.* in 2004 at 14.1 T.[11] Based on the lysine hydrochloride crystal structure, two oxygen sites were expected, and two distinct resonances for C=O* and C-O*H were indeed reported in the published work.[11] Here, when the anhydrous ^{17}O-labeled L-Lys·HCl produced by mechanochemical saponification was analysed by ^{17}O NMR at 14.1 T, no features characteristic of quadrupolar lineshapes were detected. Instead, one broad resonance representing an average of different oxygen environments was observed (Figure 4.23c). This could be due to the fact that the L-Lys·HCl formed upon lyophilisation is essentially an amorphous phase, as apparent from the XRD powder pattern (which only shows very weak diffraction peaks corresponding to an anhydrous α-form, Figure 4.23c).[91] This could imply that the carboxylic oxygens have distinct ^{17}O NMR parameters compared to the crystalline phase, which could be averaged in the amorphous phase, for instance because of local dynamics around the carboxylate groups. In an attempt to see if the presence of dynamics around the oxygen atoms could also be responsible, at least in part, for this featureless signal, additional 1D ^{17}O NMR experiments were performed lowering the temperature (down to -70 °C), but with no effect on the peak appearance.

As mentioned previously, the enriched anhydrous phase was then converted to the crystalline L-Lys·HCl·$2H_2O$ form, and this form was confirmed by XRD, its pattern matching the powder patter simulated for the crystalline dihydrate compound (Figure 4.23c). Also the ^{13}C MAS NMR spectrum recorded at 14.1 T showed sharp resonances expected for a crystalline phase (Figure 4.23b). However, when ^{17}O solid-state NMR analysis was performed, only minor changes in the lineshape were observed compared to the amorphous compound, with a few discontinuities appearing on the spectrum (Figure 4.23c). In fact, the previously published work[11] may not be the best for comparison, due to the lack of important information. For example, it was not specified, whether the study concerned L- or D- lysine, nor if the product was analysed in its anhydrous or its hydrated form. Another question is related to the experimental protocol. Based on the information provided, lysine was enriched *via* acid-catalysed exchange, but no comment regarding pH adjustment was included. It is therefore possible, that the isolated phase of lysine is in fact the dihydrochloride salt. Indeed, it was observed that when an α-COOH group is coordinated with HCl, the δ_{iso} of C=O group tends to higher chemical shifts, whereas δ_{iso} of C-OH group tends to lower chemical shifts (compared

to the zwitterionic form), resulting in splitting of these two resonances.[92] This could explain why the oxygen sites are nicely resolved for the "Lys·HCl" sample, as well as for all other AA·HCl in the published study,[11] whereas they are clearly overlapping in this work (Figure 4.23c).

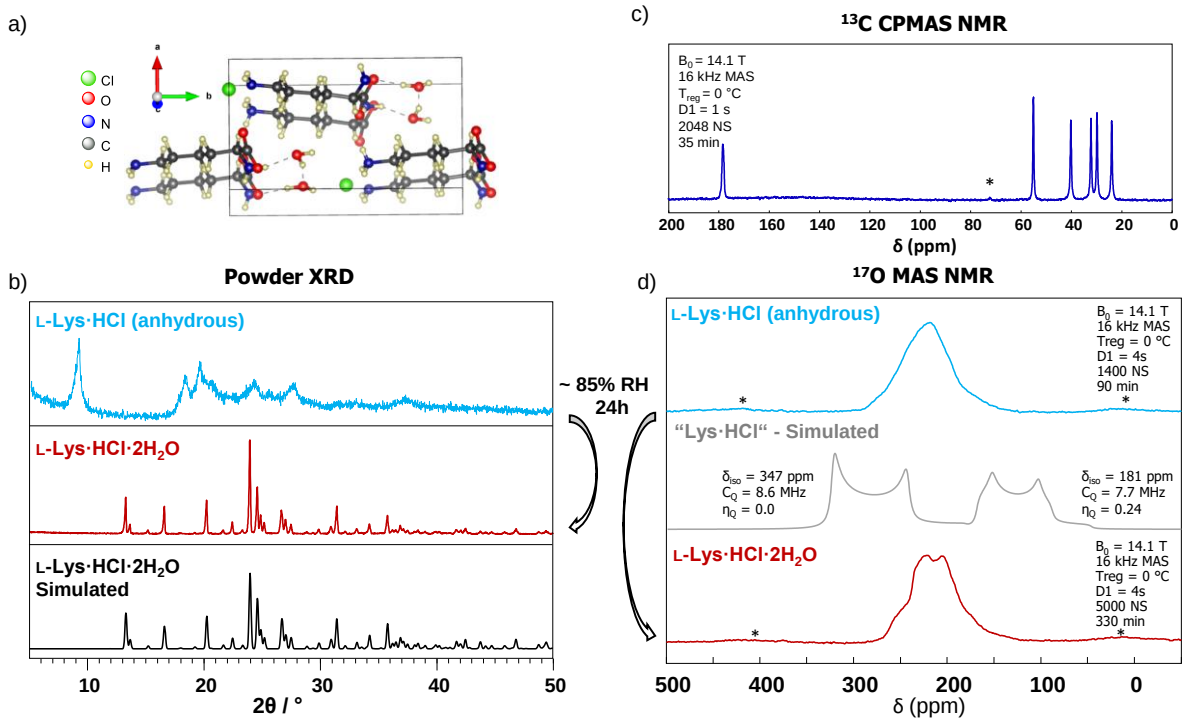

Figure 4.23: a) Crystal structure of L-Lys·HCl·2H_2O (CCDC number: 1208839), b) XRD powder patters of labeled L-Lys·HCl in its anhydrous and dihydrate forms, and comparison with a simulated powder pattern for L-Lys·HCl·2H_2O (CCDC number: 1208839), c) ^{13}C CPMAS NMR spectrum of L-Lys·HCl·2H_2O recorded at 14.1 T by Dr. Ieva Goldberga), d) ^{17}O MAS NMR spectra of L-Lys·HCl in its anhydrous and dihydrate form recorded at 14.1 T, compared to a spectrum of anhydrous "Lys·HCl" simulated from published data.[11] Symbol "*"stands for spinning side bands.

4.2.5 Summary tables

Two $^{17}O/^{18}O$-enrichment protocols for amino acids labeling were proposed here: VBM saponification and acid-catalysed oxygen exchange. Five amino acids were $^{17}O/^{18}O$-labeled using mechanochemical saponification: Gly, L-leu, L -Phe, L-Asp and L-Lys.HCl. For Gly, L-Asp and L-Lys, the saponification protocols were compared to the acid-catalysed exchange procedures. For the same three molecules, saponification procedure was also scaled-up.

In the tables presented below, the reaction conditions (including different work-ups employed) and results for $^{17}O/^{18}O$-enrichment of free amino acids using VBM saponification (at both low and higher scale) and acid catalysed exchange are all summarized.

Table 4.8: Summary of reaction conditions and results obtained for amino acids enrichment *via* VBM saponification (using MM 400, 25 Hz / 0.5 h / rt) at low-scale (corresponding to 150 mg of starting ester derivatives).

Amino acid (AA)	n AA-OMe·HCl [mmol]	NaOEt eq.	H_2O* eq.	Mass/yield	EY[a] [%]	^{18}O-EL[b] [%]	^{17}O-EL[b] [%]	*ee*[c] [%]
Gly	1.2	2.5	3	49 ± 6 mg 52 ± 6 %	~ 85[d]	~ 43[d]	~ 38[d]	-
Leu	0.8	2.5	3	86 ± 4 mg 78 ± 3 %	82 ± 1	41 ± 1	29	> 99
Phe	0.7	2.5	2	71 ± 3 mg 61 ± 2 %	92 ± 2	46 ± 1	32	> 99
Asp-both[e]	0.8	2.5	4	80 ± 2 mg 76 ± 1 %	88 ± 1	44 ± 1	31	> 99
Asp-side[e]	0.8	3.5	3	77 ± 7 mg 70 ± 6 %	85 ± 1	42	31	-
Asp-main[e]	1.0	2.5	3	113 ± 12 mg 84 ± 11 %	95 ± 1	47	34	-
Lys.HCl[f]	0.6	3.5	3	64 ± 6 mg 54 ± 4 %	93 ± 1	47 ± 1	33	> 99

[a] EY = enrichment yield, [b] EL = enrichment level (for ^{18}O and ^{17}O labeling, 99% ^{18}O-enriched and 70% ^{17}O-enriched water was used, respectively), [c] enantiomeric excess (*ee*) determined for Fmoc-AA derivatives, [d] Enrichment yield and level of labeled Gly estimated from its Fmoc-Gly derivative, [e] Asp-both, Asp-side and Asp-main correspond to L-Asp labeled either on both carboxylic functions, on the side-chain only or main-chain only, and [f] data for essentially anhydrous L-Lys hydrochloride phase. Error bars calculated from repeated experiments (n = 2 - 3).

Table 4.9: Summary of work-up conditions and procedures employed for isolation of labeled amino acids after VBM saponification procedure (at low-scale).

Amino acid (AA)	H_2O wash [mL]	Final pH (°=precision)	Anti-solvent MeOH [mL]	Ice-bath time [min]	Lyoph.[a]	RC[b] MeOH + H_2O [mL]	Sonic.[c] + fridge time [h]	Overall time[d]
Gly	0.4 + 0.4	3-4°	7.9	10-15	-	-	-	< 2 h
Leu	1 + 2	5.0-5.5°°	-	-	ovnt	4 + 0.5	1 + 1	< 24 h
Phe	1 + 2	5.0-5.5°°	-	-	ovnt	3 + 0.5	1 + 1h15	< 24 h
Asp-both[e]	0.5 + 0.5	1.25-1.52°°°	-	-	-	-	-	< 2 h
Asp-side[e]	0.5 + 0.5	1.25-1.52°°°	-	-	-	-	-	< 2 h
Asp-main[e]	0.5 + 0.5	1.25-1.52°°°	-	-	-	-	-	< 2 h
Lys·HCl·anh	0.3 + 0.3	3-4°	6.0	50	x*ovnt	-	-	24-48 h
Lys·HCl·$2H_2O$	0.3 + 0.3	3-4°	6.0	50	x*ovnt	85% RH 24 h	-	48-72 h

[a] Lyoph. = lyophilisation, ovnt = overnight, [b] RC =recrystallization, RH = relative humidity, [c] Sonic. = sonication, [d]overall time spend on the work-up, [d] Asp-both, Asp-side and Asp-main correspond to L-Asp labeled either on both carboxylic functions, on the side-chain only or main-chain only. Symbol "°" is used to express the precision of pH measurement, more ° = more precise (*i.e.* °=common pH paper, °°= pH paper for specific pH zone (pH = 0-6), °°°= pH measured with pH probe).

Table 4.10: Summary of reaction conditions and results obtained for amino acids enrichment *via* VBM saponification (using MM 400, 25 Hz / 0.5 h / rt) at higher-scale (corresponding to 450 mg of Gly-OMe·HCl and 300 mg of L-Asp(OMe)-OMe·HCl and L-Lys(OMe)-OH·2HCl).

Amino acid (AA)	n AA-OMe·HCl [mmol]	NaOEt eq.	H_2O* eq.	Mass/yield	EY[a] [%]	^{18}O-EL[b] [%]
Gly	3.6	2.5	3	185 ± 17 mg 66 ± 6 %	~ 87[c]	~ 42[c]
Asp-both[d]	2.0	2.5	3	174 ± 5 mg 84 ± 3 %	95 ± 2	47 ± 1
Lys·HCl[e]	1.2	3.5	3	183 ± 7 mg 77 ± 3 %	93 ± 6	47 ± 3

[a] EY = enrichment yield, [b] EL = enrichment level (for ^{18}O-labeling, 99% ^{18}O-enriched water was used), [c] Enrichment yield and level of labeled Gly estimated from its Fmoc-Gly-OH derivative, [d] Asp-both correspond to L-Asp labeled on both carboxylic functions, and [e] data for essentially anhydrous L-Lys hydrochloride phase. Error bars calculated from repeated experiments (n = 2 - 3).

Table 4.11: Summary of reaction conditions and results obtained for amino acids enrichment *via* acid-catalysed exchange (heating in oven, 24 h / 100 °C) at low-scale.

Amino acid substrate form	n Substrate [mmol]	H_2O* eq.	Mass/yield	EY[a] [%]	^{18}O-EL[b] [%]	*ee*[c] [%]
Gly·HCl	1.2	3	72 ± 3 mg 77 ± 3 %	quantitative[d]	62 ± 1[d]	-
L-Asp-both[e]	0.8	4	79 ± 1 mg 78 ± 2 %	56	28	N.D.
L-Lys·2HCl[f]	0.6	3	73 ± 7 mg 62 ± 5 %	quantitative	60 ± 1	> 99

[a] EY = enrichment yield, [b] EL = enrichment level (for ^{18}O-labeling, 99% ^{18}O-enriched water was used), [c] enantiomeric excess (*ee*) determined for Fmoc-AA derivatives, [d] Enrichment yield and level of labeled Gly estimated from its Fmoc-Gly derivative, [e] L-Asp labeled at both carboxylic functions, N.D. = not determined, and [f] data for essentially anhydrous L-Lys hydrochloride phase. Error bars calculated from repeated experiments (n = 2 - 3).

4.3 FMOC PROTECTION IN SOLUTION

The fluorenylmethoxycarbonyl (Fmoc) group is a base-labile protecting group used in organic synthesis typically to prevent amines from reacting with electrophiles. Together with *tert*-butyl protection group (*t*Bu), Fmoc is used for orthogonal protection of amino acids, notably for the solid-phase peptide synthesis (SPPS), which will be further described in the following Chapter 5.

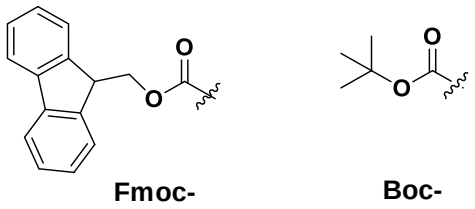

Figure 4.24: Fluorenylmethoxycarbonyl (Fmoc) and *tert*-butyloxycarbonyl (Boc) protection groups.

For their importance as peptide building blocks, several protocols for direct $^{17}O/^{18}O$-enrichment of Fmoc-protected amino acids (Fmoc-AA-OH) have also been described in the literature.

- First, Fmoc-AA-OH with no acid-labile side-chain protection groups have been enriched *via* classical H^+ catalysed oxygen exchange procedure.[23] To be more specific, Fmoc-AA-OH were labeled in H_2O*/dioxane mixture and the exchange was catalysed by HCl (generated *in-situ* by reaction of acetyl chloride with labeled water), while heated at 100 °C for 3 - 30 h (depending on the substrate). The labeled Fmoc-AA-O*H were isolated in high yields (80 - 90 %), and enrichment levels (> 90 %, when the procedure was repeated twice).[23] However, this protocol is only applicable to residues that do not require acid-labile side-chain protective groups, and due to the large excesses of water used (> 100 eq. of H_2O*), the enrichment medium had to be recovered for the procedure to be cost-efficient.
- Second, in the work of Yamada *et al.*, Fmoc/Boc-protected amino acids were enriched via hydrolysis of their pentafluorophenyl esters at room temperature and nearly neutral pH, using small excess of labeled water (5 eq.), but with long reaction times (up to several days).[55] Similarly to our VBM saponification, due to the mechanism of Yamada's enrichment procedure, only one labeled oxygen per carboxylic function was introduced in the molecule, decreasing the average enrichment levels of a single reaction.[55]

- Lastly, a completely different approach was developed by Seyfried (discussed in detail in Chapter 1, section 1.1.2), where Fmoc/Boc-AA-OH were enriched *via* multiple-turnover reaction composed of repeating carboxylic acid activations (using 1-ethyl-3-(3-dimethylaminopropyl)carbodiimide hydrochloride, EDC) and hydrolysis steps (using enriched water).[93] Here, the labeled water was used in excess (50 eq.), but the Fmoc-AA-OH were isolated with very high enrichment levels (> 92% per carboxylic oxygen). In the recent work of Michaelis *et al.*, this procedure was adapted and the excess of labeled water was reduced to 35 equivalents, keeping its enrichment efficiency.[92] However, this procedure suffers from very long reaction times (~ 20 - 40 h), and, in addition, the final products often had to be purified by column chromatography.[93]

In this thesis, amino acids were Fmoc-protected for two reasons. The first reason was to check the optical purity of previously prepared labeled amino acids by chiral HPLC, and this was more readily feasible for Fmoc-AAs than for non-protected amino acids. The second purpose was to prepare $^{17}O/^{18}O$-labeled Fmoc-protected amino acids, which will be used as building blocks for the synthesis of short $^{17}O/^{18}O$-labeled peptides in the SPPS (see Chapter 5).

The reaction procedures described in this subsection were adapted from standard published protocols for Fmoc protection of amino acids performed in solution. In general, the pre-labeled amino acid was first dissolved in a basic aqueous solution, and then N-(9-fluorenylmethoxycarbonyloxy) succinimide (Fmoc-OSu) dissolved in an organic solvent was added to the stirred solution (H_2O/organic solvent, V/V, 1/1). After the work-up, the Fmoc-protected amino acid was isolated as a white solid and characterized. Improvements to this overall approach in view of producing large quantities of $^{17}O/^{18}O$-enriched Fmoc-protected species in high yields were also looked into, by avoiding the isolation of the labeled product formed after mechanochemical saponification, as described below in section 4.3.2.

4.3.1 Fmoc-protected amino acids for chiral HPLC measurements

Except for glycine, all other amino acids $^{17}O/^{18}O$-enriched in this study were used as optically active L-enantiomers. However, naturally, over a long period of time, L-amino acids undergo slow racemization, producing D-enantiomers.[94] This process can be promoted under specific conditions, such as elevated temperature or presence of a strong base. Base-catalysed racemization can start with removal of the acidic α-proton, which leads to a formation of carbanion intermediate. This carbanion is then re-protonated with a proton restoring the original

amino acid, yet in both L- and D-forms (Scheme 4.15). Racemization under acidic condition is also possible, however its rate is generally slower than the one catalysed by a base.[95]

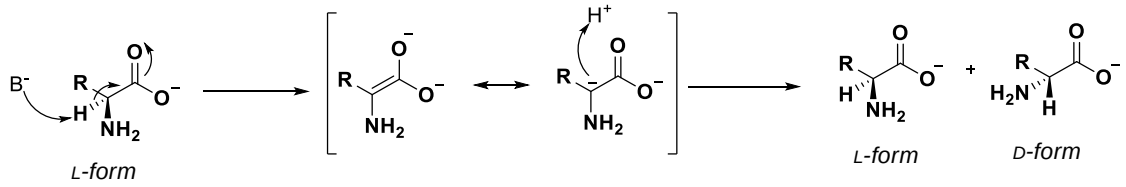

Scheme 4.15: Mechanism of base (B^-) catalysed racemization of amino acid.

To preserve the optical purity of L-amino acids upon labeling was a critical point of here proposed $^{17}O/^{18}O$-enrichment procedures. The isolated ^{18}O-labeled amino acids were at first analysed by polarimetry, to obtain primary idea of the extent of the potential racemization. Since no racemization was observed for any of the studied molecules, the labeled L-amino acids were Fmoc protected and their enantiomeric excess was determined more precisely by chiral HPLC analyses. These analyses were performed by the iSm2 institute in Marseille.

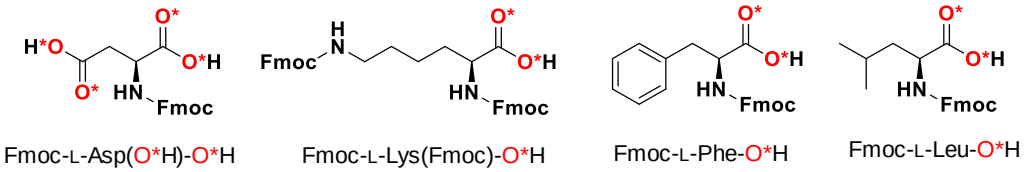

Figure 4.25: Fmoc-protected labeled amino acids prepared here for the purpose of chiral HPLC analysis. Depending on the labeling strategy used, one or both oxygens per carboxylic function were enriched.

Chiral HPLC is an analytical technique used for separation of chiral molecules. The stationary phase is composed of an optically active polymer, which, in an ideal situation, interacts more strongly with one of the two enantiomers, which is retained a bit longer on the column and therefore eluted with a longer retention time (Figure 4.26). From the integral intensity of the separated peaks, the enantiomeric excess is calculated.

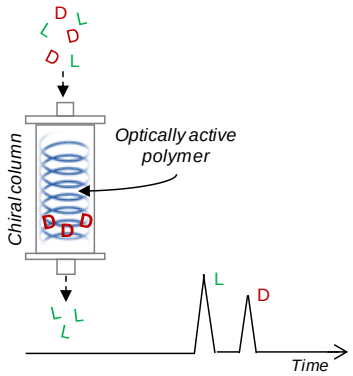

Figure 4.26: Scheme of chiral HPLC analyses of DL-amino acid mixture, allowing separation of L- and D- forms.

4.3.1.1 Fmoc-L-Asp-OH and Fmoc-L-Lys(Fmoc)-OH

The enriched Fmoc-L-Asp-O*H and Fmoc-L-Lys(Fmoc)-O*H molecules were both prepared solely for the purpose of the chiral HPLC analysis. Indeed, the side-chain carboxylic function of aspartic acid remained unprotected throughout the synthesis, and the nitrogen atoms of both the main-chain and the side-chain of lysine became protected with the Fmoc-groups during the reaction. Therefore, both of these products were not suitable for the type of peptides we were targeting for the SPPS peptide synthesis in this study (see Chapter 5).

The reaction procedure was at first tested on non-labeled racemic commercial compounds DL-Asp and DL-Lys·HCl, providing Fmoc-DL-Asp-OH and Fmoc-DL-Lys-OH, which were used to find the appropriate analytical method for chiral HPLC analysis, and which then served as a reference for the analysis of the labeled compounds. Once reaction conditions optimized, L-Asp enriched in ^{18}O only by saponification and L-Lys enriched in ^{18}O by both saponification and acid catalysed exchange were at first isolated, and then Fmoc-protected in solution following published protocols (*i.e.* Fmoc-OSu (1.0 or 2.2 eq.), Na_2CO_3 (13.5%), DMF, 1 h, rt), as described in more details in the Annexe IV.[96-97]

No loss of enrichment was observed when comparing ^{18}O-enrichment levels before and after Fmoc-protection (for L-Asp 44 % and 44 %, respectively; for L-Lys 47 % and 47 %, respectively), which is not surprising, considering that the protection reaction occurs under basic conditions and at low temperature. The products were then analysed by chiral HPLC confirming no loss of enantiomeric excess (*ee* > 99%, see Annexe IV) upon the saponification enrichment protocol and also after acid-catalysed exchange for L-Lys. This was a very important result validating the use of mechanochemical saponification for oxygen isotope labeling of these two amino acids.

4.3.1.2 Fmoc-L-Leu-OH and Fmoc-L-Phe-OH

The main objective here was to prepare the Fmoc-L-Leu-O*H and Fmoc-L-Phe-O*H for the purpose of chiral HPLC analysis, and the reaction conditions were not further optimized (see Annexe IV for details). Nevertheless, the labeled products prepared are suitable for SPPS and could be employed in the peptide synthesis in future projects.

As for the other amino acids, the enrichment levels of the protected Fmoc-L-Leu-O*H and Fmoc-L-Phe-O*H molecules correspond to the enrichment levels observed previously for ^{18}O-labeled L-Leu and L-Phe. Moreover, the products were analysed by chiral HPLC confirming no loss of enantiomeric excess upon saponification, validating the VBM saponification for oxygen isotope labeling.

4.3.2 Fmoc-protected amino acids for SPPS

In view of a future use in peptide synthesis, $^{17}O/^{18}O$-labeled Fmoc-protected Gly and Fmoc/*t*Bu orthogonally protected L-Asp and L-Lys were prepared (Figure 4.27). Especially for the Fmoc-Gly-O*H and Fmoc-L-Asp(O*t*Bu)-O*H, the reaction conditions in terms of the amount of $^{17}O/^{18}O$-enriched water used with respect to the amount of labeled product obtained, were carefully optimized. The synthesis of $^{17}O/^{18}O$-labeled Fmoc-L-Lys(Boc)-O*H was also developed, however this product was finally not included in the sequence of the peptide chosen in the following chapter.

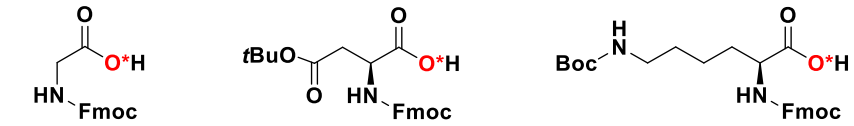

Fmoc-Gly-O*H Fmoc-L-Asp(O*t*Bu)-O*H Fmoc-L-Lys(Boc)-O*H

Figure 4.27: Fmoc-protected labeled amino acids prepared here in view of the synthesis of labeled peptides. Due to the equilibrium in carboxylic group, both oxygen sites (*i.e.* C=O* and C-O*H) are equally enriched.

For the orthogonal protection in general, different protection groups with different resistance towards reaction conditions are used. This allows to selectively deprotect only one functional group in a molecule, while keeping the rest protected and therefore inert in the subsequent reactions. One of the typical orthogonal protection strategies used for SPPS is based on the Fmoc/*t*Bu orthogonality, and it was applied here on the synthesis of Fmoc-L-Asp(O*t*Bu)-O*H and Fmoc-L-Lys(Boc)-O*H.

4.3.2.1 Fmoc-Gly-OH

The $^{17}O/^{18}O$-labeled Fmoc-Gly-O*H was prepared in view of its use for the SPPS synthesis of a tri-peptide and a penta-peptide (as discussed in the Chapter 5). Reaction conditions were therefore carefully optimized. In a typical SPPS protocol, Fmoc-AA-OH are used in a large excess (~ 10 equivalents for each coupling step). The goal was therefore to design a synthetic procedure, in which ~ 1 g of $^{17}O/^{18}O$-labeled Fmoc-glycine would be prepared in a time- and cost-efficient manner.

At the beginning, Fmoc-Gly-O*H was prepared *via* a reaction similar to those described above for the synthesis of Fmoc-AA-O*H used for chiral HPLC analysis. The Gly was enriched by mechanochemical saponification or *via* acid-catalysed exchange, isolated, and finally Fmoc-protected in solution following a published protocol (*i.e.* Fmoc-OSu (1.0 eq.), Na_2CO_3 (10%), dioxane, 20 min, rt) (Scheme 4.16).[97]

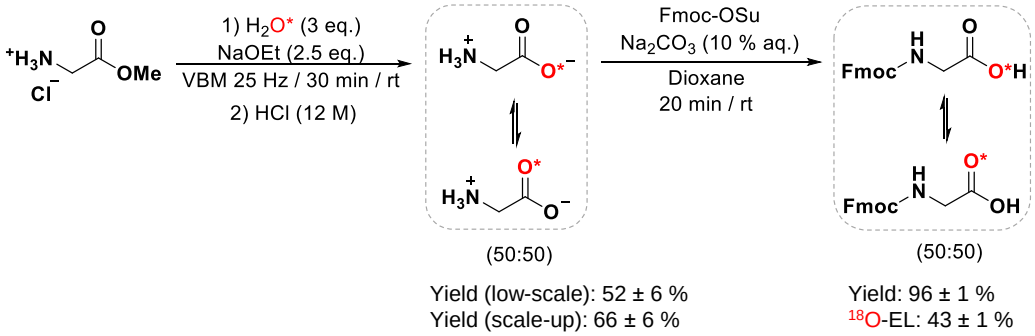

Scheme 4.16: Reaction scheme for the synthesis of Fmoc-Gly-O*H *via* isolation of labeled glycine. The yields provided here are those of the isolated pure compounds.

Despite the very high yield of the Fmoc-protection second step, such strategy would turn out to be very costly when being scaled-up for the SPPS purposes, as almost half of the labeled Gly would be lost upon its isolation. In order to increase its cost-efficiency, the $^{17}O/^{18}O$-labeled Gly was kept in the solution recovered from the jar after saponification, together with the different side-products (*e.g.* Na^+ and Cl^- ions, EtOH, etc.). This solution was then directly acidified with aqueous HCl to pH ~ 5 - 6, and finally used for the Fmoc-protection, by adapting the same published protocol described previously (Scheme 4.17).[97] This approach, where the product after saponification was not isolated, was applied as well for the preparation of other Fmoc-protected amino acids (described in the next sections).

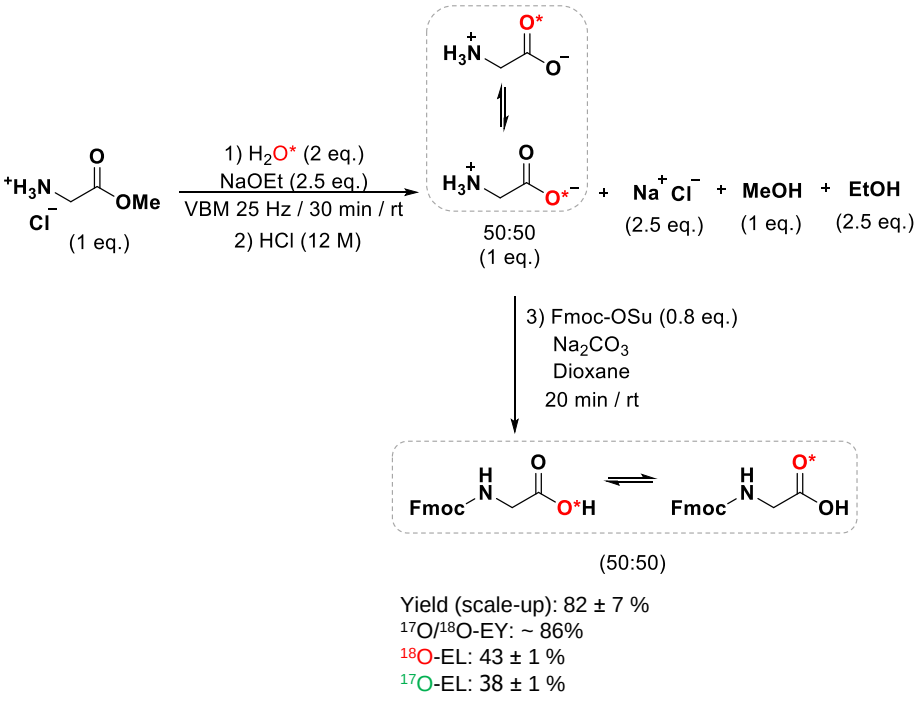

Scheme 4.17: Reaction scheme for the synthesis of Fmoc-Gly-O*H, without isolation of the enriched glycine intermediate. The dilution of labeled water after acidification with aqueous HCl is not shown in the scheme. The yields provided here are those of the isolated pure compounds (see Annexe IV for work-up and purification conditions). For the $^{17}O/^{18}O$-enrichment, 90% ^{17}O and 99% ^{18}O-enriched water was used, respectively.

Under these optimized conditions, only 2 equivalents of labeled water were finally used for the saponification step (without impacting the final enrichment yield), and the initial mass of reagents was doubled compared to the low-scale synthesis described in section 4.2.2.1 (meaning that 300 mg of Gly-OMe·HCl and 86 µL of H_2O^* (2 eq.) were engaged). In contrast to the Gly scale-up procedure (described in section 4.2.2.1.), here the amount of reagents could not be further increased as this resulted in the formation of a significant amount of Fmoc-Gly-Gly-O*H side-product, which was identified easily by LCMS analyses (see Annexe IV). The relative amount of this side-product was not reproducible, and its presence was probably caused by the inefficient mixing of the reaction mixture during saponification. This could also be the case for the scale-up synthesis of enriched Gly, with the Gly-Gly side-product being eliminated during the work-up and was therefore not detected in the isolated enriched Gly phase. As a side note, it is worth mentioning that the presence of Fmoc-Gly-Gly-O*H side product was sometimes observed also when the Fmoc-Gly-O*H was produced at low-scale (150 mg of starting Gly-OMe·HCl) without intermediate Gly isolation, but only in a very low amount, which was compatible with the SPPS syntheses and ^{17}O NMR analyses planned (see Annexe IV).

Using this approach, Fmoc-Gly-O*H was isolated in high yield (82 ± 7 %) along with a high enrichment level (43 % and 38 % for ^{18}O and ^{17}O-enriched products, respectively). Overall, using the protocol where the intermediate was not isolated, the overall water consumption was reduced by half, from 34 µL to 17.5 µL per 100 mg of labeled Fmoc-Gly-O*H. Moreover, by performing two reactions in a row without isolating the intermediate (*i.e.* using both jars of the MM400 ball-mill for the first step), ~ 1 g of $^{17}O/^{18}O$-labeled Fmoc-Gly-O*H could be prepared in only 1 day (work-up included).

4.3.2.2 Fmoc-L-Asp(OtBu)-OH

Orthogonally protected Fmoc-L-Asp(O*t*Bu)-O*H was also prepared using a 2-steps synthesis (Scheme 4.18). Here, the methyl ester of L-aspartic acid already protected with a *tert*-butyl group at the side-chain carboxylic function was used for the saponification (specifically, 290 mg of L-Asp(O*t*Bu)-OMe·HCl and 65 µL of H_2O^* (3 eq.) was engaged). The *tert*-butyl group was found to be stable under the basic saponification conditions, where exactly 2 equivalents of NaOEt base were used (one to react with the HCl and the second to form labeled hydroxides). Only negligible amounts of side-chain deprotected Fmoc-L-Asp(O*H)-O*H were detected by LCMS. As for Gly, the labeled intermediate was not isolated. Instead, the reaction mixture was recovered as an aqueous solution from the jar,

acidified with HCl solution (6M) to pH ~ 8 - 9, and finally used for the subsequent Fmoc-protection, by adapting the published protocol (*i.e.* Fmoc-OSu (0.95 eq.), Na_2CO_3, DMF, 1 h, rt), as further detailed in Annexe IV.[96]

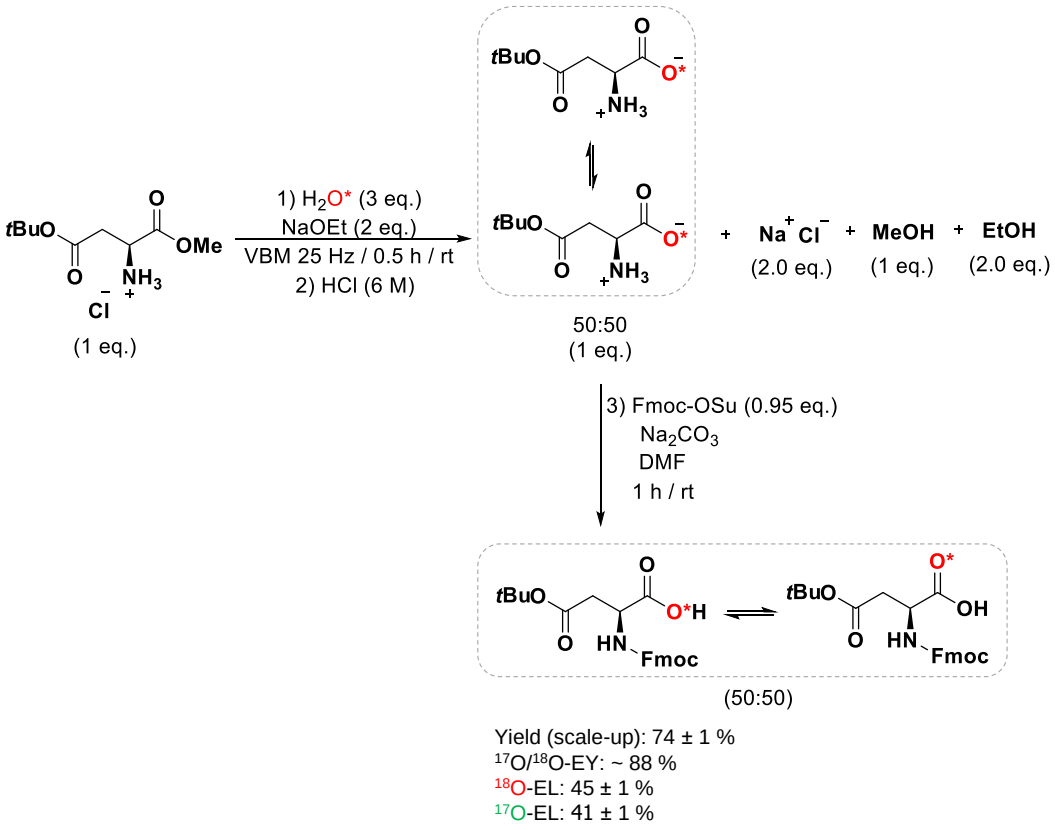

Scheme 4.18: Reaction scheme for the synthesis of Fmoc-L-Asp(O*t*Bu)-O*H. The dilution of labeled water after acidification with aqueous HCl is not shown in the scheme. The yields provided here are those of the isolated pure compounds (see Annexe IV for work-up and purification conditions). For the $^{17}O/^{18}O$-enrichment, 90% ^{17}O and 99% ^{18}O-enriched water was used, respectively.

The $^{17}O/^{18}O$-labeled Fmoc-L-Asp(O*t*Bu)-O*H was isolated with purity acceptable for the SPPS, in high yield (76 ± 2 %), and with a high enrichment level (43 ± 2 % and 40 ± 1 % for ^{18}O and ^{17}O-enriched products, respectively). The labeled water consumption was the same as for Fmoc-Gly-O*H described above, with 17.5 µL engaged per 100 mg of labeled Fmoc-L-Asp(O*t*Bu)-O*H. By performing two reactions in a row without isolating the intermediate (*i.e.* using both jars of the MM400 ball-mill for the first step), ~ 700 mg of $^{17}O/^{18}O$-labeled Fmoc-L-Asp(O*t*Bu)-O*H could be prepared in only 1 day (work-up included).

Using this synthetic scheme, only the oxygens in the main-chain carboxylic function of L-Asp are labeled. Yet, considering the engagement of L-Asp containing peptides in different biological processes (including bio-mineralization), where it is mostly the side-chain carboxylic acid that interacts with the surrounding medium,[78] and in the view of studying these interactions with ^{17}O NMR, it is of high interest to label as well the oxygens in the *side-chain* carboxylic

function of L-Asp in peptides. An alternative approach for the labeling of the L-Asp side-chain carboxylic group in peptides will be discussed in the next Chapter 5.

4.3.2.3 Fmoc-L-Lys(Boc)-OH

The orthogonally protected $^{17}O/^{18}O$-labeled Fmoc-L-Lys(Boc)-O*H was also prepared using a 2-steps procedure, in which the labeled intermediate after saponification was not isolated (Scheme 4.19). Here, L-Lysine methy lester hydrochloride already protected at the side-chain amine with a *tert*-butylcarbonyl protective group (Boc) was used as a substrate for the saponification. The Boc-protective group was found to be stable under the basic conditions used during the saponification step, and no unwanted deprotection was observed when using exactly 2 equivalents of NaOEt. The reaction mixture was recovered from the jar after saponification as an aqueous solution, which was acidified with an HCl solution (6M) to pH ~ 8-9, and finally used for the Fmoc-protection, by adapting a published protocol (*i.e.* Fmoc-OSu (1.1 eq.), $NaHCO_3$, THF, 16 h, rt), as described in Annexe IV.[98]

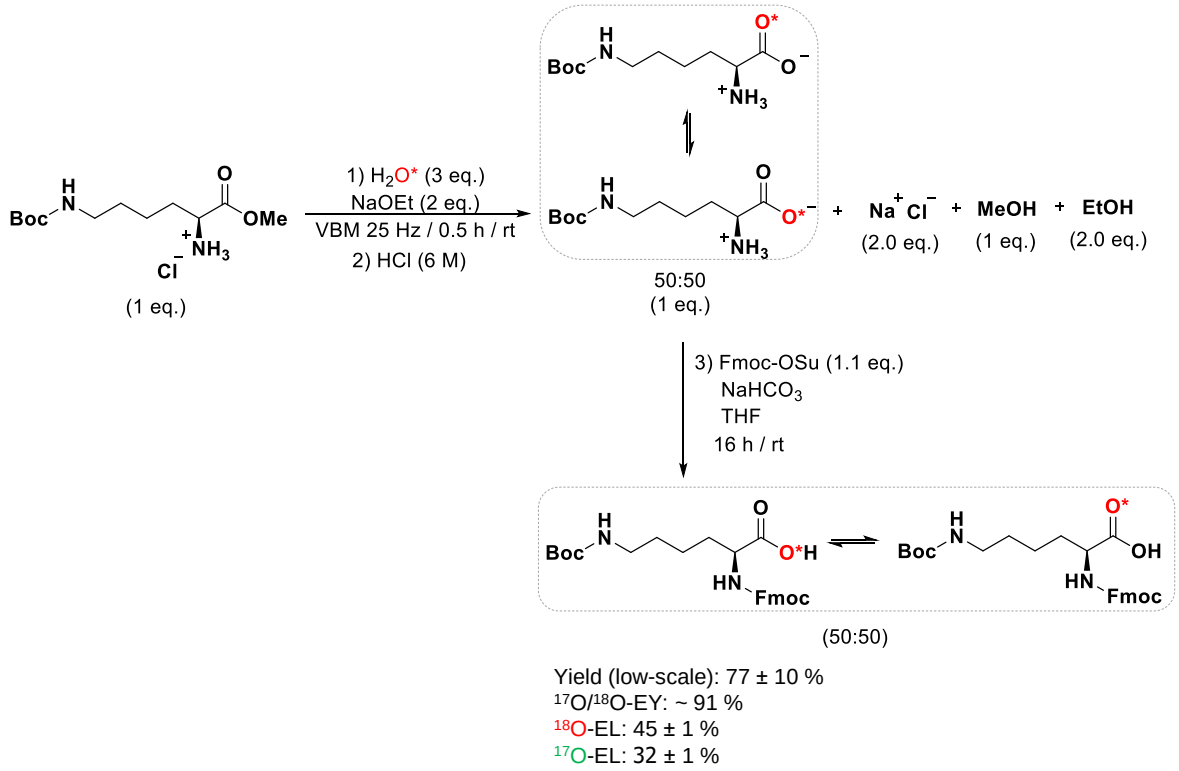

Scheme 4.19: Reaction scheme for the synthesis of Fmoc-L-Lys(Boc)-O*H. The dilution of labeled water after acidification with aqueous HCl is not shown in the scheme. The yields provided here are those of the isolated pure compounds (see Annexe IV for work-up and purification conditions). For the $^{17}O/^{18}O$-enrichment, 70% ^{17}O and 99% ^{18}O-enriched water was used, respectively.

The final Fmoc-L-Lys(Boc)-O*H was purified by flash column chromatography on silica gel, and isolated in high yield (77 ± 10 %) and with a high enrichment level (45 % and

32 % for ^{18}O and ^{17}O labeled products, respectively). It is possible, that the necessity of performing column chromatography to separate the labeled product from a fluorene-methanol side-product could be avoided by using the amino acid in excess, as it was done for Fmoc-Gly-O*H and Fmoc-L-Asp(O*t*Bu)-O*H, which were isolated pure without column chromatography. However, no further optimization of this protocol was attempted at this stage, as L-Lys does not occur in the peptide sequence selected for ^{17}O NMR study (see Chapter 5).

4.3.3 Summary table:

The $^{17}O/^{18}O$-labeled Fmoc-protected amino acids were prepared using pre-labeled reagents (enriched using mechanochemistry), and following protocols published for Fmoc-protection in solution. Fmoc-L-Leu-O*H, Fmoc-L-Phe-O*H, Fmoc-L-Asp(O*H)-O*H and Fmoc-L-Lys(Fmoc)-O*H were prepared for the enantiomeric excess measurements, whereas Fmoc-Gly-O*H, Fmoc-L-Asp(O*t*Bu)-O*H and Fmoc-L-Lys(Boc)-O*H were prepared in view of the SPPS synthesis. Special attention was dedicated to the synthetic protocols of $^{17}O/^{18}O$-labeled Fmoc-Gly-OH and Fmoc-L-Asp(O*t*Bu)-O*H, with the aim of producing up to 1 g quantities rapidly and in cost-efficient manner, as these two molecules were finally used in the peptide synthesis described in the next Chapter 5. In the table presented below, the reaction conditions and results for the synthesis of $^{17}O/^{18}O$-enriched Fmoc-AA-O*H are summarized.

Table 4.12: Summary of experimental conditions and results for Fmoc-protection of $^{17}O/^{18}O$-labeled amino acids.

Substrate	Fmoc-reagent	Aq. base	Org. solvent	Time[a] [h]	Yield	EY[b] [%]	^{18}O-EL[c] [%]	^{17}O-EL[c] [%]	*ee* [%]
Fmoc-protected amino acids prepared for the purpose of chiral measurements									
^{18}O-L-Asp (1.2 eq)	Fmoc-OSu (1.0 eq)	Na_2CO_3 (13.5%)[d]	DMF	1	470 mg 69 %	-	44	-	> 99
^{18}O-L-Lys (1.0 eq)	Fmoc-OSu (2.2 eq)	Na_2CO_3 (13.5%)[d]	DMF	1	515 mg[e] 81 %[e]	-	47[e] 60[f]	-	> 99[e] > 99[f]
L-Leu-OMe·HCl (1.0 eq)	Fmoc-OSu (1.1 eq)	$NaHCO_3$	acetone	16	255 mg 86 %	78	39	-	> 99
L-Phe-OMe·HCl (1.0 eq)	Fmoc-OSu (1.1 eq)	Na_2CO_3	DMF	1	250 mg 92 %	95	47	-	> 99
Fmoc-protected amino acids prepared for the purpose of peptide synthesis									
^{18}O-Gly (1.2 eq)	Fmoc-OSu (1.0 eq)	Na_2CO_3 (10%)[d]	dioxane	0.33	96 %[g]	96	43	-	-
Gly-(OMe)·HCl[h] (1.0 eq)	Fmoc-OSu (0.8 eq)	Na_2CO_3 (10%)[d]	dioxane	0.33	490 mg[i] 82 %[i]	86[j]	43[j]	38	-
L-Asp(O*t*Bu)-OMe·HCl[h] (1.0 eq)	Fmoc-OSu (0.95 eq)	Na_2CO_3	DMF	1	350 mg[j] 76 %[j]	91[j]	45[j]	41[j]	N.D.
L-Lys(Boc)-OMe·HCl[h] (1.0 eq.)	Fmoc-OSu (1.1 eq)	$NaHCO_3$	THF	16	180 mg 76 %	91	45	32	N.D.

[a] Reaction time at room temperature, [b] EY = enrichment yield, [c] EL = enrichment level, using 99% ^{18}O and 90% ^{17}O-enriched water for ^{18}O and ^{17}O-enrichment, respectively, [d] aqueous solution (w/w), [e] values for L-Lys enriched by saponification, [f] values for L-Lys enriched by acid-catalysed exchange, [g] different mass isolated depending on the amount of ^{18}O-Gly reagent, [h] intermediate not isolated, [i] values for the Fmoc-Gly-O*H scaled-up procedure, [j] values the Fmoc-L-Asp(O*t*Bu)-O*H scaled-up procedure, N.D. = not determined.

CONCLUSION

In total, five different amino acids (Gly, L-Leu, L-Phe, L-Asp and L-Lys) were $^{17}O/^{18}O$-labeled in this chapter, using mechanochemical saponification, and also acid-catalysed exchange for Gly, L-Asp and L-Lys. Results are summarized in Table 4.13. Using either procedure, the labeled molecules were isolated pure, in moderate to high yields (55 - 85 %), and with no loss of enantiomeric purity (for optically active species: *ee* > 99%).

The main advantages of VBM saponification approach are its rapidity and labeling efficiency. With only 30 min of milling under ambient conditions (room temperature and atmospheric pressure) and using only small excess of H_2O^* (2 - 3 eq.), amino acids were labeled with high enrichment efficiency (enrichment yield: 82 - 95 %, enrichment level per carboxylic oxygen: 41 - 41% for ^{18}O-labeling and 29 - 34 % for ^{17}O-labeling). This fact clearly distinguishes the mechanochemical approach from other solution based saponification protocols published, where more than 12 h was required to provide a similar labeling efficiency. The saponification protocol was also scaled-up (only for Gly, L-Asp and L-Lys) providing around 180 - 200 mg of labeled amino acids in just one reaction.

In the acid catalysed oxygen exchange, which is to date still the protocol used the most in the literature for the labeling of amino acids, the application of HCl gas, commonly employed in H^+ catalysed exchange, was successfully avoided here by using HCl salts of amino acids as starting compounds (for Gly and L-Lys). Moreover, for the first time, the oxygen exchange was catalysed by a Lewis acid (Li^+), used here for the labeling of L-Asp. In the former case, a quantitative oxygen exchange was reached for Gly and L-Lys using small excess of H_2O^* (3 eq.). This led to overall higher enrichment levels, compared to the saponification, yet with a rather long reaction time: 24 h of heating at 100 °C.

Table 4.13: Summary of results for $^{17}O/^{18}O$-enrichment of amino acids using saponification and acid catalysed exchange.

Labeled Amino acid (AA)	Labeling protocol	H_2O^* eq.	Mass/yield	EY[a] [%]	^{18}O-EL[b] [%]	^{17}O-EL[b] [%]	*ee*[c] [%]
Gly	VBM saponification	3	49 ± 6 mg 52 ± 6 %	~ 85[d]	~ 43[d]	~ 38[d]	-
Gly	H^+ catalysed exchange	3	72 ± 3 mg 77 ± 3 %	quant.[d]	62 ± 1[d]	-	-
L-Leu	VBM saponification	3	86 ± 4 mg 78 ± 3 %	82 ± 1	41 ± 1	29	> 99
L-Phe	VBM saponification	2	71 ± 3 mg 61 ± 2 %	92 ± 2	46 ± 1	32	> 99
L-Asp-both[e]	VBM saponification	4	80 ± 2 mg 76 ± 1 %	88 ± 1	44 ± 1	31	> 99
L-Asp-both[e]	Li^+ catalysed exchange	4	79 ± 1 mg 78 ± 2 %	56	28	-	N.D.
L-Asp-side[e]	VBM saponification	3	77 ± 7 mg 70 ± 6 %	85 ± 1	42	31	-
L-Asp-main[e]	VBM saponification	3	113 ± 12 mg 84 ± 11 %	95 ± 1	47	34	-
L-Lys.HCl[f]	VBM saponification	3	64 ± 6 mg 54 ± 4 %	93 ± 1	47 ± 1	33	> 99
L-Lys.HCl[f]	H^+ catalysed exchange	3	73 ± 7 mg 62 ± 5 %	quant.	60 ± 1	-	> 99

[a] EY = enrichment yield, quant. = quantitative, [b] EL = enrichment level (for ^{18}O and ^{17}O labeling, 99% ^{18}O-enriched and 70% ^{17}O-enriched water was used, respectively), [c] enantiomeric excess (*ee*) determined for Fmoc-AA derivatives, [d] Enrichment yield and level of labeled Gly estimated from its Fmoc-Gly derivative, [e] Asp-both, Asp-side and Asp-main correspond to L-Asp labeled either on both carboxylic functions, on the side-chain only or main-chain only, N.D. = not determined, and [f] concerns essentially anhydrous L-Lys hydrochloride phase. Error bars calculated from repeated experiments (n = 2 - 3).

$^{17}O/^{18}O$-labeled Fmoc-protected amino acids were prepared by common solution-based Fmoc-protection protocols applied on pre-labeled molecules. For the Fmoc-Gly-O*H and Fmoc-L-Asp(O*t*Bu)-O*H, species used for the subsequent $^{17}O/^{18}O$-labeled peptide syntheses, the protocols were scaled-up producing up to ~ 1 g and ~ 700 mg of labeled molecules, respectively, in a cost-efficient manner (17.5 µL of H_2O^* for 100 mg of Fmoc-AA-O*H), and in just one day (work-up included). In addition, no loss in optical purity nor in enrichment levels was observed.

Regarding ^{17}O solid-state NMR analyses, thanks to the high enrichment levels of ^{17}O-labeled amino acids, high-resolution 1D spectra with a good signal-to-noise ratio were generally obtained within 6 h, when recorded at 14.1 T, and within less than seventy minutes,

when recorded at higher fields (18.8 and 20.0 T). The ^{17}O NMR parameters of L-Asp (both main-chain and side-chain oxygen sites) and of L-Phe were tentatively extracted. Moreover, ^{17}O solid-state NMR spectra of L-Asp labeled at both carboxylic functions, L-Asp labeled only at the side-chain and of L-Lys·HCl were reported for the first time.

In terms of future improvement of the presented enrichment protocols for free amino acids, the amount of H_2O* employed in the saponification of Gly, L-Asp and L-Lys could probably be further reduced, not changing the enrichment efficiency, as the syntheses were note optimized in this work regarding this aspect. The second important point to be addressed in the future is the rather lower yield (< 60%) for some of the labeled products (*e.g.* Gly and L-Lys). Some enhancement was already observed for Gly and L-Lys, when performing the labeling at higher scale and this trend will probably continue with further increasing the scale of their production. Alternatively, a different two-step procedure could be looked into, composed of enrichment of Boc-protected AA using CDI-activation/hydrolysis protocol followed by Boc-deprotection of labeled molecules.

Regarding the acid-catalysed exchange, a quantitative exchange, which was observed for Gly and L-Lys after 24 h, suggests that reducing the reaction time should be possible here. On the other hand, in the case of Li^+ catalysed exchange of L-Asp, only ~ 56% exchange yield was achieved. This may be enhanced, in the contrary, by prolonging the reaction time.

Nevertheless, it was shown here, that both of the labeling schemes are efficient approaches for the production of some highly $^{17}O/^{18}O$-enriched amino acids, in time- and cost-efficient manner. The efficiency of these protocols opens up positive promises for their application to other amino acids. Moreover, it is worth highlighting that in the contrary to the majority of previously published studies, great attention was given here to develop and build reproducible and robust protocols, in view of further development of ^{17}O NMR studies for the benefit of a better understanding of oxygen environment in oxygen-containing biomolecules.

REFERENCES

1. Wage, L. G., *Organic chemistry*. 8th ed.; Boston : Pearson: 2013.
2. Craik, D. J.; Fairlie, D. P.; Liras, S.; Price, D., The Future of Peptide-based Drugs. *Chem. Biol. Drug. Des.* **2013,** *81* (1), 136-147.
3. Levin, A.; Hakala, T. A.; Schnaider, L.; Bernardes, G. J. L.; Gazit, E.; Knowles, T. P. J., Biomimetic peptide self-assembly for functional materials. *Nat. Rev. Chem.* **2020,** *4* (11), 615-634.
4. Reid, C. M.; Sutherland, A., Synthesis of Isotopically Labeled α-Amino Acids. In *Amino Acids, Peptides and Proteins in Organic Chemistry*, pp 473-494.
5. Ghosh, A.; Ostrander, J. S.; Zanni, M. T., Watching Proteins Wiggle: Mapping Structures with Two-Dimensional Infrared Spectroscopy. *Chem. Rev.* **2017,** *117* (16), 10726-10759.
6. Middleton, C.; Woys, A.; Mukherjee, S.; Zanni, M., Residue-Specific Structural Kinetics of Proteins through the Union of Isotope Labeling, Mid-IR Pulse Shaping, and Coherent 2D IR Spectroscopy. *Methods* **2010,** *52*, 12-22.
7. Tian, X.; Permentier, H. P.; Bischoff, R., Chemical isotope labeling for quantitative proteomics. *Mass Spectrom. Rev.* **2021,** *n/a* (n/a).
8. Ning, L.; Lichun, Z.; Chengyan, H.; Zongwei, C., Advances in Technologies and Biological Applications of 18O Labeling Strategies in LC-MS Based Proteomics: An Updated Review. *Curr. Anal. Chem.* **2012,** *8* (1), 22-34.
9. Wu, G., Solid-State 17O NMR studies of organic and biological molecules: Recent advances and future directions. *Solid State Nucl. Magn. Reson.* **2016,** *73*, 1-14.
10. Theodorou, V.; Biris, N.; Sakarellos, C.; Tsikaris, V., A convenient and rapid method for the selective oxygen-17 enrichment of aspartyl peptides during solid-phase synthesis. *Tetrahedron Lett.* **2001,** *42*, 7703-7705.
11. Pike, K. J.; Lemaitre, V.; Kukol, A.; Anupõld, T.; Samoson, A.; Howes, A. P.; Watts, A.; Smith, M. E.; Dupree, R., Solid-State 17O NMR of Amino Acids. *J. Phys. Chem. B* **2004,** *108* (26), 9256-9263.
12. Ponnusamy, E.; Jones, C. C.; Fiat, D., Synthesis of oxygen-18 isotope labeled amino acids and dipeptides and its effects on carbon-13 NMR. *J. Labelled Compd. Rad.* **1987,** *24* (7), 773-778.
13. Murphy, R. C.; Clay, K. L., Synthesis and back exchange of 18O labeled amino acids for use as internal standards with mass spectrometry. *Biomed. Mass Spectrom.* **1979,** *6* (7), 309-314.
14. Yano, Y.; Kondo, K.; Watanabe, Y.; Zhang, T. O.; Ho, J.-J.; Oishi, S.; Fujii, N.; Zanni, M. T.; Matsuzaki, K., GXXXG-Mediated Parallel and Antiparallel Dimerization of Transmembrane Helices and Its Inhibition by Cholesterol: Single-Pair FRET and 2D IR Studies. *Angew. Chem. Int. Edit.* **2017,** *56* (7), 1756-1759.
15. Lin, B.; Hung, I.; Gan, Z.; Chien, P.-H.; Spencer, H. L.; Smith, S. P.; Wu, G., 17O NMR studies of yeast ubiquitin in aqueous solution and in the solid state. *Chem. Bio. Chem.* **2021,** *22* (5), 826.
16. Gerothanassis, I. P.; Hunston, R. N.; Lauterwein, J., 17O NMR chemical shifts of the twenty protein amino acids in aqueous solution. *Magn. Res. Chem.* **1985,** *23* (8), 659-665.
17. Yamada, K.; Yamazaki, T.; Asanuma, M.; Hirota, H.; Yamamoto, N.; Kajihara, Y., Solid-state 17O NMR in Biological Solids: Efficient 17O Labeling of Amino Acids and Peptides. *Chem. Lett.* **2007,** *36*, 192-193.
18. Špačková, J.; Fabra, C.; Cazals, G.; Hubert-Roux, M.; Schmitz-Afonso, I.; Goldberga, I.; Berthomieu, D.; Lebrun, A.; Métro, T.-X.; Laurencin, D., Cost-efficient and user-friendly 17O/18O labeling procedures of fatty acids using mechanochemistry. *Chem. Commun.* **2021**.
19. Mears, W. H., The Oxygen Exchange Reaction of Glycine Hydrochloride and Water. *J. Chem. Phys.* **1938,** *6* (5), 295-295.
20. Métro, T.-X.; Martinez, J.; Lamaty, F., 1,1′-Carbonyldiimidazole and Mechanochemistry: A Shining Green Combination. *ACS Sustain. Chem. Eng.* **2017,** *5* (11), 9599-9602.
21. Métro, T. X.; Gervais, C.; Martinez, A.; Bonhomme, C.; Laurencin, D., Unleashing the potential of 17O NMR spectroscopy using mechanochemistry. *Angew. Chem., Int. Ed.* **2017,** *56* (24), 6803-6807.
22. Steinschneider, A.; Burgar, M. I.; Buku, A.; Fiat, D., Labeling of amino acids and peptides with isotopic oxygen as followed by 17O-N.M.R.*. *Int. J. Pept. Protein Res.* **1981,** *18* (3), 324-333.
23. Marecek, J.; Song, B.; Brewer, S.; Belyea, J.; Dyer, R. B.; Raleigh, D. P., A Simple and Economical Method for the Production of 13C,18O-Labeled Fmoc-Amino Acids with High Levels of Enrichment: Applications to Isotope-Edited IR Studies of Proteins. *Org. Lett.* **2007,** *9* (24), 4935-4937.
24. Haynes, W. M., *Handbook of Chemistry and Physics*. 92nd ed.; 2011-2012.
25. Amend, J. P.; Helgeson, H. C., Solubilities of the common L-α-amino acids as a function of temperature and solution pH. In *Pure Appl. Chem.* 1997; Vol. 69, p 935.
26. de Namor, A. F. D.; Ritt, M.-C.; Schwing-Weill, M.-J.; Arnaud-Neu, F.; Lewis, D. F. V., Solution thermodynamics of amino acid–18-crown-6 and amino acid–cryptand 222 complexes in methanol and ethanol. Linear enthalpy–entropy compensation effect. *J. Chem. Soc. Faraday T.* **1991,** *87* (19), 3231-3239.
27. Bowden, N. A.; Sanders, J. P. M.; Bruins, M. E., Solubility of the Proteinogenic α-Amino Acids in Water, Ethanol, and Ethanol–Water Mixtures. *J. Chem. Eng. Data* **2018,** *63* (3), 488-497.

28. Zhou, X.; Fan, J.; Li, N.; Du, Z.; Ying, H.; Wu, J.; Xiong, J.; Bai, J., Solubility of l-phenylalanine in water and different binary mixtures from 288.15 to 318.15 K. *Fluid Phase Equilibr.* **2012,** *316*, 26-33.
29. Pertzoff, V. In *The solubility of glutamic acid in water and certain organic solvents*, 2003.
30. Zhao, D.; Li, Q.; Duan, E.; Li, H.; Shen, X., Solubility of l-Lysine Hydrochloride in Dimethyl Sulfoxide, Methanol, Ethanol, Water, and Glycol between (283 and 323) K. *J. Chem. Eng. Data* **2009,** *54* (7), 2126-2127.
31. Zhang, L.; Huang, Z.; Wan, X.; Li, J.; Liu, J., Measurement and Correlation of the Solubility of Febuxostat in Four Organic Solvents at Various Temperatures. *J. Chem. Eng. Data* **2012,** *57* (11), 3149-3152.
32. Zhdanov, A. A.; Sergienko, N. V.; Trankina, E. S., New method for the synthesis of cage and polymeric metallosiloxanes. *Russ. Chem. Bull.* **1998,** *47* (12), 2448-2450.
33. Tang, Y.; Jiang, Z.; Xing, G.; Li, A.; Kanhere, P. D.; Zhang, Y.; Sum, T. C.; Li, S.; Chen, X.; Dong, Z.; Chen, Z., Efficient Ag@AgCl Cubic Cage Photocatalysts Profit from Ultrafast Plasmon-Induced Electron Transfer Processes. *Adv. Funct. Mater.* **2013,** *23* (23), 2932-2940.
34. Carta, R.; Tola, G., Solubilities of l-Cystine, l-Tyrosine, l-Leucine, and Glycine in Aqueous Solutions at Various pHs and NaCl Concentrations. *J. Chem. Eng. Data* **1996,** *41* (3), 414-417.
35. Tseng, H.-C.; Lee, C.-Y.; Weng, W.-L.; Shiah, I. M., Solubilities of amino acids in water at various pH values under 298.15K. *Fluid Phase Equilibr.* **2009,** *285* (1), 90-95.
36. Wang, J.; Wang, J.; Liu, J.; Wang, S.; Pei, J., Solubility of d-Aspartic Acid and l-Aspartic Acid in Aqueous Salt Solutions from (293 to 343) K. *J. Chem. Eng. Data* **2010,** *55* (4), 1735-1738.
37. Boldyreva, E. V.; Drebushchak, V. A.; Drebushchak, T. N.; Paukov, I. E.; Kovalevskaya, Y. A.; Shutova, E. S., Polymorphism of glycine, Part I. *J. Therm. Anal. Calorim.* **2003,** *73* (2), 409-418.
38. Yang, X.; Wang, X.; Ching, C. B., Solubility of Form α and Form γ of Glycine in Aqueous Solutions. *J. Chem. Eng. Data* **2008,** *53* (5), 1133-1137.
39. He, G.; Bhamidi, V.; Wilson, S. R.; Tan, R. B. H.; Kenis, P. J. A.; Zukoski, C. F., Direct Growth of γ-Glycine from Neutral Aqueous Solutions by Slow, Evaporation-Driven Crystallization. *Cryst. Growth. Des.* **2006,** *6* (8), 1746-1749.
40. Torbeev, V. Y.; Shavit, E.; Weissbuch, I.; Leiserowitz, L.; Lahav, M., Control of Crystal Polymorphism by Tuning the Structure of Auxiliary Molecules as Nucleation Inhibitors. The β-Polymorph of Glycine Grown in Aqueous Solutions. *Cryst. Growth. Des.* **2005,** *5* (6), 2190-2196.
41. Bhat, M. N.; Dharmaprakash, S. M., Effect of solvents on the growth morphology and physical characteristics of nonlinear optical γ-glycine crystals. *J. Cryst. Growth* **2002,** *242* (1), 245-252.
42. Towler, C. S.; Davey, R. J.; Lancaster, R. W.; Price, C. J., Impact of Molecular Speciation on Crystal Nucleation in Polymorphic Systems: The Conundrum of γ Glycine and Molecular 'Self Poisoning'. *J. Am. Chem. Soc.* **2004,** *126* (41), 13347-13353.
43. Iitaka, Y., The crystal structure of γ-glycine. *Acta Crystallogr.* **1961,** *14* (1), 1-10.
44. Tóth, J.; Kardos-Fodor, A.; Halász-Péterfi, S., The formation of fine particles by salting-out precipitation. *Chem. Eng. Process.* **2005,** *44* (2), 193-200.
45. Juramy, M.; Chèvre, R.; Cerreia Vioglio, P.; Ziarelli, F.; Besson, E.; Gastaldi, S.; Viel, S.; Thureau, P.; Harris, K. D. M.; Mollica, G., Monitoring Crystallization Processes in Confined Porous Materials by Dynamic Nuclear Polarization Solid-State Nuclear Magnetic Resonance. *J. Am. Chem. Soc.* **2021,** *143* (16), 6095-6103.
46. Moggach, S. A.; Parsons, S.; Wood, P. A., High-pressure polymorphism in amino acids. *Crystallogr. Rev.* **2008,** *14* (2), 143-184.
47. Kitamura, M., Polymorphism in the crystallization of L-glutamic acid. *J. Cryst. Growth* **1989,** *96* (3), 541-546.
48. Widyarani; Bowden, N. A.; Kolfschoten, R. C.; Sanders, J. P. M.; Bruins, M. E., Fractional Precipitation of Amino Acids from Agro-industrial Residues Using Ethanol. *Ind. Eng. Chem. Res.* **2016,** *55* (27), 7462-7472.
49. Orten, J. M.; Hill, R. M., A Simple Method for the Preparation of Glycine. *J. Am. Chem. Soc.* **1931,** *53* (7), 2797-2799.
50. McGlone, S. J.; Elmes, P. S.; Brown, R. D.; Godfrey, P. D., Molecular structure of a conformer of glycine by microwave spectroscopy. *J. Mol. Struct.* **1999,** *485-486*, 225-238.
51. Stievano, L.; Tielens, F.; Lopes, I.; Folliet, N.; Gervais, C.; Costa, D.; Lambert, J.-F., Density Functional Theory Modeling and Calculation of NMR Parameters: An ab Initio Study of the Polymorphs of Bulk Glycine. *Cryst. Growth. Des.* **2010,** *10* (8), 3657-3667.
52. Harris, K. D. M., New in situ solid-state NMR strategies for exploring materials formation and adsorption processes: prospects in heterogenous catalysis. *Appl. Petrochem. Res.* **2016,** *6* (3), 295-306.
53. Veinberg, S. L.; Friedl, Z. W.; Harris, K. J.; O'Dell, L. A.; Schurko, R. W., Ultra-wideline 14N solid-state NMR as a method for differentiating polymorphs: glycine as a case study. *Cryst. Eng. Comm* **2015,** *17* (28), 5225-5236.
54. Folliet, N.; Gervais, C.; Costa, D.; Laurent, G.; Babonneau, F.; Stievano, L.; Lambert, J.-F.; Tielens, F., A Molecular Picture of the Adsorption of Glycine in Mesoporous Silica through NMR Experiments Combined with DFT-D Calculations. *J. Phys. Chem. C* **2013,** *117* (8), 4104-4114.

55. Yamada, K.; Honda, H.; Yamazaki, T.; Yoshida, M., Solid-state 17O NMR study of the electric-field-gradient and chemical shielding tensors in polycrystalline γ-glycine. *Solid State Nucl. Magn. Reson.* **2006,** *30* (3), 162-170.
56. Kazuhiko, Y.; Tadashi, S.; Toshio, Y.; Akira, S., A Solid-state 17O NMR Study of β-Glycine: High Sensitivity of 17O NMR Parameters to Hydrogen-bonding Interactions. *Chem. Lett.* **2008,** *37* (4), 472-473.
57. Wong, A.; Hung, I.; Howes, A. P.; Anupõld, T.; Past, J.; Samoson, A.; Brown, S. P.; Smith, M. E.; Dupree, R., The determination of 17O NMR parameters of hydroxyl oxygen: A combined deuteration and DOR approach. *Magn. Res. Chem.* **2007,** *45* (S1), S68-S72.
58. Howes, A.; Anupold, T.; Lemaitre, V.; Kukol, A.; Watts, A.; Samoson, A.; Smith, M.; Dupree, R., Enhancing resolution and sensitivity of 17O solid-state NMR through combining double rotation, 1H decoupling and satellite modulation for biomolecular applications. *Chem. Phys. Lett.* **2006,** *421* (1-3), 42-46.
59. Görbitz, C.; Dalhus, B., Redetermination of L-Leucine at 120K. *Acta Crystallogr. C* **1996,** *52* (7), 1754-1756.
60. Harding, M. M.; Howieson, R., L-leucine. *Acta Crystallogr. B-Stru.* **1976,** *32* (2), 633-634.
61. Façanha Filho, P. F.; Jiao, X.; Freire, P. T. C.; Lima Jr, J. A.; dos Santos, A. O.; Henry, P. F.; Yokaichiya, F.; Kremner, E.; Bordallo, H. N., Structure–property relations in crystalline l-leucine obtained from calorimetry, X-rays, neutron and Raman scattering. *Phys. Chem. Chem. Phys.* **2011,** *13* (14), 6576-6583.
62. Ihlefeldt, F. S.; Pettersen, F. B.; von Bonin, A.; Zawadzka, M.; Görbitz, C. H., The Polymorphs of L-Phenylalanine. *Angew. Chem., Int. Edit.* **2014,** *53* (49), 13600-13604.
63. Williams, P. A.; Hughes, C. E.; Buanz, A. B. M.; Gaisford, S.; Harris, K. D. M., Expanding the Solid-State Landscape of l-Phenylalanine: Discovery of Polymorphism and New Hydrate Phases, with Rationalization of Hydration/Dehydration Processes. *J. Phys. Chem. C* **2013,** *117* (23), 12136-12145.
64. Cuppen, H. M.; Smets, M. M. H.; Krieger, A. M.; van den Ende, J. A.; Meekes, H.; van Eck, E. R. H.; Görbitz, C. H., The Rich Solid-State Phase Behavior of l-Phenylalanine: Disappearing Polymorphs and High Temperature Forms. *Cryst. Growth. Des.* **2019,** *19* (3), 1709-1719.
65. Steinschneider, A.; Burgar, M. I.; Buku, A.; Fiat, D., Labeling of mamino acids and peptides with isotopic oxygen as followed by 17O-NMR. *Int. J. Pept. Protein Res.* **1981,** *18* (3), 324-333.
66. Prasad, S.; Clark, T. M.; Sharma, R.; Kwak, H.-T.; Grandinetti, P. J.; Zimmermann, H., A combined 17O RAPT and MQ-MAS NMR study of l-leucine. *Solid State Nucl. Magn. Reson.* **2006,** *29* (1), 119-124.
67. Batchelder, L. S.; Sullivan, C.; Jelinski, L. W.; Torchia, D., Characterization of leucine side-chain reorientation in collagen-fibrils by solid-state 2H NMR. *Proc. Natl. Acad. Sci.* **1982,** *79* (2), 386-389.
68. Gibson, J. M.; Popham, J. M.; Raghunathan, V.; Stayton, P. S.; Drobny, G. P., A Solid-State NMR Study of the Dynamics and Interactions of Phenylalanine Rings in a Statherin Fragment Bound to Hydroxyapatite Crystals. *J. Am. Chem. Soc.* **2006,** *128* (16), 5364-5370.
69. Li, K.; Emani, P. S.; Ash, J.; Groves, M.; Drobny, G. P., A Study of Phenylalanine Side-Chain Dynamics in Surface-Adsorbed Peptides Using Solid-State Deuterium NMR and Rotamer Library Statistics. *J. Am. Chem. Soc.* **2014,** *136* (32), 11402-11411.
70. Frey, M.; DiVerdi, J.; Opella, S., Dynamics of phenylalanine in the solid state by NMR. *J. Am. Chem. Soc.* **1985,** *107* (25), 7311-7315.
71. Schaefer, J.; Stejskal, E. O.; McKay, R. A.; Dixon, W. T., Phenylalanine ring dynamics by solid-state 13C NMR. *J. Magn. reson.* **1984,** *57* (1), 85-92.
72. Yamada, K.; Asanuma, M.; Honda, H.; Nemoto, T.; Yamazaki, T.; Hirota, H., Experimental determination of the carboxylate oxygen electric-field-gradient and chemical shielding tensors in l-alanine and l-phenylalanine. *J. Mol. Struct.* **2007,** *843* (1), 45-56.
73. Derissen, J.; Endeman, H.; Peerdeman, A., The crystal and molecular structure of L-aspartic acid. *Acta Crystallogr. B-Stru.* **1968,** *24* (10), 1349-1354.
74. Roelands, C. P. M.; ter Horst, J. H.; Kramer, H. J. M.; Jansens, P. J., Precipitation mechanism of stable and metastable polymorphs of L-glutamic acid. *AIChE J.* **2007,** *53* (2), 354-362.
75. Wikner, C.; Meshalkina, L.; Nilsson, U.; Nikkola, M.; Lindqvist, Y.; Sundström, M.; Schneider, G., Analysis of an invariant cofactor-protein interaction in thiamin diphosphate-dependent enzymes by site-directed mutagenesis. Glutamic acid 418 in transketolase is essential for catalysis. *J. Biol. Chem.* **1994,** *269* (51), 32144-32150.
76. Howell, E. E.; Villafranca, J. E.; Warren, M. S.; Oatley, S. J.; Kraut, J., Functional role of aspartic acid-27 in dihydrofolate reductase revealed by mutagenesis. *Science* **1986,** *231* (4742), 1123-1128.
77. Gotliv, B.-A.; Kessler, N.; Sumerel, J. L.; Morse, D. E.; Tuross, N.; Addadi, L.; Weiner, S., Asprich: A Novel Aspartic Acid-Rich Protein Family from the Prismatic Shell Matrix of the Bivalve Atrina rigida. *Chem. Bio. Chem.* **2005,** *6* (2), 304-314.
78. Li, S.; Wang, L., Phosphorylated osteopontin peptides inhibit crystallization by resisting the aggregation of calcium phosphate nanoparticles. *Cryst. Eng. Comm.* **2012,** *14* (23), 8037-8043.

79. Zou, Z.; Bertinetti, L.; Politi, Y.; Fratzl, P.; Habraken, W. J. E. M., Control of Polymorph Selection in Amorphous Calcium Carbonate Crystallization by Poly(Aspartic Acid): Two Different Mechanisms. *Small* **2017,** *13* (21), 1603100.
80. Wang, Y.; Wilson, D.; Harbison, G. S., Solid-State NMR and the Crystallization of Aspartic and Glutamic Acids. *Cryst. Growth. Des.* **2016,** *16* (2), 625-631.
81. Ben Shir, I.; Kababya, S.; Zax, D. B.; Schmidt, A., Resilient Intracrystalline Occlusions: A Solid-State NMR View of Local Structure as It Tunes Bulk Lattice Properties. *J. Am. Chem. Soc.* **2020,** *142* (32), 13743-13755.
82. Yamada, K.; Shimizu, T.; Tansho, M.; Nemoto, T.; Asanuma, M.; Yoshida, M.; Yamazaki, T.; Hirota, H., Solid-state 17O NMR study of the electric-field-gradient and chemical shielding tensors in polycrystalline amino acids. *Magn. Res. Chem.* **2007,** *45* (7), 547-556.
83. Wright, D. A.; Marsh, R., The crystal structure of L-lysine monohydrochloride dihydrate. *Acta Crystallogr.* **1962,** *15* (1), 54-64.
84. Petrosyan, A. M.; Ghazaryan, V. V., Vibrational spectra of l-lysine monohydrochloride dihydrate and its two anhydrous forms. *J. Mol. Struct.* **2009,** *917* (1), 56-62.
85. Wada, N.; Horiuchi, N.; Nakamura, M.; Nozaki, K.; Nagai, A.; Yamashita, K., Controlled Crystallization of Calcium Carbonate via Cooperation of Polyaspartic Acid and Polylysine Under Double-Diffusion Conditions in Agar Hydrogels. *ACS Omega* **2018,** *3* (12), 16681-16692.
86. Zamani, F.; Rezapour, M.; Kianpour, S., ChemInform Abstract: Immobilization of L-Lysine on Zeolite 4A as an Organic-Inorganic Composite Basic Catalyst for Synthesis of α,β-Unsaturated Carbonyl Compounds under Mild Conditions. *Bull. Korean Chem. Soc.* **2013,** *34*, 2367.
87. Hunston, R.; Gerothanassis, I. P.; Lauterwein, J., 17O nuclear magnetic resonance studies of some enriched amino acids. *Org. Magn. Res.* **1982,** *18* (2), 120-121.
88. Manríquez, R.; López-Dellamary, F. A.; Frydel, J.; Emmler, T.; Breitzke, H.; Buntkowsky, G.; Limbach, H.-H.; Shenderovich, I. G., Solid-State NMR Studies of Aminocarboxylic Salt Bridges in l-Lysine Modified Cellulose. *J. Phys. Chem. B* **2009,** *113* (4), 934-940.
89. Maeda, S.; Mori, T.; Sasaki, C.; Kunimoto, K.-K.; Kuwae, A.; Hanai, K., Structural investigation of microbial poly (ε-L-lysine) derivatives with azo dyes by solid-state 13 C and 15 N NMR. *Polym. Bull.* **2005,** *53* (4), 259-267.
90. Dos, A.; Schimming, V.; Tosoni, S.; Limbach, H.-H., Acid−Base Interactions and Secondary Structures of Poly-l-Lysine Probed by 15N and 13C Solid State NMR and Ab initio Model Calculations. *J. Phys. Chem. B* **2008,** *112* (49), 15604-15615.
91. Y. Takayanagi, K. I., M. Miyazawa, N. Yamaya, H. Tamura Anhydrous L-lysine monohydrochloride in alpha-cyrstalline form and preparation thereof. 1981.
92. Klein, B. A.; Tkachuk, D. G.; Terskikh, V. V.; Michaelis, V. K., Expanding the NMR toolkit for biological solids: oxygen-17 enriched Fmoc-amino acids. *New J. Chem.* **2021,** *45* (28), 12384-12398.
93. Seyfried, M. S.; Lauber, B. S.; Luedtke, N. W., Multiple-Turnover Isotopic Labeling of Fmoc- and Boc-Protected Amino Acids with Oxygen Isotopes. *Org. Lett.* **2010,** *12* (1), 104-106.
94. Bada, J. L., Racemization of Amino Acids in Nature. *Interdiscip. Sci. rev.* **1982,** *7* (1), 30-46.
95. Cartus, A., Chapter 12 - d-Amino Acids and Cross-Linked Amino Acids in Food. In *Chemical Contaminants and Residues in Food (Second Edition)*, Schrenk, D.; Cartus, A., Eds. Woodhead Publishing: 2017; pp 251-278.
96. Bruno Perly, S. M., Florence Pilard Amphiphilic cyclodextrin derivatives, method for preparation thereof and uses thereof. 2007.
97. Lapatsanis, L.; Milias, G.; Froussios, K.; Kolovos, M., Synthesis of N -2,2,2-(Trichloroethoxycarbonyl)-L-amino Acids and N -(9-Fluorenylmethoxycarbonyl)-L-amino Acids Involving Succinimidoxy Anion as a Leaving Group in Amino Acid Protection. *Synthesis-Stuttgart* **1983,** *1983*, 671-673.
98. Schramma, K. R.; Bushin, L. B.; Seyedsayamdost, M. R., Structure and biosynthesis of a macrocyclic peptide containing an unprecedented lysine-to-tryptophan crosslink. *Nat. Chem.* **2015,** *7* (5), 431-437.

ANNEXE IV

AMINO ACIDS LABELING - EXPERIMENTAL PART

IV-A) MATERIALS AND METHODS

IV-A1) Reagents

The following reagents were used as received: glycine methylester hydrochloride (Gly-OMe·HCl, Alfa Aesar, 99%), glycine hydrochloride (Gly·HCl, Alfa Aesar, 98%), L-phenylalanine methylester hydrochloride (L-Phe-OMe·HCl, Iris), L-leucine methylester hydrochloride (L-Leu-OMe·HCl, Alfa Aesar, 99%), L-aspartic acid dimethylester hydrochloride (L-Asp(OMe)-OMe·HCl, Alfa Aesar, 98%), L-aspartic acid 1-methylester (L-Asp-OMe, Alfa Aesar, 98%), L-aspartic acid 4-methylester monohydrochloride (L-Asp(OMe)-OH·HCl, Alfa Aesar, 95%), L-aspartic acid (L-Asp, Acros Organics, >98%), L-aspartic acid 4-*tert*-butyl-1-methyl ester hydrochloride (L-Asp(O*t*Bu)-OMe·HCl, Fluorochem, 95%), L-lysine methylester dihydrochloride (L-Lys-OMe·2HCl, Alfa Aesar, 99%), L-lysine dihydrochloride (L-Lys-OH·2HCl, Alfa Aesar, 99%), *N*-ε-*tert*-butoxycarbonyl-L-lysine methyl ester hydrochloride (L-Lys(Boc)-OMe·HCl, Fluorochem, 97%), sodium ethoxide (NaOEt, Sigma-Aldrich, >95%), lithium chloride anhydrous (LiCl, Alfa-Aesar, >99%), Fmoc *N*-hydroxysuccinimide ester (Fmoc-OSu, Alfa Aesar, >95%), sodium carbonate (Na_2CO_3, VWR, >99%), sodium hydrogen carbonate ($NaHCO_3$, Fluka, >99%). Reagent grade solvents were used in all purification protocols.

The ~ 70% ^{17}O-labeled water was purchased from CortecNet. The isotopic composition, as indicated in the certificate of analysis, is 26.34 % ^{18}O, 70.37 % ^{17}O, 3.29 % ^{16}O. The ~ 90% ^{17}O-labeled water was purchased from Eurisotop. The isotopic composition, as indicated in the certificate of analysis, is 1.0 % ^{18}O, 91.0 % ^{17}O, 8.0 % ^{16}O.

^{18}O-labeled water was purchased from CortecNet. Its isotopic composition, as indicated in the certificate of analysis, is 99.3 % ^{18}O, 0.2 % ^{17}O, 0.5 % ^{16}O).

IV-A2) Synthetic equipment

Milling treatments were carried out in a Retsch Miller Mill 400 apparatus, using 10 mL screw-type stainless steel grinding jars, containing two 10 mm diameter stainless steel. All protocols were first tested using non-labeled water and then optimized using ^{18}O-labeled water, before performing experiments with ^{17}O-labeled H_2O.

IV-A3) Characterization protocols

Infrared (IR) spectra were recorded on a Perkin Elmer Spectrum 2 FT-IR instrument. The attenuated total reflectance (ATR) measurement mode was used (diamond crystal), and measurements were performed in the 400-4000 cm^{-1} range.

Powder XRD analyses were carried out on a X'Pert MPD diffractometer using Cu $K_{\alpha 1}$ radiation (λ = 1.5406 Å) with the operation voltage and current maintained at 40 kV and 25 mA, respectively. Diffractograms were recorded between 5°and 50° in 2θ, with step size of 0.017°, and a time per step of 40 s.

Determinations of enantiomeric excesses were performed by HPLC on chiral support with an Agilent 1260 Infinity unit (pump G1311B, autosampler G1329B, DAD G1315D) and Agilent OpenLAB Chemstation. The different analytical columns (250 x 4.6 mm) used Chiralpak AZ-H (amylose tris(3-chloro-4-methylphenylcarbamate) coated on silica), Chiralpak IC (cellulose tris(3,5-dichlorophenylcarbamate) immobilized on silica) and Chiralpak IE (amylose tris(3,5-dichloro-phenylcarbamate) immobilized on silica) from Chiral Technology Europa (Illkirch, France). Retention times Rt in minutes, retention factors $k_i = (Rt_i - Rt_0)/Rt_0$ and

enantioselectivity factor $\alpha = k_2/k_1$ and resolution $Rs = 1.18\ (Rt_2 - Rt_1) / (w_1 + w_2)$ are given. Rt_0 was determined by injection of tri-tertio-butyl benzene and w_i was the peak width at half-height.

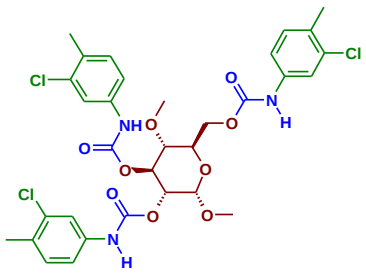	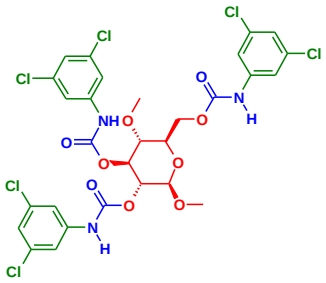	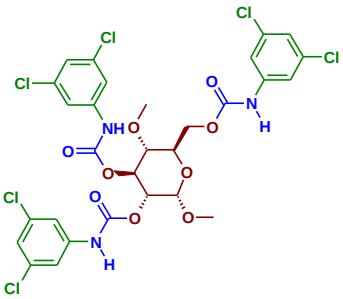
Chiralpak AZ-H	Chiralpak IC	Chiralpak IE

LC-MS analysis were done using a Acquity H-Class (Waters) system equipped with a Kinetex EVO C18 column (1.9 µm particle size, 50 x 2.1 mm, Phenomenex). Mobile phase A consisted of water while mobile phase B was acetonitrile both containing 0.1% formic acid. The gradient started at 0% mobile phase B and increase to 100% mobile phase B over 3 min. After holding for 0.6 min the gradient returned to 0% B before re-equilibration for 1.4 min, to give a total run time of 5 min. The flow rate was 0.5 mL/min and the eluent was directed to the atmospheric pressure ionisation source of a Synapt G2-S (Waters) operating in negative or positive electrospray ionization mode depending of the sample. Capillary and cone voltage were respectively 3000V and 30V. Source and desolvation temperatures were respectively 450°C and 140°C.

MS analysis were done by infusion of the sample in the electrospray source of a Synapt G2-S (Waters, SN: UEB205) mass spectrometer operating in positif or negative mode. Capillary and cone voltage were respectively 3000V and 30V. Source and desolvation temperatures were respectively 250°C and 100°C. All data were processed by Masslynx 4.2 software.

The $^{17}O/^{18}O$-enrichement *level* was estimated based on the calculation of an apparent average atomic weight for oxygen in the isolated phase, from which enrichment level per carboxylic oxygen was subsequently derived using $^{18}O/^{17}O$ isotopic ratio of the labeled water. Reported error bars correspond either to the standard deviation coming from the analysis of different batches (for $n > 1$). Enrichment *yields* correspond to the ratio between the average enrichment level per carboxylic oxygen determined by MS and the maximum average enrichment level per carboxylic oxygen which could have been obtained, considering the composition of enriched water used for the hydrolysis, and assuming that each carboxylic group is enriched on one of the 2 oxygen atoms.

^{1}H and ^{13}C solution NMR spectra were recorded on an Avance III Bruker 600 MHz NMR spectrometer equipped with a TCI Prodigy cryoprobe or on an Avance III Bruker 500 MHz NMR spectrometer equipped with a BBO Helium cryoprobe, using D_2O as a solvent. Chemical shifts were referenced to the peak of added DSS (sodium trimethylsilylpropanesulfonate) standard at 0 ppm (^{1}H NMR spectra) and 0 ppm (^{13}C NMR spectra).

^{13}C solid-state NMR experiments were performed on a VNMRS 600 MHz (14.1 T) NMR spectrometer at the University of Montpellier (France) by Dr. Ieva Goldberga, using a Varian 3.2 mm HX probe tuned to ^{1}H (599.82 MHz) and ^{13}C (150.81 MHz). The experiment performed at 20.0 T was acquired at the UK High-Field solid-state NMR facility in Warwick with the help of Dr Dinu Iuga on a Bruker Avance NEO NMR spectrometer equipped with a

3.2 mm HXY probe operating at a 13C frequency of 213.81 MHz and 1H frequency of 850.23 MHz. The temperature was regulated at 0 °C. All ^{13}C NMR spectra were recorded under MAS (Magic Angle Spinning) with a spinning frequency of 10, 12 or 16 kHz (see Table IV-1). A ^{1}H-^{13}C CPMAS NMR sequence was used with a 3 µs ^{1}H excitation pulse, followed by a ramped CP pulse of 2 or 2.5 ms contact time, and applying SPINAL-64 ^{1}H-decoupling (75 kHz) during acquisition. All acquisition parameters for CPMAS experiments are summarized in Table IV-1. ^{1}H and ^{13}C chemical shifts were referenced to adamantane at 1.8 ppm and 38.5 ppm (high frequency peak), respectively.

Table IV-1: ^{13}C CPMAS NMR acquisition parameters

Sample	Field [T]	Probe	CT [ms]	MAS [kHz]	D1 [s]	NS	Time	Temp. [°C]
Glycine	14.1	Phoenix	2	12	1	3750	1h05	0
Glycine	20.0	HXY	2	10	4	80	0h05	0
L-Leu	14.1	HXY	2.5	16	2	120	0h04	0
L-Phe	14.1	HXY	2.5	16	8	140	0h19	0
L-Asp-main	14.1	HX	2.5	16	16	256	1h08	0
L-Lys·HCl·2H_2O	14.1	HX	2.5	16	1	2048	0h35	0

^{17}O solid-state NMR experiments were acquired at multiple magnetic fields (9.4, 14.1, 18.8 and 20.0 T) at different NMR facilities.

Experiments performed at 9.4 and 14.1 T were carried out at University of Montpellier (France) with the help of Dr. Ieva Goldberga. At 9.4 T, the experiments were performed on a VNMRS 400 MHz (9.4 T) NMR spectrometer using a 3.2 mm HX probe tuned to ^{1}H (399.68 MHz) and ^{17}O (54.18 MHz). At 14.1 T, the experiments were performed on a VNMRS 600 MHz (14.1 T) NMR spectrometer using a 3.2 mm probe tuned to ^{1}H (599.82 MHz) and ^{17}O (81.31 MHz). Three types of probes were used, depending on the availability of the equipment: Varian HX, HXY or a Phoenix probe equipped with a 3.2 mm probe head. The spectra were recorded under MAS conditions, using spinning frequencies of 16 or 20 kHz (see Table IV-2) with temperature regulation at 0 °C. The ^{17}O MAS one pulse NMR experiments (Bloch decay) were performed using 1.0 µs for CT selective 90^0 pulse. Some of the ^{17}O NMR experiments were recorded using DFS excitation scheme to enhance the ^{17}O signal.[1] The parameters were as follows: DFS pulse of 500 µs, with sweep between 200 and 80 kHz, followed by a 90° "solid" pulse of 2 µs. ^{1}H decoupling (RF ~ 75 kHz) (SPINAL-64) was applied during acquisition.

At 18.8 T, ^{17}O NMR spectra were acquired at two different facilities on a Bruker Avance NEO NMR spectrometers operating at a ^{17}O frequency of 108.49 MHz and a ^{1}H frequency of 800.12 MHz. Experiments recorded at IMEC-ISB-UCCS in Lille (France) were acquired with the help of Dr. Julien Trébosc and Dr. Ieva Goldberga. The ^{17}O MAS one pulse NMR experiment (Bloch decay) was performed using a 1.25 µs for CT selective 90^0 pulse. The experiment recorded at MagLab in Tallahassee (USA) was with the help of Dr. Ivan Hung. The ^{17}O MAS 1D spectrum was recorded using the WURST pulse sequence.[2-3] The 2D MQMAS experiment was recorded using a 3Q z-filtered experiment.[4] The length of the excitation, conversion and soft excitation pulses were 3, 1 and 5 µs, respectively, ^{1}H decoupling was applied during acquisitions for both experiments.

At 20.0 T, ^{17}O NMR spectra were acquired at two different facilities on a Bruker Avance NEO NMR spectrometers operating at a ^{17}O frequency of 115.26 MHz and a ^{1}H frequency of 850.23 MHz. Experiments performed at the UK High-Field solid-state NMR facility in

Warwick were acquired with the help of Dr. Dinu Iuga. The ^{17}O MAS one pulse NMR experiment (Block decay) was performed using 1.5 µs for CT selective 90^0 pulse. The experiment performed at CEMHTI in Orléans (France) was recorded by Dr. Ieva Goldberga and Dr César Leroy. The parameters for the DFS experiment were as follows: DFS pulse of 1000 µs, with sweep between 1 MHz and 50 kHz, followed by a 90° "solid" pulse of 8.33 µs. Experiment was performed on 4.0 mm HX probe with the MAS frequency of 14.286 kHz with temperature regulation at 0 °C.

More details on acquisition conditions are reported in table IV-2. ^{17}O chemical shifts were referenced to D_2O at -2.7 ppm (which corresponds to tap-water at 0 ppm). The ^{17}O MAS NMR spectra were presented (and fitted) using DMfit software (using Q MAS ½ model).[5]

Table IV-2: ^{17}O solid-state NMR acquisition parameters

Sample	Field [T]	Probe	Exp. type	H-dec.	MAS [kHz]	D1 [s]	NS	Time	Temp [°C]
Glycine	14.1	Phoenix	DFS	no	16	2	8000	4h27	0
Glycine	20.0	HXY[a]	OnePulse	no	20	1	2048	0h34	0
L-Leu	9.4	HX	DFS	yes	20	0.5	32600	4h42	0
L-Leu	14.1	HX	DFS	yes	20	0.5	2000	0h17	0
L-Leu	14.1	HX	DFS	yes	20	0.5	4000	0h34	0
L-Leu	18.8	Phoenix[b]	DFS	no	20	0.5	5120	0h42	5.5
L-Leu	18.8	HXY[c]	WURST	yes	16	0.5	2048	0h17	N.R.
L-Leu	18.8	HXY[c]	2D MQMAS	yes	16	0.05	4512/ 80[e]	5h00	N.R.
L-Phe	9.4	HX	DFS	yes	20	4	35900	40h05	0
L-Phe	14.1	HX	DFS	yes	20	4	13350	14h56	0
L-Phe	18.8	Phoenix[b]	OnePulse	no	20	1	4096	1h08	5.5
L-Asp-both	14.1	Phoenix	DFS	no	20	4	2000	2h14	0
L-Asp-side	14.1	Phoenix	DFS	no	20	4	2000	2h14	0
L-Asp-main	14.1	HXY	DFS	no	20	4	2000	2h14	0
L-Asp-main	20.0	HX[d]	DFS	yes	14	4	1024	1h08	0
L-Lys.HCl.anh	14.1	Phoenix	DFS	no	16	4	1400	1h33	0
L-Lys·HCl·$2H_2O$	14.1	HXY	DFS	no	16	4	5000	5h35	0

[a] Experiments were performed at the UK High-Field solid-state NMR facility in Warwick.
[b] Experiments were performed at the IMEC-ISB-UCCS in Lille, France.
[c] Experiments were performed at the MagLab in Tallahassee, USA.
[d] Experiments were performed at the CEMHTI in Orléans, France.
[e] The ^{17}O z-filtered 2D MQ MAS experiment was recorded using 4515 transients per increment, in total 80 increments were acquired in F1 dimension.
N.R. = not regulated (temperature), DFS stands for Double Frequency Sweep, to indicate that this signal-enhancement was used just before the excitation pulse.

IV-B) $^{17}O/^{18}O$-LABELED AMINO ACIDS PREPARED BY SAPONIFICATION

IV-B1) Glycine (Gly, G)

a) Labeling protocols

- *Low-scale synthesis:*

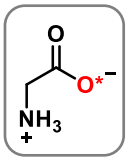

^{18}O-labeled water (98%, 65 µL, 3.6 mmol, 3.0 eq.), two stainless steel balls (10 mm diameter), glycine methyl ester monohydrochloride (150 mg, 1.2 mmol, 1.0 eq.) and sodium ethoxide (203 mg, 3.0 mmol, 2.5 eq.) were introduced successively into a screw-top stainless steel grinding jar (10 mL inner volume). The jar was closed and subjected to grinding for 30 min in the MM400 mixer mill operated at 25 Hz. The yellowish paste obtained was dissolved in water in order to recover the product from the jar, as described in the following paragraph.

At first, non-labeled water (400 µL) was added into the jar, and the content was subjected to grinding for 2 min at 25 Hz. Then, the yellow solution was transferred to a round-bottom flask, the jar was rinsed with non-labeled water (400 µL) and the aqueous phases were combined and sonicated for 5 min. The medium was stirred and gradually acidified to pH = 3 - 4 using concentrated aqueous HCl (12M) added in several steps (total volume ~ 180 µL), and then sonicated for 5 min (to properly dissolve all particles, if necessary). Afterwards, the solution was stirred, and methanol was slowly added drop-by-drop (7.88 mL total volume added) in order to precipitate the labeled glycine. The suspension was then stirred in an ice-bath for 10-15 min. The off-white product was collected by filtration using glass frit (pore-size P3), washed with MeOH and Et_2O and finally dried under vacuum. Labeled glycine was mostly obtained as pure *β-form*, in rare cases as a mixture of polymorphs with predominant *β-form*. Due to the equilibrium in the carboxylic function, both oxygen sites (*i.e.* C=O* and C-O*H) are equally enriched. **Average yield (n = 2):** 52 ± 5 mg, 55 ± 5 %.

For the ^{17}O-labeling, 70% ^{17}O-enriched water (65 µL, 3.0 eq.) was used. **Yield (n = 1):** 43 mg, 46 %.

- *Scale-up procedure:*

^{18}O-labeled water (98%, 195 µL, 10.8 mmol, 3.0 eq.), two stainless steel balls (10 mm diameter), glycine methyl ester monohydrochloride (450 mg, 3.6 mmol, 1.0 eq.) and sodium ethoxide (610 mg, 9.0 mmol, 2.5 eq.) were introduced successively into the screw-top stainless steel grinding jar (10 mL inner volume). The jar was closed and subjected to grinding for 30 min in the MM400 mixer mill operated at 25 Hz. The yellowish paste obtained was dissolved in water in order to recover the product from the jar, as described in more detail below.

At first, non-labeled water (1 mL) was added into the jar, and the content was subjected to grinding for 2 min at 25 Hz. Then, the yellow solution was transferred to a round-bottom flask, the jar was rinsed with non-labeled water (500 µL) and the aqueous phases were combined and sonicated for 10 min. The medium was stirred and gradually acidified to pH = 3 - 4 using concentrated aqueous HCl (12M) added in several steps (total volume ~500 µL) and sonicated for 10 min. Afterwards, the solution was stirred and labeled glycine precipitated by slow drop-by-drop addition of methanol (15 mL). The suspension was then stirred in an ice-bath for 25-30 min. The off-white product was collected by filtration using a glass frit (pore-size P3), washed with MeOH (2 x 5 mL) and Et_2O, and finally dried under vacuum. Labeled glycine was mostly obtained as pure *β-form*, in rare cases as a mixture of polymorphs with predominant *β-form*. **Average yield (n = 3):** 185 ± 17 mg, 66 ± 6 %.

Enrichment of glycine: Estimated enrichment level per carboxylic oxygen: ~ 43 % for ^{18}O-labeled products and ~ 38 % for ^{17}O-labeled products. The estimated enrichment yield: ~ 87 % for ^{18}O-labeled products, ~ 84 % for ^{17}O-labeled products (calculated from HRMS analyses of Fmoc-protected glycine, see Annexe IV-D1).

Figure IV-1: ATR-IR analysis of the starting material, reaction intermediate and final labeled products compared to non-labeled commercial compound. The ^{17}O/^{18}O-labeled products are β-polymorphs of glycine, and the commercial non-labeled compound is a mixture of polymorphs.

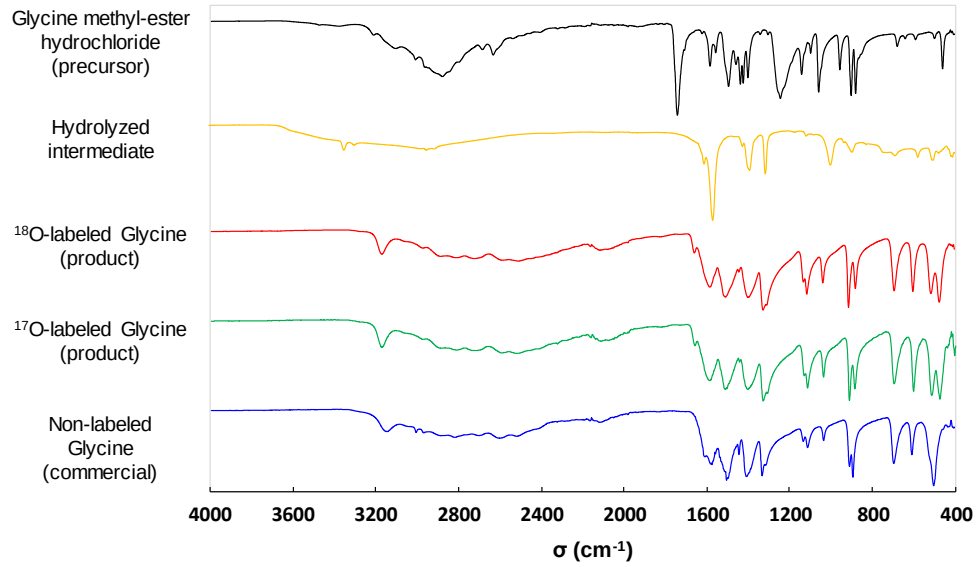

b) Characterization of the ^{18}O/^{17}O-labeled Gly

Figure IV-2: ^{13}C NMR spectra of non-labeled Glycine in comparison to ^{18}O/^{17}O-enriched products (D_2O/1% DSS, 500 MHz). Solvent peak and peaks of DSS (used here to reference the spectrum) are crossed out.

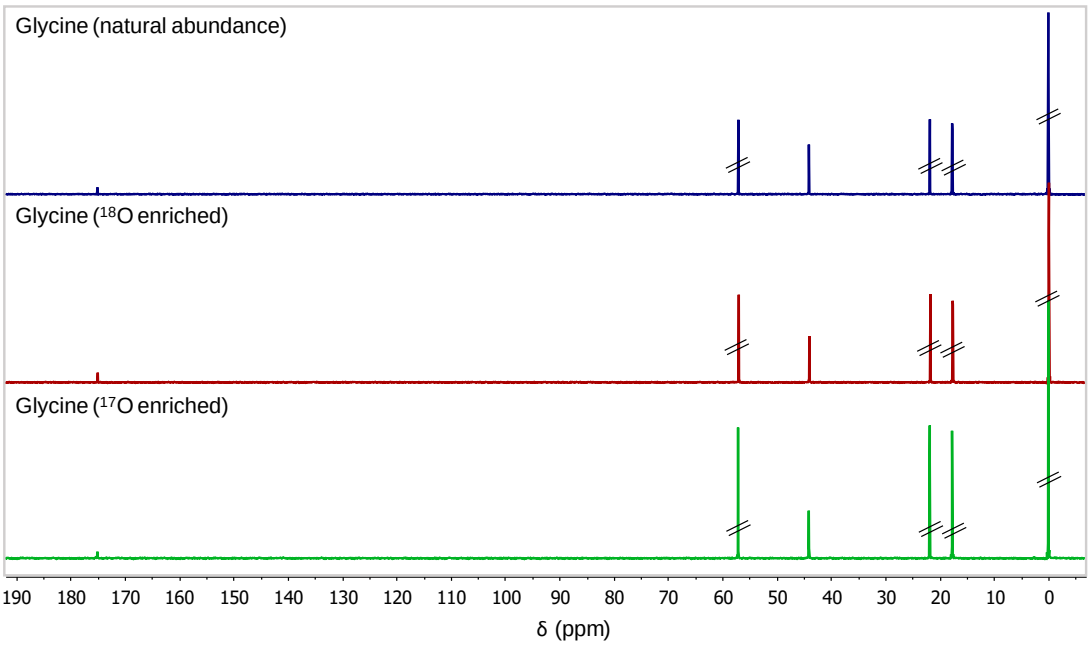

^{1}H NMR spectra of ^{18}O/^{17}O-enriched products were also recorded (in D_2O/1% DSS, at 500 MHz), and no impurities were observed.

Figure IV-3: Zoom in carboxylic region in ^{13}C NMR spectra of non-labeled Glycine in comparison to ^{18}O-enriched product (D_2O/1% DSS, 500 MHz). The isotope effect on the shift of carboxylic peak is visible for the labeled compound.

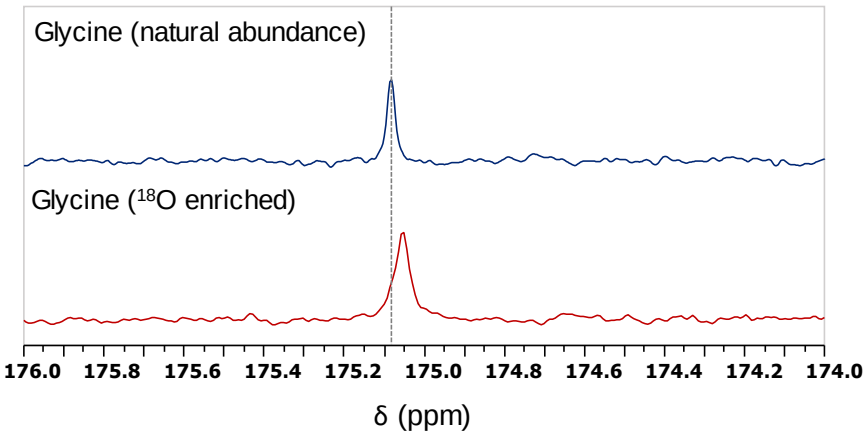

Figure IV-4: XRD powder pattern of $^{18}O/^{17}O$-enriched products in comparisons with simulated powder pattern of β-Glycine (COD-5000008). The relative intensities in isolated products varies due to preferential orientation effects.

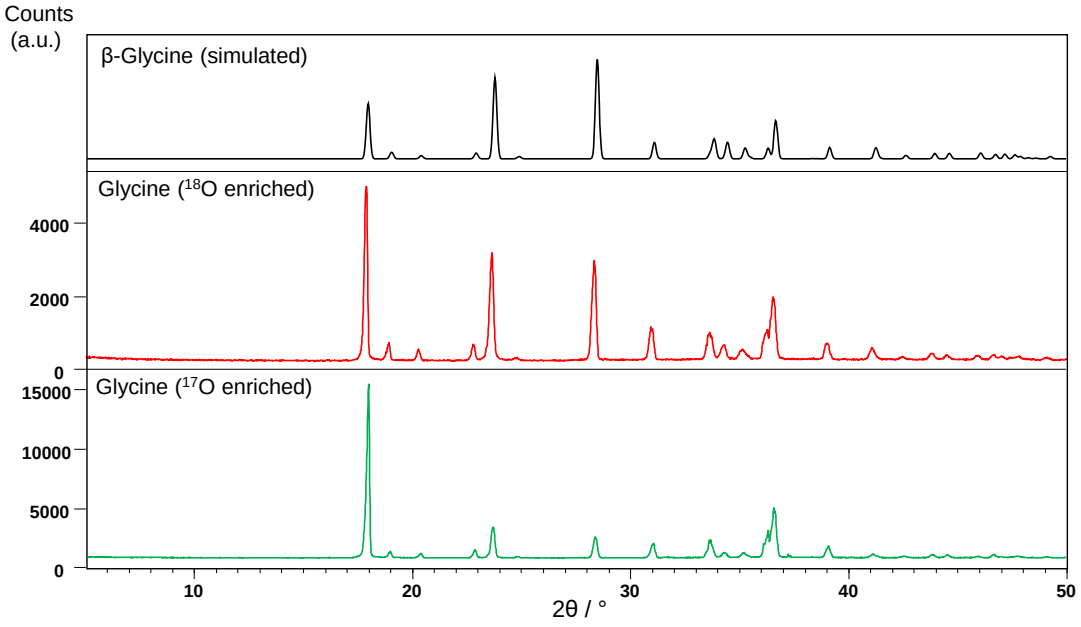

IV-B2) L-Leucine (Leu, L)

a) Labeling protocol

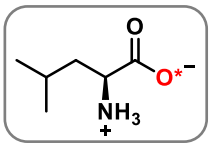

^{18}O-labeled water (99%, 44.5 µL, 2.5 mmol, 3.0 eq.), two stainless steel balls (10 mm diameter), L-leucine methyl ester monohydrochloride (150 mg, 0.83 mmol, 1.0 eq.) and sodium ethoxide (140.5 mg, 2.1 mmol, 2.5 eq.) were introduced successively into the screw-top stainless steel grinding jar (10 mL inner volume). The jar was closed and subjected to grinding for 30 min in the MM400 mixer mill operated at 25 Hz. The yellowish paste/suspension obtained was dissolved in water in order to recover the product from the jar, as further detailed below.

At first, non-labeled water (1 mL) was added into the jar, and the content was subjected to grinding for 2 min at 25 Hz. Then, the yellow solution was transferred to a round-bottom flask, the jar was rinsed with non-labeled water (2 mL) and the aqueous phases were combined. The medium was stirred and gradually acidified to pH = 5.0 - 5.5 using aqueous HCl (6M) added in several steps (total volume ~200 µL). Sometimes, precipitation was observed upon acidification. Afterwards, the solution was lyophilized over the night. The dry mixture was then resuspended in a MeOH/H_2O mixture (4 mL of MeOH and 500 µL of non-labeled H_2O), sonicated for 1 h and placed in the fridge for another 1 h. The solid product was collected by filtration using a glass frit (pore-size P3), washed with MeOH (2x 2 mL), and dried under vacuum. Labeled L-leucine was isolated in a form of beige shiny plate-like solid. Due to the equilibrium in the carboxylic function, both oxygen sites (*i.e.* C=O* and C-O*H) are equally enriched. $[\alpha]_D^{20}$ = + 13.5 ± 1.0 ° (c 4, 6M HCl); lit.[6] $[\alpha]_D^{20}$ = + 15.1 ° (c 4, 6M HCl). **Average yield (n = 2):** 87 ± 3 mg, 79 ± 3 %.

For the ^{17}O-labeling, 70% ^{17}O-enriched water (44.5 µL, 3.0 eq.) was used. **Yield (n = 1):** 83 mg, 75 %.

Figure IV-5: ATR-IR analysis of the starting material, reaction intermediate and final labeled products compared to non-labeled commercial compound.

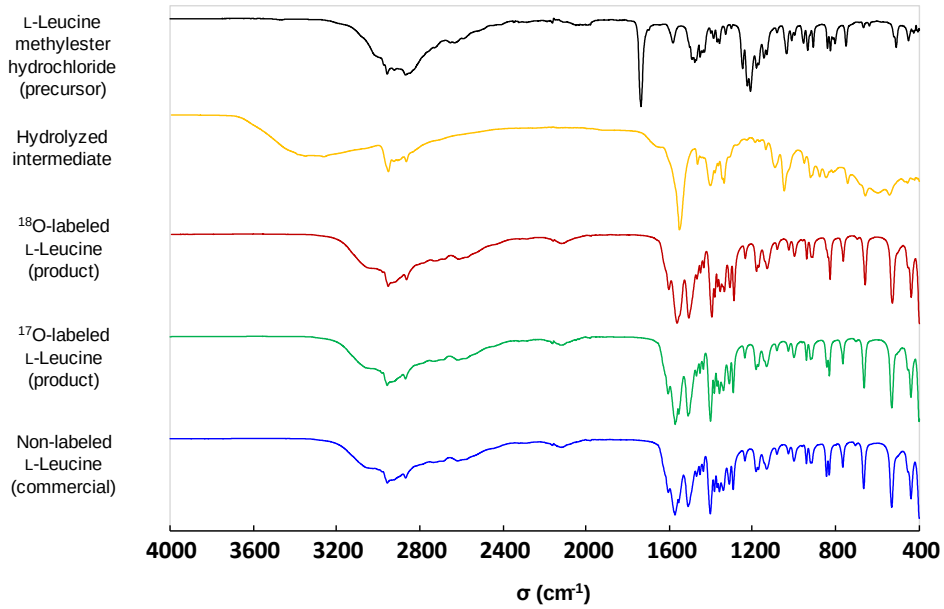

b) Characterization of the $^{18}O/^{17}O$-labeled L-Leucine

Figure IV-6: HRMS (ESI^-) analyses of non-labeled L-Leucine (dissolved in H_2O) in comparison to $^{18}O/^{17}O$-enriched products. Average enrichment per carboxylic oxygen determined by MS for ^{18}O-labeled product: 41.4 ± 0.1 % (n = 2), enrichment yield: ~ 83 %; for ^{17}O-labeled product: 28.7 % (n = 1), enrichment yield: ~ 81 %.

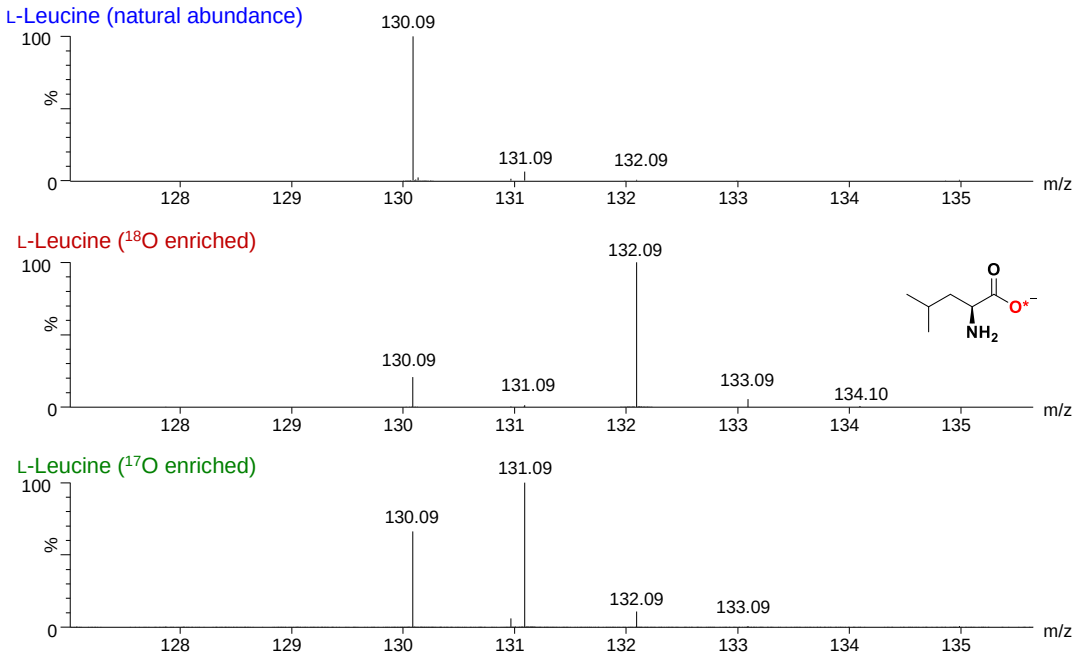

Figure IV-7: ^{13}C NMR spectra of non-labeled L-Leucine in comparison to $^{18}O/^{17}O$-enriched products (D_2O/1% DSS, 600 MHz). Peaks of DSS (used here to reference the spectrum) are crossed out.

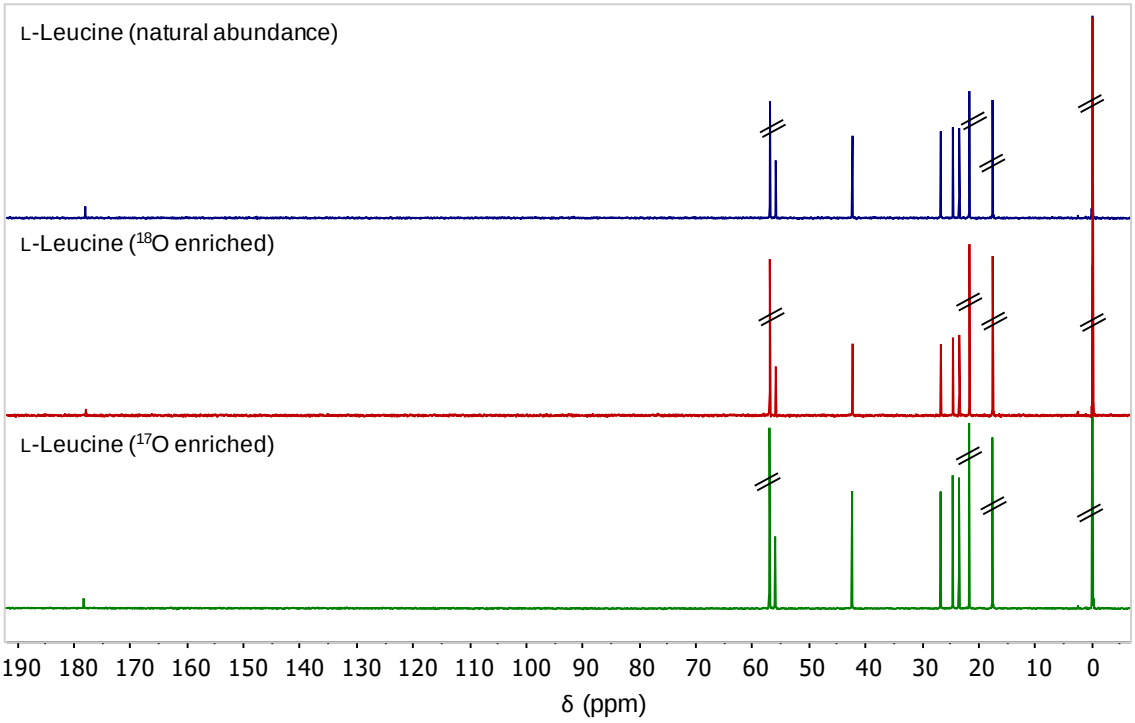

^{1}H NMR spectra of $^{18}O/^{17}O$-enriched products were also recorded (in D_2O/1% DSS, at 500 MHz), and no impurities were observed.

Figure IV-8: Zoom in carboxylic region in ^{13}C NMR spectra of non-labeled L-Leucine in comparison to ^{18}O-enriched product (D_2O/1% DSS, 500 MHz). The isotope effect on the shift of carboxylic peak is visible for the labeled compound.

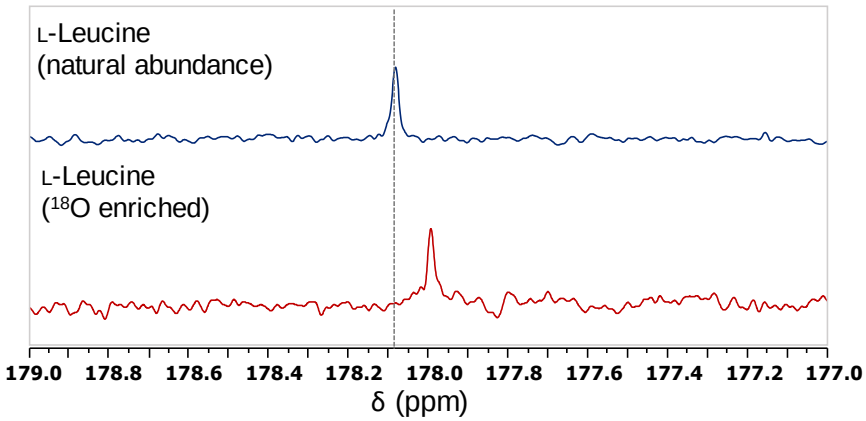

Figure IV-9: XRD powder pattern of $^{18}O/^{17}O$-enriched products in comparison with non-labeled commercial L-Leucine.

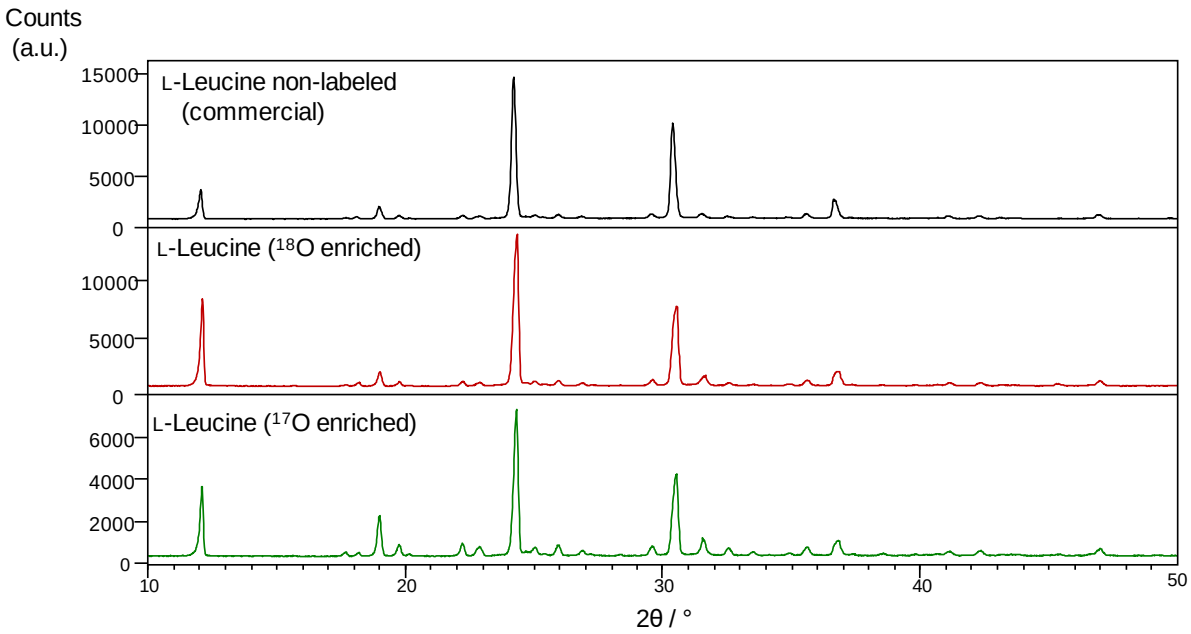

IV-B3) L-Phenylalanine (Phe, F)

a) Labeling protocol

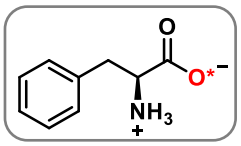

^{18}O-labeled water (99%, 25 µL, 1.4 mmol, 2.0 eq.), two stainless steel balls (10 mm diameter), L-phenylalanine methyl ester monohydrochloride (150 mg, 0.7 mmol, 1.0 eq.) and sodium ethoxide (118.3 mg, 1.8 mmol, 2.5 eq.) were introduced successively into the screw-top stainless steel grinding jar (10 mL inner volume). The jar was closed and subjected to grinding for 30 min in the MM400 mixer mill operated at 25 Hz. A yellowish paste/suspension was obtained and dissolved in water in order to recover the product from the jar, as further detailed below.

At first, non-labeled water (1 mL) was added into the jar, and the content was subjected to grinding for 2 min at 25 Hz. Then, the yellow solution was transferred to a round-bottom flask (25 mL), the jar was rinsed with non-labeled water (2 mL) and the aqueous phases were combined. The medium was stirred and gradually acidified to pH = 5.0 - 5.5 using aqueous HCl (6M) added in several steps (total volume ~ 175 µL). Sometimes, precipitation was observed upon acidification. Afterwards, the solution was freeze-dried overnight. The dry mixture was then suspended in a MeOH/H_2O mixture (with 3 mL of MeOH + 500 µL of non-labeled H_2O), sonicated for 1h and placed in the fridge for another 1h15. The solid product was collected by filtration using a glass frit (pore-size P3), washed with MeOH (1x 2 mL, 1x 1 mL), and dried under vacuum. Labeled L-phenylalanine was isolated as a beige solid. Due to the equilibrium in the carboxylic function, both oxygen sites (*i.e.* C=O* and C-O*H) are equally enriched. $[\alpha]_D^{20}$ = - 32.7 ± 0.6 ° (c 2, water); lit.[6] $[\alpha]_D^{20}$ = - 34.3 ° (c 2, water). **Average yield (n = 2):** 72 ± 3 mg, 62 ± 3 %.

For the ^{17}O-labeling, 70% ^{17}O-enriched water (25 µL, 2.0 eq.) was used. **Yield (n = 1):** 69 mg, 60 %.

Figure IV-10: ATR-IR analysis of the starting material, reaction intermediate and final labeled products compared to non-labeled commercial compound.

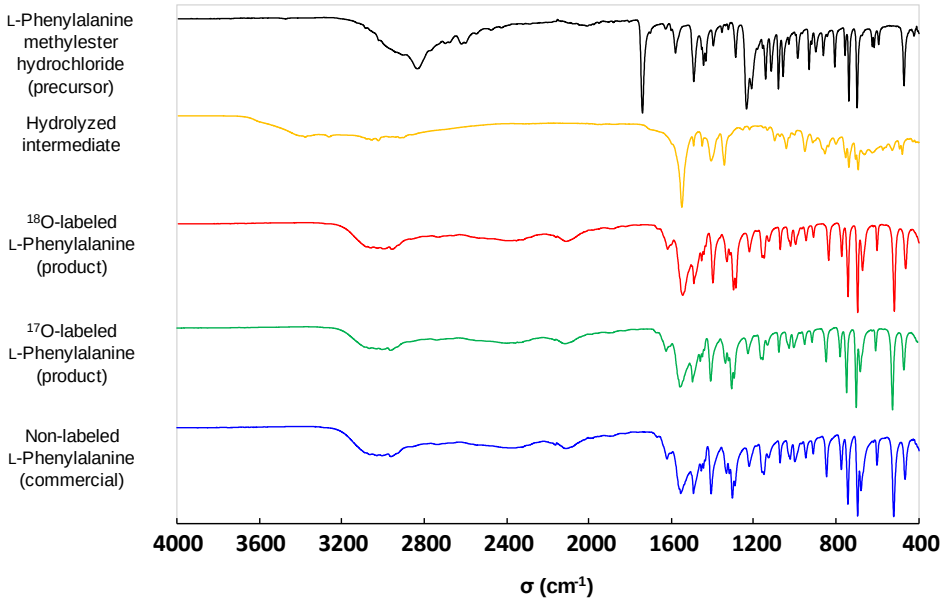

b) Characterization of the $^{18}O/^{17}O$-labeled L-Phenylalanine

Figure IV-11: HRMS (ESI^-) analyses of non-labeled L-Phenylalanine (dissolved in H_2O) in comparison to $^{18}O/^{17}O$-enriched products. Average enrichment per carboxylic oxygen determined by MS for ^{18}O-labeled product: 46.3 ± 0.4 % (n = 2), enrichment yield: ~ 93 %; for ^{17}O-labeled product: 32.0 % (n = 1), enrichment yield: ~ 90 %.

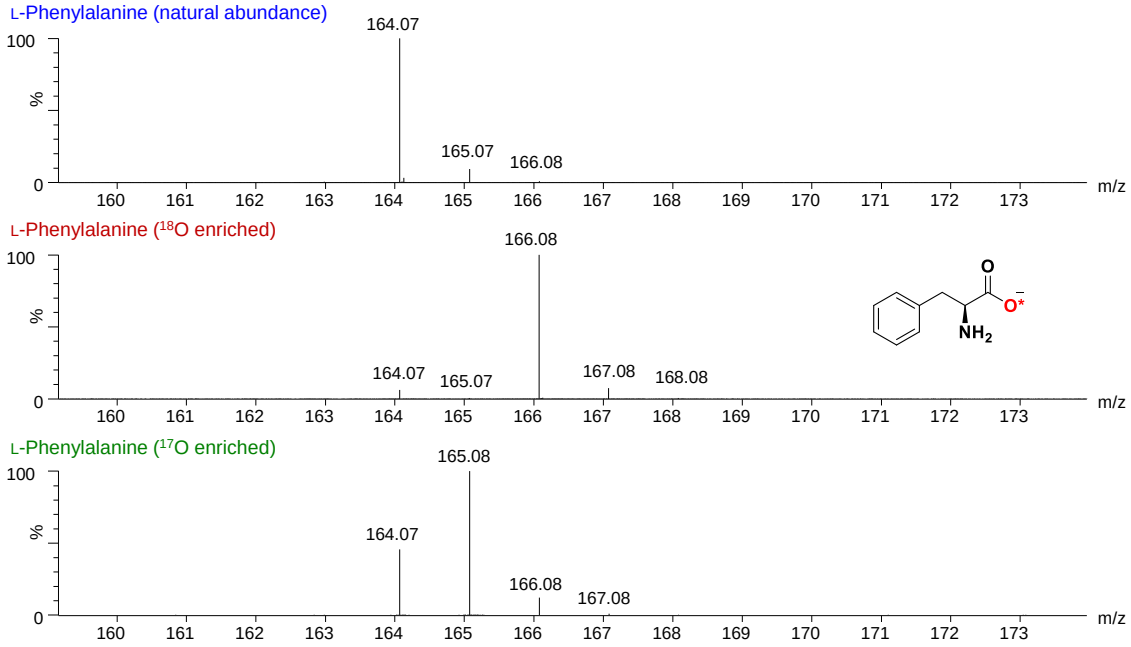

Figure IV-12: ^{13}C NMR spectra of non-labeled L-Phenylalanine in comparison to $^{18}O/^{17}O$-enriched products (D_2O/1% DSS, 600 MHz). Peaks of DSS (used here to reference the spectrum) are crossed out.

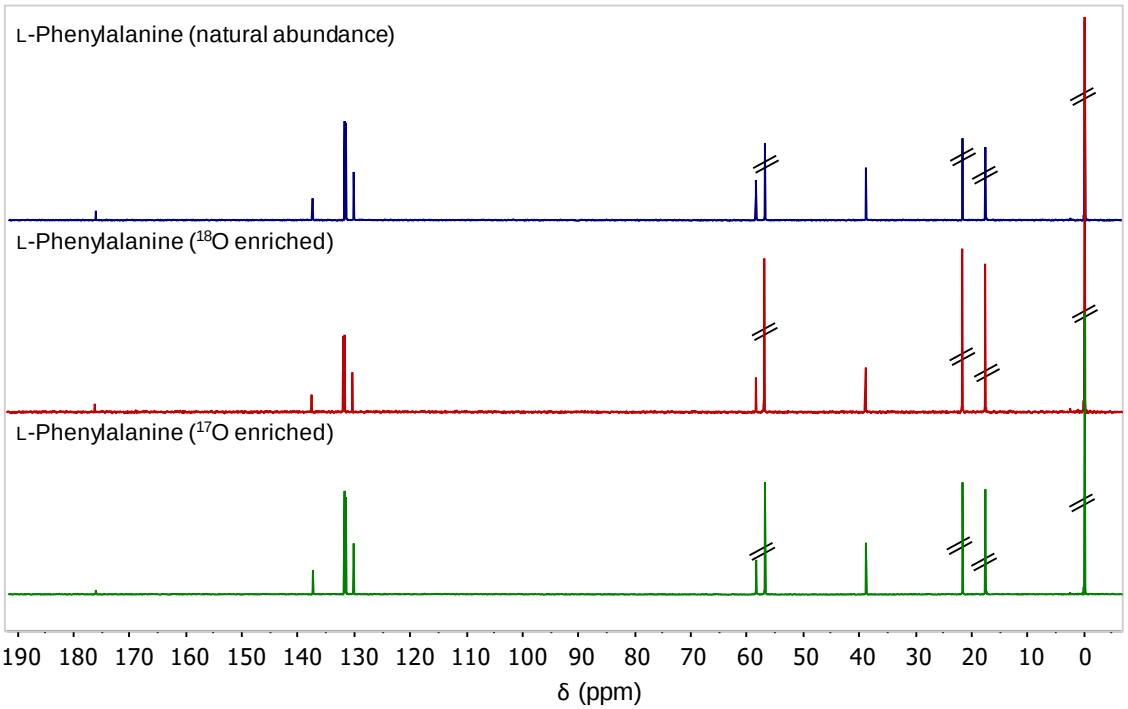

^{1}H NMR spectra of $^{18}O/^{17}O$-enriched products were also recorded (in D_2O/1% DSS, at 500 MHz), and no impurities were observed.

Figure IV-13: Zoom in carboxylic region in ^{13}C NMR spectra of non-labeled L-Phenylalanine in comparison to ^{18}O-enriched product (D_2O/1% DSS, 500 MHz). The isotope effect on the shift of carboxylic peak is visible for the labeled compound.

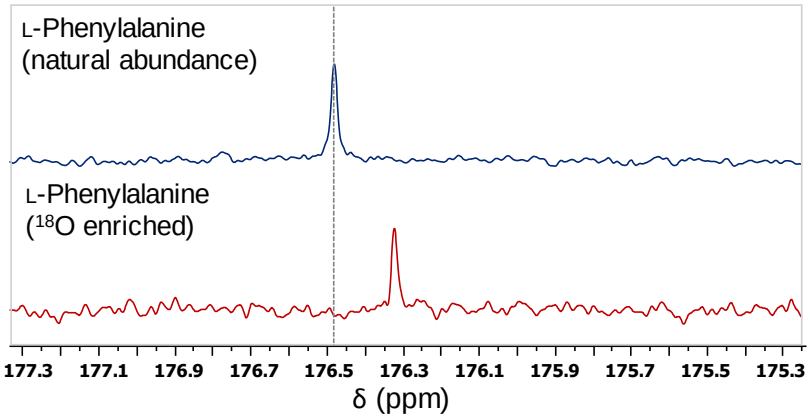

Figure IV-14: XRD powder pattern of $^{18}O/^{17}O$-enriched products in comparison with non-labeled commercial L-Phenylalanine.

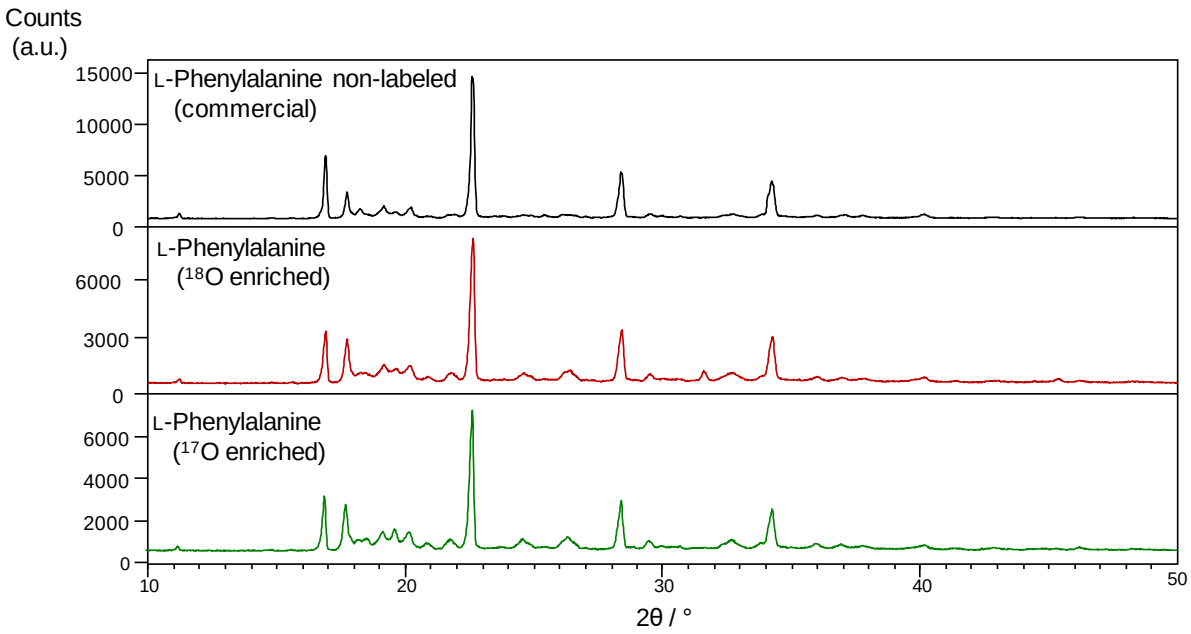

IV-B4) L-Aspartic acid (Asp, D)

a-1) Labeling protocols for L-Aspartic acid labeled on both carboxylic groups

- *Low-scale synthesis:*

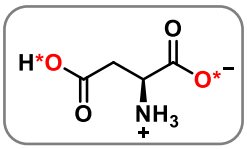

^{18}O-labeled water (98%, 55 µL, 3.1 mmol, 4.0 eq.), two stainless steel balls (10 mm diameter), L-aspartic acid dimethyl ester monohydrochloride (150 mg, 0.8 mmol, 1.0 eq.) and sodium ethoxide (181 mg, 2.7 mmol, 3.5 eq.) were introduced successively into a screw-top stainless steel grinding jar (10 mL inner volume). The jar was closed and subjected to grinding for 30 min in the MM400 mixer mill operated at 25 Hz. A yellowish sticky solid was obtained, which was dissolved in water in order to recover the product from the jar, as further detailed below.

At first, non-labeled water (500 µL) was added into the jar, and the content was subjected to grinding for 2 min at 25 Hz. Then, the yellow solution was transferred to a hemolysis tube containing stirring bar. The jar was rinsed with non-labeled water (500 µL) and the aqueous phases were combined. The medium was stirred and gradually acidified using concentrated aqueous HCl (12M). After addition of 120 µL of HCl (12M), the pH dropped to ~ 3.9, and a precipitate started to form. This precipitation induced an increase of pH reaching to ~ 4.7. Subsequent addition of HCl (12M) in several steps (total volume 60 - 120 µL) resulted in a final pH ~ 1.25 - 1.52. The snow-white product was collected by filtration using a glass frit (pore-size P3), washed with MeOH (2x 3 mL) and Et_2O, and finally dried under vacuum. Due to the equilibrium in the carboxylic function, both oxygen sites (*i.e.* C=O* and C-O*H) are equally enriched. $[\alpha]_D^{20}$ = + 24.2 ± 0.4 ° (c 5, 2.5M HCl); lit.[6] $[\alpha]_D^{20}$ = + 26.2 ° (c 10, 2 - 3 M HCl). **Average yield (n = 2):** 80 ± 2 mg, 76 ± 1 %.

For the ^{17}O-labeling, 70% ^{17}O-enriched water (55 µL, 4.0 eq.) was used. **Yield (n = 1):** 79 mg, 77 %.

- *Scale-up procedure:*

^{18}O-labeled water (98%, 110 µL, 6.1 mmol, 4.0 eq.), two stainless steel balls (10 mm diameter), L-aspartic acid dimethyl ester monohydrochloride (300 mg, 1.5 mmol, 1.0 eq.) and sodium ethoxide (362 mg, 5.3 mmol, 3.5 eq.) were introduced successively into the screw-top stainless steel grinding jar (10 mL inner volume). The jar was closed and subjected to grinding for 30 min in the MM400 mixer mill operated at 25 Hz. A yellowish sticky solid was obtained, which was dissolved in water in order to recover the product from the jar, as further described below.

At first, non-labeled water (1 mL) was added into the jar, and the content was subjected to grinding for 2 min at 25 Hz. Then, the yellow solution was transferred to a round-bottom flask containing a stirring bar. The jar was further rinsed with non-labeled water (1 mL) and the aqueous phases were combined. The medium was stirred and gradually acidified using concentrated aqueous HCl (12M, total volume 50 - 90 µL) up to pH 1.95 - 2.20. The same "buffering behavior" as for the low scale synthesis was observed. The snow-white product was collected by filtration using a glass frit (pore-size P3), washed with MeOH (2x 5 mL) and Et_2O, and finally dried under vacuum. **Average yield (n = 3):** 174 ± 5 mg, 84 ± 3 %.

Figure IV-15: ATR-IR analysis of the starting material, reaction intermediate and final labeled products compared to non-labeled commercial compound.

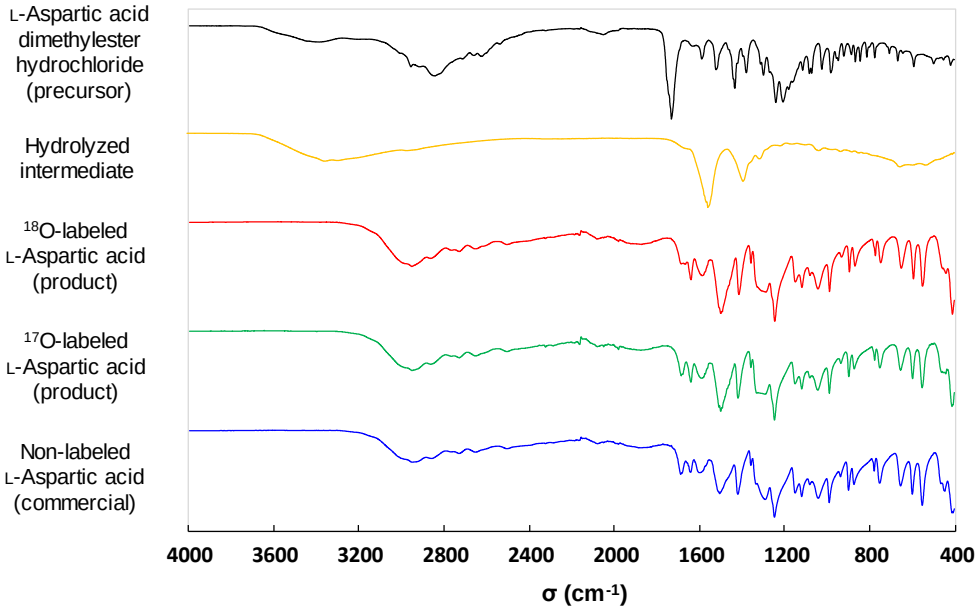

a-2) Labeling protocol for L-Aspartic acid selectively $^{18}O/^{17}O$-labeled at side-chain carboxylic group

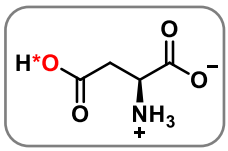

For the selective labeling at the side chain, L-aspartic acid 4-methylester monohydrochloride (150 mg, 0.8 mmol, 1.0 eq.), sodium ethoxide (195 mg, 2.9 mmol, 3.5 eq.) and ^{18}O-labeled water (98%, 45 µL, 2.5 mmol, 3.0 eq.) were used. The reaction procedure and the work-up remain identical as for the doubly labeled aspartic acid protocol described above. **Yield (n = 1)**: 82 mg, 74 %.

For the ^{17}O-labeling, 70% ^{17}O-enriched water (45 µL, 3.0 eq.) was used. **Yield (n = 1)**: 72 mg, 66 %.

a-3) Labeling protocol for L-Aspartic acid selectively labeled at main-chain carboxylic group

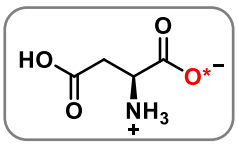

For the selective labeling at the main chain, L-aspartic acid 1-methylester (150 mg, 1.0 mmol, 1.0 eq.), sodium ethoxide (173 mg, 2.5 mmol, 2.5 eq.) and ^{18}O-labeled water (98%, 55 µL, 3.0 mmol, 3.0 eq.) were used. The reaction procedure and the work-up remain identical as for the doubly labeled aspartic acid protocol described above. **Yield (n = 1)**: 104 mg, 76 %.

For the ^{17}O-labeling, 70% ^{17}O-enriched water (55 µL, 3.0 eq.) was used. **Yield (n = 1)**: 122 mg, 91 %.

b-1) Characterization of the $^{18}O/^{17}O$-labeled L-Asp, enriched on both carboxylic functions

Figure IV-16: HRMS (ESI^-) analyses of non-labeled L-Aspartic acid (dissolved in H_2O) in comparison to $^{18}O/^{17}O$-enriched products. Average enrichment per carboxylic oxygen determined by MS for ^{18}O-labeled product: 43.9 ± 0.3 % (n = 2), enrichment yield: ~ 88 %; for ^{17}O-labeled product: 30.7 % (n = 1), enrichment yield: ~ 87 %.

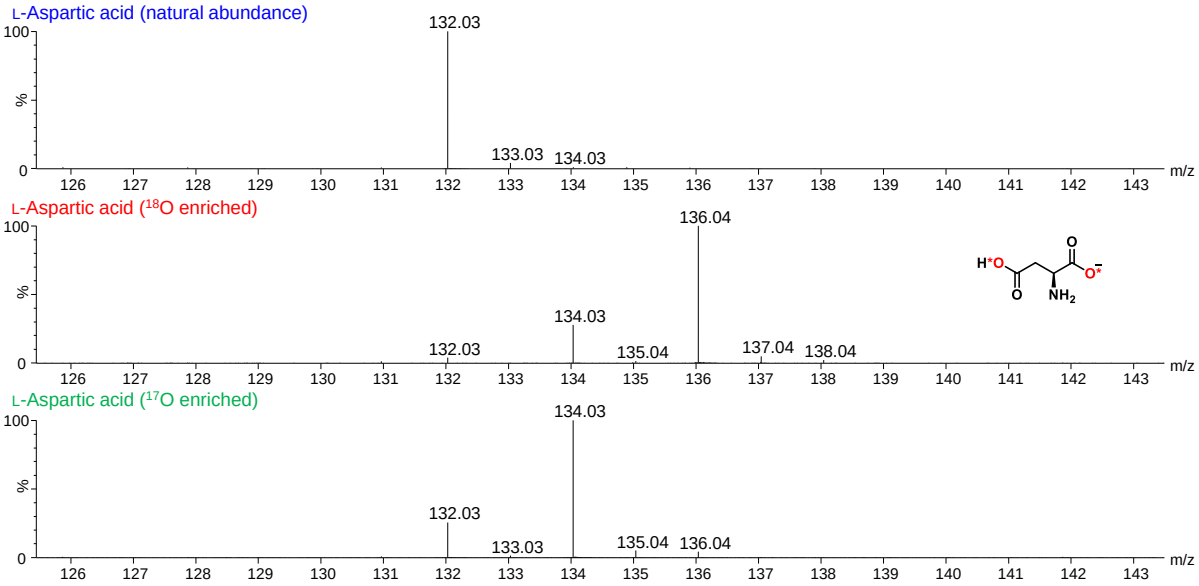

Figure IV-17: ^{13}C NMR spectra of non-labeled L-Aspartic acid in comparison to $^{18}O/^{17}O$-enriched products (D_2O/1% DSS, 500 MHz). Peaks of DSS (used here to reference the spectrum) are crossed out.

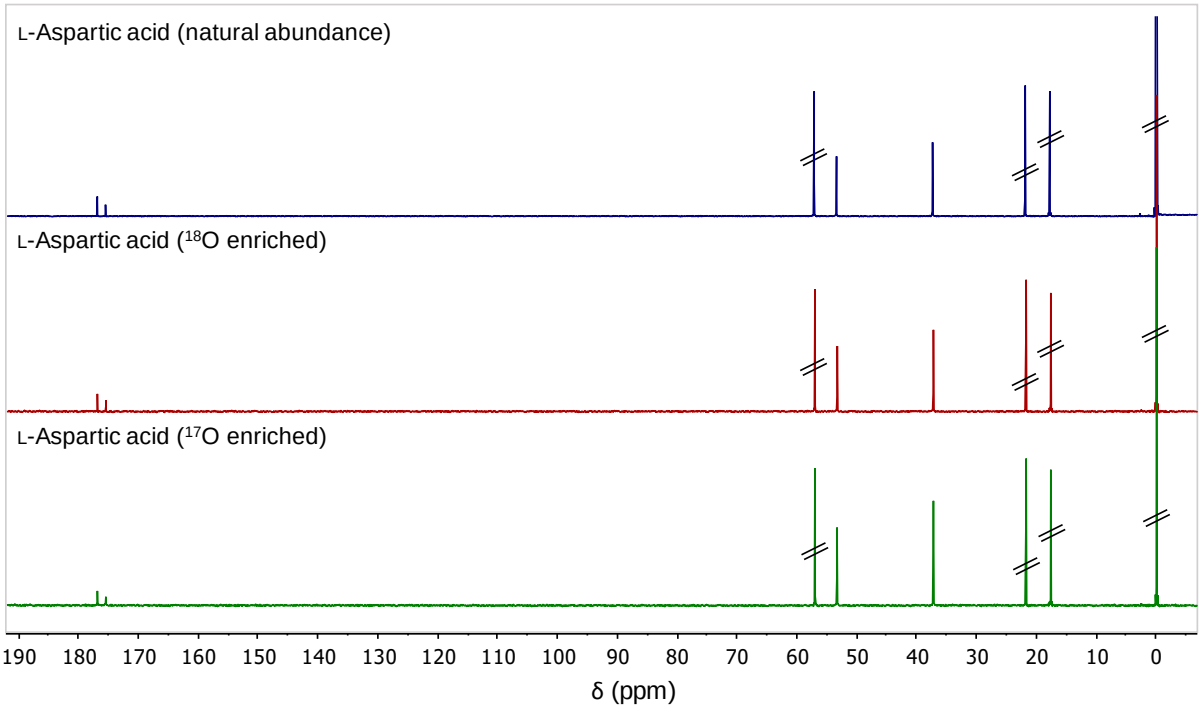

^{1}H NMR spectra of $^{18}O/^{17}O$-enriched products were also recorded (in D_2O/1% DSS, at 500 MHz), and no impurities were observed.

Figure IV-18: Zoom in carboxylic region in ^{13}C NMR spectra of non-labeled L-Aspartic acid in comparison to ^{18}O-enriched product (D_2O/1% DSS, 500 MHz). The isotope effect on the shift of both carboxylic peaks is visible for the labeled compound.

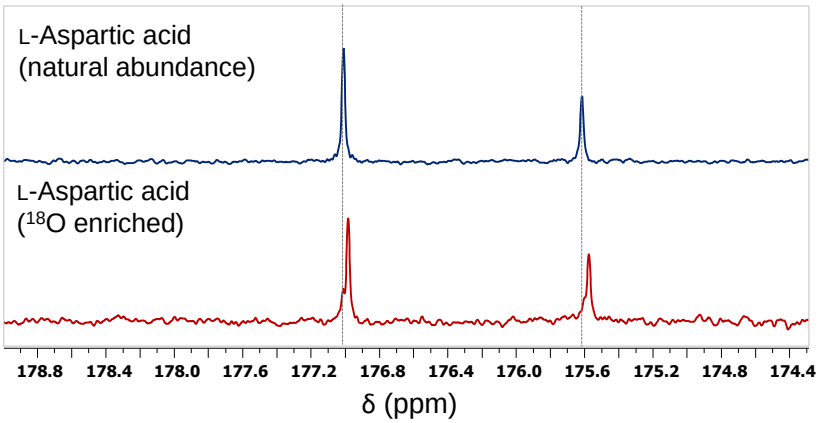

Figure IV-19: XRD powder pattern of $^{18}O/^{17}O$-enriched products in comparisons with simulated powder pattern of L-Aspartic acid (CSD-LASPRT).

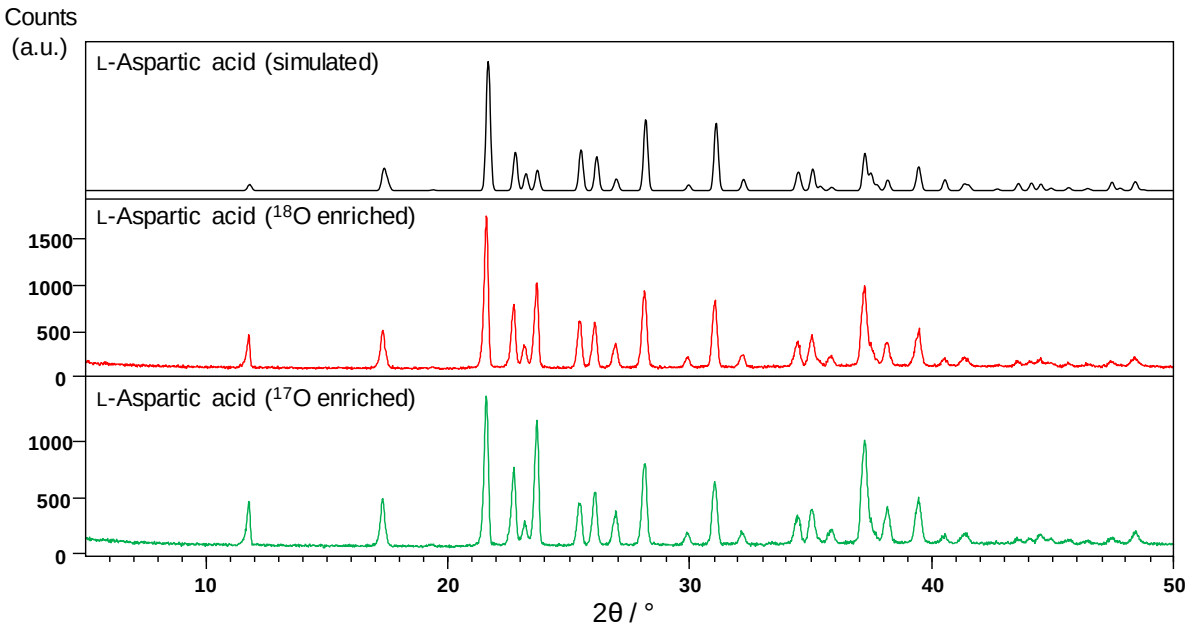

b-2) Characterization of L-Aspartic acid selectively $^{18}O/^{17}O$-labeled at side-chain carboxylic group

Figure IV-20: HRMS (ESI^-) analyses of non-labeled L-Aspartic acid (dissolved in H_2O) in comparison to $^{18}O/^{17}O$-enriched products. Average enrichment per carboxylic oxygen (side-chain) determined by MS for ^{18}O-labeled product: 42.3 % (n = 1), enrichment yield: ~ 85 %; for ^{17}O-labeled product: 30.9 % (n = 1), enrichment yield: ~ 86 %.

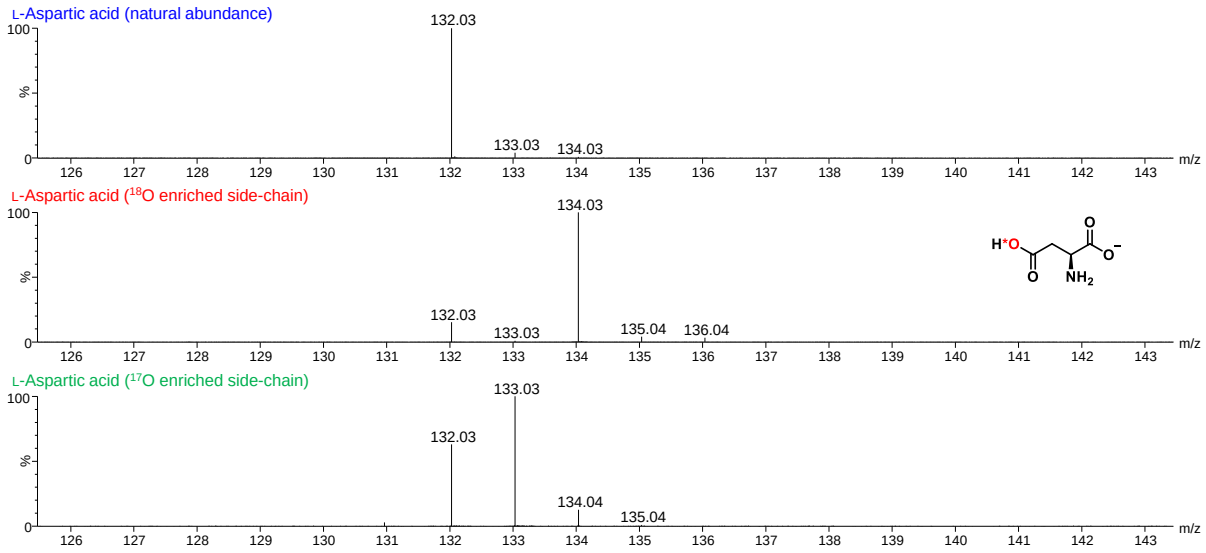

Figure IV-21: ^{13}C NMR spectra of non-labeled L-Aspartic acid in comparison to $^{18}O/^{17}O$-enriched products (D_2O/1% DSS, 500 MHz). Peaks of DSS (used here to reference the spectrum) are crossed out.

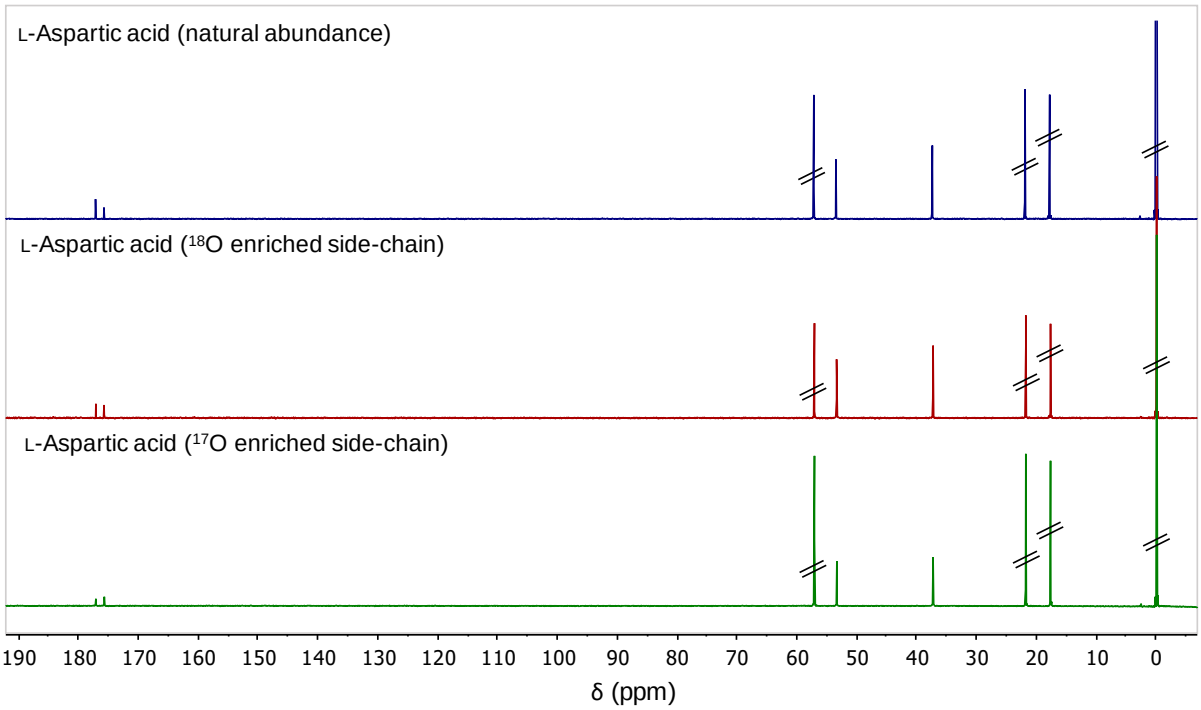

^1H NMR spectra of $^{18}O/^{17}O$-enriched products were also recorded (in D_2O/1% DSS, at 500 MHz), and no impurities were observed.

Figure IV-22: Zoom in carboxylic region in ^{13}C NMR spectra of non-labeled L-Aspartic acid in comparison to ^{18}O-enriched product (D_2O/1% DSS, 500 MHz). The isotope effect on the shift of the left carboxylic peak is visible for the labeled side of the compound.

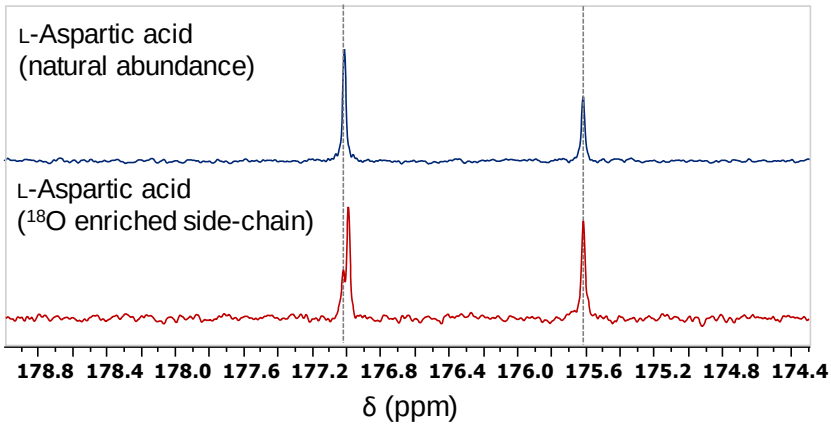

Figure IV-23: XRD powder pattern of ^{18}O/^{17}O-enriched products in comparison with the simulated powder pattern of L-Aspartic acid (CSD-LASPRT). The relative intensities in isolated products varies due to preferential orientation effects.

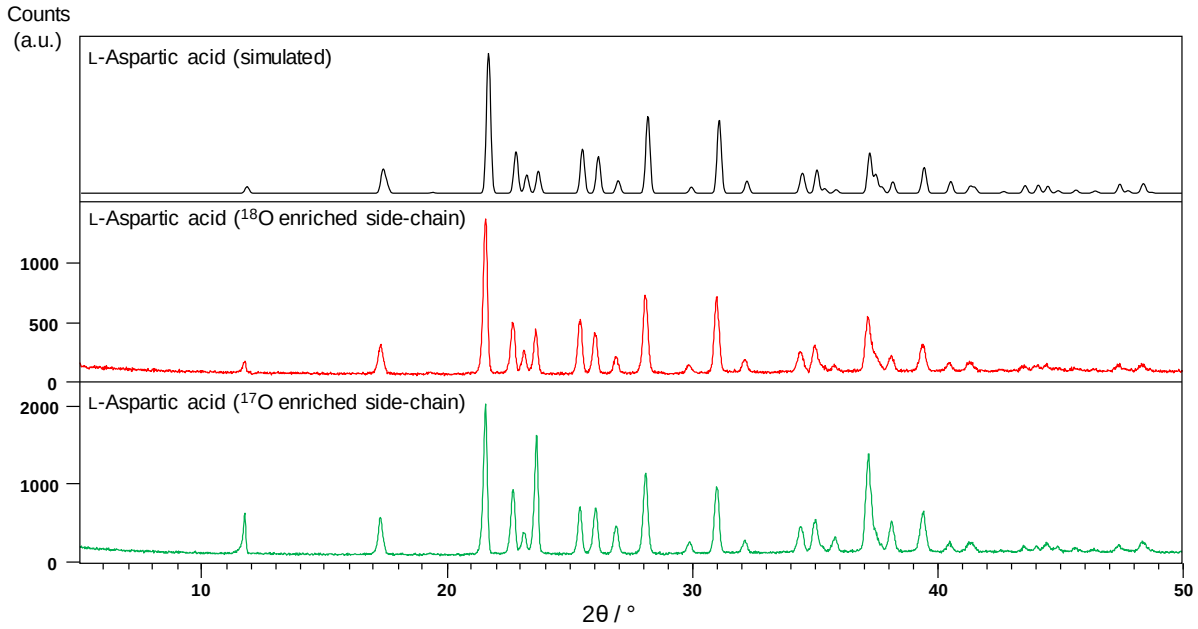

b-3) Characterization of L-Aspartic acid selectively $^{18}O/^{17}O$-labeled at main-chain carboxylic group

Figure IV-24: HRMS (ESI^-) analyses of non-labeled L-Aspartic acid (dissolved in H_2O) in comparison to $^{18}O/^{17}O$-enriched products. Average enrichment per carboxylic oxygen (main-chain) determined by MS for ^{18}O-labeled product: 47.3 % (n = 1), enrichment yield: ~ 95 %; for ^{17}O-labeled product: 34.0 % (n = 1), enrichment yield: ~ 95 %.

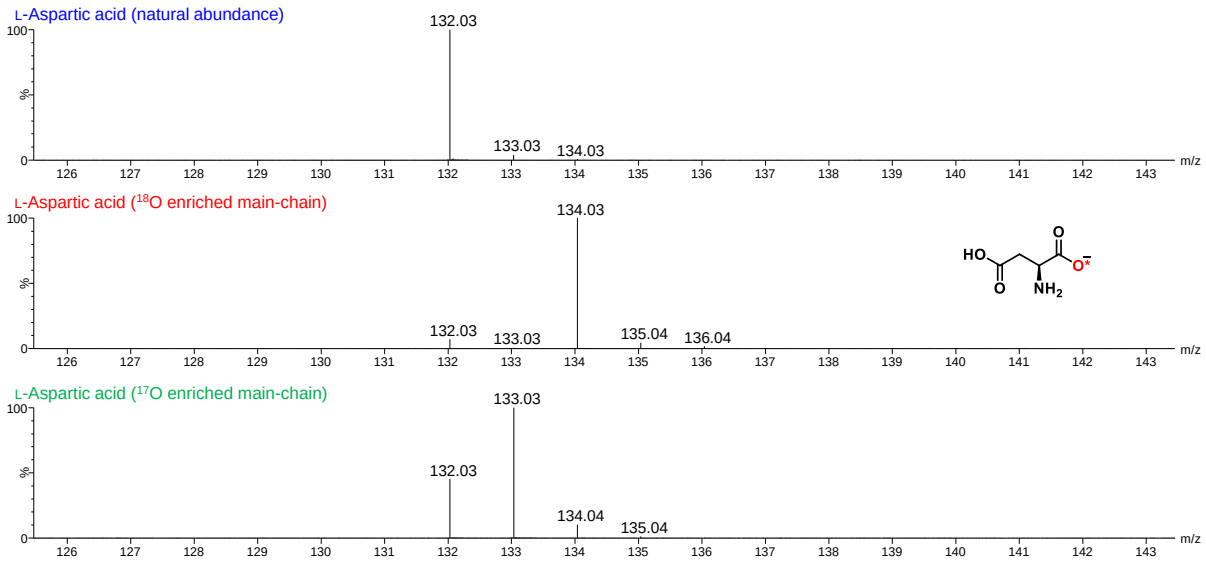

Figure IV-25: ^{13}C NMR spectra of non-labeled L-Aspartic acid in comparison to $^{18}O/^{17}O$-enriched products (D_2O/1% DSS, 500 MHz). Peaks of DSS (used here to reference the spectrum) are crossed out.

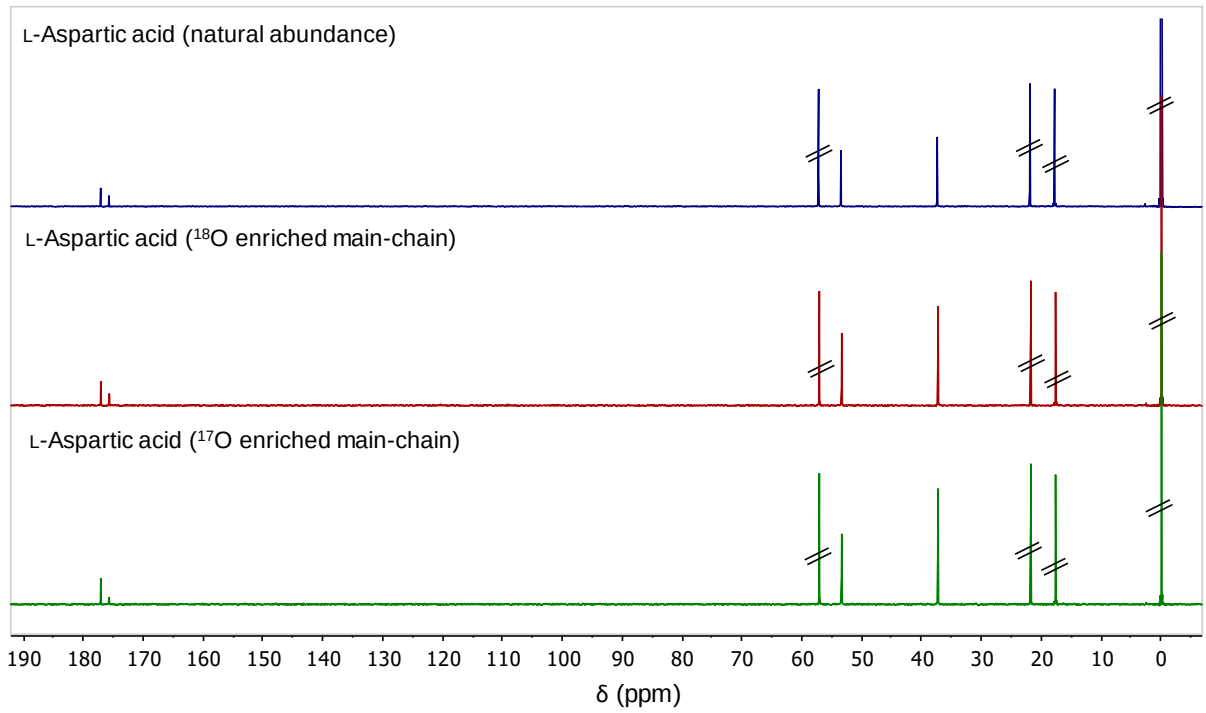

^1H NMR spectra of $^{18}O/^{17}O$-enriched products were also recorded (in D_2O/1% DSS, at 500 MHz), and no impurities were observed.

Figure IV-26: Zoom in carboxylic region in ^{13}C NMR spectra of non-labeled L-Aspartic acid in comparison to ^{18}O-enriched product (D_2O/1% DSS, 500 MHz). The isotope effect on the shift of the right carboxylic peak is visible for the labeled side of the compound.

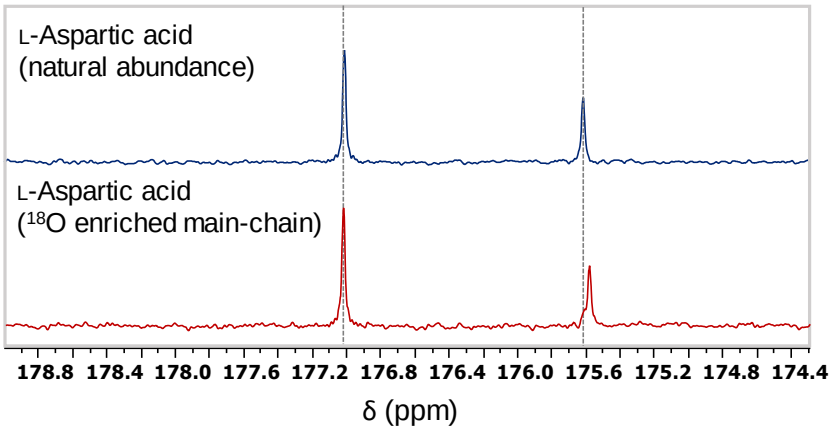

Figure IV-27: XRD powder pattern of $^{18}O/^{17}O$-enriched products in comparisons with simulated powder pattern of L-Aspartic acid (CSD-LASPRT). The relative intensities in isolated products varies due to preferential orientation effects.

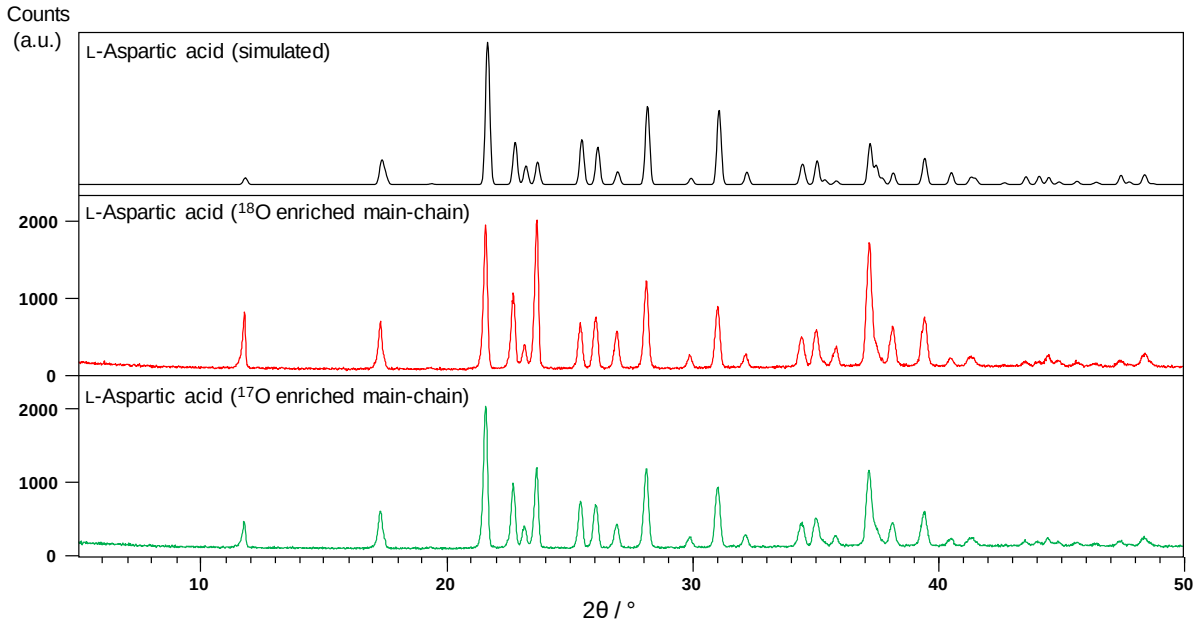

Figure IV-28: Zoom in carboxylic region in ^{13}C NMR spectra of non-labeled L-Aspartic acid in comparison to ^{18}O-enriched products (D_2O/1% DSS, 500 MHz). The isotope effect on the shift of the carboxylic peaks is visible for the labeled site of the compounds.

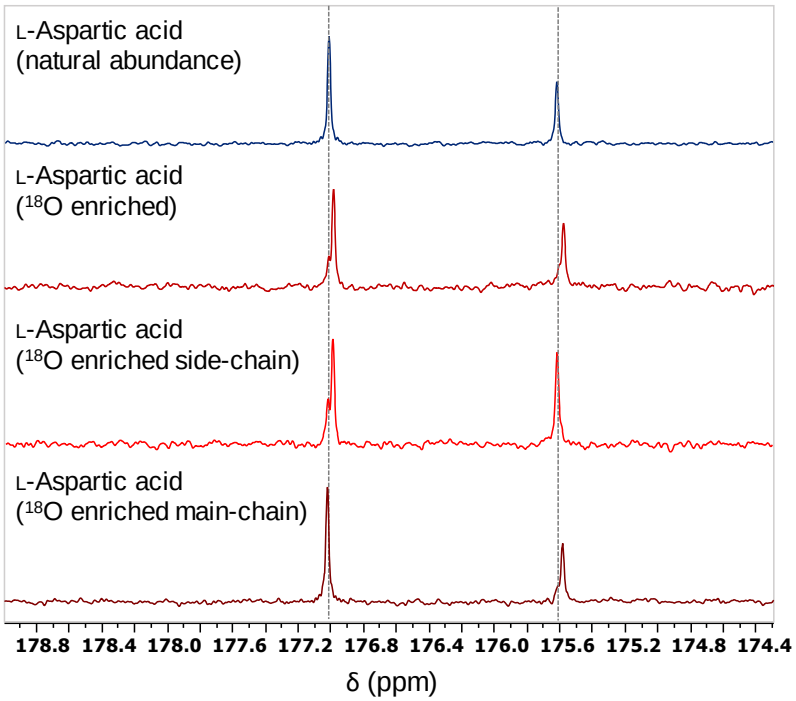

IV-B5) L-Lysine monohydrochloride (Lys, K)

a) Labeling protocols

- *Low-scale synthesis:*

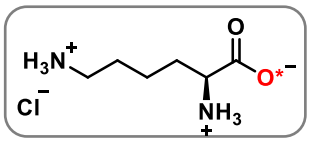

^{18}O-labeled water (98%, 35 µL, 1.9 mmol, 3.0 eq.), two stainless steel balls (10 mm diameter), L-Lysine methyl ester dihydrochloride (150 mg, 0.6 mmol, 1.0 eq.) and sodium ethoxide (153 mg, 2.2 mmol, 3.5 eq.) were introduced successively into the screw-top stainless steel grinding jar (10 mL inner volume). The jar was closed and subjected to grinding for 30 min in the MM400 mixer mill operated at 25 Hz. A yellowish paste was obtained, which was dissolved in water in order to recover the product from the jar, as further detailed below.

At first, non-labeled water (300 µL) was added into the jar, and the content was subjected to grinding for 2 min at 25 Hz. Then, the yellow suspension was transferred to a round-bottom flask, the jar was rinsed with non-labeled water (300 µL) and the aqueous phases were combined and sonicated for 5 min resulting in yellow solution. The medium was stirred and gradually acidified to ~ pH = 3-5 using concentrated aqueous HCl (12M), which was added in several steps (total volume ~ 140 µL), and then sonicated for 5 min (to properly dissolve all particles, if necessary). Afterwards, the solution was stirred, and MeOH (6 mL) was slowly added drop-by-drop to precipitate the labeled L-Lysine·HCl. The suspension was then stirred in an ice-bath for 50 min. The off-white precipitate was collected by filtration using a glass frit (pore-size P3), washed with MeOH and Et_2O, and finally dried under vacuum.

The L-Lysine monohydrochloride obtained by this protocol is in a form of dihydrate but contaminated with methanol (~ 0.8 eq.). In order to eliminate the residual methanol, the product was dissolved in 2 - 3 mL of non-labeled water and lyophilized (repeatedly if necessary). Pure essentially anhydrous L-Lysine monohydrochloride was thus obtained as a white amorphous fluffy solid. Due to the equilibrium in the carboxylic function, both oxygen sites (*i.e.* C=O* and C-O*H) are equally enriched. $[\alpha]_D^{20}$ = + 19.9 ± 1.1 ° (c 4, 6M HCl); lit.[6] $[\alpha]_D^{20}$ = + 21.2 ° (c 8, 6M HCl). **Average mass (n = 2):** 67 ± 3 mg.

For the ^{17}O-labeling, 70% ^{17}O-enriched water (35 µL, 3.0 eq.) was used. **Yield (n = 1)**: 58 mg, 50 %.

- *Scale-up procedure:*

^{18}O-labeled water (98%, 70 µL, 3.9 mmol, 3.0 eq.), two stainless steel balls (10 mm diameter), L-Lysine methylester dihydrochloride (300 mg, 1.3 mmol, 1.0 eq.) and sodium ethoxide (307 mg, 4.5 mmol, 3.5 eq.) were introduced successively into the screw-top stainless steel grinding jar (10 mL inner volume). The jar was closed and subjected to grinding for 30 min in the MM400 mixer mill operated at 25 Hz. A yellowish paste was obtained and dissolved in water in order to recover the product from the jar, as further detailed below.

At first, non-labeled water (500 µL) was added into the jar, and the content was subjected to grinding for 2 min at 25 Hz. Then, the yellow suspension was transferred to a round-bottom flask, the jar was rinsed with non-labeled water (500 µL) and the aqueous phases were combined and then sonicated for 5 min (to properly dissolve all particles, if necessary) resulting in a yellow solution. The medium was stirred and gradually acidified to pH = 3 - 5 using concentrated aqueous HCl (12M), which was added in several steps (total volume ~ 280 µL), and sonicated for 5 min. Afterwards, the solution was stirred, and MeOH (10 mL) was slowly added drop-by-drop to precipitate the labeled L-Lysine·HCl. The suspension was then stirred in an ice-bath for 50 min. The off-white precipitate was collected by filtration using

a glass frit (pore-size P3), washed with MeOH (2x 4 mL) and Et_2O, and dried under vacuum. In order to eliminate the residual methanol, the product was dissolved in 3 - 4 mL of non-labeled water and lyophilized (repeatedly if necessary). Pure essentially anhydrous L-lysine monohydrochloride was obtained as a white amorphous fluffy solid. **Average mass (n = 2):** 183 ± 7 mg. This solid was placed in a chamber with controlled humidity[7] 85% RH for 24 h, furnishing crystalline L-lysine monohydrochloride dihydrate as a white solid. **Average yield (n = 2):** 197 ± 12 mg, 69 ± 5 %.

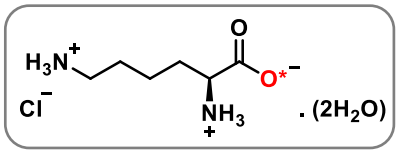

Figure IV-29: ATR-IR analysis of the starting material, reaction intermediate and final products compared to non-labeled commercial compound.

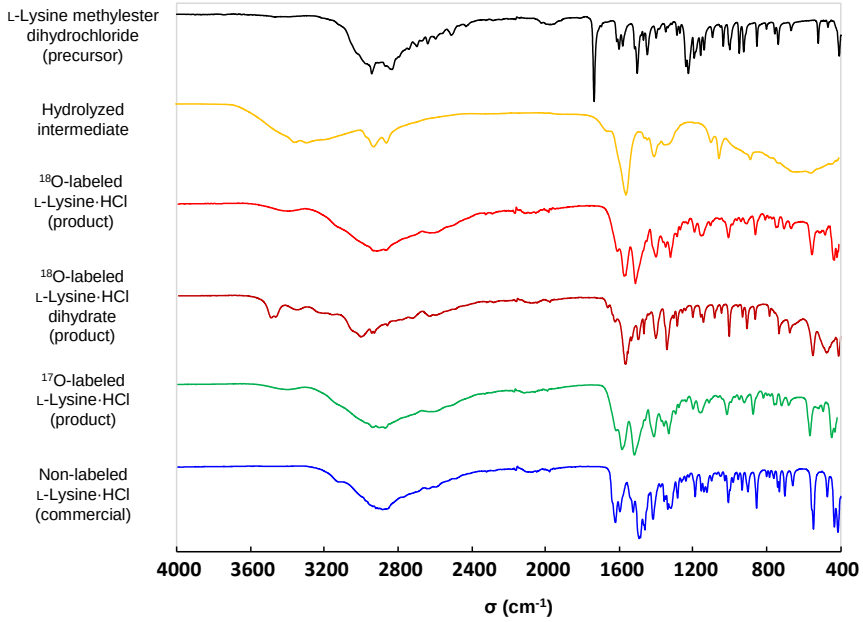

b) Characterization of the $^{18}O/^{17}O$-labeled L-Lysine monohydrochloride

Figure IV-30: HRMS (ESI^+) analyses of non-labeled L-Lysine monohydrochloride (dissolved in H_2O) in comparison to $^{18}O/^{17}O$-enriched products. Average enrichment per carboxylic oxygen determined by MS for ^{18}O-labeled product: 46.7 ± 0.1 % (n = 2), enrichment yield: ~ 94 %; for ^{17}O-labeled product: 32.5 % (n = 1), enrichment yield: ~ 92 %.

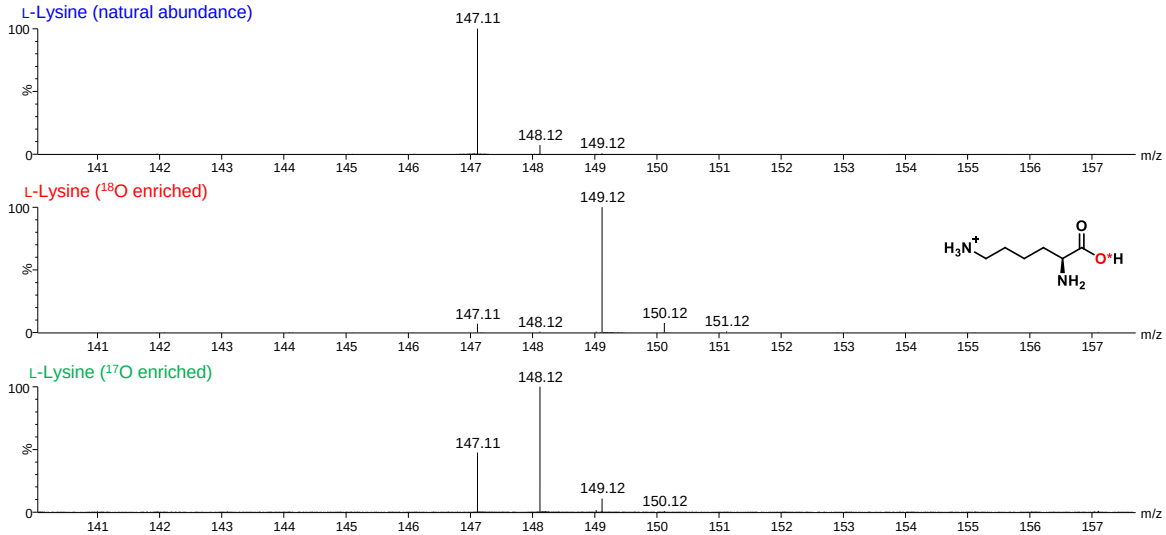

Figure IV-31: ^{13}C NMR spectra of non-labeled L-Lysine monohydrochloride in comparison to $^{18}O/^{17}O$-enriched anhydrous products (D_2O/1% DSS, 500 MHz). Peaks of DSS (used here to reference the spectrum) are crossed out.

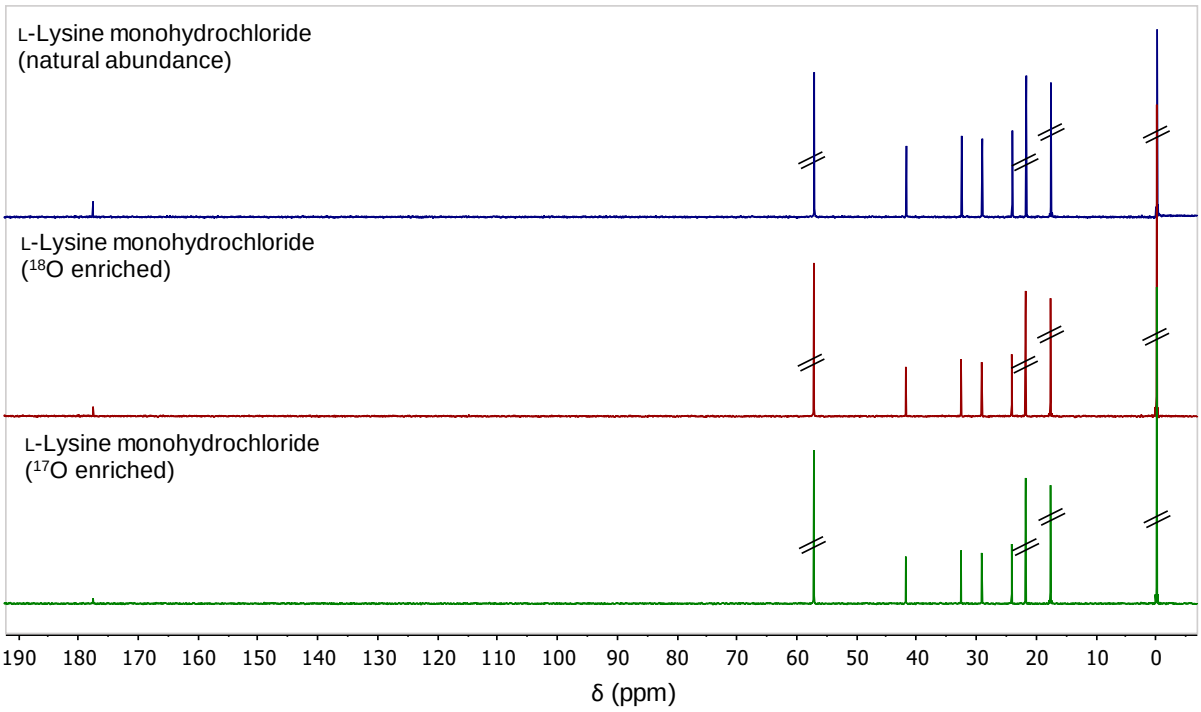

^{1}H NMR spectra of $^{18}O/^{17}O$-enriched products were also recorded (in D_2O/1% DSS, at 500 MHz), and no impurities were observed.

Figure IV-32: Zoom in carboxylic region in ^{13}C NMR spectra of non-labeled L-Lysine monohydrochloride in comparison to ^{18}O-enriched products (D_2O/1% DSS, 500 MHz). The isotope effect on the shift of the carboxylic peaks is visible for the labeled site of the compounds.

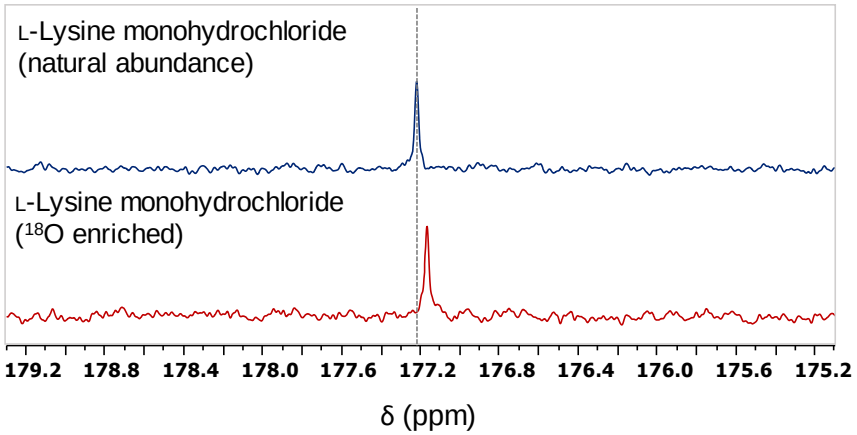

Figure IV-33: XRD powder pattern of $^{18}O/^{17}O$-enriched products in comparison with simulated powder pattern of L-Lysine monohydrochloride dihydrate (CSD-LYSCLH). Labeled anhydrous products isolated in amorphous form were transformed to their crystalline dihydrate form (indicated by red/green arrows - see experimental procedure above).

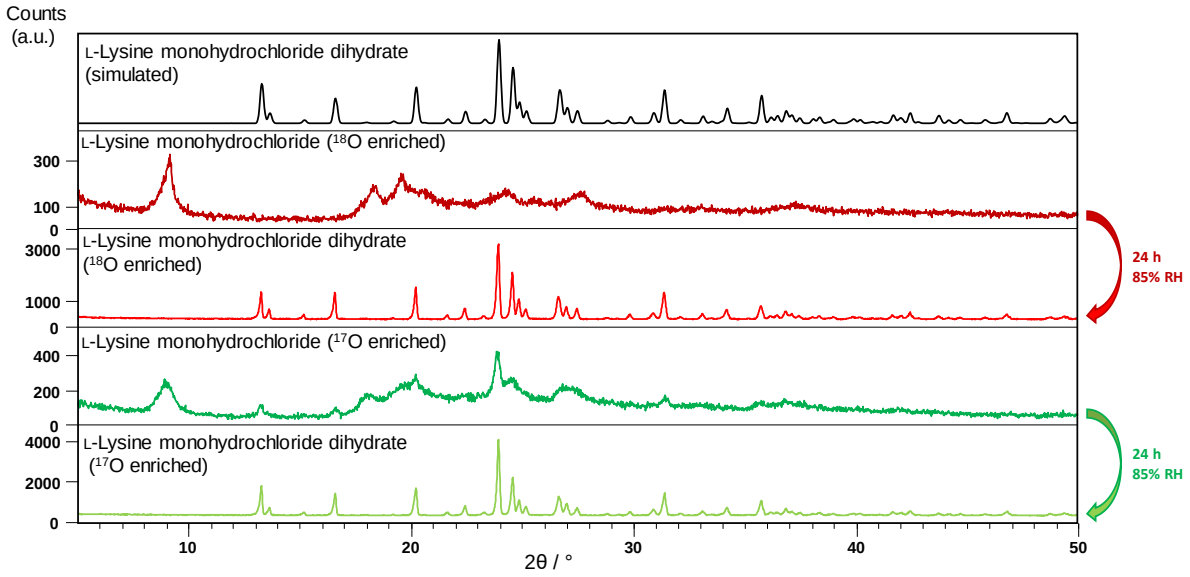

IV-C) $^{17}O/^{18}O$-LABELED AMINO ACIDS PREPARED *VIA* ACID CATALYSED EXCHANGE

IV-C1) Glycine (Gly, G)

a) Labeling protocol[8-9]

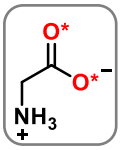

Glycine hydrochloride (132 mg, 1.2 mmol, 1 eq.) was placed on the bottom of a 2 mL brown glass HPLC vial, ^{18}O-labeled H_2O* (99%, 65 µL, 3.6 mmol, 3 eq.) was added leading to the wetting of the solid. The vial was closed by a lid with septum and placed in an oven heated at 100 °C for 24 h.

To recover the product, the liquid reaction mixture was transferred to a round-bottom flask, and the vial was washed with non-labeled water (500 µL). Using an aqueous solution of NH_4OH (28 - 30%, w/w), the pH was set to 4 -5, and the glycine precipitated upon dropwise addition of *i*-PrOH (5 mL). The precipitate was collected by filtration using a glass frit (pore-size P3), washed with MeOH (2x 2 mL), and dried under vacuum. The pure labeled glycine was isolated in the form of a white powder, which appeared to be mixture of polymorphs. **Average yield (n = 2):** 72 ± 3 mg, 77 ± 3 %.

Enrichment of glycine: Estimated enrichment level per carboxylic oxygen: ~ 62 % for ^{18}O-labeled products. The enrichment yield was quantitative (calculated from HRMS analyses of Fmoc-protected glycine, see Annexe IV-D1).

b) Characterization of the $^{18}O/^{17}O$-labeled Gly

Figure IV-34: XRD powder pattern of ^{18}O-enriched product (mixture of polymorphs) in comparison with simulated powder pattern of β-Glycine (COD-5000008) and non-labeled commercial glycine (mixture of polymorphs).

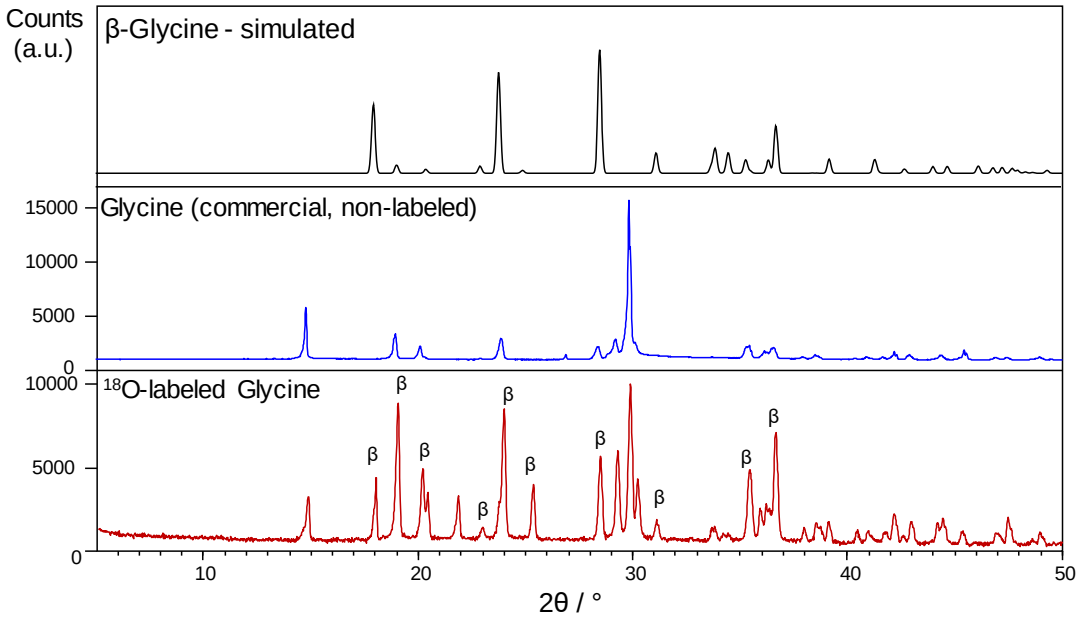

IV-C2) L-Aspartic acid (Asp, D)

a) Labeling protocol for L-Aspartic acid labeled at both carboxylic groups

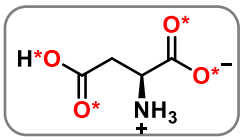

Commercial non-labeled L-Aspartic acid (101 mg, 0.8 mmol, 1 eq.) and anhydrous LiCl (33 mg, 0.8 mmol, 1 eq.) were placed on the bottom of a 2 mL brown glass HPLC vial and mixed with a spatula. ^{18}O-Labeled H_2O* (99%, 55 µL, 3.0 mmol, 4 eq.) was quickly added leading to the wetting of the solids. The vial was closed by a lid with septum, and placed in an oven heated at 100 °C for 24 h.

The product was then transferred on a glass frit (pore-size P4) and the vial was washed with non-labeled water (3x 500 µL), which was used to wash directly the product on the frit. The solid was then washed with MeOH (2x 1 mL) and Et_2O, and dried under vacuum. The pure labeled L-aspartic acid was isolated in the form of white solid. **Average yield (n = 2):** 79 ± 1 mg, 78 ± 2 %.

b) Characterization of the ^{18}O-labeled L-Aspartic acid

Figure IV-35: HRMS (ESI$^-$) analyses of non-labeled L-Aspartic acid (dissolved in H_2O) in comparison to ^{18}O-enriched product. Average enrichment level per carboxylic oxygen determined by MS: 28.2 % (n = 1), enrichment yield: ~ 56 %.

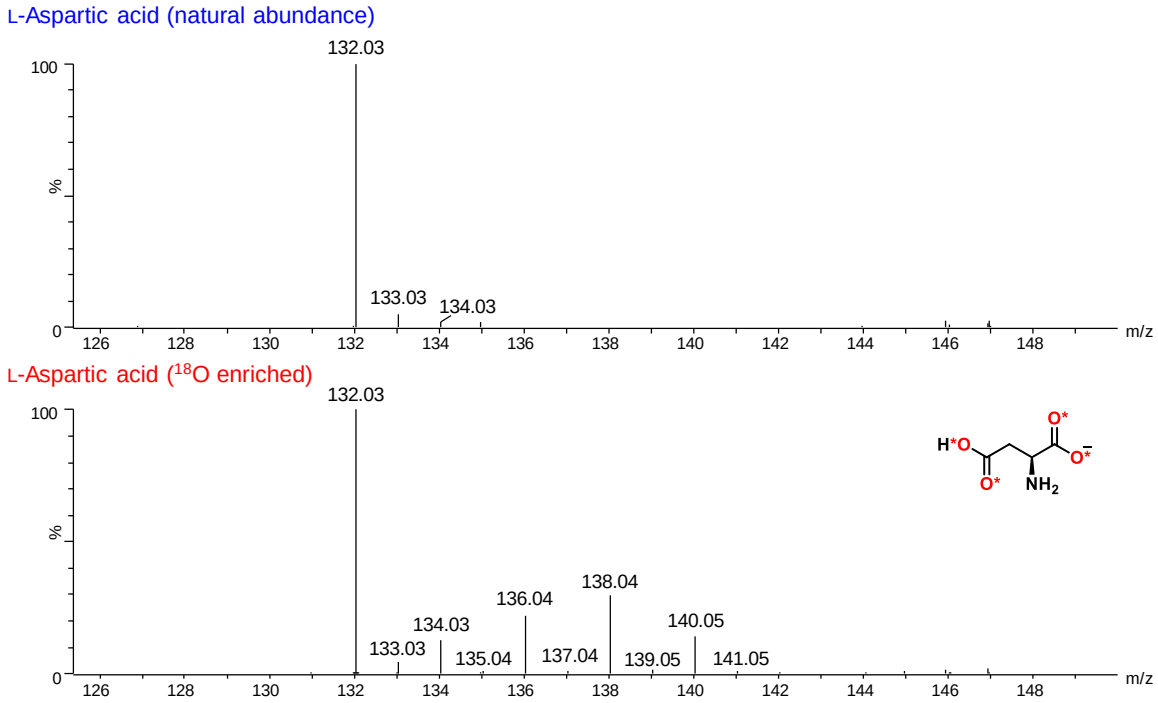

Figure IV-36: XRD powder pattern of ^{18}O-enriched product in comparison with simulated powder pattern of L-Aspartic acid (CSD-LASPRT) and non-labeled commercial compound. The relative intensities in isolated products varies due to preferential orientation effects.

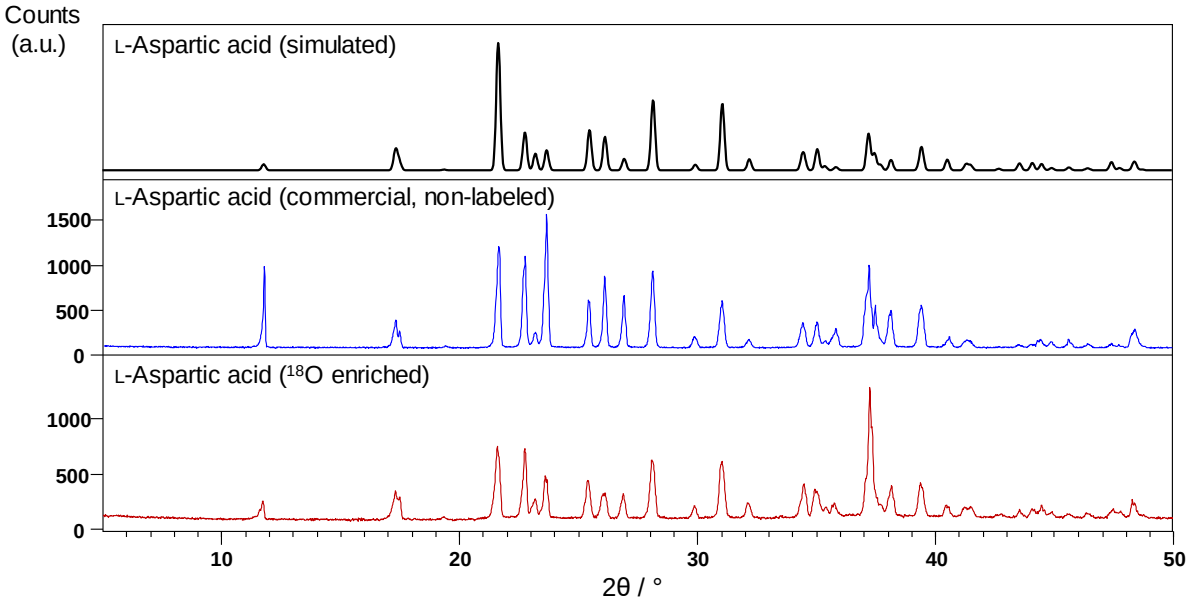

IV-C3) L-Lysine monohydrochloride (Lys, K)

a) Labeling protocol

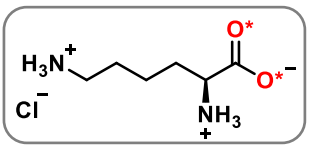

Commercial non-labeled L-Lysine dihydrochloride (140 mg, 0.6 mmol, 1 eq.) was placed on the bottom of a 2 mL brown glass HPLC vial, ^{18}O-labeled H_2O* (99%, 34.5 µL, 1.9 mmol, 3 eq.) was added leading to the wetting of the solid. The vial was closed by a lid with a septum and placed in an oven heated at 100 °C for 24 h.

To recover the product, the viscous liquid was transferred to a round-bottom flask with non-labeled water (2x 300 µL), which was used to both dissolve the product and wash the vial. The pH was then adjusted to ~ 3 - 4 by progressive addition of small amounts of sodium ethoxide. The product was then precipitated upon dropwise addition of MeOH (6 mL). The solution with precipitate was stirred in an ice-bath for 30 min. Then, the precipitate was collected by filtration using a glass frit (pore-size P3) and washed with MeOH (2x 3 mL). The product was first dried under vacuum, then dissolved in non-labeled H_2O (3 mL) and finally lyophilized. Pure essentially anhydrous labeled L-lysine monohydrochloride was thereby isolated in a form of snow-white amorphous solid. **Average mass (n = 2):** 73 ± 7 mg.

b) Characterization of the ^{18}O-labeled L-Lysine monohydrochloride

Figure IV-37: HRMS (ESI$^+$) analyses of non-labeled L-Lysine (dissolved in H_2O) in comparison to ^{18}O-enriched product. Average enrichment per carboxylic oxygen determined by MS: 59.8 ± 0.7 % (n = 2), enrichment yield: quantitative.

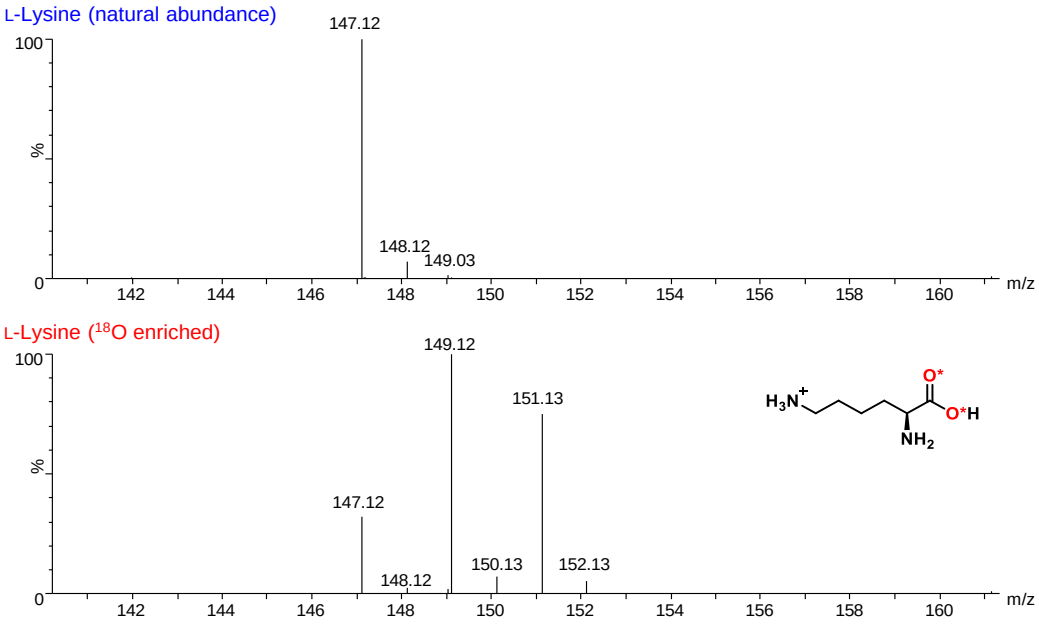

IV-D) $^{17}O/^{18}O$-LABELED FMOC-PROTECTED AMINO ACIDS

IV-D1) Fmoc-L-Asp-OH

a) Synthetic protocol[10]

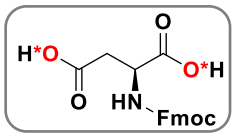

^{18}O-Enriched L-Aspartic acid (311 mg, 2.3 mmol, 1.2 eq.) prepared by mechanochemistry was dissolved in an aqueous solution of Na_2CO_3 (13.5% w/w, 5.4 mL) and cooled down in an ice-bath (< 4 °C). A solution of Fmoc *N*-hydroxysuccinimide ester (Fmoc-OSu, 641 mg, 1.9 mmol, 1.0 eq.) in DMF (4.4 mL) was then added dropwise, inducing precipitation, and the suspension was stirred at room temperature for 1h15. After dilution with water (50 mL), the solution was washed with Et_2O (20 mL) and EtOAc (2x 15 mL). The aqueous phase was cooled down in an ice-bath and acidified with HCl (6M, 4 mL) to pH ~ 1.5, which led to the precipitation. The product was extracted to EtOAc (6x 15 mL), organic phases were combined, washed with water and brine, dried over $MgSO_4$, and evaporated to dryness. The residue was suspended in petroleum-ether, the white precipitate was collected by filtration using a glass frit (pore-size P3), and dried under vacuum. The ^{18}O-labeled Fmoc-L-Aspartic acid was isolated in the form of a white solid. Due to the equilibrium in the carboxylic function, both oxygen sites (*i.e.* C=O* and C-O*H) are equally enriched. **Yield (n = 1):** 468 mg, 69 %.

b) Characterization of the ^{18}O-labeled Fmoc-L-Aspartic acid

Figure IV-38: ^{13}C NMR spectrum of ^{18}O-labeled Fmoc-L-Asp-OH (DMSO-*d6*, 600 MHz) corresponds to the published structure.[11] Peak of DMSO (used to reference the spectrum) is crossed out.

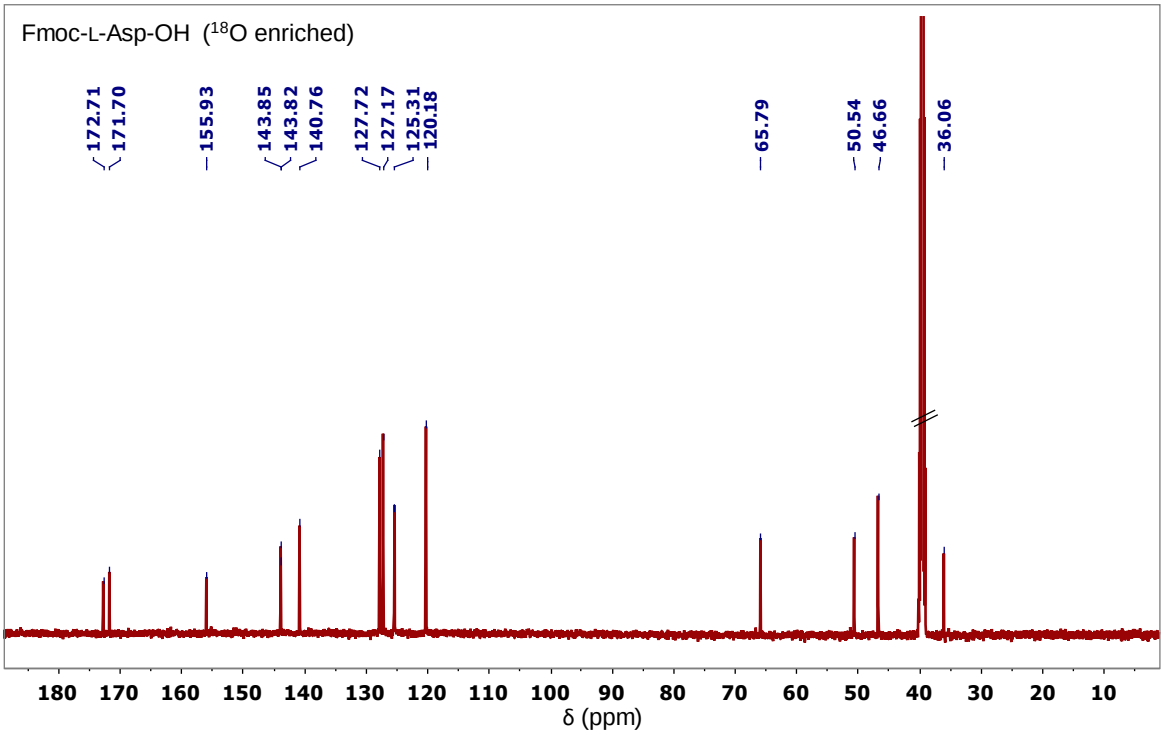

Figure IV-39: HRMS (ESI$^-$) analyses of non-labeled Fmoc-L-Aspartic acid (dissolved in MeOH) in comparison to ^{18}O-enriched product. Average enrichment per carboxylic oxygen determined by MS for ^{18}O-labeled product: 43.9 % (n = 1).

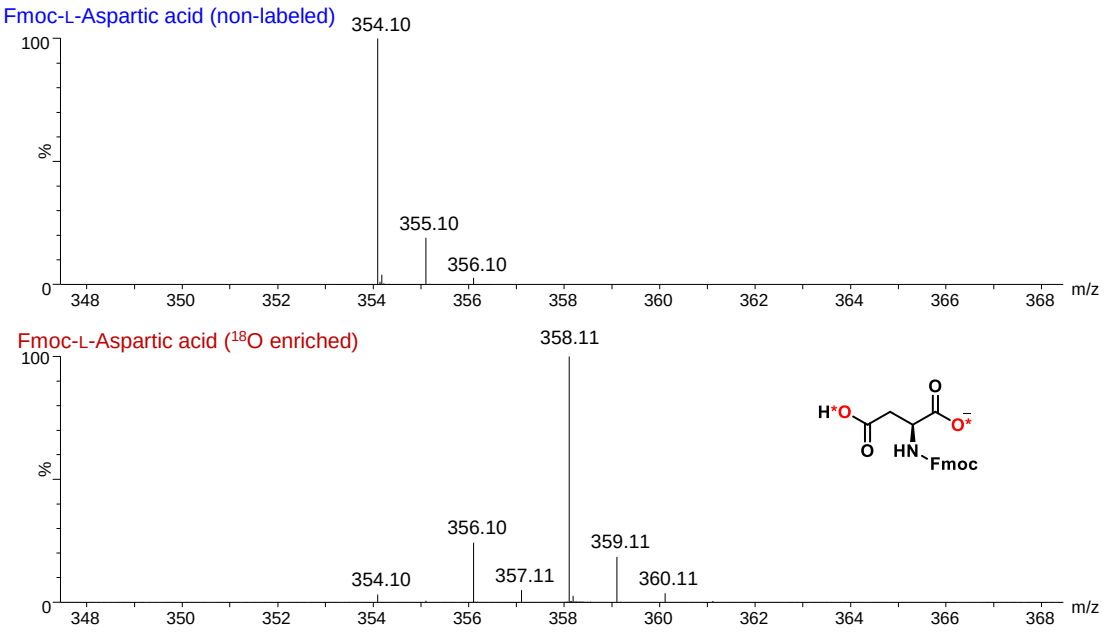

Figure IV-40: Chiral HPLC analyses of ^{18}O-L-product (enriched *via* saponification, *ee* > 99%) compared to non-labeled DL-compound.

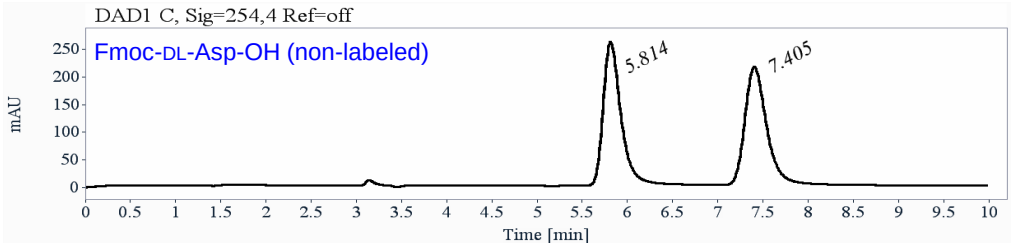

Signal: DAD1 C, Sig=220,4 Ref=off

RT [min]	Area	Area%	Capacity Factor	Enantioselectivity	Resolution (USP)
9.61	13116	49.51	2.26		
11.68	13377	50.49	2.96	1.31	3.91
Sum	26493	100.00			

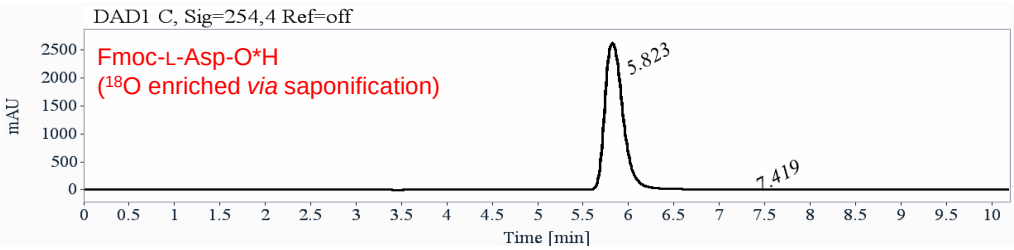

Signal: DAD1 C, Sig=254,4 Ref=off

RT [min]	Area	Area%	Capacity Factor	Enantioselectivity	Resolution (USP)
5.82	36150	99.83	0.97		
7.42	61	0.17	1.52	1.56	4.13
Sum	36211	100.00			

IV-D2) Fmoc-L-Lys(Fmoc)-OH

a) Synthetic protocol[12]

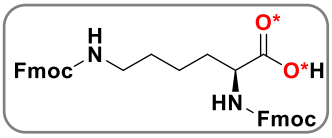

^{18}O-enriched L-Lysine monohydrochloride (200 mg, 1.1 mmol, 1.0 eq.) labeled by saponification or by H^+ catalyzed exchange was dissolved in an aqueous solution of Na_2CO_3 (13.5% w/w, 8 mL), and cooled down in an ice-bath (< 4 °C). A solution of Fmoc *N*-hydroxysuccinimide ester (Fmoc-OSu, 804 mg, 2.4 mmol, 2.2 eq.) in DMF (4.4 mL) was then added dropwise to the vigorously stirred solution, inducing precipitation, and the suspension was stirred at room temperature for 1h15. After dilution with water (100 mL), the solution was washed with Et_2O (2x 45 mL) and EtOAc. The aqueous phase was cooled down in an ice-bath and acidified with HCl (6M, 4 mL) to pH ~ 1.5, which led to the precipitation. The product was extracted with EtOAc (1x 30 mL, 4x 20 mL), organic phases were combined, washed with water and brine, dried over $MgSO_4$ and evaporated to dryness. The residual oil was dissolved in small amount of EtOAc and product precipitated upon addition of petroleum-ether. The white precipitate was collected by filtration using a glass frit (pore-size P3), and dried under vacuum. The ^{18}O-labeled Fmoc-L-Lys(Fmoc)-OH was isolated in the form of a white solid. Depending on the labeling scheme, one or both oxygens per carboxylic function were enriched. **Yield (n = 1):** 515 mg, 81 %.

*b) Characterization of the ^{18}O-labeled Fmoc-L-Lys(Fmoc)-O*H*

Figure IV-41: ^{13}C NMR spectrum of ^{18}O-labeled Fmoc-L-Lys(Fmoc)-OH (DMSO-*d6*, 600 MHz) corresponds to the published structure.[13] Peak of DMSO (used to reference the spectrum) is crossed out.

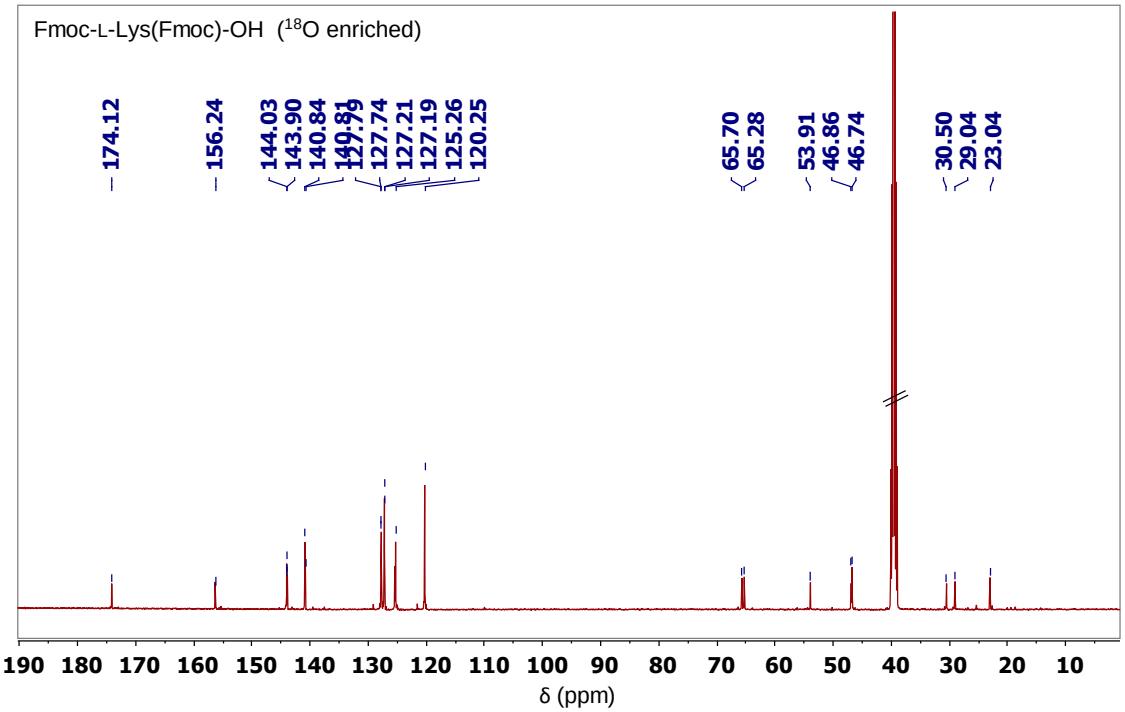

Figure IV-42: HRMS (ESI^-) analyses of non-labeled Fmoc-L-Lys(Fmoc)-OH (dissolved in EtOH) in comparison to ^{18}O-enriched product. Average enrichment per carboxylic oxygen determined by MS for ^{18}O-labeled products: 47.0 % (n = 1, L-Lys-O*H·HCl prepared *via* saponification), 59.8 % (n = 1, L-Lys-O*H·HCl prepared *via* H^+ catalyzed exchange).

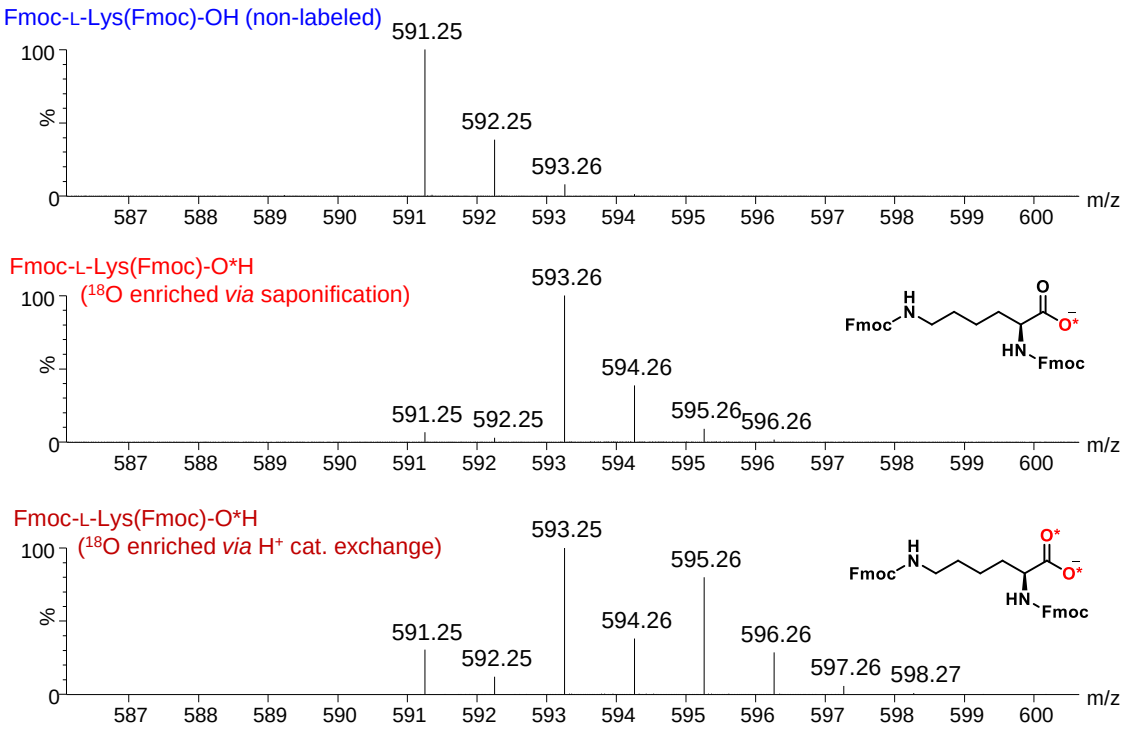

Figure IV-43: Chiral HPLC analyses of ^{18}O-L-products (enriched *via* saponification or H^+ catalyzed exchange, *ee* > 99%) compared to non-labeled DL-compound.

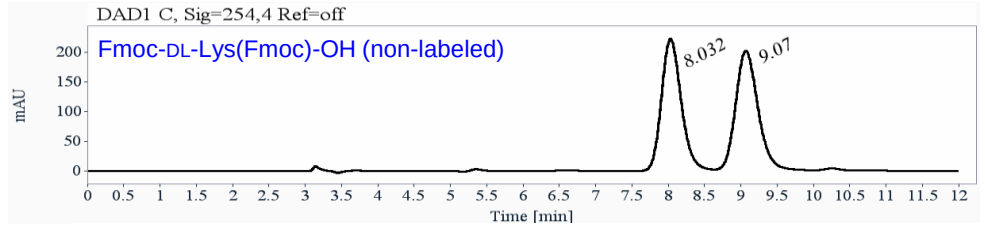

Signal: DAD1 C, Sig=254,4 Ref=off

RT [min]	Area	Area%	Capacity Factor	Enantioselectivity	Resolution (USP)
8.03	4222	49.36	1.72		
9.07	4331	50.64	2.07	1.20	1.98
Sum	8553	100.00			

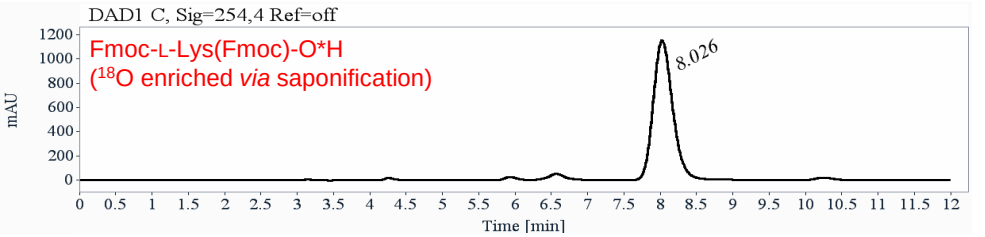

Signal: DAD1 C, Sig=254,4 Ref=off

RT [min]	Area	Area%	Capacity Factor	Enantioselectivity	Resolution (USP)
8.03	21542	100.00	1.72		
Sum	21542	100.00			

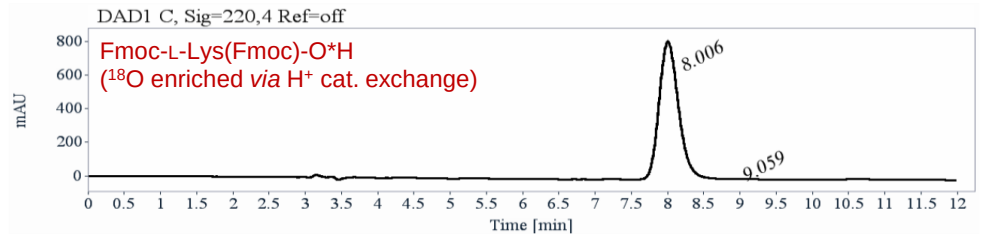

Signal: DAD1 C, Sig=220,4 Ref=off

RT [min]	Area	Area%	Capacity Factor	Enantioselectivity	Resolution (USP)
8.01	15511	99.54	1.71		
9.06	71	0.46	2.07	1.21	2.08
Sum	15582	100.00			

IV-D3) Fmoc-L-Leu-OH

*a) Synthetic protocol (2-steps, but with the labeled L-Leu-O*H intermediate not isolated)*

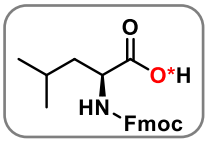

At first, L-leucine was labeled *via* mechanochemical saponification. For ^{18}O-labeling, ^{18}O-labeled water (99%, 44.5 µL, 2.5 mmol, 3.0 eq.), two stainless steel balls (10 mm diameter), L-leucine methylester monohydrochloride (150 mg, 0.83 mmol, 1.0 eq.) and sodium ethoxide (140.5 mg, 2.1 mmol, 2.5 eq.) were introduced successively into the screw-top stainless steel grinding jar (10 mL inner volume). The jar was closed and subjected to grinding for 30 min in the MM400 mixer mill operated at 25 Hz. To recover the product, non-labeled water (1 mL) was added into the jar, and the content was subjected to grinding for 2 min at 25 Hz. Then, the yellow solution was transferred to a round-bottom flask, the jar was rinsed with non-labeled water (3 mL), the aqueous phases were combined and gradually acidified to pH ~ 5 - 6 using concentrated aqueous HCl (12M, total volume ~ 200 µL), resulting in leucine precipitation.

For the Fmoc-protection,[14] at first $NaHCO_3$ (90 mg, 1.1 mmol, 1.1 eq.) and acetone (4 mL) were added to the leucine suspension. While stirred at room temperature, solid Fmoc *N*-hydroxysuccinimide ester (Fmoc-OSu, 303 mg, 0.9 mmol, 1.1 eq.) was then added in one portion, and the suspension was stirred overnight, resulting in complete dissolution of reaction mixture. The solution was acidified with HCl (1 M, 3x 500 µL) to pH ~ 1.5, the precipitate was collected by filtration (glass frit, pore-size P3), washed with water (2x 3 mL), and finally dried under vacuum. ^{18}O-labeled Fmoc-L-Leucine was isolated in the form of a white solid. Due to the equilibrium in the carboxylic function, both oxygen sites (*i.e.* C=O* and C-O*H) are equally enriched. **Yield (n = 1):** 255 mg, 86 %.

b) Characterization of the ^{18}O-labeled Fmoc-L-leucine

Figure IV-44: LCMS analyses of ^{18}O-enrcihed product compared to non-labeled commercial compound. The retention times are slightly shifted due to a different calibration of the mass spectrometer.

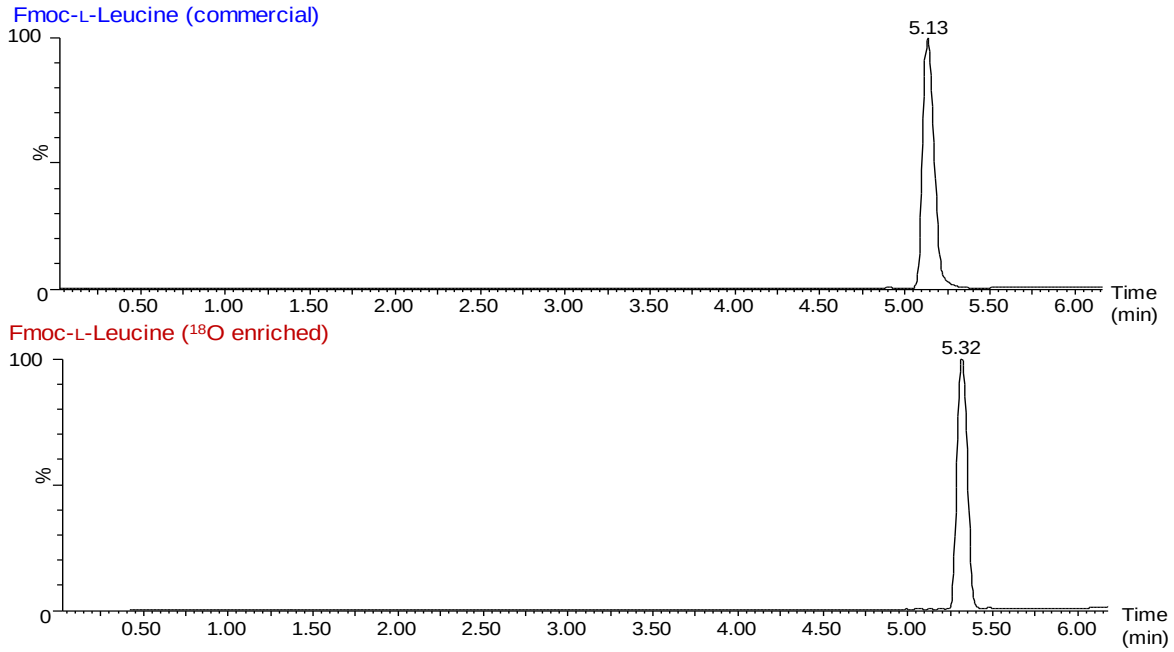

Figure IV-45: HRMS (ESI$^-$) analyses of non-labeled Fmoc-L-leucine (dissolved in MeOH) in comparison to ^{18}O-enriched products. Average enrichment per carboxylic oxygen determined by MS for ^{18}O-labeled products: 38.8 % (n = 1), enrichment yield: ~ 78 %.

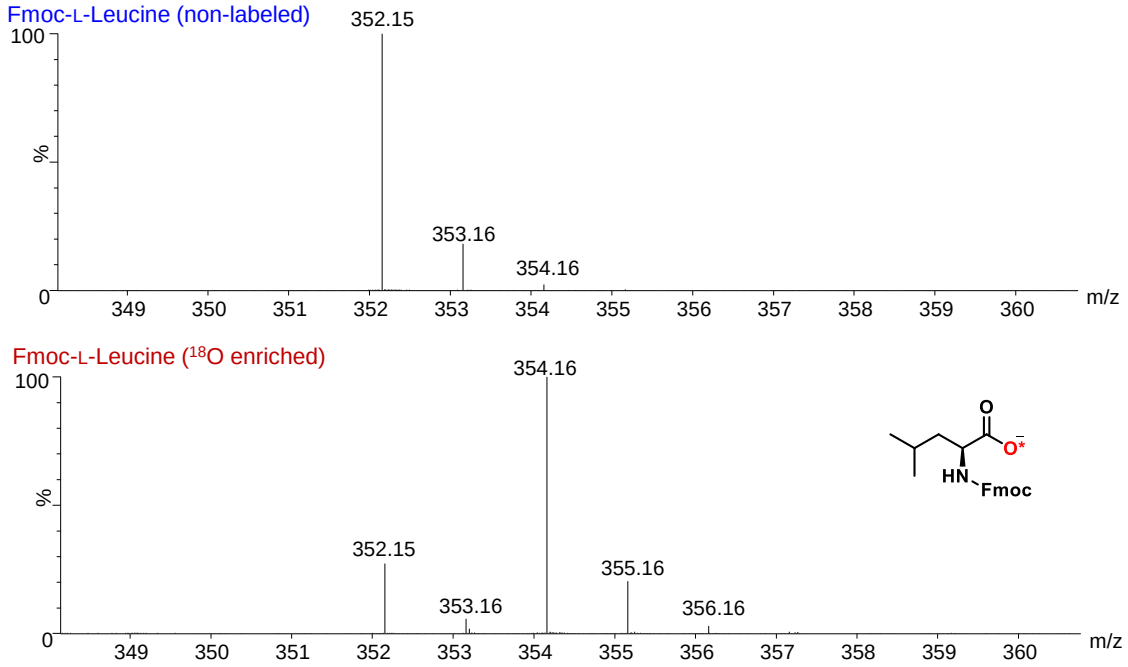

Figure IV-46: Chiral HPLC analyses of ^{18}O-L-product (enriched *via* saponification, *ee* > 99%) compared to non-labeled DL-compound.

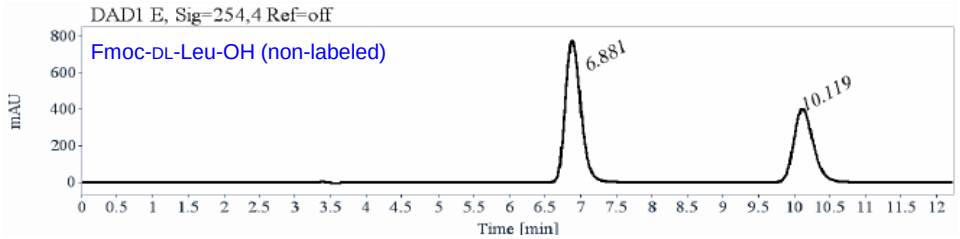

Signal: DAD1 E, Sig=254,4 Ref=off

RT [min]	Area	Area%	Capacity Factor	Enantioselectivity	Resolution (USP)
6.88	11864	60.49	1.33		
10.12	7749	39.51	2.43	1.82	7.23
Sum	19613	100.00			

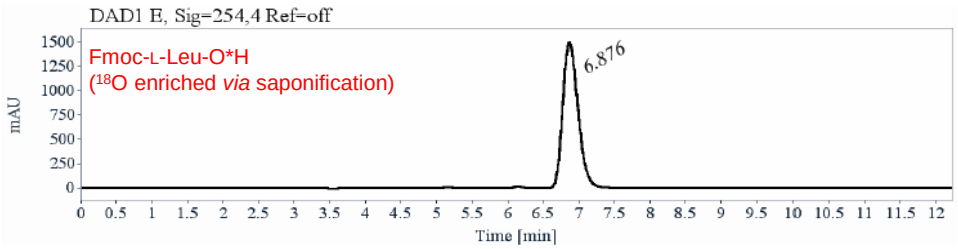

Signal: DAD1 E, Sig=254,4 Ref=off

RT [min]	Area	Area%	Capacity Factor	Enantioselectivity	Resolution (USP)
6.88	14862	100.00	1.33		
Sum	14862	100.00			

IV-D4) Fmoc-L-Phe-OH

*a) Synthetic protocol (2-steps, but with the labeled L-Phe-O*H intermediate not isolated)*

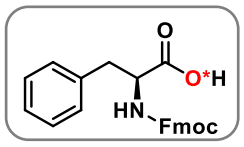

At first, L-phenylalanine was labeled via mechanochemical saponification. For ^{18}O-labeling, ^{18}O-labeled water (99%, 25 µL, 1.4 mmol, 2.0 eq.), two stainless steel balls (10 mm diameter), L-phenylalanine methyl ester monohydrochloride (150 mg, 0.7 mmol, 1.0 eq.) and sodium ethoxide (118 mg, 1.7 mmol, 2.5 eq.) were introduced successively into the screw-top stainless steel grinding jar (10 mL inner volume). The jar was closed and subjected to grinding for 30 min in the MM400 mixer mill operated at 25 Hz. To recover the product, non-labeled water (1 mL) was added into the jar, and the content was subjected to grinding for 2 min at 25 Hz. Then, the yellow solution was transferred to a round-bottom flask, the jar was rinsed with non-labeled water (3 mL), the aqueous phases were combined, and gradually acidified to pH ~ 5 - 6 using aqueous HCl (6M, total volume ~ 160 µL).

For the Fmoc-protection,[15] at first Na_2CO_3 (440 mg, 4.2 mmol, 4.2 eq.) was dissolved in the phenylalanine solution, and the flask was placed in an ice-bath to cool down (< 4 °C). A solution of Fmoc *N*-hydroxysuccinimide ester (Fmoc-OSu, 260 mg, 0.8 mmol, 1.1 eq.) in DMF (4 mL) was then added dropwise under stirring to the cold phenylalanine solution, inducing precipitation, and the suspension was stirred at room temperature for 1 h. After dilution with water (30 mL), the solution was washed with EtOAc (15 mL). The aqueous phase was then cooled down in an ice-bath and acidified with HCl (12M, 900 µL) to pH ~ 1.5, and precipitation was observed. The suspension was then extracted with EtOAc (1x 20 mL, 3x 10 mL), organic phases were combined, washed with water and brine, dried over $MgSO_4$, and solvent was evaporated under reduced pressure. The product was finally dried under vacuum. The ^{18}O-labeled Fmoc-L-Phenylalanine was isolated as a white solid. Due to the equilibrium in the carboxylic function, both oxygen sites (*i.e.* C=O* and C-O*H) are equally enriched. **Yield (n = 1):** 250 mg, 92 %.

b) Characterization of the ^{18}O-labeled Fmoc-L-phenylalanine

Figure IV-47: LCMS analyses of ^{18}O-enriched product compared to non-labeled commercial compound.

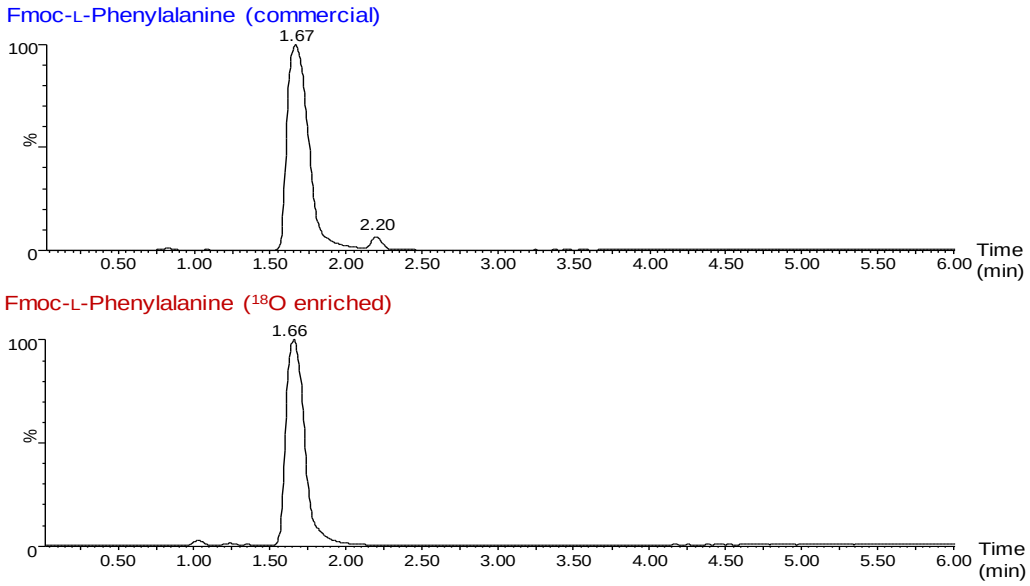

Figure IV-48: HRMS (ESI$^-$) analyses of non-labeled Fmoc-L-phenylalanine (dissolved in EtOH) in comparison to ^{18}O-enriched product. Average enrichment per carboxylic oxygen determined by MS for ^{18}O-labeled product: 46.9 % (n = 1), enrichment yield: ~ 95 %.

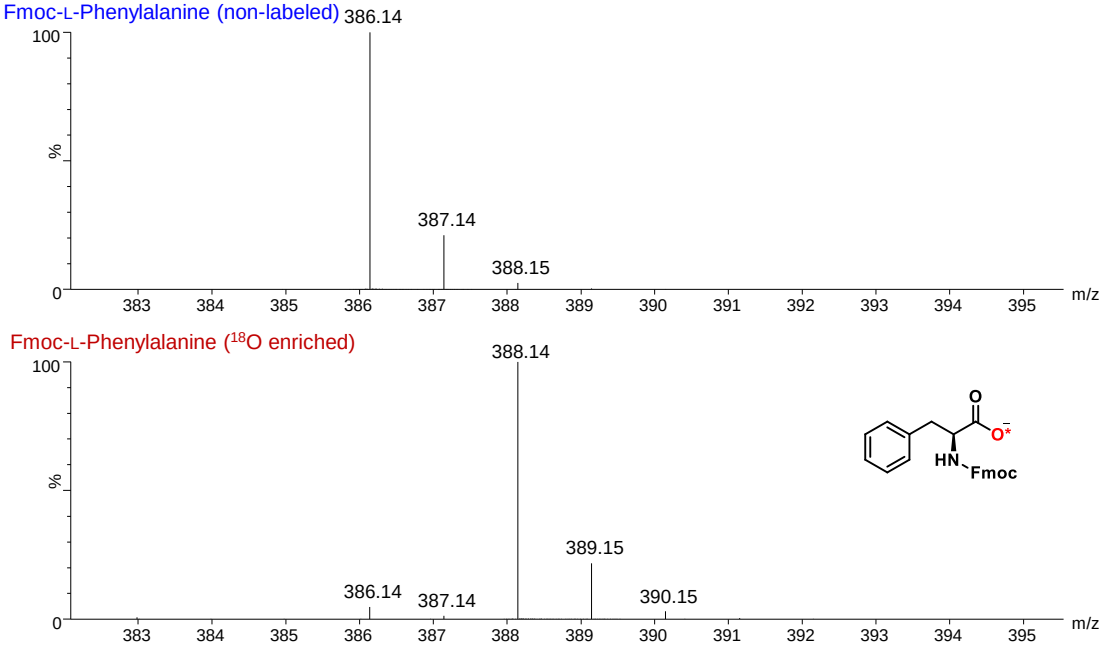

Figure IV-49: Chiral HPLC analyses of ^{18}O-L-product (enriched *via* saponification, *ee* > 99%) compared to non-labeled DL-compound.

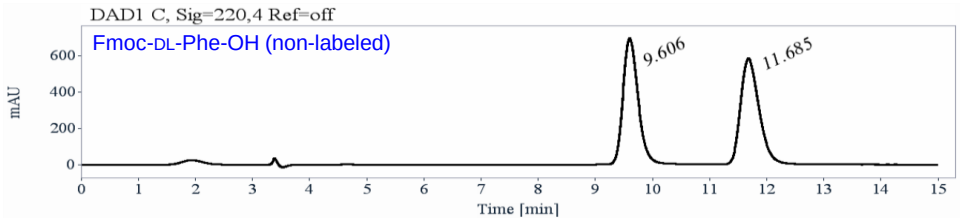

Signal: DAD1 C, Sig=220,4 Ref=off

RT [min]	Area	Area%	Capacity Factor	Enantioselectivity	Resolution (USP)
9.61	13116	49.51	2.26		
11.68	13377	50.49	2.96	1.31	3.91
Sum	26493	100.00			

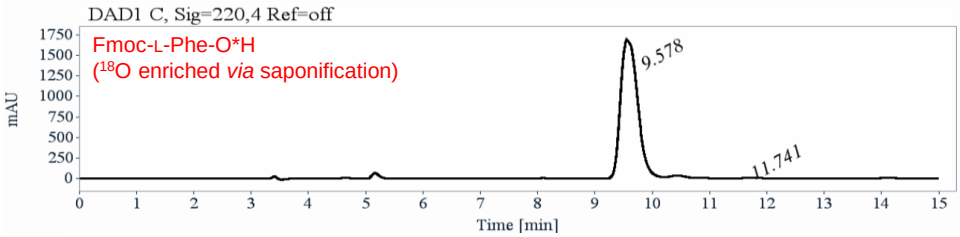

Signal: DAD1 C, Sig=220,4 Ref=off

RT [min]	Area	Area%	Capacity Factor	Enantioselectivity	Resolution (USP)
9.59	26481	99.65	2.25		
11.96	93	0.35	3.05	1.36	3.24
Sum	26574	100.00			

IV-D5) Fmoc-Gly-OH

*a) Synthetic protocols (2-steps, but with the labeled Gly-O*H intermediate not isolated)*

- *Low-scale synthesis:*

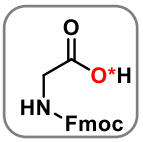

At first, glycine was labeled via mechanochemical saponification. For ^{18}O-labeling, ^{18}O-labeled water (99%, 43 µL, 2.4 mmol, 2.0 eq.), two stainless steel balls (10 mm diameter), glycine methyl ester monohydrochloride (150 mg, 1.2 mmol, 1.0 eq.) and sodium ethoxide (203 mg, 3.0 mmol, 2.5 eq.) were introduced successively into the screw-top stainless steel grinding jar (10 mL inner volume). The jar was closed and subjected to grinding for 30 min in the MM400 mixer mill operated at 25 Hz. To recover the product, non-labeled water (1 mL) was added into the jar, and the content was subjected to grinding for 2 min at 25 Hz. Then, the yellow solution was transferred to a round-bottom flask, the jar was rinsed with non-labeled water (1.5 mL), and the aqueous phases were combined and sonicated for 5 min (to dissolve all the particles, if necessary). The medium was stirred and gradually acidified to pH ~ 5 - 6 using concentrated aqueous HCl (12M, total volume ~ 140 µL).

For the Fmoc-protection,[12] at first Na_2CO_3 (280 mg, 2.6 mmol, 2.6 eq.) was dissolved in the glycine solution, and the flask was placed in an ice-bath to cool down (< 4 °C). A solution of Fmoc *N*-hydroxysuccinimide ester (Fmoc-OSu, 336 mg, 1.0 mmol, 0.8 eq.) in dioxane (2.5 mL) was then added in one portion to the stirred glycine solution. Immediate precipitation was observed. The suspension was stirred at room temperature for 20 min, then diluted with 20 mL of water. The cloudy solution was then washed with Et_2O (7 mL) and EtOAc (2x 7 mL) using a separating funnel. The aqueous phase was then separated from the organic phase, cooled down in an ice-bath and acidified to pH ~ 1 - 2 with concentrated HCl (12M, total volume ~ 550 µL) leading to precipitation. The resulting suspension was extracted with EtOAc (1x 10 mL, 5x 5 mL), organic phases were combined, washed with brine, dried over $MgSO_4$ and concentrated to dryness. To eliminate residual dioxane, the dry white solid was re-dissolved in EtOAc, solvent was re-evaporated and the product was dried under vacuum. ^{18}O-enriched Fmoc-Gly-OH was thereby obtained in the form of a white solid. Due to the equilibrium in the carboxylic function, both oxygen sites (*i.e.* C=O* and C-O*H) are equally enriched. **Average yield (n = 2):** 237 ± 2 mg, 79 ± 1 %.

For the ^{17}O-labeling, 90% ^{17}O-enriched water (34 µL, 2.0 eq.) was used. **Yield (n = 1):** 233 mg, 78 %.

- *Scale-up procedure:*

For the scale-up synthesis, all reagents and solvents used were doubled in mass/volume. The reaction times and work-up conditions remained exactly the same; 30 min/25 Hz for saponification and 20 min for Fmoc-protection. **Average yield (n = 2):** 488 ± 40 mg, 82 ± 7 %.

b) Characterization of the $^{17}O/^{18}O$-labeled Fmoc-Glycine

Figure IV-50: LCMS analyses of $^{17}O/^{18}O$-enriched products compared to non-labeled commercial compound. The peak at 2.19 min belongs to a Fmoc-Gly-Gly-OH side-product.

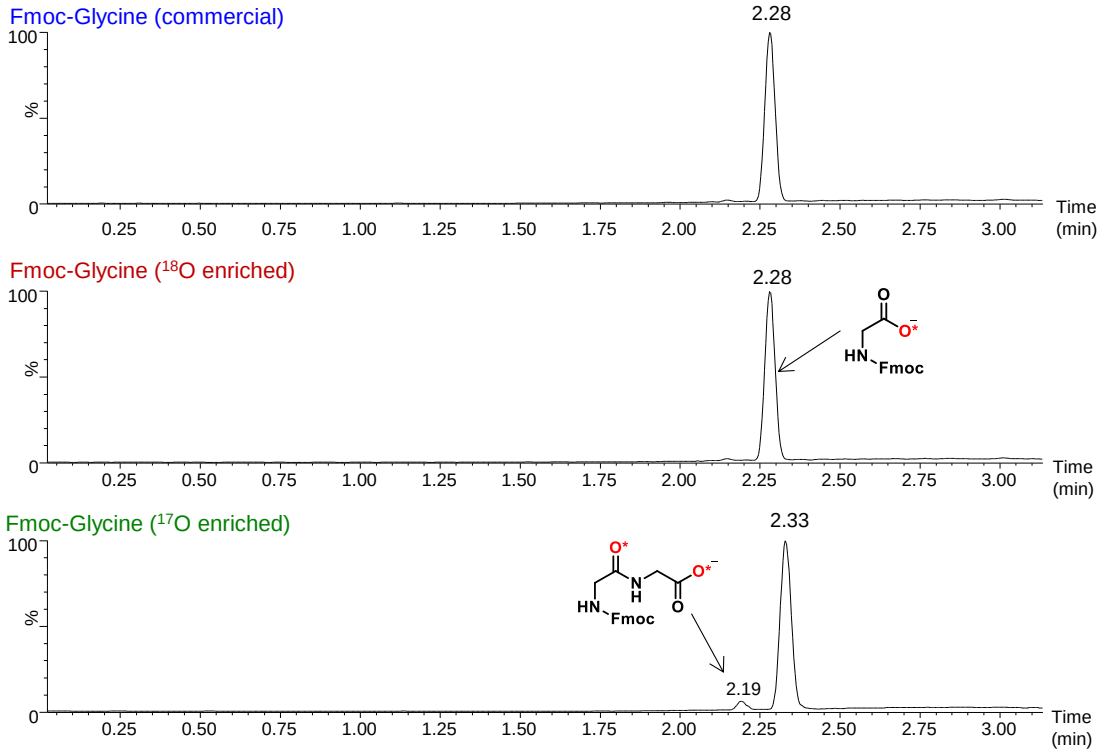

Figure IV-51: HRMS (ESI^-) analyses of non-labeled Fmoc-Glycine (dissolved in EtOH) in comparison to $^{18}O/^{17}O$-enriched products. Average enrichment per carboxylic oxygen determined by MS for ^{18}O-labeled products: 43.4 ± 1.2 % (n = 2), enrichment yield: ~ 87 %; for ^{17}O-labeled products: 38.2 ± 0.5 % (n = 2), enrichment yield: ~ 84 %.

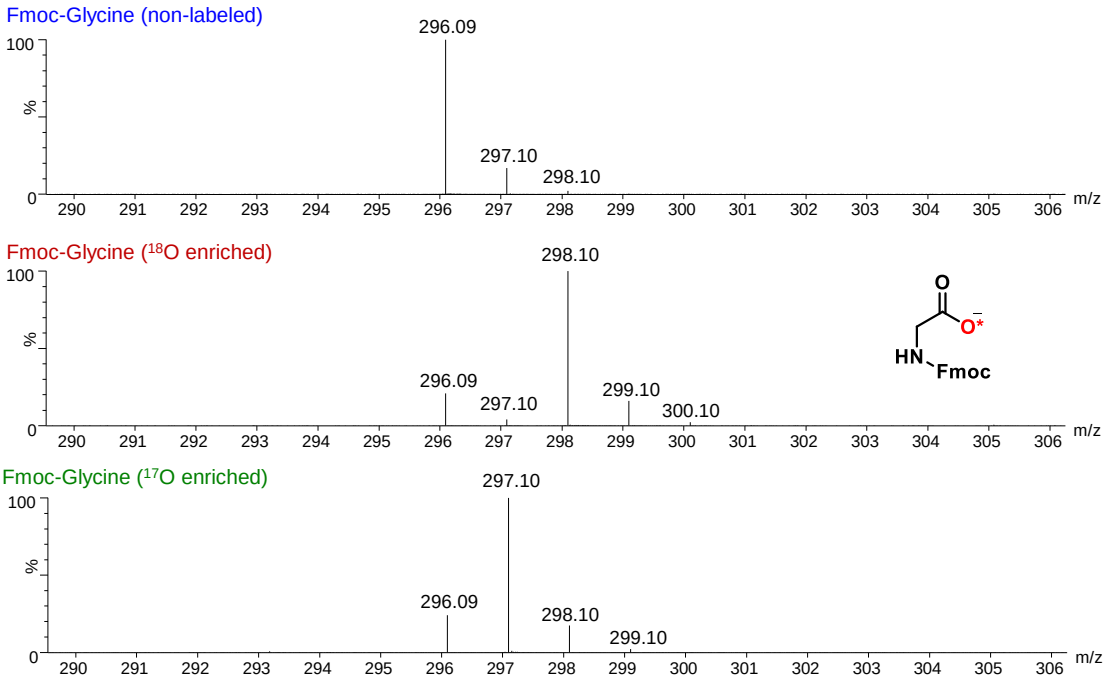

IV-D6) Fmoc-L-Asp(O*t*Bu)-OH

*a) Synthetic protocols (2-steps, with the labeled L-Asp(OtBu)-O*H intermediate not isolated)*

- *Low-scale synthesis:*

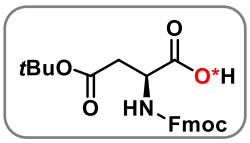

At first, L-Asp(O*t*Bu)-O*H was $^{17}O/^{18}O$-labeled using mechanochemical saponification. For the ^{18}O-labeling, ^{18}O-labeled water (99%, 34 µL, 1.9 mmol, 3.0 eq.), two stainless steel balls (10 mm diameter), L-Asp(O*t*Bu)-OMe·HCl (150 mg, 0.6 mmol, 1.0 eq.) and sodium ethoxide (85 mg, 1.3 mmol, 2.0 eq.) were introduced successively into the screw-top stainless steel grinding jar (10 mL inner volume). The jar was closed and subjected to grinding for 30 min in the MM400 mixer mill operated at 25 Hz. To recover the product, non-labeled water (1 mL) was added into the jar, and the content was subjected to grinding for 2 min at 25 Hz. Then, the yellow solution was transferred to a round-bottom flask, the jar was rinsed with non-labeled water (2 mL), and the aqueous phases were combined and gradually acidified to pH ~ 8 - 9 using aqueous HCl (6M, total volume ~ 60 µL).

For the Fmoc-protection,[10] at first Na_2CO_3 (320 mg, 3.0 mmol, 3 eq.) was added to the solution, and the flask was placed in an ice-bath to cool down (< 4 °C). A solution of Fmoc *N*-hydroxysuccinimide ester (Fmoc-OSu, 200 mg, 0.6 mmol, 0.95 eq.) in DMF (3 mL) was then added dropwise under stirring to this solution, inducing precipitation, and the suspension was stirred at room temperature for 1 h. After dilution with water (30 mL), the solution was washed with Et_2O (10 mL) and EtOAc (15 mL). The aqueous phase was then cooled down in an ice-bath, and acidified with HCl (1M, 6.5 mL) to pH ~ 1.5, which led to the precipitation. The suspension was extracted to EtOAc (1x 20 mL, 2x 15 mL), organic phases were combined, washed with water and brine, dried over $MgSO_4$, and solvent evaporated under reduced pressure. The residual solid was dried under vacuum. The ^{18}O-labeled Fmoc-L-Asp(O*t*Bu)-^{18}OH was isolated as a white solid. Due to the equilibrium in the carboxylic function, both oxygen sites (*i.e.* C=O* and C-O*H) are equally enriched. **Average yield (n = 2):** 169 ± 5 mg, 73 ± 5 %.

- *Scale-up procedure:*

For the scale-up synthesis, the amount of reagents was almost doubled. For the saponification step: L-Asp(O*t*Bu)-OMe·HCl (288 mg, 1.2 mmol, 1 eq.), labeled H_2O* (65 µL, 3.6 mmol, 3 eq.) and NaOEt (164 mg, 2.4 mmol, 2 eq.) were used. The milling time remained the same, 30 min at 25 Hz. For the Fmoc-protection, Na_2CO_3 (555 mg) was dissolved in 5 mL of H_2O and Fmoc-OSu (365 mg, 1.1 mmol, 0.9 eq.) was dissolved in 5 mL of DMF. Reaction time remained the same, 1h of stirring at room temperature. **Average yield (n = 3):** 347 ± 5 mg, 74 ± 1 %.

For the ^{17}O-labeling, 90% ^{17}O-enriched water (65 µL, 3.0 eq.) was used. **Average yield (n = 2):** 354 ± 8 mg, 78 ± 1 %.

*b) Characterization of the ^{18}O-labeled Fmoc-L-Asp(OtBu)-O*H*

Figure IV-52: LCMS analyses of ^{17}O/^{18}O-enriched products compared to non-labeled commercial compound. The peak at 2.19 min belongs to the Fmoc-L-Asp-OH side-product issuing from partial side-chain deprotection during the saponification step.

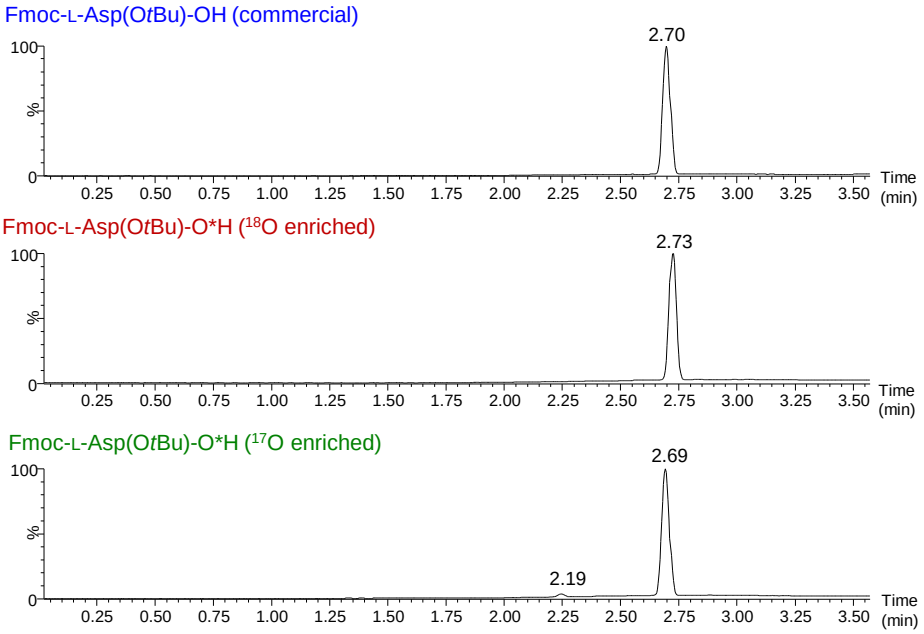

Figure IV-53: HRMS (ESI$^-$) analyses of non-labeled Fmoc-L-Asp(O*t*Bu)-OH (dissolved in MeOH) in comparison to ^{17}O/^{18}O-enriched products. Average enrichment per carboxylic oxygen determined by MS for ^{18}O-labeled products: 45.1 ± 1.0 % (n = 3), enrichment yield: ~ 91 %; for ^{17}O-labeled products: 40.5 ± 0.2 % (n = 2), enrichment yield: ~ 86 %.

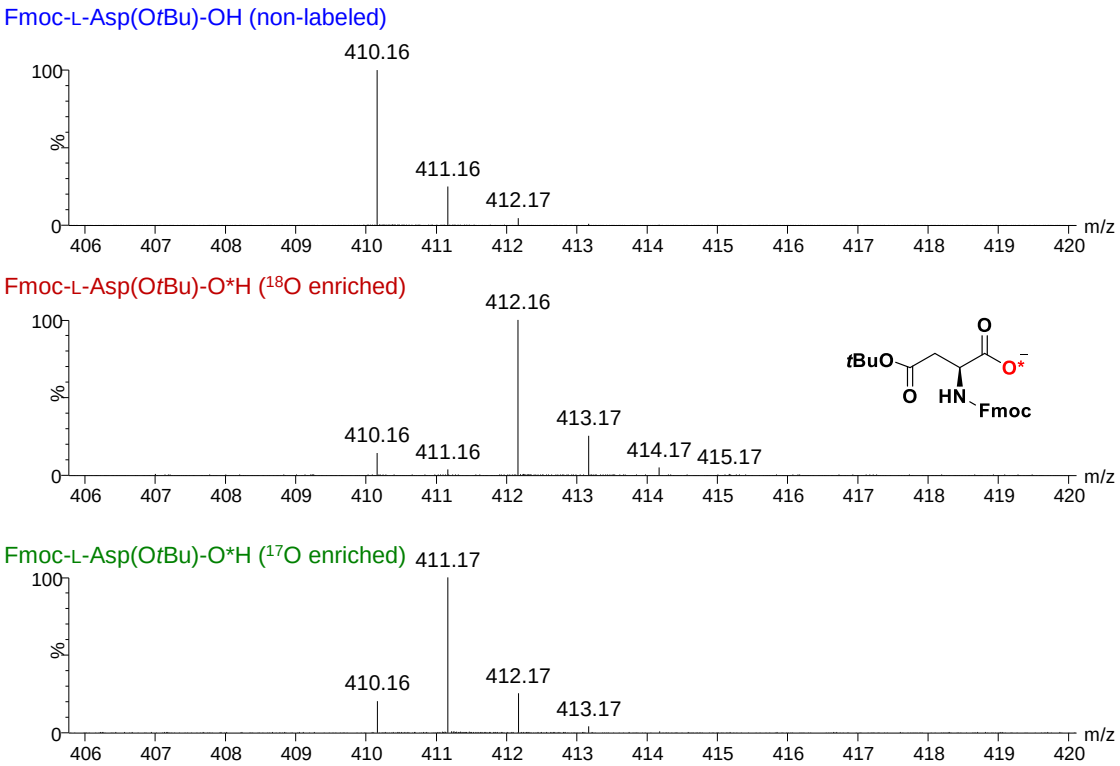

IV-D7) Fmoc-L-Lys(Boc)-OH

*a) Synthetic protocol (2-steps, with the labeled L-Lys(Boc)-O*H intermediate not isolated)*

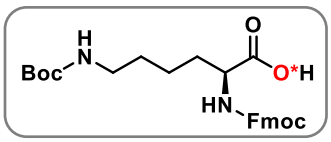

At first, L-Lys(Boc)-O*H was $^{17}O/^{18}O$-labeled using mechanochemical saponification. For ^{18}O-labeling, ^{18}O-labeled water (99%, 27.5 µL, 1.5 mmol, 3.0 eq.), two stainless steel balls (10 mm diameter), L-Lys(Boc)-OMe·HCl (150 mg, 0.5 mmol, 1.0 eq.) and sodium ethoxide (69 mg, 1.0 mmol, 2.0 eq.) were introduced successively into the screw-top stainless steel grinding jar (10 mL inner volume). The jar was closed and subjected to grinding for 30 min in the MM400 mixer mill operated at 25 Hz. To recover the product, non-labeled water (1 mL) was added into the jar, and the content was subjected to grinding for 2 min at 25 Hz. Then, the yellow solution was transferred to a round-bottom flask, the jar was rinsed with non-labeled water (500 µL) and the aqueous phases were combined and gradually acidified to pH ~ 8-9 using aqueous HCl (6M, total volume ~ 70 µL).

For the Fmoc-protection[16], at first the precipitated L-Lys(Boc)-O*H was dissolved in a saturated aqueous solution of $NaHCO_3$ (4 mL). A solution of Fmoc *N*-hydroxysuccinimide ester (Fmoc-OSu, 185 mg, 0.6 mmol, 1.1 eq.) in THF (4 mL) was then added dropwise under stirring, inducing precipitation. The suspension was stirred at room temperature overnight. The THF was evaporated under reduced pressure and the product was extracted from the aqueous phase with EtOAc (3x 10 mL). Organic phases were combined, dried over $MgSO_4$, and evaporated to dryness. The crude residue was purified by flash column chromatography on silica gel (DCM/MeOH, gradient 0 -> 10% MeOH), providing the desired product in the form of a white solid. Due to the equilibrium in the carboxylic function, both oxygen sites (*i.e.* C=O* and C-O*H) are equally enriched. **Average yield (n = 2):** 189 ± 26 mg, 80 ± 11 %.

For the ^{17}O-labeling, 70% ^{17}O-enriched water (27.5 µL, 3.0 eq.) was used. **Yield (n = 1):** 354 ± 8 mg, 78 ± 1 %.

*b) Characterization of the ^{18}O-labeled Fmoc-L-Lys(Boc)-O*H*

Figure IV-54: LCMS analyses of $^{17}O/^{18}O$-enriched products compared to non-labeled commercial compound. The retention times are slightly shifted due to a different calibration of the mass spectrometer.

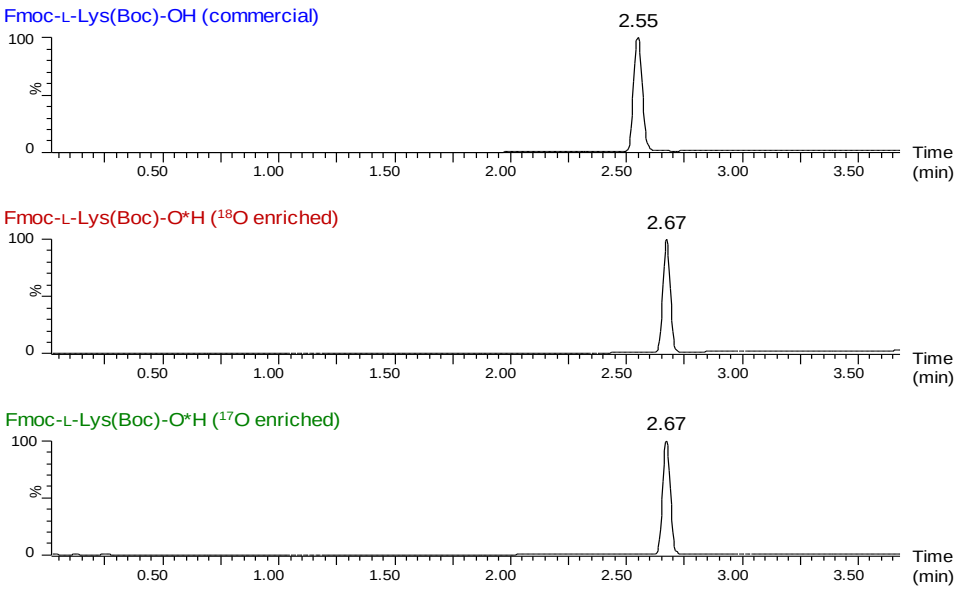

Figure IV-55: HRMS analyses (ESI^-) of non-labeled Fmoc-L-Lys(Boc)-OH (dissolved in MeOH) in comparison to $^{17}O/^{18}O$-enriched products. Average enrichment per carboxylic oxygen determined by MS for ^{18}O-labeled products: 45.1 ± 0.1 % (n = 2), enrichment yield: ~ 91 %; for ^{17}O-labeled product: 32.3 % (n = 1), enrichment yield: ~ 91 %.

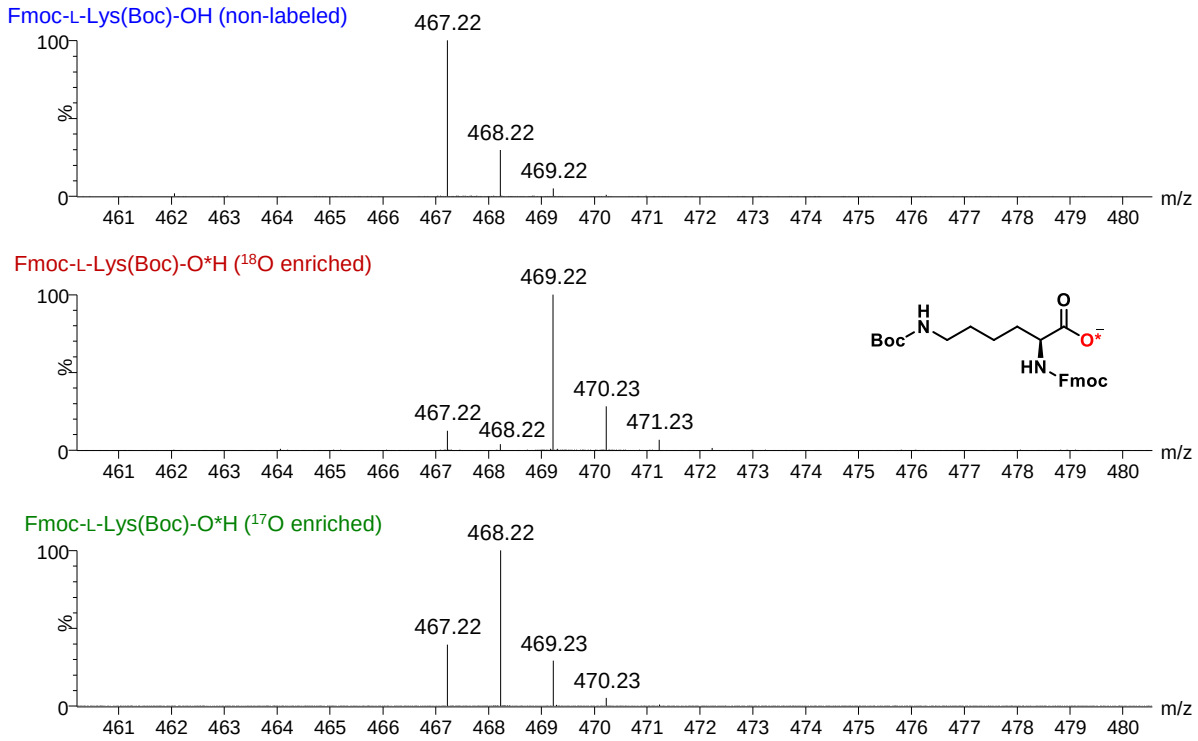

REFERENCES

1. Perras, F. A.; Viger-Gravel, J.; Burgess, K. M.; Bryce, D. L., Signal enhancement in solid-state NMR of quadrupolar nuclei. *Solid State Nucl. Magn. Reson.* **2013,** *51*, 1-15.
2. Kupce, E.; Freeman, R., Adiabatic pulses for wideband inversion and broadband decoupling. *J. Magn. reson.* **1995,** *115* (2), 273-276.
3. Dey, K. K.; Prasad, S.; Ash, J. T.; Deschamps, M.; Grandinetti, P. J., Spectral editing in solid-state MAS NMR of quadrupolar nuclei using selective satellite inversion. *J. Magn. Reson.* **2007,** *185* (2), 326-330.
4. Amoureux, J.-P.; Fernandez, C.; Steuernagel, S., ZFiltering in MQMAS NMR. *J. Magn. Reson.* **1996,** *123* (1), 116-118.
5. Massiot, D.; Fayon, F.; Capron, M.; King, I.; Le Calvé, S.; Alonso, B.; Durand, J.-O.; Bujoli, B.; Gan, Z.; Hoatson, G., Modelling one- and two-dimensional solid-state NMR spectra. *Magn. Res. Chem.* **2002,** *40* (1), 70-76.
6. Hayashi, K.; Fujii, Y.; Saito, R.; Kanao, H.; Hino, T., The Influence of Measurement Parameters on the Specific Rotation of Amino Acids. *Agr. Biol. Chem.* **1966,** *30* (12), 1221-1237.
7. Haynes, W. M., *Handbook of Chemistry and Physics*. 92nd ed.; 2011-2012.
8. Mears, W. H., The Oxygen Exchange Reaction of Glycine Hydrochloride and Water. *J. Chem. Phys.* **1938,** *6* (5), 295-295.
9. McGlone, S. J.; Elmes, P. S.; Brown, R. D.; Godfrey, P. D., Molecular structure of a conformer of glycine by microwave spectroscopy. *J. Mol. Struct.* **1999,** *485-486*, 225-238.
10. Bruno Perly, S. M., Florence Pilard Amphiphilic cyclodextrin derivatives, metho d for preparation thereof and uses thereof. 2007.
11. Berthet, M.; Davanier, F.; Dujardin, G.; Martinez, J.; Parrot, I., MgI2 -Mediated Chemoselective Cleavage of Protecting Groups: An Alternative to Conventional Deprotection Methodologies. *Chem. Eur. J.* **2015,** *21* (31), 11014-11016.
12. Lapatsanis, L.; Milias, G.; Froussios, K.; Kolovos, M., Synthesis of N -2,2,2-(Trichloroethoxycarbonyl)-L-amino Acids and N -(9-Fluorenylmethoxycarbonyl)-L-amino Acids Involving Succinimidoxy Anion as a Leaving Group in Amino Acid Protection. *Synthesis-Stuttgart* **1983,** *1983*, 671-673.
13. Morin, B.; Bubb, W. A.; Davies, M. J.; Dean, R. T.; Fu, S., 3-Hydroxylysine, a Potential Marker for Studying Radical-Induced Protein Oxidation. *Chem. Res. Toxicol.* **1998,** *11* (11), 1265-1273.
14. Djedaïni-Pilard, F.; Azaroual-Bellanger, N.; Gosnat, M.; Vernet, D.; Perly, B., Potential formation of intramolecular inclusion complexes in peptido-cyclodextrins as evidenced by NMR spectroscopy. *J. Chem. Soc. Perk. T. 2* **1995,** (4), 723-730.
15. Chaiyakunvat, P.; Anantachoke, N.; Reutrakul, V.; Jiarpinitnun, C., Caged xanthones: Potent inhibitors of global predominant MRSA USA300. *Bioorg. Med. Chem. Lett.* **2016,** *26* (13), 2980-2983.
16. Schramma, K. R.; Bushin, L. B.; Seyedsayamdost, M. R., Structure and biosynthesis of a macrocyclic peptide containing an unprecedented lysine-to-tryptophan crosslink. *Nat. Chem.* **2015,** *7* (5), 431-437.

CHAPTER 5

SYNTHESIS OF $^{17}O/^{18}O$-LABELED SHORT PEPTIDES

INTRODUCTION

Peptides are an important and thoroughly studied class of biomolecules composed of amino acid residues connected *via* amide bonds (named peptide bonds), which play structural and functional roles in the human body. As was already mentioned in the previous chapter, due to the irreplaceable role of peptides and proteins in the living organisms, a lot of effort was invested to better understand their reactivity and to explore their structure, as a crucial prerequisite for the development of new drugs[1] or biomimetic materials.[2] Solid-state NMR spectroscopy is a versatile analytical tool frequently used to study the structure, function and dynamics of peptides and proteins. Looking at different nuclei, typically ^{1}H, ^{13}C or ^{15}N, NMR spectroscopy enables to collect and combine complementary information. However, one last major component of proteins remains largely neglected: oxygen. Despite the fact that oxygen is a key participant in many biological functions, through enzyme-substrate interactions or hydrogen bonding, biological ^{17}O NMR studies are still rare.

To date, only a few ^{17}O NMR studies have focused on the characterization of simple small tri-peptides such as Gly-Gly*-Gly[3] or Ala-Ala*-Ala.[4] Other works have targeted much bigger structures, such as a 15-residue polypeptide gramicidine A (studied at 14.1 and 18.8 T),[5] a 23-residue transmembrane peptide WALP23 (analysed at 19.6 and 35.2 T),[6] or even a 72-residue containing phospholemann protein (PLM) (analysed using a 14.1 T instrument),[7] providing structural insights, such as the number of inequivalent oxygen sites in the studied samples, and/or information regarding site-specific interactions of labeled carbonyl with water molecules and metal cations. Peptides for these studies were typically synthesized using solid-phase peptide synthesis (SPPS) with only one ^{17}O-labeled amino acid introduced in the peptide chain, which had been initially ^{17}O-enriched under the form of a Fmoc-protected amino acid.

Only very recently, a ^{17}O NMR study of a recombinant protein, yeast ubiquitin, prepared via expression with *E.coli* was published.[8] In this 76-residues containing peptide, all the glycine, phenylalanine or tyrosine units, present in the sequence, were ^{17}O-labeled and the protein was studied by ^{17}O solution and solid-state NMR spectroscopy (recorded at 16.4 and 35.2 T, respectively). From the solid-state experiments, ^{17}O parameters were extracted for the multiple oxygen sites detected in the protein.

Selection of the peptide to label in ^{17}O

The aim of this work was to prepare a ^{17}O-labeled peptide, which could then be used to study biological processes using ^{17}O solid-state NMR, such as the surface interactions between the peptide and inorganic materials (such as hydroxyapatite) during bio-mineralization. Indeed, these surface interactions are an important feature of mineral formation in biological systems, and their closer characterization could provide a better understanding of pathological bio-mineralisation processes, such as a kidney stone formation,[9] or could bring new information which could be used for development of more efficient bone-implants.[10-12] We have decided to use the SPPS approach, which enables to selectively label only the chosen amino acid positions within a peptide of interest, compared to the recombinant protein expression strategy, which is a less selective labeling strategy. Since the peptide synthesis was a new experimental technique for our research group, in this initial study we focused on a selection of short peptide sequences of interest, to gain a synthetic insight first.

One of the frequently studied sequences (which is also present in more complex proteins involved in bio-mineralization processes) is Arginyl-glycyl-aspartic acid (Arg-Gly-Asp, RGD) and its longer derivative Gly-Arg-Gly-Asp-Ser (GRGDS). It serves as a structural recognition motif for cell transmembrane protein receptors (integrins), which facilitate cell-cell and cell-extracellular matrix adhesion.[13] Integrins recognize and bind to this sequence found in multiple matrix proteins, including fibronectin, fibrinogen or osteopontin. The RGD motif is also frequently used in drug development (including drug delivery systems or tumor-targeting nanoparticles)[14] and bioengineering (*e.g.* for inclusion or coating of implants).[15-16] Moreover, both RGD and GRGDS peptides are commercially available, which is an indication of their general interest to the research community.

Several solid-state ^{13}C NMR studies have been published with the aim to better understand the structure and dynamics in the RGD-motif-containing proteins and to explain their cell adhesion behaviour.[16-18] Yet, to the best of our knowledge, only one example of a ^{17}O solution spectrum of RGD derivative (Ac-Arg-Asp-Gly-NH_2) labeled at the aspartic acid side-chain *via* saponification of the peptide, was published.[19] However, no ^{17}O solid-state NMR study of this motif was reported so far.

Here, the short peptides RGD (H-Arg-Gly-Asp-OH) and GRGDS (H-Gly-Arg-Gly-Asp-Ser-OH), were prepared selectively $^{17}O/^{18}O$-labeled at glycine and aspartic acid units using $^{17}O/^{18}O$-labeled precursors Fmoc-Gly-O*H and Fmoc-L-Asp(O*t*Bu)-O*H (labeled only at the main-chain) (Figure 5.1). The syntheses of these labeled Fmoc-protected amino acids were described in the previous Chapter (section 4.3.2). For the GRGDS penta-peptide, two

^{17}O-labeled products with both or only one Gly unit being enriched were synthesised and analysed by solid-state NMR spectroscopy (Figure 5.1). Furthermore, a synthesis of GRGDS penta-peptide with Asp labeled at the side-chain was also attempted (Figure 5.1).

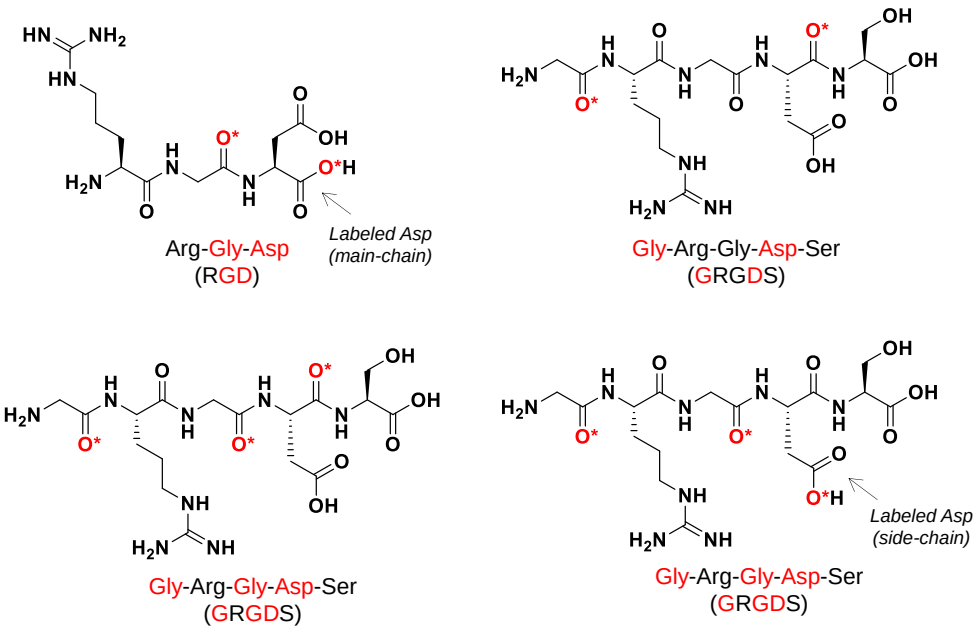

Figure 5.1: Targeted tri-peptide RGD and penta-peptides GRGDS labeled in ^{17}O/^{18}O at Gly and Asp (labeled at the main-chain or side-chain) units. Labeled amino acids are displayed in red colour, and the red oxygen atoms marked with asterisk correspond to the oxygen positions, which will be labeled with a given enrichment level. In the side-chain of Asp in the GRGDS peptide and in the main-chain of Asp in the RGD peptide, the label is equally distributed between both carboxylic oxygens (C=O and C-OH, 50:50).

5.1 SOLID PHASE ^{17}O/^{18}O-PEPTIDE SYNTHESIS (SPPS)

The synthesis of ^{17}O/^{18}O-labeled RGD and GRGDS peptides was performed at the SynBio3 platform in Montpellier,[20] which has the expertise in SPPS. On site, Pascal Verdié and Manon Maurel kindly provided me with the necessary training so I could prepare the targeted peptides. Yet, these non-labeled RGD and GRGDS peptides had not been previously synthesized at the SynBio3 platform, so all the reaction steps needed to be optimized prior to the synthesis of the ^{17}O/^{18}O-labeled molecules.

In general, the SPPS is composed of a series of rather simple steps, which lead to complex final products (peptides):

a) attachment of the first amino acid to the polymer beads,

b) peptide chain building by attaching amino acids to the growing peptide chain,

c) cleavage of the peptide chain from the polymer beads and side-chain deprotections,

d) purification and peptide isolation.

These steps are summarized in the Figure 5.2 and will be discussed in more detail in the following subsections.

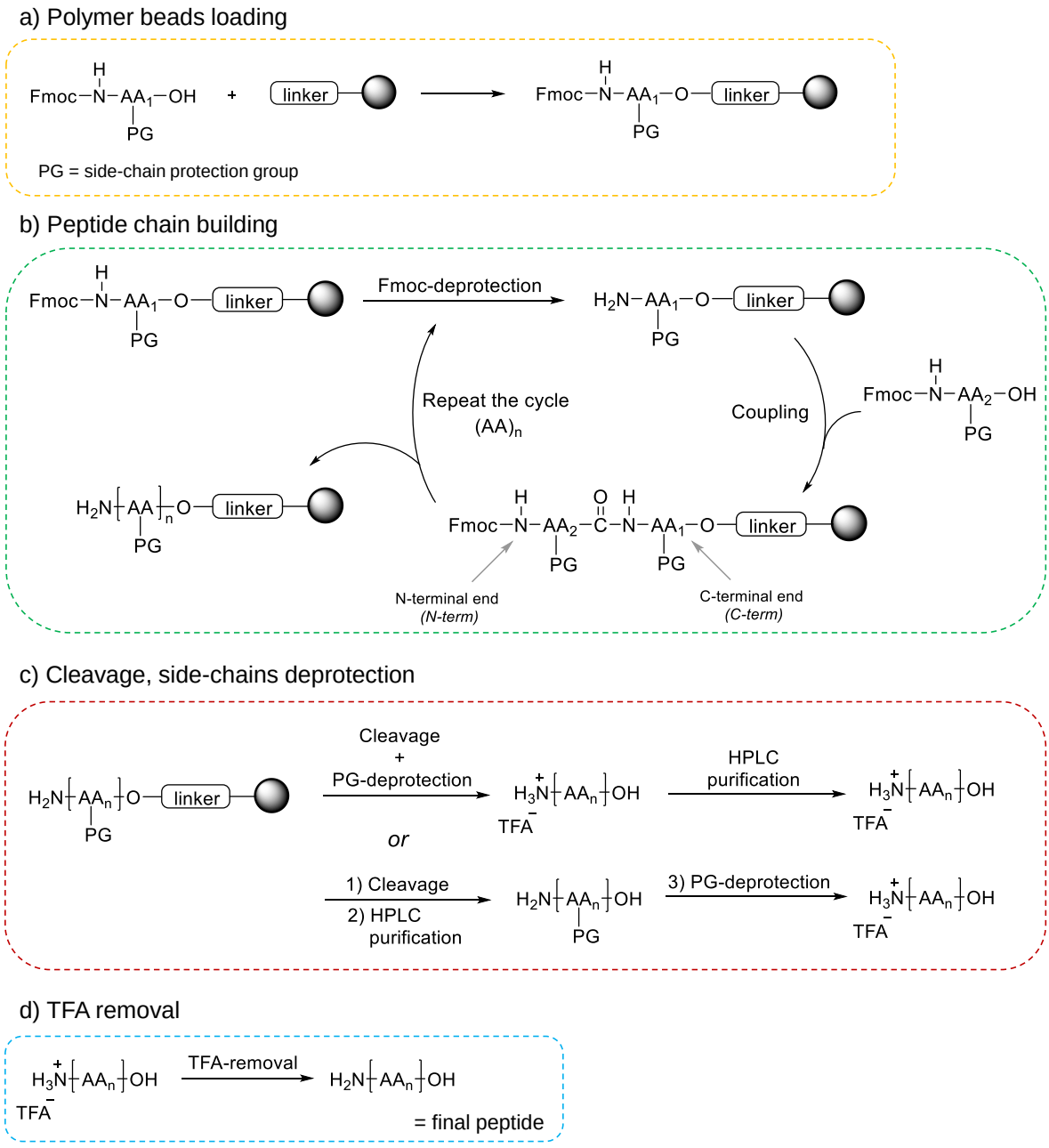

Figure 5.2: General scheme summarizing different parts of the peptide synthesis. a) Polymer beads loading, b) Peptide chain building on a solid-support, c) Cleavage of a peptide from a resin and side-chain deprotection, d) Removal of trifluoroacetate (TFA) ions (desalt procedure).

In the SPPS, a peptide chain is built on a solid-support (polymer beads) typically going from the C-terminal end (C-term, carboxylic group) to the N-terminal end (N-term, amine group) of the peptide *via* a sequence of deprotections and coupling steps of amino acids. Due to the presence of at least two reactive functions per amino acid (the amine and the carboxylic

groups, plus eventually functions on the side-chain), orthogonal protection is required in the SPPS protocols.[21] For the orthogonal protection in general, different protective groups with different resistance towards reaction conditions are used. This allows to selectively deprotect only one functional group in a molecule, while keeping the rest protected and therefore inert in the subsequent reactions. A Fmoc/*t*Bu orthogonal protection (Fmoc for the amine protection and *t*Bu for the side-chain protections) was employed here in the synthesis of RGD and GRGDS peptides, and more details will be provided later in this chapter.

Several aspects had to be thought through in view of the synthesis of the labeled peptides, such as the scale of the synthesis or the functionality on the C-terminal end of the targeted peptide. It was important to keep in mind that the scale of the synthesis will affect not only the mass of the isolated labeled peptide, but as well the amount of labeled reactants consumed. During SPPS, amino acid reactants are typically used in large excess (typically ~ 10 equivalents with respect to the peptide chain being built). Here, the targeted mass was 20 mg of pure labeled RGD and GRGDS peptides, and to achieve this value, the syntheses were performed at 0.1 mmol scale. Considering the high-cost of ^{17}O-labeled water, the equivalents of amino acid reactants were also reduced in the steps involving labeled precursors (compared to classical conditions employing non-labeled amino acids). Another important aspect was related to the enrichment level of the final products. Due to the strongly acidic conditions employed in the cleavage and deprotection steps during the synthesis, the loss of oxygen enrichment might have occurred, and this point had to be verified after isolation of the labeled peptides.

Considering the above mentioned specific aspects of the synthesis of ^{17}O/^{18}O-labeled peptides, the synthetic procedures were first designed and optimized on non-labeled compounds, and further adapted for the synthesis of ^{17}O/^{18}O-labeled molecules, using Fmoc-Gly-O*H and Fmoc-L-Asp(O*t*Bu)-O*H, which were pre-labeled in oxygen-^{17}O/^{18}O using mechanochemistry (synthesis described in the previous Chapter 4). The potential loss of enrichment level was first verified on the synthesis of ^{18}O-labeled peptides, before producing more expensive ^{17}O-labeled products.

5.1.1 Resin preparation

In SPPS, the peptide chain is built on a solid support composed of polymer beads, most frequently made of cross-polymerized polystyrene. The polymer beads will be referred to by the commonly used term “resin” from now onwards. The choice of the chemical functionality bonding the solid-support to the growing peptide chain will depend on the type of C-terminal

end (C-term) of the targeted peptide. The RGD and GRGDS peptides in this study contained a carboxylic acid function at the C-term. Therefore, a resin containing a 2-chlorotrityl chloride function was selected.

The use of 2-chlorotrityl chloride functionalized resin is advantageous for several reasons: *i)* the first amino acid can be attached easily *via* fast and racemization-free esterification under basic conditions (see Scheme 5.1a),[22] *ii)* the final peptide can be easily cleaved from the resin under mild acidic conditions, keeping the side chains protected for further purification (more details are provided in the following subsection 5.1.3), and *iii)* the sterical hindrance of the large trityl group prevents the formation of a diketopiperazine side-product during the Fmoc-deprotection step (Scheme 5.1b).[23]

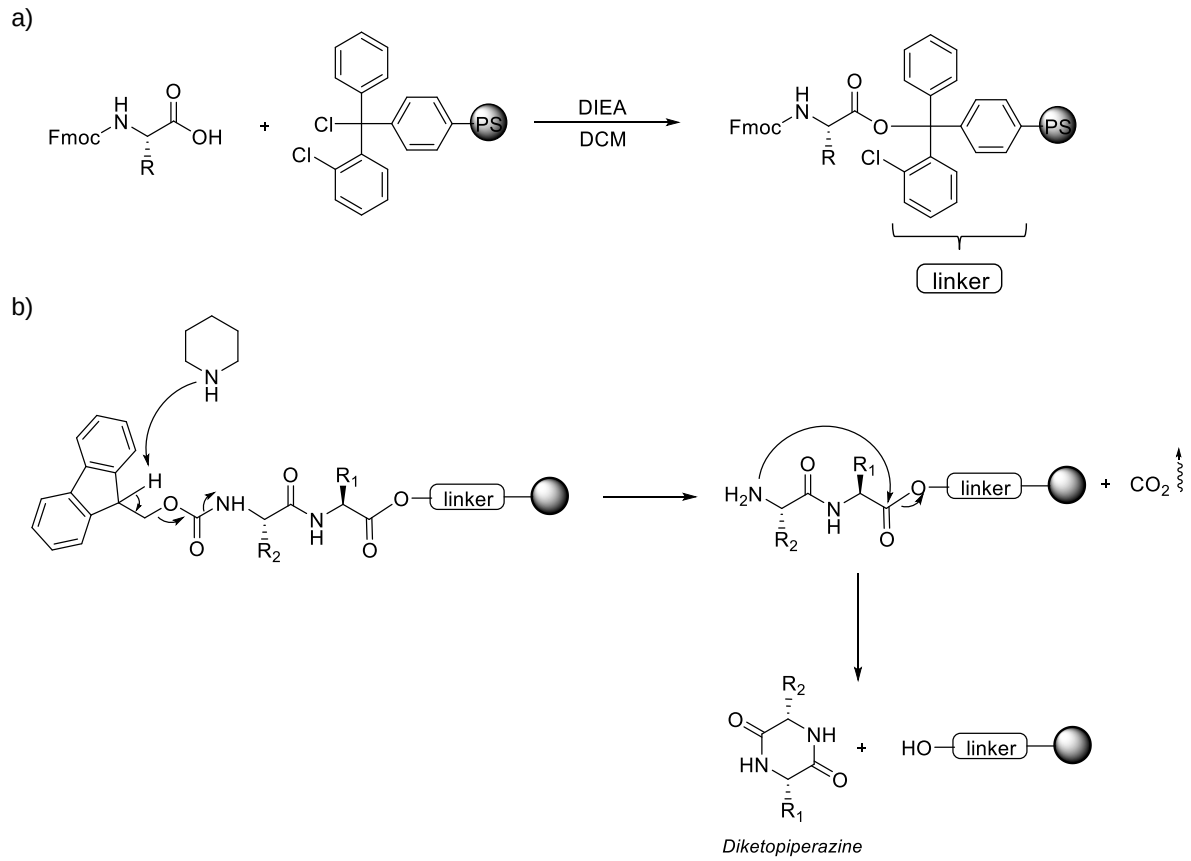

Scheme 5.1: a) Functionalization of 2-chlorotrityl resin with the first Fmoc-AA-OH under basic conditions (DIEA = *N*,*N*-diisopropylethylamine, DCM = dichloromethane, PS = polystyrene), b) Diketopiperazine formation during Fmoc-deprotection step of the second amino acid attached to the resin.

Here, four different resins functionalized with the first amino acid of the peptide chain were prepared: the non-labeled Fmoc-L-Asp(O*t*Bu)-O-2-chlorotrityl resin, the ^{17}O-labeled and ^{18}O-labeled Fmoc-L-Asp(O*t*Bu)-O*-2-chlorotrityl resins (for the non-labeled, ^{17}O-labeled and

^{18}O-labeled tri-peptides RGD), and the non-labeled Fmoc-L-Ser(*t*Bu)-O-2-chlorotrityl resin (for the penta-peptides GRGDS).

In practice, the non-labeled and the ^{17}O/^{18}O-labeled Fmoc-L-Asp(O*t*Bu)-O*-2-chlorotrityl resins were produced by reaction of non-labeled Fmoc-L-Asp(O*t*Bu)-OH or ^{17}O/^{18}O-labeled Fmoc-L-Asp(O*t*Bu)-O*H (1 eq.) with 2-chlorotrityl chloride resin (1 eq.) in dry dichloromethane (DCM) under basic conditions (*N*,*N*-diisopropylethylamine (DIEA), 4 eq.) during 2 - 4 hours at room temperature, providing 4.9 g of the non-labeled Fmoc-L-Asp(O*t*Bu)-O-2-chlorotrityl resin, and 0.4 g or 0.9 g of Fmoc-L-Asp(O*t*Bu)-O*-2-chlorotrityl resins labeled in ^{17}O or ^{18}O, respectively. The non-labeled Fmoc-L-Ser(*t*Bu)-O-2-chlorotrityl resin was produced by reaction of Fmoc-L-Ser(*t*Bu)-OH (1 eq.) with 2-chlorotrityl chloride resin (1 eq.) in dry dichloromethane (DCM) under basic conditions (DIEA, 4 eq.) during 2 hours at room temperature, providing 1.6 g of the non-labeled Fmoc-L-Ser(*t*Bu)-O-2-chlorotrityl resin. The loading (mmol of attached Fmoc-AA-OH per 1 g of the resin) of thus prepared resin was determined *via* absorbance measurements using a UV-Vis spectrometer, and it was typically ~0.5 - 0.6 mmol/g (value corresponded to the loadings typically obtained at the SynBio3 platform).[24]

A significant loss of loading (< 0.01 mmol/g instead of 0.6 mmol/g), which had a crucial impact on the amount of peptide produced, was observed for one of the resins, the Fmoc-L-Ser(*t*Bu)-O-2-chlorotrityl resin, when re-analysed after 3 months of storage. In general, the 2-chlorotrityl resins are known to be sensitive to humidity, which triggers their partial decomposition over time. However, the extent and rapidity of the decomposition observed here was surprising and was probably caused by inefficient drying of the prepared resin in the first place. Based on this experience, the resins used subsequently were either prepared fresh just before the peptide synthesis, or their loading was verified just before being engaged in a reaction. After careful drying procedure, the Fmoc-L-Ser(*t*Bu)-O-2-chlorotrityl resin was found to be stable for at least 4 weeks, as no loss of loading was observed for another batch, which was re-analysed after 1 month of storage.

5.1.2 Peptide chain building

As described in the previous subsection, the prepared resin already contains the first amino acid of the future peptide. In order to extend the peptide chain *via* coupling reaction with another amino acid and formation of a peptide bond, the amine group of the last amino acid attached to the resin first needs to be deprotected (see general scheme in Figure 5.2). Fmoc/*t*Bu orthogonal protection is one of the commonly used strategies and was employed here in the

synthesis of RGD and GRGDS peptides. In this strategy, the Fmoc-groups protecting the α-NH_2 functions are labile under basic conditions, whereas the side-chain protection groups (*t*Bu) are labile under strongly acidic conditions. The orthogonal protection enables to: *i)* keep the side chains protected, and thus inert, through the whole process of peptide chain building, *ii)* remove all the side chain protections simultaneously when the peptide is cleaved from the resin.

For the Fmoc-deprotection step, typically, a solution of mild base (secondary amine piperidine - noted here as pip) in an aprotic polar solvent (typically *N,N*-dimethylformamide, DMF) is used in excess in SPPS. At first, the acidic proton at the 9-position of fluorene ring system is removed by piperidine resulting in a stabilized carbanion. The lone pair then moves to the neighbouring carbon atom forming dibenzofulvene (DBF) intermediate and triggers elimination of carbon dioxide, leaving the amino acid deprotected. Finally, DBF reacts with piperidine resulting in a dibenzofulvene-piperidine adduct (Scheme 5.2a).[25]

When aspartic acid is present in the peptide chain, formation of an aspartimide side-product under the basic conditions used for Fmoc-removal can be observed (Scheme 5.2b). This side-reaction is prevalent in the peptides containing Asp-Gly, Asp-Asn or Asp-Ser sequences and is promoted at elevated temperatures.[26] To prevent the formation of this unwanted aspartimide side-product, an acidic reagent ethyl 2-cyano-2-(hydroxyimino)acetate (commercial name: Oxyma pure) was added to the Fmoc-removal solution (pip/DMF) reducing the pH of the reaction mixture during the deprotection step (Scheme 5.2a).[27]

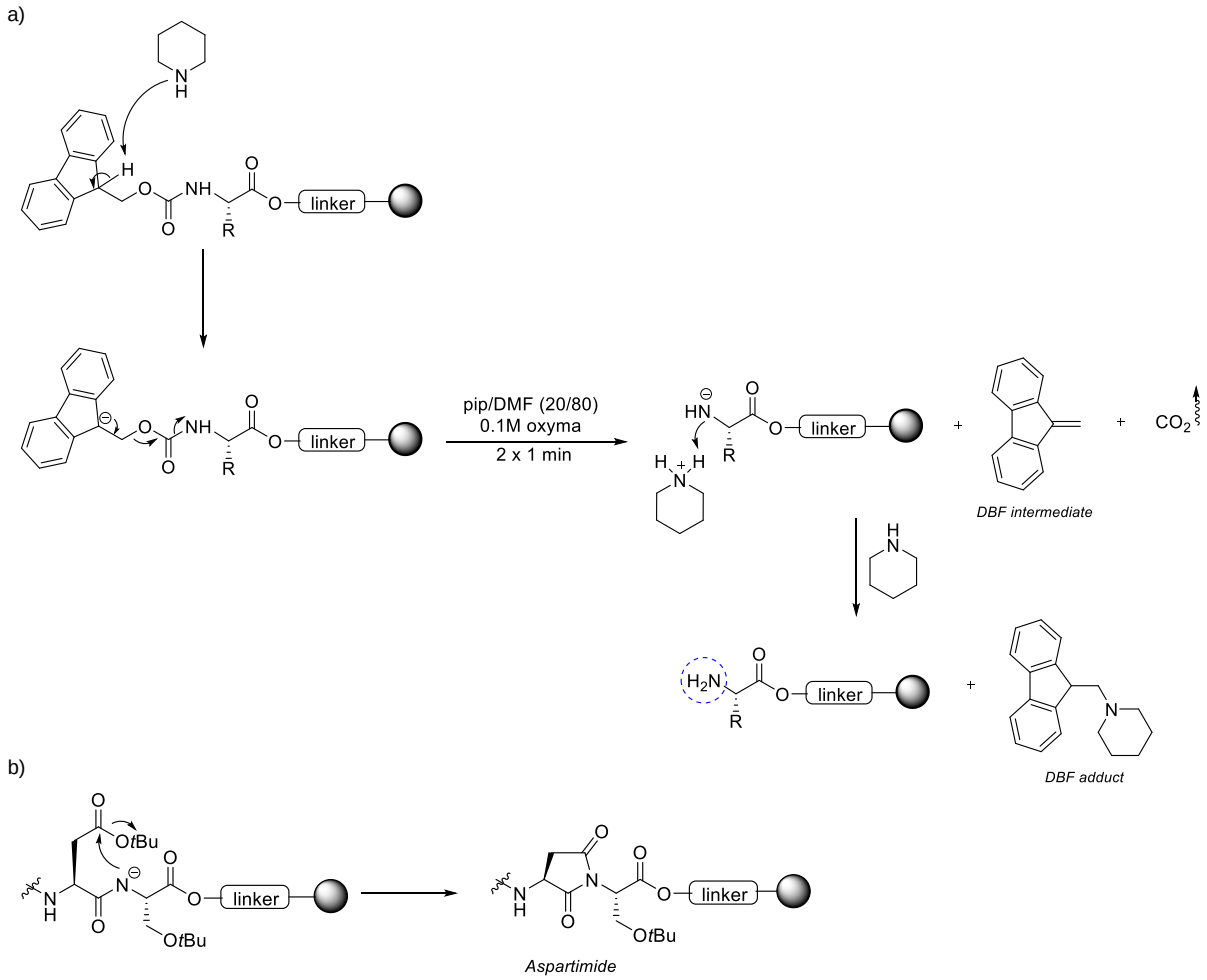

Scheme 5.2: a) Mechanism of the Fmoc-deprotection, DMF = dimethylformamide, DBF = dibenzofulvene, b) Mechanism of the unwanted aspartimide side-product formation during the Fmoc-deprotection step.

Based on the above, for the Fmoc-deprotection step, a solution of pip/DMF (20/80, V/V) containing Oxyma pure (0.1 M) was used here in the synthesis of non-labeled and $^{17}O/^{18}O$-labeled RGD and GRGDS peptides. The suspension was stirred at room temperature for 1 min. This step was performed twice. Under these conditions, no aspartimide formation was observed in the synthesis of RGD and GRGDS peptides.

Once the Fmoc-deprotection step achieved, then the coupling step can be performed to elongate the peptide chain. Under the standard coupling conditions used in SPPS, a solution of Fmoc-AA-OH in DMF is added to the resin (where AA corresponds to the amino acid added here to elongate the chain), followed by addition of an organic base (DIEA) and a solution of activation reagent, namely 1-[bis(dimethylamino)methylene]-1H-1,2,3-triazolo[4,5-b]pyridinium 3-oxid hexafluorophosphate (HATU) in DMF. The carboxylic function in the Fmoc-AA-OH added is first deprotonated by the base and then activated *via* reaction with

HATU. The ester thus formed then reacts with the free amine group of the last amino acid in the peptide attached to the resin forming a peptide bond (Scheme 5.3).

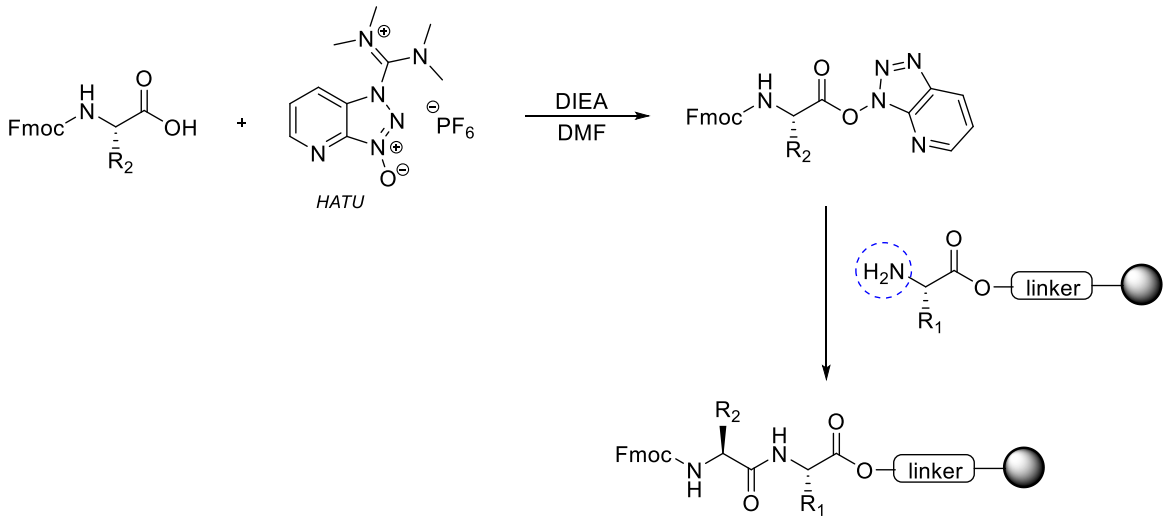

Scheme 5.3: Coupling reaction using HATU as an activating reagent.

Specifically, for the coupling of non-labeled arginine, excess of Fmoc-Arg(Pbf)-OH (5 eq.), DIEA (10 eq.) and HATU (5 eq.) was used in both RGD and GRGDS peptide syntheses (see Table 5.1). The equivalents were calculated with respect to the scale of the synthesis (here 0.1 mmol scale was used). The Arg-coupling step took 5 min and was performed twice. For the coupling of $^{17}O/^{18}O$-labeled amino acids (Gly and Asp), in order to limit the consumption of labeled species, the amount of $^{17}O/^{18}O$-labeled Fmoc-protected amino acids had to be reconsidered. For this reason, the amounts of reagents for the Gly and Asp-coupling steps were reduced by half to 2.5 equivalents of Fmoc-AA-O*H, 5 equivalents of DIEA and 2.5 equivalents of HATU. For the Asp-coupling, the reaction step took 5 min and was performed twice. For the glycine addition, to further reduce the amount of Fmoc-Gly-O*H consumed, the Gly-coupling step was typically done only once with the reaction time prolonged to 10 min (see Table 5.1). These conditions, described above, were finally applied on the synthesis of both, the GRGDS peptide (non-labeled and $^{17}O/^{18}O$-labeled) and the RGD peptide (only the non-labeled).

Table 5.1: Optimized reaction conditions of Fmoc-AA-OH coupling reactions (equivalents and time).

Peptide sequence	Asp Eq. / time	Acetylation[a]	Gly_1 Eq. / time	Acetylation[a]	Arg Eq. / time	Gly_2 Eq. / time
RG_1D	-	-	1x 2.5 eq. 1x 10 min	-	2x 5 eq. 2x 5 min	-
^{18}O-RG_1D	-	-	2x 2.5 eq. 2x 5 min	2x 5 mL 2x 0.5 min	2x 5 eq. 2x 5 min	-
^{17}O-RG_1D	-	-	2x 2.5 eq. 2x 5 min	-	2x 5 eq. 2x 5 min	-
G_2RG_1DS	2x 2.5 eq 2x 5min	2x 5 mL 2x 1 min	1x 2.5 eq. 1x 10 min	-	2x 5 eq. 2x 5 min	1x 2.5 eq. 1x 10 min
^{18}O-G_2RG_1DS	2x 2.5 eq 2x 5min	2x 5 mL 2x 1 min	1x 2.5 eq. 1x 10 min	-	2x 5 eq. 2x 5 min	1x 2.5 eq. 1x 10 min
^{17}O-G_2RG_1DS	2x 2.5 eq 2x 5min	2x 5 mL 2x 1 min	1x 2.5 eq. 1x 10 min	-	2x 5 eq. 2x 5 min	1x 2.5 eq. 1x 10 min
^{17}O-G_2RG_1DS	2x 2.5 eq 2x 5min	2x 5 mL 2x 1 min	2x 2.5 eq. 2x 5 min	-	2x 5 eq. 2x 5 min	1x 2.5 eq. 1x 10 min
$G_2RG_1D(OMe)S$	2x 2.5 eq 2x 5min	2x 5 mL 2x 1 min	1x 2.5 eq 1x 10 min	-	2x 5 eq. 2x 5 min	1x 2.5 eq. 1x 10 min

"Gly_1 (G_1)" and "Gly_2 (G_2)" represent the order in which Gly were coupled to the chain. [a] Acetic anhydride (Ac_2O)/DCM (50/50, V/V) mixture was used for acetylation capping step.

During the optimization of the reaction conditions for the synthesis of the GRGDS penta-peptide, it was observed that a small amount of Asp-deleted side-product (peptide chain with missing Asp unit, *i.e.* GRGS) formed as well, due to the incomplete Asp-coupling step (see Scheme 5.4), and this impurity could not be separated *via* HPLC purification. Although Fmoc-Asp(O*t*Bu)-OH had been used in excess (2.5 eq.), it is hypothesized that the sterical hindrance of *t*Bu protective groups caused, that not all free amino groups of serine reacted with Asp under these conditions, and thus remained available for the subsequent coupling reaction with Fmoc-Gly-OH. The formation of this Asp-deleted peptide was avoided by acylation of the remaining free amino groups of serine using an acetic anhydride (Ac_2O) solution, following the Asp-coupling reaction (Scheme 5.4). Although this additional acetylation reaction did not lead to the targeted peptide, the acetylated side-product was easier to remove than the Asp-deleted peptide GRGS.

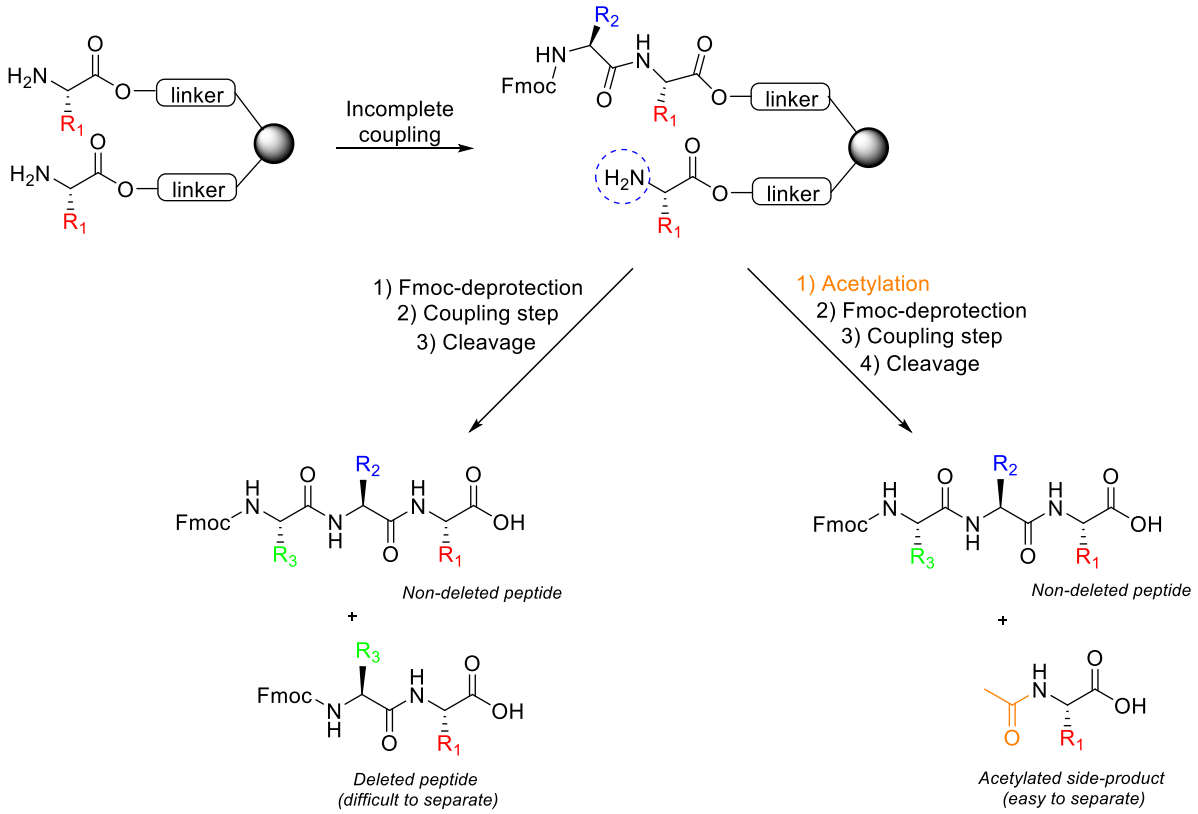

Scheme 5.4: Deleted peptide formation and its avoidance using an acetylation step. Cleavage procedure (releasing a peptide from the resin) will be discussed in more details in the following subsection 5.1.3.

In the synthesis of the shorter non-labeled RGD tri-peptide, no deleted peptide was observed. However, when the synthesis of ^{18}O-labeled RGD was attempted, using the same reaction conditions as for the non-labeled RGD, a side-product was observed in LCMS analysis of the peptide cleaved from the resin. This side-product was identified as Gly-deleted di-peptide (RD) and its amount was estimated by ^{1}H solution NMR to be 45 ± 5 %. In order to avoid its formation, in the future syntheses of labeled RGD, the Gly-coupling step was performed twice with 2.5 equivalents of ^{17}O/^{18}O-labeled Fmoc-Gly-O*H used in each step. Moreover, in the case of a new batch of ^{18}O-labeled RGD, an acetylation step was introduced following the Gly-coupling step. Despite these additional efforts, it was revealed by the HRMS analyses of the final ^{17}O/^{18}O-labeled RGD, that the formation of the Gly-deleted di-peptide RD was still not fully prevented (as will be discussed in more detail later in this chapter, subsection 5.1.5).

5.1.3 Cleavage of the peptide chain from the resin, side-chain deprotection and HPLC purification

Once the elongation of a peptide chain is complete, it needs to be cleaved from the solid-support to allow its subsequent purification and isolation. For the SPPS strategy described above, strongly acidic conditions are typically used to cleave the peptide from the resin. The

common cleavage cocktail consists of concentrated trifluoroacetic acid (TFA) with added scavengers, namely triisopropylsilane (TIS) and water. These scavengers can trap released carbocations and thus prevent formation of alkylated peptide side-products. The acid-labile protection groups are at the same time removed from the side-chains (see Scheme 5.5, red arrow). Alternatively, as already mentioned above, one of the advantages of using 2-chlorotrityl resin lies in its high acid-lability, which allows to cleave a peptide from the resin under mild acidic conditions without removing the protective groups of the peptide side-chains. Using this approach, the peptide is first isolated with the side-chains still protected for the subsequent steps (see Scheme 5.5, blue arrows).

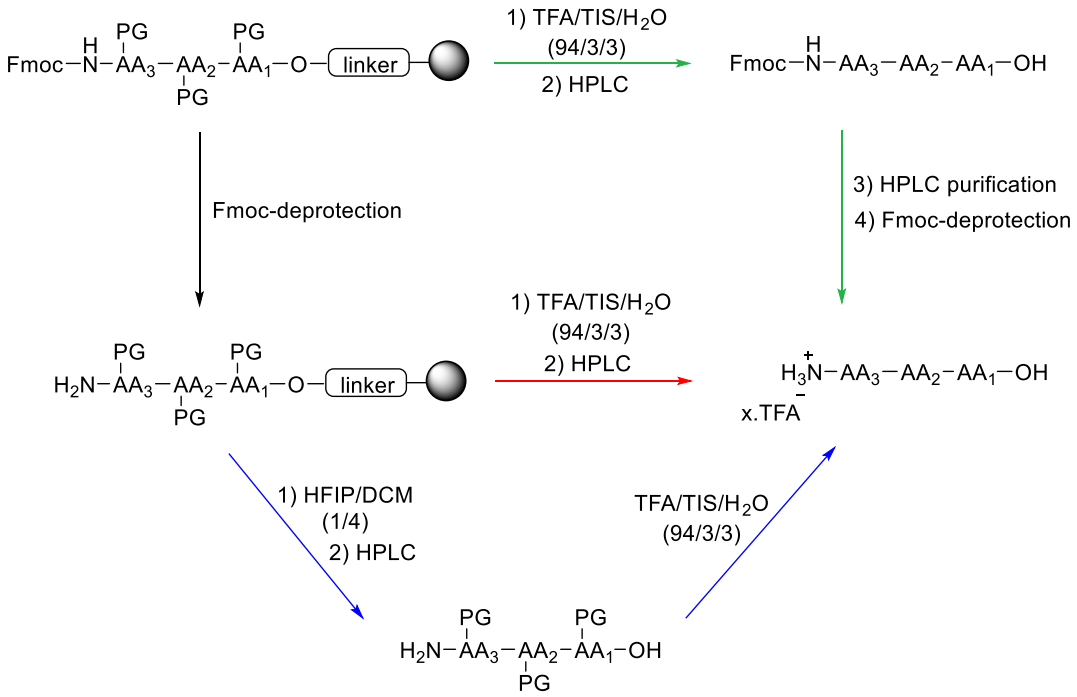

Scheme 5.5: General scheme of possible ways for a tri-peptide isolation. TFA = trifluoroacetic acid, TIS = triisopropylsilane, HFIP = 1,1,1,3,3,3-hexafluoro-2-propanol, DCM = dichloromethane, PG = side-chain protective group.

Here, due to a very short length of the RGD and GRGDS peptides, which are in addition composed of amino acids with polar side chains, the fully deprotected peptides obtained by classical cleavage using TFA/TIS/H_2O mixture were eluted together with the dead volume of the hydrophobic reverse-phase C18 column used for the preparative HPLC, thus making it impossible to purify the peptide (Scheme 5.5, red arrow strategy). Two different strategies for the isolation of pure RGD and GRGDS peptides were then tested:

I) On one hand, the last amino acid in the chain was kept Fmoc-protected (Scheme 5.5, green arrow strategy). The Fmoc-NH-peptide was then cleaved from the resin by stirring the

resin suspension in the conventional TFA/TIS/H_2O (94/3/3, V/V/V) mixture for 30 min at 38 °C. The side-chains were no longer protected in the cleaved peptide, but the remaining presence of Fmoc-protection at the N-terminal end was sufficient for a suitable retention of the peptide on the preparative HPLC column. Several different reaction conditions were then applied for the final Fmoc-deprotection in solution: excess of pip/DMF (20/80, V/V), excess of diethylamine (DEA) in DCM (1/9, V/V) or in DMF (DEA/DMF, 1/9, V/V), all stirred at room temperature for 1 h. Unfortunately, none of them provided a pure product without a need for additional purification. Such purifications were not attempted at this stage.

II) On the other hand, a cleavage procedure under mild-acidic conditions using a solution of 1,1,1,3,3,3-hexafluoro-2-propanol (HFIP) in dichloromethane (DCM) was tested (Scheme 5.5, blue arrow strategy). The resin suspension was stirred in the reaction mixture (HFIP/DCM, 1/4, V/V) at room temperature for 1 hour, producing a peptide with fully protected side-chains.[28] The presence of the side-chain protective groups enabled to purify the peptide by preparative HPLC. The isolated phases were analysed by LCMS analyses and revealed to be pure (> 98 %). In the following step, the purified peptide was dissolved in a solution of TFA/TIS/H_2O (94/3/3, V/V/V) mixture and its side-chains were deprotected within 30 min of stirring at 38 °C (see Scheme 5.5 - blue arrows). Altogether, this strategy led to the isolation of the pure fully deprotected non-labeled peptides (confirmed by LCMS), and was then employed as well for the synthesis of $^{17}O/^{18}O$-labeled RGD and GRGDS peptides.

Under the acidic conditions used for the side-chain deprotection (described above), the arginine side-chain and as well the amine group at the N-terminal end of the peptides remained partially protonated and the peptides were isolated as TFA salts containing ~ 0.4 - 2.4 equivalents of TFA per peptide chain. The amount of TFA was estimated by ^{19}F solution NMR with respect to trifluoroethanol (TFE) internal standard (see Table 5.2 in the next subsection).[29] For our study, due to the intended future application of labeled peptides towards the study of surface-interaction of peptide chains with inorganic biomaterials (*e.g.* hydroxyapatite or other calcium phosphates), the presence of another carboxylic acid-containing molecule, such as TFA, was unwanted. As a consequence, an additional purification step was implemented to remove the remaining TFA.

5.1.4 TFA removal

One of the possibilities to remove the TFA anions, which remain in close interaction with the peptide isolated after the side-chain deprotection step, is to flush the peptide-TFA salt solution on a polymer-supported quaternary ammonium resin, bearing bicarbonate counter ions HCO_3^- (Figure 5.3). The trifluoroacetate anions are retained by the quaternary ammonium ions on the column, while the TFA-free desalted peptides are eluted. The protonated bicarbonate ions then decompose into water and CO_2 molecules.[30]

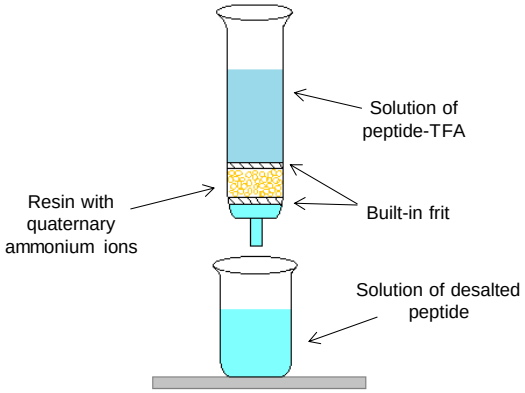

Figure 5.3: Desalting procedure for the removal of TFA anions using a syringe with a pre-packed quaternary ammonium resin.

Here, a commercial pre-packed *N,N,N*-trimethyl-1-phenylmethanaminium containing resin with bicarbonate counter ion (Vari-Pure IPE, loading 0.18 mmol/100 mg) was used for the TFA anions removal. For the non-labeled RGD and GRGDS peptides, at least 4 equivalent excess of quaternary ammonium ions per peptide were used (excess recommended by the resin provider), and the amount of residual TFA anions after desalt procedure was estimated by ^{19}F solution NMR analyses, compared to the trifluoroethanol (TFE) internal standard (Figure 5.4).[29]

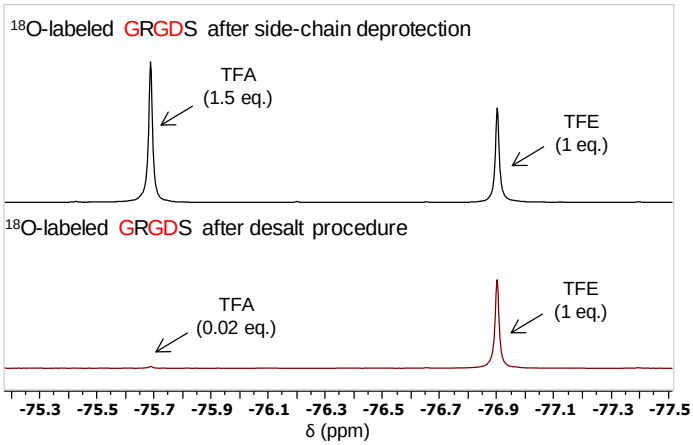

Figure 5.4: Example of TFA-salt quantification using ^{19}F solution NMR spectra of ^{18}O-labeled GRGDS penta-peptide before (1.5 eq. TFA) and after (0.02 eq. TFA) desalt procedure.

As evident from the results summarized in Table 5.2, the resin was highly efficient in removing the TFA anions (typically < 0.1 equivalents of TFA anions remained). On the other hand, the mass of desalted peptide obtained was lower than theoretically expected (see Table 5.2). This can be possibly explained by a strong interaction between the ammonium ions on the resin and the carboxylate functions in the aspartic acid side-chains, resulting in partial retention of the peptide on the column, which caused a low yield of the desalt step (*e.g.* only 23% desalt yield for non-labeled RGD). In order to avoid a substantial loss of labeled peptides, the excess of active ammonium sites was reduced to ~ 2 equivalents per peptide. Under these conditions, the resin remained its high efficiency and the desalt yield increased (*e.g.* from 23 % to 53 % for the RGD and from 56 % up to 80 % for the GRGDS).

Overall, the desalt procedure provided the final peptides containing less than 0.1 equivalents of TFA anions per peptide chain, which poses no problems for the future scientific goals of our group. The purity of isolated desalted peptides was also confirmed by LCMS analyses, as shown in Annexe V.

Table 5.2: Summary of the conditions and results of the desalt procedure for RGD and GRGDS peptides.

Peptide sequence	Quaternary ammonium ions (eq.)[a]	TFA eq. before desalt[b]	TFA eq. after desalt[b]	Initial peptide-TFA mass	Peptide mass expected[c]	Peptide mass obtained	Desalt yield[d]
RGD	4.2	0.4	0.05	44 mg	39 mg	9 mg	23 %
^{18}O-RGD	1.6	2.4	0.35	57 mg	32 mg	24 mg	75 %
^{17}O-RGD	1.8	2.0	0.01	50 mg	30 mg	16 mg	53 %
GRGDS	5.0	1.0	0.20	48 mg	39 mg	22 mg	56 %
^{18}O-GRGDS	2.5	1.5	0.02	47 mg	34 mg	21 mg	62 %
^{17}O-GRGDS	2.1	1.0	0.01	56 mg	45 mg	27 mg	60 %
^{17}O-GRGDS	2.3	2.2	0.01	53 mg	35 mg	28 mg	80 %
GRGD(OMe)S	7.5	0.6	0.01	19 mg	17 mg	11 mg[e]	65 %

[a] Equivalents of quaternary ammonium ions with respect to 1 eq. of a peptide chain, [b] TFA eq. with respect to 1 eq. of peptide chain, [c] TFA mass (estimated from ^{19}F solution NMR) was subtracted from the initial peptide-TFA salt mass, [d] yield of the desalt procedure, [e] partial removal of methyl ester protective group observed in LCMS.

5.1.5 Isolated products

All reaction steps described in previous sections were at first optimized and applied on the synthesis of non-labeled RGD and GRGDS peptides. These were isolated in moderate to high yield: 22 % for the RGD (9 mg) and 45 % for the GRGDS (22 mg) (see Table 5.3). Indeed, the typical SPPS-yield of short polar peptides is in general around 30 %. Regarding their purity, both peptides were obtained pure according to LCMS analyses (> 98 %). However, for the non-

labeled RGD, small amounts of grease and other unidentified impurities were detected by ^{1}H and ^{13}C solution NMR (see Annexe V).

Table 5.3: Summary table with isolated yields and enrichment levels of RGD and GRGDS peptides.

Product	Isolated mass/yield	$^{17}O/^{18}O$-EL[a]
RGD	9 mg / 22 %	-
^{18}O-RGD	16 mg[b]	-
^{17}O-RGD	24 mg[c]	-
GRGDS	22 mg / 45 %	-
^{18}O-GRGDS	20 mg / 41 %	43 %
^{17}O-GRGDS	27 mg / 55 %	38 %
^{17}O-GRGDS	28 mg / 57 %	39 %

[a]Average $^{17}O/^{18}O$-enrichment level per labeled carbonyl groups, [b] ^{18}O-labeled RGD contained 30 ± 5 % of Gly-deleted RD di-peptide (estimated from ^{1}H solution NMR) and ~ 0.35 eq. of TFA salt (estimated from ^{19}F solution NMR), [c] ^{17}O-labeled RGD contained 23 ± 5 % of Gly-deleted RD di-peptide (estimated from ^{1}H solution NMR).

Regarding the *enriched RGD* compounds, unfortunately, HRMS analyses of the final isolated $^{17}O/^{18}O$-labeled products surprisingly revealed that these labeled species are contaminated with the Gly-deleted (RD) by-products. The amount of RD di-peptide was estimated from ^{1}H solution NMR analyses, as 30 ± 5 % of RD in ^{18}O-labeled RGD and 23 ± 5 % of RD in ^{17}O-labeled RGD. Due to this high contamination, the enrichment level of $^{17}O/^{18}O$-labeled RGD products was not calculated at this stage.

The presence of Gly-deleted di-peptide in the labeled RGD compounds was unexpected for several reasons: *i)* No Gly-deleted peptide had been observed in the synthesis of non-labeled RGD, where only 1x 2.5 equivalents of Fmoc-Gly-OH excess had been used in the Gly-coupling reaction. *ii)* For the $^{17}O/^{18}O$-labeled RGD, the reaction conditions had been further modified to avoid Gly-deleted peptide formation. More specifically, 2x 2.5 equivalents of Fmoc-Gly-O*H were used, and the acetylation capping step was introduced following Gly-coupling (for ^{18}O-labeled RGD). *iii)* All the LC analyses performed on the labeled RGD intermediates (*i. e.* side-protected products after HPLC purification, side-deprotected products and desalted products) had shown only one peak (Figure 5.5a). However, based on the results of the HRMS data recorded on the final products, retrospectively for all steps, all the lower-resolution MS data obtained during the synthesis of $^{17}O/^{18}O$-labeled RGD were then re-analysed more closely. In doing so, it appeared that the Gly-deleted di-peptide could have been detected much sooner. Due to the rather complicated MS pattern of enriched species, which was not

fully resolved under the routine LCMS conditions used at the SynBio3 platform, the peak at 599.3 m/z had been firstly mistakenly assigned to the monoisotopic mass of the targeted peptide fragment RGD, with Asp being deprotected (Figure 5.5b). This deprotection is indeed commonly observed in MS spectra of protected peptides and results from the fragmentation of the analysed molecule during the analysis. However, the small peak at 598.3 m/z had been overlooked. This peak actually corresponds to the monoisotopic mass of the fully protected H-Arg(Pbf)-Asp(O*t*Bu)-OH di-peptide (with a deleted Gly fragment), and only appears clearly in higher resolution MS analyses (Figure 5.5c).

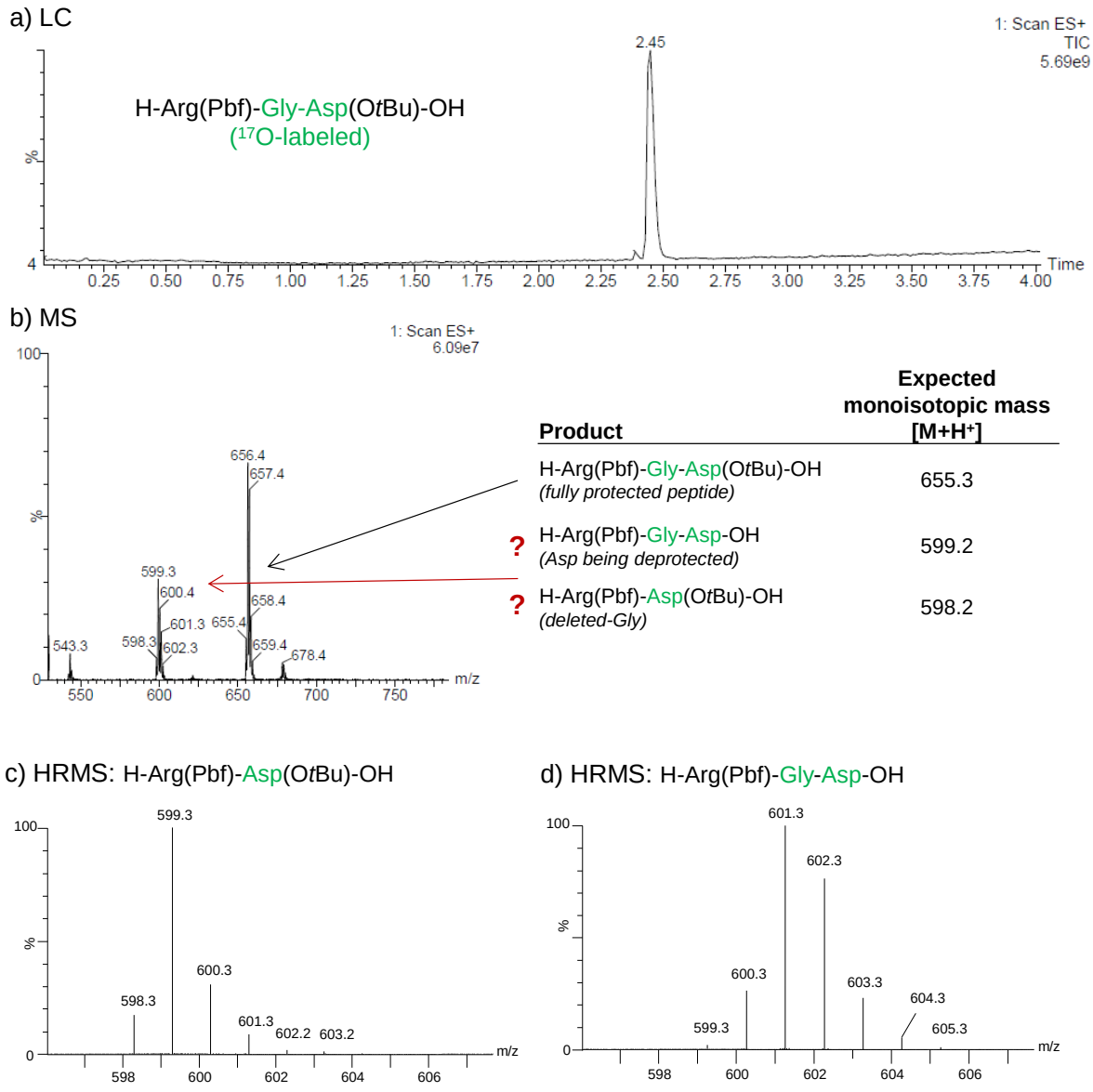

Figure 5.5: a) LC analysis of fully protected HPLC purified ^{17}O-labeled RGD, b) MS (ESI$^+$) spectrum associated to the compound eluted at 2.45 min retention time and table with possible products and their monoisotopic masses, c) high-resolution MS (ESI$^+$) spectrum of Gly-deleted side-product, d) high-resolution MS (ESI$^+$) spectrum of the Asp-deprotected species. Pbf is a side-chain protective group (2,2,4,6,7-pentamethyldihydrobenzofuran-5-sulfonyl).

Based on the analyses of the final $^{17}O/^{18}O$-labeled RGD compounds, it can be concluded that neither doubling the amount of Fmoc-Gly-O*H used for the coupling, nor introducing acetylation capping step, avoided the Gly-deleted RD peptide formation. However, since the Gly-deleted RD content in ^{17}O-labeled RGD decreased when 2x 2.5 equivalents of Fmoc-Gly-O*H were used (from 45 ± 5 % to 23 ± 5 %), it is probable, that further increasing of the Fmoc-Gly-O*H excess and prolonging the coupling reaction time could solve this problem. However, it would also mean consuming more costly ^{17}O-labeled Fmoc-Gly-O*H. Moreover, since no Gly-deleted RD peptide had been observed initially, when non-labeled RGD was synthesized using only 2.5 equivalent excess of Fmoc-Gly-OH, this unwanted by-product formation may also be linked to other factors, such as the quality of the resin prepared using pre-labeled Fmoc-L-Asp(O*t*Bu)-O*H compounds. At this point of the study, additional investigations would be necessary to provide a final conclusion on the formation of undesired Gly-deleted di peptide.

Regarding the *enriched GRGDS* compounds, the $^{17}O/^{18}O$-labeled GRGDS peptides were also isolated pure (LCMS: > 98 %) and in high yields: 41 % (20 mg) for the ^{18}O-labeled GRGDS, and in average 56 % (28 mg) for the two ^{17}O-labeled species (Table 5.3). A complete structural assignment of ^{1}H and ^{13}C solution NMR signals of GRGDS penta-peptide was performed using data recorded for the ^{18}O-labeled GRGDS (see Annexe V). Based on the HRMS results (see Figure 5.6b,c), the average enrichment level of labeled carbonyl oxygens remained the same as in the starting Fmoc-protected amino acids: ~ 43 % for the ^{18}O-labeled GRGDS, ~ 38 % for the ^{17}O-labeled GRGDS and ~ 39 % for the ^{17}O-labeled GRGDS, enriched selectively only at the aspartic and the last glycine carbonyl functions (Table 5.3). Using the oxygen isotope composition calculated from the measured MS spectra, the MS patterns of ^{17}O-labeled GRGDS compounds were simulated using program IsoPro 3.1. The simulated patterns are shown in Figure 5.6b,c, and they match the experimentally recorded MS spectra. From this comparison it can be concluded, that the calculated enrichment level is correct. Moreover, the high $^{17}O/^{18}O$-enrichment levels achieved demonstrate, that the amino acids labeling protocols (described in the Chapter 4) are fully suitable for the preparation of ^{17}O-labeled peptides, and their subsequent application in ^{17}O NMR studies.

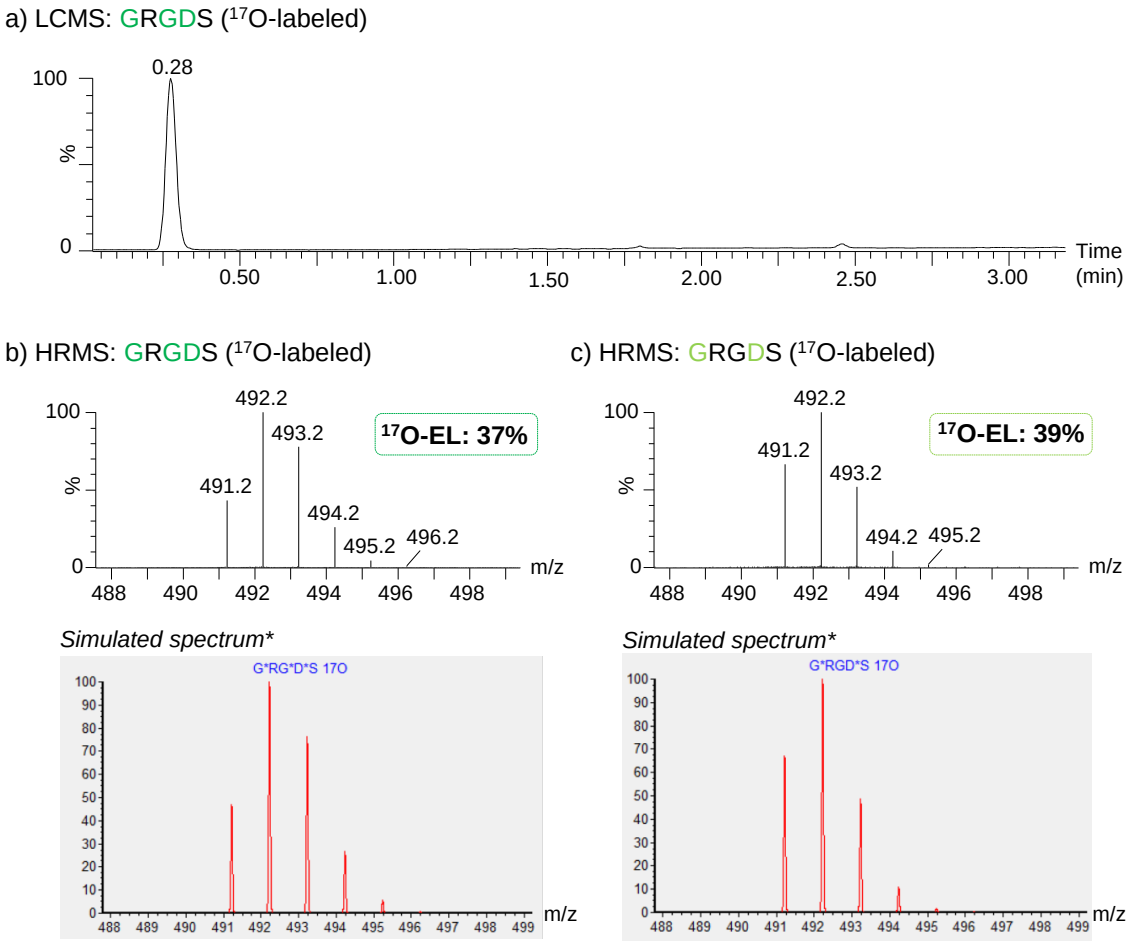

Figure 5.6: a) LC analyses of ^{17}O-labeled GRGDS, b) HRMS (ESI$^+$) spectrum of ^{17}O-labeled GRGDS compared to the simulations of corresponding MS pattern, c) HRMS (ESI$^+$) spectrum of ^{17}O-labeled GRGDS (labeled only on one Gly) compared to the simulation of corresponding MS pattern. *Simulations of the MS patterns were performed using program IsoPro 3.1, ^{17}O-EL = average enrichment level of labeled carbonyls (using 90% ^{17}O-enriched water).

5.1.6 GRGDS peptide ^{17}O/^{18}O-labeled at the aspartic acid side chain

Using the labeled Fmoc-L-Asp(O*t*Bu)-O*H for the synthesis of labeled GRGDS peptide (as discussed in the previous sections) only allows the carbonyl oxygen in the peptide back-bone chain to be labeled. Nevertheless, it is the *side-chain* carboxylic function which interacts more with the surrounding environment. The synthesis of GRGDS peptide labeled at the side-chain of aspartic acid is therefore of high interest. An alternative synthetic pathway was looked into here to achieve this goal, and first steps were carried out.

As already mentioned in the introduction of this chapter, a procedure for selective labeling of aspartic acid side-chain in Ac-Arg-Gly-Asp-NH_2 had been published in the literature, where the tri-peptide was synthesised by SPPS using Boc/Bzl orthogonal protection, and then enriched in ^{17}O *via* saponification of the benzyl ester of the aspartic acid side-chain of the peptide still attached to the resin.[19] Off note, this saponification had been performed in

solution (absolute MeOH) using 4.7 equivalents of $H_2{}^{17}O$ (10 % ^{17}O-enriched). An alternative strategy was developed here. The idea was to use non-labeled Fmoc-L-Asp(OMe)-OH instead of Fmoc-L-Asp(O*t*Bu)-OH, which should allow the non-labeled GRGD(OMe)S peptide with a methyl ester side-chain to be prepared by SPPS. The methyl ester installed on the side-chain of aspartic acid could be then saponified by ball-milling with sodium ethoxide and $^{17}O/^{18}O$-labeled water, thereby introducing the labeled oxygen selectively in the side-chain of the aspartic acid (Scheme 5.6).

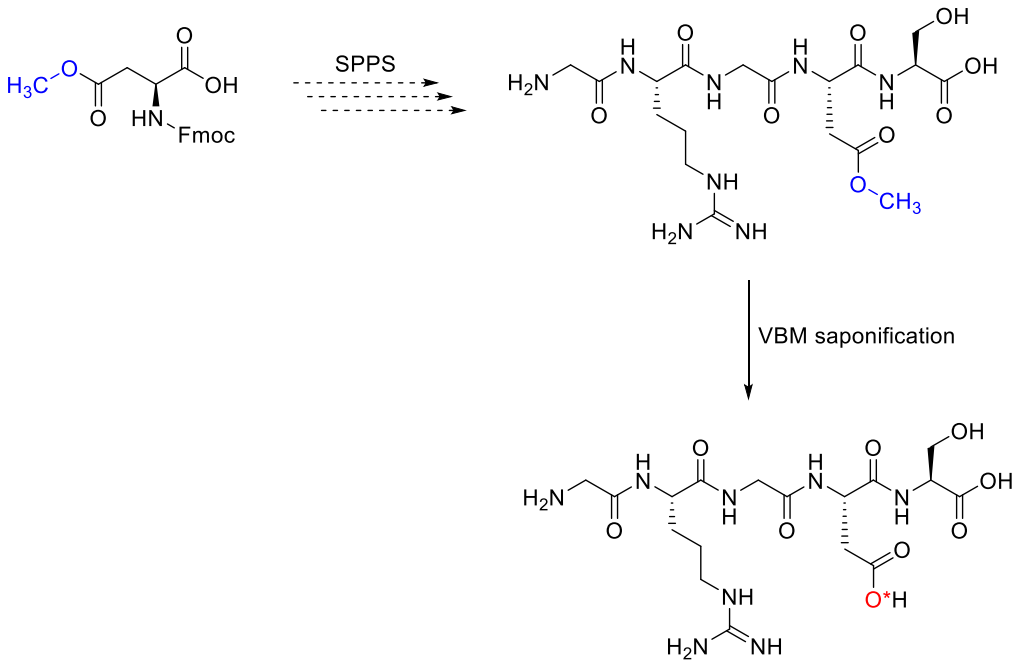

Scheme 5.6: General scheme showing the synthetic approach for GRGDS peptide selectively $^{17}O/^{18}O$-labeled at the side-chain of the aspartic acid. The label is equally (50:50) distributed between both oxygens in the side-chain carboxylic function of Asp (*i.e.* C=O* and C-O*H).

However, in order for this procedure to work, two points needed to be verified. First, the methyl ester protection had to last throughout the whole peptide synthesis procedure, and second, the peptide chain needed to survive the mechanochemical saponification conditions.

Regarding the first point, a pilot SPPS synthesis was performed using identical steps as described above for the GRGDS synthesis, yet with Fmoc-L-Asp(OMe)-OH instead of Fmoc-L-Asp(O*t*Bu)-OH for the Asp-coupling step. The methyl ester protective group was found to be stable under the mild basic conditions used in SPPS for the Fmoc-deprotection steps (pip/DMF/0.1M Oxyma pure (20/80, V/V), room temperature, 2x 1 min, 8 Fmoc-deprotection cycles in total). Fortunately, it was also stable under acidic conditions used for the cleavage (HFIP/DCM (1/4, V/V), room temperature, 2x 30 min), the side-chain deprotection step (TFA/TIS/H_2O (94/3/3, V/V/V), 30 min, 38 °C) and also throughout the TFA removal

procedure (using resin bearing quarternary ammonium cations with bicarbonate anions). The final peptide protected only at the aspartic acid side-chain was isolated pure and will therefore be used in the near future for the subsequent trial saponification.

Overall, up to now, this alternative procedure remains an attractive possibility to prepare side-chain $^{17}O/^{18}O$-labeled GRGDS peptides. Yet, the stability of the peptide chain upon mechanochemical saponification treatment still needs to be verified before the final conclusion can be made. However, based on the results of the published work,[19] we remain optimistic.

5.2 Solid-state NMR analyses of ^{17}O-labeled RGD and GRGDS peptides

The ^{17}O-labeled RGD and GRGDS peptides prepared in this study were characterized by ^{13}C and ^{17}O solid-state NMR at 14.1 T (Figure 5.6). In the recorded ^{13}C CPMAS spectra, broad and poorly resolved signals were observed due to the amorphous nature of the lyophilized peptide samples (Figure 5.7a). In the ^{13}C CPMAS spectra of the shorter tri-peptide RGD (contaminated with ~ 23 % of the di-peptide RD) two resonances were resolved between 190 - 160 ppm, whereas for the GRGDS and Gly-selectively labeled GRGDS penta-peptides (recorded under identical conditions) only one broad resonance was observed, representing all different overlapping carbonyl and carboxyl groups in the penta-peptide structure. The resonance located at ~ 158 ppm in all three spectra then corresponds to the quaternary carbon of the guanidine group in arginine, and the peaks between 70 - 15 ppm represent the remaining aliphatic carbons in the respective peptide chains (Figure 5.7a).

Regarding ^{17}O NMR, MAS spectra could be recorded in just a few hours for both types of peptides (Figure 5.7c). No features characteristic for quadrupolar lineshapes were observed for both types of peptides. Instead, all recorded spectra showed broad resonances, which correspond to different overlapping oxygen sites, *i.e.* two or three depending on the studied sample. Also here, the broad signals are not surprising for the amorphous lyophilized samples, and their shape is comparable with other ^{17}O-labeled lyophilized peptides reported in the literature.[31] The chemical shift range of this broad resonance also corresponds to the region expected for carbonyls in secondary amides. This is illustrated in Figure 5.7d, where ^{17}O NMR spectrum of GRGDS penta-peptide is compared to the simulated spectra of two secondary amides: acetanilide (Amide A) and *N*-methylbenzamide (Amide B).[32]

In the previously published studies of other ^{17}O-labeled peptides, typically only one amino acid in the peptide was labeled, which enabled to fit the spectrum and extract oxygen parameters.[6-7, 31, 33] Here, due to the overlapping sites, such deconvolution was not attempted.

However, comparing all three spectra and mainly looking at the decrease in relative intensity of the high-frequency contribution in the GRGDS signal (indicated with an arrow, Figure 5.7c), this part can be tentatively assigned to the carbonyl in labeled Gly units.

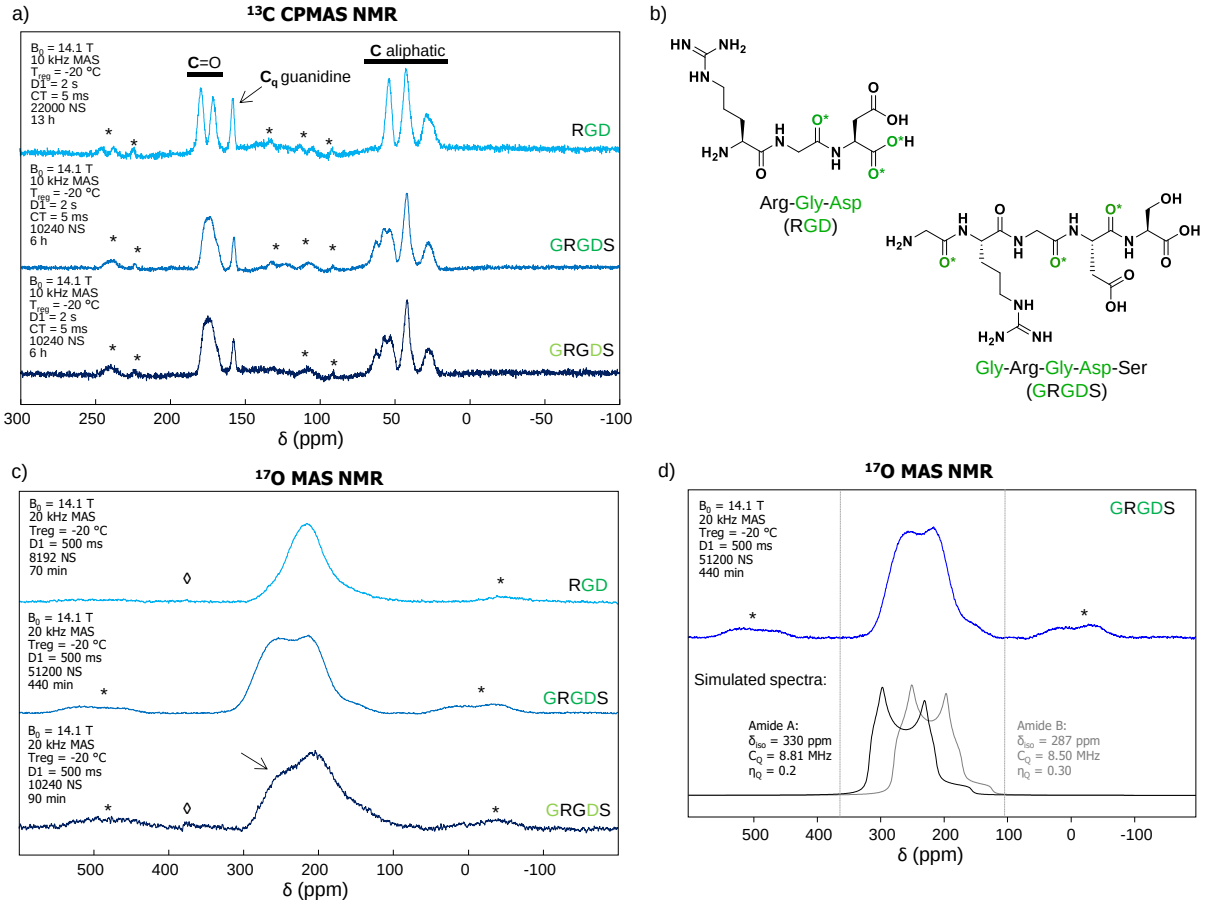

Figure 5.7: a) ^{13}C CPMAS NMR spectra of ^{17}O-labeled RGD (contaminated with RD di-peptide, 23 ± 5%), GRGDS and Gly-selectively labeled GRGDS peptides, b) Chemical structures of RGD and GRGDS peptides. Only one carboxylic oxygen was enriched in the ending carboxylic function of RGD, but globally the label is distributed between both C=O* and C-O*H sites (50 : 50). c) ^{17}O MAS NMR spectra of ^{17}O-labeled RGD (contaminated with RD di-peptide, 23 ± 5%), GRGDS and Gly-selectively labeled GRGDS peptides, line broadening (LB = 50) was applied on all three spectra, average ^{17}O-EL ~ 38 % per labeled carbonyl, d) Simulated spectra of secondary amides (Amide A = acetanilide, Amide B = N-methylbenzamide)[32] compared to the recorded ^{17}O MAS NMR spectrum of ^{17}O-labeled GRGDS.

CONCLUSION

The development of efficient $^{17}O/^{18}O$-labeling protocols of amino acids based on mechanochemistry, together with the successful scalability of these procedures, have enabled to prepare $^{17}O/^{18}O$-labeled short peptides: RGD and GRGDS. These peptides were synthesized manually by SPPS using Fmoc/*t*Bu strategy at the SynBio3 platform in Montpellier.

Regarding the shorter tri-peptide RGD, only the non-labeled product was obtained pure (LCMS, > 98%). Indeed, the synthesis of $^{17}O/^{18}O$-labeled RGD provided impure products contaminated with Gly-deleted di-peptide (RD) by-product. The reason for the presence of this by-product could not be fully understood and explained yet, and additional experiments are required.

The GRGDS peptides were all isolated pure (LCMS: > 98 %) and with high yields (> 40 %, 20 - 28 mg; for details of the masses and yields see Table 5.3). The average enrichment level of labeled carbonyls was calculated based on HRMS analyses of the final isolated compounds and reached ~ 43 % and ~ 38 %, for the ^{18}O-labeled and ^{17}O-labeled species, respectively. These obtained enrichment levels correspond to the enrichment levels of the labeled Fmoc-AA-O*H reactants, which confirms that no loss of enrichment occurred during the peptide synthesis. The overall time required for the synthesis and isolation of one pure labeled peptide was one week. In terms of the cost of the ^{17}O-labeled GRGDS peptides, altogether, only 113 µL of 90% ^{17}O-enriched water was involved in the preparation of the ^{17}O-labeled Fmoc-AA-O*H reactants used in the synthesis of both ^{17}O-labeled GRGDS and GRGDS peptides. The cost of the ^{17}O-labeled water, as the most expensive reagent (1800 - 2900 €/1g of 90% ^{17}O-water compared to ~ 5 - 30 €/1 g of the other reagents), was ~ 230 € for 55 mg of ^{17}O-labeled peptides isolated. This is seven times less than the cost of the same amount of commercially available non-labeled GRGDS peptide (≥ 97% purity, Sigma Aldrich).

Compared to the recombinant protein expression approach, where all identical amino acids of the peptide chain are necessarily labeled in the final peptide sequence, using SPPS enables to prepare peptide chains selectively labeled at only the chosen amino acid units, which makes the future assignments of ^{17}O signals easier. Here, RGD and GRGDS were prepared in a cost-efficient manner, but their short length and polar side-chains implied that extra steps had to be implemented, thereby prolonging the time for preparation and potentially reducing the yields. Further elongating the peptide sequence with two/three non-polar residues might already be sufficient to simplify the isolation and purification process. Alternatively, the extra steps

could be avoided using optimized conditions for purification of short polar peptides by preparative HPLC, however, such optimization was not possible at the SynBio3 platform.

Two ^{17}O-labeled GRGDS peptides (namely GRGDS and GRGDS), and the impure RGD compound were for the first time analysed by ^{17}O solid-state NMR spectroscopy. The average enrichment level achieved here (~ 38 % per labeled carbonyl oxygen) is completely sufficient for the intended ^{17}O NMR studies. Indeed, it corresponds to the mean value of the ^{17}O-enrichment levels of peptides studied by ^{17}O NMR in the literature (^{17}O-EL being typically 15 - 60 %).[7, 33-34] However, thanks to the efficient enrichment scheme leading to ^{17}O-labeled Fmoc-AA*-OH reactants, the enrichment level ~ 38 % was reached here in significantly shorter time (< 4 hours compared to ~ 24 hours), and with more than a half lower price, compared to the published studies.[35-36] Due to the presence of multiple labeled oxygen sites within a peptide, their resonances were overlapping and could not be resolved at 14.1 T. However, additional analyses at higher-field, which can provide higher resolution, are planned. Another way to simplify the assignment, would be to prepare GRGDS and RGD peptides selectively labeled only at one amino acid.

The preparation and ^{17}O NMR characterization of the ^{17}O-labeled RGD and GRGDS peptides was a first step and a pre-requisite for their future application in the study of their interactions with biologically-relevant species using ^{17}O solid-state NMR spectroscopy, and in the investigation of their structural and functional roles when present in proteins such as those involved in bio-mineralization processes.

REFERENCES

1. Craik, D. J.; Fairlie, D. P.; Liras, S.; Price, D., The Future of Peptide-based Drugs. *Chem. Biol. Drug. Des.* **2013,** *81* (1), 136-147.
2. Levin, A.; Hakala, T. A.; Schnaider, L.; Bernardes, G. J. L.; Gazit, E.; Knowles, T. P. J., Biomimetic peptide self-assembly for functional materials. *Nat. Rev. Chem.* **2020,** *4* (11), 615-634.
3. Chekmenev, E. Y.; Waddell, K. W.; Hu, J.; Gan, Z.; Wittebort, R. J.; Cross, T. A., Ion-Binding Study by 17O Solid-State NMR Spectroscopy in the Model Peptide Gly-Gly-Gly at 19.6 T. *J.Am.Chem.Sc.* **2006,** *128* (30), 9849-9855.
4. Yamauchi, K.; Okonogi, M.; Kurosu, H.; Tansho, M.; Shimizu, T.; Gullion, T.; Asakura, T., High field 17O solid-state NMR study of alanine tripeptides. *J. Mag. Reson.* **2008,** *190* (2), 327-332.
5. Paulino, J.; Yi, M.; Hung, I.; Gan, Z.; Wang, X.; Chekmenev, E. Y.; Zhou, H.-X.; Cross, T. A., Functional stability of water wire–carbonyl interactions in an ion channel. *Proc. Natl. Acad. Sci.* **2020,** *117* (22), 11908-11915.
6. Lemaître, V.; de Planque, M. R. R.; Howes, A. P.; Smith, M. E.; Dupree, R.; Watts, A., Solid-State 17O NMR as a Probe for Structural Studies of Proteins in Biomembranes. *J.Am.Chem.Soc.* **2004,** *126* (47), 15320-15321.
7. Wong, A.; Beevers, A. J.; Kukol, A.; Dupree, R.; Smith, M. E., Solid-state 17O NMR spectroscopy of a phospholemman transmembrane domain protein: Implications for the limits of detecting dilute 17O sites in biomaterials. *Solid State Nucl. Magn. Reson.* **2008,** *33* (4), 72-75.
8. Lin, B.; Hung, I.; Gan, Z.; Chien, P.-H.; Spencer, H. L.; Smith, S. P.; Wu, G., 17O NMR studies of yeast ubiquitin in aqueous solution and in the solid state. *Chem.Bio.Chem.* **2021,** *22* (5), 826.
9. Tsolaki, E.; Bertazzo, S., Pathological Mineralization: The Potential of Mineral omics. *Materials* **2019,** *12* (19), 3126.
10. Ferris, D. M.; Moodie, G. D.; Dimond, P. M.; Giorani, C. W. D.; Ehrlich, M. G.; Valentini, R. F., RGD-coated titanium implants stimulate increased bone formation in vivo. *Biomaterials* **1999,** *20* (23), 2323-2331.
11. Anselme, K., Osteoblast adhesion on biomaterials. *Biomaterials* **2000,** *21* (7), 667-681.
12. Mavropoulos, E.; Hausen, M.; Costa, A. M.; Alves, G.; Mello, A.; Ospina, C.; Mir, M.; Granjeiro, J. M.; Rossi, A. M., The impact of the RGD peptide on osteoblast adhesion and spreading on zinc-substituted hydroxyapatite surface. *J. Mater. Sci. Mater. Med.* **2013,** *24* (5), 1271-1283.
13. Plow, E. F.; Haas, T. A.; Zhang, L.; Loftus, J.; Smith, J. W., Ligand Binding to Integrins*. *J. Biol. Chem.* **2000,** *275* (29), 21785-21788.
14. Sun, Y.; Kang, C.; Liu, F.; Zhou, Y.; Luo, L.; Qiao, H., RGD Peptide-Based Target Drug Delivery of Doxorubicin Nanomedicine. *Drug Develop. res.* **2017,** *78* (6), 283-291.
15. Meyers, S. R.; Grinstaff, M. W., Biocompatible and Bioactive Surface Modifications for Prolonged In Vivo Efficacy. *Chem. Rev.* **2012,** *112* (3), 1615-1632.
16. Gilbert, M.; Shaw, W. J.; Long, J. R.; Nelson, K.; Drobny, G. P.; Giachelli, C. M.; Stayton, P. S., Chimeric peptides of statherin and osteopontin that bind hydroxyapatite and mediate cell adhesion. *J. Biol. Chem.* **2000,** *275* (21), 16213-16218.
17. Tanaka, C.; Asano, A.; Kurotsu, T.; Asakura, T., Structural Study of Silk-like Peptides Modified by the Addition of the Cell Adhesive Sequence, RGD, Using 13 C CP/MAS NMR. *Polym. J.* **2009,** *41* (1), 18-19.
18. Asakura, T.; Nishi, H.; Nagano, A.; Yoshida, A.; Nakazawa, Y.; Kamiya, M.; Demura, M., NMR Analysis of the Fibronectin Cell-Adhesive Sequence, Arg-Gly-Asp, in a Recombinant Silk-Like Protein and a Model Peptide. *Biomacromolecules* **2011,** *12* (11), 3910-3916.
19. Theodorou-Kassioumis, V.; Biris, N.; Sakarellos, C.; Tsikaris, V., A convenient and rapid method for the selective oxygen-17 enrichment of aspartyl peptides during solid-phase synthesis. *Tetrahedron Lett.* **2001,** *42* (43), 7703-7705.
20. https://ibmm.umontpellier.fr/?Plate-forme-Analyse-et-Synthese,324&lang=fr.
21. Amblard, M.; Fehrentz, J.-A.; Martinez, J.; Subra, G., Methods and protocols of modern solid phase peptide synthesis. *Mol. Biotech.* **2006,** *33* (3), 239-254.
22. Barlos, K.; Chatzi, O.; Gatos, D.; Stavropoulos, G., 2-Chlorotrityl chloride resin. *Int. J. Pept. Protein Res.* **1991,** *37*, 513-520.
23. Ieronymaki, M.; Androutsou, M. E.; Pantelia, A.; Friligou, I.; Crisp, M.; High, K.; Penkman, K.; Gatos, D.; Tselios, T., Use of the 2-chlorotrityl chloride resin for microwave-assisted solid phase peptide synthesis. *Pept. Sci.* **2015,** *104* (5), 506-514.
24. Eissler, S.; Kley, M.; Bächle, D.; Loidl, G.; Meier, T.; Samson, D., Substitution determination of Fmoc-substituted resins at different wavelengths. *J. Pept. Sci.* **2017,** *23* (10), 757-762.
25. Luna, O. F.; Gomez, J.; Cárdenas, C.; Albericio, F.; Marshall, S. H.; Guzmán, F., Deprotection Reagents in Fmoc Solid Phase Peptide Synthesis: Moving Away from Piperidine? *Molecules* **2016,** *21* (11), 1542.
26. Yang, Y.; Sweeney, W. V.; Schneider, K.; Thörnqvist, S.; Chait, B. T.; Tam, J. P., Aspartimide formation in base-driven 9-fluorenylmethoxycarbonyl chemistry. *Tetrahedron Lett.* **1994,** *35* (52), 9689-9692.

27. Subirós-Funosas, R.; El-Faham, A.; Albericio, F., Use of Oxyma as pH modulatory agent to be used in the prevention of base-driven side reactions and its effect on 2-chlorotrityl chloride resin. *Pept. Sci.* **2012,** *98* (2), 89-97.
28. Bollhagen, R.; Schmiedberger, M.; Barlos, K.; Grell, E., A new reagent for the cleavage of fully protected peptides synthesised on 2-chlorotrityl chloride resin. *J. Chem. Soc. Chem. Comm.* **1994,** (22), 2559-2560.
29. Roux, S.; Zékri, E.; Rousseau, B.; Paternostre, M.; Cintrat, J.-C.; Fay, N., Elimination and exchange of trifluoroacetate counter-ion from cationic peptides: a critical evaluation of different approaches. *J. Pept. Sci.* **2008,** *14* (3), 354-359.
30. Linda Lloyd; Boguszewski, P. *Freebasing of Peptide Salts and the Removal of Acidic Ion-Pairing Reagents from Fractions after HPLC purification*.
31. Hu, J.; Chekmenev, E. Y.; Gan, Z.; Gor'kov, P. L.; Saha, S.; Brey, W. W.; Cross, T. A., Ion Solvation by Channel Carbonyls Characterized by 17O Solid-State NMR at 21 T. *J.Am.Chem.Soc.* **2005,** *127* (34), 11922-11923.
32. Yamada, K.; Dong, S.; Wu, G., Solid-State 17O NMR Investigation of the Carbonyl Oxygen Electric-Field-Gradient Tensor and Chemical Shielding Tensor in Amides. *J.Am.Chem.Soc.* **2000,** *122* (47), 11602-11609.
33. Antzutkin, O. N.; Iuga, D.; Filippov, A. V.; Kelly, R. T.; Becker-Baldus, J.; Brown, S. P.; Dupree, R., Hydrogen Bonding in Alzheimer's Amyloid-β Fibrils Probed by 15N{17O} REAPDOR Solid-State NMR Spectroscopy. *Angew. Chem. Int. Ed. Engl.* **2012,** *51* (41), 10289-10292.
34. Wei, J.; Antzutkin, O. N.; Filippov, A. V.; Iuga, D.; Lam, P. Y.; Barrow, M. P.; Dupree, R.; Brown, S. P.; O'Connor, P. B., Amyloid Hydrogen Bonding Polymorphism Evaluated by 15N{17O}REAPDOR Solid-State NMR and Ultra-High Resolution Fourier Transform Ion Cyclotron Resonance Mass Spectrometry. *Biochem.* **2016,** *55* (14), 2065-2068.
35. Keeler, E. G.; Michaelis, V. K.; Colvin, M. T.; Hung, I.; Gor'kov, P. L.; Cross, T. A.; Gan, Z.; Griffin, R. G., 17O MAS NMR Correlation Spectroscopy at High Magnetic Fields. *J.Am.Chem.Soc.* **2017,** *139* (49), 17953-17963.
36. Klein, B. A.; Tkachuk, D. G.; Terskikh, V. V.; Michaelis, V. K., Expanding the NMR toolkit for biological solids: oxygen-17 enriched Fmoc-amino acids. *New J. Chem.* **2021,** *45* (28), 12384-12398.

ANNEXE V

PEPTIDE SYNTHESIS - EXPERIMENTAL PART

V-A) MATERIALS AND METHODS

V-A1) Reagents

2-Chlorotrityl chloride resin (Iris Biotech), Fmoc-Gly-OH (Iris Biotech), $^{17}O/^{18}O$-labeled Fmoc-Gly-O*H (synthesis in Annexe 1), Fmoc-L-Asp(O*t*Bu)-OH (Iris Biotech $^{17}O/^{18}O$-labeled Fmoc-L-Asp(O*t*Bu)-O*H (synthesis in Annexe 1), Fmoc-L-Asp(OMe)-OH (Fluorochem, 95%), Fmoc-L-Arg(Pbf)-OH (Iris Biotech), Fmoc-L-Ser(*t*Bu)-OH (Iris Biotech), 1-[Bis(dimethylamino)methylene]-1H-1,2,3-triazolo[4,5-b]pyridinium 3-oxide hexafluorophosphate (HATU, Fluorochem, 99.5%), *N*,*N*-diethylisopropylamine (DIEA, Sigma Aldrich, 99%), ethyl 2-cyano-2-(hydroxyimino)acetate (Oxyma pure, Fluorochem, 98%), piperidine (Analytic Lab, 99%), trifluoroacetic acid (TFA, Analytic Lab, 99%), triisopropylsilane (TIS, Sigma Aldrich, 98%), 1,1,1,3,3,3,-hexafluoro-2-propanol (HFIP, Fluorochem, 99%), acetic anhydride (Ac_2O, Sigma Aldrich, 99%). Reagent grade solvents were used for all the syntheses. Commercial dichloromethane (DCM) anhydrous was used for the resin loading. HPLC grade solvents were used for HPLC purification.

V-A2) Synthetic equipment

Solid phase peptide syntheses were performed in fritted syringes placed in an orbital shaker using a 2-chlorotrityl resin loaded at ~ 0.5 - 0.6 mmol/g, and the Fmoc/*t*Bu strategy. Side-chain deprotections were performed in a Carousel 12 Plus Reaction Station - Radleys.

V-A3) Characterization protocols

Routine LCMS analyses of the reaction intermediates were performed on a system composed of a Waters Alliance 2690 HPLC, coupled to a Micromass (Manchester, UK) ZQ spectrometer (electrospray ionization mode, ESI^+). All the analyses were carried out using a C18 Chromolith Flash 25 x 4.6 mm column. A flow rate of 3 mL/min and a gradient of (0-100)% B over 2.5 min were used: eluent A, water/0.1% HCOOH; eluent B, acetonitrile/0.1% HCOOH. Positive-ion electrospray mass spectra were acquired at a solvent flow rate of 100-200 µL/min. Nitrogen was used for both the nebulizing and drying gas. The data were obtained in a scan mode ranging from 200 to 1700 m/z in 0.1 s intervals; 10 scans were summed up to get the final spectrum. Samples were prepared in ultra-pure water or acetonitrile/water (50/50, V/V) mixture containing 0.1% TFA.

Final peptide products were analysed using UPLCMS Acquity Analysis. The identification was carried out by liquid chromatography (UPLC, Waters Acquity mode) coupled to a high-resolution mass spectrometer (SQD2 model), equipped with an electrospray ionization source and controlled by MassLynx v.4.2 software for data acquisition. All the analyses were carried out using an Acquity UPLC BEH C18 2.1 x 50 mm column. A flow rate of 0.6 mL/min and a gradient of (0 - 100)% B over 5 min were used: eluent A, water/0.1% HCOOH; eluent B, acetonitrile/0.1% HCOOH. The mass spectrometer parameters were set as follows: ionization mode: electrospray positive ion; capillary voltage: 3.0 kV; source block temperature: 150 °C; desolvation temperature: 650 C; nebulizer nitrogen flow rate: 50 L/h; desolvation nitrogen gas flow: 650 L/h; and cone voltage: 20 V. The spectra were recorded by scanning the mass range from m/z 100 to 1300 with scan time of 0.5 s. In view of these analyses, peptides were dissolved in ultra-pure water containing 0.1% TFA.

Samples for HPLC purification were prepared in acetonitrile/water (4/10, V/V) mixture, containing 0.1% TFA. The purifications were carried out using a PLC2050 Armen-Gilson purification system either on a reverse-phase Luna 5 µm C18 100Å Axia 100 x 21.2 mm, column, with a flow rate of 20 mL/min, or a C18 Waters Delta-Pack column (100 x 40 mm,

100 Å), with a flow rate of 50 mL/min, both using a gradient of 30–50% B over 20 min. Eluent A: water/0.1% TFA; eluent B: acetonitrile/0.1% TFA.

UV-Vis analyses. Absorbance measurements for resin loading determination were carried out using a UV-Vis spectrometer CARY60.

For the final products characterization, LC-MS analysis were done using an Acquity H-Class (Waters) system equipped with a Kinetex EVO C18 column (1.9 µm particle size, 50 x 2.1 mm, Phenomenex). Mobile phase A consisted of water while mobile phase B was acetonitrile both containing 0.1% formic acid. The gradient started at 0% mobile phase B and increase to 100% mobile phase B over 3 min. After holding for 0.6 min the gradient returned to 0% B before re-equilibration for 1.4 min, to give a total run time of 5 min. The flow rate was 0.5 mL/min and the eluent was directed to the atmospheric pressure ionisation source of a Synapt G2-S (Waters) operating in negative or positive electrospray ionization mode depending of the sample. Capillary and cone voltage were respectively 3000 V and 30 V. Source and desolvation temperatures were respectively 450 °C and 140 °C.

HRMS analysis were done by infusion of the sample in the electrospray source of a Synapt G2-S (Waters, SN : UEB205) mass spectrometer operating in positif or negative mode. Capillary and cone voltage were respectively 3000 V and 30 V. Source and desolvation temperatures were respectively 250°C and 100°C. All data were processed by Masslynx 4.2 software.

The $^{17}O/^{18}O$-enrichement *level* was estimated based on the calculation of an apparent average atomic weight for oxygen in the isolated phase, from which enrichment level per carboxylic oxygen was subsequently derived using $^{18}O/^{17}O$ isotopic ratio of the labeled water.

^{1}H and ^{13}C solution NMR spectra were recorded on an Avance III Bruker 600 MHz NMR spectrometer equipped with a TCI Prodigy cryoprobe or on an Avance III Bruker 500 MHz NMR spectrometer equipped with a BBO Helium cryoprobe, using DMSO-d_6 as a solvent. Chemical shifts were referenced to DMSO-d_6 resonances, centred at 2.50 ppm (^{1}H NMR spectra) and 39.52 ppm (^{13}C NMR spectra).

^{13}C solid-state NMR experiments were performed on a VNMRS 600 MHz (14.1 T) NMR spectrometer, using a Varian 3.2 mm HX probe tuned to ^{1}H (599.82 MHz) and ^{13}C (150.81 MHz). The temperature was regulated at -20 °C. All ^{13}C NMR spectra were recorded under MAS (Magic Angle Spinning) with a spinning frequency of 10 kHz. A ^{1}H-^{13}C CPMAS NMR sequence was used with a 3.3 µs ^{1}H excitation pulse, followed by a ramped CP pulse of 5 ms contact time, and applying SPINAL-64 ^{1}H-decoupling (75 kHz) during acquisition. All acquisition parameters for CPMAS experiments are summarized in Table V-1. ^{1}H and ^{13}C chemical shifts were referenced to adamantane at 1.8 ppm and 38.5 ppm (high frequency peak), respectively.

Table V-1: Acquisition parameters for ^{13}C CPMAS NMR measurements.

Sample	Field	Probe	Sequence	CT	MAS	D1	NS	Time	Temp
RGD	14.1 T	V-HX	CP MAS	5ms	10 kHz	2s	22000	12h40	-20 °C
GRGDS	14.1 T	V-HX	CP MAS	5ms	10 kHz	2s	10240	5h45	-20 °C
GRGDS	14.1 T	V-HX	CP MAS	5ms	10 kHz	2s	10240	5h45	-20 °C

^{17}O solid-state NMR experiments were performed on a VNMRS 600 MHz (14.1 T) NMR spectrometer, using a 3.2 mm probe tuned to ^{1}H (599.82 MHz) and ^{17}O (81.31 MHz). Two types of probes were used, depending on the availability of the equipment: a 3.2 mm Varian HX probe, or a 3.2 mm Varian HXY probe equipped with a 3.2 mm probe head. The temperature was regulated at -20 °C. Spectra were recorded under MAS (Magic Angle Spinning) conditions, using a spinning frequency of 20 kHz. The ^{17}O MAS one pulse NMR

experiments (Bloch decay) were recorded using 1.0 µs for CT selective 90°pulse with ^{1}H decoupling (RF ~ 75 kHz) (SPINAL-64) applied during acquisition. More details on acquisition conditions are reported in Table V-2. ^{17}O chemical shifts were referenced to D_2O at -2.7 ppm (which corresponds to tap-water at 0 ppm). The ^{17}O MAS NMR spectra were presented using DMfit software.[1]

Table V-2: Acquisition parameters for ^{17}O MAS NMR measurements.

Sample	Field	Probe	Sequence	Hdec	MAS	D1	NS	Time	Temp
RGD	600	V-HX	OnePulse	yes	20kHz	500ms	8192	1h10	-20°C
GRGDS	600	V-HXY	OnePulse	yes	20kHz	500ms	51200	7h20	-20°C
GRGDS	600	V-HX	OnePulse	yes	20kHz	500ms	10240	1h30	-20°C

V-B) RESIN PREPARATION AND CHARACTERIZATION

V-B1) Fmoc-L-Asp(O*t*Bu)-O-2-chlorotrityl resin[2]

a) Non-labeled Fmoc-L-Asp(OtBu)-O-2-chlorotrityl resin

The non-labeled commercial Fmoc-L-Asp(O*t*Bu)-OH precursor (2.0 g, 4.8 mmol, 1 eq.) was dissolved in anhydrous DCM (25 mL) with DIEA (3.3 mL, 19.2 mmol, 4 eq.) and the solution was added to polymer-bound 2-chlorotrityl chloride (3.0 g, loading 1.6 mmol of Cl/g, 1 eq.). The suspension was magnetically stirred at room temperature for 2 h. The resin was collected by filtration using a syringe with built-in glass frit, and washed three times with a DCM/MeOH/DIEA (17/2/1, V/V/V) solution, three times with DMF, and finally twice with DCM. The resin was dried under vacuum overnight. 4.9 g of the Fmoc-L-Asp(O*t*Bu)-O-2-chlorotrityl resin was obtained. Loading: 0.58 mmol/g. Resin was stored in a parafilmed vial in a fridge. The stability of the loading was not verified.

b) ^{18}O-labeled Fmoc-L-Asp(OtBu)-O-2-chlorotrityl resin*

The ^{18}O-labeled Fmoc-L-Asp(O*t*Bu)-O*H precursor (394 mg, 1.0 mmol, 1 eq.) was dissolved in anhydrous DCM (20 mL) with DIEA (650 µL, 4.0 mmol, 4 eq.) and the solution was added to polymer-bound 2-chlorotrityl chloride (600 mg, loading 1.6 mmol of Cl/g, 1 eq.). The suspension was magnetically stirred at room temperature for 4 h. The resin was collected by filtration using a syringe with built-in glass frit, and washed three times with a DCM/MeOH/DIEA (17/2/1, V/V/V) solution, three times with DMF, and finally twice with DCM. The resin was dried under vacuum overnight. 896 mg of ^{18}O-labeled Fmoc-L-Asp(O*t*Bu)-O*-2-chlorotrityl resin was obtained. Loading: ~ 0.5-0.8 mmol/g. Resin was stored in a parafilmed vial in a fridge. The stability of loading was not verified.

c) ^{17}O-labeled Fmoc-L-Asp(OtBu)-O-2-chlorotrityl resin*

The ^{17}O-labeled Fmoc-L-Asp(O*t*Bu)-O*H precursor (198 mg, 0.5 mmol, 1 eq.) was dissolved in anhydrous DCM (10 mL) with DIEA (327 µL, 1.9 mmol, 4 eq.) and the solution was added to polymer-bound 2-chlorotrityl chloride (300 mg, loading 1.6 mmol of Cl/g, 1 eq.). The suspension was stirred at room temperature for 4 h. The resin was collected by filtration using a syringe with built-in glass frit, and washed three times with DCM/MeOH/DIEA (17/2/1, V/V/V) solution, three times with DMF, and finally twice with DCM. The resin was dried under vacuum overnight. 442 mg of ^{17}O-labeled Fmoc-L-Asp(O*t*Bu)-O*-2-chlorotrityl resin was obtained. Loading: ~ 0.5-0.8 mmol/g. Resin was stored in a parafilmed vial in a fridge. The stability of loading was not verified.

V-B2) Fmoc-L-Ser(*t*Bu)-O-2-chlorotrityl resin[2]

The Fmoc-L-Ser(*t*Bu)-OH precursor (613 mg, 1.6 mmol, 1 eq.) was dissolved in anhydrous DCM (15 mL) with DIEA (1 mL, 7.7 mmol, 4 eq.), and the solution was added to polymer-bound 2-chlorotrityl chloride (1.0 g, loading 1.6 mmol of Cl/g, 1 eq.). The suspension was magnetically stirred at room temperature for 2 h. The resin was collected by filtration using syringe with built-in glass frit, and washed three times with a DCM/MeOH/DIEA (17/2/1, V/V/V) solution, three times with DMF, and finally twice with DCM. The resin was dried under vacuum overnight. 1.56 g of Fmoc-L-Ser(*t*Bu)-O-2-chlorotrityl resin was obtained. Loading: 0.55 mmol/g. Resin was stored in a parafilmed vial in a fridge and the loading was found to be stable for at least 4 weeks.

V-B3) Resin loading determination[3]

To determine the loading of the prepared resins, three samples containing approximately 10 mg (weighed precisely) of pre-dried resin were dispersed in 1 mL of a piperidine/DMF (20/80, V/V) solution, and placed in benchtop horizontal rotating shaker for 30 min at room temperature. Then, after letting suspension of the resin to set, 100 µL of solution above the resin beads was diluted with 9.9 mL of DMF, and the absorbance at the wavelength of 289.8 nm was measured three times for each sample using a CARY60 UV/Vis spectromete. A blank solution of 100 µL of piperidine/DMF in 9.9 mL of DMF was used to substract the contribution of piperidine and DMF to the UV absorbance of the mixture. The loading [mmol/g] was calculated *via* a modified equation based on the Lambert-Beer law:

$$loading = \frac{10^6 \cdot A \cdot V \cdot D}{m_r \cdot \varepsilon_\lambda \cdot d}$$

where A is absorbance, V [L] is a volume of piperidine/DMF solution added to the resin, D is a dilution factor of the solution analysed (here equals to 100), m_r is a mass of the resin sample [mg], ε_λ is a molar absorbance coefficient [$L.mol^{-1}.cm^{-1}$] (here at wavelength 289.8 nm) and d is the thickness of the cuvette [cm].

V-C) SOLID-PHASE PEPTIDE SYNTHESIS (SPPS)

The reaction conditions were first tested and optimized on the synthesis of non-labeled peptides, followed by preparation of ^{18}O-labeled version, and finally the ^{17}O-labeled equivalent was prepared. The peptides were synthesized by manual SPPS synthesis at the SynBio3 platform in Montpellier (see general scheme in Figure 5.2 in the Chapter 5.1). Some of the instruments used in the peptide synthesis are shown in Figure V-1.

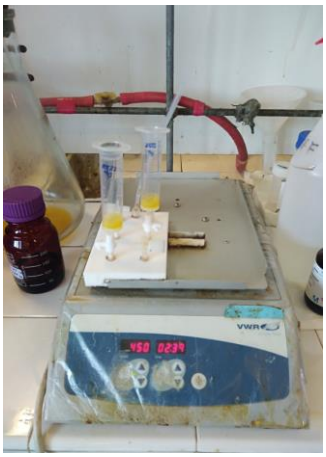

SPPS platform

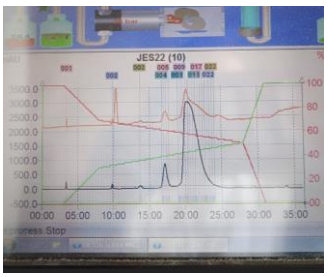

HPLC purification

Side-deprotection step

Lyophilisator

Ongoing lyophilisation

Lyophilised product

TFA-removal procedure

Final product

Figure V-1: Photos of some of the instruments and procedures used during the SPPS synthesis, including purification steps and lyophilisation and photo of a final product.

V-C1) RGD tri-peptide

a) Non-labeled RGD tri-peptide synthesis

Peptide chain building

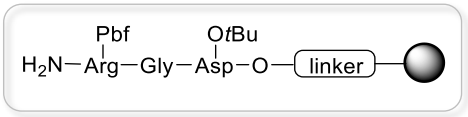

The Fmoc-L-Asp(O*t*Bu)-O-2-chlorotrityl resin (174 mg, 0.1 mmol) was placed in a syringe with a built-in glass frit, and properly swelled in DMF while stirred with an orbital shaker at 450 rpm during ~ 15 min. The solvent was filtered out.

1) For the Fmoc-deprotection, 5 mL of pip/DMF (20/80, V/V) containing Oxyma pure (0.1M) was added and the resin was stirred at 450 rpm for 1 min. The solvent was filtered out and this process was repeated once. The solvent was filtered out and the resin was then washed with ~ 5mL of DMF (3x).

2) For the Gly-coupling, 500 µL of a Fmoc-Gly-OH solution in DMF (0.5M, 2.5 eq.) was added followed by addition of 87.6 µL of DIEA (5 eq.) and 500 µL of HATU solution in DMF (0.5M, 2.5 eq.). The suspension was stirred at 450 rpm for 10 min. The solvent was filtered out and the resin was then washed with ~ 5mL of DMF (2x).

3) Fmoc-deprotection step was identical to the step 1).

4) For the Arg-coupling, 1 mL of a Fmoc-L-Arg(Pbf)-OH solution in DMF (0.5M, 5 eq.) was added followed by addition of 176 µL of DIEA (10 eq.) and 1 mL of HATU solution in DMF (0.5M, 5 eq.). The suspension was stirred at 450 rpm for 5 min. The solvent was filtered out, the resin was washed with DMF (1x), and the process was repeated once. The resin was then washed with ~ 5mL of DMF (2x).

5) Fmoc-deprotection step was identical to the step 1).

Finally, the resin was washed with ~ 5mL of DCM (2x).

Cleavage under mild conditions[4]

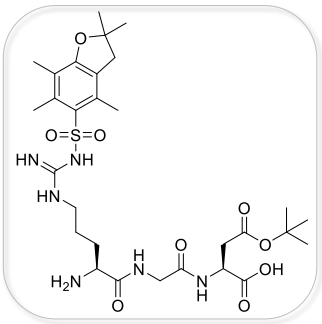

The previously recovered resin was dispersed in 960 µL of DCM and 240 µL of HFIP was added. The suspension was stirred at room temperature for 30 min. The solution containing the cleaved peptide was obtained by filtration using a syringe with built-in glass frit, and the resin was subjected once again to cleavage under the same conditions. The filtrates were combined and evaporated to dryness. The peptide was purified using preparative HPLC with an acetonitrile gradient in water (0-0-30-50-100-100%, 3-5-20-5-10 min), and was eluted at 38 % of acetonitrile. The solution was finally lyophilised, providing 60 mg of the side-chain protected peptide in a form of a white fluffy solid.

Side-chain deprotection

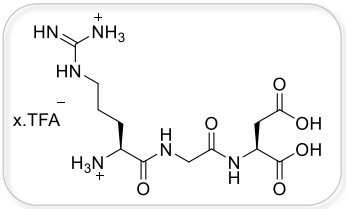

The side-chain protected peptide was dissolved in ~ 2 mL of DCM and 10 mL of a solution of TFA/TIS/H_2O (94/3/3, V/V/V) was added. The solution was stirred in an incubator heated at 38 °C for 30 min. The solvent was then evaporated almost to dryness under reduced pressure, and cold Et_2O was added to the warm residual solution (~ 2 mL) inducing precipitation. The precipitate was separated by centrifugation, washed once with Et_2O, re-dissolved in ultra-pure water, and finally lyophilised. The deprotected peptide.xTFA salt was obtained pure in the form of a white solid. Isolated mass: 44 mg.

TFA salt removal

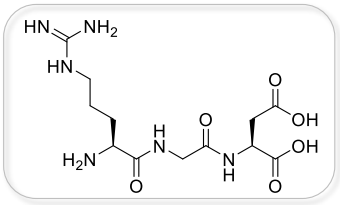

The previously deprotected peptide.xTFA (0.085 mmol, 1 eq. supposing two TFA molecules/peptide chain) was dissolved in 10 mL of acetonitrile/H_2O (20/80, V/V). Two commercially pre-packed syringes containing polymer-supported quaternary ammonium resin with bicarbonate counter ions on a frit (VariPure IPE, volume of the beads 150 - 300 µm, 1 syringe: 0.18 mmol/100 mg; > 4 eq.) were at first conditioned with MeOH (3x syringe volume), and then with the mobile phase (acetonitrile/H_2O, (20/80, V/V); 3x syringe volume). Half of the product solution in the mobile phase (5 mL) was then introduced to each syringe and filtrates were collected. Each resin was washed with mobile phase (5x syringe volume) and with pure acetonitrile (3x syringe volume). Filtrates from the mobile phase washings and from the first syringe volume of acetonitrile washing were combined with the previously collected phases, and lyophilised together.

Final peptide was isolated pure with less than 0.1 eq. of TFA salt (determined by ^{19}F solution NMR), and no deleted peptide detected. Yield (n = 1): 9 mg (27 %).

b) $^{17}O/^{18}O$-labeled RGD tri-peptides

For the preparation of $^{17}O/^{18}O$-labeled RGD peptide, the same reaction and purification conditions were used with a few modifications:

- The $^{17}O/^{18}O$-labeled Fmoc-L-Asp(O*t*Bu)-O*-2-chlorotrityl resin was used.
- For the Gly-coupling, 500 µL of $^{17}O/^{18}O$-labeled Fmoc-Gly-O*H solution in DMF (0.5M, 2.5 eq.) was added, followed by addition of 87.6 µL of DIEA (5 eq.) and 500 µL of HATU solution in DMF (0.5M, 2.5 eq.). The suspension was stirred at 450 rpm for 5 min. Then, the solvents were filtered out, the resin was washed once with ~ 5mL of DMF, and the coupling step was repeated once.
- Only one VariPure IPE syringe was used for TFA-removal.

Deleted glycine was detected by LCMS analysis of the side-protected product and it was not possible to be separated by preparative HPLC. The final $^{17}O/^{18}O$-labeled RGD was therefore found to be contaminated with the deleted glycine side-product. For the ^{18}O-labeled RGD, isolated mass: 15 mg, for the ^{17}O-labeled RGD, isolated mass: 16 mg.

c) Characterizations of RGD tri-peptides

Figure V-2: ^{19}F solution NMR spectra of non-labeled, ^{18}O-labeled and ^{17}O-labeled RGD peptide (400 MHz, D_2O). 3mM of peptide was dissolved in D_2O containing 3 mM of trifluoroethanol (TFE) as an internal standard.[5] For the non-labeled RGD, 0.06 eq. of TFA was detected. For the $^{17}O/^{18}O$-labeled products, less than 0.05 eq. of TFA was detected.

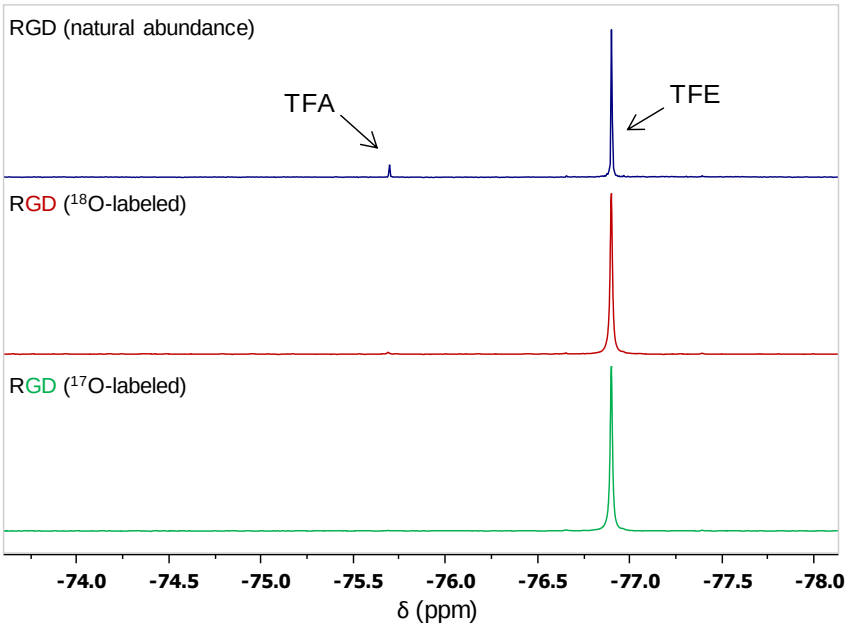

Figure V-3: LC analyses of non-labeled and $^{18}O/^{17}O$-labeled RGD tri-peptide (dissolved in H_2O).

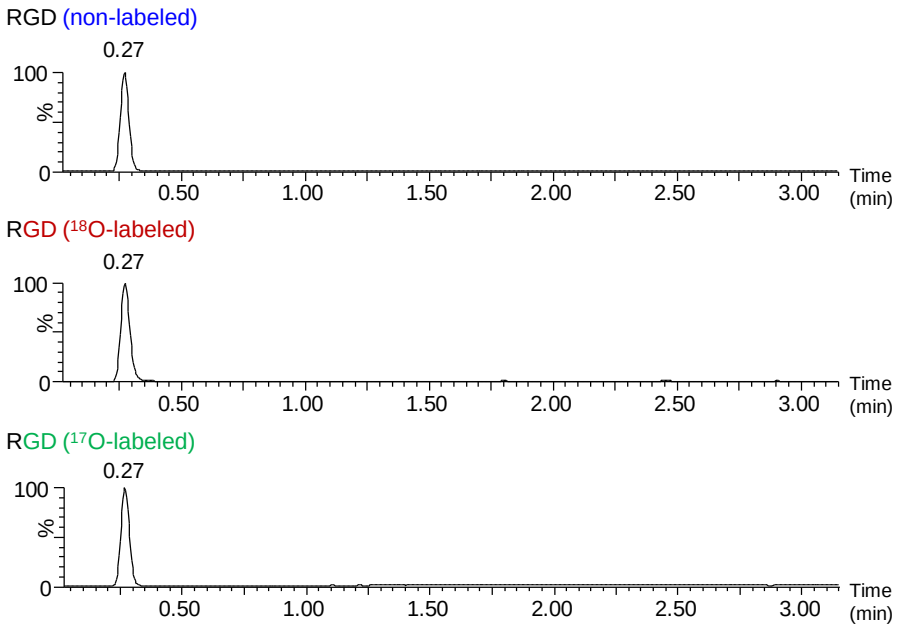

Figure V-4: HRMS (ESI$^+$) analyses of non-labeled and $^{17}O/^{18}O$-labeled RGD tri-peptide. The monoisotopic mass at 290.15 m/z belongs to the Gly-deleted di-peptide RD by-product, which was eluted at the same retention time as the main product. The Gly-deleted di-peptide was only detected in the $^{17}O/^{18}O$-labeled RGD products.

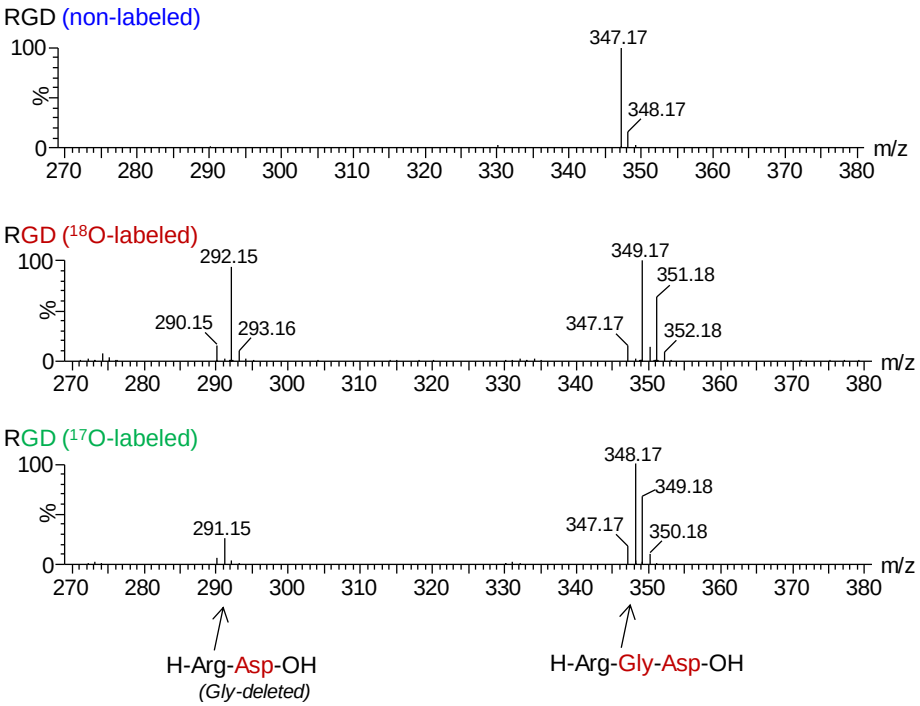

Figure V-5: HRMS (ESI$^+$) analyses of non-labeled and $^{18}O/^{17}O$-labeled RGD tri-peptide (zoom on the 340-358 m/z region). Average enrichment for the labeled carbonyl oxygen level estimated: ~ 42.2 %, for the ^{18}O-labeled RGD and ~ 39.8 %, for the ^{17}O-labeled RGD.

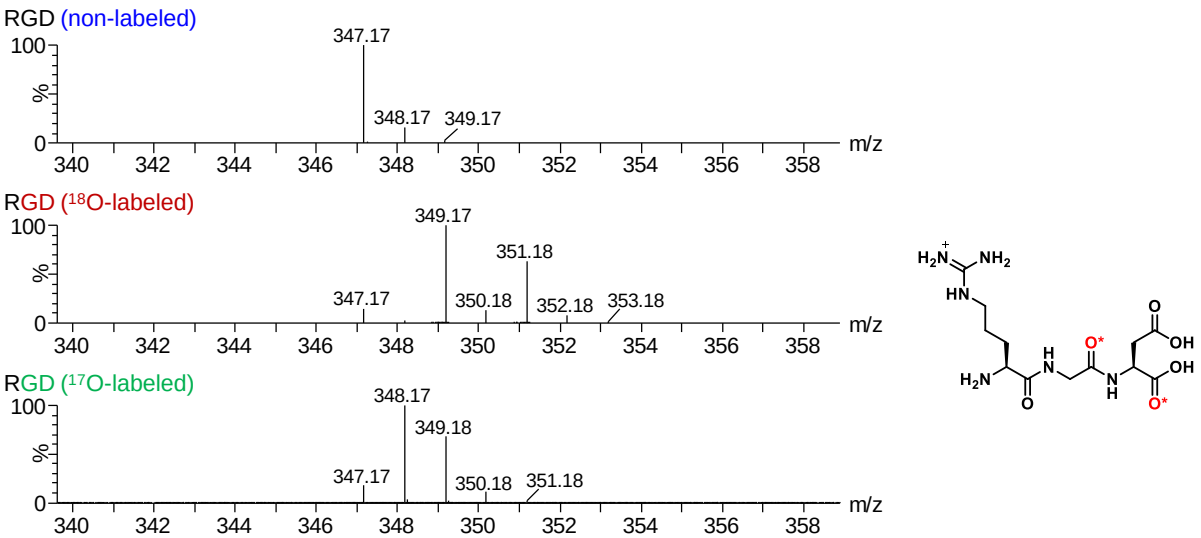

Figure V-6: ^{1}H solution NMR spectrum of non-labeled RGD peptide (DMSO-d_6, 600 MHz). The solvent peaks are crossed out.

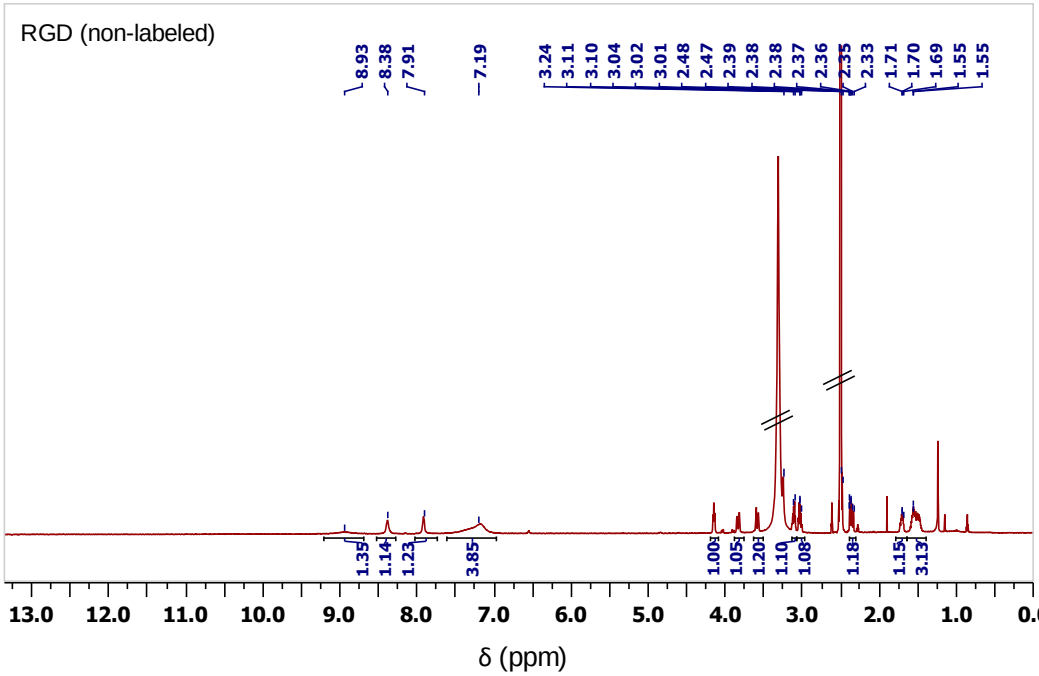

Figure V-7: ^{13}C solution NMR spectrum of non-labeled RGD peptide (DMSO-d_6, 600 MHz). The solvent peak is crossed out.

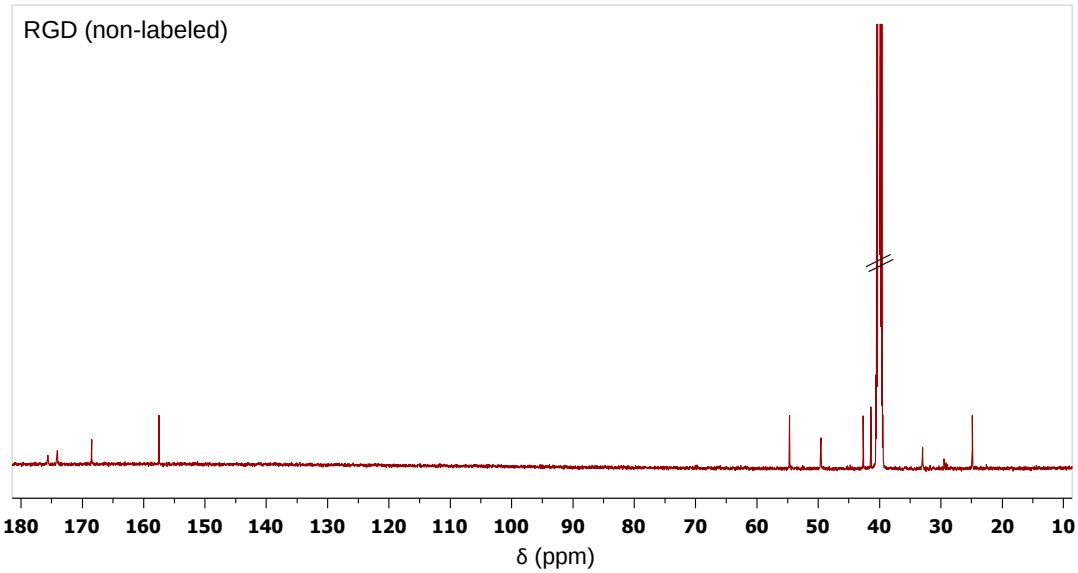

V-C2) GRGDS penta-peptide

a) Non-labeled GRGDS synthesis

Peptide chain building

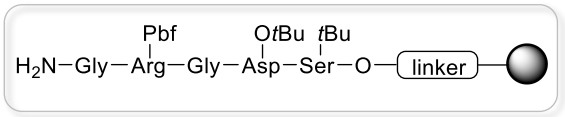

The Fmoc-L-Ser(*t*Bu)-O-2-chlorotrityl resin (185 mg, 0.1 mmol) was placed in a syringe with a built-in glass frit, and properly swelled in DMF while stirred with an orbital shaker at 450 rpm for 5 min. The solvent was filtered out.

1) For the Fmoc-deprotection, 5 mL of pip/DMF (20/80, V/V) containing Oxyma pure (0.1M) was added and the resin was stirred at 450 rpm for 1 min. The solvent was filtered out and this process was repeated once. The solvent was filtered out and the resin was then washed with ~ 5 mL of DMF (3x).

2) For the Asp-coupling, 500 µL of a Fmoc-L-Asp(O*t*Bu)-OH solution in DMF (0.5M, 2.5 eq.) was added followed by addition of 87.6 µL of DIEA (5 eq.) and 500 µL of HATU solution in DMF (0.5M, 2.5 eq.). The suspension was stirred at 450 rpm for 5 min. The solvent was filtered out, the resin was then washed with ~5 mL of DMF (1x), and the coupling process was repeated once. The resin was then washed with ~5 mL of DMF (2x).

3) For the acetylation step, 5 mL of a Ac_2O/DCM (50/50, V/V) solution was added, and the suspension was stirred at 450 rpm for 1 min. The solvents were filtered out and the resin was then washed with ~ 5 mL of DMF (2x).

4) Fmoc-deprotection step was identical to the step 1).

5) For the Gly-coupling, 500 µL of a Fmoc-Gly-OH solution in DMF (0.5M, 2.5 eq.) was added followed by addition of 87.6 µL of DIEA (5 eq.) and 500 µL of HATU solution in DMF (0.5M, 2.5 eq.). The suspension was stirred at 450 rpm for 10 min. The solvent was filtered out and the resin was then washed with ~ 5 mL of DMF (2x).

6) Fmoc-deprotection step was identical to the step 1).

7) For the Arg-coupling, 1 mL of a Fmoc-L-Arg(Pbf)-OH solution in DMF (0.5M, 5 eq.) was added followed by addition of 176 µL of DIEA (10 eq.) and 1 mL of HATU solution in DMF (0.5M, 5 eq.). The suspension was stirred at 450 rpm for 5 min. The solvent was filtered out, the resin was then washed with ~ 5 mL of DMF (1x), and the process was repeated once. The resin was then washed with ~ 5 mL of DMF (2x).

8) Fmoc-deprotection step was identical to the step 1).

9) The Gly-coupling step was identical to the step 5).

10) Fmoc-deprotection step was identical to the step 1).

Finally, the resin was washed with ~ 5 mL of DCM (2x).

Cleavage under mild conditions

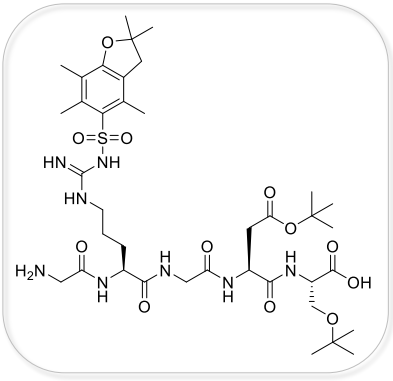

The previously recovered resin was dispersed in 960 µL of DCM and 240 µL of HFIP was added. The suspension was stirred at room temperature for 30 min. The solution containing the cleaved peptide was obtained by filtration using a syringe with a built-in glass frit, and the resin was subjected once again to cleavage under the same conditions. The filtrates were combined and evaporated to dryness. The peptide was purified using preparative HPLC with an acetonitrile gradient in water (0-0-30-50-100-100%, 3-5-20-5-10 min), and was eluted at 42 % of acetonitrile. The solution was finally lyophilised, providing 69 mg of the side-chain protected peptide in a form of a white fluffy solid.

Side-chain deprotection

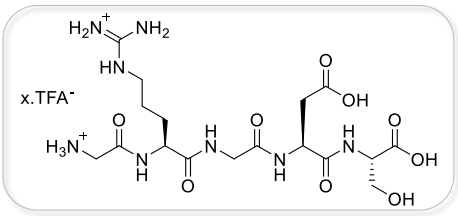

The side-chain protected peptide was dissolved in ~ 2 mL of DCM and 10 mL of solution of TFA/TIS/H_2O (94/3/3, V/V/V) was added. The solution was stirred in an incubator heated at 38 °C for 30 min. The solvent was then evaporated almost to dryness under reduced pressure, and cold Et_2O was added to the warm residual solution (~ 2 mL) inducing precipitation. The precipitate was separated by centrifugation, washed once with Et_2O, re-dissolved in ultra-pure water, and finally lyophilised. The deprotected peptide.xTFA salt was obtained pure in the form of a white solid. Isolated mass: 48 mg.

TFA salt removal

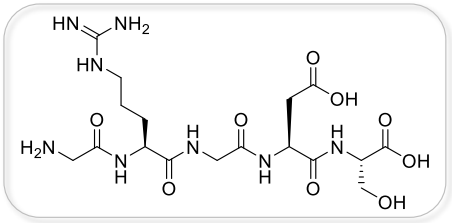

The previously deprotected peptide.xTFA (0.072 mmol, 1 eq. supposing 2TFA molecules/peptide chain) was dissolved in 10 mL of acetonitrile/H_2O (20/80, V/V). Two commercially pre-packed syringes containing polymer-supported quaternary amine resin with a bicarbonate counterion on a frit (VariPure IPE, polymer beads volume 150 - 300 µm, 1 syringe: 0.18 mmol/100 mg; > 4 eq.) were at first conditioned with MeOH (3x syringe volume), and then with the mobile phase (acetonitrile/H_2O (20/80, V/V); 3x syringe volume). Half of the product solution in the mobile phase (5 mL) was then introduced to each syringe and filtrates were collected. Each resin was washed with mobile phase (5x syringe volume) and with pure acetonitrile (3x syringe volume). Filtrates from the mobile phase washings and from the first syringe volume of acetonitrile washing were combined with the previously collected phases, and lyophilised together.

Final peptide was isolated pure with only 0.2 eq. of TFA anion (determined by ^{19}F solution NMR), and no deleted peptide was detected. Yield (n = 1): 22 mg (45 %).

b) $^{17}O/^{18}O$-labeled GRGDS penta-peptides

For the preparation of $^{17}O/^{18}O$-labeled GRGDS peptides, the same reaction and purification conditions were used with one modification:

- Only one VariPure IPE syringe was used for the TFA-removal.

Final peptides were isolated pure with less than 0.05 eq. of TFA anion (determined by ^{19}F solution NMR), and no deleted peptide was detected. Yield (n = 1): 20 mg (41 %) for the ^{18}O-labeled GRGDS, 27 mg (55 %) for the ^{17}O-labeled GRGDS.

c) ^{17}O-labeled G_2RG_1DS penta-peptide

For the preparation of G_2RG_1DS peptide ^{17}O-labeled selectively only at the Asp and the last Gly_2 unit, the same reaction and purification conditions were used with a few modifications:

- For the first Gly_1-coupling, 500 µL of a non-labeled Fmoc-Gly-OH solution in DMF (0.5M, 2.5 eq) was added followed by addition of 87.6 µL of DIEA (5 eq) and 500 µL of HATU solution in DMF (0.5M, 2.5 eq). The suspension was stirred at 450 rpm for 5 min. The solvent was filtered out, the resin was then washed with ~ 5 mL of DMF (1x), and the process was repeated once. The resin was then washed with ~ 5 mL of DMF (2x).
- Only one VariPure IPE syringe was used for TFA-removal.

The final peptide was isolated with no TFA salt and no deleted peptide detected. Yield (n = 1): 28 mg (57 %).

d) Characterizations of GRGDS penta-peptides

Figure V-8: ^{19}F solution NMR spectra of non-labeled, ^{18}O-labeled and ^{17}O-labeled GRGDS peptides (400 MHz, D_2O). 3 mM of peptide was dissolved in D_2O containing 3 mM of trifluoroethanol (TFE) as internal standard.[5] For the non-labeled GRGDS, 0.2 eq. of TFA was measured. For the $^{17}O/^{18}O$-labeled products, less than 0.05 eq. of TFA was detected.

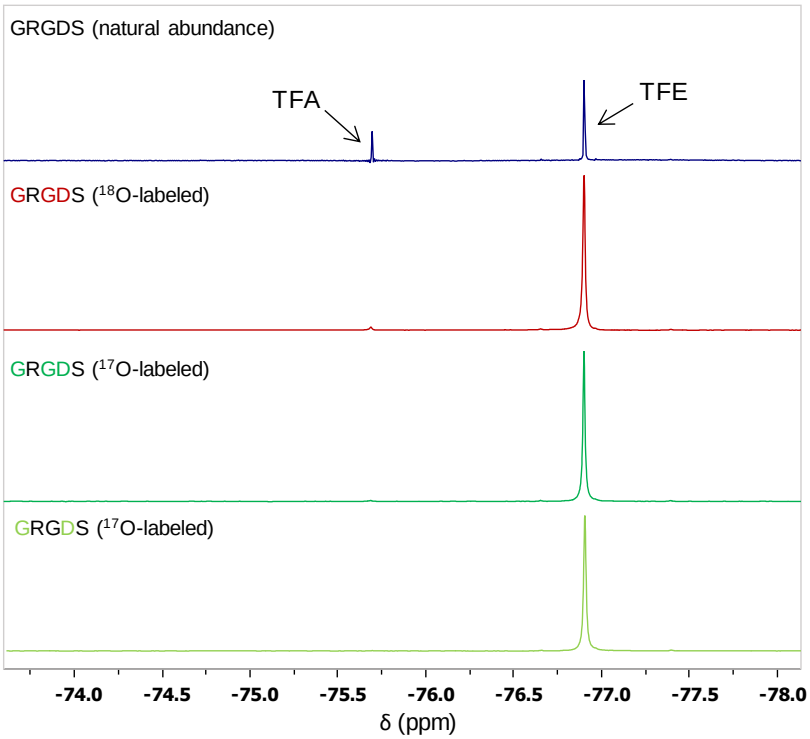

Figure V-9: LC analyses of non-labeled and $^{18}O/^{17}O$-labeled GRGDS penta-peptides (dissolved in H_2O, retention time 0.28 min).

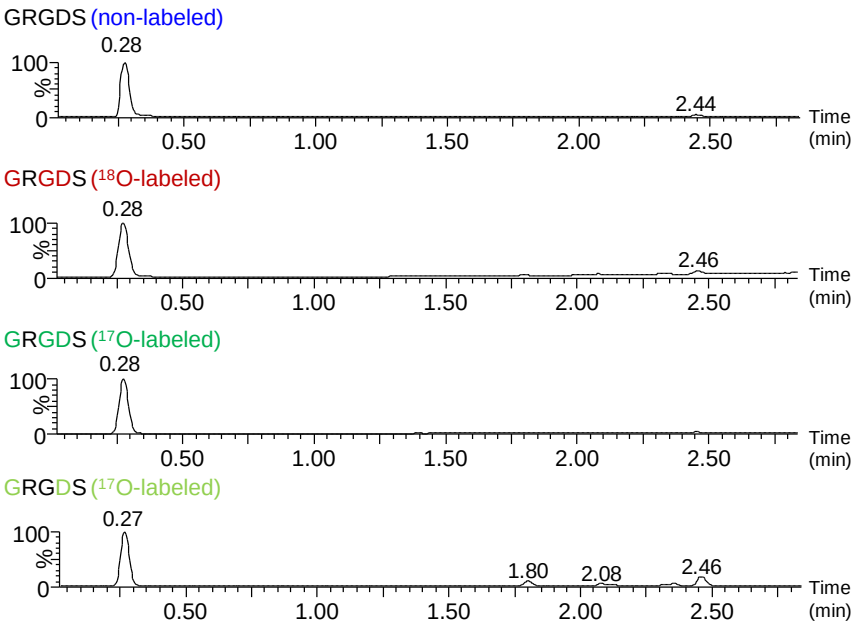

Figure V-10: HRMS (ESI$^+$) analyses of non-labeled and ^{18}O/^{17}O-labeled GRGDS penta-peptides. Average enrichment level for the labeled carbonyl oxygen measured: ~ 42.9 %, for the ^{18}O-labeled GRGDS, ~ 37.9 %, for the ^{17}O-labeled GRGDS, and ~ 39.2 %, for the selectively ^{17}O-labeled GRGDS.

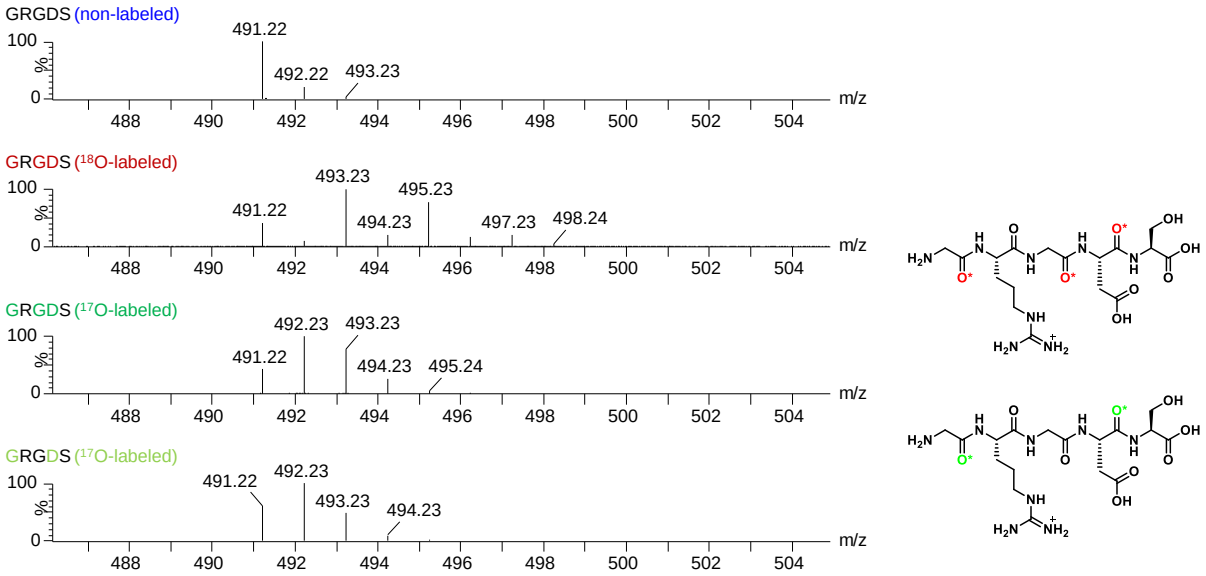

Figure V-11: ^{1}H solution NMR spectrum of ^{18}O-labeled GRGDS peptide (DMSO-d_6, 600 MHz). The solvent peak is crossed out.

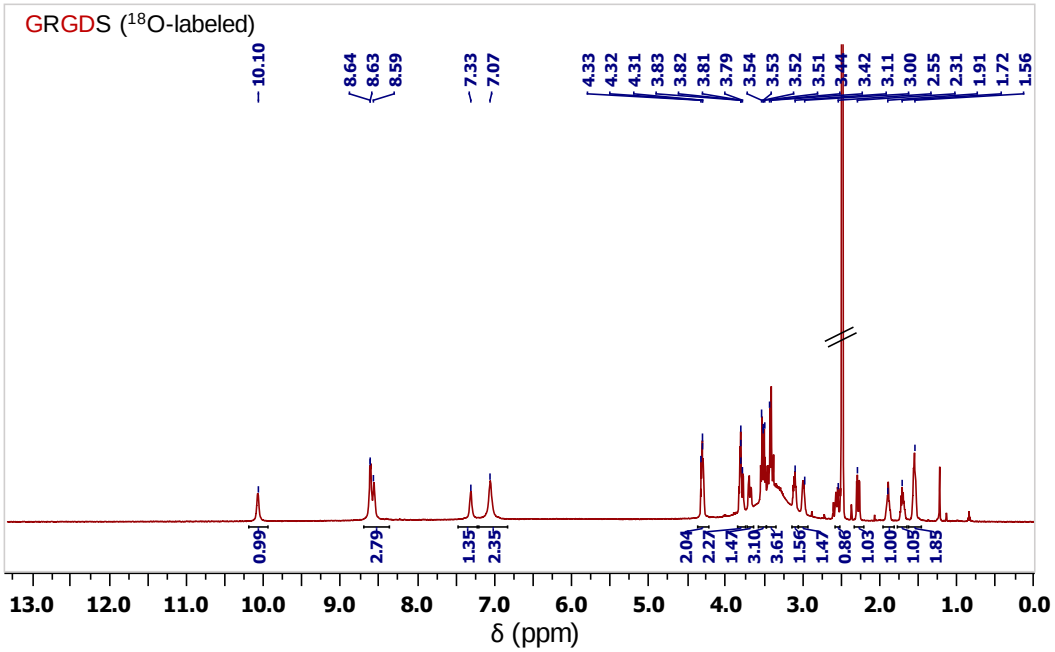

Figure V-12: ^{13}C solution NMR spectrum of ^{18}O-labeled GRGDS peptide (DMSO-d_6, 600 MHz). Isotope effect of ^{18}O on the ^{13}C carbonyl peak shift is displayed in the zoomed region. The solvent peak is crossed out.

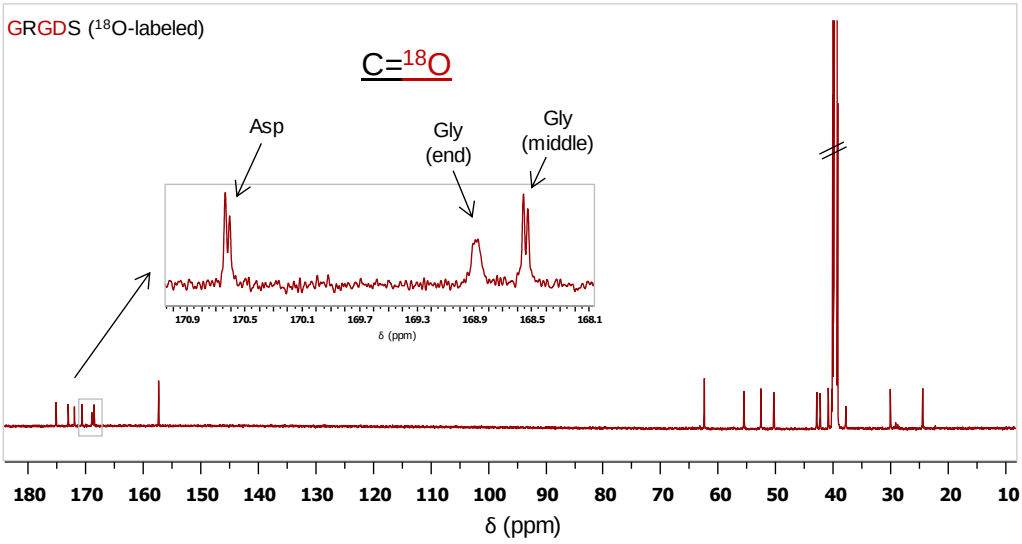

Figure V-13: COSY (^1H-^1H correlation) solution NMR spectrum of ^{18}O-labeled GRGDS peptide (DMSO-d_6, 600 MHz). The solvent peaks are crossed out in the projections.

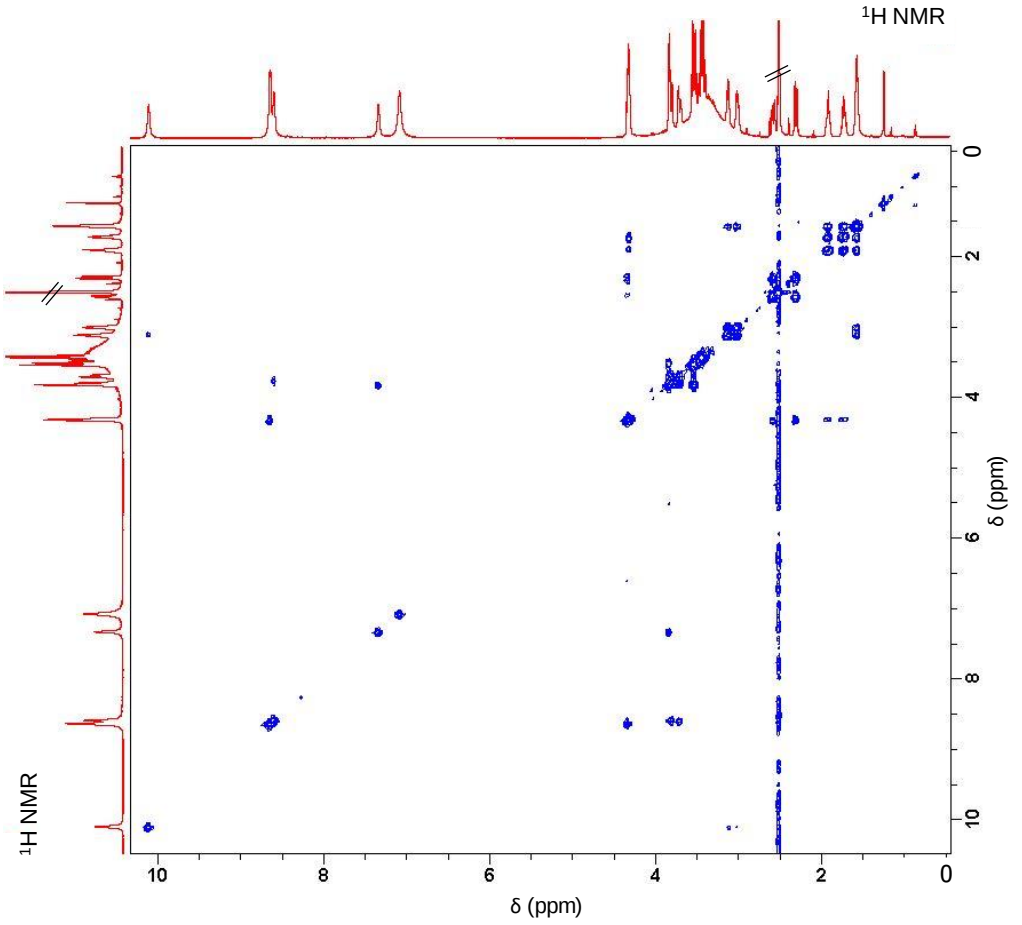

Figure V-14: HSQC (^{1}H-^{13}C correlation) solution NMR spectrum of ^{18}O-labeled GRGDS peptide (DMSO-d_6, 600 MHz). The solvent peaks are crossed out in the projections.

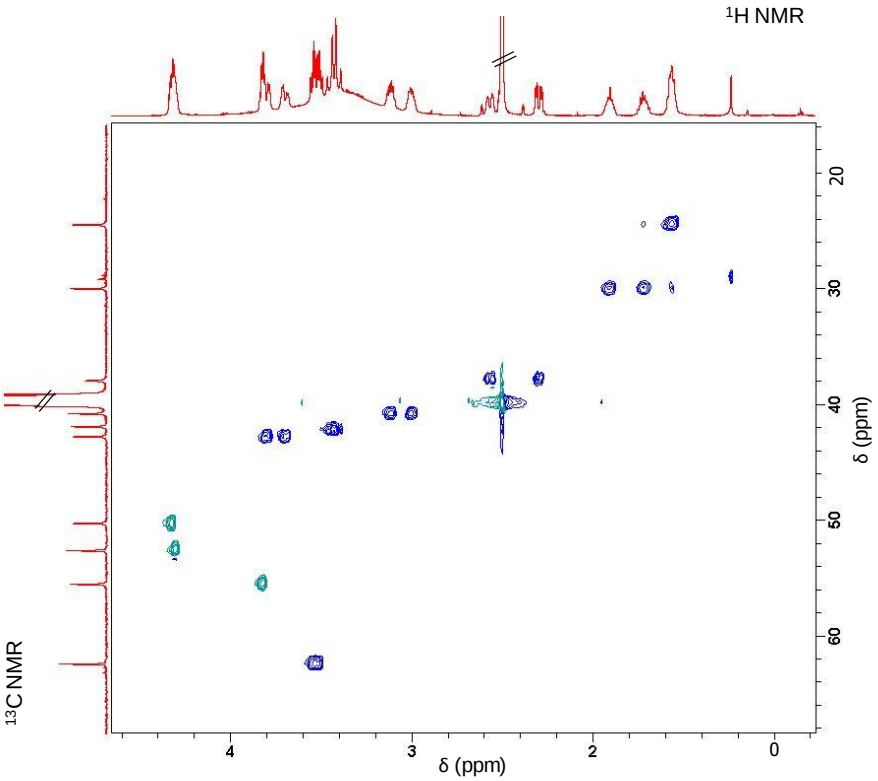

Figure V-15: HMBC (^{1}H-^{13}C correlation) solution NMR spectrum of ^{18}O-labeled GRGDS peptide (DMSO-d_6, 600 MHz). The solvent peaks are crossed out in the projections.

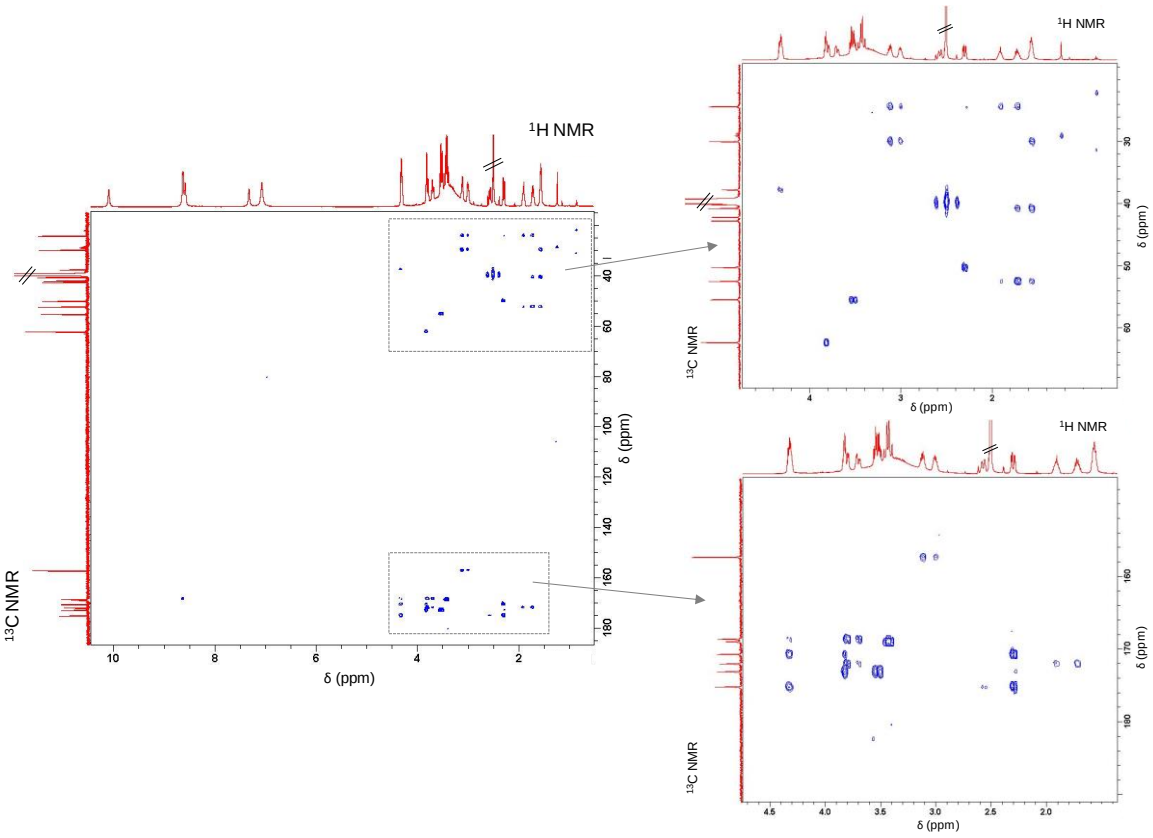

Table V-3: Complete ^{1}H and ^{13}C structural assignments of ^{18}O-labeled GRGDS peptide.

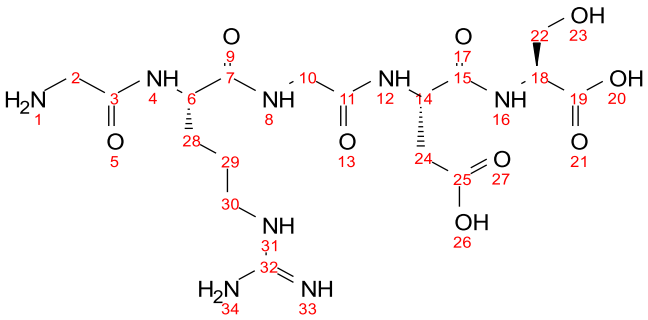

Atom number	^{13}C shift [ppm]	Carbon type	Protons attached [ppm]	Multiplicity	J-coupling	Assignment	HMBC correlation
29	24.5	CH_2	1.56	m		middle CH_2 in Arg	CH_2-next to guanidine CH_2-next to C*-Arg
28	30.0	CH_2	1.72 1.92	m m		CH_2 next to C* in Arg	CH_2-middle Arg CH_2-next to guanidine
24	37.9	CH_2	2.30 2.58	dd dd	4.9 Hz, 15.9 Hz 3.3 Hz, 15.9 Hz	CH_2 next to C* in Asp	C*H-Asp
30	40.7	CH_2	3.00 3.12	m m		CH_2 next to guanidine in Arg	CH_2-middle Arg CH_2-next to C*-Arg
2	41.9	CH_2	3.43	dd	16.1 Hz	CH_2 in ending Gly	
10	42.8	CH_2	3.70 3.79	dd dd	5.7 Hz, 16.3 Hz 5.1 Hz, 16.3 Hz	CH_2 in middle Gly	
14	50.2	CH	4.33	m		C*H in Asp	CH_2-Asp
6	52.6	CH	4.31	m		C*H in Arg	CH_2-next to C*-Arg CH_2-middle Arg
18	55.5	CH	3.83	"t"	5.6 Hz	C*H in Ser	CH_2-Ser
22	62.5	CH_2	3.50 3.54	dd dd	5.9 Hz, 10.4 Hz 5.1 Hz, 10.4 Hz	CH_2 between OH and C* in Ser	C*H-Ser
32	157.4	C_q	-	-		$NH_2(NH)C$=NH in guanidine	CH_2-next to guanidine
11	168.5	C=^{18}O	-	-		Labeled C=^{18}O in middle Gly	CH_2 in middle Gly, C*H-Asp
3	168.9	C=^{18}O	-	-		Labeled C=^{18}O in ending Gly	CH_2 in ending Gly

15	170.8	C=^{18}O	-	-		Labeled C=^{18}O in Asp-main	C*H-Asp, CH_2-Asp, C*H-Ser
7	172.1	C=O	-	-		C=O in Arg	CH_2-Arg, CH_2 in middle Gly
19	173.3	C=O	-	-		C=O in Ser	C*H-Ser, CH_2-Ser
25	175.4	COOH	-	-		COOH in Asp-side	CH_2-Asp, C*H-Asp
33, 34	-	C(*NH_2*) =*NH* (2xH)	7.08	br s		C(N*H_2*)=N*H* in guanidine	
16	-	NH	7.33	br s		NH in Ser	
8	-	NH	8.60	br s		NH in middle Gly	
4, 12	-	2xNH	8.63	br s, ovlp		NH in Arg, NH in Asp	
31	-	NH	10.10	br s		NH in guanidine	
1	-	NH_2	labile -> exchanged			NH_2 in ending Gly	
34	-	NH_2	labile -> exchanged			NH_2 in guanidine	
23	-	OH	labile -> exchanged			OH in Ser	
20, 26	-	CO*OH*	labile -> exchanged			acidic OH in Asp-side and ending Ser	

REFERENCES

1. Massiot, D.; Fayon, F.; Capron, M.; King, I.; Le Calvé, S.; Alonso, B.; Durand, J.-O.; Bujoli, B.; Gan, Z.; Hoatson, G., Modelling one- and two-dimensional solid-state NMR spectra. *Magn. Res. Chem.* **2002,** *40* (1), 70-76.
2. AG, C.-N., *Novabiochem catalog & peptide synthesis handbook*.
3. Eissler, S.; Kley, M.; Bächle, D.; Loidl, G.; Meier, T.; Samson, D., Substitution determination of Fmoc-substituted resins at different wavelengths. *J. Pept. Sci.* **2017,** *23* (10), 757-762.
4. Bollhagen, R.; Schmiedberger, M.; Barlos, K.; Grell, E., A new reagent for the cleavage of fully protected peptides synthesised on 2-chlorotrityl chloride resin. *J. Chem. Soc. Chem. Comm.* **1994,** (22), 2559-2560.
5. Roux, S.; Zékri, E.; Rousseau, B.; Paternostre, M.; Cintrat, J.-C.; Fay, N., Elimination and exchange of trifluoroacetate counter-ion from cationic peptides: a critical evaluation of different approaches. *J. Pept. Sci.* **2008,** *14* (3), 354-359.

FINAL CONCLUSION AND PERSPECTIVES

The objective of this work was to develop and optimize new $^{17}O/^{18}O$-enrichment protocols for carboxylic acids, which would be fast, user-friendly and cost-efficient, with the emphasis being laid on the ^{17}O-labeling and applications of labeled species, illustrating the capacity of the proposed $^{17}O/^{18}O$ labeling protocols to provide answers to key scientific questions.

In this work, new enrichment schemes for $^{17}O/^{18}O$-labeling of carboxylic acids based on mechanochemistry were developed, focusing on two families of molecules: fatty acids and amino acids. All enrichment protocols were carefully optimized in order to provide the labeled products in moderate to high yields and with high enrichment levels, but also in a highly reproducible manner. The enriched molecules were thoroughly characterized in order to verify their purity, and to determine their enrichment level.

To be more specific, for the labeling of fatty acids two mechanochemical protocols were used: the CDI-activation/hydrolysis protocol and the saponification protocol. Compared to the CDI-activation/hydrolysis strategy, the saponification approach enabled to further speed up and facilitate the labeling process, and to access other species by broadening the scope of substrates. A total of nine fatty acids, including the polyunsaturated and highly sensitive fatty acids, such as EPA and DHA, were isolated pure with high yields (80 - 96 %) and with high enrichment levels (39 - 45 % for the ^{18}O-enriched acids using 97% $H_2{}^{18}O$, and 37 - 42 % for the ^{17}O-enriched acids using 90% $H_2{}^{17}O$). These results are based on reproducible protocols (n = 3 the most often). Moreover, the labeling schemes were successfully scaled-up producing up to 1 gram quantities of oleic acid and ~ 500 milligrams of stearic acids within half of a day.

^{17}O-Enriched oleic acid was then used for the preparation of ^{17}O-enriched material systems: ^{17}O-enriched zinc oleate and the ZnO-NPs grafted with ^{17}O-labeled oleic acid. Thanks to the high enrichment level, ^{17}O solid-state NMR spectroscopy could provide unprecedented insights into the structure and reactivity of these materials. In particular, a relationship between the ^{17}O NMR parameters and Zn···O distances in coordination polymers like zinc-oleate was determined (~ 6 ppm difference observed between two sets of ^{17}O resonances in zinc-oleate was estimated to be ~ 0.01 Å difference in distances between two types of Zn···O bonds), and, in addition, an oxygen isotopic exchange from the ^{17}O-enriched oleate to the surface layer of ZnO-NPs upon UV irradiation was observed for the first time.

The second part of the thesis focused on the $^{17}O/^{18}O$-enrichment of amino acids. Here, five amino acids were $^{17}O/^{18}O$-labeled using mechanochemical saponification and isolated pure

with medium to high yields (52 - 84 %) and with high enrichment levels (41 - 47 % for the ^{18}O-enriched acids using 99% $H_2{}^{18}O$, and 29 - 34 % for the ^{17}O-enriched acids using 70% $H_2{}^{17}O$). These results are based on reproducible protocols (n = 3 the most often). Moreover, no loss of enantiomeric excess upon the enrichment procedure was observed by chiral HPLC analysis. The efficiency of the mechanochemical labeling scheme was compared with an acid-catalysed oxygen exchange procedure, which is the protocol used the most frequently in the literature for the labeling of amino acids. In the latter case, a higher enrichment level was achieved for Gly and L-Lys molecules, reaching the maximal possible level under the reaction conditions used (*i.e.* ~ 60 % enrichment when starting from 99% $H_2{}^{18}O$). Moreover, in the case of L-Asp, Lewis acid was used for the first time to catalyse the oxygen exchange, leading to 28% enrichment yield (using 99% $H_2{}^{18}O$).

Furthermore, the protocols for preparation of ^{17}O/^{18}O-labeled Fmoc-Gly-O*H and Fmoc-L-Asp(O*t*Bu)-O*H, used as building blocks for the synthesis of ^{17}O/^{18}O-enriched peptides, were scaled-up, producing up to ~ 1 g and ~ 700 mg of labeled molecules, respectively, in a cost-efficient manner (17.5 µL of H_2O* for 100 mg of Fmoc-AA-O*H), and in just one day (work-up included). Using such protected amino acids for SPPS, the ^{17}O/^{18}O-labeled GRGDS peptides were then synthesized and isolated pure in high yields (41 - 57 %) and with high enrichment levels (43 % for ^{18}O-enriched peptide and 38 - 39 % for the ^{17}O-enriched peptides). The GRGDS peptides enriched in ^{17}O were also characterized for the first time by ^{17}O solid-state NMR spectroscopy.

Perspectives

Despite the many achievements of this work, some aspects of the early work could further be improved based on the knowledge acquired later during the process. To give a few specific examples, the reaction times used for the CDI-activation of fatty acids and for the hydrolysis of the unsaturated fatty acids, could be further optimized and probably reduced. Regarding the labeling of the amino acids, room for improvement is left in the enrichment procedures based on the acid-catalysed oxygen exchange. No optimization was yet performed in these processes, and it is therefore possible that the long time for the exchange (24 h) could be reduced, providing the same enrichment level. Also, in the case of L-Asp, where the reaction was catalysed by a Lewis acid (LiCl), further optimization in terms of the LiCl equivalents or the reaction time could potentially lead to higher enrichment levels. Moreover, if applied on L-Leu and L-Phe, the oxygen exchange reaction could probably also lead to higher isolated yields.

Regarding the synthesis of $^{17}O/^{18}O$-labeled peptides, additional investigation, which would explain the presence of the di-peptide (RD) side-product in the synthesis of tri-peptide RGD, and subsequently prevent its formation, is necessary. In addition, in the synthesis of GRGDS peptide enriched selectively on the side-chain of the aspartic acid, the very final step of saponification remains to be completed.

Regarding the future paths of this project, in terms of labeling, other carboxylic acids which serve for example as ligands or surfactants in (nano)materials synthesis are foreseen to be enriched. In addition, the enrichment protocols for other oxygen-containing functions in organic molecule, such as alcohols or carbonyls, will need to be looked into, as these functional groups are also very frequently found in biomolecules and organic ligands. Regarding future objectives of this work in terms of applications, studies of biological processes will be looked into, by looking at the interaction between the ^{17}O-labeled RGD or GRGDS peptides and biologically-relevant species, using ^{17}O solid-state NMR spectroscopy. In addition, other peptide sequences involved in biomineralization processes, such as polyaspartic acid, will also be considered to be enriched in $^{17}O/^{18}O$, and their role in mineralization will be studied by high-resolution ^{17}O solid-state NMR spectroscopy.

RÉSUMÉ EN FRANÇAIS

CONTEXTE ET OBJECTIFS DE L'ETUDE

L'oxygène est un élément omniprésent dans notre environnement, qui se trouve dans un grand nombre de composés organiques et inorganiques. Il participe à la formation des liaisons chimiques essentielles, telles que la liaison hydrogène qui, entre autres, définit la structure des protéines ou de l'ADN, ou encore la liaison de coordination, qui peut servir à la construction de matériaux moléculaires tels que les MOFs (Metal Organic Frameworks). Du fait de son importance, l'oxygène a fait l'objet de nombreuses études, afin d'examiner son environnement et déterminer la structure et la réactivité des composés qui le contiennent.

L'oxygène se trouve naturellement sous la forme de trois isotopes: l'oxygène-16 (qui est le plus abondant, 99.76 % d'abondance naturelle), l'oxygène-17 (qui est le plus rare avec ~ 0.04 % d'abondance naturelle) et enfin l'oxygène-18 (qui présente une abondance naturelle de 0.2 %) (voir Tableau F1).[1] Les très faibles variations de teneur en oxygène-18 sont étudiées par spectrométrie de masse à haute résolution pour déterminer l'évolution de la température sur la Terre (dans le domaine de la paléoclimatologie),[2] ou pour contrôler l'origine et la qualité d'aliments (dans le domaine de la chimie forensique).[3] Concernant les autres domaines d'application qui utilisent des techniques analytiques avancées pour étudier des molécules et des matériaux, et qui reposent sur la signature d'isotopes stables, l'enrichissement en oxygène-17/18 des composés est souvent indispensable. C'est le cas notamment pour l'oxygène-17 qui est le seul isotope stable de l'oxygène ayant un spin nucléaire non-nul, et qui est donc observable par la spectroscopie RMN (Résonance Magnétique Nucléaire).[4]

Tableau F1 : Isotopes stables de l'oxygène, leur abondance naturelle et le prix de l'eau enrichie en $^{17}O/^{18}O$.

Isotope	Masse atomique[1]	Abondance naturelle[1]	Spin nucléaire (I)	Prix de 1 mL de H_2O*
Oxygène-16	15.9949	99.757 %	0	-
Oxygène-17	16.9991	0.038 %	5/2	1800 - 2900 € (90 % de ^{17}O)
Oxygène-18	17.9992	0.205 %	0	60 - 150 € (97 - 99 % de ^{18}O)

Plusieurs voies de synthèse existent pour enrichir les molécules organiques en isotopes de l'oxygène-17/18, mais celles-ci sont généralement chères, car elles nécessitent d'utiliser de grands excès de précurseurs coûteux enrichis en $^{17}O/^{18}O$. En effet, de l'eau enrichie à 90 % en ^{17}O, qui est un précurseur souvent utilisé pour l'enrichissement des molécules organiques, peut

coûter entre 1800 et 2900 € par millilitre (voir Tableau F1). De plus, la durée de ces synthèses est souvent longue avec des conditions contraignantes (acides fortes, températures élevées).[5] Dans ce contexte, la mécanochimie est récemment apparue comme une approche très intéressante pour l'enrichissement des molécules en $^{17}O/^{18}O$, car elle permet de réduire considérablement les quantités d'eau enrichie utilisées ainsi que la durée des synthèses. De plus les réactions se font à température ambiante.[6]

L'objectif de cette thèse était double : *i)* développer de nouvelles voies d'enrichissement en $^{17}O/^{18}O$ de molécules organiques contenant la fonction acide carboxylique, plus précisément d'acides gras et d'acides aminés, par mécanochimie, et *ii)* utiliser certains des composés marqués au ^{17}O pour préparer et étudier la structure de biomolécules et de nanomatériaux fonctionnels. En outre, la thèse comprend une part importante de données analytiques, telles que la RMN (y compris la RMN ^{17}O à l'état solide), et la spectrométrie de masse.

CHAPITRE F1 - ÉTAT DE L'ART

F1.1 VOIES D'ENRICHISSEMENT EN $^{17}O/^{18}O$

Dans le contexte de cette thèse, seules les voies d'enrichissement des fonctions acide carboxylique seront décrites et discutées. Une revue dédiée spécifiquement à l'enrichissement de molécules organiques en $^{17}O/^{18}O$ peut être trouvée dans l'article rédigé par Theodorou *et al.* en 2014.[5] Ces procédures peuvent être divisées en deux groupes : *i)* les voies d'enrichissement basées sur un équilibre thermodynamique entre le substrat et de l'eau enrichie, et *ii)* les voies d'enrichissement utilisant des réactions irréversibles entre un acide carboxylique activé et de l'eau enrichie. Dans ce manuscrit, les atomes d'oxygène enrichis seront marqués par une étoile (O*) et avec la couleur rouge (pour l'oxygène enrichi en général ou pour l'enrichissement en ^{18}O) ou la couleur verte (pour l'enrichissement en ^{17}O).

a) Équilibre thermodynamique - échange d'oxygène catalysé par un acide

L'échange d'oxygène sous équilibre thermodynamique est une méthode très souvent utilisée pour l'enrichissement d'acides carboxyliques. Ici, les trois isotopes de l'oxygène sont échangés entre le substrat non-enrichi et l'eau enrichie, *via* un « scrambling » isotopique (mélange des isotopes conduisant à une distribution isotopique équilibrée). A l'état d'équilibre, chaque atome d'oxygène échangeable a la même composition isotopique (^{16}O, ^{17}O et ^{18}O), et le produit final est un mélange de molécules non-enrichies, de molécules avec un oxygène enrichi (mono-marquées) et de molécules avec deux oxygènes enrichis (doublement marquées) (Schéma F1).

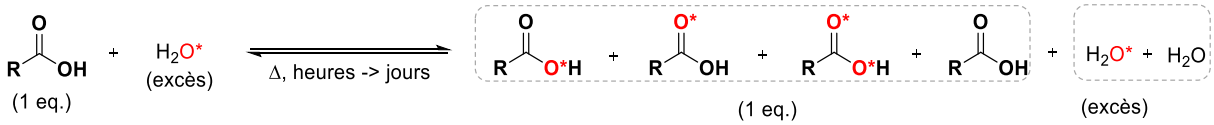

Schéma F1 : Synthèse d'acides enrichis par la voie d'échange d'oxygène.

Cette méthode peut fournir des produits avec un taux d'enrichissement très élevé, en fonction de l'excès d'eau enrichie utilisé et de sa composition isotopique. Par contre, cette méthode présente quelques désavantages:

- Un grand excès d'eau enrichie est fréquemment utilisé (20 - 50 eq.). Dans un certain nombre de cas d'enrichissement en ^{17}O, un processus additionnel de recyclage de l'eau enrichie a été implémenté, afin de rendre la procédure moins coûteuse.

- Les durées des réactions sont longues, afin d'atteindre l'équilibre thermodynamique. Pour accélérer les réactions, un acide fort est ajouté (souvent de l'acide chlorhydrique), et les synthèses sont réalisées à haute température. Ces conditions contraignantes ne sont pas compatibles avec tous les substrats ou produits, et peuvent provoquer leur décomposition.

- Les réactions sont souvent réalisées sous atmosphère inerte (afin d'empêcher l'eau non-enrichie présente dans l'air de réagir avec le substrat), et dans les cas où il est nécessaire d'utiliser des solvants organiques (pour augmenter la solubilité du substrat), ces solvants doivent être séchés au préalable pour que la composition isotopique de l'eau enrichie ne se retrouve pas abaissée.

Des exemples de cette voie d'enrichissement sont discutés dans la version anglaise de cette manuscrit (Chapitre 1.1.1).

b) Réactions irréversibles - hydrolyse

Des réactions irréversibles sont également utilisées pour l'enrichissement d'acides carboxyliques. Ici, un réactif activé (par exemple sous la forme d'ester ou de chlorure d'acyle) est hydrolysé par de l'eau enrichie, généralement sous conditions modérées. En utilisant cette méthode, en seul des deux atomes d'oxygène de la fonction acide carboxylique peut être enrichi, ce qui réduit le taux d'enrichissement maximal accessible (Schéma F2).

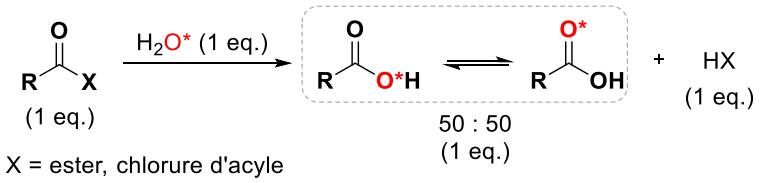

Schéma F2 : Synthèse d'acides enrichis utilisant des réactions irréversibles.

Afin d'enrichir les deux oxygènes et d'augmenter le taux d'enrichissement, des nitriles (qui peuvent aussi servir de précurseurs d'acides carboxyliques) ont été hydrolysés par de l'eau enrichie. Cependant, ces réactions ont été réalisées dans des conditions contraignantes (haute température, acides forts). Une autre possibilité est d'isoler le produit enrichi, puis de réactiver la fonction carboxylique et enfin répéter l'hydrolyse avec de l'eau enrichie. Il est également possible de faire des cycles de réactivation et d'hydrolyse *in-situ*, sans isoler les produits intermédiaires.[7]

Des exemples de ce type sont discutés dans la version anglaise de ce manuscrit (Chapitre 1.1.2).

Dans l'ensemble, les voies synthétiques d'enrichissement d'acides carboxyliques accessibles dans la bibliographie présentent un certain nombre de limitations : de grandes quantités d'eau enrichie sont utilisées (donc les synthèses sont coûteuses), les conditions réactionnelles sont contraignantes (hautes températures, acides forts, temps de réaction élevés), et/ou les protocoles expérimentaux sont incomplets ou non détaillés. De ce fait, l'utilisation et la dissémination de ces procédures au sein de la communauté scientifique restent très limitées. Il y a donc un réel besoin de développer des protocoles nouveaux d'enrichissement en $^{17}O/^{18}O$ qui soient plus faciles, plus rapides, plus efficaces et moins chers. Dans cette thèse, il a été envisagé de répondre à cette demande en enrichissant les acides carboxyliques en $^{17}O/^{18}O$ par mécanochimie (principalement des acides gras, des acides aminés et des peptides).

F1.2 MECANOCHIMIE

La mécanochimie est le domaine de la chimie qui correspond aux réactions chimiques induites par des forces mécaniques. Ce domaine est en plein développement.[8] Historiquement, elle était plutôt utilisée pour la préparation de matériaux inorganiques, mais depuis quelques dizaines d'années elle est aussi appliquée dans les synthèses de molécules organiques.[9] Le plus grand avantage de la mécanochimie est que l'utilisation des solvants de réaction est réduite au minimum. La réaction est ainsi réalisée dans un milieu réactionnel très concentré et grâce à cet aspect, elle est très souvent beaucoup plus rapide qu'en solution.

La réaction mécanochimique se déroule dans un réacteur qui contient des billes et des réactifs, et qui est lui-même placé dans un broyeur (Figure F1). Les réacteurs ainsi que les billes sont fabriqués en matériaux variés (par exemple en acier inoxydable ou en Téflon), et avec des tailles variables. Le mouvement rapide du broyeur est transmis aux billes dans le réacteur, et le déplacement de celles-ci favorise la réduction de la taille des particules des réactifs solides, l'homogénéisation du milieu réactionnel, et la création des nouvelles surfaces disposées à réagir. En ajoutant un additif liquide en très petite quantité (quelques microlitres), il est possible de faciliter encore davantage l'homogénéisation et le déplacement des réactifs solides. Cette technique s'appelle le « Liquid Assisted Grinding » (LAG). Au démarrage de cette thèse, la technique LAG avait déjà été utilisée au laboratoire, pour l'enrichissement isotopique en ^{17}O de précurseurs organiques et inorganiques.[6, 10] Au cours de cette thèse, elle a également été appliquée pour enrichir des composés en ^{17}O.

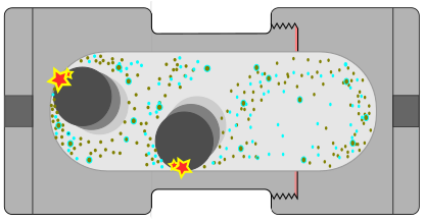

Figure F1 : Schéma d'un réacteur contenant deux billes, des réactifs introduits et des intermédiaires et produits progressivement formés.

F1.3 ANALYSES DES MOLECULES ENRICHIES EN $^{17}O/^{18}O$

Les acides carboxyliques enrichis en oxygène $^{17}O/^{18}O$ ont été caractérisés, entre autres, par des techniques d'analyses qui reposent sur la signature d'isotopes stables: RMN solide de l'oxygène-17, spectroscopie infrarouge (IR) et spectrométrie de masse (MS).

a) RMN solide de l'oxygène-17

La spectroscopie de Résonance Magnétique Nucléaire (RMN) est une technique potentiellement puissante pour analyser le voisinage local des atomes. Ayant la possibilité d'analyser finement le voisinage local des atomes d'oxygène, cette méthode peut aider à comprendre la structure et la réactivité d'un grand nombre de systèmes.[4] En particulier, la RMN ^{17}O peut être utilisée pour examiner les modes de liaison des ligands situés au niveau des surfaces et des interfaces dans des (bio)matériaux composites et des (nano)matériaux. Cependant, elle est très peu sensible dans le cas de l'oxygène, majoritairement à cause de la très faible abondance naturelle de l'oxygène-17 (0.04%), qui est le seul isotope actif en RMN. Il est donc souvent nécessaire d'enrichir au préalable les composés d'intérêt en oxygène-17. De plus, l'oxygène-17 est un noyau quadripolaire (il a un spin nucléaire I = 5/2), ce qui entraîne des difficultés additionnelles (discutées en détails dans la version anglaise de ce manuscrit).

b) Spectroscopie infrarouge

La spectroscopie infrarouge (IR) permet de déterminer la présence des groupements fonctionnels ou la nature de certaines liaisons chimiques dans les composés organiques et inorganiques. Certaines liaisons particulières (C=O, O-H…) vibrent en effet à une fréquence caractéristique, appelée ‘‘bande de vibration’’, qui dépend des atomes de la liaison. En remplaçant un atome dans un groupe fonctionnel avec son isotope plus lourd (par exemple ^{16}O remplacé par ^{18}O), on va provoquer un déplacement de la bande de vibration caractéristique vers les basses fréquences, et ce déplacement peut être utilisé pour l'attribution de tous les bandes associées avec le groupe fonctionnel contenant de l'oxygène enrichi.[11]

c) Spectrométrie de masse

La spectrométrie de masse est utilisée pour la détection, l'identification et la quantification de composés (en se basant sur leur rapport masse/charge (m/z)), et permet parfois d'accéder à la structure chimique de molécules complexes (*via* l'exploration des fragments formés par exemple). Seules les molécules chargées (positivement ou négativement) peuvent être analysées par spectrométrie de masse. En utilisant une source d'ionisation douce (comme l'ionisation par électrospray (ESI)), la molécule est peu fragmentée, et les ions moléculaires sont formés en majorité.

À cause de la présence de différents isotopes dans les molécules analysées (naturellement abondants ou introduits artificiellement), la molécule n'est pas identifiée seulement par le rapport m/z, mais aussi grâce à son profil isotopique caractéristique. En utilisant les données obtenues par l'analyse par spectrométrie de masse de produits enrichis en $^{17}O/^{18}O$ (rapports m/z et abondance relative), les taux d'enrichissement ont pu être déterminés.

CHAPITRE F2 - ENRICHISSEMENT D'ACIDES GRAS

Le contenu de ce Chapitre F2 est basé sur une partie du travail publié dans:

- Špačková, J.; Fabra, C.; Cazals, G.; Hubert-Roux, M.; Schmitz-Afonso, I.; Goldberga, I.; Berthomieu, D.; Lebrun, A.; Métro, T.-X.; Laurencin, D., Cost-efficient and user-friendly $^{17}O/^{18}O$ labeling procedures of fatty acids using mechanochemistry. *Chem. Commun.* **2021**, *57*, 6812-6815

- Špačková, J.; Fabra, C.; Mittelette, S.; Gaillard, E.; Chen, C.-H.; Cazals, G.; Lebrun, A.; Sene, S.; Berthomieu, D.; Chen, K.; Gan, Z.; Gervais, C.; Métro, T.-X.; Laurencin, D., Unveiling the Structure and Reactivity of Fatty-Acid Based (Nano)materials Thanks to Efficient and Scalable ^{17}O and ^{18}O-Isotopic Labeling Schemes. *J. Am. Chem. Soc.* **2020**, *142* (50), 21068-21081.

Les acides gras sont des biomolécules très importantes avec des applications nombreuses, par exemple dans les domaines de la métabolomique ou de la lipidomique. Ils sont également utilisés comme surfactants pour la synthèse de nanoparticules, en jouant un rôle sur leur forme et leurs propriétés finales. La bibliothèque complète des acides gras enrichis en $^{17}O/^{18}O$ dans cette thèse est affichée dans la Figure F2.

a) Acides gras saturés

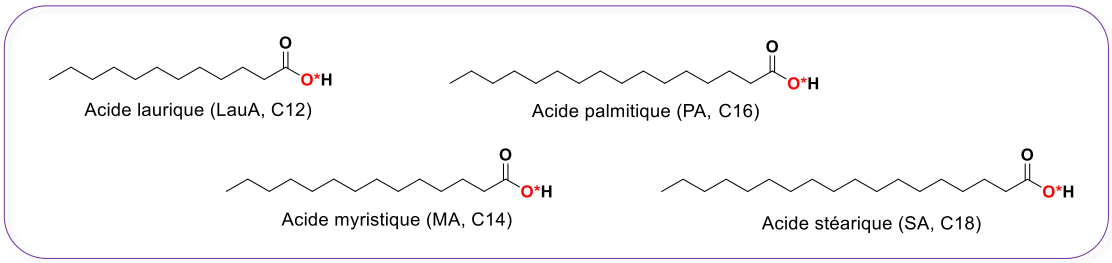

b) Acides gras insaturés

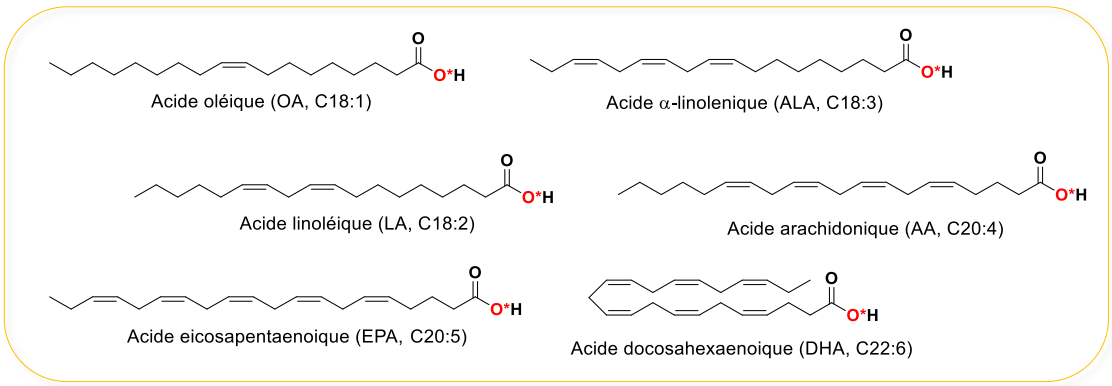

Figure F2: Les acides gras enrichis en $^{17}O/^{18}O$ au cours de cette thèse. Les deux oxygènes des fonctions acides carboxyliques sont enrichis avec la même probabilité (50 : 50, entre le C=O* et le C-O*H).

F2.1 ACIDES GRAS ENRICHIS PAR ACTIVATION AU CDI SUIVI D'UNE HYDROLYSE

L'enrichissement en $^{17}O/^{18}O$ d'acides gras à chaîne saturée (ne contenant pas de double liaison), avec une longueur de chaîne variable entre C12 et C18, ainsi que d'acides gras insaturés ayant jusqu'à quatre double liaisons, a été réalisé en adaptant et en optimisant les protocoles déjà publiés qui sont basés sur l'activation de la fonction acide carboxylique à l'aide du 1,1'-carbonyldiimidazole (CDI), suivi d'une hydrolyse par de l'eau enrichie (Schéma F3).[12]

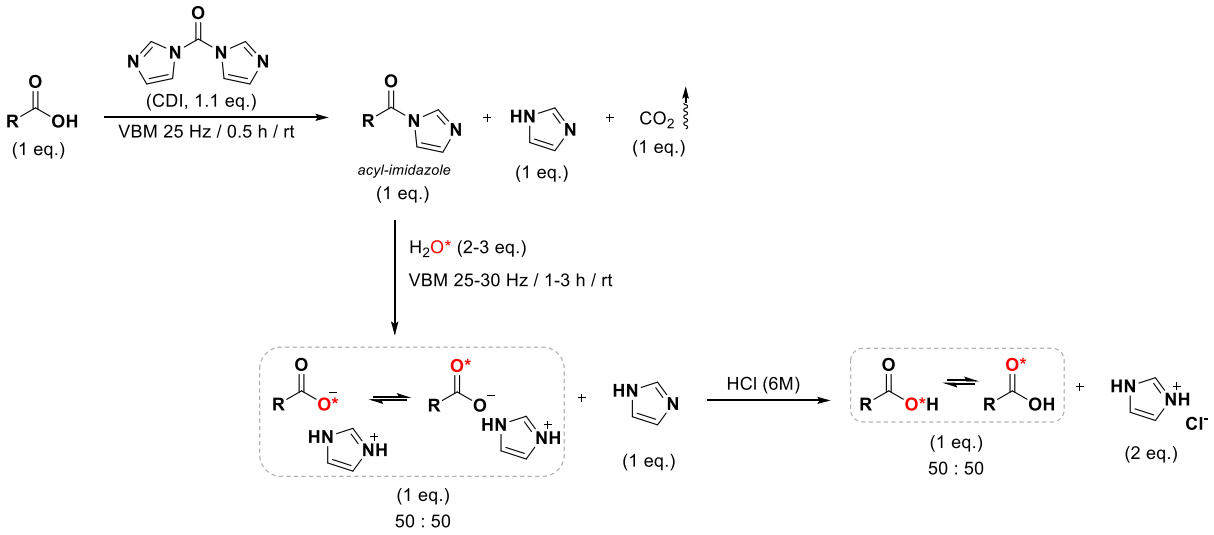

Schéma F3 : Le protocole d'enrichissement d'acides gras basé sur l'activation au CDI suivi par l'hydrolyse. R = la chaîne aliphatique spécifique. VBM = broyage vibrant, rt = température ambiante.

a) Enrichissement en $^{17}O/^{18}O$ d'acides gras saturés

Les acides gras saturés ont été enrichis par la méthode mentionnée ci-dessus (Schéma F3). Tous les acides gras saturés ont été activés par broyage pendant 30 min à 25 Hz en présence de CDI dans un réacteur en acier inoxydable contenant deux billes du même matériau. Cependant, la durée et la fréquence à appliquer pour permettre l'hydrolyse complète de l'intermédiaire activé par trois équivalents d'eau enrichie ont dû être adaptées selon le substrat. Dans le cas de l'acide stéarique, il n'était pas possible de finir l'hydrolyse sans addition de base (carbonate de potassium). Tous les produits ont été isolés purs avec des rendements corrects (80 - 91 %) et des taux d'enrichissement élevés (taux d'enrichissement moyen des atomes d'oxygène 44 - 47 % et 42 - 44 %, en utilisant de l'eau enrichie à 97% en ^{18}O ou à 90% en ^{17}O, respectivement) (voir Tableau F2).

Tableau F2 : Récapitulatif des acides gras saturés enrichis en $^{17}O/^{18}O$ en utilisant le protocole d'activation au CDI suivi d'une hydrolyse.

Produit enrichi	**Rendement [%]**	**EY[a] [%]**	**^{18}O-EL[b] [%]**	**^{17}O-EL[c] [%]**
Acide laurique (LauA, C12)	82	97	47	44
Acide myristique (MA, C14)	80	96	46	44
Acide palmitique (PA, C16)	88	96	47	43
Acide stéarique (SA, C18)	84	91	44	42
Acide stéarique-^{13}C (^{13}C-SA, C18)	91	94	44	43

[a] EY = Rendement d'enrichissement en $^{17}O/^{18}O$, [b] ^{18}O-EL = Taux d'enrichissement en utilisant de l'eau enrichie à 97 % en ^{18}O, [c] ^{17}O-EL = Taux d'enrichissement en utilisant de l'eau enrichie à 90 % en ^{17}O. Toutes les valeurs correspondent à la moyenne de plusieurs expériences (voir Annexe II pour plus de détails).

b) Enrichissement en $^{17}O/^{18}O$ d'acides gras insaturés

Les acides insaturés ont également été enrichis par le protocole d'activation au CDI suivi d'une hydrolyse. Plus spécifiquement, l'acide oléique a été activé par broyage en présence de CDI pendant 30 min à 25 Hz dans un réacteur en acier inoxydable avec deux billes du même matériau, et l'intermédiaire activé a été hydrolysé pendant 60 min de broyage à 25 Hz. Dans le cas d'acides gras polyinsaturés, l'enrichissement a été réalisé en utilisant un réacteur en téflon. La durée d'activation était de 20 min, et la durée de l'hydrolyse de 90 min, pour un broyage à 25 Hz. Tous les produits ont été isolés purs avec des rendements corrects (88 - 90 %) et des taux d'enrichissement élevés (taux d'enrichissement moyen de l'oxygène 39 - 44 % et 37 - 42 %, en utilisant de l'eau enrichie à 97% en ^{18}O ou à 90% en ^{17}O, respectivement) (voir Tableau F3).

Tableau F3 : Récapitulatif des acides gras insaturés enrichis en $^{17}O/^{18}O$, en utilisant le protocole d'activation au CDI suivi d'une hydrolyse.

Produit enrichi	**Rendement [%]**	**EY[a] [%]**	**^{18}O-EL[b] [%]**	**^{17}O-EL[c] [%]**
Acide oléique (OA, C18:1)	90	90	44	42
Acide linoléique (LA, C18:2)	90	87	41	40
Acide α-linolénique (ALA, C18:3)	88	87	43	40
Acide arachidonique (AA, C20:4)	89	81	39	37

[a] EY = Rendement d'enrichissement en $^{17}O/^{18}O$, [b] ^{18}O-EL = Taux d'enrichissement en utilisant de l'eau enrichie à 97 % en ^{18}O, [c] ^{17}O-EL = Taux d'enrichissement en utilisant de l'eau enrichie à 90 % en ^{17}O. Toutes les valeurs correspondent à moyenne de plusieurs expériences (voir Annexe II pour plus de détails).

c) Enrichissement en $^{17}O/^{18}O$ d'acides gras: montée en échelle

Afin de produire des quantités d'acides gras enrichis suffisantes pour l'utilisation de ces acides gras dans la synthèse de nanoparticules ou de matériaux moléculaires, les protocoles d'enrichissement de l'acide oléique (enrichi en ^{17}O) et de l'acide stéarique (enrichi en ^{18}O) à échelle plus élevée ont été développés. L'acide oléique a ainsi été produit sous forme pure, avec un rendement (92%) et un taux d'enrichissement (43%) comparables à ceux obtenus à petite échelle. Ici, un gramme d'acide oléique enrichi en ^{17}O a été produit en seulement ~ 2 heures (traitement compris). L'acide stéarique a également été produit pur, avec un rendement plus élevé (95 %) et un taux d'enrichissement (46%) comparable de celui obtenu à petite échelle. Ici, ~ 500 mg d'acide stéarique ont été produits en seulement ~ 4 heures (traitement compris).

F2.2 ACIDES GRAS ENRICHIS PAR SAPONIFICATION

Afin d'accéder aux autres acides gras polyinsaturés importants (comprenant jusqu'à six liaisons doubles), et pour élargir également la gamme de substrats utilisables pour l'enrichissement en $^{17}O/^{18}O$ d'acides carboxyliques par méchanochimie, une nouvelle voie d'enrichissement basée sur la saponification a été développée. Ici, l'enrichissement se fait en une seule étape, par broyage de l'ester d'éthyle de l'acide gras avec de l'eau enrichie, en présence d'éthanolate de sodium. Dans un premier temps, l'éthanolate de sodium réagit avec H_2O^* pour former un hydroxyle enrichi (O^*H^-), qui va ensuite réagir avec l'ester d'éthyle de l'acide gras, fournissant l'acide gras enrichi sous forme de carboxylate de sodium (Schéma F4).

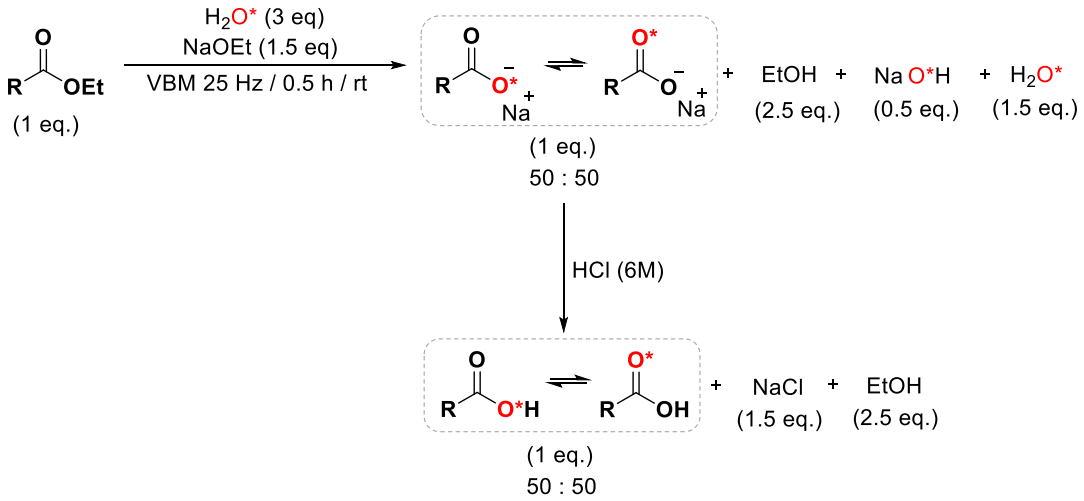

Schéma F4: Le protocole d'enrichissement d'acides gras polyinsaturés basé sur la saponification. R = la chaîne aliphatique spécifique. VBM = broyage vibrant, rt = température ambiante.

Les acides polyinsaturés ont été enrichis en 30 min de broyage à 25 Hz dans un réacteur en acier inoxydable avec deux billes du même matériau. Tous les produits ont été isolés purs avec des rendements très corrects (93 - 96 %) et des taux d'enrichissement élevés (taux d'enrichissement moyen de l'oxygène 45 % et 41 - 42 %, en utilisant de l'eau enrichie à 97% en ^{18}O ou à 90% en ^{17}O, respectivement) (voir Tableau F4).

Tableau F4 : Récapitulatif des acides gras polyinsaturés enrichis en $^{17}O/^{18}O$, en utilisant la saponification.

Produit enrichi	Rendement [%]	EY[a] [%]	^{18}O-EL[b] [%]	^{17}O-EL[c] [%]
Acide α-linolénique (ALA, C18:3)	96	93	45	42
Acide eicosapentaenoique (EPA, C20:5)	96	92	45	42
Acide docosahexaenoique (DHA, C22:6)	93	91	45	41

[a] EY = Rendement d'enrichissement en $^{17}O/^{18}O$, [b] ^{18}O-EL = Taux d'enrichissement utilisant de l'eau enrichie à 97 % en ^{18}O, [c] ^{17}O-EL = Taux d'enrichissement utilisant de l'eau enrichie à 90 % en ^{17}O. Toutes les valeurs correspondent à une moyenne de plusieurs expériences (voir Annexe II pour plus de détails).

F2.3 ANALYSES DES PRODUITS ENRICHIS EN $^{17}O/^{18}O$

Les acides gras enrichis en oxygène $^{17}O/^{18}O$ ont été caractérisés, entre autres, par les analyses qui reposent sur la signature d'isotopes stables : RMN solide de l'oxygène-17, spectroscopie infrarouge (IR) et spectrométrie de masse (MS).

Seuls les acides gras saturés et l'acide oléique enrichi en ^{17}O ont été analysés par la spectroscopie RMN solide ^{17}O dans le cadre de cette thèse. Dans tous les cas, du fait de l'enrichissement élevé, des spectres RMN ^{17}O ont été obtenus en quelques heures seulement sur un spectromètre 600 MHz.

Les bandes de vibration liées aux fonctions acides carboxyliques enrichies ont été attribuées dans le spectre IR de l'acide stéarique, par comparaison des données obtenues sur les composés marqués en ^{17}O et ^{18}O.

Les structures fines isotopiques d'acides gras enrichis en $^{17}O/^{18}O$ ont été attribuées dans des spectres de masse de très-haute résolution, enregistrés sur un spectromètre FT-ICR (Fourier-Transform Ion Cyclotron Resonance). De plus, dans le cas de l'acide α-linolénique qui avait été enrichi en utilisant les deux méthodes mécanochimiques décrites ci-dessus (CDI/hydrolyse et saponification), il a été observé que le produit issu de l'activation au CDI suivi d'une hydrolyse contenait environ dix fois plus des molécules enrichies sur les deux oxygènes en comparaison avec le produit obtenu par la saponification.

Par ailleurs, l'effet isotopique sur le déplacement chimique des atomes de carbone des acides carboxyliques en RMN ^{13}C liquide a été remarqué dans tous les produits enrichis en ^{18}O. A cause de la présence d'un isotope ^{18}O dans un groupe acide carboxylique, un décalage de signal du carbone de l'acide de ~ 0.025 ppm a été observé.

CHAPITRE F3 - UTILISATION DE L'ACIDE OLEIQUE ENRICHI EN ^{17}O DANS L'ELUCIDATION STRUCTURALE DE MATERIAUX

Le contenu de ce Chapitre F3 est basé sur le travail publié dans:

- Špačková, J.; Fabra, C.; Mittelette, S.; Gaillard, E.; Chen, C.-H.; Cazals, G.; Lebrun, A.; Sene, S.; Berthomieu, D.; Chen, K.; Gan, Z.; Gervais, C.; Métro, T.-X.; Laurencin, D., Unveiling the Structure and Reactivity of Fatty-Acid Based (Nano)materials Thanks to Efficient and Scalable ^{17}O and ^{18}O-Isotopic Labeling Schemes. *J. Am. Chem. Soc.* **2020**, *142* (50), 21068-21081.

L'une des applications des acides gras se trouve dans les (nano)matériaux. Les acides gras sont utilisés pour préparer des savons,[13] des formulations pour des médicaments,[14] ou pour la fonctionnalisation de la surface de matériaux inorganiques et de (nano)particules (NPs).[15-16] Pour illustrer les applications potentielles des acides gras enrichis en ^{17}O, deux types de matériaux ont été préparés : un polymère de coordination (l'oléate de zinc - Zn-OA) et des nanoparticules d'oxyde de zinc fonctionnalisées par l'acide oléique. Leurs structures et leur réactivité sous irradiation UV ont été étudiées par RMN solide ^{17}O.

F3.1 OLEATE DE ZINC - POLYMERE DE COORDINATION

a) Synthèse d'oléate de zinc par mécanochimie

L'oléate de zinc (Zn-OA, $Zn(C_{18}H_{33}O_2)_2$) a été produit en deux étapes en utilisant la mécanochimie. Premièrement, l'oléate de sodium a été créé par réaction entre l'acide oléique enrichi en ^{17}O et l'hydroxyde de sodium, en 10 minutes de broyage à 25 Hz. Après, le chlorure de zinc a été ajouté dans le réacteur et l'oléate de zinc a été formé en 15 min de broyage à 25 Hz (Schéma F5).

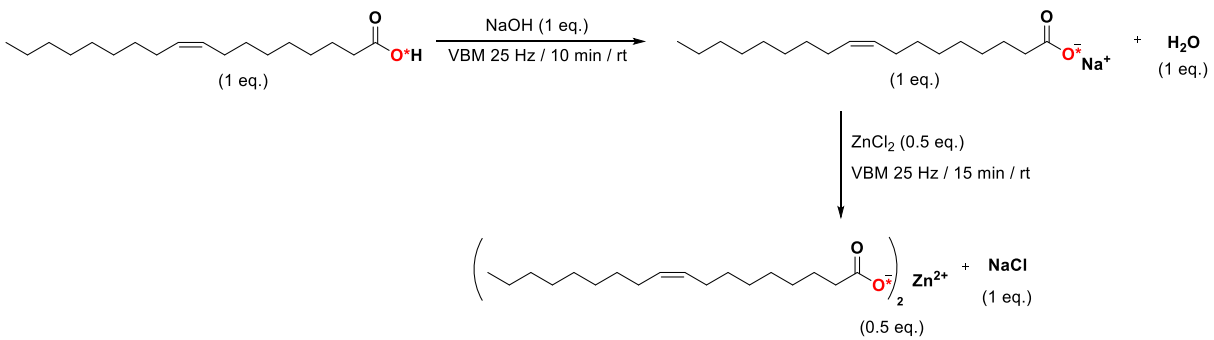

Schéma F5 : Mécanosynthèse d'oléate de zinc enrichi en ^{17}O. Les deux oxygènes sont enrichis avec le même taux d'enrichissement moyen (50 : 50) dans le produit final. Le produit final a été obtenu en mélange avec le chlorure de sodium. VBM = broyage vibrant, rt = température ambiante.

b) Analyses structurales de l'oléate de zinc

Afin de déterminer le mode de liaison entre le cation de zinc et les ligands oléate, l'oléate de zinc enrichi en ^{17}O a été analysé par spectroscopie IR et par RMN solide ^{13}C et ^{17}O. Dans le spectre IR, les bandes de vibration liées au groupe acide carboxylique ont été attribuées et comparées avec la bibliographie,[17] et il a été conclu que les ligands oléate sont coordonnés à deux cations de zinc différents, dans un mode de liaison bidentate. Ensuite, l'analyse RMN solide ^{13}C a montré dans la région des acides carboxyliques la présence de deux résonances séparées, qui peuvent être expliquées par l'existence de deux ligands carboxylates inéquivalents dans la structure crystalline de l'oléate de zinc. Enfin, l'analyse des spectres RMN solide ^{17}O a montré deux résonances correspondant à deux oxygènes avec des environnements différents, et ceux-ci ont été résolus en faisant l'expérience bidimensionnelle (MQMAS) (Figure F3). La différence de déplacement chimique isotrope n'était que de 6 ppm. Il a été déterminé par calculs DFT complémentaires que cette différence en ppm correspond à une très petite différence de ~ 0.01 Å dans la distance Zn···O.

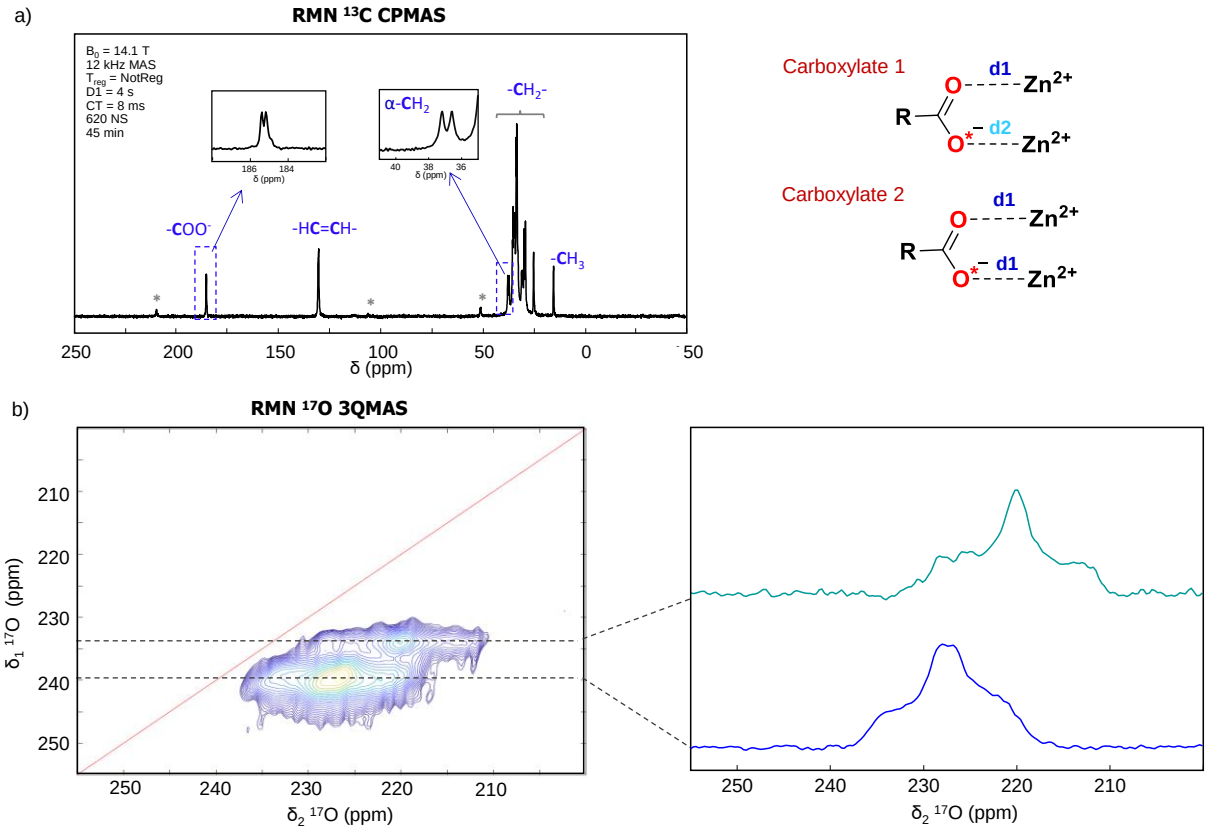

Figure F3 : a) Spectre RMN solide ^{13}C de l'oléate de zinc enrichi en ^{17}O enregistré sous 14.1 T, montrant la présence de deux carboxylates et deux groupes α-CH_2 inéquivalents (régions agrandies), b) Spectre RMN ^{17}O 3QMAS enregistré à ultra-haut champ (35.2 T, MagLab, Tallahassee, USA) (à gauche), et les deux résonances résolues (à droite).

F3.2 NANOPARTICULES D'OXYDE DE ZINC

a) Synthèse de (nano)particules de ZnO fonctionnalisées avec de l'acide oléique enrichi en ^{17}O

Les (nano)particules (NPs) d'oxyde de zinc ont été synthétisées par réaction entre l'acétate de zinc et l'hydroxyde de potassium.[18] Ensuite, la surface a été fonctionnalisée avec de l'acide oléique enrichi en ^{17}O. En parallèle, les NPs ont aussi été fonctionnalisées avec de l'acide oléique non-enrichi et utilisées comme échantillon témoin. Les NPs isolées ont été analysées par DRX, ATG, MET, IR et RMN solide multi-nucléaire.

b) Analyses des (nano)particules fonctionnalisées

D'abord, les (nano)particules ont été analysées par des méthodes analytiques couramment utilisées dans le domaine des (nano)matériaux, afin de déterminer leur forme et la densité de fonctionnalisation de surface. Ensuite, des analyses plus avancées par RMN solide ont été réalisées pour décrire le mode de liaison des molécules d'acide oléique à la surface des NPs.

Il a été montré par les analyses DRX et MET que les NPs ont pu être préparées sous la forme de « nanorods » (nano-bâtonnets), et que leur forme n'était pas changée après la fonctionnalisation de leur surface. La densité de la fonctionnalisation a été évaluée par analyse ATG, qui a montré une perte de masse correspondant à une densité de 2 molécules par nm^2.

Concernant le mode de coordination de l'acide oléique à la surface des NPs, il a été conclu que les ligands issus de l'acide oléique sont majoritairement sous leur forme déprotonée (oléate), et qu'ils sont attachés par une liaison de coordination entre les atomes d'oxygène carboxyliques et les cations Zn^{2+}, avec une très faible contribution des espèces interagissant par liaison hydrogène. Leur mode de liaison est différent de celui de l'oléate de zinc, avec des distances Zn···O plus importantes. Pour être un peu plus spécifique concernant les analyses effectuées :

- Sur le spectre IR, la bande de vibration caractéristique de la fonction acide carboxylique protonée (-COOH) n'est pas observée pour les NPs greffées.

- Sur le spectre de RMN solide ^{13}C, si le déplacement chimique du carbone de l'acide carboxylique est plus proche de celui d'un acide protoné, il reste compatible avec celui d'un acide déprotoné à cause de la variation possible des déplacements chimiques des carboxylates, en fonction de leur mode de liaison. De plus, aucune corrélation

hétéronucléaire ^{1}H-^{13}C n'a été observée et aucun proton acide n'a été détecté dans les spectres enregistrés à très basse température (jusqu'à -100 °C).

- Sur le spectre de RMN solide ^{17}O qui est montré sur la Figure F4, une résonance large centrée à ~ 200 ppm a été observée, cette région étant typique des acides carboxyliques ainsi que des carboxylates. Cependant, contrairement à ce qui a pu être observé pour l'acide oléique, elle n'est pas plus résolue à très basse température. Les autres pics plus petits correspondent quant à eux aux oxygènes en abondance naturelle dans le cœur des NPs (à ~ -18 ppm) et aux oxygènes en abondance naturelle dans un rotor en zircone (à ~ 380 ppm).

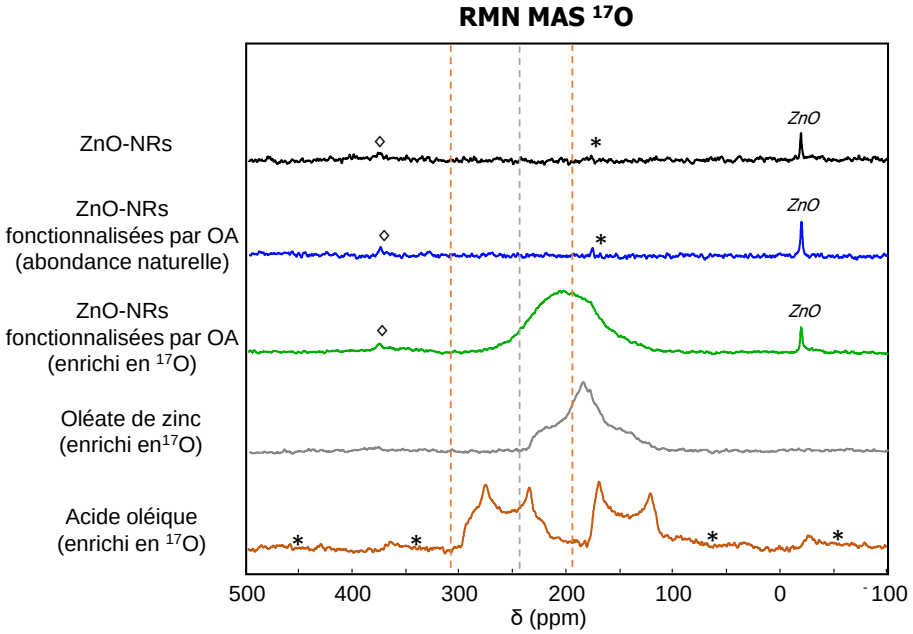

Figure F4: Les spectres de RMN MAS ^{17}O de ZnO-NPs non-fonctionnalisés (noir), ZnO-NPs fonctionnalisées par l'acide oléique (OA) non-enrichi (bleu), ZnO-NPs fonctionnalisées par l'acide oléique enrichi en ^{17}O (vert), comparés aux spectres de l'oléate de zinc enrichi en ^{17}O (gris), et de l'acide oléique enrichi en ^{17}O (marron). Tous les spectres ont été enregistrés à 14.1 T. Le symbole "*" correspond aux bandes de rotation, et le symbole "◊" correspond aux oxygènes en abondance naturelle dans le rotor en zircone. Les lignes en pointillé indiquent les positions des résonances isotropes des groupes C=O et C-OH de l'acide oléique (marron) et des carboxylates de l'oléate de zinc (gris).

F3.3 REACTIVITE DES NANOPARTICULES FONCTIONNALISEES SOUS IRRADIATION UV

Les études consécutives concernant la réactivité de la surface des NPs fonctionnalisées par l'acide oléique ont été réalisées en exposant les composés décrits ci-dessus à une irradiation UV. Sous UV, la modification de la forme de NPs non-fonctionnalisées a été observée par DRX et MET. A contrario, la forme de NPs fonctionnalisées a été maintenue, mais la dégradation d'acide oléique attachés sur la surface de ZnO a été observée par ATG, IR, et RMN solide ^{13}C

et ^{17}O. Cette dégradation est en accord avec la bibliographie publiée concernant les propriétés photophysiques de nanoparticules de ZnO.[19]

Par contre, les études de RMN solide ^{17}O ont montré pour la première fois l'échange d'oxygène entre le ligand enrichi en ^{17}O et la surface de ZnO-NPs, avec une nouvelle résonance apparaissant à ~ -28 ppm (voir Figure F5), et qui a été attribuée aux oxygènes situés à la surface des ZnO-NPs.[20]

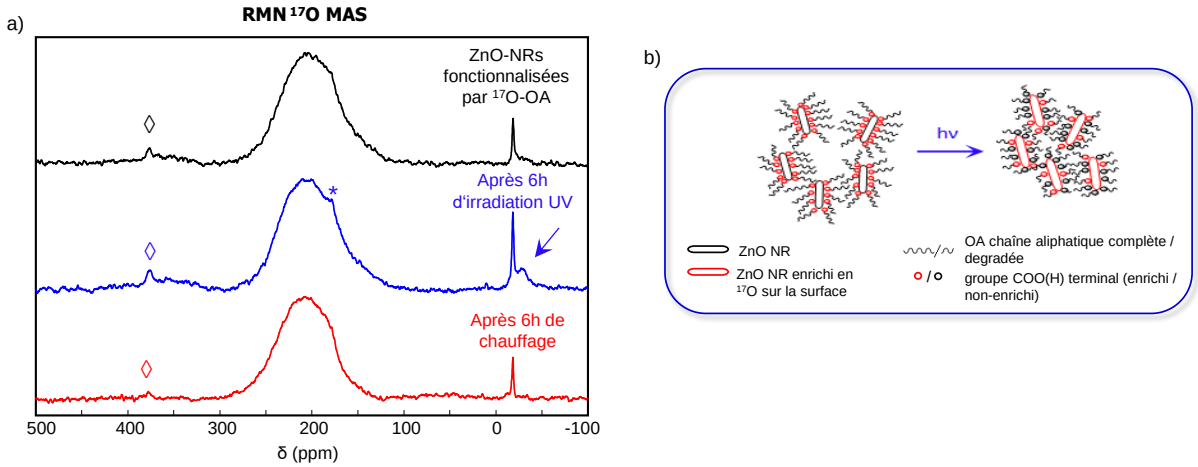

Figure F5 : a) Les spectres de RMN solide ^{17}O de ZnO-NPs fonctionnalisées par l'acide oléique (OA) enrichi en ^{17}O, avant (noir) et après 6 heures d'irradiation UV (bleu) ou de chauffage (rouge). La flèche bleue indique les oxygènes situés à la surface du ZnO enrichi. Le symbole "*" correspond aux bandes de rotation, et le symbole "◊" correspond aux oxygènes en abondance naturelle dans le rotor en zircone. b) Schéma illustrant décrivant le processus d'échange d'oxygènes sur la surface des NPs.

CHAPITRE F4 - ENRICHISSEMENT D'ACIDES AMINES

Les acides aminés (AA) sont des molécules organiques importantes, qui contiennent un groupe amine (-NH_2), un groupe acide carboxylique (-COOH) et une chaîne latérale spécifique (R-) positionnée en α de la fonction acide carboxylique (dans le cas des acides α-aminés). Les plus importants de ces acides aminés sont au nombre de 20. Ils sont protéinogènes, c'est-à-dire qu'ils se retrouvent très majoritairement dans les structures des peptides et des protéines. A part la glycine, tous les acides aminés sont des molécules chirales ayant une activité optique. Dans ce manuscrit, les acides aminés ont été enrichis en $^{17}O/^{18}O$ en utilisant principalement la méchanochimie. Certains de ces acides aminés ont ensuite été protégés par un groupe Fmoc (dans ce cas les réactions ont été réalisées en solution) en vue de leur utilisation pour la préparation des peptides courts enrichis en $^{17}O/^{18}O$. Le répertoire complet des produits enrichis dans ce chapitre est montré dans la Figure F6.

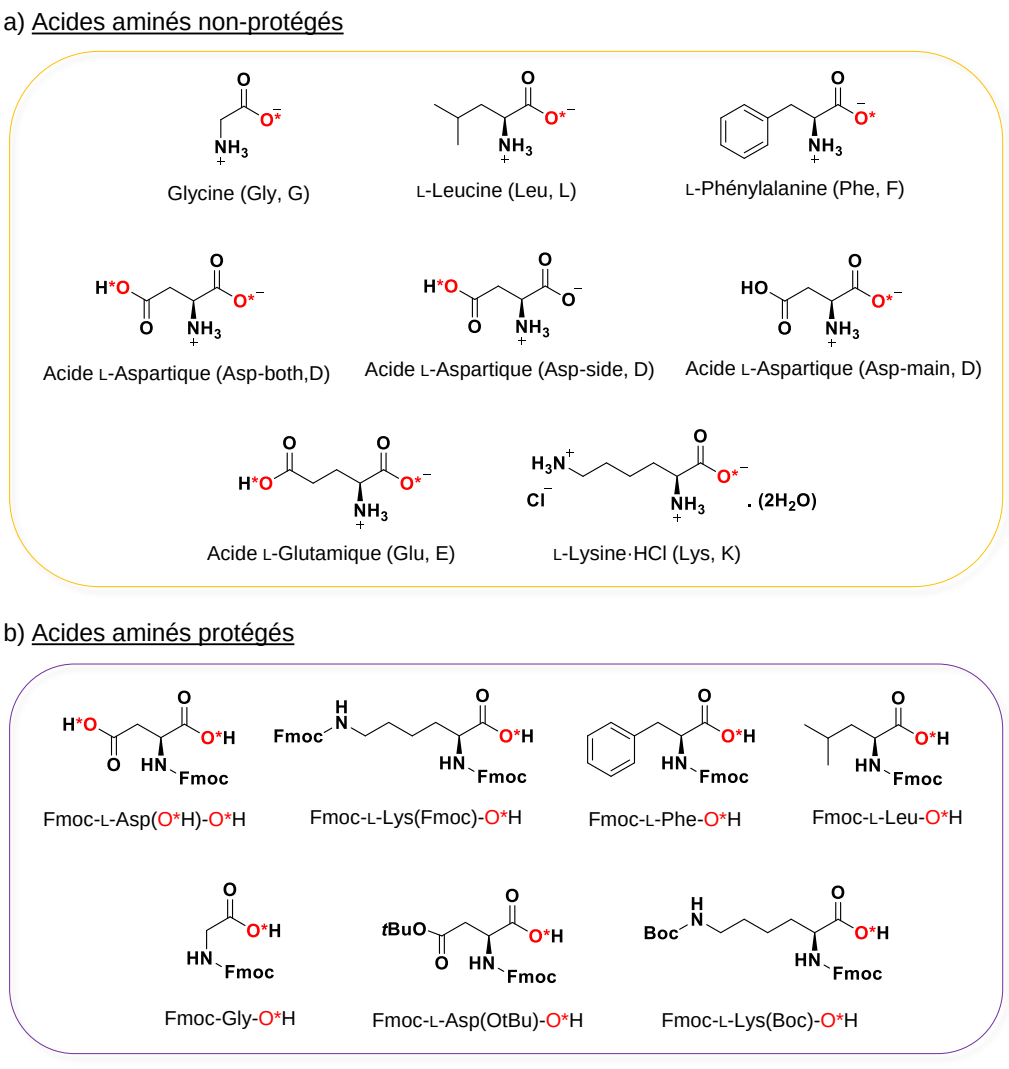

Figure F6 : Répertoire des acides aminés a) non-protégés et b) protégés enrichis en $^{17}O/^{18}O$.

F4.1 ACIDES AMINES NON-PROTEGES

a) Voies d'enrichissement en $^{17}O/^{18}O$

Deux voies différentes ont été appliquées pour l'enrichissement des acides aminés (AA) en $^{17}O/^{18}O$: la saponification mécanochimique et l'échange d'oxygènes catalysé par un acide (Schéma F6) :

- Pour ce qui est de la saponification, contrairement aux acides gras enrichis en $^{17}O/^{18}O$ par cette méthode, les esters d'acides aminés disponibles commercialement étaient sous forme de sels de chlorure d'hydrogène. Cela a nécessité d'utiliser une quantité plus importante d'éthanolate de sodium. Une autre différence est liée au processus d'isolement des acides aminés (traitement ou « work-up ») qui sont très solubles dans l'eau et qui ne pouvaient pas être facilement séparés par extraction du produit secondaire NaCl.

- Le deuxième protocole (l'échange d'oxygènes par catalyse) est dans la littérature le protocole le plus utilisé pour l'enrichissement d'acides aminés en $^{17}O/^{18}O$. Il a été utilisé ici majoritairement pour effectuer une comparaison directe avec l'enrichissement par voie mécanochimique.[21] Pour la catalyse, le chlorure d'hydrogène compris dans la structure des acides aminés (AA·HCl) ou un acide de Lewis (Li^+) ont été utilisés.

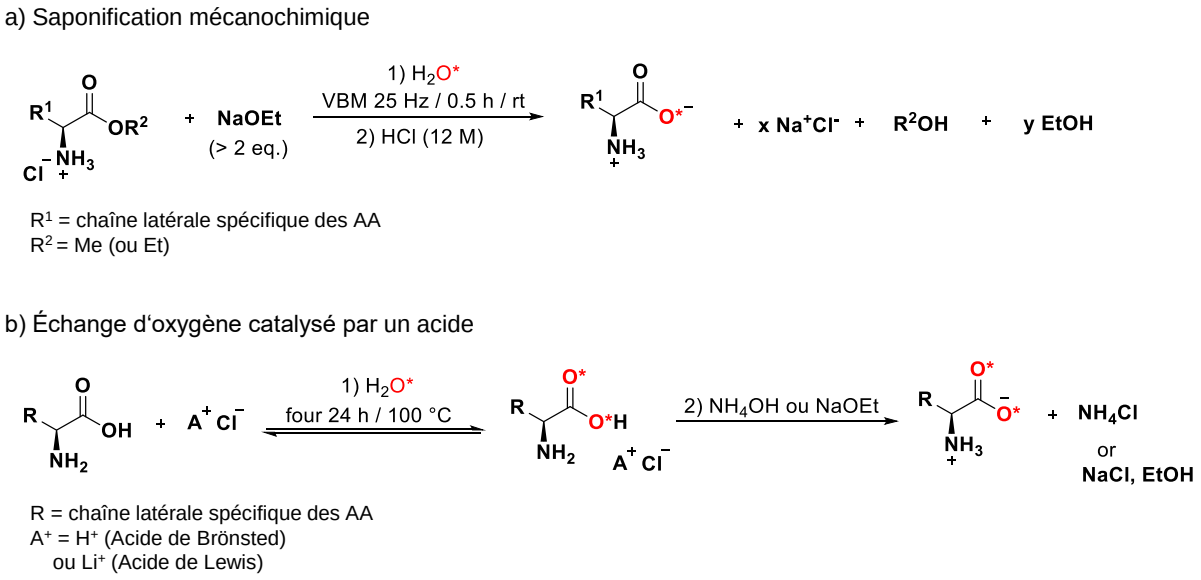

Schéma F6 : Les voies d'enrichissement d'acides aminés en $^{17}O/^{18}O$ en utilisant a) la saponification mécanochimique, ou b) l'échange d'oxygène catalysé par un acide. La procédure d'isolement n'est pas présentée dans ce schéma.

b) Acides aminés enrichis par saponification

Au total, cinq acides aminés ont été enrichis en $^{17}O/^{18}O$ par la saponification mécanochimique en 30 min de broyage à 25 Hz dans le réacteur en acier inoxydable contenant deux billes du même matériau. Les conditions d'isolement ont dû être optimisées pour chaque acide aminé afin d'obtenir les produits purs en absence du sous-produit NaCl. Tous les acides aminés (sauf l'acide glutamique) ont été isolés avec un rendement allant de moyen à élevé et avec un taux d'enrichissement élevé. L'excès énantiomérique a été contrôlé pour tous les acides aminés optiquement actifs par analyse HPLC chirale (sous leur forme protégée Fmoc-AA-OH) et aucune racémisation n'a été détectée. Les résultats sont résumés dans le Tableau F5.

Tableau F5 : Récapitulatif des conditions réactionnelles et des résultats obtenus pour les acides aminés enrichis en $^{17}O/^{18}O$ par saponification mécanochimique (30 min, 25 Hz, température ambiante) réalisée à petite échelle (correspondant à 150 mg d'ester d'acide aminé).

Acide aminé (AA)	n AA-OMe·HCl [mmol]	NaOEt eq.	H_2O* eq.	Masse/ rendement	EY[a] [%]	^{18}O-EL[b] [%]	^{17}O-EL[b] [%]	*ee*[c] [%]
Gly	1.2	2.5	3	49 ± 6 mg 52 ± 6 %	~ 85[d]	~ 43[d]	~ 38[d]	-
Leu	0.8	2.5	3	86 ± 4 mg 78 ± 3 %	82 ± 1	41 ± 1	29	> 99
Phe	0.7	2.5	2	71 ± 3 mg 61 ± 2 %	92 ± 2	46 ± 1	32	> 99
Asp-both[e]	0.8	2.5	4	80 ± 2 mg 76 ± 1 %	88 ± 1	44 ± 1	31	> 99
Asp-side[e]	0.8	3.5	3	77 ± 7 mg 70 ± 6 %	85 ± 1	42	31	-
Asp-main[e]	1.0	2.5	3	113 ± 12 mg 84 ± 11 %	95 ± 1	47	34	-
Lys·HCl[f]	0.6	3.5	3	64 ± 6 mg 54 ± 4 %	93 ± 1	47 ± 1	33	> 99

[a] EY = rendement d'enrichissement, [b] EL = taux d'enrichissement (en utilisant de l'eau enrichie à 99% en ^{18}O ou à 70% en ^{17}O), [c] excès énantiomérique (*ee*) déterminé pour les Fmoc-AA-OH produits, [d] Le rendement et le taux d'enrichissement de la Gly enrichie ont été estimés sur sa forme Fmoc-protégée (Fmoc-Gly-O*H), et de l'eau enrichie à 90% en ^{17}O a été utilisée ici pour l'enrichissement en ^{17}O, [e] Asp-both, Asp-side and Asp-main correspondent à l'acide L-aspartique enrichi sur les deux fonctions acides carboxyliques, sur la fonction acide carboxylique de la chaîne latérale ou de la chaîne principale, respectivement, et [f] valeurs correspondent à L-Lys·HCl essentiellement sous sa forme d'anhydre. Les barres d'erreurs ont été estimées en réalisant plusieurs expériences (n = 2,3).

Dans le cas particulier de l'acide L-aspartique, celui-ci a été enrichi *i)* sur les deux fonctions acides carboxyliques (Asp-both), *ii)* sélectivement sur la fonction acide carboxylique de la chaîne principale (Asp-main), et *iii)* sur la fonction acide carboxylique de la chaîne latérale

(Asp-side). La L-lysine a été isolée sous la forme du sel de chlorure d'hydrogène anhydre ou comme un dihydrate. Dans le cas de l'acide L-glutamique, un sous-produit indésirable (l'acide pyro-glutamique) a été formé pendant la saponification et le protocole n'a pas été encore optimisé afin de prévenir sa formation.

Afin de produire les quantités suffisantes pour la préparation d'acides aminés enrichis en $^{17}O/^{18}O$ et protégés avec le groupe Fmoc qui seront utilisés pour la synthèse de peptides enrichis en $^{17}O/^{18}O$, les protocoles d'enrichissement de la glycine, de la L-lysine et de l'acide L-aspartique ont été optimisés à une échelle plus élevée utilisant 300 ou 450 mg de substrats de départ. Les résultats sont récapitulés dans le Tableau F6.

Tableau F6 : Récapitulatif des conditions réactionnelles et des résultats obtenus pour les acides aminés enrichis en $^{17}O/^{18}O$ par saponification mécanochimique (30 min, 25 Hz, température ambiante) à échelle élevée (correspondant à 450 mg de Gly-OMe·HCl et 300 mg de L-Asp(OMe)-OMe·HCl et L-Lys(OMe)·2HCl).

Acide aminé (AA)	n AA-OMe·HCl [mmol]	NaOEt eq.	H_2O^* eq.	Masse/ rendement	EY[a] [%]	^{18}O-EL[b] [%]
Gly	3.6	2.5	3	185 ± 17 mg 66 ± 6 %	~ 87[c]	~ 42[c]
Asp-both[d]	1.6	2.5	3	174 ± 5 mg 84 ± 3 %	95 ± 2	47 ± 1
Lys·HCl[e]	1.3	3.5	3	183 ± 7 mg 77 ± 3 %	93 ± 6	47 ± 3

[a] EY = rendement d'enrichissement, [b] EL = taux d'enrichissement (utilisant de l'eau enrichie à 99% en ^{18}O), [c] Le rendement et le taux d'enrichissement de la Gly enrichie ont été estimé sur sa forme Fmoc-protégée (Fmoc-Gly-O*H), [d] Asp-both correspond à l'acide aspartique enrichi sur les deux fonctions acides carboxyliques, et [e] valeurs correspondant à L-Lys·HCl essentiellement sous sa forme anhydre. Les barres d'erreurs ont été estimées en réalisant plusieurs expériences (n = 2,3).

c) Acides aminés enrichis par échange d'oxygène catalysé par un acide

Le protocole d'enrichissement de la glycine à partir de son sel de chlorure d'hydrogène a été adapté pour être comparé directement avec les protocoles basés sur la saponification mécanochimique.[21] Ici, trois acides aminés ont été enrichis par la voie d'échange d'oxygènes catalysé par un acide: la glycine, l'acide L-aspartique et la L-lysine. L'échange a été réalisé pendant 24 heures de chauffage au four à 100 °C. L'acide chlorhydrique présent dans les composés initiaux a été utilisé afin de catalyser l'enrichissement de la Gly et de la L-Lys. Par ailleurs, l'acide de Lewis Li^+ (LiCl) a été utilisé pour l'enrichissement de L-Asp. Les résultats sont récapitulés dans le Tableau F7.

Tableau F7 : Récapitulatif des conditions réactionnelles et des résultats obtenus pour l'enrichissement d'acides aminés en ^{18}O par échange d'oxygène catalysé par un acide (24 h, 100 °C, four) à petite échelle.

Substrat	n Substrat [mmol]	H_2O^* eq.	Masse/ rendement	EY[a] [%]	^{18}O-EL[b] [%]	*ee*[c] [%]
Gly·HCl	1.2	3	72 ± 3 mg 77 ± 3 %	quantitatif[d]	62 ± 1[d]	-
L-Asp-both[e]	0.8	4	79 ± 1 mg 78 ± 2 %	56	28	N.D.
L-Lys·2HCl[f]	0.6	3	73 ± 7 mg 62 ± 5 %	quantitatif	60 ± 1	> 99

[a] EY = rendement d'enrichissement, [b] EL = taux d'enrichissement (utilisant de l'eau enrichie à 99% en ^{18}O), [c] excès énantiomérique (*ee*) déterminé pour les Fmoc-AA-OH produits, [d] Le rendement et le taux d'enrichissement de la Gly enrichie ont été estimés sur sa forme Fmoc-protégée (Fmoc-Gly-O*H), [e] Asp-both correspond à l'acide aspartique enrichi sur les deux fonctions acides carboxyliques, N.D. = non-déterminé, et [e] valeurs correspondant à L-Lys·HCl essentiellement sous sa forme anhydre. Les barres d'erreurs ont été estimées en réalisant plusieurs expériences (n = 2,3).

d) Analyses des produits enrichis

Les acides aminés enrichis en $^{17}O/^{18}O$ ont été analysés par RMN liquide ^{1}H et ^{13}C pour évaluer leur pureté, et ensuite par DRX pour évaluer la présence de NaCl comme sous-produit de la réaction, ou pour déterminer le polymorphisme de l'acide aminé isolé, et enfin par spectrométrie de masse pour déterminer le taux d'enrichissement. Toutes ces analyses sont présentées dans l'Annexe IV.

Les acides aminés enrichis en ^{17}O ont été analysés par RMN solide ^{17}O et les résultats sont présentés et décrits dans la version anglaise de ce manuscrit.

F4.2 ACIDES AMINES PROTEGES AVEC LE GROUPEMENT FMOC

Les acides aminés enrichis en $^{17}O/^{18}O$ ont ensuite été protégés par le groupe Fmoc pour deux raisons : *i)* pour pouvoir analyser l'éventuelle perte d'excès énantiomérique suite à la procédure d'enrichissement et *ii)* pour produire les substrats enrichis pour la synthèse des peptides enrichis. Toutes les réactions de protection ont été réalisées en solution en suivant des protocoles déjà publiés. Les conditions réactionnelles et les résultats sont récapitulés dans le Tableau F8.

Tableau F8 : Récapitulatif des conditions réactionnelles et des résultats obtenus pour la préparation d'acides aminés enrichis en $^{17}O/^{18}O$ et protégés avec le groupe Fmoc.

Substrat	Réactif	Base aq.	Solvant org.	Temp[a] [h]	Rendement	EY[b] [%]	^{18}O-EL[c] [%]	^{17}O-EL[c] [%]	*ee* [%]
Acides aminés protégés avec le groupe Fmoc préparés pour les analyses chirales									
^{18}O-L-Asp (1.2 eq)	Fmoc-OSu (1.0 eq)	Na_2CO_3 (13.5%)[d]	DMF	1	470 mg 69 %	-	44	-	> 99
^{18}O-L-Lys (1.0 eq)	Fmoc-OSu (2.2 eq)	Na_2CO_3 (13.5%)[d]	DMF	1	515 mg[e] 81 %[e]	-	47[e] 60[f]	-	> 99[e] > 99[f]
L-Leu-OMe·HCl (1.0 eq)	Fmoc-OSu (1.1 eq)	$NaHCO_3$	acétone	16	255 mg 86 %	78	39	-	> 99
L-Phe-OMe·HCl (1.0 eq)	Fmoc-OSu (1.1 eq)	Na_2CO_3	DMF	1	250 mg 92 %	95	47	-	> 99
Acides aminés protégés avec le groupe Fmoc préparés pour la synthèse des peptides enrichis									
^{18}O-Gly (1.2 eq)	Fmoc-OSu (1.0 eq)	Na_2CO_3 (10%)[d]	dioxane	0.33	96 %[g]	96	43	-	-
Gly-(OMe)·HCl [h] (1.0 eq)	Fmoc-OSu (0.8 eq)	Na_2CO_3 (10%)[d]	dioxane	0.33	490 mg[i] 82 %[i]	86[i]	43[i]	38	-
L-Asp(O*t*Bu)-OMe·HCl [h] (1.0 eq)	Fmoc-OSu (0.95 eq)	Na_2CO_3	DMF	1	350 mg[j] 76 %[j]	91[j]	45[j]	41[j]	N.D.
L-Lys(Boc)-OMe·HCl[h] (1.0 eq.)	Fmoc-OSu (1.1 eq)	$NaHCO_3$	THF	16	180 mg 76 %	91	45	32	N.D.

[a] Durée de la réaction à température ambiante, [b] EY = rendement d'enrichissement, [c] EL = taux d'enrichissement (en utilisant de l'eau enrichie à 99% en ^{18}O ou à 90% en ^{17}O), [d] solution aqueuse (w/w), [e] valeurs pour la L-Lys enrichie par saponification, [f] valeurs pour la L-Lys enrichie par l'échange d'oxygènes catalysé par un acide, [g] masse isolée variée dépendant de la quantité de ^{18}O-Gly utilisée, [h] intermediaire non-isolé, [i] valeurs pour le Fmoc-Gly-O*H à échelle élevée, [j] valeurs pour le Fmoc-L-Asp(O*t*Bu)-O*H à échelle élevée, N.D. = non-déterminé.

CHAPITRE F5 - SYNTHESE DES PEPTIDES ENRICHIS

Les peptides RGD et GRGDS enrichis en $^{17}O/^{18}O$ (sur les acides aminés Gly et/ou L-Asp) ont été synthétisés par SPPS (la synthèse peptidique sur support solide) en utilisant la stratégie de la protection orthogonale « Fmoc/O*t*Bu ».[22] La synthèse a d'abord été optimisée en utilisant les acides aminés non-enrichis. Ensuite, les peptides enrichis ont été synthétisés à partir de la glycine et de l'acide L-aspartique enrichis en $^{17}O/^{18}O$ par mécanochimie, et ensuite protégés avec le groupe Fmoc par synthèse en solution (comme décrit dans le chapitre précédent). Dans ce chapitre, les étapes individuelles de la synthèse par SPPS seront d'abord expliquées sans donner tous les détails synthétiques, qui pourront être trouvés dans la version anglaise de ce manuscrit. Ensuite, les résultats concernant les peptides isolés seront présentés. Les peptides enrichis synthétisés au cours de cette thèse sont présentés dans la Figure F7.

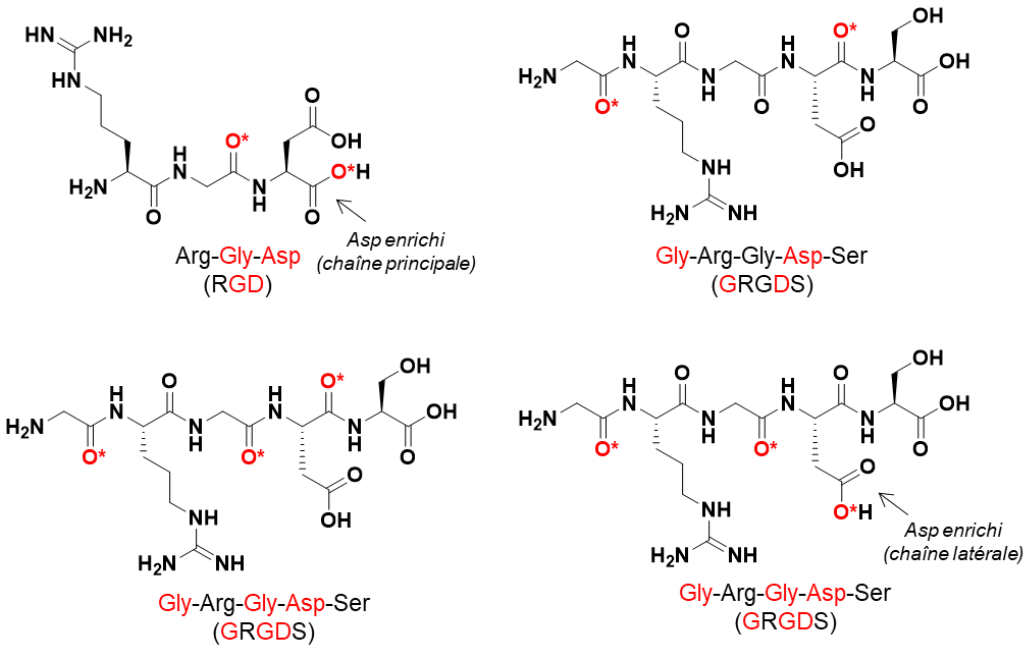

Figure F7 : Le tri-peptide RGD et les penta-peptides GRGDS enrichis en $^{17}O/^{18}O$ sur les unités Gly et L-Asp (sur la fonction acide carboxylique de la chaîne principale ou latérale). Les oxygènes enrichis (avec des taux d'enrichissement variés) sont indiqués par une étoile et la couleur rouge. Dans la fonction acide carboxylique de l'acide aspartique (de la chaîne principale pour le RGD et latérale pour le GRGDS), les deux oxygènes ont le même taux d'enrichissement.

F5.1 SYNTHESE PEPTIDIQUE SUR SUPPORT SOLIDE

La synthèse des peptides RGD et GRGDS sur support solide (SPPS) s'est déroulée en plusieurs étapes qui sont présentées dans la Figure F8 :

a) La fonctionnalisation de la résine avec le premier acide aminé du peptide envisagé.

b) La construction de la chaîne peptidique *via* une alternance de déprotections et de couplages.

c) Le clivage du peptide de la résine.

d) L'élimination du TFA du peptide, suivi par l'isolement du peptide désalé.

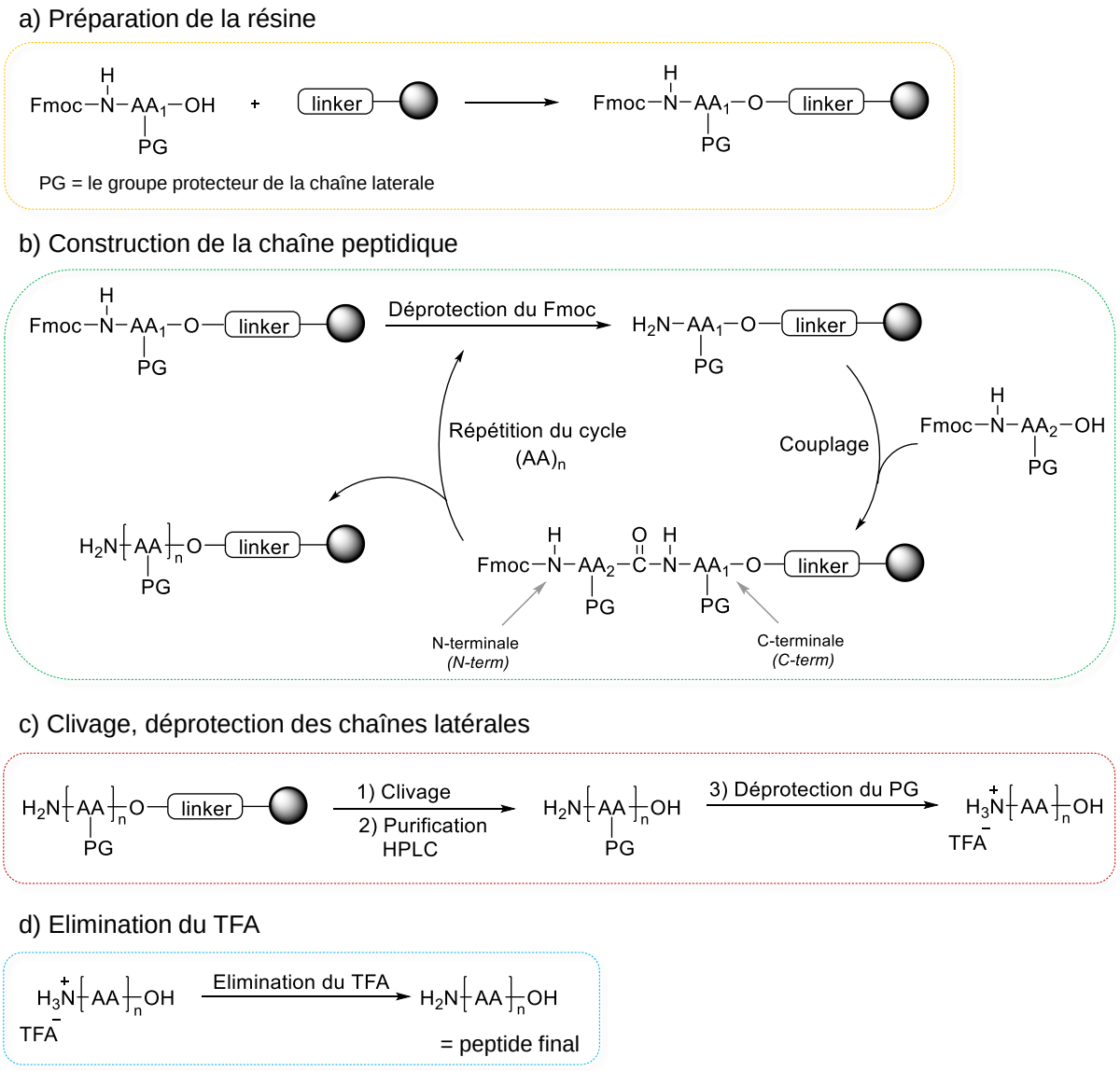

Figure F8: Schéma général avec toutes les étapes importantes de la SPPS.

a) Préparation de la résine

En total, quatre résines 2-chlorotrityle ont été préparées par réaction de la résine fonctionnalisée avec du chlorure de 2-chlorotrityle avec un acide aminé protégé avec le groupe Fmoc dans le DCM anhydre en présence de la base DIEA. Chacune contenait le premier acide aminé (Fmoc-protégé) des peptides RGD ou GRGDS : la résine Fmoc-L-Asp(O*t*Bu)-O-2-

chlorotrityle non-enrichie, les résines Fmoc-L-Asp(O*t*Bu)-O*-2-chlorotrityle enrichies en ^{18}O ou ^{17}O pour les peptides RGD, et la résine Fmoc-L-Ser(*t*Bu)-O-2-Chlorotrityl non-enrichie pour les peptides GRGDS.

b) Construction de la chaîne peptidique

La synthèse des peptides a consisté en une alternance de déprotections et de couplages. Au cours de la synthèse, les déprotections du groupement Fmoc ont été effectuées à l'aide d'une solution de pipéridine dans le DMF (20%, V/V) et d'oxyma pure (0.1M) dans le DMF. Les liaisons peptidiques ont été formées par couplage en présence de la base DIEA et de l'agent de couplage HATU. Pour le couplage d'acides aminés enrichis en $^{17}O/^{18}O$, leur quantité a été réduite en comparaison avec les acides aminés non-enrichis. Les conditions expérimentales exactes, la durée et le nombre de cycles sont détaillés dans la version anglaise de ce manuscrit.

c) Clivage du peptide et déprotection des chaînes latérales

Les peptides ont été détachés de la résine dans des conditions douces (HFIP/DCM) ce qui a permis d'obtenir les peptides avec leurs chaînes latérales toujours protégées. La préservation des protections des chaînes latérales était importante pour pouvoir facilement purifier les peptides RGD et GRGDS par HPLC préparative. Ensuite, les chaînes latérales des peptides purifiés ont été déprotégées en présence de TFA/H_2O/TIS.

d) Elimination du TFA

Les anions TFA ont été éliminés des peptides en passant les solutions des sels de peptide-TFA sur une colonne échangeuse d'ions, qui a retenu les anions TFA, mais pas le peptide libre. La présence de TFA dans le peptide après cette procédure d'élimination a été vérifiée et sa quantité a été estimée en utilisant la RMN liquide ^{19}F (évaluée entre 0.01 - 0.35 eq. de TFA par peptide).

Synthèse du peptide GRGDS enrichi sur la chaîne latérale de l'acide aspartique

La synthèse du peptide GRGDS enrichi sur la chaîne latérale de l'acide aspartique a aussi été envisagée. Afin de préparer ce peptide, un acide aminé L-Asp dont la chaîne latérale était protégée par un groupe ester de méthyl a été utilisé pour la SPPS. En suivant les mêmes étapes de synthèse décrites ci-dessus, il a été possible d'isoler un peptide déprotégé sur tous les chaînes latérales à l'exception de celle de L-Asp. Il a ensuite été envisagé de faire une saponification mécanochimique en utilisant de l'eau enrichie afin d'enrichir en $^{17}O/^{18}O$ le

groupe acide carboxylique de la chaîne latérale de l'acide aspartique. Cependant, cette dernière expérience n'a pas encore pu être réalisée.

F5.2 ANALYSE DES PEPTIDES RGD ET GRGDS ENRICHIS EN $^{17}O/^{18}O$

En suivant les protocoles décrits ci-dessus, seul le tri-peptide non-enrichi RGD a été isolé pur avec un rendement de 22%. Malheureusement, les peptides RGD enrichis en ^{17}O et ^{18}O ont été produits en mélange avec les di-peptides RD (suppression de la glycine). En revanche, les penta-peptides GRGDS ont tous été tous isolés purs avec des rendements très corrects (41 - 57 %) et des taux d'enrichissement élevés (43 % pour le peptide enrichi en ^{18}O et 38 - 39 % pour les peptides enrichis en ^{17}O). Les résultats sont récapitulés dans le Tableau F9.

Tableau F9 : Récapitulatif des résultats obtenus pour les peptides RGD et GRGDS non-enrichis et enrichis en $^{17}O/^{18}O$.

Produits	Rendements et masses isolées	TFA eq.[a]	$^{17}O/^{18}O$-EL[b]
RGD	9 mg / 22 %	0.05	-
^{18}O-RGD	16 mg[c]	0.35	-
^{17}O-RGD	24 mg[d]	0.01	-
GRGDS	22 mg / 45 %	0.2	-
^{18}O-GRGDS	20 mg / 41 %	0.02	43 %
^{17}O-GRGDS	27 mg / 55 %	0.01	38 %
^{17}O-GRGDS	28 mg / 57 %	0.01	39 %

[a] La quantité de TFA a été estimée par RMN liquide ^{19}F, [b] Taux d'enrichissement moyen, [c] RGD enrichi en ^{18}O en mélange avec 30 ± 5 % de di-peptide RD (estimé par la RMN liquide ^{1}H) et ~ 0.35 eq, de TFA (estimé par la RMN liquide ^{19}F), [d] RGD enrichi en ^{17}O en mélange avec 23 ± 5 % de di-peptide RD (estimé par la RMN liquide ^{1}H).

Les peptides finaux ont été analysés et caractérisés par LCMS et par RMN liquide ^{1}H, ^{13}C et ^{19}F afin de déterminer leur pureté, par MS afin de déterminer leur taux d'enrichissement (pour les peptides enrichis en $^{17}O/^{18}O$), et les peptides enrichis en ^{17}O ont été analysés par RMN solide ^{13}C et ^{17}O. Grâce à un taux d'enrichissement élevé, les spectres de RMN solide ^{17}O ont été enregistrés rapidement à un champ magnétique de 14.1 T.

CONCLUSION GENERALE

L'objectif de cette thèse a été de développer de nouvelles voies d'enrichissement en isotopes d'oxygène $^{17}O/^{18}O$ d'acides carboxyliques utilisant la mécanochimie. Il était envisagé que ces nouvelles procédures soient rapides, faciles à réaliser, efficaces tant en termes de rendement isolé qu'en taux d'enrichissement atteint, et abordables (aspect particulièrement important pour l'enrichissement en ^{17}O). Je crois que cet objectif a été atteint comme le montrent les résultats présentés dans ce manuscrit.

Premièrement, un total de neuf acides gras (quatre saturés et cinq insaturés) comprenant des acides polyinsaturés importants tels que l'EPA et le DHA, ont été enrichis en $^{17}O/^{18}O$ par la mécanochimie et isolés purs, avec des rendements élevés (80 - 96 %) et des taux d'enrichissement également élevés (39 - 45 % pour les acides enrichis en ^{18}O en utilisant de l'eau enrichie à 97 % en ^{18}O, 37 - 42 % pour les acides enrichis en ^{17}O en utilisant de l'eau enrichie à 90 % en ^{17}O). Les procédures ont été optimisées également sur une échelle élevée. Ainsi, ~ 1 g d'acide oléique enrichi en ^{17}O et ~ 500 mg d'acide stéarique enrichi en ^{18}O ont été produits en une demi-journée chacun. Tous les acides gras ont été enrichis en ^{17}O pour la première fois. De même, les spectres RMN solide ^{17}O des acides gras saturés et de l'acide oléique ont été reportés ici pour la première fois.

L'intérêt d'enrichir l'acide oléique en ^{17}O a été illustré dans l'étude de la structure de l'oléate de zinc et de nanoparticules d'oxyde de zinc fonctionnalisées avec l'acide oléique enrichi. Leurs structures et la réactivité de la surface des ZnO-NPs sous irradiation UV ont été examinées. Grâce au taux d'enrichissement élevé en ^{17}O, une compréhension inédite de ces systèmes a été permise par la RMN solide ^{17}O, comprenant la détermination de distances Zn···O dans l'oléate de zinc et l'observation d'échange d'oxygènes entre l'acide oléique et la surface des ZnO-NPs lors de l'irradiation.

Ensuite, un total de cinq acides aminés ont été enrichis en $^{17}O/^{18}O$ par mécanochimie et isolés purs avec des rendements moyens à élevés (52 - 84 %) et avec des taux d'enrichissement élevés (41 - 47 % pour les acides ainés enrichis en ^{18}O en utilisant de l'eau enrichie à 99 % en ^{18}O, 29 - 34 % pour les acides aminés enrichis en ^{17}O en utilisant de l'eau enrichie à 70 % en ^{17}O). Aucune perte d'excès énantiomérique n'a été détectée. Des protocoles d'enrichissement par échange d'oxygène catalysé par un acide ont été également appliqués. Dans le cas de la glycine et de la lysine, le taux d'enrichissement a atteint le maximum possible avec l'excès d'eau enrichie utilisé (~ 60 % en utilisant de l'eau enrichie à 99% en ^{18}O). Dans le cas de l'acide

aspartique, l'échange a été catalysé par un acide Lewis et un taux d'enrichissement de 28% a été obtenu (sans optimisation, en utilisant de l'eau enrichie à 99% en ^{18}O).

La synthèse de la glycine et de l'acide aspartique enrichis en $^{17}O/^{18}O$ et leurs protections par le groupe Fmoc ont été optimisées à une échelle permettant de produire les quantités nécessaires à la préparation des peptides enrichis. Ensuite, trois peptides GRGDS enrichis en $^{17}O/^{18}O$ ont été préparés et isolés purs avec des rendements corrects (41 - 57 %) et des hauts taux d'enrichissement (43 % pour le peptide enrichi en ^{18}O, 38 - 39 % pour les peptides enrichis en ^{17}O). Les peptides GRGDS enrichis en ^{17}O ont été analysés par RMN solide ^{17}O pour la première fois.

Perspectives

Ainsi, il a été montré que les procédures d'enrichissement basés sur la mécanochimie sont applicables facilement à l'enrichissement d'acides carboxyliques. Le prochain objectif de notre équipe sera de développer des procédures d'enrichissement en $^{17}O/^{18}O$ d'autres acides carboxyliques, ainsi que d'autres fonctions organiques contenant des atomes d'oxygène et qui sont présentes dans les molécules utilisées, par exemple, comme ligands ou surfactants en science des matériaux. Concernant les acides aminés, les protocoles d'enrichissement d'autres acides aminés non-mentionnés ici sont aussi envisagés par mécanosynthèse afin de les produire de façon facile et rapide. Concernant les peptides enrichis en ^{17}O, leur utilisation future pour l'étude des processus biologiques par RMN solide ^{17}O est également prévue, et sera à compléter par la synthèse d'autres peptides enrichis qui sont également actifs dans les processus de (bio)minéralisation, comme l'acide polyaspartique.

RÉFÉRENCES

1. Haynes, W. M., *Handbook of Chemistry and Physics*. 92nd ed.; 2011-2012.
2. Pearson, P. N., Oxygen isotopes in foraminifera: Overview and historical review. *The Paleontological Society Papers* **2012,** *18*, 1-38.
3. Benson, S.; Lennard, C.; Maynard, P.; Roux, C., Forensic applications of isotope ratio mass spectrometry—A review. *Forensic Sci. Int.* **2006,** *157* (1), 1-22.
4. Gerothanassis, I., Oxygen-17 NMR spectroscopy: Basic principles and applications (Part I). *Prog. Nucl. Magn. Reson. Spectrosc.* **2010,** *56*, 95-197.
5. Theodorou, V.; Skobridis, K.; Alivertis, D.; Gerothanassis, I. P., Synthetic methodologies in organic chemistry involving incorporation of [17O] and [18O] isotopes. *J. Labelled Comp. Radiopharm.* **2014,** *57* (8), 481-508.
6. Métro, T.-X.; Gervais, C.; Martinez, A.; Bonhomme, C.; Laurencin, D., Unleashing the Potential of 17O NMR Spectroscopy Using Mechanochemistry. *Angew. Chem., Int. Ed. Engl.* **2017,** *56* (24), 6803-6807.
7. Seyfried, M. S.; Lauber, B. S.; Luedtke, N. W., Multiple-Turnover Isotopic Labeling of Fmoc- and Boc-Protected Amino Acids with Oxygen Isotopes. *Org. Lett.* **2010,** *12* (1), 104-106.
8. James, S. L.; Adams, C. J.; Bolm, C.; Braga, D.; Collier, P.; Friščić, T.; Grepioni, F.; Harris, K. D.; Hyett, G.; Jones, W., Mechanochemistry: opportunities for new and cleaner synthesis. *Chem. Soc. Rev.* **2012,** *41* (1), 413-447.
9. Howard, Joseph L.; Cao, Q.; Browne, D. L., Mechanochemistry as an emerging tool for molecular synthesis: what can it offer? *Chem. Sci.* **2018,** *9* (12), 3080-3094.
10. Lukin, S.; Tireli, M.; Stolar, T.; Barišić, D.; Blanco, M. V.; di Michiel, M.; Užarević, K.; Halasz, I., Isotope Labeling Reveals Fast Atomic and Molecular Exchange in Mechanochemical Milling Reactions. *J. Am. Chem. Soc.* **2019,** *141* (3), 1212-1216.
11. Ghosh, A.; Ostrander, J. S.; Zanni, M. T., Watching Proteins Wiggle: Mapping Structures with Two-Dimensional Infrared Spectroscopy. *Chem. Rev.* **2017,** *117* (16), 10726-10759.
12. Métro, T. X.; Gervais, C.; Martinez, A.; Bonhomme, C.; Laurencin, D., Unleashing the potential of 17O NMR spectroscopy using mechanochemistry. *Angew. Chem., Int. Ed.* **2017,** *56* (24), 6803-6807.
13. Lynch, M. L., Acid-soaps. *COCIS* **1997,** *2* (5), 495-500.
14. Mehnert, W.; Mäder, K., Solid lipid nanoparticles: production, characterization and applications. *Adv. Drug Deliv. Rev.* **2012,** *64*, 83-101.
15. Zherebetskyy, D.; Scheele, M.; Zhang, Y.; Bronstein, N.; Thompson, C.; Britt, D.; Salmeron, M.; Alivisatos, P.; Wang, L.-W., Hydroxylation of the surface of PbS nanocrystals passivated with oleic acid. *Science* **2014,** *344* (6190), 1380-1384.
16. Kwak, G.; Seol, M.; Tak, Y.; Yong, K., Superhydrophobic ZnO nanowire surface: chemical modification and effects of UV irradiation. *J. Phys. Chem. C* **2009,** *113* (28), 12085-12089.
17. Zeleňák, V.; Vargová, Z.; Györyová, K., Correlation of infrared spectra of zinc (II) carboxylates with their structures. *Spectrochim. Acta A* **2007,** *66* (2), 262-272.
18. Pacholski, C.; Kornowski, A.; Weller, H., Self-assembly of ZnO: from nanodots to nanorods. *Angew. Chem., Int. Ed.* **2002,** *41* (7), 1188-1191.
19. Kenanakis, G.; Giannakoudakis, Z.; Vernardou, D.; Savvakis, C.; Katsarakis, N., Photocatalytic degradation of stearic acid by ZnO thin films and nanostructures deposited by different chemical routes. *Catal. Today* **2010,** *151* (1-2), 34-38.
20. Champouret, Y.; Coppel, Y.; Kahn, M. L., Evidence for Core Oxygen Dynamics and Exchange in Metal Oxide Nanocrystals from In Situ 17O MAS NMR. *J. Am. Chem. Soc.* **2016,** *138* (50), 16322-16328.
21. McGlone, S. J.; Elmes, P. S.; Brown, R. D.; Godfrey, P. D., Molecular structure of a conformer of glycine by microwave spectroscopy. *J. Mol. Struct.* **1999,** *485-486*, 225-238.
22. Amblard, M.; Fehrentz, J.-A.; Martinez, J.; Subra, G., Fundamentals of modern peptide synthesis. In *Peptide synthesis and applications*, Springer: 2005; pp 3-24.